Plasticity and Impact Test Studies on Thermoplastic Materials, Finite Element Analysis and Experimental Correlation.

by Aitor Arriaga Osa

Lea Artibai Ikastetxea S. Coop.

and

London Metropolitan Polymer Centre,
London Metropolitan University.

Thesis submitted for the award of the degree of Doctor Europaeus (European doctorate).

May 2012.

Abstract.

Scope of the Thesis.

This research deals with the mechanical prediction of the behaviour of two thermoplastic materials, Polypropylene (PP) and a blend of Polycarbonate + Acrilonytrile Butadiene Styrene (PC/ABS). A combined methodology of experimental work and finite element approach was used.

The thesis document is divided into two general parts. Part I concerns to the quasi-static behaviour of both materials. Here, the aim was to evaluate the validity of the elasto-plastic material constitutive models implemented in the software ANSYS. For this purpose, different testing modes were evaluated (tensile, bending, puncture) both experimentally and numerically. Acceptable results were obtained with the use of simple yield criteria models (Von Mises). The correlation level was improved using sophisticated yield models (Drucker-Prager).

Part II deals with the dynamic/impact behaviour of the selected polymers. The objective was to evaluate again elasto plastic material models but with especial consideration to strain rate effects and the use of LS-DYNA. Tensile, Charpy and Puncture test were carried out and correlated by means of numerical simulations. The correlation level was improved with the developed iterative method.

Each part of the thesis includes a short abastract and an introduction in order to describe the research carried out and the covered challenges.

As a result of the carried out research two papers were published in the journal Polymer Testing (Elsevier), which are included in the last pages of the document. The first paper reflects the work carried out in the Part I of the thesis, while the second paper covers the dynamic behaviour of a thermoplastic part developed in collaboration with a plastic component developing company.

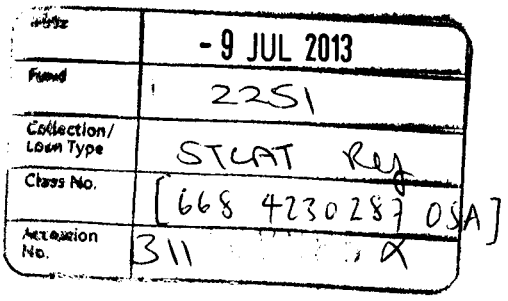

Acknowledgements.

First of all, I would like to thank all the people at the Materials Department in Leartiker and Lea-Artibai Ikastetxea S. Coop. The completion of this thesis is not only an individual achievement but also a collective success. I am especially grateful to Dr. Alex Arrillaga for his support and friendship; we both started this research journey together and finally have arrived to the final destination.

Many thanks to my different supervisors in Leartiker; Jose Mari Lazkano at the very start of the thesis, Rikardo Pagaldai for his continuous advices, and Rikardo Hernandez for his kind help. I would also like to express my sincere thank to my different research group leaders; Rafael Atxurra, Maria Madarieta, Jose Javier Egurrola, Amaia Egia and Ainara Basurko.

I especially want to express mý sincere gratitude to my supervisors in London Metropolitan University-Polymer Centre (UK), Dr. Alicia Chrysostomou, Dr. Michael O´Brien and Prof. S. Hashemi, for their helpful discussion, suggestions and corrections.

My best gratitude to Xabier Aparicio and Mario Ordoñez at Maier Technology Centre (MTC) in Ajangiz, for their kind collaboration at the experimental impact testing phase.

I would like to express my deepest thanks to my entire family and friends, for their support and motivation throughout the years.

Eskerrik asko!

Aitor Arriaga
Markina-Xemein, August 2011.

Part I: Mechanical Quasi-Static Studies in Thermoplastic Materials. Experimental Testing and Finite Element Analysis.

Index of Contents.

Index of Tables.

Index of Figures.

Abstract.

The primary aim of the study was to evaluate the validity of the elasto-plastic constitutive models implemented in the Finite Element Analysis (FEA) software ANSYS®. This was carried out comparing experimental tensile, bending and puncture or plate penetration test results with the corresponding FEA calculations. The studies were carried out in concern to the slow rate testing and finite element analysis of two thermoplastic materials. The selected materials were a blend of Polycarbonate (PC) and Acrylonitrile-Butadiene-Styrene (ABS), Bayblend® T45 from Bayer Material Science, as an amorphous polymer and a Polypropylene (PP) copolymer, BE677AI from Borealis, as a semi-crystalline polymer.

The uniaxial tensile behavior of both materials was used to generate material data input for the simulation software. Due to post yield uncertainties when measuring true values of stress and strain with conventional extensometric devices, an iterative approach was presented here as a solution for measuring large local plastic strains in tensile specimens.

The experimental three point bend test and the plate perforation test with hemispherical darts, were used as correlation tests with simulations in order to validate not only the used constitutive elasto-plastic models based on the Von Mises yield criteria, but also to check the influence of different simulation variables. The parameters studied were the element type, mesh density, friction and contact conditions between different parts. Additionally, another yielding criteria, the hydrostatic pressure sensitive Drucker-Prager model, was analysed.

It was observed that for both materials, the use of a classical approach for obtaining true values of stress and strain in conjunction with a Von Mises yielding criteria gave acceptable results for the studied testing modes. However, the input curves did not closely correlate with the tensile test results. This was overcome to using an iterative method to correct the input curves to match then to the experimental tensile tests. Being a precise procedure for uniaxial cases, it was observed that for bending or puncture problems this method offered stiffer responses than using the classical approach of stress-strain conversions.

Finally, the Drucker-Prager criterion was able to capture in a more precise way bending dominated problems than the usual Von Mises yielding criteria.

Chapter 1: Introduction.

The use of calculation codes based on the finite element method (FEM) in the design phase of new industrial products has resulted in cost reductions relative to the manufacture of physical prototypes and "trial and error" tests.

The general use software such as NASTRAN, ABAQUS or ANSYS permit the virtual modelling of a mechanical part or assembly, the input of material's mechanical properties, the solving of loading conditions and the visualisation and evaluation of the obtained results.

Nowadays, polymeric materials, and more specifically thermoplastic materials, have passed from applications where aesthetics were the principal function to strict structural requirements in sectors like automotive (substitution of metallic parts, passenger and pedestrian protection components, instrument boards, etc.) or appliances (mobile phones, TV-audio devices, etc.). Due to this, companies need to use FEA in order to predict the structural behaviour of their plastic components prior to testing trials.

One of the most challenging considerations when modelling thermoplastic materials is the inputting the calculation code, with the appropriate test data, in order to represent the material's mechanical behaviour. This involves the determination of suitable constitutive material mathematical models for plastic components.

Usually, the former is met using data from the traditional uniaxial tensile test even though the yielding behaviour in tension, compression and shear differ for thermoplastic materials [1].

The uniaxial tensile test itself presents some challenging considerations when dealing with plastics; simulation software require "true" stress-strain data up to the failure point of the specimen and this is not simple with thermoplastics since the determination of true stress-strain data above the yield point is not straightforward with conventional extensometric devices. This point will be discussed in detail in the present section.

Moreover, the vast majority of material models used in FEA software are developed for metals, and it is well known that plastics present special characteristics such as, linear viscoelastic behaviour at small strains leading to non-linearity in the stress-strain curve, differing yielding in tensile, compression and shear modes (thus, the Von Mises yielding is not satisfied), anisotropic hardening and no volume preservation in plasticity, among others.

These considerations need to be borne in mind, but from the practical engineering or industrial viewpoint the approximation of metal plasticity should not be rejected.

The validation of a constitutive model needs to be achieved in different deformation modes. If the experimental vs. simulation correlation is only performed at a uniaxial level, it is not properly calibrated the multiaxial behaviour of the material. Then these could not be adequate, for example, to represent bending or shearing states.

In the present work, it is intended to determine the multiaxial correlation level reached when contrasting the three point bending test (where tensile and compression stress zones are generated when straining the sample) and the dart penetration test (where biaxial stresses are generated in the central region of the plate) adopting the classical elastic-plastic material models (isotropic hardening with Von Mises criterion).

Additionally, more sophisticated material models (the Drucker-Prager constitutive model) will also be checked in order to evaluate the correlation level with experimental tests.

When performing the simulations, apart from the selected constitutive model and material data input, finite element related variables have to be considered. These variables can be mainly summarised in the used element type for meshing the different components, the mesh density and in the frictional and contact characteristics between different parts of the finite element model. The goal is to evaluate the influence on the simulations results with any change on the mentioned parameters.

As a result of this study, a validated working methodology will be developed for dealing with thermoplastic materials in static loading conditions.

Chapter 2: Definitions on the Mechanical Behaviour of Thermoplastic Polymers.

In this section, some basic concepts related to the quasi-static mechanical behavior of thermoplastic polymers will be described first. These include the yielding behaviour and different phenomena like crazing, shear yielding, necking and failure. The most widely used test methods for material data generation will also be described shortly.

2.1. Shear Yield, Crazing and Fracture.

2.1.1. Introduction: Ductile and Brittle behaviour.

The most common type of stress-strain tests is that in which the response (strain) of a sample subjected to a force that increases with time, at constant rate, is measured. The shape of the stress-strain curve is used to define ductile and brittle behaviour. Since polymeric materials are viscoelastic, the shape of the stress-strain curve is affected by temperature and rate of testing. Figure 2.1 illustrates two general types of stress-strain curves. The curve for a hard and brittle polymer (red) shows that the stress increases more or less linearly with the strain. This behaviour is characteristic of amorphous polymers at temperatures well below the glass transition temperature ($T<<T_g$); these materials (e.g., polystyrene, Tg aprox. 100°C) fail at low strains, leading to brittle fracture at room temperature. Some semicrystalline polymers and thermoset resins exhibit a similar behaviour at $T<<T_g$

The curve in blue represents a polymer that shows a ductile behaviour up to failure. The most ductile polymers undergo necking and cold drawing. Semicrystalline polymers are typical examples that display this behaviour at temperatures intermediate between melting and glass transition ($T_g<<T<<T_m$) (e.g. polyethylene at room temperature).

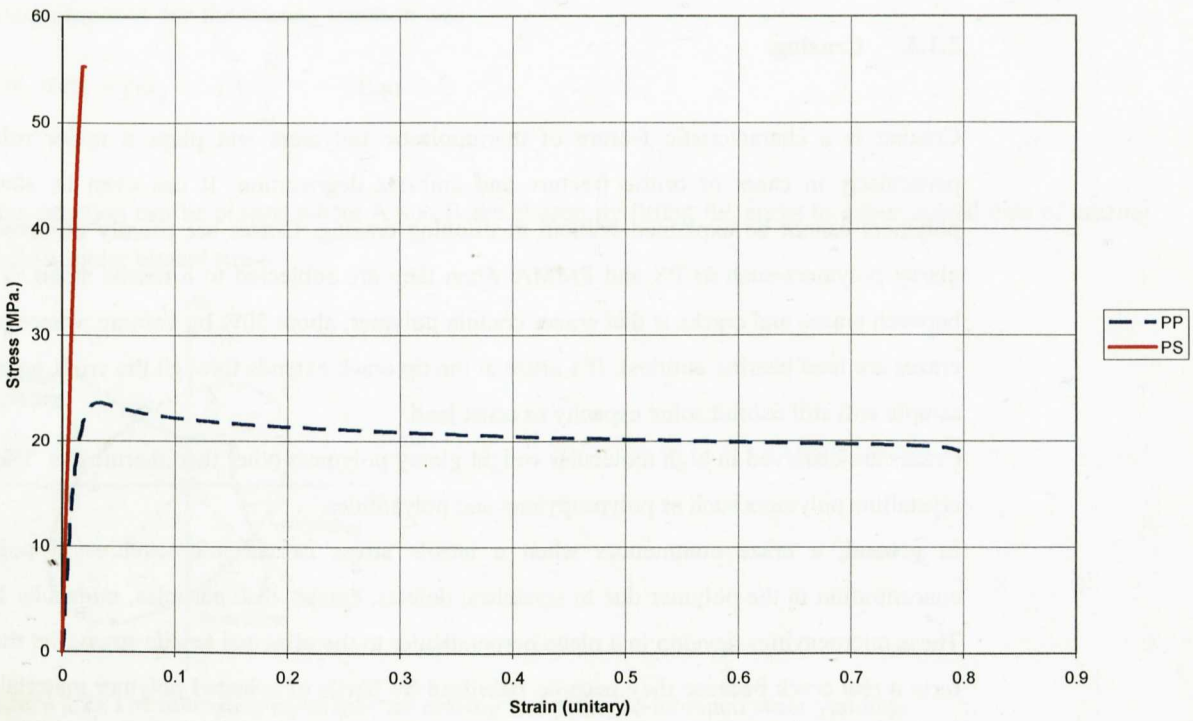

Figure 2.1: Comparison of a ductile behaviour (Polypropylene) and a brittle response (Polystyrene).

Brittle behaviour is displayed by a sample that fails at relatively small strain values (e.g. <10%), while ductile behaviour is displayed by a sample that fails at higher strains after exhibiting a yield point.
In polymer materials it is difficult to distinguish between elastic deformation (recoverable) and plastic deformation (non-recoverable), since the degree to which a sample recovers its original dimension depends on temperature and time.
The most important mechanisms that can lead to plastic deformation in polymers are shear yielding and crazing. Shear yielding takes place at constant volume and leads to a large change in specimen shape. Crazes are the results of localised yield and are formed by microcavities bridged by fibrils; crazing leads to an increase in volume and is a precursor to brittle fracture.
Moreover, the mechanical behaviour of polymers is viscoelastic. Meaning that the yielding process in polymers depends on temperature and strain rate as well as pressure. The stress-strain curve is therefore upon the type of test: tension, compression, shear, bending, etc.

2.1.2. Shear Yield. Basic Concepts.

In polymers it is possible to detect plastic deformation before the yield point, and for strains greater than the yield strain (ε_{yield}), polymers can recover the undeformed macroscopic shape if the temperature is suitably increased.
The formation of a neck always involves the concentration of permanent deformation in a small region of the specimen. This can occur in two different ways. First, if the cross section of the sample is not uniform, the volume element of smaller cross-section will be subjected to higher stresses and therefore, will reach yield faster than any other volume element. Second, a fluctuation in the properties of the material could cause a localised reduction in the yield stress in a volume element, in which case, yield occurs at a lower load value (stress softening).

2.1.3. Crazing.

Crazing is a characteristic feature of thermoplastic polymers and plays a major role in their fracture, particularly in cases of brittle fracture and ambient degradation. It can even be stated that fracture in polymers cannot be explained without mentioning crazing. Crazes are usually observed on the surface of glassy polymers such as PS and PMMA when they are subjected to a tensile stress. The basic difference between crazes and cracks is that crazes contain polymer, about 50% by volume, whereas cracks do not (i.e., crazes are load bearing entities). If a craze at the tip crack extends through the cross section of a sample, the sample will still exhibit some capacity to resist load.
Crazes are observed in high molecular weight glassy polymers other than thermosets. They can also occur in crystalline polymers such as polypropylene and polyamides.
In general, a craze commences when a tensile stress causes microcavities at points of high stress concentration in the polymer due to scratches, defects, cracks, dust particles, molecular heterogeneities, etc. These microcavities develop in a plane perpendicular to the principal tensile stress, but they do not join up to form a real crack because they become stabilised by fibrils of oriented polymer material that are plastically strained. As a result, an interpenetrating system of cavities and polymer fibrils is obtained, known as craze. Crazing occurs before the yield point is reached.

Crazing involves a localised or inhomogeneous plastic strain of the material as in the formation of shear bands. Nevertheless, while shear yielding essentially occurs at constant volume, crazing is a cavitation process and takes place with an increase in volume. The initiation of crazing normally requires the presence of a dilative component of the stress tensor and can be inhibited by applying a hydrostatic pressure, though it is favoured by the presence of triaxial tensile stresses.

Some criteria have been proposed for craze initiation in amorphous polymers. The earliest criterion states that crazing occurs when the uniaxial tensile stress reaches a critical value. Since crazing stress depends on the strain rate and temperature and can also be affected by molecular orientation and environment. This simple criterion is inadequate to describe the behaviour in multiaxial stress systems, since crazing formation is a dilatational process and therefore, criterion should include a dilatational stress component.

Sternstein-Ongchin [2] proposed the following criteria for crazing in amorphous polymers:

$$\sigma_b = A + \frac{B}{I_1} \qquad \text{Equ. 2.1.}$$

where σ_b is the stress required to orientate the fibrils, and A and B are time and temperature dependent parameters. I_1 is the first stress invariant of the stress tensor and represents the dilatational component:

$$I_1 = \sigma_1 + \sigma_2 + \sigma_3 = 3p > 0 \qquad \text{Equ. 2.2.}$$

where σ_1, σ_2, and σ_3 are the principal stresses and p is the hydrostatic pressure or mean stress. The easiest way to test craze criteria is to make measurements in plane stress. In plane stress conditions, $\sigma_1 > \sigma_2$ and $\sigma_3 = 0$, so $\sigma_b = \sigma_2 - \sigma_1$ and I_1 becomes $\sigma_1 + \sigma_2$.

This criteria is generally linked to a critical strain e_1 which depends on the hydrostatic component of stress. For small strains, for the two-dimensional stress field, e_1 is given by:

$$e_1 = \frac{1}{E}(\sigma_1 - \nu\sigma_2) \qquad \text{Equ. 2.3.}$$

where E is Young's modulus and v is Poisson's ratio.

It was proposed that the crazing criterion was

$$Ee_1 = \sigma_1 - \nu\sigma_2 = A + \frac{B}{I_1} \qquad \text{Equ. 2.4.}$$

This equation can be plotted where A and B are chosen by fitting the curve to experimental data of crazing PMMA under biaxial stress.

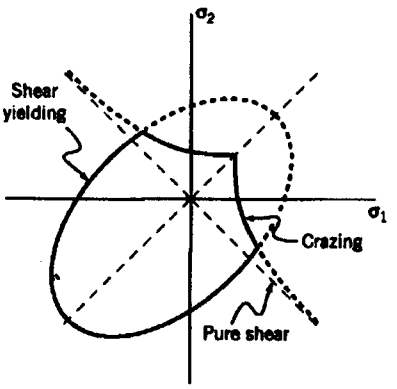

Figure 2.2: The Sternstein envelopes for crazing and pressure-inhibited shear yielding.

The yielding process in a thermoplastic is considered to be a competition between crazing and shear yielding. If crazing dominates, the behaviour of the polymer is brittle, but if shear yielding occurs, the polymer is ductile.

2.2. Mechanical Tests.

2.2.1. Uniaxial Tension Test.

The most common test procedure to obtain yielding information is uniaxial tensile deformation. The material is tested in the gauge section of reduced area A_0, which has a length L_0. The larger section zones are used as attaching points for the clamps. The clamps are separated at a constant rate, and the force F is measured as a function of this separation. The stress can be obtained as the true stress,

$$\sigma_t = F/A \qquad \text{Equ. 2.5.}$$

where A is the area of the section tested at each instant, or as the nominal-engineering stress,

$$\sigma_e = F/A_0 \qquad \text{Equ. 2.6.}$$

A_0 being the area of the original section of the tested piece. The nominal or engineering strain is calculated as the displacement of the clamps per unit length and is commonly written as

$$\varepsilon_e = (L - L_0)/L_0 = \Delta L/L_0 \qquad \text{Equ. 2.7.}$$

where L is the instantaneous measurement length, L_0 is the original gauge length and ΔL is the change in length. The true uniaxial strain is the integral of the infinitesimal nominal strains:

$$\varepsilon_t = \int_{L_0}^{L} \frac{dL}{L} = \ln\left(\frac{L}{L_0}\right) \qquad \text{Equ. 2.8.}$$

As long as the deformation is uniform along the gauge section, the true stress and strain can be calculated from the engineering quantities. With constant volume and uniform deformation assumption during plastic flow, $L\,A = L_0\,A_0$:

$$A_0/A = L/L_0 \qquad \text{Equ. 2.9.}$$

The equation for true stress can be rewritten,

$$\sigma_t = (F/A_0)(A_0/A)$$
$$\sigma_t = \sigma_e(1+\varepsilon_e) \qquad \text{Equ. 2.10.}$$

For true strain, the substitution of $L/L_0 = 1+\varepsilon_e$ gives,

$$\varepsilon_t = \ln(1+\varepsilon_e) \qquad \text{Equ. 2.11.}$$

At very low strains, the differences between true and engineering stress and strain are very small. It does not really matter whether Young's modulus is defined in terms of engineering or true stress-strain.

It must be emphasised that these expressions are valid only as long as the deformation is uniform, once necking starts, the first equation is still valid but the cross-sectional area at the base of the neck must be measured directly rather than being inferred from the length measurements. Because the true stress, thus calculated, is the true stress at the base of the neck, the corresponding true strain should also be at the base of the neck.

Equation 2.10 could still be used if the L and L_0 values were known for an extremely short gauge section centred on the middle of the neck (one so short that variations of area along it would be negligible). Of course, there will be no such gauge section, but if there were, $A_0/A = L/L_0$ would be valid. Thus the true strain could also be calculated as

$$\varepsilon_t = \ln(A_0/A) \qquad \text{Equ. 2.12.}$$

2.2.1.1. Strain Rate. Definition.

This effect will be detailed in depth in the second part of the thesis related to impact studies.

Strain rate is defined by Equ. 2.13 and it is expressed in units of s^{-1}.

$$\dot{\varepsilon} = d\varepsilon/dt \qquad \text{Equ. 2.13.}$$

If the cross-head speed of the testing machine is v=dL/dt, then the strain rate expressed in terms of conventional engineering strain is:

$$\dot{\varepsilon}_e = \frac{d\varepsilon_e}{dt} = \frac{d(L-L_0)/L_0}{dt} = \frac{1}{L_0}\frac{dL}{dt} = \frac{v}{L_0} \qquad \text{Equ. 2.14.}$$

The engineering strain rate is proportional to the crosshead speed. In a modern testing machine, in which the crosshead speed can be set accurately and controlled, it is a simple matter to carry out tensile tests at a constant engineering strain rate.

The true strain rate is given by:

$$\dot{\varepsilon}_t = \frac{d\varepsilon_t}{dt} = \frac{d[\ln(L/L_0)]}{dt} = \frac{1}{L}\frac{dL}{dt} = \frac{v}{L} \qquad \text{Equ. 2.15.}$$

This equation shows that for a constant crosshead speed the true strain rate will decrease as the specimen elongates or cross-sectional area shrinks. To run tensile tests at a constant true strain rate requires monitoring of the instantaneous cross section of the deforming region, with closed-loop control feed back to increase the crosshead speed as the area decreases. The true strain rate is related to the engineering strain rate by the following equation:

$$\dot{\varepsilon}_t = \frac{v}{L} = \frac{L_0}{L}\frac{d\varepsilon_e}{dt} = \frac{1}{1+\varepsilon_e}\frac{d\varepsilon_e}{dt} = \frac{\dot{\varepsilon}_e}{1+\varepsilon_e} \qquad \text{Equ. 2.16.}$$

2.2.1.2. Control modes.

Although testing at a constant crosshead speed is the most common method for tensile testing, there are some other control modes that can be interesting, especially when constant strain rate testing is needed.

- Constant Load Rate Testing. A load-control module allows the machine with the constant rate of extension to function as a constant load rate device. This is accomplished by a feedback signal from a load cell, which generates a signal that automatically adjusts the motion controller of the crosshead. Usually, the servomechanism system response is particularly critical when materials are loaded through the yield point.
- Constant Strain Rate Testing. These systems rely on extensometer to measure the change in the gauge length and to provide strain data as a function of time. The resulting signal is processed to determine the

current strain rate and is used to adjust the crosshead displacement rate throughout the test. Again, servomechanism response time is particularly critical when materials are taken trough yield.

The achievement of a constant strain rate test is not simple, for example, in metallic materials, at the beginning of a test, the plastic strain rate is ostensibly zero and the initial strain rate is:

$$\dot{\varepsilon}_e = \frac{\left(\frac{S_0}{L_0}\right)}{1+\left(\frac{A_0 E}{K L_0}\right)} \qquad \text{Equ. 2.17.}$$

where S_0 is the crosshead speed at the beginning of the test, L_0 is the gage length, A_0 is the initial cross-section, E is the elastic modulus of the material, and K is the stiffness of the testing system.

The strain rate at the yield point is:

$$\dot{\varepsilon}_{e_1} = \left(\frac{S_1}{L_0}\right) \qquad \text{Equ. 2.18.}$$

where S_1 is crosshead speed at yield point.

Equating these two values of strain rate shows that crosshead speed must be reduced from its initial value to its yield-point value by a factor of:

$$\frac{S_0}{S_1} = \left(1+\frac{A_0 E}{K L_0}\right) \qquad \text{Equ. 2.19.}$$

This factor is typically 20 and can be as high as 100. This equation indicates the magnitude of speed changes required only for tests in which there is no yield drop. For materials having upper and lower yield points (which is the case of some plastics), the direction of crosshead motion may have to be reversed after initial yielding to maintain a constant strain rate.

Although the uniaxial tensile test is the one most widely used, it has two drawbacks, when used to provide information on the yielding of polymers. First, the tensile stress applied can lead to brittle fracture before yield takes place, and second, yield may occur in an inhomogeneous way due to the formation of a neck accompanying the tensile test. In any case, given that the cross-section of test specimen decreases as the stress increases, the true stress is always higher than the engineering stress ($\sigma_t > \sigma_e$).

2.2.1.3. Standard Tensile Testing.

The multipurpose specimen from ISO 3167 is a very useful shape of reference when quasi-static mechanical properties are needed.

The ISO standard specifies two specimen shapes which can be used in different test types. This ensures that the test results from various types of tests refer to a uniform material condition.

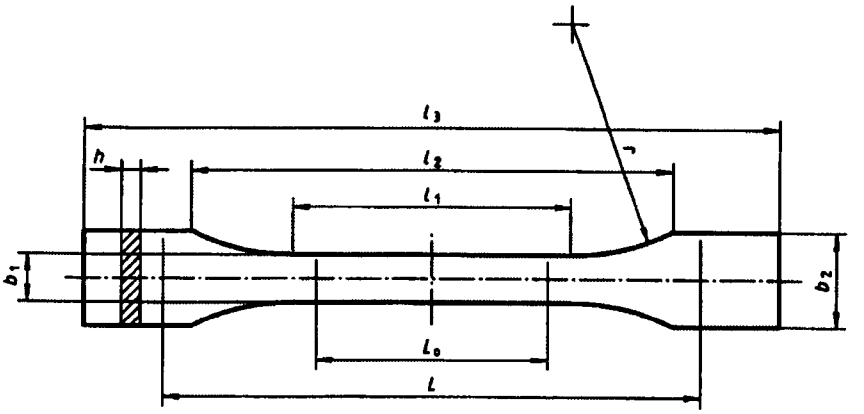

Figure 2.3: Specimen shape and dimensions according to ISO 527.

Dimension		Type A	Type B
b1	width of the narrow part	10±0.2 mm	10±0.2 mm
h	thickness	4±0.2 mm	4±0.2 mm
L1	length of the small parallel part	80±0.2 mm	60±0.5 mm
r	radius	20-25 mm 24±1 recommended	≥60 mm

Table 2.1: Specimen dimensions according to ISO 527 A and B.

In our thesis work, type A specimens were selected.

2.2.1.3.1. Test speed in the standard tensile test.

Due to the viscoelastic characteristics of thermoplastic materials, the test results depend on the rate of loading during the mechanical testing. ISO 527 (Determination of tensile characteristics) allows a speed range between 1 and 500 mm/min. ISO 10350 specifies additional definitions:

- for the modulus of elasticity 1 mm/min.
- for brittle materials (strain to break lower than a 10%) 5 mm/min.
- for all other materials 50 mm/min.

Test speeds are defined as "rate of separation of the grips" in ISO 527 as well as in ASTM D 638.
For comparative purposes, the following standardised testing speed ranges can be encountered for "static" and high rate or impact tests:

Test	Standard	Speed
Static tensile test	ISO 527, ISO 10350	1, 5, 50 mm/min.
Impact tests	ISO 179 (Charpy)	2.9 m/s.
	ISO 180 (Izod)	3.5 m/s.
	ISO 8256 (tensile impact)	3.8 m/s.

Table 2.2: Comparative table of velocities for static and impact standards on plastic materials.

Initial point of the test and calculation of the elastic modulus in the tensile test.

ISO 527 specifies recommended values for the pre-stress at the clamping of the specimens. ASTM D638 uses a Toe Compensation method for the determination of the starting point of the test.
Since the slope of the stress-strain curve is not linear for many plastics, the result of this value depends on the selected strain for the calculation. ISO specifies two strain values, 0.05 and 0.25% for calculating the secant modulus (linear progression could also be used). In ASTM no fixed strain is specified but the standard differentiates between the modulus of elasticity for materials showing linear portion and the secant modulus for materials not showing linearity.

The yield point is mathematically described as a point on the test curve for which the slope takes the value of zero. This behaviour can be observed in most unfilled thermoplastics.

For the strain measurements, direct strain determination and nominal or engineering strain measurements should be differentiated. Direct strain measurements relate to the usage of extensometers (mechanical, laser, video, etc.) while nominal strain is defined as the ratio of the increase of the distance between grips and the initial distance between grips. The results are not comparable especially after the yield point and in materials that suffer localised strains as necking.

2.2.1.3.2. Poisson's ratio determination.

This section deals with the elastic Poisson's ratio, which is a necessary input in the material data card of any FEA code.
Note: a plastic Poisson's relation could also be considered in high strain applications which is discussed in the impact part of the thesis. Section 12.2.
The main handicap is that most of the simulation software only admit as input the elastic relation and not the plastic Poisson's ratio.

A **Bayer**'s Aplication Technology Information (ATI) report [3] describes the general definition for the Poisson's ratio and presents some values for different thermoplastics from Bayer. Poisson's ratio is defined as the relation of the longitudinal and transverse strains in a tensile test and typically is represented by the symbol ν.

$$\nu = -\frac{\varepsilon_{lateral}}{\varepsilon_{longitudinal}} \qquad \text{Equ. 2.20.}$$

The Poisson's ratio hence determines the multiaxial deformation behaviour of the material. Theoretically, Poisson ratio of homogeneous and isotropic materials varies between 0.3 (steel) for elastic ideal solids to 0.5 for plastic flowing materials at constant volume (rubbers also could be considered to have a $\nu \approx 0.5$). Above 0.5 volume reduction is given and below 0.5 (for most materials) a volume increase takes place under deformation. For amorphous moulding materials a value of 0.38 is often more precise than the mechanical measurement since a high precision is required in the measurement device. For long fibre reinforced materials a measurement extensometer device is recommended.

For thermoplastics, which are neither homogeneous nor isotropic, especially the glass filled systems, a theoretical relationship could be defined as a function of the loading duration (t), the temperature (T) and the stress level (σ). This relationship is also based on the limits 0.3 and 0.5 and the Young's modulus:

$$\nu(t,T,\sigma)=\nu_0+(0.5-\nu_0)\cdot\left[1-\frac{E(t,T,\sigma)}{E_0}\right] \qquad \text{Equ. 2.21.}$$

Bayer also presents the following values for most of its thermoplastics:

Polymer	Elastic Poisson's ratio
PC	0.39
PC/ABS	0.40
PC/ABS+GF 10	0.40
TPU	0.47
PA66	0.40
PA66+GF30	0.40
PC+GF30	0.40
ABS	0.37
PBT	0.41
PBT+GF30	0.39

Table 2.3: Poisson's ratio for different thermoplastics from Bayer [3].

The given data is valid for strains up to 1% and a testing speed of 5 mm/min.
Bayer also reports a comparison of FEA results in a circular membrane under concentric load changing a 50% the Poisson's ratio value. They obtain a 7% difference in deformation results and a 14% for stresses. Hence, the usual approximation of selecting a 0.4 Poisson's elastic value for plastics can be correct from an engineering design point of view.

2.2.1.4. Stress-strain curves. Considére's Construction.

Some polymers deform by forming a stable neck during the deformation process and undergo cold drawing, as shown by curve B. In some polymers necking begins at the maximum value of stress but the neck rapidly becomes thinner, causing failure of the specimen immediately after yielding begins, curve A. In other words, the volume element that experiences yielding undergoes a reduction in area ($A<A_0$) in such a way that the true stress, σ_t, is sufficiently high to produce fracture. In polymers, chain alignment also contributes to stable or unstable neck generation.

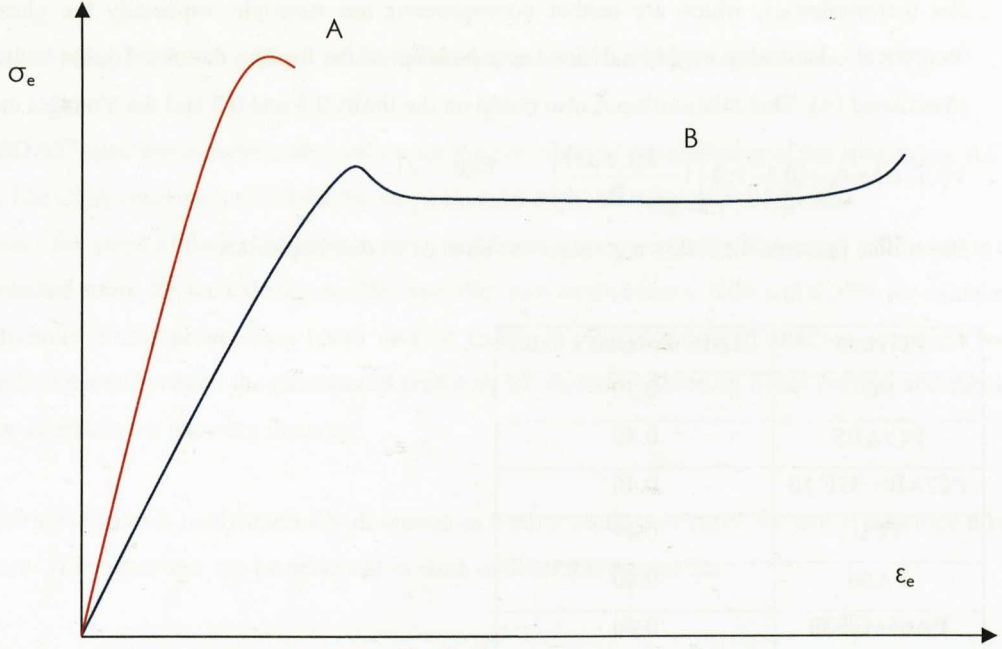

Figure 2.4: Different neck formation mechanisms for polymers. A, unstable necking causing failure rapidly, and B, stable necking propagation and cold drawing before failure.

The Considére construction, which is discussed below, considers the possibility of the formation of a stable neck as a response of polymer materials to the action of a uniaxial tensile stress.

If the strain takes place at constant volume, as previously stated, $AL = A_0 L_0$.

Additionally, we may write

$$\frac{L}{L_0} = 1 + \varepsilon_e = \lambda \qquad \text{Equ. 2.22.}$$

where λ is the extension.

Bearing in mind the definitions of true stress, σ_t, and nominal stress, σ_e, as given by Equ. 2.9, the following relationship could be deduced:

$$\sigma_e = \frac{\sigma_t}{1+\varepsilon_e} = \frac{\sigma_t}{\lambda} \qquad \text{Equ. 2.23.}$$

For a uniaxial tensile test, $\lambda > 1$.

When the development of the neck starts, the applied load on the specimen ceases to increase as strain increases, reaching a maximum in the curve of σ_e vs. ε_e. Mathematically, the condition for obtaining a maximum in nominal stress-strain curve is defined as $d\sigma_e/d\varepsilon_e = 0$. If this condition is applied to Equ. 2.22, one obtains

$$\frac{d\sigma_e}{d\varepsilon_e} = 0 = \frac{1}{1+\varepsilon_e}\frac{d\sigma_t}{d\varepsilon_e} - \frac{\sigma_t}{(1+\varepsilon_e)^2} \qquad \text{Equ. 2.24.}$$

Hence,

$$\frac{d\sigma_t}{d\varepsilon_e} = \frac{\sigma_t}{(1+\varepsilon_e)} = \frac{\sigma_t}{\lambda} \qquad \text{Equ. 2.25.}$$

This equation corresponds to the slope of the tangent to the curve σ_t vs. ε_e drawn from the point $\varepsilon_e = -1$ or $\lambda = 0$.

In practice, the Considére construction is used as a criterion to decide when a polymer will form an unstable neck or form a neck accompanied by cold drawing.

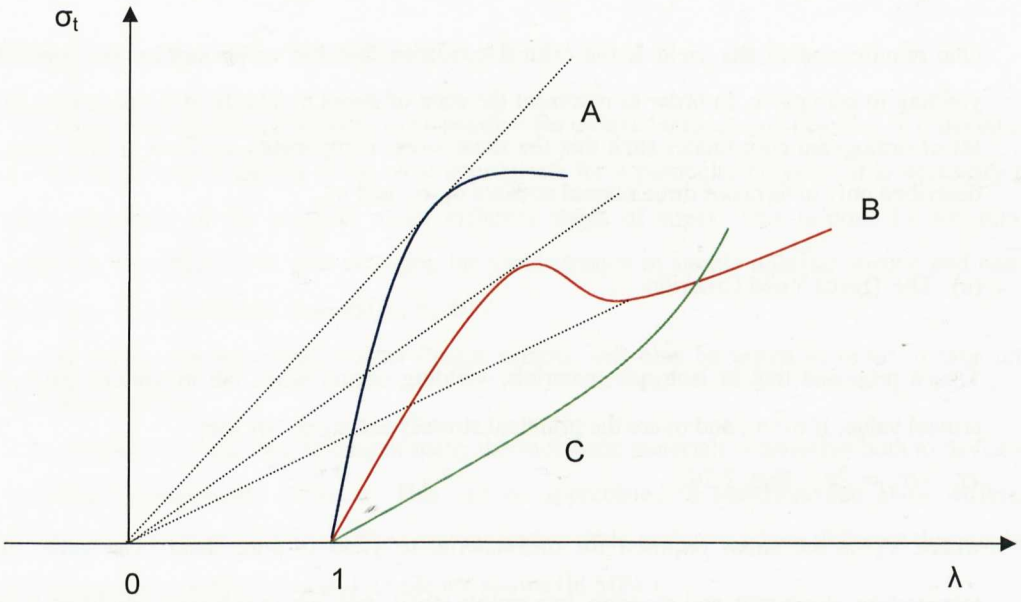

Figure 2.5: Considère's construction for three different types of stress strain curves.

For curve A, it is possible to draw only one tangent from $\lambda=0$. This implies that once the neck has started in the sample, it will continue becoming thinner until fracture is reached. In the case of the curve B there is the possibility of drawing two tangents to the curve. The second tangent corresponds to the appearance of a minimum in the curve of nominal stress versus nominal strain, which is necessary for stable necking. Therefore, the formation of a stable neck, and cold drawing, will take place when condition defined by Equ. 2.24 is met at two points.

Two phenomena can be observed once yielding starts. These are strain softening and strain hardening. Strain softening can be defined as a drop in the true stress with increasing strain. This behaviour is observed in curve B. Strain softening is an intrinsic property of a polymer and can be detected fundamentally in compression and shear tests. All glassy polymers show strain softening, although some become oriented and quickly harden. The orientation, or strain hardening, can be observed in many polymers and corresponds to the region where the true stress increases after yield. Most commercial polymers show strain hardening; those that do not display this characteristic are difficult to process and are not very reliable in service.

Curve C corresponds to a material that deforms homogeneously at all draw ratios. No tangent can be drawn and hence no necking process could be observed.

Considére's construction is equally applicable to metals (was originally developed for metals) and polymers, but the necking of polymers is affected by two physical factors which are not normally so significant in metals:

- dissipation of mechanical energy as heat can raise the temperature in the neck, causing significant softening (the magnitude of this effect increases with strain rate); and
- deformation resistance of the neck. The necking area has a higher strain rate than the surrounding polymer, this can raise the yield stress of the material which also increases the resistance to develop a neck.

The relative importance of these two (opposing) effects depends upon the material, the length and thickness of the specimen, and test conditions, especially the strain rate.

2.2.1.5. Yield criteria.

One requirement of the yield is the critical condition that has to be met by the applied stress tensor for yielding to take place. In order to represent the state of stress in a body, it is convenient to choose a suitable set of orthogonal coordinates such that the shear stress components are zero. In this case, the stress state is described only in terms of three normal stresses σ_1, σ_2, and σ_3.

(a) The Tresca Yield Criterion.

Tresca proposed that in isotropic materials, yielding occurs when the maximum shear stress τ reaches a critical value. If σ_1, σ_2, and σ_3 are the principal stresses and $\sigma_1>\sigma_2>\sigma_3$, then

$\sigma_1 - \sigma_3 = 2\tau_y$ Equ. 2.26.

where τ_y is the stress required for the material to yield in pure shear. The value of τ_y depends on temperature, strain rate, and pressure. In a simple tensile test, where $\sigma_2=\sigma_3=0$, condition for yielding becomes

$\sigma_1 = 2\tau_y = \sigma_y$ Equ. 2.27.

where σ_y is the tensile yield stress of the material. Although the Tresca yield criterion was developed for metals, most metals obey the Von Mises criterion better.

(b) The Von Mises Criterion

Conditions for shear yielding in isotropic materials are best summarised by the Von Mises criterion.

$(\sigma_1 - \sigma_2)^2 + (\sigma_2 - \sigma_3)^2 + (\sigma_3 - \sigma_1)^2 = 6\tau_y^2$ Equ. 2.28.

Yielding occurs when the elastic shear strain energy density in the stressed material reaches a critical value. In the case of simple tension, $\sigma_2=\sigma_3=0$ and therefore Equ. 2.27 becomes,

$\sigma_y = \sqrt{3}\tau_y$ Equ. 2.29.

Experimental data has shown that neither Tresca nor Von Mises can adequately describe the shear yielding behaviour in polymers [3].

(c) Pressure-Dependent Yield Behaviour.

In polymers the compressive yield stress is higher than the tensile yield stress. In addition, the yield stress in polymers increases significantly with hydrostatic pressure. The Tresca and Von Mises criteria both predict that the yield stress measured in uniaxial tension is the same as that measured in compression. The differences observed between the behaviour of polymers in uniaxial tension and uniaxial compression are due to the fact that polymeric materials are mostly van der Waals solids and therefore it is not surprising that mechanical properties of polymeric materials are affected by hydrostatic pressure.

To take into account the pressure dependence, τ_y can be expressed as a function of hydrostatic pressure P, which is the Coulomb's criterion:

$\tau_y = \tau_y^0 - \mu P$ Equ. 2.30.

where τ_y^0 is the strain rate dependent yield stress at zero pressure, μ is a material constant that describes the effect of pressure, and P is given by

$$P = \frac{1}{3}(\sigma_1 + \sigma_2 + \sigma_3) \quad \text{Equ. 2.31.}$$

The hydrostatic pressure P is taken to be positive for uniaxial tension and negative in uniaxial compression.

To determine which criteria is the most appropriate for a particular polymer, it is necessary to examine the yield behaviour of the polymer under different states of stress. This is done by assuming plane stress condition for which $\sigma_3=0$, and obtaining the yield stresses in simple uniaxial tension and compression, pure shear ($\sigma_1=-\sigma_2$) and biaxial tension (σ_1, $\sigma_2>0$).

In this thesis, the so called Drucker-Prager criteria will also be tested in order to take into account the hydrostatic effects.

It has been shown that the yielding of many thermoplastic materials is sensitive both to deviatoric (shear) and hydrostatic components of stress. This can be appreciated in materials that show different tensile and compressive yield stress values. Next a comparative table is shown where different thermoplastic materials' yield stresses in compression and tensile are shown (in MPa.):

Polymer	σ_{yC}	σ_{yT}
PVC	67.52	57.19
PE	13.47	10.02
PP	43.41	32.38
PTFE	13.47	10.71
Nylon	66.83	61.32
ABS	42.72	44.79

Table 2.4: Different yield stresses for common thermoplastics in tensile and compressive testing modes. Extracted from [5].

Additional data can be found in [6]:

Polymer	σ_{yT}	σ_{yC}
PC/ABS	56	62
PC	66	66
Noryl GTX910	55	76
Noryl EM6100	36	60
PBT	53.1	73.1
ABS	42.5	45.9
PC/Polyester	51	61

Table 2.5: Different yield stresses for common thermoplastics in tensile and compressive testing modes [6].

In compression mode, small defects have less effect on the test results and this can also lead to differences between compressive and tensile yield values.

A report from R. R. P. Rodenburg (TU/e Internship Report) [7] treated the differences in yielding criterion between metals and plastics. The Von Mises criteria was considered to be suitable for metals (unless

subjected to high pressure) but for thermoplastics not only deviatoric stress components should be considered but also hydrostatic ones. The author reported that the value of μ, a hydrostatic sensitivity parameter, was in the range of 0.1 to 0.2 for plastic materials which translates into 10.5% to 23% difference in yield strength between uniaxial tensile and compression loading conditions.

2.2.2. Uniaxial Compression Test.

The uniaxial compression test overcomes some disadvantages in relation to a tensile test. The stress is compressive, and consequently there is no possibility of brittle fracture observed in tensile deformation. In addition, the determination of the yield stress is made under conditions of homogeneous deformation since there is no geometrical reason for the formation of a neck as in tension. A problem that can arise in this test concerns the diameter/length ratio of the specimen geometry. If this ratio is too large friction between plates and sample will introduce a constraint, and if it is very small the sample could buckle. In practice, 0.5 is a good working ratio. Finally, since the cross-sectional area of the specimen increases when the test is conducted, $\sigma_t<\sigma_e$, in contrast to what occurs in a tensile test.

The ASTM standard D 695M-91 "Standard Test Method for Compressive Properties of Rigid Plastics" describes the procedure for testing thermoplastic in compression mode. Although usually this test is employed for quality control and comparison purposes, in finite element design analysis, its applicability resides on the definition of a yield criterion capable of differentiating between tensile and compressive yield stress values.

The standard test specimen shall be in the form of a right cylinder or prism whose length is twice its principal width or diameter. The recommended specimen sizes are 11.5 by 11.5 by 25 mm (prism) or a cylinder of 11.5 mm in diameter and 25 mm in length. Other specimen specifications are described in the standard for different materials and shapes. The recommended speed of testing is1 mm/min.

Buckling and yielding in compression.

Uniform compressive yielding is rare in plastics products, which are usually thin walled. It is more likely that regions under excessive compressive forces, such as the vertical sides of a bottle crate at the base of a stack, will fail by elastic buckling.

Euler buckling theory predicts collapse under a constant force. However, finite element analysis (FEA) shows that the onset of buckling causes the load bearing capability to decrease [8]. At high axial deflections, plastic hinges develop at mid-length and at the ends of slender struts.

2.2.3. Simple Shear Test.

In a simple shear deformation test, the specimen is clamped between two steel blocks that move parallel to each other in order to achieve a uniform shear strain along the waisted region. The shear stress is calculated as

$$\tau = F/A \qquad \text{Equ. 2.32.}$$

where F is the shear force acting on a plane of area A. In this test it is not necessary to distinguish between nominal and true stress since shear strain is not affected by A. The shear strain is defined as

$$\gamma = \Delta x/y \qquad \text{Equ. 2.33.}$$

where Δx is the displacement of planes separated by a distance y, Δx being measured in the direction of the applied force, which is perpendicular to y.

The main objective of shear tests is to obtain the shear stress/strain curve. Unlike the tensile test, different types of apparatus and specimen geometries are available for this purpose.

The ASTM standard D3846-02 "Standard Test Method for In-Plane Shear Strength of Reinforced Plastics" defines a procedure for testing plastics in flat sheet form (thickness range from 2.54 to 6.60 mm). In-plane shear strength is measured applying a compressive load to a notched specimen of uniform width. The specimen is loaded edgewise in a supporting jig of the same description as in the standard D695 for testing thin specimens. Failure of the specimen occurs in shear mode between two centrally located notches, halfway through its thickness, and spaced a fixed distance apart on opposing faces. The standard speed of testing shall be 1.3 mm/min. The in-plane strength is calculated by dividing the maximum shear load carried by the specimen by the product of the specimen's width and the length of the failed area. The length of the failed area is determined to the nearest 0.025 mm with respect either half of the ruptured specimen.

Additional commonly used shear test types can also be found in literature and standards:

- Iosipescu shear test.

This test is referred to the standard ASTM D 5379. A double V-notched specimen is used, which typically is 75 mm wide, 20 mm high and at least 4 mm thick. The specimen is loaded in tension or compression and a state of pure shear is established in a region between the notches. Strain gauges may be used to measure the shear strain in this region but a correction is needed for the local stiffening of the specimen by the gauge.

Interlaminar V-notched shear test

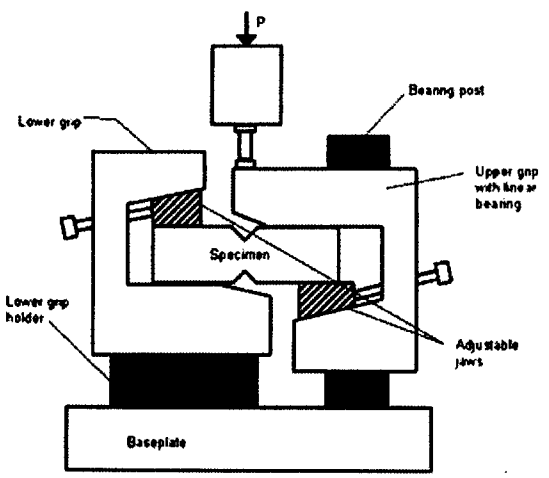

Figure 2.6: Iosipescu shear test configuration [10].

- Arcan shear test.

It is a modification of the Iosipescu test method. In this case the specimen can be thinner (more representative in plastics).

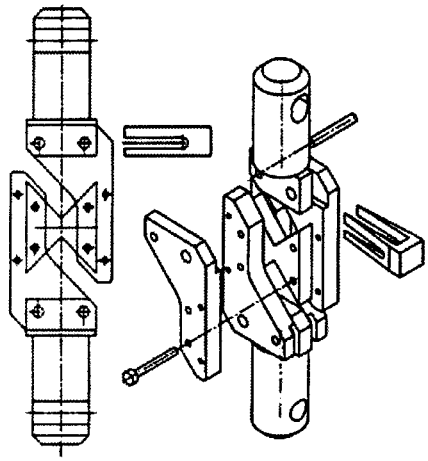

Figure 2.7: Arcan shear test configuration [11].

The strain measurement can be conducted accurately by video-extensometers.

2.2.4. Flexural Testing of Thermoplastics.

The ASTM standard D 790-03 "Standard Test Methods for Flexural Properties of Unreinforced and Reinforced Plastics and Electrical Insulating Materials" specifies a support span-to-depth ratio of 16:1 for 3 point bending test.

The analogous test to measure flexural strength in the ISO system is ISO 178. The values reported in the ASTM D790 and ISO 178 tests seldom differ significantly.

Procedure A employs a strain rate of 0.01 mm/mm/min (the preferred one) while procedure B uses a strain rate of 0.1 mm/mm/min.

Flexural properties may vary with specimen depth, temperature, atmospheric conditions, and the differences in rate of straining.

Although the preferred specimen type is 11.7 by 11.7 by 3.2 mm for moulding materials, the multipurpose specimen from ISO standard is suitable for this application.

The strain rate is calculated as follows:

$$\dot{e} = 6\dot{x}d/L^2 \qquad \text{Equ. 2.34.}$$

where,

$\dot{x}$ = rate of crosshead motion, mm/min.

$\dot{e}$ = straining rate of the outer fibre, mm/mm/min.

L= support span, mm.

d= specimen thickness, mm.

The $\dot{e}$ value is specified by the standard, depending on the A or B procedures.

2.2.4.1. Stress-Strain Calculations in Bending.

The stress calculation follows the form of a homogeneous elastic material as a simple beam supported at extreme points and centrally loaded. The maximum stress is located in the outer surface of the specimen at the midpoint. This stress can be calculated for every load-deflection point of the bending test:

$$\sigma = \frac{3PL}{2bd^2}$$ Equ. 2.35.

where:

σ= stress in the outer fibres at midpoint, MPa.

P= load at a given point on the load-deflection curve, N.

L= support span, mm.

b= width of specimen tested, mm.

d= thickness of specimen tested, mm.

This equation applies strictly to materials for which stress is linearly proportional to strain up to the point of rupture and for which the strains are small (Hookean relation is used, and this is not always true with plastics). The equation is valid for comparison purposes, but only up to a maximum fibre strain of 5% in the outer surface.

Flexural strain is calculated as the nominal fractional change in the length of an element of the outer surface of the test specimen at the centre, where the maximum strain is located. It can be calculated for any deflection using:

$$\varepsilon = \frac{6\delta d}{L^2}$$ Equ. 2.36.

where:

ε= strain in the outer surface, mm/mm.

δ= maximum deflection at the specimen's centre, mm.

d= specimen thickness, mm.

L= support span, mm.

The modulus of elasticity in bending can be calculated as the ratio of the stress and the strain in the elastic region:

$$E = \frac{PL^3}{4Dbd^3}$$ Equ. 2.37.

where:

P= load at a given point on the load-deflection curve, N.

L= support span, mm.

D= maximum deflection at the specimen's centre, mm.

b= width of specimen tested, mm.

d= specimen thickness, mm.

Flexural strength values based on these equations are typically 1.5 times greater than tensile strength data. This is due to plastic materials may not perfectly obey the classical linear theory of mechanics on which the equations are based. Modulus values may only marginally be higher than tensile modulus.

2.2.4.2. Yield in Bending.

A beam of ductile material can be bent until it stays permanently deformed. The yielded region acts as a very stiff hinge, so is referred to as a plastic hinge. In this region, one side of the beam yields in tension while the other side yields in compression. The material is assumed not to work harden after yielding (considered a good approximation for polymers for strains up to 50% [8], so the longitudinal stress is σ_0 on the tensile side

and - σ_0 on the compressive side, where σ_0 is the initial yield stress. When the two yielded zones meet at the neutral surface, the stress distribution is shown in Figure 2.8, and the bending moment at the central load point reaches a limiting plastic moment M_{pl}. For a beam, w wide and d deep, M_{pl} can be calculated by summing the internal moments of the forces acting on the cross section, as

$$M_{pl} = \frac{wd^2}{4}\sigma_0 \qquad \text{Equ. 2.38.}$$

Necking will not occur on the tensile side of the beam, because the support of the compressive side. For metals, the initial stages of yielding occur as in Fig 2.8, and the beam remains very slightly bent if the loads are removed. There is no evidence of permanent deformation in polymer beams before a plastic hinge forms. The non-linearity in the early part of the force-deflection relationship is due to non-linear viscoelasticity. Since polymer yield strains are approximately 5%, there is always a small elastic region near the neutral surface in the plastic hinge region.

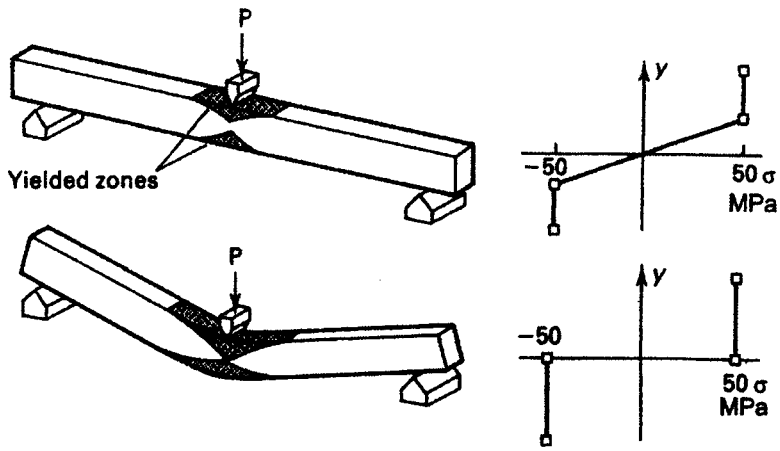

Figure 2.8: Yielded zones in a three point bend test. The upper figure represents a beam that remains elastic, and the lower picture a beam when a plastic hinge is formed [8].

The recommended short-term surface strains that can be used without causing yielding are higher for semi-crystalline plastics (ranging from 4% for polyamides to 8% for polyethylene) than for glassy plastics (1.8% for polystyrene to 4.5% for polycarbonate). To cause these large surface strains, the beam must bent to a small radius of curvature. For example, in a 2 mm thick polyethylene, the deflections involved in bending a beam to a radius smaller than 12 mm would be unacceptable for the function of any product [8].

2.3. Temperature and Strain Rate Sensitivity Analysis with the Eyring's Model.

Although temperature and strain rate effects will be covered in more detail in Part II of the thesis covering impact testing and simulation, in this part a well known theoretical model will be briefly described: the flow model of Eyring. The Eyring model was developed to describe the viscous flow in liquids. The fundamental ideas can be applied to clarify some aspects of the yield behaviour of glassy polymers. Based on thermodynamics, the final expression of the model is reduced to

$$\sigma_y = \left[R \times 2.303 \log\left(\frac{\dot{\varepsilon}_y}{\dot{\varepsilon}_0}\right) + \frac{\Delta E^*}{T} \right]\left(\frac{2T}{V^*}\right) \qquad \text{Equ. 2.39.}$$

when the study is done in terms of measured yield stresses at different temperatures and strain rates.

σ_y: is the yield stress (MPa.).

R: is the Avogadro's number (mol^{-1}).

$\dot{\varepsilon}_y$:is the strain rate at yield (s^{-1}).

$\dot{\varepsilon}_0$: is a constant or reference strain rate (s^{-1}).

ΔE^* : is the needed activation or jump energy (enthalpy).

T: is the testing temperature (°K).

V*: is the activation volume (m^3/mol).

Figure 2.9 shows plots of σ_y/T versus log $\dot{\varepsilon}_y$ for polycarbonate for a series of temperatures between 21.5 and 140°C (the Tg of PC is 160°C). [4].

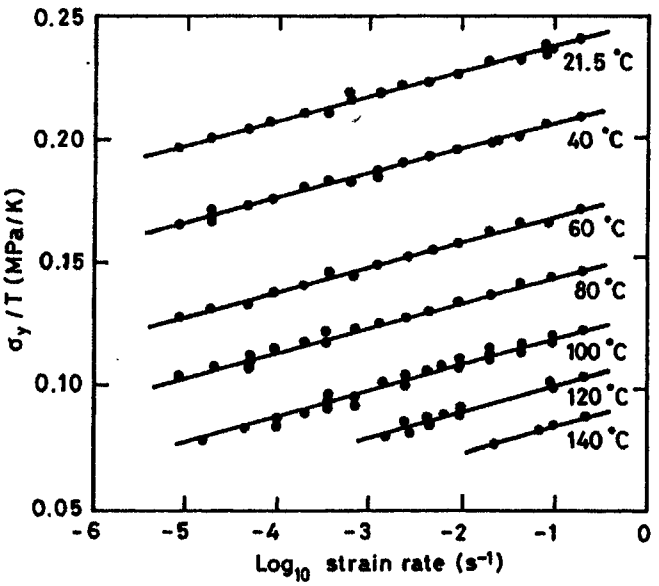

Figure 2.9: Eyring plot of σy/T versus log $\dot{\varepsilon}_y$ for polycarbonate [4].

This plot can lead to the following conclusions:

- σ_y/T increases linearly with log $\dot{\varepsilon}_y$ (the yield stress is rate dependent).
- At a constant strain rate (log $\dot{\varepsilon}_y$), σ_y/T increases with decreasing temperature (the yield stress is temperature dependent).

From the plots, the separation of the lines gives ΔE^* and the slope of the lines, V*.

The Eyring model can fail when it tries to describe the yield behaviour of polymers over a wide range of temperatures. Additionally, it has to be modified when hydrostatic effects are needed to be included.

Chapter 3: Literature Review.

This literature review is divided in two main sections. The first part is related to the quasi-static material constitutive description of plastics and the second section describes the different static characterisation methods for performing simulations in FEA software. A short appendix is also included covering the failure modelling and description of the unloading behaviour.

3.1. Quasi-Static Material Constitutive Description of Plastics.

Although the mechanical response passes through different phases during straining, the stress-strain behaviour of thermoplastic materials can be considered non linear due to the viscoelastic nature of polymers. No initial Hookean zone is observed in the majority of plastics and above the yielding point the mechanical behaviour becomes difficult to specify. At low strains, the removal of the applied load results in recoverable strains but above the yield point unrecoverable strains develop.

In spite of the development of theoretical non-linear viscoelastic material models for the description of the stress-strain behaviour of thermoplastic materials, no specific constitutive models exist in commercial finite element analysis software. The usual way of representing plastics' behaviour is by the use of elasto-plastic models developed for metals and in some cases, modified for the use with plastics.

The elasto-plastic definition of a material involves the determination of low strain material properties ($\leq$ 0.01) as the elastic Young's modulus and Poisson's ratio, together with higher strain properties (plastic strains, and in some cases, failure). The elastic part, or the onset of non-linearity, is used to calculate the yield stress of the material. This point is used as the elastic limit (the onset of plasticity) and if stress increases with plastic strains strain hardening is given in the material.

Several researches have employed elasto-plastic models in publications regarding to the design of thermoplastic made components by means of FEA codes [7, 8, 9, 10, 11, 12, 13, 14, 15, 26, 31, to cite some publications]. In fact, using FEA is a normal procedure in industry where "time" is the most important factor in design stages. User focused ease of use is also wanted when inputting material data and nowadays most elasto plastic models admit direct tabular data.

G. Dean and co-authors [9,10,11] from the National Physics Laboratory (NPL Materials Centre) in the United Kingdom, proposed different elasto-plastic material models for representing the stress-strain behaviour at low and high strain values (some other studies presented by these authors were related to strain rate sensitivity, yielding, crazing or void development in thermoplastics and adhesive materials).

According to the authors, the true stress-plastic strain curve (hardening) up to total strains of 5% and plastic strains of 3% can be represented with a function as follows:

$$\sigma_T(\varepsilon_T^p) = \sigma_0 + (\sigma_f - \sigma_0)\cdot\left[1 - e^{-\left(\varepsilon^p/\varepsilon_s^p\right)^\beta}\right] \qquad \text{Equ. 3.1.}$$

Here, σ_0 is the true stress at zero plastic strain, σ_f is the limiting stress at high plastic strains, $\varepsilon^p{}_s$ and β are parameters that define the mean strain and the strain range over which a sudden increase in σ_T (true stress) with $\varepsilon^p{}_T$ (true plastic strain) takes place.

Additional functions could be added for the reproduction of the stress decay after yielding in some materials:

$$\sigma_T(\varepsilon_T^p) = \sigma_0 + (\sigma_f - \sigma_0)\cdot\left[1 - e^{-\left(\varepsilon^p/\varepsilon_s^p\right)^\beta}\right] - 2\frac{\delta}{\varepsilon_s^p}\varepsilon^p + \frac{\delta}{\varepsilon_s^{p^2}}\varepsilon^{p2} \qquad \text{Equ. 3.2.}$$

where δ is the decay in stress.

For a description of the stress-strain curve at higher strain levels, the authors used modified models of the Equ. 3.1.

$$\sigma_T(\varepsilon_T^p) = \sigma_0 + (\sigma_f - \sigma_0)\cdot\left[1 - e^{-\left(\varepsilon^p/\varepsilon_s^p\right)^\beta}\right](1 + g\varepsilon^p) \qquad \text{Equ. 3.3.}$$

or

$$\sigma_T(\varepsilon_T^p) = \sigma_0 + (\sigma_f - \sigma_0)\cdot\left[1 - e^{-\left(\varepsilon^p/\varepsilon_s^p\right)^\beta}\right] + f\varepsilon^p \qquad \text{Equ. 3.4.}$$

where g and f are additional parameters that are negative if σ_T decreases with ε_p.

The strain rate dependency of the yield and flow stresses and the parameter $\varepsilon^p{}_s$ can be described by Eyring type relations:

$$\sigma_0 = \sigma_{00} + c\log\dot{\varepsilon}_p \qquad \text{Equ. 3.5.}$$

$$\sigma_f = \sigma_{f0} + b\log\dot{\varepsilon}_p \qquad \text{Equ. 3.6.}$$

$$\varepsilon_{ps} = \varepsilon_{s0} - d\log\dot{\varepsilon}_p \qquad \text{Equ. 3.7.}$$

In all these cases, a linear relationship is established between the logarithm of the plastic strain rate, $\dot{\varepsilon}_p$, and the mentioned parameters in order to fit the experimental data.

From tensile tests conducted at low and moderate strain rates, higher straining rate ranges (those that are not tested but are of interest) can be covered by extrapolations, combining Equ. 3.1 and Equ. 3.5, 3.6 and 3.7.

The validity of these equations was demonstrated by the authors using different materials like rubber toughened propylene-ethylene copolymer or polycarbonate.

The proposed relationships will be used in this work for the generation of stress-strain curves at different strain rates as input in the ANSYS and LS-DYNA codes.

The authors also remarked the difficulties when specifying a modulus value for elastic-plastic analysis in thermoplastics: the ISO 527 standard specifies recording the gradient of the secant between 0.0005 and 0.0025 strain. This upper strain limit is too low for elastic-plastic analyses which requires a strain limit that identifies the onset of material non-linear behaviour that is attributed to plastic deformation. The inability to define the elastic modulus with less ambiguity results from the need to represent viscoelastic behaviour as elastic-plastic.

Associated with viscoelastic behaviour is the dependence of modulus on strain rate. Finite element systems suitable for simulating the impact performance of plastics do not generally take into account the rate-dependency of the elastic behaviour. It is therefore worthwhile, in opinion of the authors, to determine the tensile properties at a strain rate corresponding to some mean value for the range of rates generated in the event to be simulated.

The next reference deals with another constitutive model developed for thermoplastic materials. The equations presented in this reference have not been used in this thesis work for data generation.

Y. Duan, A. Saigal, R. Greif and M.A. Zimmerman [12, 13] developed the so called "DSGZ model" for describing the deformation behaviour of amorphous and semi-crystalline polymers under monotonic (non-cyclic) loading mode. The work was oriented to impact applications, putting special emphasis on rate and temperature effects. In this section the basics for this model will be briefly mentioned, which could also be applied in quasi-static situations. Their work was mainly centred on the study of ABS and PC/PBT materials. Related to the quasi-static testing, Duan et al. predominantly used the uniaxial compression test in cylindrical specimens of 6.4 mm in diameter and 3.2 mm in thickness. Tensile tests were also carried out for the evaluation of the hydrostatic sensitivity, especially in amorphous polymers were this effect is more pronounced.

The following equations were used to describe the stress-strain behaviour in compression and tensile mode with strain rate and temperature dependency:

- Under compressive loading,

$$\sigma_c(\varepsilon,\dot{\varepsilon},T)=\left(\frac{K}{1-\frac{\gamma}{3}}\right)\left\{f(\varepsilon)+\left[\frac{\varepsilon\cdot e^{\left(1-\frac{\varepsilon}{C_3 h(\dot{\varepsilon},T)}\right)}}{C_3 h(\dot{\varepsilon},T)}-f(\varepsilon)\right]\times e^{[\ln(g(\dot{\varepsilon},T))-C_4]\varepsilon}\right\}h(\dot{\varepsilon},T)$$

Equ. 3.8.

- and under tensile loading,

$$\sigma_t(\varepsilon,\dot{\varepsilon},T)=\left(\frac{K}{1-\frac{\gamma}{3}}\right)\left\{f(\varepsilon)+\left[\frac{\varepsilon\cdot e^{\left(1-\frac{\varepsilon}{C_3 h(\dot{\varepsilon},T)}\right)}}{C_3 h(\dot{\varepsilon},T)}-f(\varepsilon)\right]\times e^{[\ln(g(\dot{\varepsilon},T))-C_4]\varepsilon}\right\}h(\dot{\varepsilon},T)$$

Equ. 3.9.

where,

$$\gamma=3\frac{\sigma_{cy}-\sigma_{ty}}{\sigma_{cy}+\sigma_{ty}}$$ Equ. 3.9.

σ_{cy} is the yield stress in uniaxial compression test and σ_{ty} is the yield stress in uniaxial tensile test.

$$f(\varepsilon)=\left(e^{-C_1\varepsilon}+e^{C_2}\right)\cdot\left(1-e^{-\alpha\varepsilon}\right)$$ Equ. 3.10.

and

$$h(\dot{\varepsilon},T)=\dot{\varepsilon}^m e^{\frac{a}{T}}$$ Equ. 3.11.

$g(\dot{\varepsilon},T)$ is defined to be the dimensionless form of $h(\dot{\varepsilon},T)$.

Nine coefficients are needed to define the DSGZ model: K (Pa s m), C_1, C_2, C_3 (s m), C_4, a(K), m, α, and γ. The procedure for calibrating the material coefficients was described in the different articles published by the corresponding authors [12,13].

The comparison of the measured compressive stress-strain curves and the predicted curves with the proposed model are in agreement at slow strain rates (around 0.001/s). At high strain rates disparity is more marked, in opinion of the authors, probably due to uncertainties in measurements at high strain rates (a Split-Hopkinson Bar system was used at 1000/s).

Another frequently used model is the following expression proposed by G'Sell and Jonas [14]. The model gives rise to the following relationship:

$$\sigma = k\left[1 - e^{(-w\varepsilon)}\right] \cdot e^{h\varepsilon^2} \left(\dot{\varepsilon} / \dot{\varepsilon}_0 \right)^m \quad \text{Equ. 3.12.}$$

where σ and ε are the effective stress and strain, k is a scaling factor and is responsible of the first plateau of the stress-strain curve, $\left[1 - e^{(-w\varepsilon)}\right]$ represents the initial small strain viscoelastic region, $e^{h\varepsilon^2}$ describes the strain hardening at large strains and the last part $(\dot{\varepsilon} / \dot{\varepsilon}_0)^m$ expresses the strain rate sensitivity in a power law form. The material constants needed for modelling the stress strain behaviour are k, w, h and m. These coefficients can be calculated for tensile tests at different temperatures and a linear interpolation could be used for any other temperature.

Different modifications to this constitutive model can be found in literature [20].

Hubert Lobo and Juan A Hurtado [15] described the non-linear elastic behavior and its interrelationship with plastic behavior in thermoplastic materials. Special attention was given to the differentiation between visco-elastic (recoverable) strain and plastic (non-recoverable) strain. The aim of the work was to have a model that could describe both loading and unloading behavior in thermoplastics accurately, and provide an accurate measure of damage accumulation during complex loading operations.

The theoretical information exposed below is extracted from their research.

Plastic deformations cause irreversible damage in the component part and it is not safe to assume that the plastic material is stable up to its yield point. This places considerable difficulty for the analyst because first, it is not trivial to differentiate between recoverable strain and plastic strain. Secondly, it is important to know at what strain and stress level these deformations start to be significant. Thirdly, simulation of damage accumulation and recovery after loading are not feasible unless the relationship between recoverable strain and plastic strain is known.

Often, the yield point, the first the maximum point in the stress strain curve, is assumed to be synonymous with the onset of plastic deformation. But this maximum on the curve actually corresponds to the point where specimen becomes unstable and a neck is formed. The stress-strain curve can then be divided into the following regions as shown in Figure 3.1.

- The first region corresponds to viscoelastic (recoverable) deformations.
- The second region starts at what the authors call the "plastic point" of the material. Plastic deformations become significant, through crazes formations and/or homogeneous flow (shear bands).
- The third region corresponds to the formation of a neck in the specimen. The deformation is dominated by a massive homogeneous flow in the drawing regions.

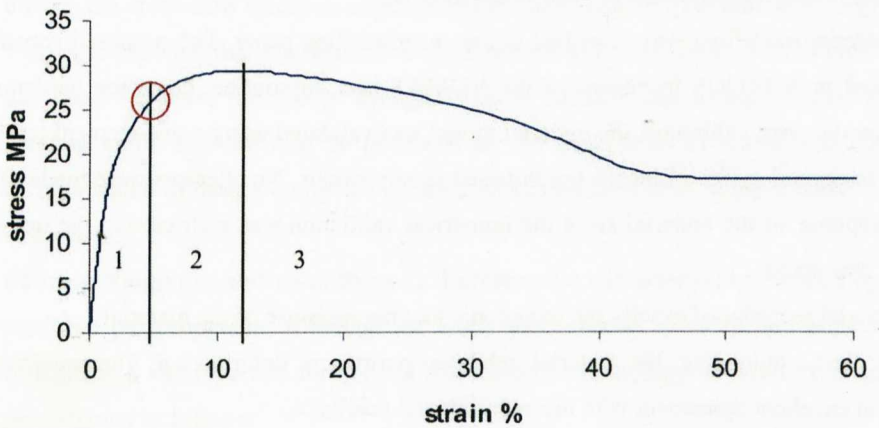

Figure 3.1: Different zones in a stress-strain curve of a thermoplastic material with yielding.

The authors stated that even in the so-called elastic region, the recovery of a plastic subjected to deformation is not instantaneous. Rather, the plastic returns to its original state after a period of time that is dependent on its visco-elastic characteristics, as described by a stress-relaxation curve. This time dependency is well characterised by visco-elastic experiments and can be modeled well in high end FEA applications via Prony series. However, visco-elastic theory implemented in most CAE programs is a linear theory and therefore, unsuitable for large-strains where visco-elastic behaviour becomes non-linear. As permanent irrecoverable plastic strain occurs, the material changes its characteristics and behaves entirely different from its original state. Accordingly, linear visco-elastic models will not work beyond the plastic point.

The general procedure is to load the specimen, allow the specimen to relax and measure the residual deformations after a fixed period of time. This procedure has been used previously by Quinson (1996, 1997) with success on PMMA, PS and PC. The residual strains could then be plotted as a function of the initially applied strains. When the initial deformation had exceeded the plastic limit of the material, a dramatic increase of residual strain was observed. It had also been shown by Quinson (1997) that this limit was independent on the time allowed for the material to recover.

The experimental procedure employed by the authors was described in the corresponding paper.

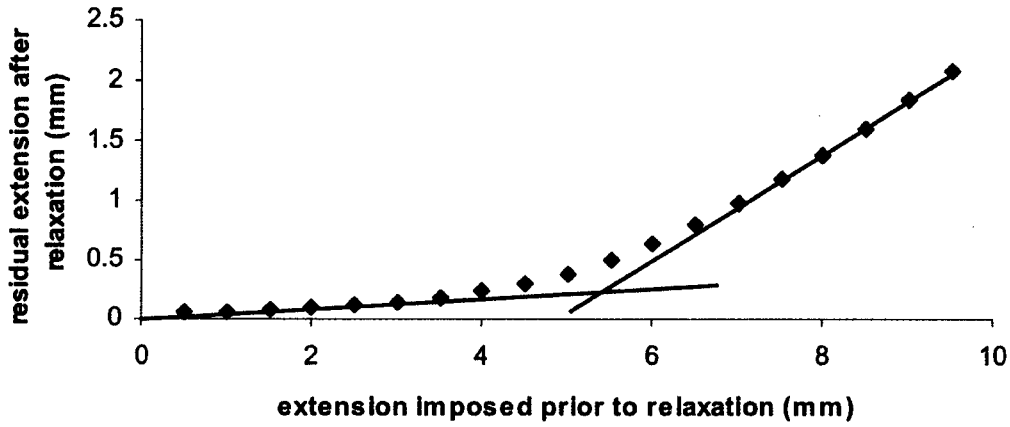

Figure 3.2: Determination of the plastic point from residual strain measurements [15].

To measure the plastic point from the curve, the initial few points are fitted with a straight line. The plastic point is the imposed strain at which where the data deviates from the straight line by a fixed percentage.

This points clearly to the importance of knowing the plastic point and using it as a fundamental basis for placing stress limits on a design. From the authors' viewpoint, the plastic point could potentially have implications related to endurance life and stress recovery.

Further material modelling was described in the corresponding paper. The proposed constitutive model was implemented in ABAQUS by means of the VUMAT user subroutine. Once the hardening curve and the elastic potential were calibrated, the material model was validated using a one-element test. The element was subjected to several cycles of increasing imposed tensile strains. No attempts were made to capture the post-necking response of the material since the numerical validation was restricted to the one-element test. The following was noted:

- The model reproduced exactly the monotonic loading response of the material.
- Upon elastic unloading, the material exhibited permanent deformation. The predicted residual strains were in excellent agreement with the experimental results.
- The model was rate-independent and, therefore, could not capture viscoelastic effects.

Additional constitutive models could also be found in literature but the most referenced and used ones are the described in this section.

3.2. Characterisation Methods and Finite Element Procedures in Quasi-Static Analyses.

This section describes the principal testing procedures and finite element modelling implications found in the literature for thermoplastic materials under static applications.

Joseph T. Woods and Gerald G. Trantina [6] presented the general special characteristics of plastics that have to be taken into account when modelling in FEA. Some ideas extracted from their work are detailed below:

- hydrostatic effects on the yielding of the material can be neglected (using the Von Mises yield criterion) since most thermoplastic made components are thin-walled and usually no large hydrostatic stresses are developed under loads.
- in rubber containing materials (ABS, PP/EPDM, ...), elastomer particles act like cavitation agents in tensile testing, giving lower tensile stresses. In shear and compression mode, cavitation does not occur and the calculated stresses differ from the tensile values in a higher amount. If these type of materials are subjected to compressive loads, hydrostatic effects should not be avoided in the FEA code.
- for the determination of the post-yield behaviour (material softening or hardening, necking and failure) the authors proposed two measurement techniques: optical recording systems and compression testing. For a correct measurement of the necking process in tensile testing, the optical system was considered a precise method but they choosed compression testing for simplicity.
- to minimise barrelling and buckling in compression, a length to diameter ratio of 1.5-2.0 was recommended for the cylindrical specimens.
- to avoid specimen heating, strain rates between $1x10^{-4}$ and $1x10^{-3}$ s^{-1}were recommended to be used.

The authors proposed a method for combining tensile and compression data: a tensile stress-strain curve was used up to the yield point and the post yield behaviour was characterised using compression data. In this way, problems associated with necking in tensile tests could be avoided.

Failure was also an important subject in their research work which was based on the experimental testing of different specimens (un-notched and notched) and the correlation with FEA using different criteria.

These authors [16] also reported on the influence of the employed processing system (gate location) on mechanical properties of glass reinforced thermoplastics (high differences in flow aligned directions and transversal to the filling). They measured that this anisotropy gives a tensile modulus and strength value of 60% in the cross-flow direction compared to the flow aligned direction, in 30% glass filled materials.

They also reported that the flexural strength measured in unfilled and filled materials is in a vast majority of the cases 1.5 times the tensile strength. This is partially due to the selected stress conversion method in bending mode and can also be produced by the differences in tensile and compressive properties. They recommended to design components based on tensile data or to apply a correction of 2/3 to flexural stress-strain data.

Pádraig Naughton and co-authors [17] presented a characterisation method tested with talc-filled impact-modified polypropylene. Although the work was oriented to creep and impact characterisation, it can be considered a valid method for general correlation methodology between experimental results and FEA. The procedure is as follows:

- Tensile tests are conducted to obtain stress-strain data.

- Simple calibrated geometries (plates, specimens) containing small details as ribs, gussets, notches, ...) are tested.
- Finite element analyses are conducted in the calibrated geometries using the data from the tensile tests.
- Depending on the correlation level, the input data is adjusted for a better approximation to test results.
- Real components are tested and simulated with the adjusted material data. A good agreement should be reached in different components, loading conditions and materials to consider the reliability of the material model.

Note: a similar methodology was used in the present thesis work.

Early studies of FEA and experimental correlation from **Menges and co-workers** [18] were performed on PMMA and PP. Based on previously developed material models (the so called "deformation model") and with the aid of strain controlled short-term tensile tests, they correlated notched tensile tests and three point bending tests using the software ABAQUS and the auxiliary software UMAT. It can be seen in their results that the prediction of the stress values in the notched tensile tests were somewhat higher than the experimental results. They reported that in the bending test the discrepancies were even greater but this could be due to the contact definitions between plates and supports.

W. Michaeli and co-workers [19] developed a study based on strain controlled tensile tests (with additional control on temperature and humidity) due to the obtained advantages in comparison with the standard speed controlled probes:

- Areas of constant stress and strains are generated in the specimen.
- Lower distortion in measurements.
- Lower scatter of the measured values.

Based on previous work, they presented a general equation for the description of the stress-strain behaviour of plastics as a function of time (strain rate) and temperature:

$$\sigma = E_0 \cdot \varepsilon \cdot \frac{(1 - D_1 \cdot \varepsilon)}{(1 + D_2 \cdot \varepsilon)} \quad \text{Equ. 3.13.}$$

where the characteristic values E_0, D_1 and D_2 were determined by approximation of stress-strain curves from strain-controlled short-term accelerated tensile tests, for different temperatures and rates of straining.

E_0 is the initial Young's modulus and the coefficients D_1 and D_2 describe the nonlinear path of the curve.

They differentiated between amorphous and semi-crystalline polymers presenting two variations to Equ. 3.14:

- for amorphous thermoplastics,

$$\sigma = E_0 \cdot \varepsilon \cdot (1 - D_1 \cdot \varepsilon) \quad \text{Equ. 3.14}$$

- for partially crystalline plastics the decline of the curvature as strain increases can be modelled with:

$$\sigma = \frac{(E_0 \cdot \varepsilon)}{(1 + D_2 \cdot \varepsilon)} \quad \text{Equ. 3.15.}$$

These equations could be used for stress-strain curves up to the yield point. In practice, they observed that for amorphous polymers good approximation is obtained for tangent modulus up to a 15% of the initial value and for semi-crystalline polymers for modulus up to 5% of the initial tangent slope. They also recommended that for applications above the Tg the general equation should be applied.

In conjunction with these equations, Time Temperature Superposition (TTS) principle could be used for obtaining the stress-strain behaviour at different strain rates and temperatures. A way for describing the time-temperature shift is using the Arrhenius equation,

$$\log(\dot{\varepsilon}_{ref}/\varepsilon) = K(1/T - T_{ref}) \quad \text{Equ. 3.17.}$$

where T_{ref} is the reference temperature (e.g. 23°C), $\dot{\varepsilon}_{ref}$ is the straining rate at the reference temperature and K is a material-specific time-temperature shift factor. K can be determined from tests at different straining rates and temperatures maintaining the other test parameters fixed.

This work was essentially focused on creep studies (high temperature-low straining rate equivalence) but the method should not be discarded for correlating low temperatures and high straining rates. The main disadvantage of these equations resides in the weakness for describing high strain ranges.

A further investigation on this area was performed by **Walter Michaeli and Markus Gliβmann [20]**. Their work was centred on the determination of true stress-strain properties of some polymers (mainly, PC, PET, PVC and PE) using video measurements. Then they modelled the obtained curves with suitable material models and finally the validity of the TTS principle was evaluated. The description formulas for the true stress-strain material behaviour were based on the Duffo's formula (similar to the G'Sell law):

$$\sigma(\varepsilon,\dot{\varepsilon}) = k\left[1 - e^{-w\varepsilon}\right]e^{h\varepsilon^2}\left(\frac{\dot{\varepsilon}}{\dot{\varepsilon}_0}\right) \quad \text{Equ. 3.18.}$$

where k is the proportionality factor, w is the visco-elastic coefficient and h is the strain hardening coefficient.

They proposed a modification to this formula in order to account for the input of experimental true data and TTS principle:

$$\sigma(\varepsilon,\dot{\varepsilon},\vartheta) = E_0(\dot{\varepsilon},\vartheta)\frac{1}{w(\dot{\varepsilon},\vartheta)}\left[1 - e^{-w(\dot{\varepsilon},\vartheta)\varepsilon}\right]e^{h(\dot{\varepsilon},\vartheta)\varepsilon^2} \quad \text{Equ. 3.19.}$$

where E_0 is the initial elastic modulus and ϑ denotes temperature dependency.

The authors pointed out that although the TTS principle has been traditionally used in the linear-elastic and linear visco-elastic regions, its suitability in the visco-plastic area has not been studied in depth. Moreover, the representation of the parameters from the modified formula (E_0, w and h) against strain rate at different temperatures gave no sufficient overlaps and therefore the Williams, Landel and Ferry or the Arrhenius superpositions could not be used. Consequently, the authors employed a numerical TTS formula developed at IKV (Institut für Kunststoffverarbeitung, Aachen, Germany).

The results obtained when comparing experimental true stress-strain curves and those obtained from TTS principle showed a good agreement in the linear-elastic and visco-elastic regions but not in the visco-plastic area for all temperatures, and especially, for the low ones.

They summarised that for example at a temperature of 23°C, different true stress-strain curves could be generated at different strain rates up to 100%/h and then TTS principle could be used for the generation of curves at different temperatures.

As part of the development process of a ISO standard (ISO 17282) related to test methods and analyses for determining design data for plastics (structural performance prediction and processing simulation), **Dean and co-workers** [21] presented a report which on part was dedicated to the description of the quasi-static behaviour of thermoplastics oriented to FEA. Different material models were employed for the analysis of a dart penetration test. Related to the static work, linear-elastic, hypo-elastic or non-linear elastic, non-linear elasto-plastic and linear-elastic anisotropic studies where performed by FEA. Non-linear elasto-plastic models were the preferred ones for correlating the experimental puncture results. Related to yielding, no significant effect was observed using a Von Mises or a modified criterion as the linear Drucker-Prager model

in the force-displacement response. The authors commented that the main differences were in the generated strain levels which could be noticeable if selecting a failure model based on critical strains.

Recent works are related to the implementation of constitutive laws in software like LS-DYNA [22, 26, refer to the second part of the thesis work]. The model implemented by **Torodd Berstad** [22] **and co-workers** was based in previous work performed by Boyce et al. Predictions from the model were compared with uniaxial tensile and compression tests on a Polypropylene. The tests were performed at constant slow velocities obtaining strain rates of $0.002s^{-1}$, both in tension and compression. The simulations in LS-DYNA gave acceptable correlation levels specially related to the capability of simulating the cold drawing behaviour in tensile mode and the pressure sensitivity in yielding (tension/compression differences).

Additional reference works will be shortly detailed relating to two important characteristics to be taken into account when dealing with thermoplastic materials and FEA: failure of the material and the unloading behaviour of some polymers.

3.2.1. Elasto-Plasticity and Failure.

Although elasto-plastic material models take into account the stiffness and strength of the material, failure is also an important aspect to consider in the evaluation of the part's performance since it will determine the load carrying limit. In literature, some attempts to combine elasto-plasticity and failure can be found.

Paul Wyluda and Dan Wolf [23] used an elasto-plastic material definition for the study of strength and failure behaviour of quasi-statically loaded acetal copolymer gears. They employed the FEA code MSC.MARC considering the material behaviour extracted from a uniaxial tensile test at laboratory temperature. They used two approaches for the modelling of failure:

1. deactivation of the elements when the maximum tensile stress was reached. It permitted "loss" of material.
2. by permitting the elements to separate along a defined path when the maximum stress was reached. It did not permit material loss but a failure path had to be defined previously. For their application this assumption was more realistic.

They concluded that these approximations gave bounds were experimental response was located and that the use of a non-linear elasto-plastic material model with a failure criterion was an acceptable choice for modelling these types of polymers.

Gervais Milcent [24] presented the existing laws in the software PAM-CRASH for the modelling of thermoplastic materials from two viewpoints: constitutive modelling and rupture or failure determination. The principal experimental tests performed at Visteon Corporation for the characterisation of thermoplastics were the so called Sablier test (tensile test in a waisted specimen), the multiaxial test (puncture test with a dart) and a specific Arcan test developed at Visteon. This Arcan test was carried out at different angles. The used material model was the G' Sell model, calibrated specifically for their applications and evaluated with the Arcan test. However, similar simulation results were obtained by using simpler elasto-plastic material models.

They performed trials with Hill's anisotropic hardening criterion in conjunction with optimisation techniques and the results were in an acceptable accordance with previous material models, but more material thinning was observed in tensile tests.

Related to the rupture model, they performed different modelling trials using various failure criteria for element elimination depending on the selected material law: maximum plastic strain, maximum principal strain, damage law, thinning criteria, etc.

Milcent concluded that the best results were obtained using an anisotropic hardening law with thinning criteria.

They also evaluated the specific rupture model implemented in PAM-CRASH (the so called ESI-Wilkins-Kamaulakos (EWK) model) which potentially gave good results but needed a deeper study for plastics.

3.2.2. Modelling the Unloading Behaviour.

One of the main problems with elasto-plastic material models resides in the description of the unloading behaviour. The models implemented in commercial codes assume that the unloading path follows the initial elastic modulus path which is not true for thermoplastics where damage has occurred in service due to the generated plastic strains.

Related to this effect, **Frank J. Ferfecki** [25] described a method for calculating the post-impact shape of an automotive bumper subjected to multiple impacts. The studied material was a Polycarbonate/Polybutylene-terephthalate (PC/PBT) and the author proposed a material model that used a secant return modulus that was a function of the plastic strain. For PC/PBT the following behaviour was observed:

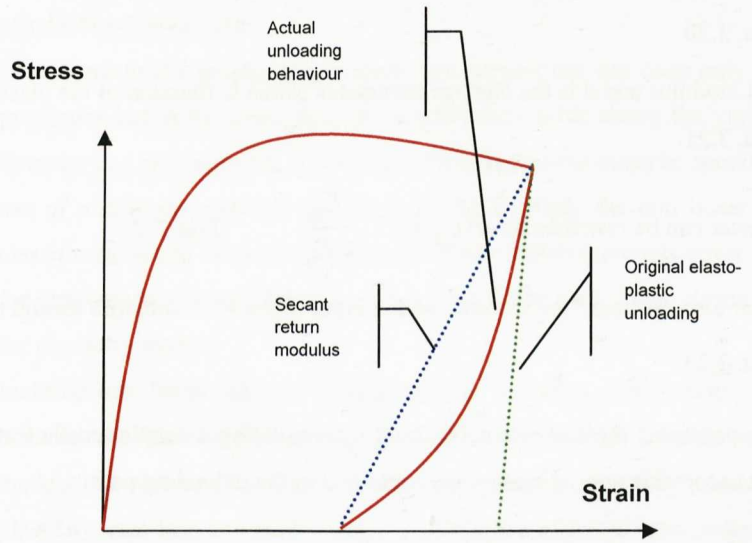

Figure 3.3: Comparison of actual unloading behavior and elasto-plastic approximations [25].

If a typical elasto-plastic approach is used (return modulus=elastic modulus) the FEA code over-predicts the permanent set.

The authors proposed a material model for LS-DYNA which was based on the use of return modulus values as a function of the generated plastic strains in tensile test mode. This model reflected in a more precise way the multiple impacts and deformed shapes in bumper systems.

P.A. du Bois et al. [26] discussed the importance of modelling the unloading behaviour of thermoplastics especially in pedestrian protection simulations (leg impact against bumper fascia). The internal energy generated in the bumper fascia must be calculated in order to get the correct bending angle of the leg during impact. As the generated strains are small, elastic loading and unloading properties are important. In the most used elasto-plastic material models, linearity is considered up to the yield point and this is not true for plastics being viscoelastic in nature.

They presented the stress-strain behaviour for a PP-EPDM where an initial material softening can be observed due to the generation of a neck and a posterior hardening due to the stabilisation of the necked area:

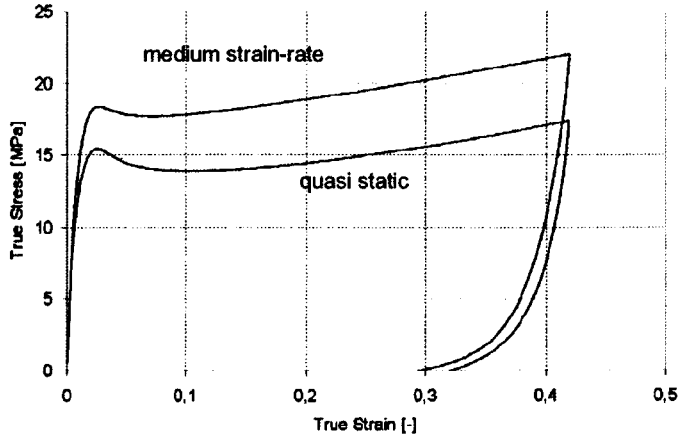

Figure 3.4: Stress-strain response of PP-EPDM, including rate dependency and non-linear unloading [26].

The non linear unloading path can be observed very clearly in the tensile test.

They proposed a method for describing the unloading path using a damage model based on the use of a decreasing modulus E_{eff} with a damage parameter d.

The effective Young's modulus is described as

$E_{eff} = E_0(1-d)$ Equ. 3.20.

where E_0 is the initial modulus and d is the damage parameter which is function of the plastic strains:

$d = \hat{d}(\varepsilon_{pl})$ Equ. 3.21.

so the damage parameter can be rewritten as $d(\varepsilon_{pl}) = 1 - \frac{E_{eff}}{E_0}$ Equ. 3.22.

The damage parameter also "softens" the stresses, so the input to the FEA software should be corrected:

$\sigma_{FEA} = \frac{\sigma_{TEST}}{1-d}$ Equ. 3.23.

The validation of the presented method was carried out by simulating a simple tensile test with loading and unloading cycles. An acceptable approximation was obtained in the unloading path.

Chapter 4: Elasto Plastic Constitutive Models in Finite Element Analysis. ANSYS Software.

In this section, different elasto-plastic models will be described in order to clarify the possibilities that these constitutive models offer in codes such as ANSYS.

4.1. Introduction.

The FEA code ANSYS offers a huge variety of material models. Inside the structural analysis group (thermal, fluid, electromagnetic, acoustic, piezoelectric, piezoresistive and thermoelectric materials could also be defined), mainly linear or nonlinear materials can be defined. For linear materials, elastic properties are defined which can be further classified in isotropic, orthotropic or anisotropic. Although the behavior in injection moulded thermoplastic materials with some fiber reinforcement is known to be anisotropic due to flow orientation, the simplest option is to consider the material isotropic since only two constants are needed to define the material card. These two constants are the elastic modulus (E in ANSYS) and the Poisson's ratio (PRXY in ANSYS). In the case of the orthotropic behavior, 9 constants are needed to be defined. And in the case of the anisotropic behavior, up to 21 constants could be specified.

For an elastic isotropic consideration, the elastic modulus and Poisson's ratio can be calculated from a standardised tensile test.

In concern to the present thesis work, the interest has not been only centred in the definition of the elastic properties but in the generation of material data cards above the yield point up to failure. Due to this, non linearity and plasticity has to be also considered in the material specification. This can be carried out by the use of non linear material models in ANSYS. Inside the non linear material models, elastic and inelastic classifications can be found. Elastic non linear material models cover mainly hyperelastic material equations for elastomeric material behavior. They also cover multilinear elastic behavior, but none of them are useful for plasticity studies.

Inelastic non linear material models are the so called elasto-plastic material constitutive equations. These material models were originally created to characterise metallic materials behavior. These constitutive models can also be classified into different groups in ANSYS: rate independent, rate dependent, non metal plasticity, cast-iron and shape memory alloy (these last two behaviours are above the scope of our work).

The rate independent consideration does not take into account testing rate effects in the stress-strain properties of the material. This approach is not very precise for thermoplastic materials since they are very sensitive to any change in the straining rate but is an adequate choice when the component to be studied is required to support quasi-static loading conditions with no change with time (no transient effects).

The hardening rule describes the changing of the yield surface with progressive yielding, so that the conditions (i.e. stress states) for subsequent yielding can be established.

4.2. Yielding.

The yield criteria is used to relate multiaxial stress state with the uniaxial case. Tensile testing on specimens provide uniaxial data, which can easily be plotted on one-dimensional stress-strain curves.

The actual structure usually exhibits a multiaxial stress state. The yield criterion provides a scalar invariant measure of the stress state of the material which can be compared with the uniaxial case.

A common yield criterion is the von Mises equation (also known as the octahedral shear stress or distortion energy criterion). In ANSYS notation, the von Mises equivalent stress for a 3D space with normal (σ) and shear (τ) stresses is defined as:

$$\sigma_0 = \sqrt{\frac{1}{2}\left(\sigma_x - \sigma_y\right)^2 + \left(\sigma_y - \sigma_z\right)^2 + \left(\sigma_z - \sigma_x\right)^2 + 6\left(\tau^2_{xy} + \tau^2_{yz} + \tau^2_{xz}\right)} \quad \text{Equ. 4.1.}$$

In tensor form, Equ. 4.1 can be expressed as

$$\sigma_0 = \sqrt{\frac{3}{2} s : s} \quad \text{Equ. 4.2.}$$

where s is the deviatoric stress, defined as the stress tensor plus the hydrostatic stress

$$s = \sigma + pI$$

$$p = -\frac{1}{3}\left(\sigma_x + \sigma_y + \sigma_z\right)\Big) \quad \text{Equ. 4.3.}$$

The stress state can be separated into hydrostatic (dilatational) and deviatoric (distortional) components. The hydrostatic stress p is associated with the energy of volume change whereas the deviatoric stress s is associated with the change in shape.

$$\sigma = s - pI \quad \text{Equ. 4.4.}$$

The von Mises yield criterion states that only the deviatoric component causes yielding. If plotted in 3D principal stress space, the von Mises yield surface is a cylinder. The cylinder is aligned with the axis $\sigma_1=\sigma_2=\sigma_3$. Note that if the stress state is inside the cylinder, no yielding occurs. This means that if the material is under hydrostatic pressure ($\sigma_1=\sigma_2=\sigma_3$), no amount of hydrostatic pressure will cause yielding.

Another way to view this is that stresses which deviate from the axis ($\sigma_1=\sigma_2=\sigma_3$) contribute to the von Mises stress calculation s.

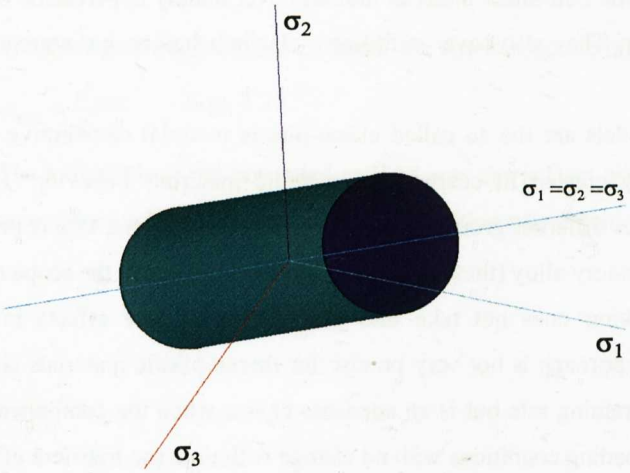

Figure 4.1: Von Mises yield surface in 3D space.

If viewed normal to the axis $\sigma_1=\sigma_2=\sigma_3$, the von Mises yield criterion will look as shown below.

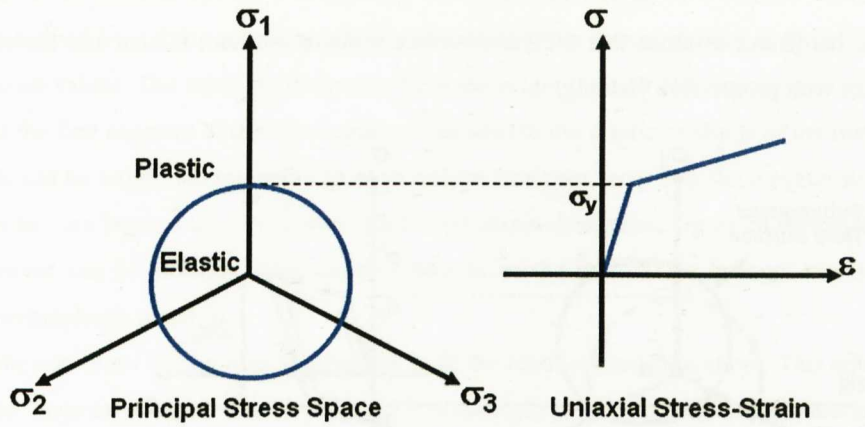

Figure 4.2: Von Mises yield surface in $\sigma_1=\sigma_2=\sigma_3$ axis.

Inside the yield surface, as noted earlier, behavior is elastic. Note that the multiaxial stress state can exist anywhere inside of the cylinder. At the edge of the cylinder (circle), yielding will occur. No stress state can exist outside of the cylinder. Instead, hardening rules will describe how the cylinder changes with respect to yielding.

4.3. Hardening Rules.

The hardening rule determines how the yield surface changes (size, center, shape) with plastic deformation. The hardening rule determines when the material will yield again if the loading is continued or reversed. This is in contrast to elastic-perfectly-plastic materials which exhibit no hardening – i.e., the yield surface remains fixed.

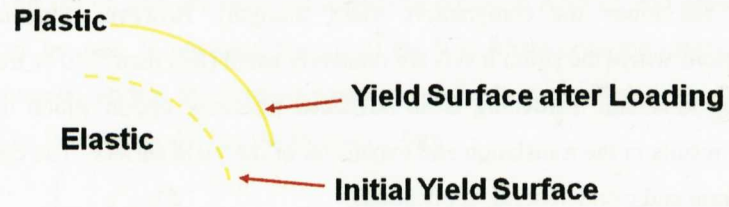

Figure 4.3: Evolution of yield surface as plastic deformation is being produced.

Two hardening rules are available: work or isotropic hardening and kinematic hardening. In work hardening, the yield surface remains centered about its initial centerline and expands in size as the plastic strains develop.

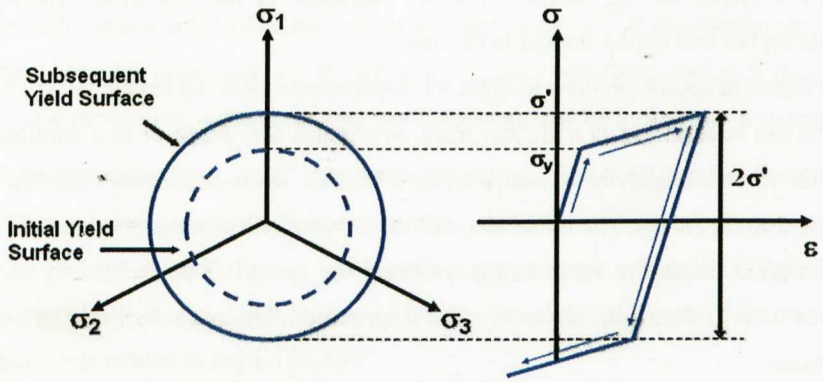

Figure 4.4: Isotropic hardening, evolution of yield surface.

Kinematic hardening assumes that the yield surface remains constant in size and the surface translates in stress space with progressive yielding.

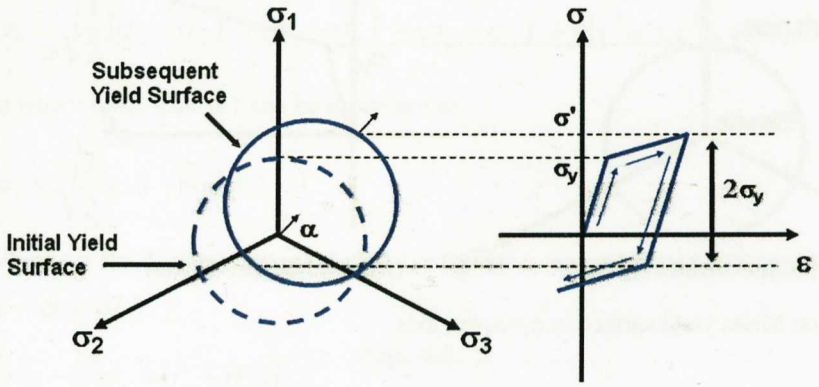

Figure 4.5: Kinematic hardening, evolution of yield surface.

This is in contrast to elastic-perfectly-plastic materials which exhibit no hardening – i.e., the yield surface remains fixed.

Different hardening behaviours can be specified inside the rate independent formulation in ANSYS:

- Isotropic Hardening Plasticity.
- Kinematic Hardening Plasticity.
- Combined Kinematic and Isotropic Hardening Plasticity.

Isotropic Hardening is appropriate for large strains with proportional loading. It is not suitable for cyclic loading applications.

Kinematic Hardening can be used for cyclic loading since it includes the Bauschinger effect (the greater the tensile cold working, the lower the compressive yield strength). However, kinematic hardening is recommended for situations where the strain levels are relatively small (less than 5-10 % true strain).

Combined isotropic and kinematic hardening is an advanced plasticity option which uses the Chaboche Hardening model. This results in the translation and expansion of the yield surface. The combined hardening can be used for large strain and cyclic loading applications.

When thermoplastic components are subjected to high straining under monotonic loads, as it will be the case of the studies performed in this thesis project, the isotropic hardening option seems to be the adequate choice.

In all the hardening models two different yielding criteria can de used in ANSYS: the Von Mises yield criterion and the anisotropic Hill´s yield criterion.

Historically, the Von Mises criterion has been used as a standard both for metallic and thermoplastic materials. Hill's criterion can be thought of as an extension of the von Mises yield criterion to cover anisotropic yielding but will not be studied in this thesis.

ANSYS offers different approximations to input the experimental uniaxial tensile tests. The input true stress-true strain curve can be modeled as a bilinear trace, as a multilinear curve or as a nonlinear curve. With the bilinear trace, the material behavior is described by a bilinear stress-strain curve starting at the origin with positive stress and strain values. The initial slope of the curve is taken as the elastic modulus of the material. At the specified yield stress, the curve continues along the second slope defined by the tangent modulus (having the same units as the elastic modulus). The tangent modulus cannot be less than zero nor greater than the elastic modulus.

In the multilinear option, a multilinear curve is used instead of a bilinear curve. The uniaxial behavior is described by a piece-wise linear total stress-total strain curve, starting at the origin, with positive stress and strain values. The curve is continuous from the origin through 100 (maximum) stress-strain points. The slope of the first segment of the curve must correspond to the elastic modulus of the material and no segment slope should be larger. No segment can have a slope less than zero. The slope of the stress-strain curve is assumed to be zero beyond the last user-defined stress-strain data point. Up to 20 temperature-dependent stress-strain curves can be included. This option seems to be the best choice to input true stress-true strain curve of a thermoplastic material.

The non linear option uses an equation to fit the input stress-strain curve. This equation can be of the form of the Voce or power law hardening and it is specially indicated to metallic materials where there is a smooth pass from the elastic to the plastic zone.

The rate dependent consideration takes into account the effect of testing rate on the stress-strain properties of the material. This is a useful approach for thermoplastic materials due to their strain rate sensitivity. When thermoplastic made components are subjected to time varying loads, especially in impact related applications, strain rate dependency has to be taken into account in order to define correctly the material properties. In contrast to the rate-independent plasticity discussed earlier, the rate-dependent plasticity is dependent upon the strain rate or time.

From a material standpoint, viscoplasticity and creep are the same. Usually, for engineering purposes, creep is used to describe the evolution of strain under a constant load. In the present work creep studies are irrelevant since time periods are very short.

4.4. Rate-dependent Plasticity (Viscoplasticity).

This option uses the isotropic hardening option in ANSYS and again, the Von Mises or Hill's yield criterion can be used. In our case, the use of the Von Mises criterion offers the possibility to select two viscoplastic material models, the Perzyna equation and the Peirce model.

The Perzyna model has the following form:

$$\sigma = \left[1 + \left(\frac{\dot{\varepsilon}^{pl}}{\gamma}\right)^{m}\right]\sigma_0 \quad \text{Equ. 4.5.}$$

and the Peirce model:

$$\sigma = \left[1 + \left(\frac{\dot{\varepsilon}^{pl}}{\gamma}\right)\right]^{m}\sigma_0 \quad \text{Equ. 4.6.}$$

In both cases σ is the (dynamic) material yield stress, $\dot{\varepsilon}^{pl}$ is the equivalent plastic strain rate, m is the strain rate hardening parameter, γ is the material viscosity parameter, and σ_0 is the static yield stress of the material. σ_0 is a function of some hardening parameter and can be defined by isotropic plasticity. As γ approaches ∞, or m approaches zero, or $\dot{\varepsilon}^{pl}$ approaches zero, the solution approaches the static (rate-independent) solution. When m is very small, the Peirce model has less difficulty in converging compared to the Perzyna model.

The Perzyna model offers a much steeper initial stage which sometimes is adequate for a correct fit of thermoplastic material data in terms of strain rate and yield stress. This model will we used in the Part II of this thesis related to impact studies.

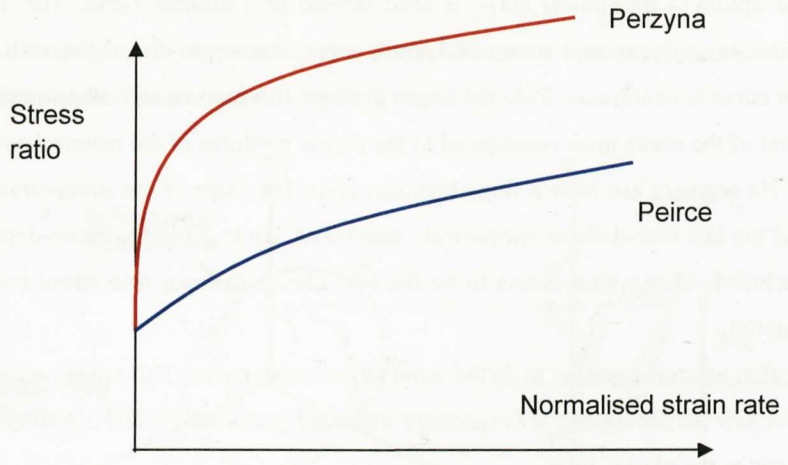

Figure 4.6: Idealised fits of the Perzyna and Peirce models. The Perzyna model offers a steeper initial fit at low strain rates.

The rate-dependent models require a rate-independent constitutive model to define the static yield stress. The viscoplastic response can be thought of as a multiplier on the static yield stress to obtain an effective stress. The rate-independent models can be bilinear-isotropic, multilinear-isotropic or non linear-isotropic.

Anand's viscoplasticity option is another rate-dependent plasticity model in ANSYS for simulations such as metal forming.

Inside the non-metal plasticity group, there is a material model that has been applied in thermoplastic materials [9,10,26] since it is able to capture the differences in yielding in compression and tensile modes. This model is called the **Drucker-Prager model** and it is in principle applicable to granular (frictional) materials such as soils, rock, and concrete.

4.5. The Drucker-Prager Plasticity Model.

This model is different from typical metal plasticity models since it considers the hydrostatic pressure. For metal plasticity (assuming von Mises or similar yield surface), only the deviatoric stress is assumed to cause yielding – if one plots the yield surface in principal stress space, the result is a cylinder whose axis is the hydrostatic pressure line, thus indicating that yielding is independent of the hydrostatic stress state. For the Mises yield surface, one could theoretically have infinite hydrostatic compression, with no yielding.

On the other hand, the Drucker-Prager plasticity model has a term that is dependent on the hydrostatic pressure. For a linear yield surface ("linear" referring to the linear shape when plotted in the plane of effective stress vs. hydrostatic pressure), this means that in the presence of hydrostatic tension, the yield strength would be smaller. Conversely, as hydrostatic compression increases, so would the yield strength. When the yield surface is plotted in principal stress space, it would look like a cone.

The two main characteristics of the model are (a) the yield strength changes, depending on the hydrostatic stress state and (b) some inelastic volumetric strain can occur, as defined by the flow potential.

Plotted in principal stress space, the yield surface is a cone.

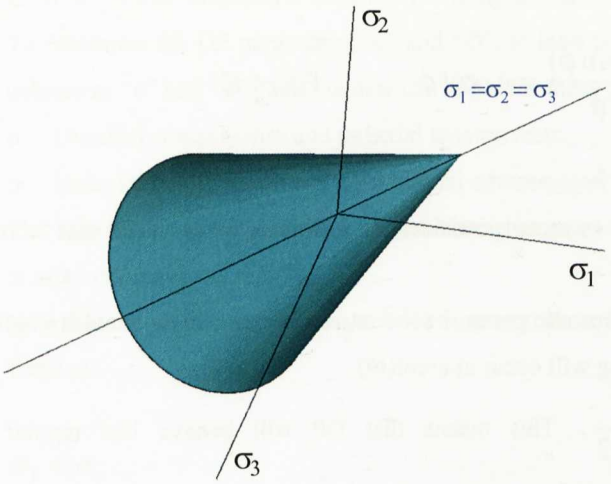

Figure 4.7: Yield surface for the Drucker-Prager model in 3D space.

The yield function is as described,

$$F = \sqrt{3}\beta\sigma_m + \frac{\sigma_{equiv}}{\sqrt{3}} - \sigma_y = 0 \quad \text{Equ. 4.7.}$$

where,

$$\sigma_{equiv} = \sqrt{\frac{3}{2} s : s} \quad \text{Equ. 4.8.} \quad \text{Von Mises stress}$$

$$\sigma_m = \frac{1}{3}\left(\sigma_x + \sigma_y + \sigma_z\right) \quad \text{Equ. 4.9.} \quad \text{Hydrostatic (mean) stress}$$

$$\sigma_y = \frac{6(c)\cos\phi}{\sqrt{3}(3 - \sin\phi)} \quad \text{Equ. 4.10.} \quad \text{Material yield parameter}$$

$$\beta = \frac{2\sin\phi}{\sqrt{3}(3 - \sin\phi)} \quad \text{Equ. 4.11.} \quad \text{Material parameter } \beta$$

The cohesion value "c" is a required input for the DP model (units of stress). And the angle of internal friction "Φ" is also a required input (units of degrees).

Instead of plotting in principal stress space, plotting the yield surface on the meridional plane provides additional insight. From Figure 4.8, the following equation can be described:

$$\sigma_{equiv} = -3\sqrt{3}\beta\sigma_m + \sqrt{3}\sigma_y \quad \text{Equ. 4.12.}$$

If σ_{equiv} is plotted vs. σ_m, the following graph is obtained:

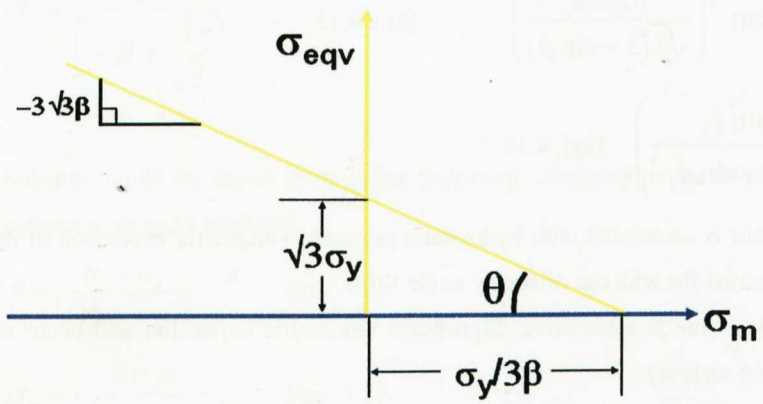

Figure 4.8: σ_{equiv} vs. σ_m plot for Drucker-Prager parameter identification.

$$\frac{\sigma_y}{3\beta} = \frac{6(c)\cos\phi}{\sqrt{3}(3-\sin\phi)} \cdot \frac{\sqrt{3}(3-\sin\phi)}{6\sin\phi} = c \cdot \cot\phi \qquad \text{Equ. 4.13.}$$

$$\theta = \tan^{-1}(3\beta) \neq \phi \qquad \text{Equ. 4.14.}$$

To better understand this constitutive model, consider the following cases (recall that "c" and "Φ" are input parameters):

In compression, an increase in hydrostatic pressure produces an increase in the yield strength.

In pure hydrostatic tension, yielding will occur at c•cot(Φ).

If Φ=0, then β=0, $\sigma_y = 2c/\sqrt{3}$. This means that DP will behave like regular metal plasticity (incompressible) with yield strength=2c.

In the limiting (fictitious) case of Φ=90, then $\beta = 1/\sqrt{3}$, σ_y=0. In this situation, yielding would occur at -$3\sigma_m$, so it would be unstable unless in a hydrostatic compressive state.

Remember that for Drucker-Prager, no hardening is assumed, so the material behavior is always elasto-perfectly plastic. If a plastic hinge develops in the finite element model (plasticity throughout a given section), then a physical instability would occur.

The flow rule for Drucker-Prager can be associative or non-associative, depending on a 3rd input parameter, the dilatancy angle, Φ_f. The dilatancy angle Φ_f controls the amount of volumetric expansion that occurs. On the meridional plane below, Φ_f indicates the direction of plastic flow (dilation angle), as shown in red. On the other hand, Φ describes the direction of the outward normal to the yield surface (angle of internal friction), as shown in yellow.

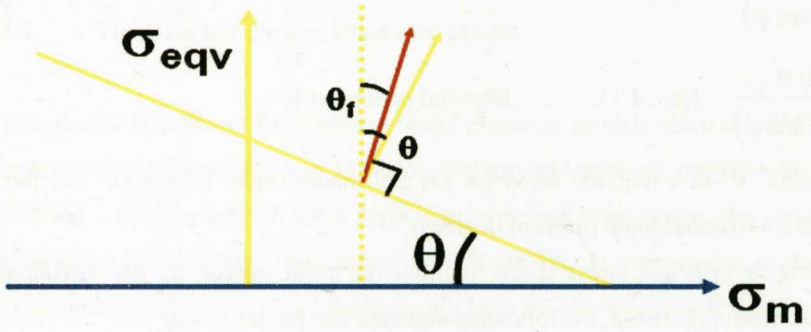

Figure 4.9: Plastic flow according to θ_f and Drucker-Prager parameter identification.

$$\theta = \tan^{-1}(3\beta) = \tan^{-1}\left(\frac{6\sin\phi}{\sqrt{3}(3-\sin\phi)}\right) \qquad \text{Equ. 4.15.}$$

$$\theta_f = \tan^{-1}\left(\frac{6\sin\phi_f}{\sqrt{3}(3-\sin\phi_f)}\right) \qquad \text{Equ. 4.16.}$$

Since volumetric strain is associated with hydrostatic pressure, volumetric expansion of the material due to yielding can be accounted for with the dilatancy angle Φf.

If Φf=Φ, then the flow rule is associative. Significant volumetric expansion will occur as a result (plastic flow is normal to yield surface).

If Φf<Φ, then the flow rule is nonassociative. Less volumetric expansion will occur.

If Φf=0, then no volumetric expansion will occur. This is usually more conservative.

To determine the DP parameters "c" and "Φ", at least two types of tests should be performed. There are two unknowns "c" and "Φ", and the user can solve for these unknowns based on yield strengths of different tests:

- Uniaxial compression and uniaxial tension tests.
- Uniaxial compression and equi-biaxial compression tests.

The calculation of the dilatancy angle Φf may be somewhat more involved. Assuming Φf=0 usually results in more conservative results.

Note that the yield stress in compression is greater than the yield stress in tension.

Tension:

$$\sigma_1 = \sigma_t$$
$$\sigma_2 = \sigma_3 = 0$$
$$\sigma_{equiv} = \sigma_t \qquad \text{Equ. 4.17.}$$
$$\sigma_m = \sigma_t/3$$

$$F = 3\beta\frac{\sigma_t}{3} + \frac{\sigma_t}{\sqrt{3}} - \sigma_y = 0$$
$$\sigma_t = \frac{\sigma_y}{\left(\beta + \frac{1}{\sqrt{3}}\right)} \qquad \text{Equ. 4.18.}$$

Compression:

$$\sigma_3 = -\sigma_c$$
$$\sigma_1 = \sigma_2 = 0$$
$$\sigma_{equiv} = \sigma_c \qquad \text{Equ. 4.19.}$$
$$\sigma_m = -\sigma_c/3$$

$$F = -3\beta\frac{\sigma_c}{3} + \frac{\sigma_c}{\sqrt{3}} - \sigma_y = 0$$
$$\sigma_c = \frac{\sigma_y}{\left(-\beta + \frac{1}{\sqrt{3}}\right)} \qquad \text{Equ. 4.20.}$$

Substitution of the above leads to the following relationships for Φ and c if the user has data of tensile and compressive yield strengths:

$$\beta = \frac{\sigma_c - \sigma_t}{\sqrt{3}(\sigma_c + \sigma_t)} \qquad \text{Equ. 4.21.}$$

$$\sigma_y = \frac{2\sigma_c\sigma_t}{\sqrt{3}(\sigma_c + \sigma_t)} \qquad \text{Equ. 4.22.}$$

$$\phi = \sin^{-1}\left(\frac{3\sqrt{3}\beta}{2+\sqrt{3}\beta}\right) \qquad \text{Equ. 4.23.}$$

$$c = \left(\frac{\sigma_y\sqrt{3}(3-\sin\phi)}{6\cos\phi}\right) \qquad \text{Equ. 4.24.}$$

Uniaxial compression:

$$\sigma_3 = -\sigma_c$$
$$\sigma_1 = \sigma_2 = 0$$
$$\sigma_{equiv} = \sigma_c \qquad \text{Equ. 4.25.}$$
$$\sigma_m = -\sigma_c/3$$

$$F = -3\beta\frac{\sigma_c}{3} + \frac{\sigma_c}{\sqrt{3}} - \sigma_y = 0$$
$$\sigma_c = \frac{\sigma_y}{\left(-\beta + \frac{1}{\sqrt{3}}\right)} \qquad \text{Equ. 4.26.}$$

Biaxial compression:

$$\sigma_3 = \sigma_2 = -\sigma_c$$
$$\sigma_1 = 0$$
$$\sigma_{equiv} = \sigma'_c \qquad \text{Equ. 4.27.}$$
$$\sigma_m = -2\sigma_c/3$$

$$F = -3\beta\frac{2\sigma'_c}{3} + \frac{\sigma'_c}{\sqrt{3}} - \sigma_y = 0$$
$$\sigma'_c = \frac{\sigma_y}{\left(-2\beta + \frac{1}{\sqrt{3}}\right)} \qquad \text{Equ. 4.28.}$$

From this,

$$\beta = \frac{\sigma'_c - \sigma_c}{\sqrt{3}(2\sigma'_c - \sigma_c)} \qquad \text{Equ. 4.29.}$$

$$\sigma_y = \frac{\sigma'_c\sigma_c}{\sqrt{3}(2\sigma'_c - \sigma_c)} \qquad \text{Equ. 4.30.}$$

and again,

$$\phi = \sin^{-1}\left(\frac{3\sqrt{3}\beta}{2+\sqrt{3}\beta}\right) \quad \text{Equ. 4.31.}$$

$$c = \left(\frac{\sigma_y\sqrt{3}(3-\sin\phi)}{6\cos\phi}\right) \quad \text{Equ. 4.32.}$$

All constants should be input (i.e., the cohesion value cannot be zero). Note that elastic material properties (Young's Modulus EX, Poisson's ratio NUXY) also need to be input. No temperature-dependency is allowed for this material law in ANSYS.

Drucker-Prager is a rate-independent plasticity model. For solution options, the same considerations apply for models with other rate-independent plasticity.

In ANSYS, there is an extension to this model, the so called Extended Drucker-Prager model. The Extended Drucker-Prager is meant to address some shortcomings of the basic Drucker-Prager model – namely, the use of perfectly-plastic behavior and the requirement of a linear yield surface.

A linear, power law, or hyperbolic yield surface can be specified with the TBOPT argument of the TB, EDP command in ANSYS. Strain-hardening behavior is specified by adding an isotropic hardening plasticity model to the same material.

In the present thesis work the extended Drucker-Prager model has been used in the form of a linear yield surface. In this case the following constants are needed as an input:

$$C_1 = \alpha = \frac{6\sin\phi}{3-\sin\phi} \quad \text{Equ. 4.33.}$$

$$C_2 = \sigma'_y = \sqrt{3}\sigma_y \quad \text{Equ. 4.34.}$$

Additionally, the true stress-true strain curve has to be input in order to model the plastic area of the tensile curve.

The last interesting material model option in ANSYS is inside the inelastic non linear group and is related to the modeling of viscoelasticity. This approach is very useful for thermoplastic materials being viscoelastic in nature.

However, the load requirements studied in this work force the material to large plastic straining regions where other concepts as

- the proper modeling of the plastic part of the stress-strain curve,
- yieldingand rate dependency on yielding,
- the determination of failure strains,

are more important than viscoelastic effects. In fact, the vast majority of elasto-plastic material models does not take into account viscoelasticity but other factors, for example viscoplasticity is considered in Perzyna and Peirce models.

In ANSYS, experimental viscoelastic data can be fitted to Maxwell or Prony mathematical series.

It has to be remarked that an advanced material model should take into account both the viscoelastic and viscoplastic effects in order to be suitable for simulating time dependent events with plastic materials.

Chapter 5: Finite Element Analysis Techniques and Nonlinear Issues.

5.1. Introduction.

Finite Element Analysis (FEA) is a computer simulation technique used in engineering analysis. It uses a numerical technique called the finite element method (FEM).

It was first developed in 1943 by Richard Courant, who utilized the Ritz method of numerical analysis and minimization of variational calculus to obtain approximate solutions to vibration systems. Shortly thereafter, a paper published in 1956 by M. J. Turner, R. W. Clough, H. C. Martin, and L. J. Topp established a broader definition of numerical analysis. The paper centered on the "stiffness and deflection of complex structures".

In its application, the object or system being investigated is represented by a geometrically similar model consisting of multiple, linked, simplified representations of discrete regions—i.e., finite elements on an unstructured grid. Equations of equilibrium, in conjunction with applicable physical considerations such as compatibility and constitutive relations, are applied to each element, and a system of simultaneous equations is constructed. The system of equations is solved for unknown values using the techniques of linear algebra or nonlinear numerical schemes, as appropriate. While being an approximate method, the accuracy of the FEA method can be improved by refining the mesh in the model using more elements and nodes.

A common use of FEA is for the determination of stresses and displacements in mechanical objects and systems. However, it is also routinely used in the analysis of many other types of problems, including those in heat transfer, fluid dynamics and electromagnetism. FEA is able to handle complex systems that defy closed-form analytical solutions.

There exist many finite element software packages, both free and proprietary.

Over the past years, one of the most significant developments in analytical methods, directed at overcoming the issues of geometric complexity and non linearity, has been the FEM. This method has been used successfully in a wide range of industries, including aerospace, automotive, and consumer products, to name a few. Just as with other engineering materials, the finite element method has become an extremely important tool for analysis of components made of thermoplastic. Part fabrication processes such as injection moulding provide means of creating geometrically complex parts that make simple handbook formulas difficult to apply. Furthermore, the low material stiffness and yield strengths of thermoplastics create situations where nonlinear behaviour is often commonplace.

In this section, a general description of the basic theory behind finite element analysis will be followed by a discussion on element types commonly available for application. The generic procedure for applying finite elements will also be summarised in terms of geometry definition and mesh creation, material properties, boundary and loads conditions, and interpretation of results.

Since the ability to account for nonlinear behaviour is one of the reasons that finite element techniques are being used, a basic understanding of some of the nonlinear structural behaviour that is significant when dealing plastics will be described.

5.2. Structural Finite Element Analysis. Theoretical Basis.

A structure can be idealised as being composed of many small, discrete pieces called finite elements. The problem can now be characterised by large numbers of simultaneous equations. The advent of the first generation of computers soon made the solution of these equations straightforward.

As linear solutions (Hooke's law application) became routine, techniques for the application of FEA approach to nonlinear problems received increased attention.

FEA simulation has become a very important tool in engineering part design. Advantages of the FEA include:

- improved performance and quality of the final plastic product.
- optimum use of materials.
- weight savings.
- improved probability of successful performance of prototype parts
- faster time to market and therefore a competitive edge.
- reduced development, production and part costs.

5.2.1. Fundamentals.

FEA reduces a large, complex structure into a network of small, simple geometric elements, such as beams, two dimensional (2-D) elements, shells, or solids (3-D) elements. Within any of these elements, relatively simple equations can be used to describe the measures of deformation, e.g., stress, strain and displacement. The behaviour of the entire structure is calculated by combining the element equations into a large set of simultaneous equations representing the behaviour of the structure.

Linear analysis applies to problems where stress and strain are related in a linear fashion and deflections are small. In contrast, nonlinear analysis is required when material constitutive relations or boundary conditions become nonlinear in nature or when strains and displacements become large.

A finite element model can be thought as a system of springs.

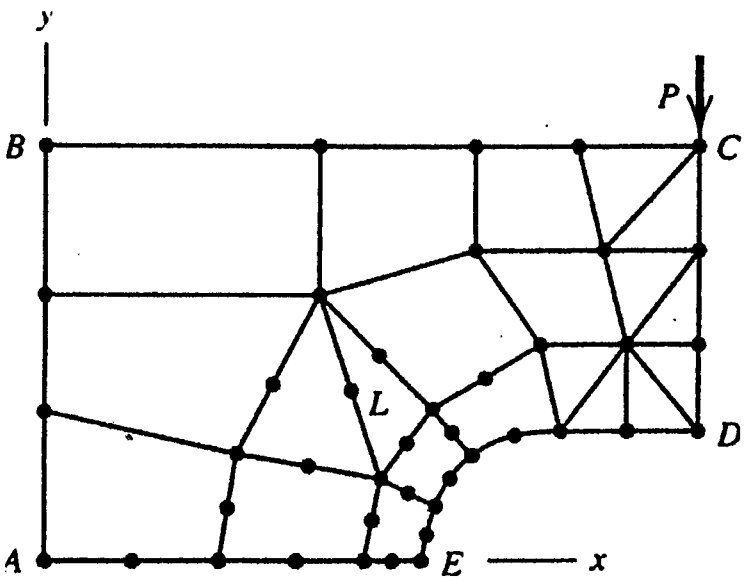

Figure 5.1: Example of a finite element model in 2D [30].

When a load is applied to the structure, all of the elements must deform in a fashion that guarantees equilibrium of forces between the elements. In addition, the deformation of the modelled structure must remain compatible.

The first step in developing equations is to establish the expression for element stiffness, relating forces and displacements at the nodes of an element. The sequence is as follows:

1. assume an approximate displacement function for the element. This function is defined in terms of the displacements at the nodes of the element and should ensure compatibility of displacements with neighbouring elements along its entire boundary.
2. apply the kinematic equations defining strain in terms of the approximate displacement functions.
3. use the constitutive relationship appropriate for the material to determine stresses in terms of strains.
4. develop equilibrium equations relating internal element nodal forces to externally applied nodal forces.

5.2.2. Displacement function.

Characterises the displacements within an element as a function of space. The choice of displacement function affects the accuracy of the element in approximating actual displacements, strain, and stress behaviour over the volume of the element. Since strains are first derivatives of displacements, a linear displacement function leads to the approximation of constant strains and stresses within the element. Similarly, a quadratic displacement function simulates linear stress and strain fields within an element. For the three-node triangular elements shown in Figure 5.1, with the x axis lying along one edge of the triangle, and with displacements (U_i, V_i) in two coordinate directions (x,y) at each node (i), a total of six nodal displacements (degrees of freedom) can be defined in terms of the deformation field for the element. This requires functions with a total of six coefficients:

$$u = a + bx + cy \qquad \text{Equ. 5.1.}$$

$$v = d + ex + fy \qquad \text{Equ. 5.2.}$$

where a, b, c, d, e, and f are unknown constants.

Element displacements in terms of nodal displacements.

Using the previous equations 5.1 and 5.2 to evaluate the displacement at each node (i),

$$U_i = a \qquad \text{Equ. 5.3.}$$

$$U_i = a + bX_j \qquad \text{Equ. 5.4.}$$

$$U_i = a + bX_k + cY_k \qquad \text{Equ. 5.5.}$$

where X_j, X_k and Y_k define known coordinate locations. A similar set of equations can be written to define the coefficients d, e, and f in terms of the nodal y displacements. Using matrix manipulation it is possible to represent the u and v displacements within an element in terms of nodal displacements as

$$\begin{Bmatrix} u(x,y) \\ v(x,y) \end{Bmatrix} = [N] \begin{Bmatrix} Ui \\ Vij \\ Vj \\ Uk \\ Vk \end{Bmatrix} = [N]\{\delta\} \qquad \text{Equ. 5.6.}$$

where [*N*] is the shape function matrix and $\{\delta\}$ is the vector of nodal displacements.

5.2.3. Strains as a function of nodal displacements.

The two dimensional definitions of strain in terms of displacement are:

$$\varepsilon_x = \frac{\partial u}{\partial x} \qquad \text{Equ. 5.7.}$$

$$\varepsilon_y = \frac{\partial u}{\partial y} \qquad \text{Equ. 5.8.}$$

$$\gamma_{xy} = \frac{\partial u}{\partial y} + \frac{\partial v}{\partial x} \qquad \text{Equ. 5.9.}$$

Equ. 5.7-5.9 are used to calculate the strains within the element in terms of its nodal displacements. Using matrix notation again, the above relationships can be expressed as

$$\{\varepsilon\} = \begin{Bmatrix} \varepsilon_x \\ \varepsilon_y \\ \gamma_{xy} \end{Bmatrix} = [B]\{\delta\} \qquad \text{Equ. 5.9.}$$

where [B] is a matrix that can be defined in terms of derivatives of the shape function elements.

5.2.4. Stresses in terms of strains.

In order to relate stresses to strains, a material constitutive model is necessary. For simple linear elasticity, the plane stress constitutive relations are

$$\sigma_x = \frac{E}{1-\nu^2}\left(\varepsilon_x + \nu\varepsilon_y\right) \qquad \text{Equ. 5.10.}$$

$$\sigma_y = \frac{E}{1-\nu^2}\left(\varepsilon_y + \nu\varepsilon_x\right) \qquad \text{Equ. 5.11.}$$

$$\tau_{xy} = \frac{E}{2(1+\nu)}\gamma_{xy} \qquad \text{Equ. 5.12.}$$

where E is the elastic modulus and ν is the Poisson's ratio. Using matrix notation,

$$\begin{Bmatrix} \sigma_x \\ \sigma_y \\ \tau_{xy} \end{Bmatrix} = [D]\begin{Bmatrix} \varepsilon_x \\ \varepsilon_y \\ \gamma_{xy} \end{Bmatrix} = [D][B]\{\delta\} \qquad \text{Equ. 5.13.}$$

where [D] is the material matrix formed using Equ. 5.11-5.12.

5.2.5. Nodal forces in terms of displacements.

Load is transmitted from one finite element to another trough forces at the node points of the elements, which can be represented as $\{F\}$. These nodal forces in the two coordinate directions are related to the nodal displacements through a set of element equilibrium equations. These equilibrium equations can be defined by equating the external work accomplished by the nodal forces when subjected to an arbitrary set of virtual nodal displacements, $d\{\delta\}$, to that of the internal energy stored in the element's volume as its stress is subjected to the virtual strain field, resulting from the same nodal displacements.

This relationship can be expressed as:

$$(d\{\delta\})^T\{F\} = \int_{Vol} d\{\varepsilon\}^T\{\sigma\}dVol \qquad \text{Equ. 5.14}$$

Since the virtual strains can be related to the virtual nodal displacements as

$$d\{\varepsilon\} = [B]d\{\delta\} \qquad \text{Equ. 5.15.}$$

the element equilibrium takes the form

$$(d\{\delta\})^T\{F\} = d\{\delta\}^T \int_{Vol} [B]^T[D][B]\{\delta\}dVol \qquad \text{Equ. 5.17.}$$

The relationship between the nodal forces $\{F\}$ and the nodal displacements $\{\delta\}$ can be written as,

$$\{F\} = [K]_e\{\delta\} \qquad \text{Equ. 5.18.}$$

where $[K]_e$ is the element stiffness matrix defined as

$$[K]_e = \int_{Vol} [B]^T[D][B]dVol \qquad \text{Equ. 5.19.}$$

5.2.6. Global equilibrium.

Individual elements stiffnesses are assembled using matrix algebra techniques into a global stiffness matrix representing the stiffness of the entire structure.
If the externally applied forces are known, a solution for the nodal degrees of freedom can be obtained using linear algebra once the required boundary equations are applied.
Equilibrium is only guaranteed at a finite number of nodal points in the structure, so the finite element method is a numerical approximation rather than an exact solution. The accuracy of the approximation will depend on the number of nodes and elements in the structure (mesh density).

5.3. Types of Finite Elements.

The choice of the type of element to use for a particular problem is often a trade off between reality and simplicity. Elements can be categorised as one, two and three dimensional solid elements and beam, plate and shell elements.

The complexity of the analysis and the amount of engineering and computer time increase significantly when moving from 1-D to 2-D and 3-D analysis. Many real part geometries and loadings are certainly 3-D in nature. When 2-D and 1-D elements are used, assumptions must be made relative to the distribution of stress and strain in the other directions. Since plastic parts tend to have thin walls relative to their overall dimensions, the most suitable types of elements are plates and shells. Plate or shell analysis can treat the geometric complexity adequately and offer the flexibility to change the wall thickness of the model easily during engineering parameter studies. In 3-D analysis, a thickness change requires a complete change of the finite element mesh, which is usually a more time consuming process. However, plate and shell elements are complex and vary widely in their formulations.

- One dimensional elements.

Bar or truss elements are simple, one dimensional elements. Their length is calculated from the nodal positions defining the bar ends. The cross-sectional area is defined by the modeller. These elements are simple spring elements and have very limited use in plastic part modelling.

- Two dimensional elements.

Include plane stress, plane strain and axisymmetric elements. The plane stress assumption (that stress in the thickness direction is zero) is used when the component's deformation is independent of the dimension perpendicular to the plane of description and its thickness in that direction is small (thin snap fits). The plane strain assumption (that strain in the thickness direction is zero) is used when the component is thick relative to the planar dimensions (long plastic boxes).

In the axisymmetric elements, the stresses, strains, and loads do not vary in the circumferential direction. These elements are often quite useful because they account for fully 3-D behaviour (parts that offer the possibility to only model the revolution cross-sectional area, plastic bottles).

- Three dimensional elements.

3-D elements are typically either tetrahedrons or hexahedrons. One of the most common is the rectangular hexahedron with eight nodes, one at each corner. Normally it is not necessary to model plastic parts with 3-D elements because of the thin-walled nature of their structure. However such elements will be used when precise studies of local stress distributions around geometric details like notches are needed.

In this thesis work 3-D elements will be evaluated for simple geometries as beam and plates.

- Shell elements.

All the nodes describing the geometry of these elements are at the midsurface of the component. The thickness of the element is usually specified as either a nodal or element parameter.

The degrees of freedom associated with the nodes of these elements now include rotations as well as translations.

In this thesis, 3-D shell elements will be evaluated for simple geometries as beam and plates.

Many of these elements are formulated under the assumption that the transverse shear deformation within the element can be neglected, as this is normally a valid approximation. However, if the shell is relatively thick, the shear deformation may be significant. There are specifically formulated shell elements that can be used to account for shear deformation if it is significant.

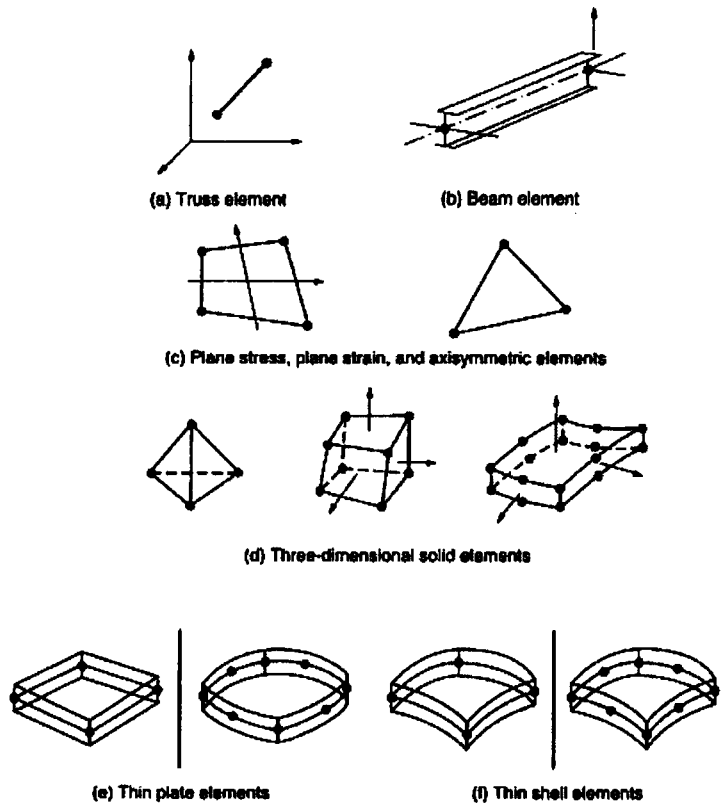

Figure 5.2: Basic element types found in FEA software.

5.4. Finite Element Analysis Procedure.

The study of a component or a system of different parts (an assembly) requires in any finite element based software three main steps:

- Preprocessing.
- Solution.
- Postprocessing.

The preprocessing step is related to the preparation of the geometry and mesh. In some cases no geometry is available since the mesh is directly imported from another FEA code. When the geometry is modelled, it can be imported from a CAD software or can be directly created in the finite element programme. In both cases, the general aim of the geometrical modellisation is to obtain the simplest representation of the part (eliminating small details that will not affect the overall response) in order to make the meshing process easier.

Meshing consists of dividing the geometry into elements that are connected to one another at the nodal points. The meshing of the part is automatic in most of the codes and the user has to specify the element type and the mesh size to be used. Selecting a coarser meshes results in a faster solution time but limits the accuracy of the analysis.

As described previously, engineering judgment is necessary for the selection of the element types and dimensionality of the problem: when simulating plastic components, 3-D calculations are mainly performed due to the geometrical complexities (using adequate 3-D hexahedral or tetrahedral elements). However, since thickness values are generally much smaller than other dimensions of the component, "shell" type 3-D elements are the preferred choice to be used, where the thickness is removed from the original geometry (the component is represented with skin type 3-D surfaces). This requires an additional extra work when

preparing the model (if there is not a CAD model previously prepared in an all-surface type geometry) but solution time is shortened due to the lower number of nodes and elements than in a complete 3D analysis.

The preprocessing step also comprises the specification of material properties, which can be complicated depending on the materials to be studied and the complexity of the analysis.

For simple isotropic, linear-elastic stress analysis, only elastic modulus and Poisson' ratio are needed. For highly loaded parts, elastic-plastic behaviour may be included. In some cases, nonlinear stress-strain relationships may be represented through a multilinear approximation of the curve. Some material models allow for the definition of strain rate or time dependence of a yield condition. Such material models may be useful in modelling impact events or creep situations, respectively. Increased capability in material modelling implies that more material data must be available (tested).

The solution phase is related to the specification of the boundary conditions and loads that are imposed to the component or system of components and the solving of the problem.

The boundary conditions can be in the form of restrictions of degrees of freedom (DOF) in the X, Y, Z directions, or in the form of contact regions in between different areas of the same part or between different parts.

The load type varies with the analysis type but in general structural problems, forces, displacements, pressures, temperatures, velocities or accelerations are applied.

Each software uses different solution types for the calculation of the equations below the analysis. The time needed for obtaining results depends on many factors as:

- mesh size (number of nodes and elements).
- problem complexity: contacts, material laws, friction, high strains; non-linear behaviour.
- solvers and time integration method (implicit-explicit).

The postprocessing phase is related to the visualization of the results in a graphical form. Deformed shapes, stresses, strains, reaction results and graphs can be plotted between other quantities and the output should be compared with admissible parameters in our design (for example, comparing the obtained Von Mises stresses with the material's yield point). An adequate postprocess should evaluate critically the validity of the obtained results, for example, in a static analysis the applied forces and the obtained reaction results should be in equivalence or in a crash event the total energy should be maintained constant along time. Evaluating the obtained results, design modification or optimization works can be carried out.

5.5. Nonlinear Issues in Analysis.

There are several different types of nonlinear behaviour that are important to plastics. The most obvious nonlinearity associated with plastics is the nonlinear constitutive relationship relating stress to strain for some plastics.

However, some nonlinearities are geometric in nature and are associated with the strain-displacement equations. This nonlinearity is especially significant in beam, plate and shell structures, when rotations associated with transverse displacements become moderately large. The behaviour associated with this nonlinearity can be either stiffening or softening.

A third nonlinearity may be associated with the application of load. In some situations both the magnitude and location of load application depend upon the structure's deformation and cannot be explicitly defined beforehand. In such cases, the contact loads must be calculated as part of the solution process, thus making the problem nonlinear.

Chapter 6: Experimental Work. Quasi-Static Testing and Simulation of Thermoplastic Materials.

In this chapter, the general characteristics of thermoplastic materials will be presented first, and more specifically, the mechanical properties of the materials used in the thesis work. It will also be described shortly the processing considerations to obtain the desired specimens.

The experimental work comprised two aspects:

a) Static or slow rate testing of tensile, bending and puncture specimens in both materials.
b) FEA of the tensile, bending and puncture tests,
    a. to correlate and validate the tensile test as a method to generate material data input.
    b. to correlate the bending and puncture tests and evaluate the validity of the different elasto-plastic constitutive models.

In each section, both testing and simulation results will be presented for both materials as well as some final conclusions and considerations especially focused on the use of elasto-plastic models.

6.1. Thermoplastic Materials.

The vast majority of plastics are synthetic compounds having a carbon-carbon backbone modified by other organic side groups. Plastics are differentiated chemically from other materials by their extremely long, chainlike molecules and high molecular weights. The process of joining together tens of thousands of smaller molecular units, known as monomers, into these long molecules is called polymerisation. A plastic material is a polymer plus reinforcements, fillers, and additives, such as mineral and glass fillers, flame retardants, and stabilisers. The resultant plastics are then shape and solidified, thus producing a plastic part.

In general, plastic materials can be divided into two major classes: thermoplastics and thermosets. The fundamental difference between these two types of plastic materials can be described with respect to the bonds that exist between long molecular chains and their consequent response to temperature increase.

When raised to a sufficiently high temperature, a solid thermoplastic will become viscous and pliable in nature. In this state, it can be formed into useful geometric shapes and will retain these shapes when cooled. If reheated to a high enough temperature, a thermoplastic again will become viscous and can be reshaped and then cooled and resolidified. This characteristic behaviour is related to the fact that the long molecular chains of thermoplastics are not significantly cross-linked through covalent bonds, similar to those bonds that hold each chain together.

On the other hand, the first application of sufficient heat or a catalyst to a thermoset initiates covalent bonding between these polymer chains, leading to a more rigid, cross-linked coupling between the constituent molecules. Before this cross-linking occurs, a thermoset can be very fluid in nature, allowing it to fill moulds defining the desired component's shape easily. However, unlike thermoplastics, if a thermoset is subsequently reheated, it will not return to its fluid like shape. Sufficient application of temperature will eventually degrade the thermoset.

Crystalline and amorphous polymers.

There are also two major thermoplastic material types: crystalline and amorphous polymers. A crystalline polymer is a polymer chain that exhibits an ordered molecular structure. The term crystalline is actually a misnomer since crystalline polymers are actually only semi-crystalline in nature. They have regions of ordered molecular structure and also have regions of no order of form (amorphous). Characteristics:

- a well-defined melting point.
- more resistant to solvents than amorphous polymers.
- more shrinkage and more likely to warp due to anisotropic shrinkage during processing than amorphous polymers.
- low melt viscosity (long flow lengths) in comparison to amorphous thermoplastics for similar molecular weights.
- low melt strength and , as a result, not as readily blow-moldable.
- more temperature dependant mechanical properties than amorphous thermoplastics.

Amorphous polymers are composed of randomly oriented polymer chains with minimal ordered molecular structure. Amorphous polymers rely on increased polymer chain lengths (higher molecular weights) and physical entanglements of those chains for structural integrity. Some general characteristics:

- undergo a second order transition.
- more uniform and quantitatively lower shrinkage during processing as well as greater dimensional stability.
- high melt viscosities.
- more susceptible to chemical attack than semicrystalline polymers.
- option of optical transparency.

Polymer blends and alloys.

These materials are becoming increasingly important material subgroups because they offer unique combinations of properties of each of their parent polymers. Polymer blends fall into three main categories: miscible, immiscible, and partially miscible. Miscible blends consist of a single polymer phase containing two or more polymers that are completely soluble in each other (for example, polyethylene ether PPE and polystyrene PS blends).

Immiscible blends result from mixing two materials with little affinity to each other. The most practiced example of combining two immiscible polymers is for the purpose of impact resistance; examples of such immiscible blends are high-impact polystyrene (HIPS) and some ABS materials.

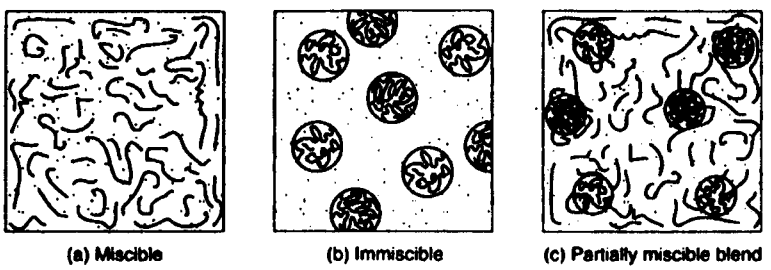

Figure 6.1: Different options for miscibility in polymer blends.

The PC/ABS blend studied in this thesis falls in the range of partially miscible blends. It can be considered to have miscible PC/SAN phases with immiscible PC/PB phases. The PC contributes impact and heat distortion resistance, while the ABS contributes processability and chemical stress resistance, and cost reduction below PC.

In this thesis study, two material types have been employed: a semi-crystalline polypropylene (PP) and an amorphous PC/ABS. The thermoplastic materials employed are described below.

6.1.1. Polypropylene (PP).

The grade used in this study is PP-BE677AI from the material manufacturer Borealis.

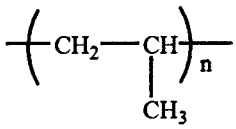

Figure 6.2: Molecular structure of Polypropylene.

This material grade is under the trademark Xmod ™. It is a highly crystallinity standard block copolymer, with ethylene as comonomer. It is UV stabilised and impact modified.

The principle application is injection moulded automotive interior and appliance parts, it possesses an excellent balance between impact strength and stiffness as well as good surface quality. Typical application areas are:

Automotive interior parts,

- Pillar trims, door panels and pockets, central consoles.

Appliances parts,

- Internal and external parts for vacuum cleaners, accessory parts for vacuum cleaners like nozzles extension tubes etc., parts of refrigerators.

The main physical properties extracted from the material manufacturer data sheets are described in the following table:

Property	Typical value	Test Method
Density	905 Kg/m^3	ISO 1183
Melt Flow Rate (230°C/ 2.16 Kg.)	14 g/10 min.	ISO 1183
Flexural Modulus (2 mm/min.)	1500 MPa.	ISO 178
Tensile Modulus (1 mm/min.)	1500 MPa.	ISO 527-2
Tensile Strain at Yield (50 mm/min.)	5%	ISO 527-2
Tensile Stress at Yield (50 mm/min.)	26 MPa.	ISO 527-2
Heat Deflection Temperature A (1.80 MPa.)	56°C	ISO 75-2
Heat Deflection Temperature B (0.45 MPa.)	110°C	ISO 75-2
Vicat softening temperature (10N)	150°C	ISO 306
Vicat softening temperature (50N)	72°C	ISO 306
Charpy Impact Strength, notched (23°C)	9 KJ/m^2	ISO 179/1eA
Charpy Impact Strength, notched (-20°C)	4.5 KJ/m^2	ISO 179/1eA
Charpy Impact Strength, unnotched (23°C)	110 KJ/m^2	ISO 179/1eU
Charpy Impact Strength, unnotched (-20°C)	62 KJ/m^2	ISO 179/1eU
Hardness, Ball Indentation H 358/30	62 MPa	ISO 2039

Table 6.1: Mechanical properties for the selected PP BE677AI from Borealis.

These values were determined on standard injection moulded specimens conditioned at 23°C and 50% relative humidity after at least 96 hours storage time.

The material manufacturer also offers an engineering stress-strain curve (at 23°C) which could be useful for structural simulations.

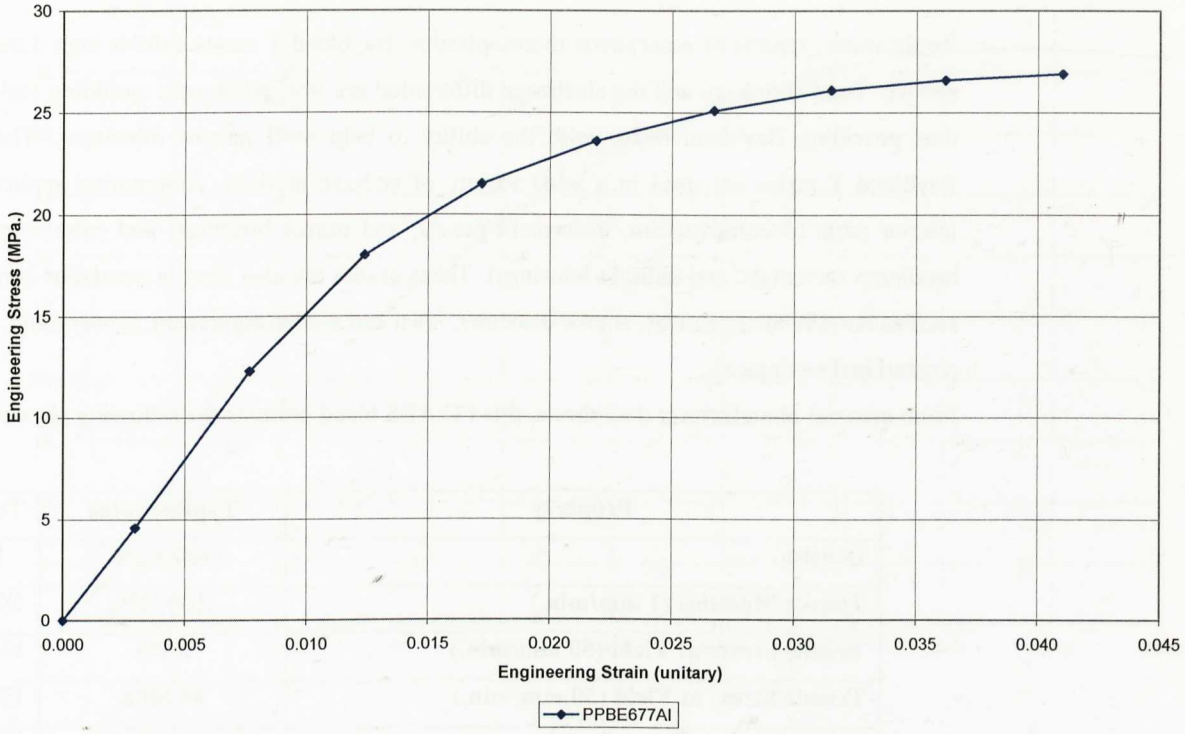

Figure 6.3: Engineering stress-strain curve provided in the CAMPUS software for the selected PP.

For our purpose, the main disadvantage of this curve is that the stress-strain values are given only up to low strain values. Approximately above the yield point (26 MPa.) no material data points are given, probably due to the initialisation of the plastic region and the necking phenomena. From this point, it is difficult to obtain adequate stress-strain data which is one of the objectives of the present thesis work.

Anyway, this curve will be used as reference for comparison purposes with experimentally obtained stress-strain curves.

6.1.2. Polycarbonate+Acrylonitrile Butadiene-Styrene (PC+ABS).

PC/ABS Bayblend T45 from the material manufacturer Bayer Material Science.

It is a general purpose, unreinforced, injection moulding grade PC/ABS blend.

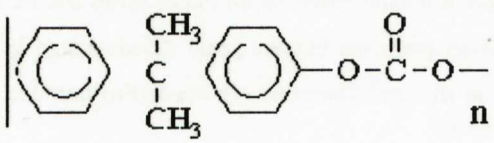

Figure 6.4: Polycarbonate's molecular structure.

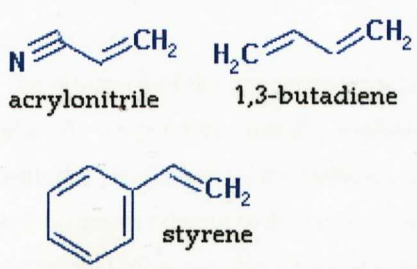

Figure 6.5: Molecular structure of Acrylonitrile-Butadiene-Styrene.

Applications: typical of amorphous thermoplastics, Bayblend T resins exhibit high dimensional stability in service. Total shrinkage and the shrinkage differential are low, while post moulding shrinkage is negligible, thus providing Bayblend resins with the ability to help meet narrow tolerances. These general-purpose Bayblend T resins are used in a wide variety of end-use markets. Automotive applications include both interior parts (decorative trim, instrument panels, and mirror housings) and exterior parts (wheel covers, headlamp surrounds, and taillight housings). These grades are also used in numerous consumer applications, such as household appliances, smoke detectors, lawn and garden equipment, power tools, sporting goods, and recreational equipment.

From material manufacturer data sheets, this PC/ABS blend presents the following physical characteristics:

Property	Typical value	Test Method
Density	1100 Kg/m^3	ISO 1183
Tensile Modulus (1 mm/min.)	2100 MPa.	ISO 527-1/-2
Tensile Strain at Yield (50 mm/min.)	3.7%	ISO 527-1/-2
Tensile Stress at Yield (50 mm/min.)	49 MPa.	ISO 527-1/-2
Stress at break (50 mm/min.)	40 MPa.	ISO 527-1/-2
Strain at break (50 mm/min.)	> 50%	ISO 527-1/-2
Izod impact strength (KJ/m^2)	non break (at 23°C)	ISO 180-U
Izod impact strength (KJ/m^2)	non break (at -30°C)	ISO 180-U
Izod notched impact strength (KJ/m^2)	40 (at 23°C)	ISO 180-U
Izod notched impact strength (KJ/m^2)	36 (at -30°C)	ISO 180-U
Temperature of deflection under load (1.80 MPa.)	95°C	ISO 75-1,-2
Temperature of deflection under load (0.45 MPa.)	112°C	ISO 75-1,-2
Vicat softening temperature (50 N;50 °C/h)	110°C	ISO 306
Vicat softening temperature (50 N;120 °C/h)	112°C	ISO 306

Table 6.2: Mechanical properties of the selected PC/ABS T45 from Bayer.

In the next graphs, additional material properties are plotted corresponding to the selected PC/ABS blend. Bayer Material Science offers for example a tensile stress-strain curve up to 5% of strain (tested at 23°C). This curve could be suitable for simulation purposes but the main disadvantage is that this material can withstand strains greater than a 50% up to rupture. Therefore we needed to produce our own experimental testing to cover the plasticity range.

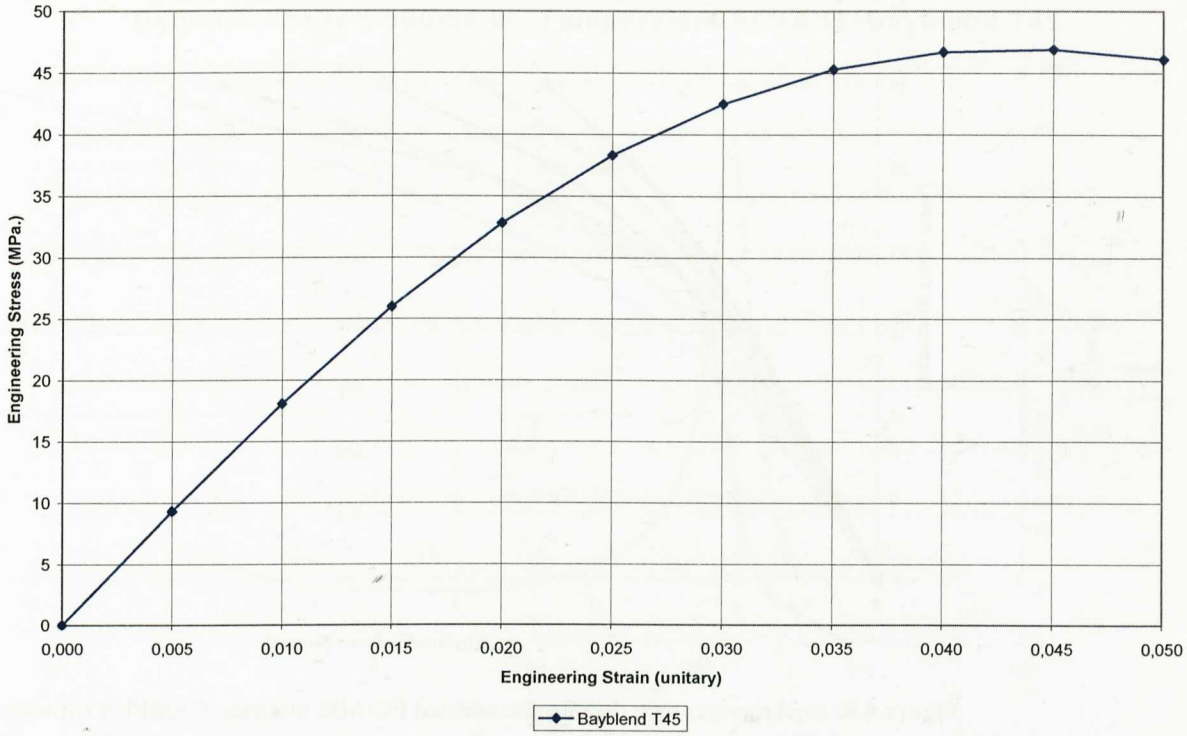

Figure 6.6: Engineering stress-strain curve provided in the CAMPUS software for the selected PC/ABS.

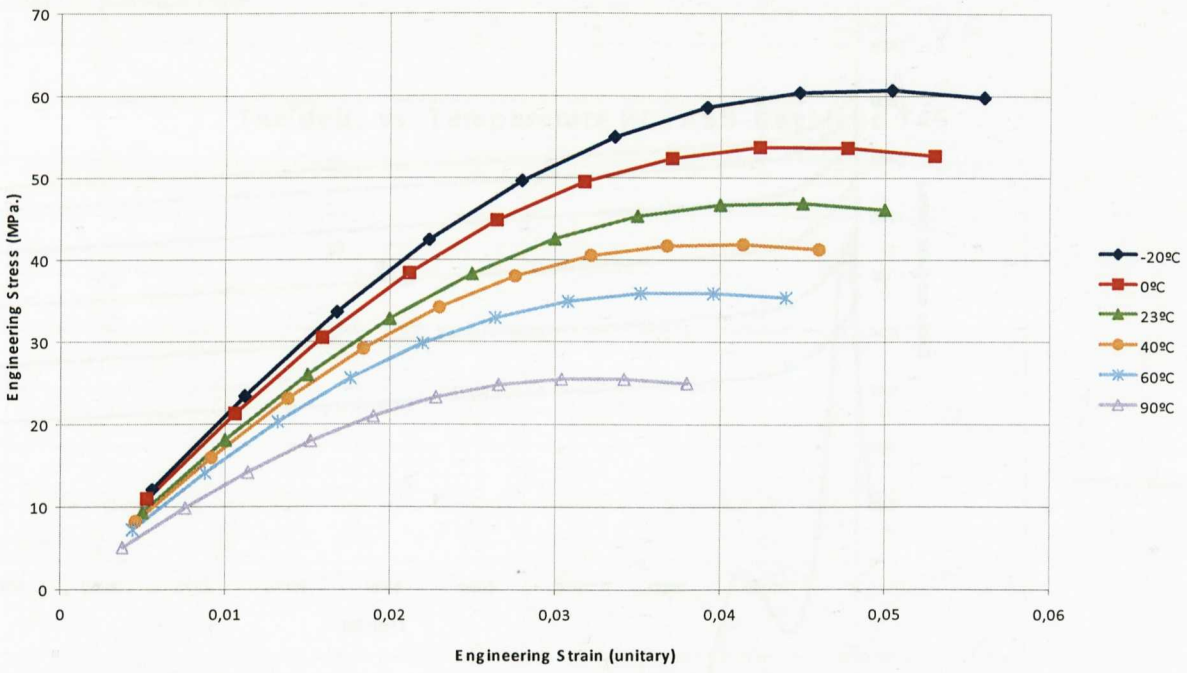

Figure 6.7: Effect of changing the temperature on the stress-strain behaviour, provided in the CAMPUS software for the selected PC/ABS.

The influence of the temperature on the stress-strain properties of the material can be seen in the preceding plot. As temperature rises the stiffness of the thermoplastic material is redweed. The same effect happens with the yield stress of the material, as temperature is increased, the yield point decreases. No conclusions can be drawn relating to the failure strain since the data points where not considered up to rupture.

Additional plots are also offered by the material manufacturer. For informative purposes some creep data is presented here.

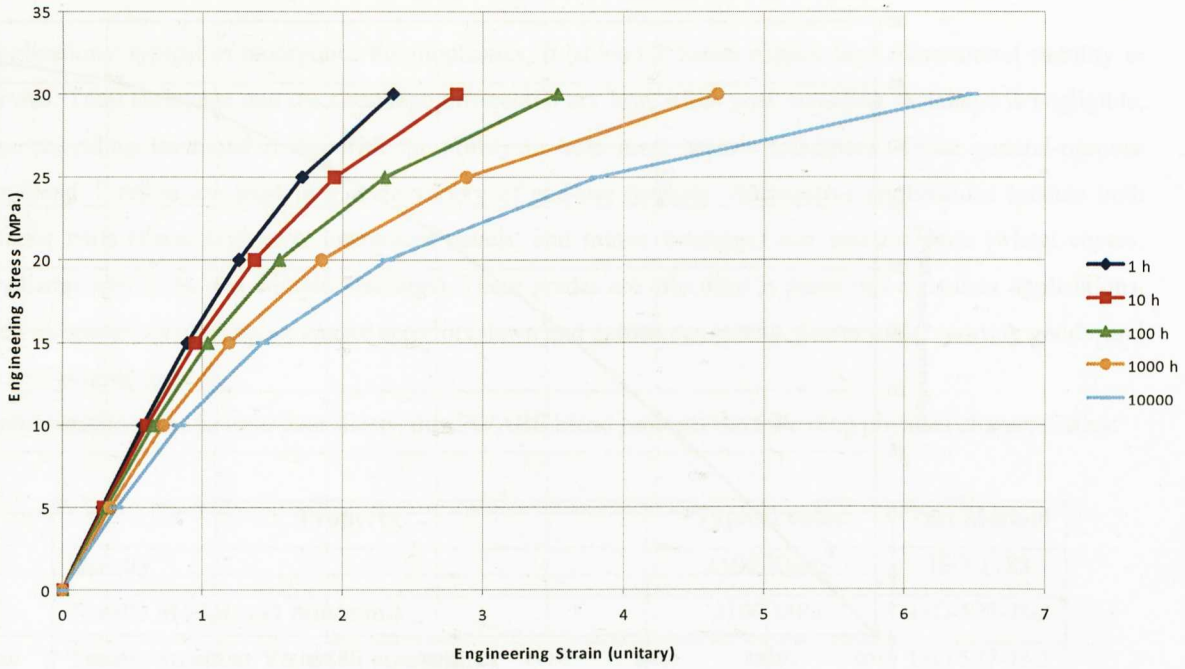

Figure 6.8: Isochronous creep data for the selected PC/ABS material. CAMPUS software data.

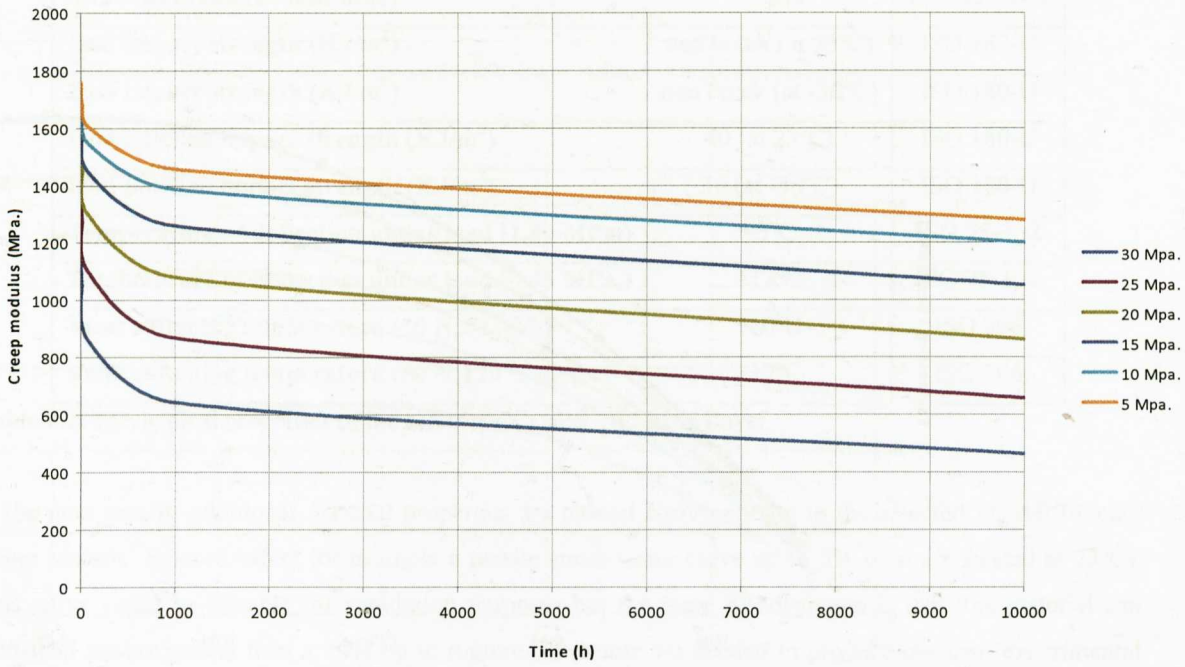

Figure 6.9: Creep modulus data for the selected PC/ABS material. CAMPUS software data.

Creep data is not relevant to our simulation purposes, since the loading conditions used correspond to instantaneous static conditions or high speed testing events.

Viscoelastic properties are also given by the material manufacturer according to the standard ISO 6721-1,-2. These properties are not considered as material input for the simulations in this thesis work.

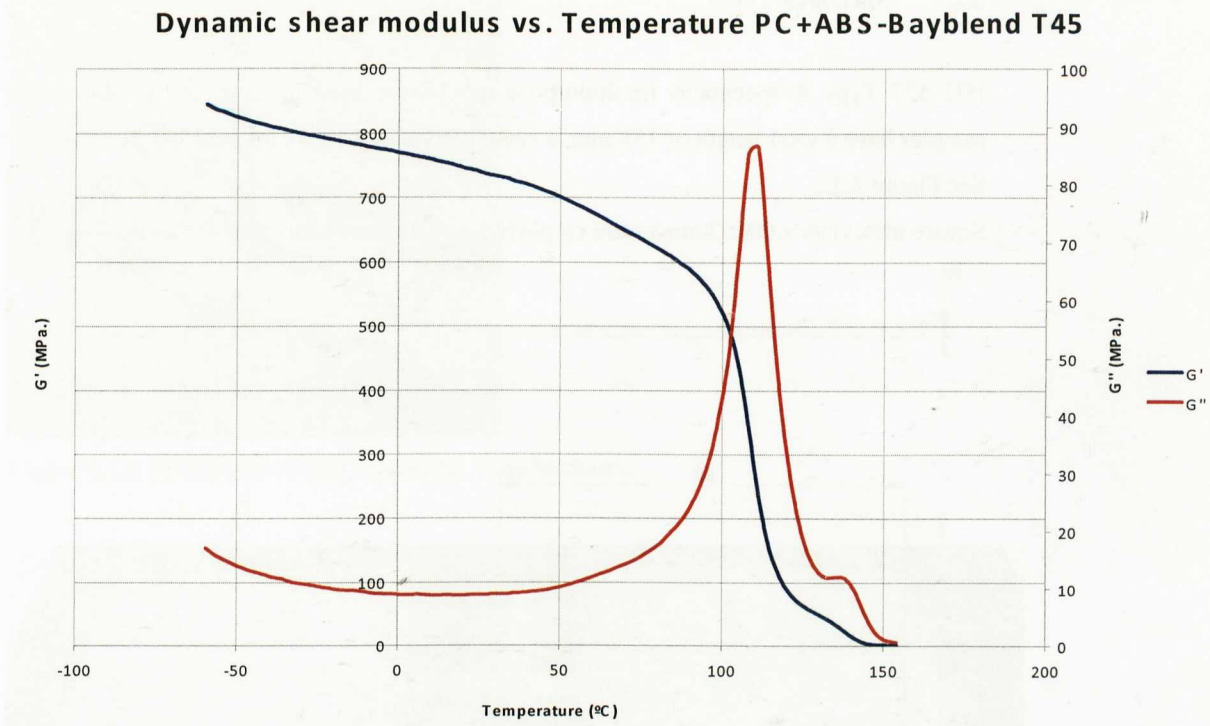

Figure 6.10: Viscoelastic properties of PC/ABS. Evolution of the storage modulus G' and Loss modulus G''. CAMPUS software data.

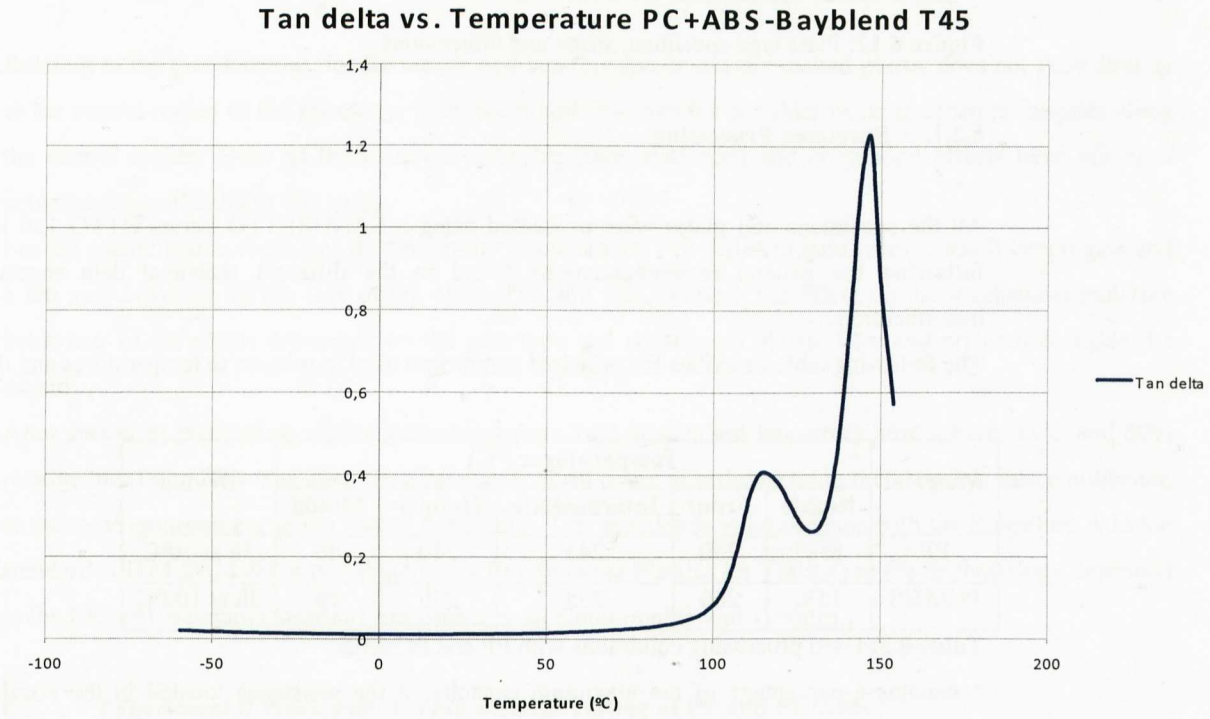

Figure 6.11: Viscoelastic properties of PC/ABS. Evolution of Tan delta. CAMPUS software data.

These dynamic properties are indicating a glass transition region between 100-150ºC for the selected PC/ABS blend. The first peak in the tan delta graph at around 115ºC corresponds to the ABS phase while the second peak at around 145ºC corresponds to the Tg of PC.

6.2. Specimen Types.

ISO 527 Type A specimens (multipurpose type) were used in slow rate tensile and bending tests. The samples have a total length of 158 mm, a cross section of 10 x 4 mm^2 and a straight central length of 80 mm. See Figure 2.3.

Square plates (90 x 90 x 2 mm) were employed in quasi-static dart perforation tests.

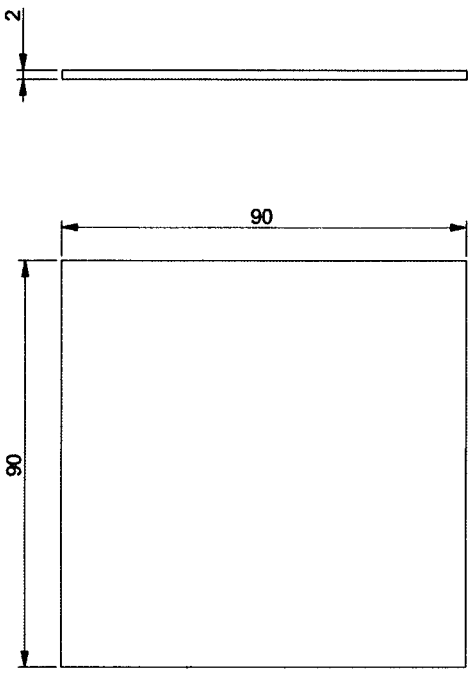

Figure 6.12: Plate type specimen, shape and dimensions.

6.2.1. Specimen Processing.

All the specimens and plates were processed using a SANDRETTO Series OTTO 150 injection machine following the general recommendations found in the different technical data sheets from materials manufacturers.

The following table describes the principal parameters used in relation to temperatures and drying conditions:

Material	Temperatures (°C)					Drying
	Nozzle	Front	Intermediate	Hopper	Mould	
PP	8%*	250	245	240	40	1h at 70°C
PC/ABS	15%	260	255	250	70	3h at 100°C

Table 6.3: Used processing conditions with PP and PC/ABS.

* denotes a percentage of the maximum capacity of the resistance located in the nozzle. The following pictures show the gate locations for the multipurpose and the plate type specimens:

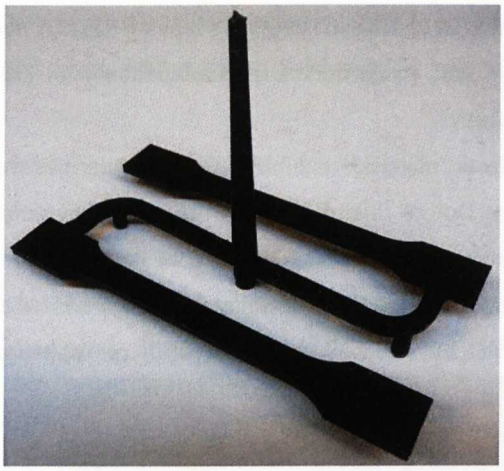

Figure 6.13: Multipurpose type specimens. Gate locations.

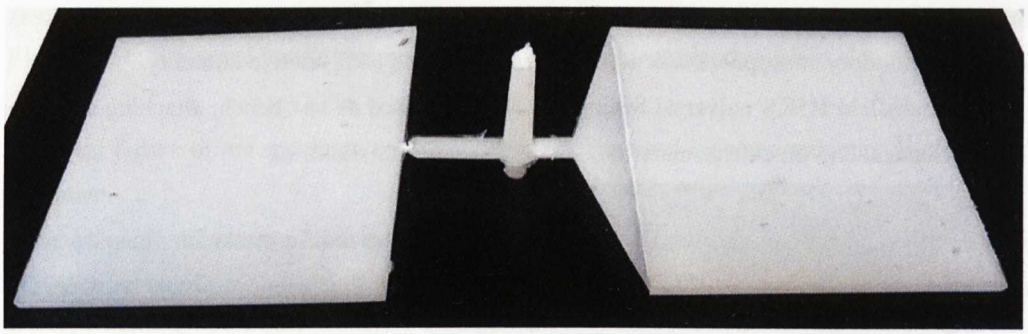

Figure 6.14: Square plate specimens. Two type of gates were used: lateral and fan.

Relating to the gate location, for the tensile and bending specimens the melted plastic does not flow directly to the central region of the geometry. First, the liquid flow hits the shoulder walls and then propagates along the central region. None of the materials used are fibre reinforced and orientation effects have not been considered specifically in this study.

For the square plates, there was the possibility of evaluating two different gate types: a small lateral gate and a fan gate covering all the side of the plate. The aim was to check the effect on the mechanical puncture behaviour of the plates depending on the gate type and consequent plastic flow and orientation inside the mould.

After specimen processing, all the geometries were kept at standard laboratory atmosphere: 23°C and 50% relative humidity. This was done for a minimum of 40 hours in order to bring the materials into equilibrium at the same environment as the testing conditions. This practice is in accordance with the Procedure A in the standard ASTM D618 (Standard Practice for Conditioning Plastics for Testing) as the methodology described in the ISO 291 standard (Standard Atmospheres for Conditioning and Testing).

6.3. Experimental Work Part 1: Quasi-Static Testing of PP and PC/ABS.

This section describes the slow rate testing carried out both in the semi-crystalline polypropylene (PP) and the amorphous Polycarbonate+Acrylonitrile-Butadiene-Styrene (PC/ABS).

The first testing method used, is the common uniaxial tensile test, which is known to be a simple way of evaluating material mechanical properties. In this thesis it was used as a general method to generate stress-strain data for FEA codes.

The different elasto-plastic models implemented in codes such as ANSYS or LS-DYNA need this data in the form of true strain (total or plastic strain) vs. true stress curves in combination with elastic data (tensile modulus of elasticity and elastic Poisson's ratio).

As described in previous sections, thermoplastic materials exhibit some particularities that complicate the measurement of true stress and strain values. Due to this, different procedures were employed in order to generate the most adequate data for finite element calculations.

As the constitutive model used in simulations is needed to be correlated with experimental tests in order to evaluate its validity, additional tests were carried out in 3-point bend and puncture or plate perforation.

6.3.1. Tensile Testing of Polypropylene.

In the present work tensile data was generated according to the standard "ISO 527. Plastics - Determination of tensile properties." [27].

The laboratory atmosphere was adjusted to be 23ºC and 50% relative humidity.

A Hounsfield H5KS universal testing machine was used as test bench, attaching a load cell of 5KN. and a mechanical clip-on extensometer model 100R from Hounsfield.

Figure 6.15: Testing machine, clamps and extensometer for tensile testing of specimens.

The use of a clip-on extensometer has a principal drawback when used with plastic materials: once the deformation becomes non homogeneous in the measuring gage length, which is related to the necking formation, the measured strain values are not local values but some average or global values of the strains generating along the gage section.

Due to this, initially, strain values obtained by the extensometer were evaluated and after that, corrections and different procedures were proposed in order to take into account the non homogeneous and local strains above the yield point.

6.3.1.1. Testing conditions.

A minimum number of five specimens were tested at each condition. According to the ISO 527 standard, different testing velocities could be used (1, 2, 5, 10, 20, 50, 100, 200 and 500 mm/min.). In this case, three

testing speeds were selected in order to evaluate the effect of the testing rate on the mechanical behaviour of the selected PP material: 5, 50 and 500 mm/min.

6.3.1.2. Results.

The selected polypropylene clearly showed a crazing or stress-whitening behaviour (Figure 6.16) when tensile tested. This denoted the presence of some impact modification with rubber addition. The crazes were developed perpendicularly to the direction of the tensile stress.

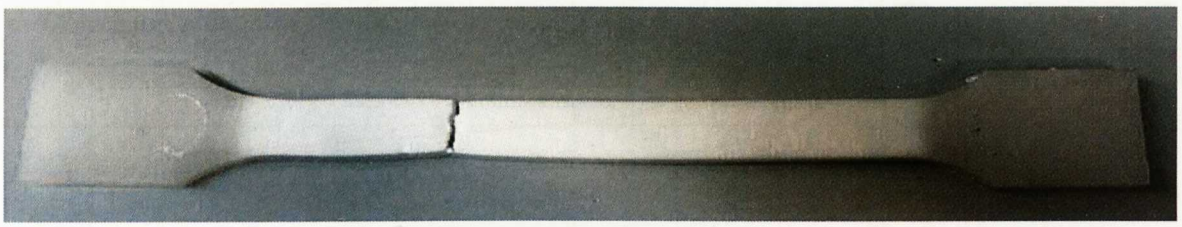

Figure 6.16: Fractured tensile specimen. A whitened area was clearly visible along the gage section.

The final failure of the specimen was previously accompanied by some reduction in the cross section of the specimen.

Note: although the elasto-plastic models that were selected did not take into account the crazing phenomena; the intention was to evaluate their validity from the simulation viewpoint to correlate force-displacement data and then perform additional validation simulations rather than from micro-structure aspects.

Tensile force-displacement data was collected at the three testing velocities of 5, 50 and 500 mm/min.

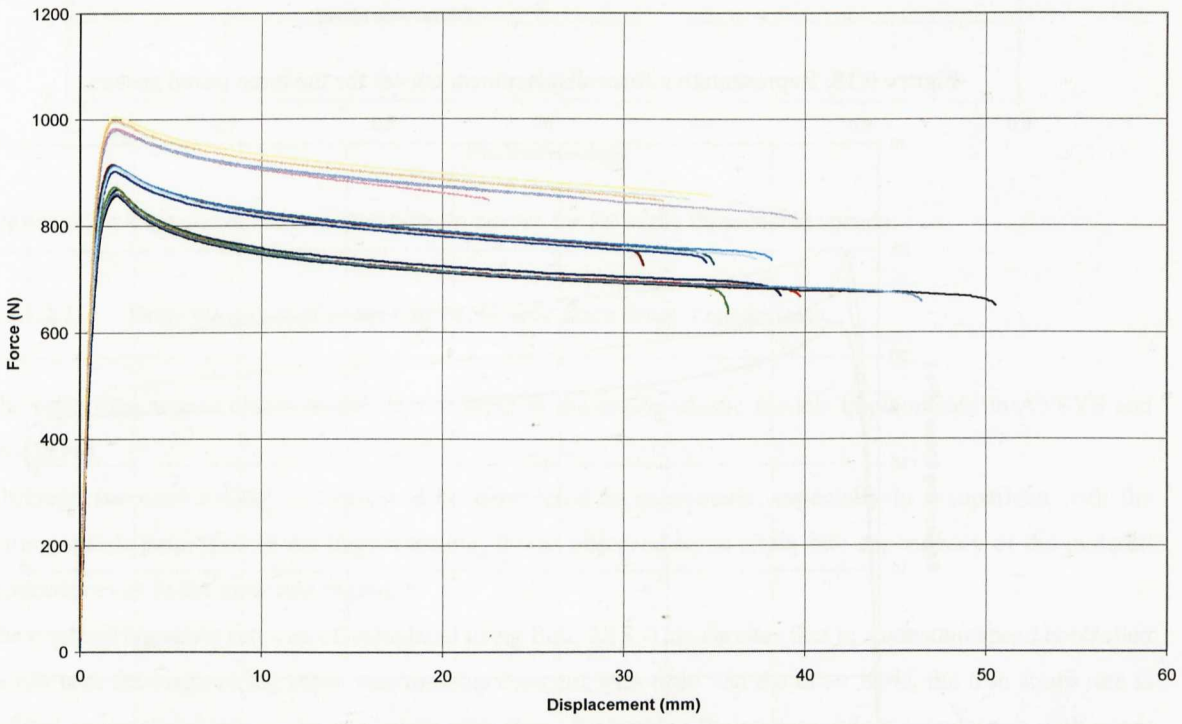

Figure 6.17: Force-displacement curves for PP at testing speeds of 5, 50 and 500 mm/min.

In general, the tests at each speed offered a good repeatability even though failure displacement values showed a higher dispersion.

The higher the testing speed, the higher the maximum force recorded, thus indicating a positive dependence of yield values with increasing testing rate. On the other hand, as testing rate increased, the material's tendency was to break at lower displacement values but this is always more difficult to determine due to the usual dispersion in failure values.

From the curves in Figure 6.17, one was selected for each testing speed. The selected curves were then used for the calculation of engineering and true stress-strain curves.

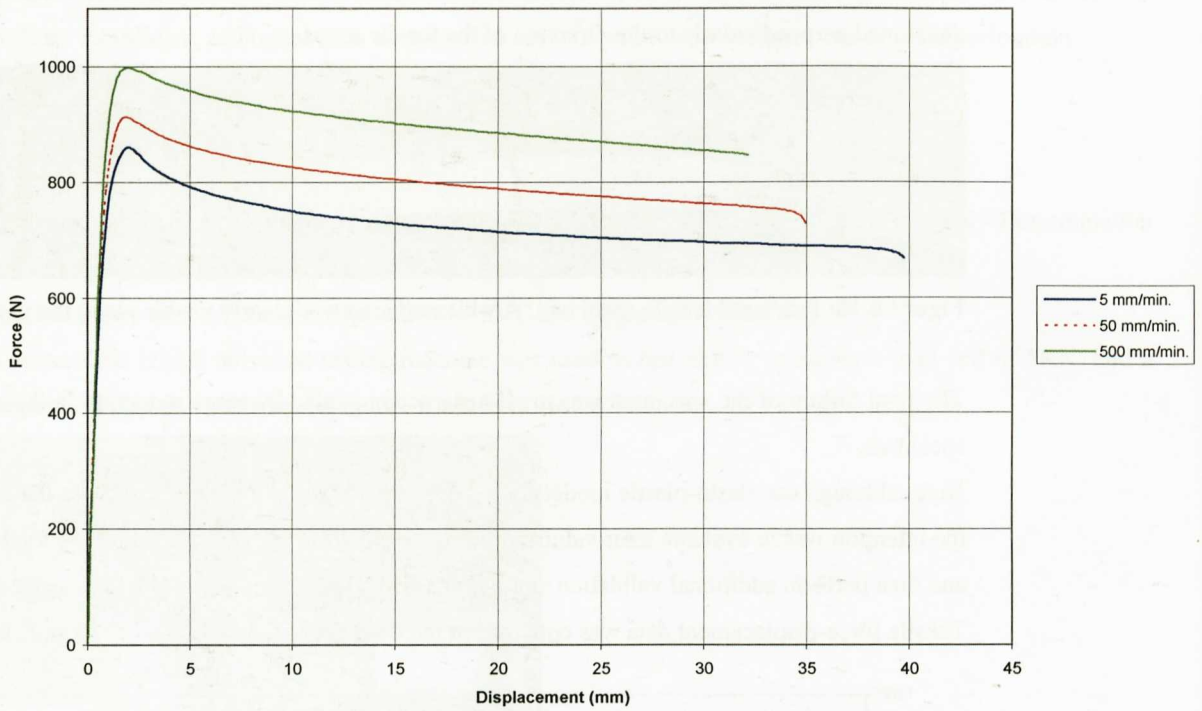

Figure 6.18: Representative force-displacement curves for the three tested speeds.

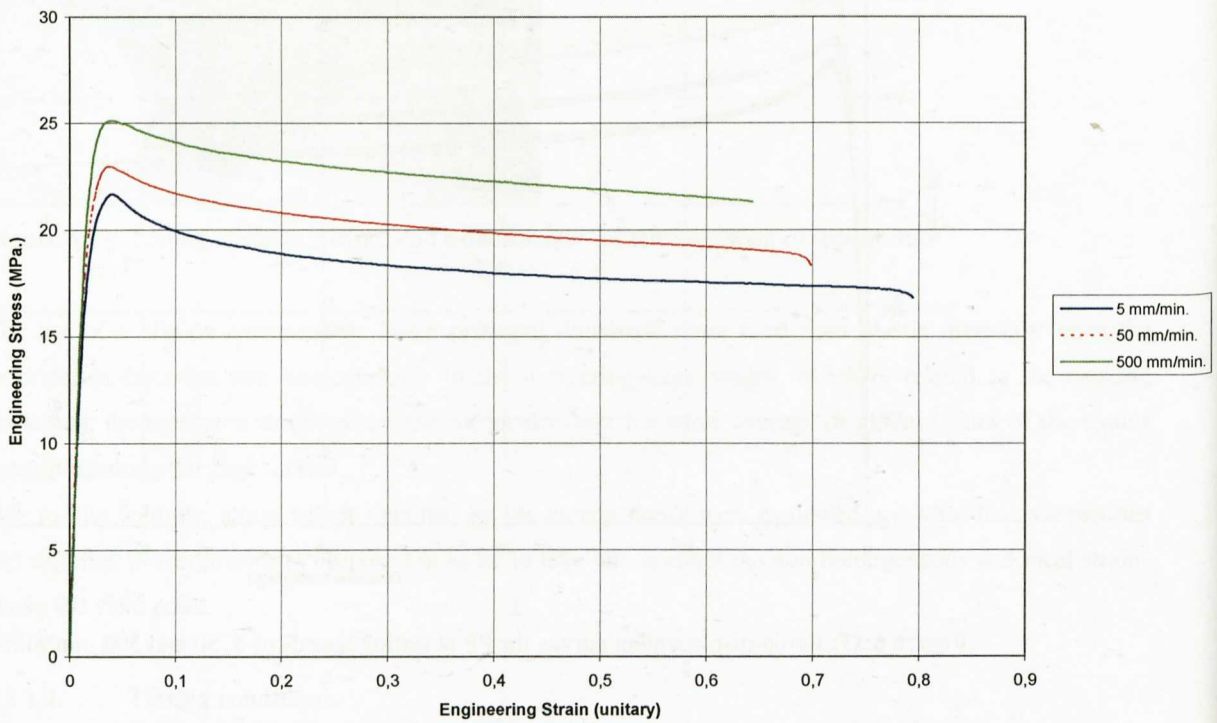

Figure 6.19: Representative engineering stress-strain curves for the three tested speeds.

The calculation of engineering (also known as nominal or technical) stress and strain was performed using equations 2.6 and 2.7.

As in the case of force-displacement curves, engineering stress-strain curves offered continuously reducing stress from maximum values in yield to rupture. This indicated the presence of softening mechanisms after yielding but also some plateau-like shape after the first initial decrease.

The calculation of true values of strain and stress data was performed using equations 2.10 and 2.11.

The calculated true stress-strain curves showed some softening, especially at the testing speed of 5 mm/min. A strain hardening behaviour was observed after this initial reduction in stress values which could be related to the neck formation and evolution.

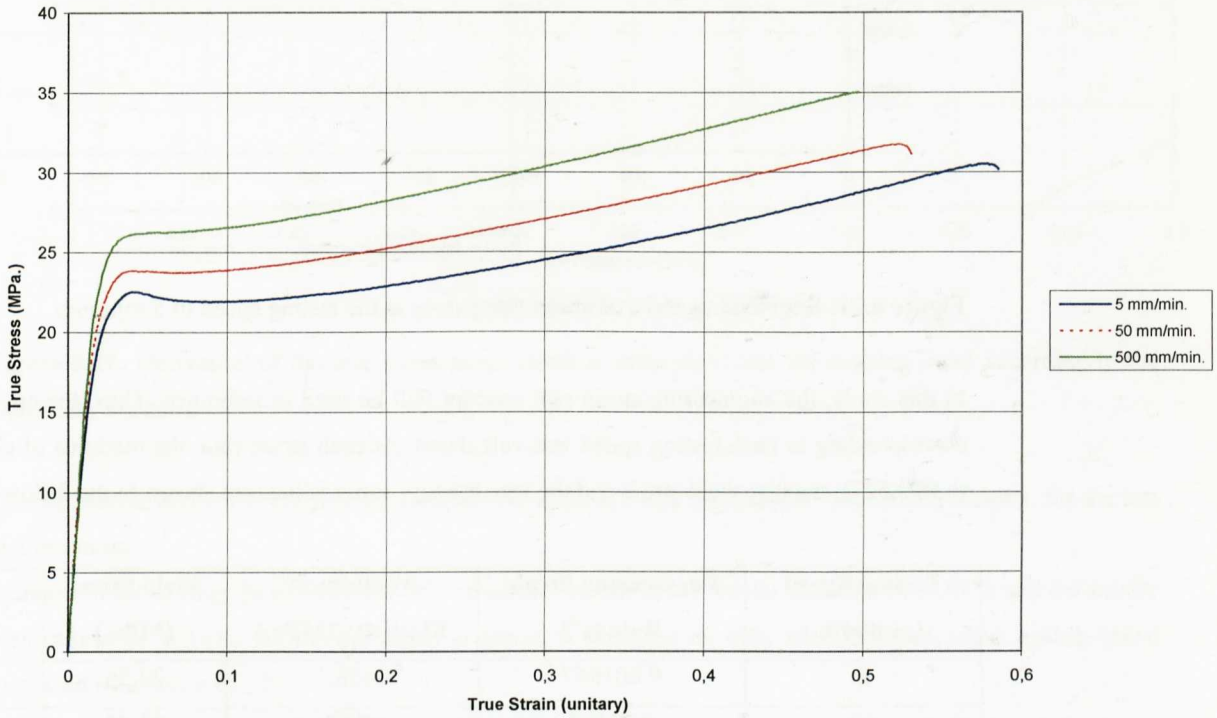

Figure 6.20: Representative true stress-strain curves for PP at the three tested speeds.

6.3.1.2.1. Determination of some Characteristic Data from Tensile tests.

The main idea was to obtain useful data to input in the elastic-plastic models implemented in ANSYS and LS-DYNA.

Although the used testing speeds could be considered as quasi-static, especially in comparison with the testing speeds employed in the impact testing, it was observed some strain rate dependency of the material properties even in the slow rate regime.

The engineering strain rate can be calculated using Equ. 2.13. This denotes that in a constant speed controlled tensile test, the engineering strain rate remains constant with time. On the other hand, the true strain rate is defined as the derivative of the true strain with time. Performing the correspondent calculations with every true strain point from the calculated curve, it can be observed that in a constant speed test, the true strain rate decreases exponentially as the specimen is stretched. This demonstrates than in a real tensile experiment, if it is required to achieve a constant true strain rate, the test speed should be changed gradually. One option could be to increase the stretching speed exponentially.

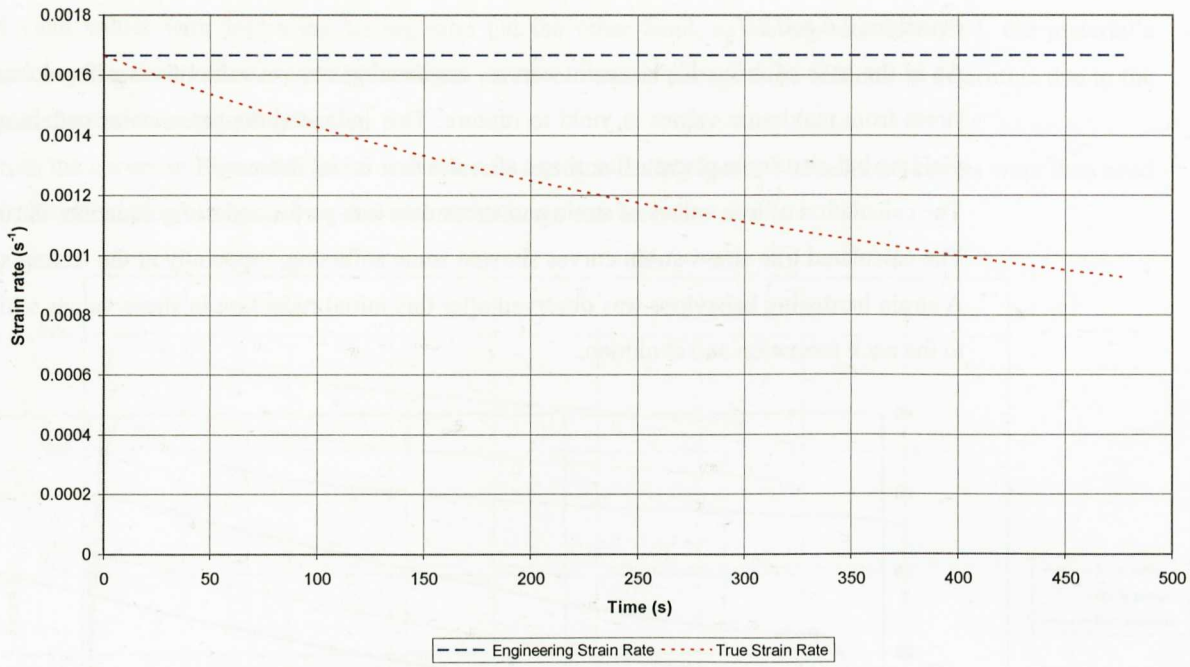

Figure 6.21: Engineering and true strain rate curves at the testing speed of 5 mm/min.

In this study, the engineering strain rate concept will be used as reference. Thus, the engineering strain rate corresponding to each testing speed was calculated. At each strain rate, the modulus of elasticity (according to ISO 527), the true yield stress and the true fracture strain values are shown in the following table.

Testing Speed (mm/min.)	Engineering Strain Rate (s^{-1})	Modulus of Elasticity (MPa.)	Yield Stress (MPa.)	True Strain at Break (unitary)
5	0.001667	1458.1	22.56	0.58
50	0.01667	1688.6	23.88	0.53
500	0.1667	1826.7	26.16	0.49

Table 6.4: Evolution of modulus, yield stress and strain at break with strain rate.

Yield stress was considered as the maximum point after the proportional limit of the initial stage of the stress-strain curve plot.

This is in accordance with the Considére's construction (section 2.2.1.4): taking the derivative of the true stress-strain curve, the point at which the curve is cut by the derivative curve can be considered the yield point.

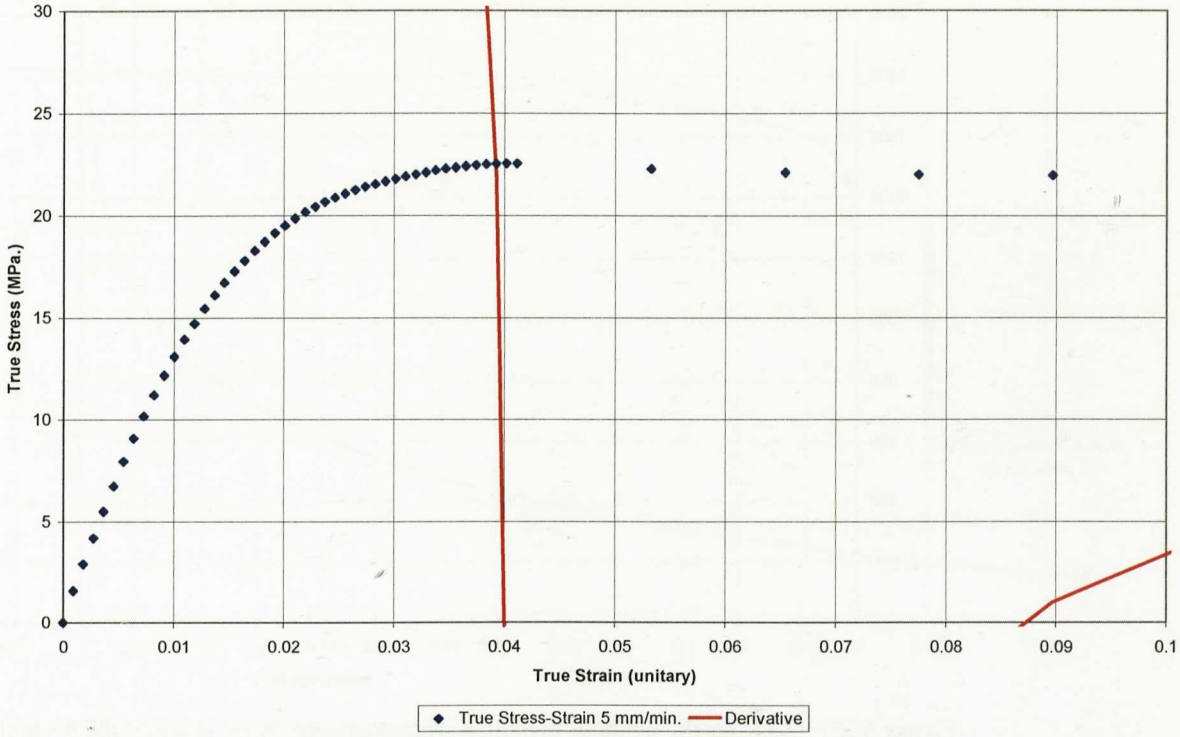

Figure 6.22: Derivation of the true stress-strain curve in order to obtain the necking point according to the Considére's criterion.

This derivation and cut of the true stress-strain curve gave a true yield stress value of 22.56 MPa. for the test at 5 mm/min.

Increase in the testing speed from 5 to 500 mm/min. increased the tensile modulus by a 20 % and the tensile yield stress by a 14%. As far the strain at break, a decrease of 18% was observed when testing speed increased by a factor of 100.

This shows the importance of strain rate and its effect in tensile properties even at low strain rate regime.

The graphical evolution of each property can now be observed. It is necessary to take into account that the evolution is corresponding to three testing speeds. This number was sufficient since the goal was to check tendencies when changing the rate of testing in the quasi-static regime.

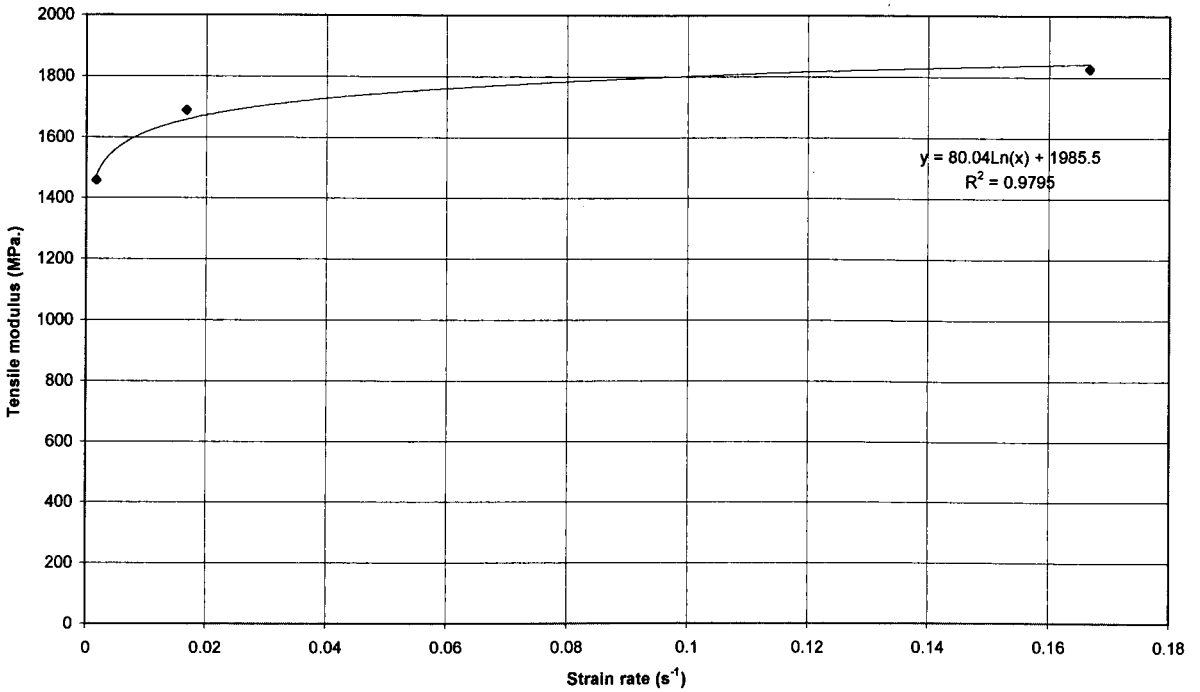

Figure 6.23: Elastic tensile modulus evolution with strain rate.

The elastic modulus and yield stress for PP offered a natural logarithmic tendency with strain rate, although more test data should be recomendable for a more representative and accurate data fit.

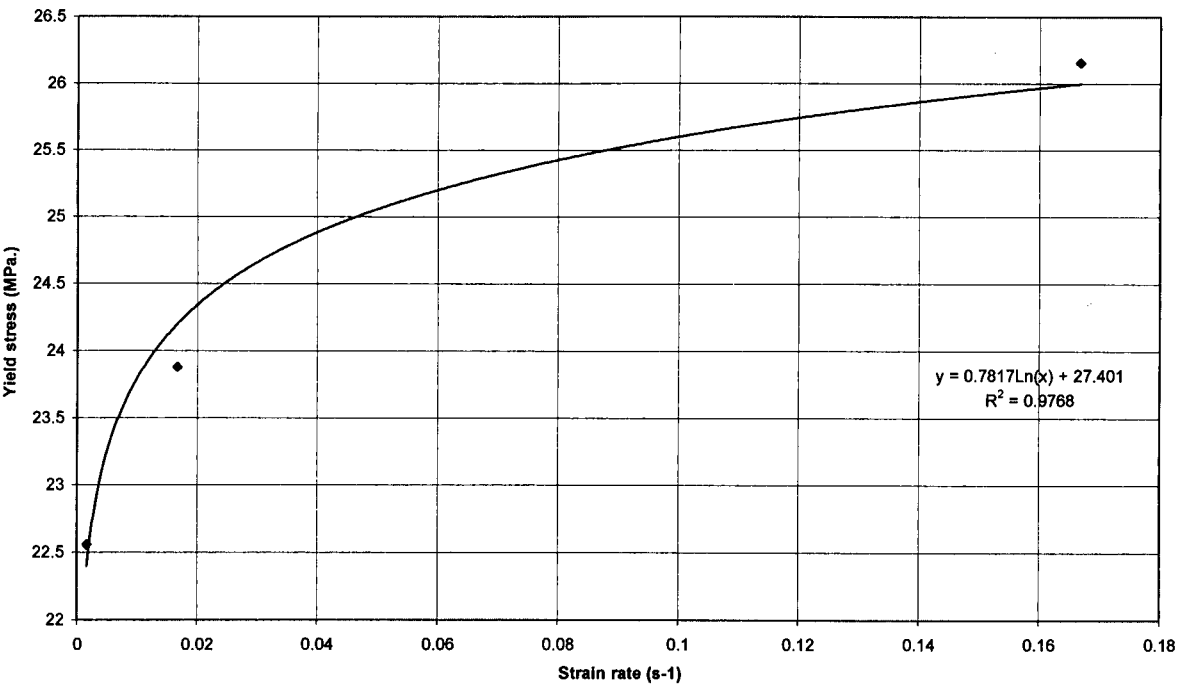

Figure 6.24: Yield stress evolution with strain rate.

Again, the evolution of the strain at break values with changing strain rates offered a logarithmic tendency.

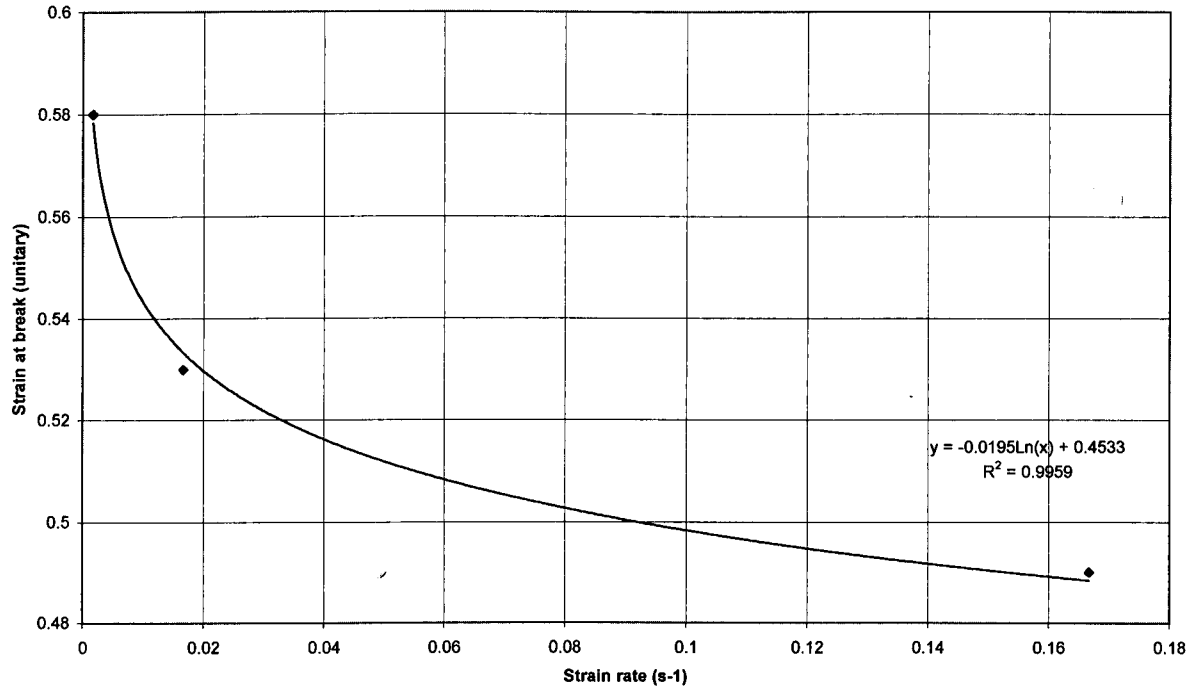

Figure 6.25: Strain at break versus strain rate.

In relation to the modelling of the yield stress rate sensitivity with the Eyring's model, discussed in Equ. 2.39, a linear fit to the yield stress data with the logarithm of the strain rate, gave a similar degree of correlation as the previous fits with natural logarithms. It seems to be possible to establish a logarithmic relation between the yield stress and the strain rate. Interpolations between the tested strain rates could be achieved with little loss of precision, but extrapolation to higher strain rates should be performed carefully. First, additional data should be tested in the slow rate regime and secondly, the use of some data from higher testing speeds for contrast should be preferable.

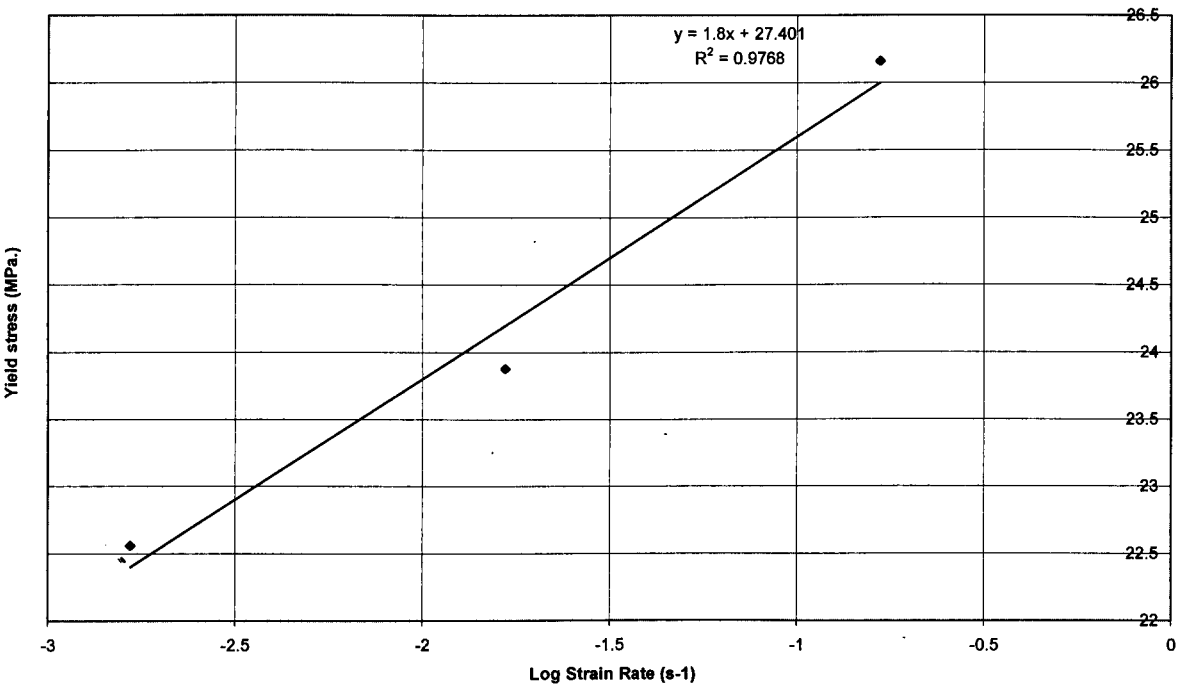

Figure 6.26: Yield stress versus strain rate according to the Eyring's equation.

With elasto-plastic models it is always difficult to define accurately the yield stress and elastic modulus. By definition, yield stress is the maximum stress in the curve after the linear region, but this region is not actually linear in thermoplastics due to viscoelastic effects. On the other hand, elasto-plastic models require a tensile modulus which defines the linear portion and then, a yield stress which delimitates the plastic onset.

In the present work the definition of the elastic region has been done up to the proportionality limit using the value of a tensile modulus calculated according to the ISO 527 standard. The first data point defines the yield stress followed by the plastic curve. This gives a yield point which is lower than one obtains for real materials but offers a way of overcoming the problem associated with elasto-plastic definitions [28].

A tensile modulus of 1454.7 MPa. gave an accurate fit for the linear region of the PP curve at 5 mm/min. This gave a proportional-limit yield stress value of 9.183 MPa. It is assumed that after this point, plastic strain will be generated in the material.

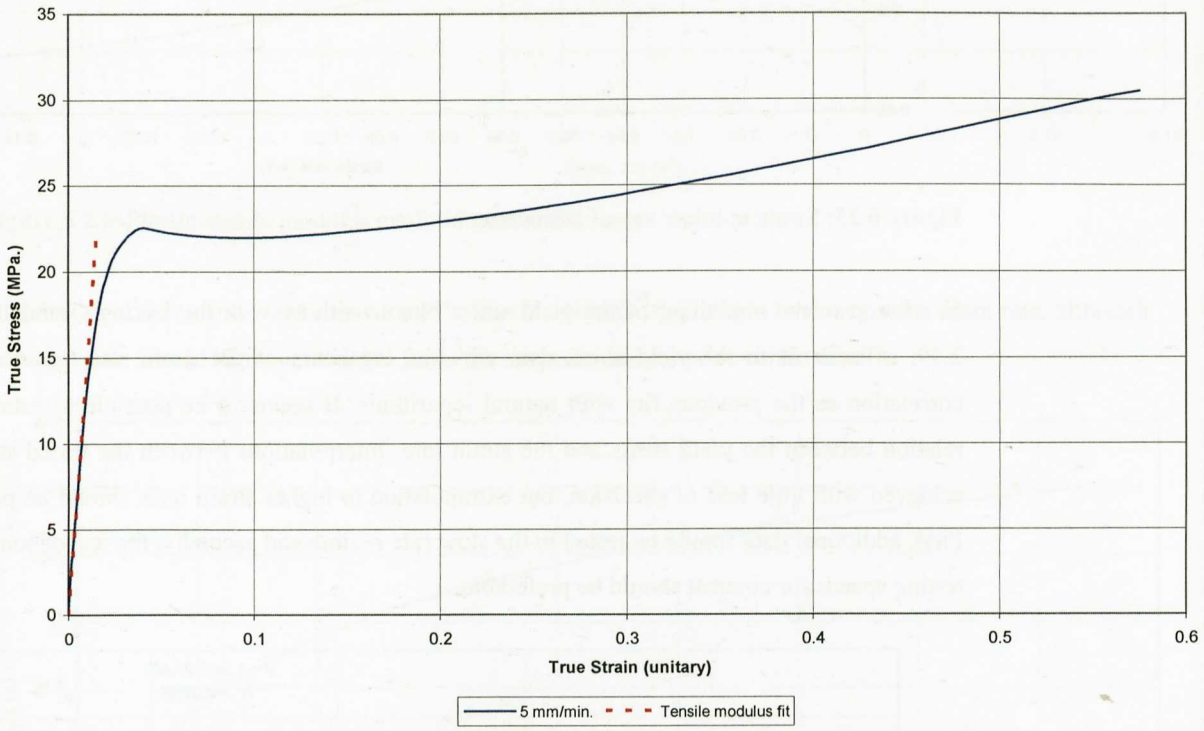

Figure 6.27: Tensile modulus fit to the true stress-strain curve for PP at 5 mm/min.

Similarly, taking into consideration the elastic modulus of each curve, the proportional-limit yield stress values were generated for the testing velocities of 50 and 500 mm/min.

Testing speed (mm/min.)	Engineering Strain Rate (s^{-1})	Modulus of elasticity (MPa.)	Proportional Yield Stress (MPa.)
5	0.001667	1458.1	9.183
50	0.01667	1688.6	10.99
500	0.1667	1826.7	12.217

Table 6.5: Proportional-limit yield stress values obtained from cutting the curve with the slope of the tensile modulus.

In this case, an increase of a 100% in the testing speed resulted in 23% increase in the yield stress at the proportional limit point.

It was noted that the proportional limit yield stress followed once again a logarithmic tendency with strain rate.

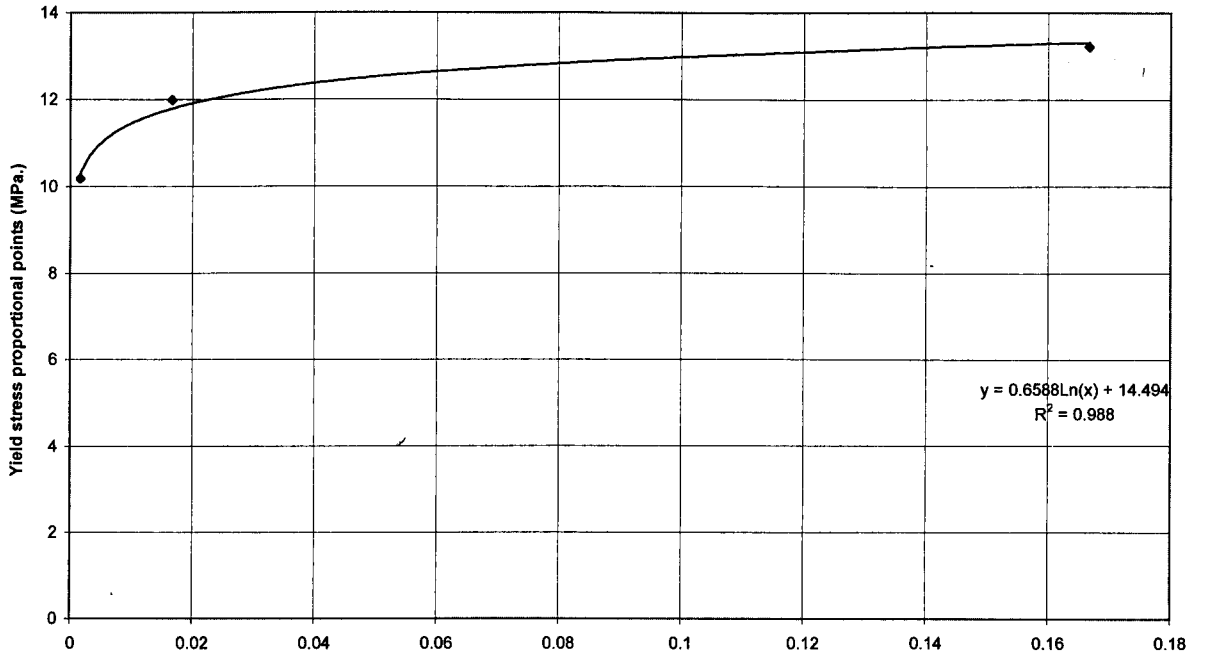

Figure 6.28: Yield stress (proportional point) evolution with strain rate.

The use of proportional limit values for the determination of the yield stress, gave a slight improvement to the fits with natural logarithmic values at different strain rates.

The Eyring's model also offered an improvement to the fit to the yield stress data values:

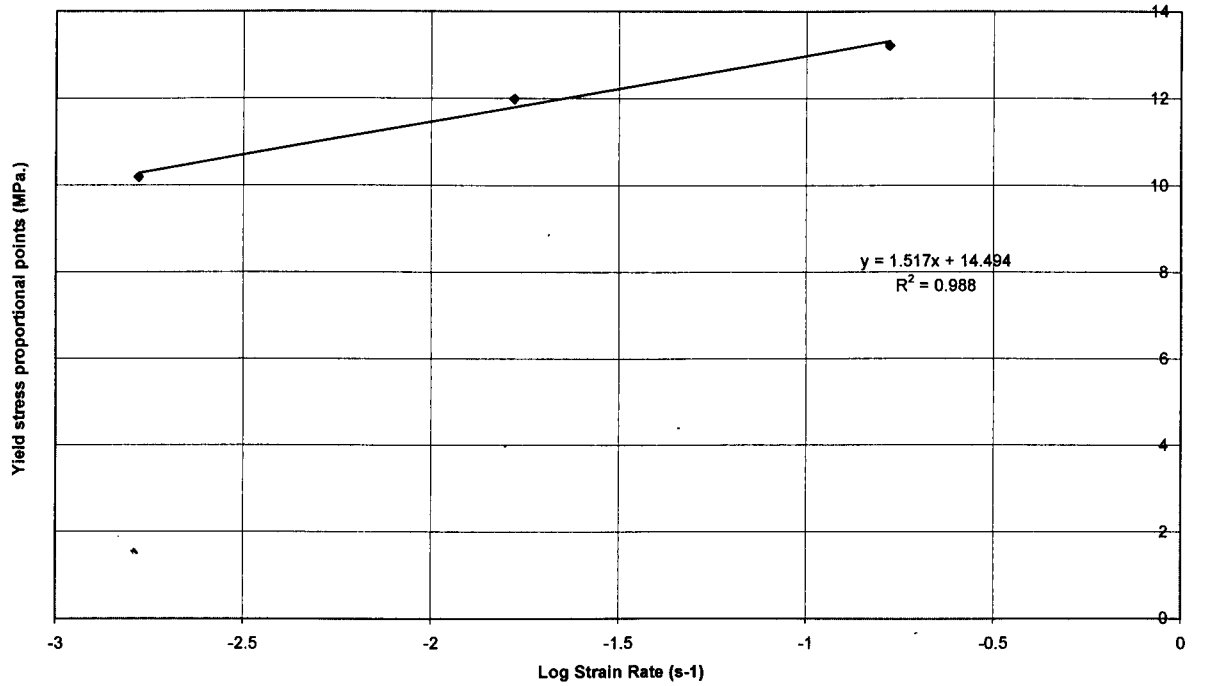

Figure 6.29: Yield stress (proportional point) evolution with strain rate. Eyring's model fit.

6.3.1.2.2. Data preparation for ANSYS.

As described in previous sections, this should be the necessary data to implement the tensile data in the elasto-plastic constitutive model of ANSYS (taking as reference the curve at 5 mm/min.):

- Elastic modulus: 1458.1 MPa.
- Elastic Poisson's ratio: 0.38. This data comes from the material manufacturers' data sheets.

Here, it was assumed the use of a multilinear isotropic hardening behaviour, so,

- A set of true stress vs. true strain points up to failure were needed.

This description offered a yield stress value of 9.183 MPa. and the post yield true behaviour was directly calculated from engineering data without any consideration being given to non-homogeneities due to necking. The result is shown in Figure 6.30 for the test speed of 5 mm/min.

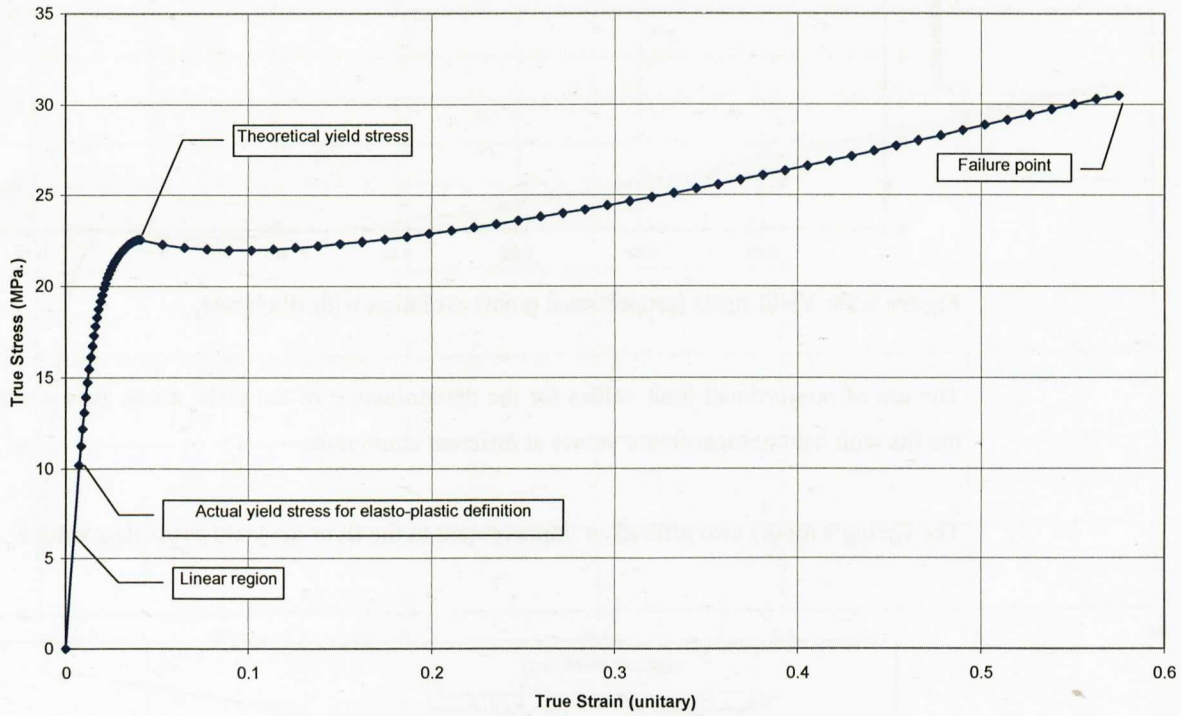

Figure 6.30: Definition of the elasto-plastic curve for ANSYS.

The first choice for converting engineering data to true curves was to use the assumption of incompressibility in the plastic region. This is a reasonable assumption for metallic materials but not so for thermoplastic materials [26].

A more precise method is based on the use of the classical conversion method up to the maximum point on the curve; this point could be considered the start of the necking process. Above this point, some corrections are performed in order represent the growing of the neck at the specimen [28, 29].

6.3.1.2.3. Corrections for the plastic zone from the maximum point in stress.

From the maximum stress, the conversion from engineering data to "true" values is not straight forward. For most of plastic materials, "necking" begins at maximum load point for a strain value where the true stress equals the slope of the plasticity region curve. Beyond this point, the engineering data conversion should be

completed iteratively simulating the tensile test and correcting the plastic part of the curve until adequately representing the force-displacement curve obtained in the tensile test.

The engineering stress at the maximum point is:

$$\sigma_e = F_{\max} / A_0 \qquad \text{Equ. 6.1.}$$

and the true stress:

$$\sigma_t = F_{\max} / A_t \qquad \text{Equ. 6.2.}$$

substituting Fmax,

$$\sigma_t = \sigma_e A_0 / A_t \qquad \text{Equ. 6.3.}$$

or

$$\sigma_t = \sigma_e e^{\varepsilon} \qquad \text{Equ. 6.4.}$$

where ε is the true strain at the maximum load point.

Starting from the maximum load point, a series of corrections can be carried out depending on the shape of the experimental engineering stress-strain curves.

Correction 1: the case of a constant engineering stress. Supposing that the engineering stress-strain curve follows the form represented in Figure 6.31. Until the point of maximum load the classical conversion from engineering to "true" values is used, and from this point, the formula utilised for stress conversion is as follows:

$$\sigma_t = \sigma_e e^{(\varepsilon - \varepsilon_{\max})} \qquad \text{Equ. 6.5.}$$

Correction 2: in the case of a plateau zone, additional exponents can be used for correcting different zones within the engineering stress-strain curve. This correction could be applied to the case when a plateau region appears beyond the maximum load point. See Figure 6.32.

$$\sigma_t = \sigma_e e^{(\varepsilon - \varepsilon_{\max})^2} \qquad \text{Equ. 6.6.}$$

Correction 3: case of a more pronounced plateau zone. See Figure 6.32.

$$\sigma_t = \sigma_e e^{(\varepsilon - \varepsilon_{\max})^3} \qquad \text{Equ. 6.7.}$$

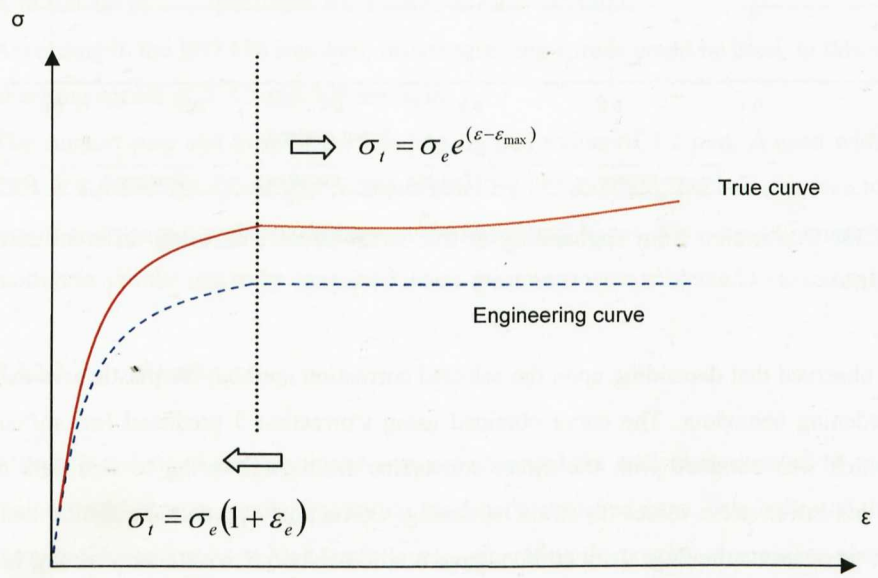

Figure 6.31: Idealised conversion from engineering data to true stress-strain values using correction 1.

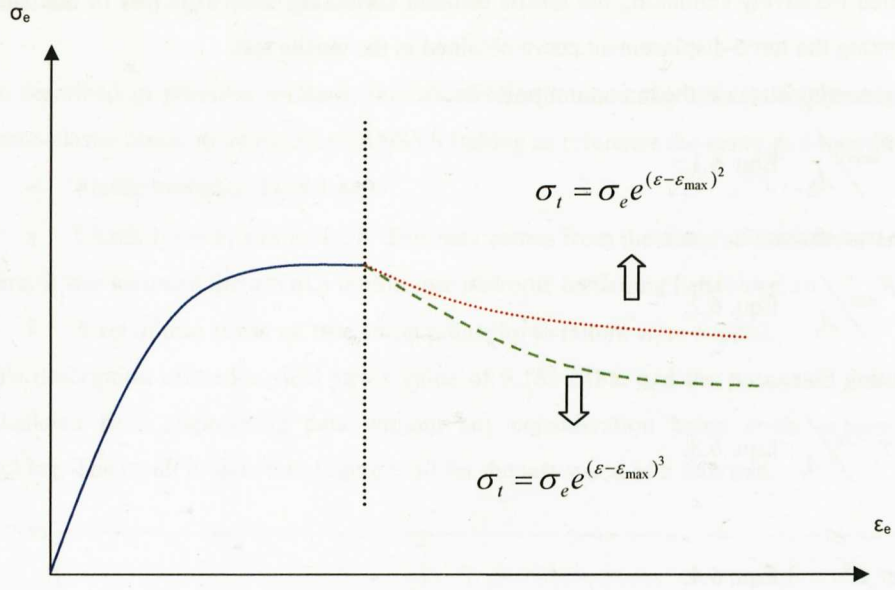

Figure 6.32: Engineering data conversion using corrections 2 and 3.

For the selected PP, the following true stress-strain curves were obtained using these conversion methods at the testing speed of 5 mm/min.

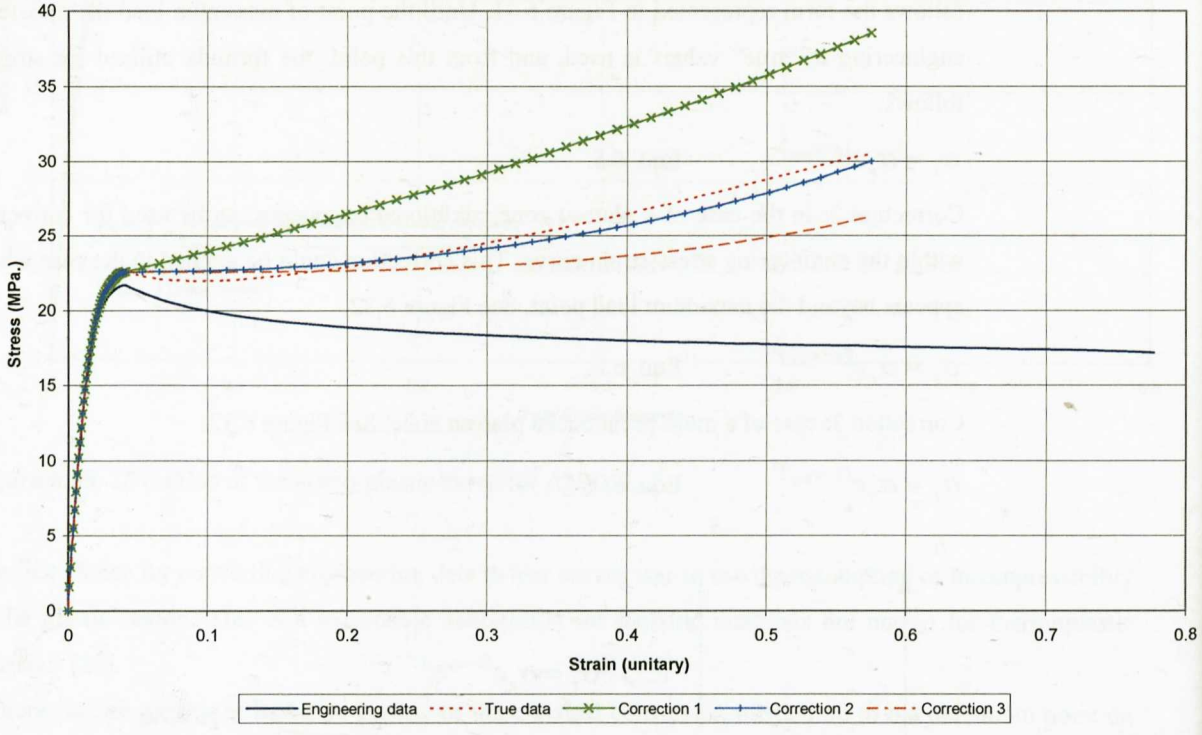

Figure 6.33: Conversion from engineering to true stress-strain data using different corrections above the yield point.

It can be observed that depending upon the selected correction method, the plastic area exhibits a higher or a lower hardening behaviour. The curve obtained using Correction 3 predicted less softening than the True curve (which was obtained with the direct conversion from engineering to true data using the classical formula) and lower stress values for strain hardening. Correction 2 predicted a similar behaviour to the True curve but gave less softening. Correction 1 gave a stiff behaviour with a very strong hardening response. These curves are to be used later in bending and puncture test simulations.

6.3.2. Bending Testing of Polypropylene.

The three point bending testing along with the tensile test, is the most common mechanical test for thermoplastic materials. The flexural test measures the force required to bend a beam under three point loading configuration. The data is often used to select materials for components that will support loads without flexing. Flexural modulus is used as an indication of a material's stiffness when flexed.

Most commonly, the specimen lies on a support span and the load is applied to the centre by the loading "nose" producing three point bending at a specified rate. The parameters for this test are the support span, the speed of the loading, and the maximum deflection in the beam. These parameters are based on the test specimen thickness and are defined differently by ASTM and ISO standards. In the present work, the ISO 178 standard (Plastics-Determination of flexural properties) was taken as reference.

The laboratory atmosphere was set to 23°C and 50% relative humidity.

The multipurpose specimens were cut in order to have testing bars of 10x4x80 mm. The three point bend tests have been performed in an Hounsfield H5KS universal testing machine with a load cell capacity of 5KN. and a 3 point bending device as shown in Figure 6.34.

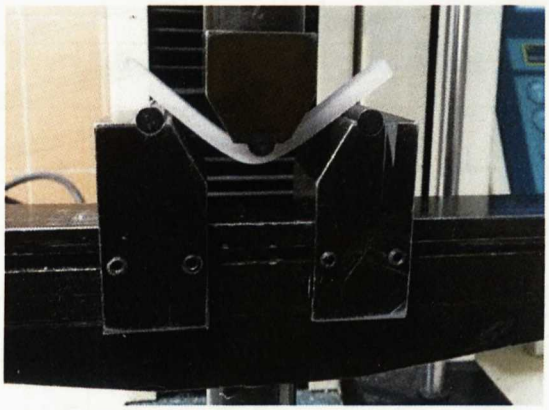

Figure 6.34: 3 point bend test of Polypropylene.

6.3.2.1. Testing conditions.

A minimum of five specimens were tested at each condition.

According to the ISO 178 standard, different testing speeds could be used. In this study, tests were performed at testing speeds of 5, 50 and 500 mm/min.

The support pins and nose of the bending rig had radius of 3.2 mm. A span width of 52 mm was selected. This is a lower span than that recommended by the standard, but the aim was to generate higher levels of strains and consequently, strain rates in the tested specimens. This should permit the validity of elasto-plastic models in simulations to be examined when specimens were subjected to extreme levels of straining.

6.3.2.2. Results.

Although failure of the specimens was not observed for a displacement of 18 mm, a clear stress whitened region could be seen, especially within the tensile stretched area. This indicated that the material had passed through the yield point at high strain levels, generating the crazing phenomena observed in the tensile tests.

Figure 6.35: Bending specimen after the test.

Figure 6.36 displays the force-displacement traces of the selected testing velocities.

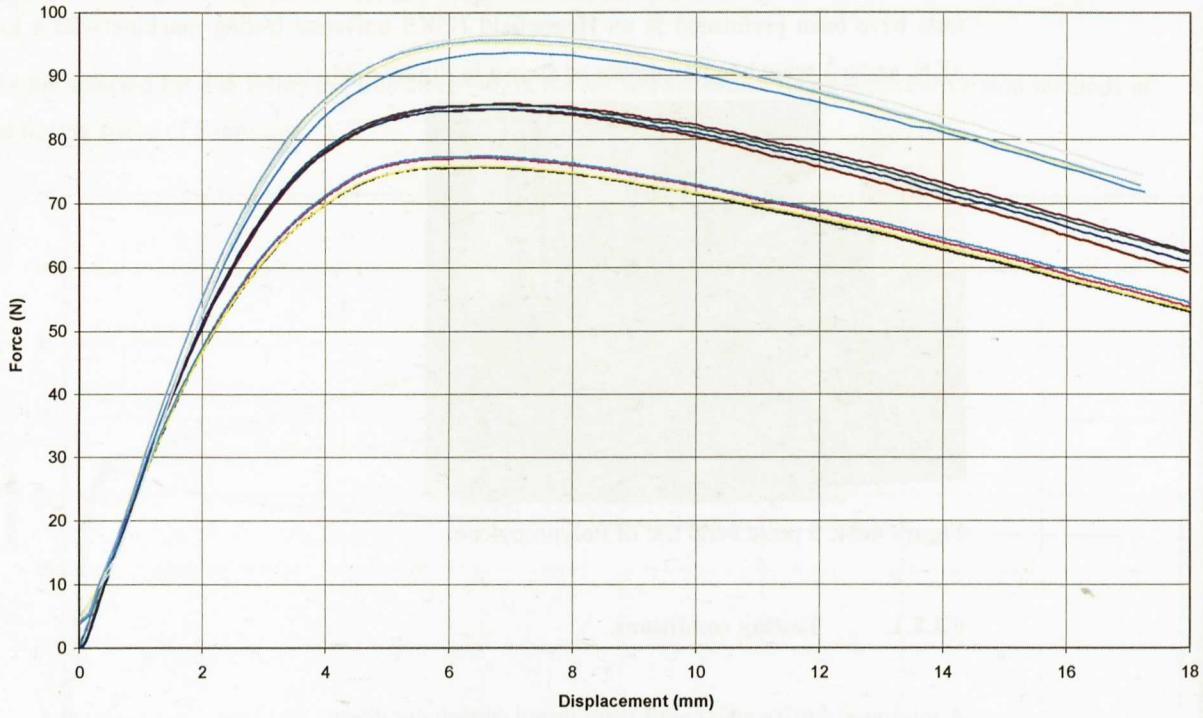

Figure 6.36: Force-displacement curves at testing speeds of 5, 50 and 500 mm/min.

It can be observed that increase in the testing speed increased the maximum bending force. No breakage was observed in the specimens.

From the five tested specimens, a representative curve was selected for each testing speed. The selected curve was then used in the calculation of bending stresses and strains and the flexural modulus.

The stress-strain curves were calculated using equations 2.35 and 2.36.

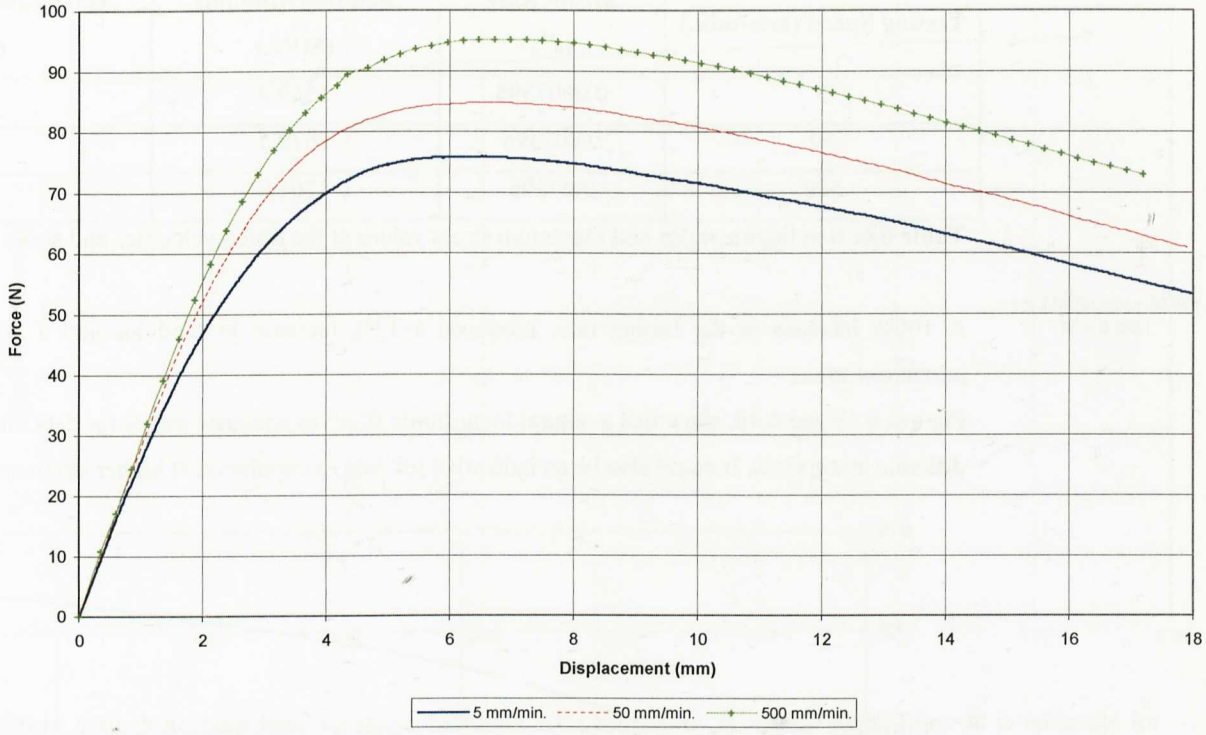

Figure 6.37: The selected force-displacement curves for testing velocities of 5, 50 and 500 mm/min.

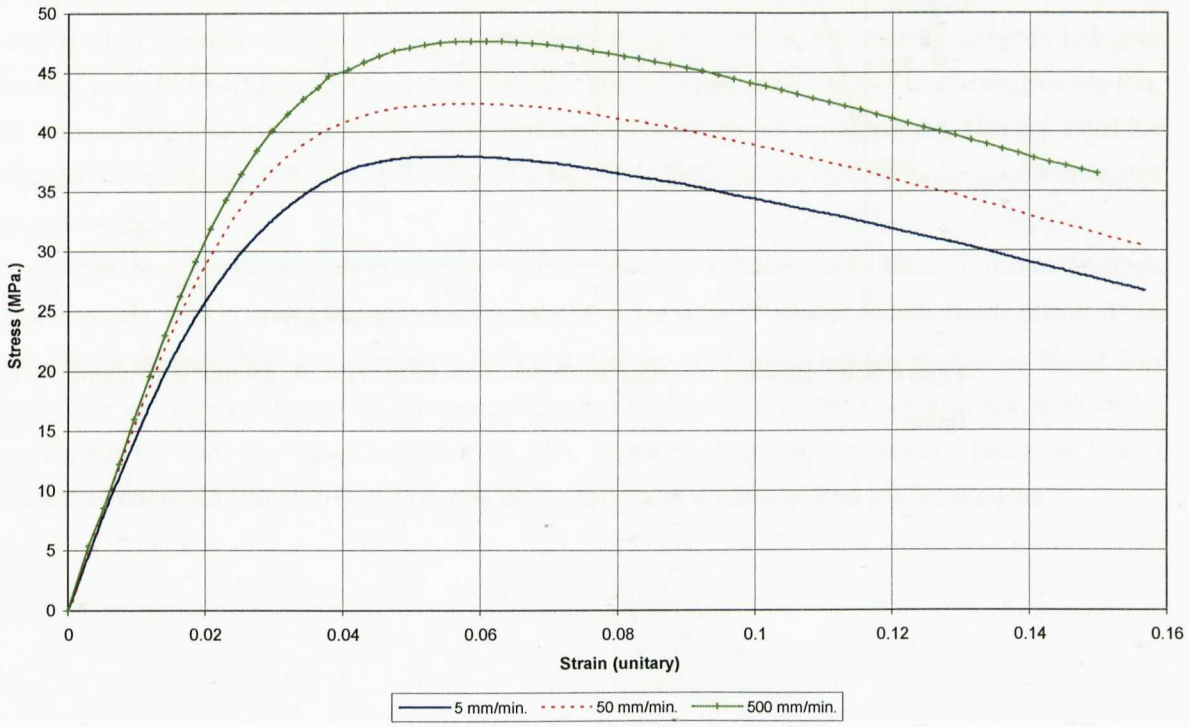

Figure 6.38: Representative stress-strain results for increasing testing velocities of 5, 50 and 500 mm/min.

The rate of straining could be calculated using Equ. 2.34, thus bending modulus and the maximum bending stress could be described in terms of rate.

Bending modulus values were calculated according to ISO 178.

Testing Speed (mm/min.)	Strain Rate (s^{-1})	Bending Modulus (MPa.)	Maximum Bending Stress (MPa.)
5	0.0007396	1549.4	37.88
50	0.007396	1679.5	42.38
500	0.07396	1767.9	47.54

Table 6.6: Bending modulus and maximum stress values at the tested velocities and strain rates.

A 100% increase in the testing rate, produced a 12% increase in modulus and a 20% increase in the maximum stress.

Figures 6.39 and 6.40, show that a natural logarithmic fit gives adequate trends for data interpolation between different strain rates. It could also be an indicative for data extrapolation at higher strain rates.

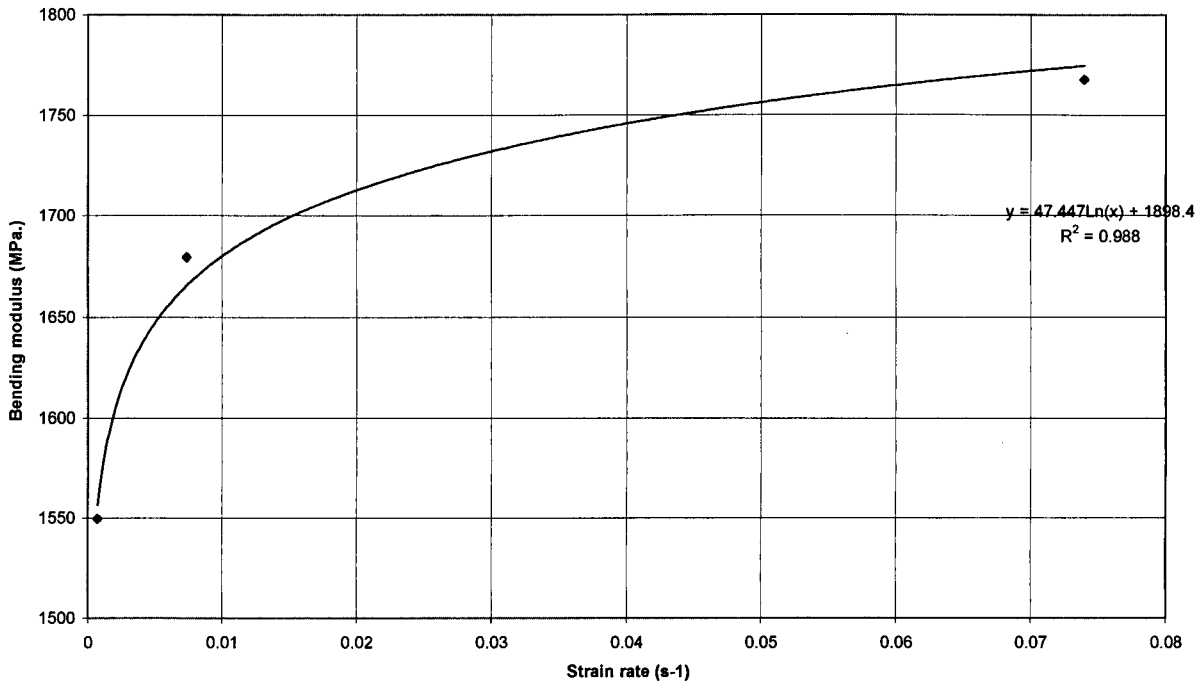

Figure 6.39: Bending modulus evolution with strain rate. A natural logarithmic fit is adequate for data fitting.

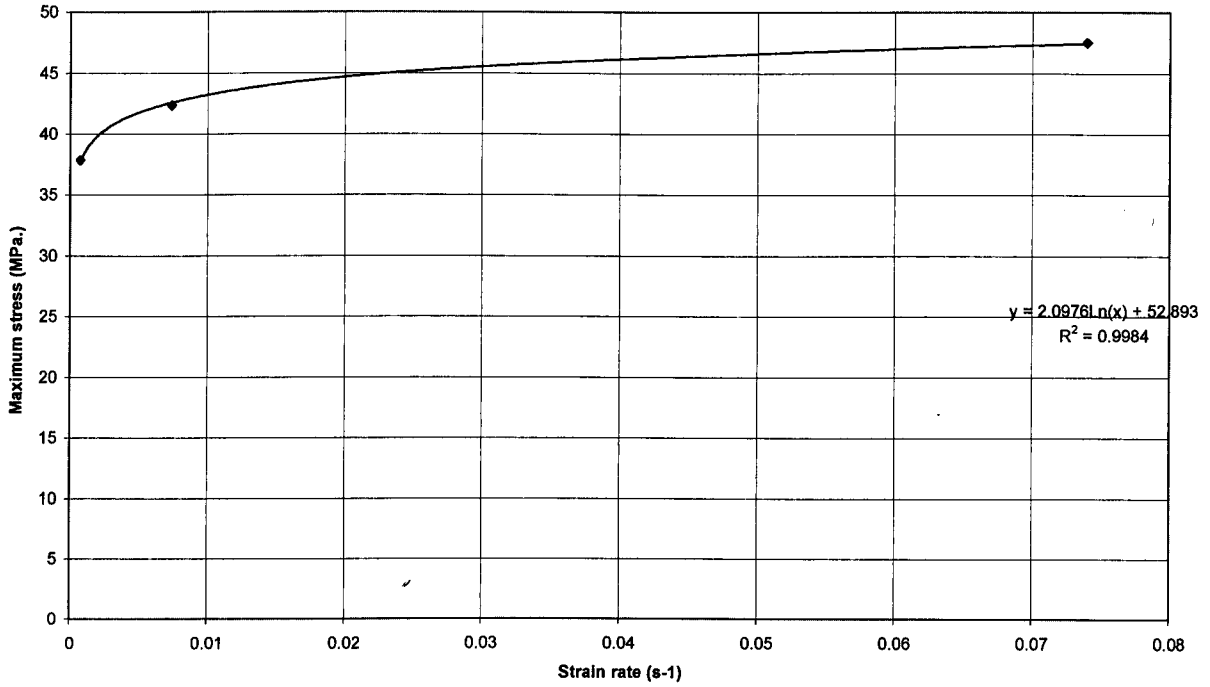

Figure 6.40: Maximum bending stress evolution with strain rate. A natural logarithmic fit is adequate for data fitting.

A comparison of tensile and bending stress-strain curves shows the different mechanical behaviour of the material when subjected to different loading conditions. In the tensile test, the material elongates to higher levels of strain (the necking effect contributes to this). This is in part due to the fact that in the bending test, the test was controlled by velocity and a limit displacement of 18 mm was programmed. This generated the limit strains represented in Figure 6.37 (around 0.156), while in the tensile test, the experiment was carried out up to rupture.

On the other hand, the stress-strain calculation for the bending test is limited to the linear portion of the curve (approximately, 0.05 in strain), beyond which calculation is not accurate enough. For the elastic region, it can be noted that the initial modulus is similar to the tensile test. Up to this point, bending stresses are higher than tensile stresses. In the tensile test the maximum stress is around 22 MPa. for the 5 mm/min. test, while in the bending test the maximum stress is around 38 MPa. In the bending test, compressive behaviour is also present and this could also contribute to having higher maximum stresses up from the linear region.

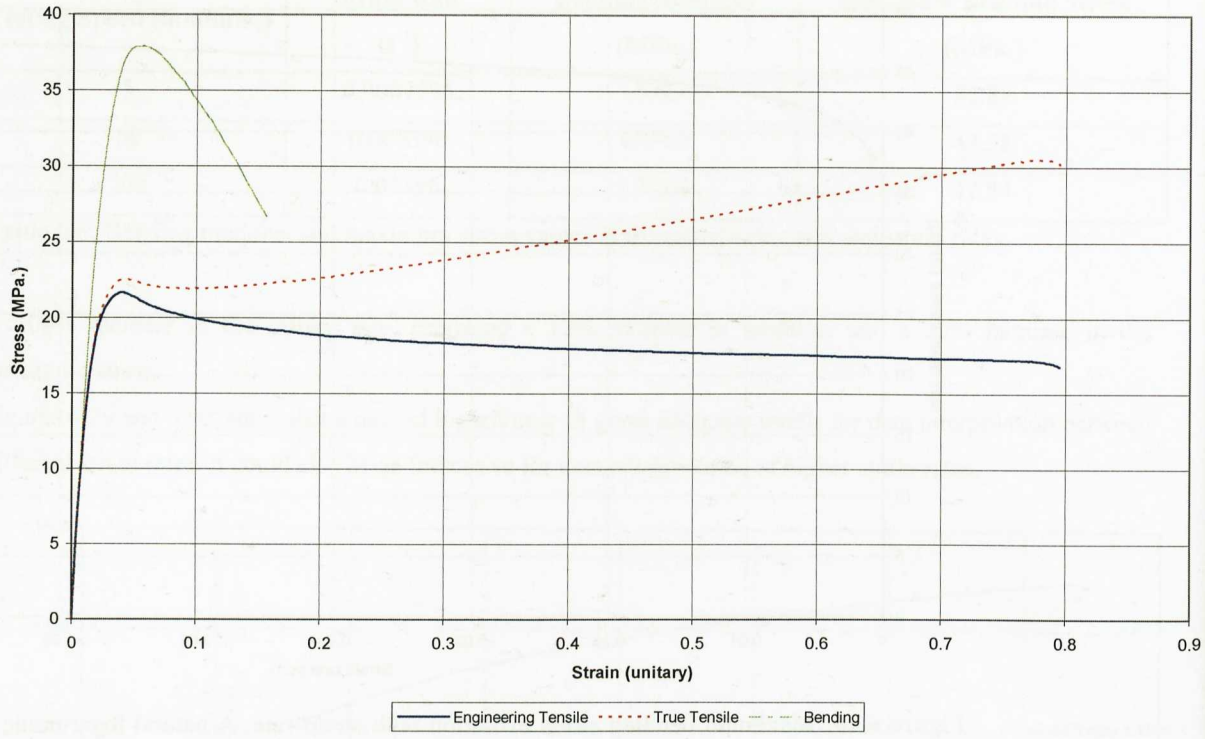

Figure 6.41: Comparison of tensile and bending stress-strain results at 5 mm/min.

Additionally, the generated strain rates also differ considerably in the tensile and bending tests. This could also contribute to the difference in maximum stresses due to strain rate sensitivity effects, but in this case bending strain rates were lower than tensile rates. This is related to the selected reference lengths and support spans.

Testing Speed (mm/min).	Tensile Strain Rate (s-1)	Bending Strain Rate (s-1)
5	0.001667	0.0007396
50	0.01667	0.007396
500	0.1667	0.07396

Table 6.7: Strain rates generated in tensile and bending mode at the selected testing velocities.

The strain rate in tension is 56% higher than in bending.

From the simulation viewpoint, the objective was to correlate the obtained experimental bending force-displacement curves with the input of true stress-strain data from tensile tests.

6.3.3. Puncture or Plate Penetration Testing of Polypropylene.

The plate perforation test used in this study is based on the dart impact test standard ISO 6603-2:2000 Plastics-Determination of puncture impact behaviour of rigid plastics. In this case, the testing speeds are very low in comparison with the ISO 6603 but geometrical characteristics of the specimen supports and strikers are identical to the standard. The main objective of this test is to have a correlation experiment with simulations in order to validate the elasto-plastic models implemented in ANSYS and LS-DYNA.

6.3.3.1. Testing Conditions.

The test specimens were square shaped with the following dimensions: 90x90x2 mm. The specimen could be located as simply supported or clamped between the support plates.

Figure 6.42: Puncture or plate perforation test configuration. Left, simply supported configuration. Right, clamped configuration.

The base support annulus has an external diameter of 60 mm and an internal diameter of 40 mm.
Two dart-indenter shapes were considered: a dart diameter of 20 mm and a smaller one of 11.7 mm diameter.
The laboratory conditions were established at 23°C and a 50% of relative humidity.
A Hounsfield H5KS universal testing machine was used for the tests, attaching a load dell of 5KN, and the described puncture system.
The first experimental tests were carried out at testing speeds of 2, 20 and 200 mm/min. The test speeds were lower than those used in tensile and bending tests since the 500 mm/min. speed was considered dangerous for the testing device. Initially, the utilised hemispherical dart had a diameter of 20 mm. The polypropylene plates were simply supported round its edges on a base annular stand. The test was stopped at a displacement value of 13 mm. No failure of the specimens was achieved at this displacement, however, the straining level of the plates was considerable hence validation of the elasto-plastic models could be examined.
Five plates were tested per test speed.

6.3.3.2. Results.

No failure in terms of total breakage was observed in the specimens, but the Polypropylene plates showed a clear whitening effect when puncture tested.

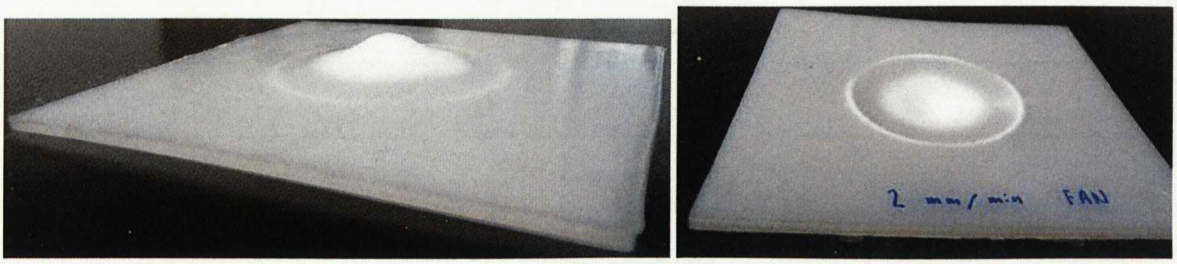

Figure 6.43: Plate specimens after a puncture test up to 13mm of penetration. A 20 mm dart was used at 2 mm/min.

The following graph of force-displacement behaviours displays three curves at different speeds.

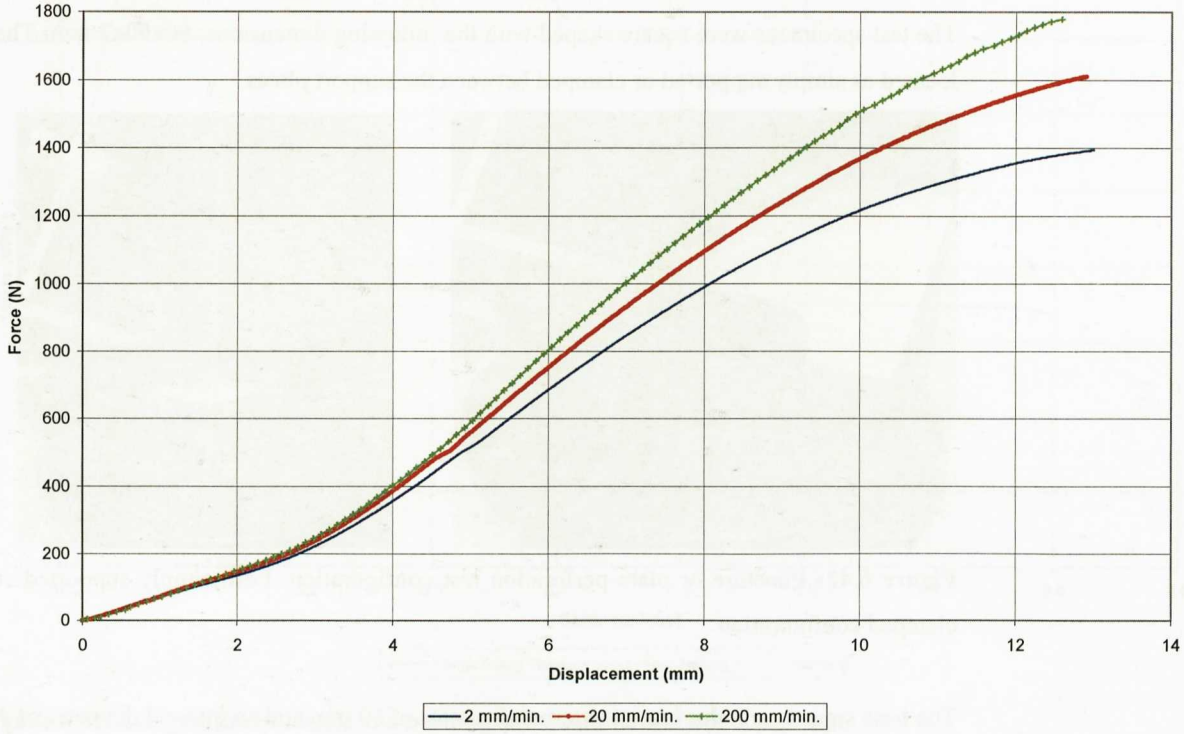

Figure 6.44: Force-displacement results for a 20 mm dart-indenter and simply supported plates at three testing velocities.

A 100% increase in the testing speed produced a 22% increase in maximum force for a displacement of 13 mm. Up to 2 mm displacement, the curve could be considered linear and was similar for all three testing velocities. This could be considered the elastic behaviour of the material. Beyond this point, a non-linear behaviour was noted with load level increasing with speed. This non linear behaviour corresponded to the plastic and necking response of polypropylene when subjected to puncture action.

Another aspect that was considered is the effect of the processing gate type on the specimens. The plates could be processed with lateral or fan type gates and although the base material did not have reinforcing fibres that could give some anisotropic behaviour, it was thought to be interesting to perform a comparison between lateral and fan gated specimens.

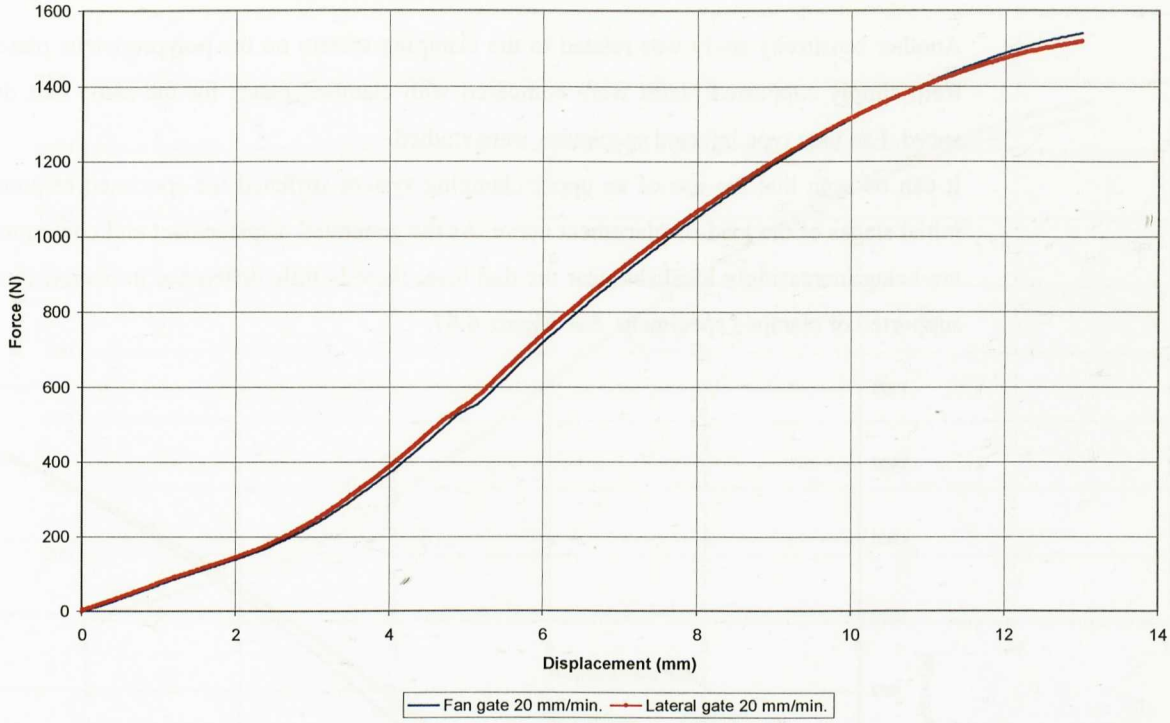

Figure 6.45: Force-displacement curves for 20 mm dart and simply supported plates at 20 mm/min. Fan and lateral gated plates are compared.

It can be seen that there was no considerable difference in the force-displacement behaviour of the two specimen types up to the studied displacement. The difference was within the experimental scatter of each group of tests.

The effect of using darts of two different diameters was also checked. The 20 mm hemispherical dart gave higher force levels than the 11.7 mm diameter dart. This is due to the fact that the 11.7 mm dart, having less contact surface, perforated the polypropylene plate more easily, thus lower force levels were registered.

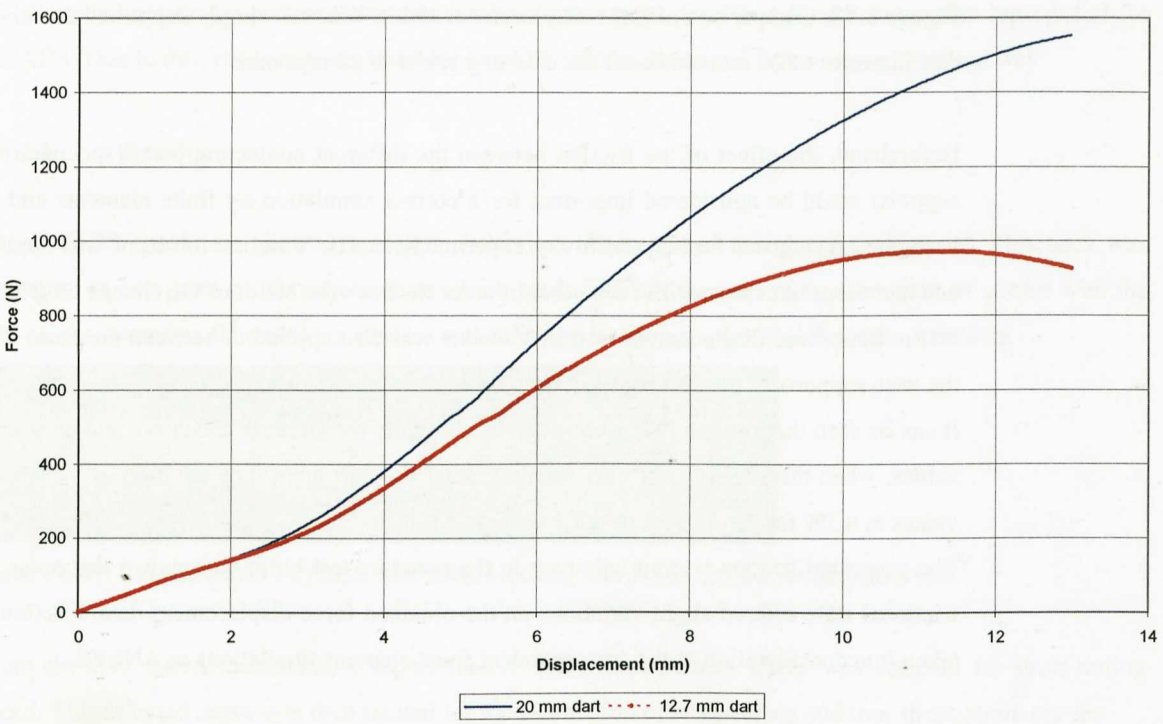

Figure 6.46: Comparison of force-displacement results between 20 and 11.7 mm diameter darts. Simply supported fan-gated plates were tested at 20 mm/min.

Another sensitivity study was related to the clamping system on the polypropylene plates. Results obtained from simply supported plates were compared with clamped plates for the same dart diameter and testing speed. Fan gate type injected specimens were studied.

It can be seen that the use of an upper clamping system stiffened the specimen response especially in the initial stages of the load-displacement curve. As the generated displacement and consequently, plastic strains, are being increasingly localised near the dart area, there is little difference in overall forces between simply supported or clamped specimens. See Figure 6.47.

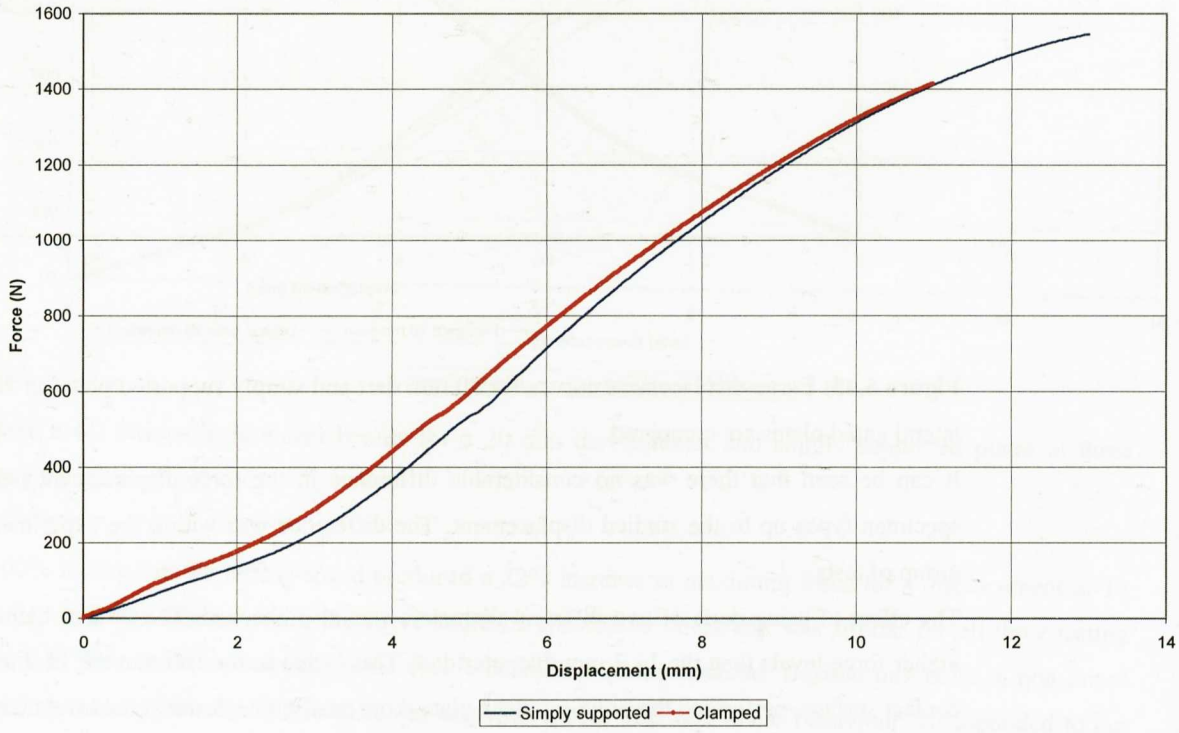

Figure 6.47: Comparison of force-displacement results between simply supported and clamped specimens. A dart diameter of 20 mm was used and a testing speed of 20 mm/min.

Beforehand, the effect of the friction between the different contacting parts (specimen-dart, specimen-base support) could be considered important for a correct simulation by finite elements and this was taken into account carrying out further sensitivity experimental tests. Vaseline lubricant was applied to the specimen and dart faces in contact with each other in order to check the effect of the change on frictional characteristics on the final force-displacement results. Vaseline was also applied in between the faces of the specimens and the base supports. Fan gate type injected specimens were studied.

It can be seen that the use of Vaseline changed slightly the shape of the curve and only for high displacement values, when the strains were very localised near the dart nose. The addition of Vaseline lowered the force values in a 3% for displacement values around 13 mm.

The generated friction was an unknown in the puncture test but it was shown that some modification of the frictional state offered slight variations on the obtained force-displacement data. Frictional effects were also taken into consideration in the correspondent finite element simulations in ANSYS.

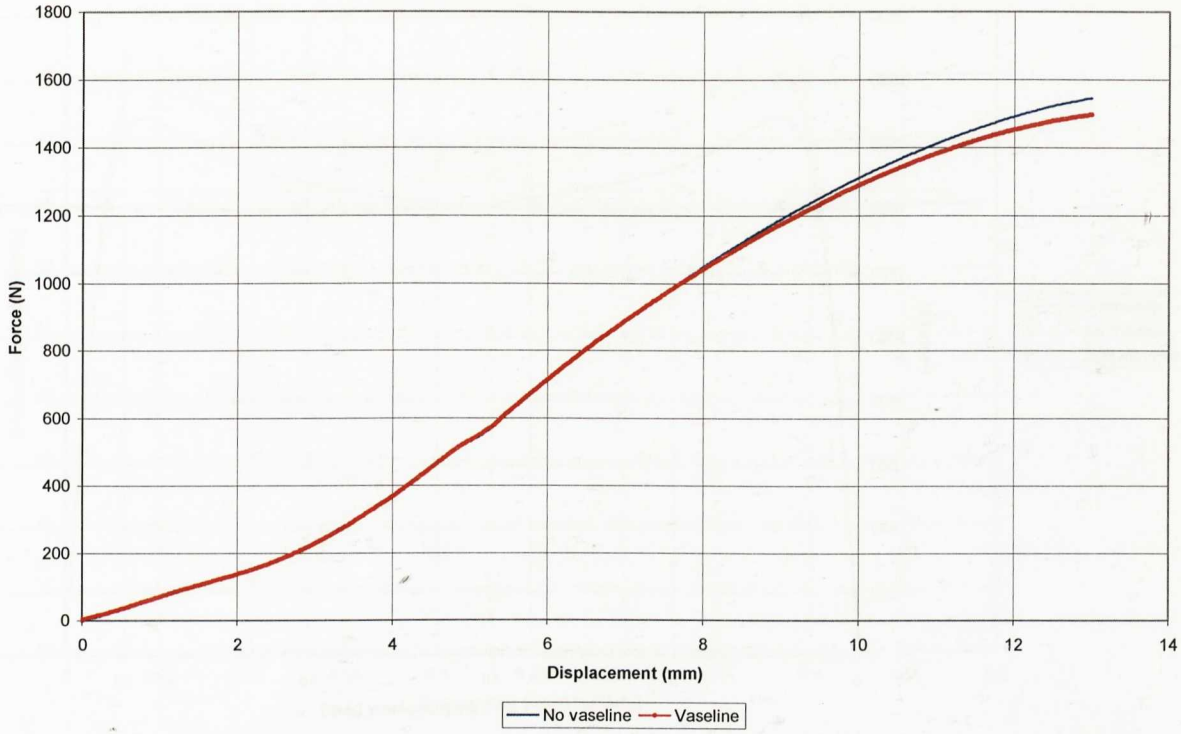

Figure 6.48: Comparison of force-displacement results between lubricated and non-lubricated surfaces (in simply supported specimens). A dart diameter of 20 mm was used and a testing speed of 20 mm/min.

The main goal of the experimental tests in the puncture test was to generate force-displacement data in order to be later correlated with simulations in ANSYS and LS-DYNA.

6.3.4. Tensile Testing of PC/ABS.

All the tensile testing conditions and data analysis procedures described for PP, were also reproduced for PC/ABS. Due to this, the results obtained for PC/ABS will be described in a more summarised way.

6.3.4.1. Results.

The PC/ABS specimens showed a necking behaviour when passed trough the yield point. This neck was generated in any point of the gage section which made difficult the correct measurement of strains with the clip-on extensometer. The necking process was followed by the complete failure of the specimen.

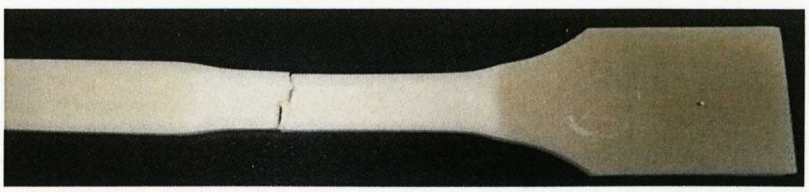

Figure 6.49: Tensile tested PC/ABS specimen. Necking and failure processes are observed.

From the five tested specimens, a representative force-displacement curve was selected for each testing speed. This selected curve was then treated for the calculation of engineering and true stress-strain curves.

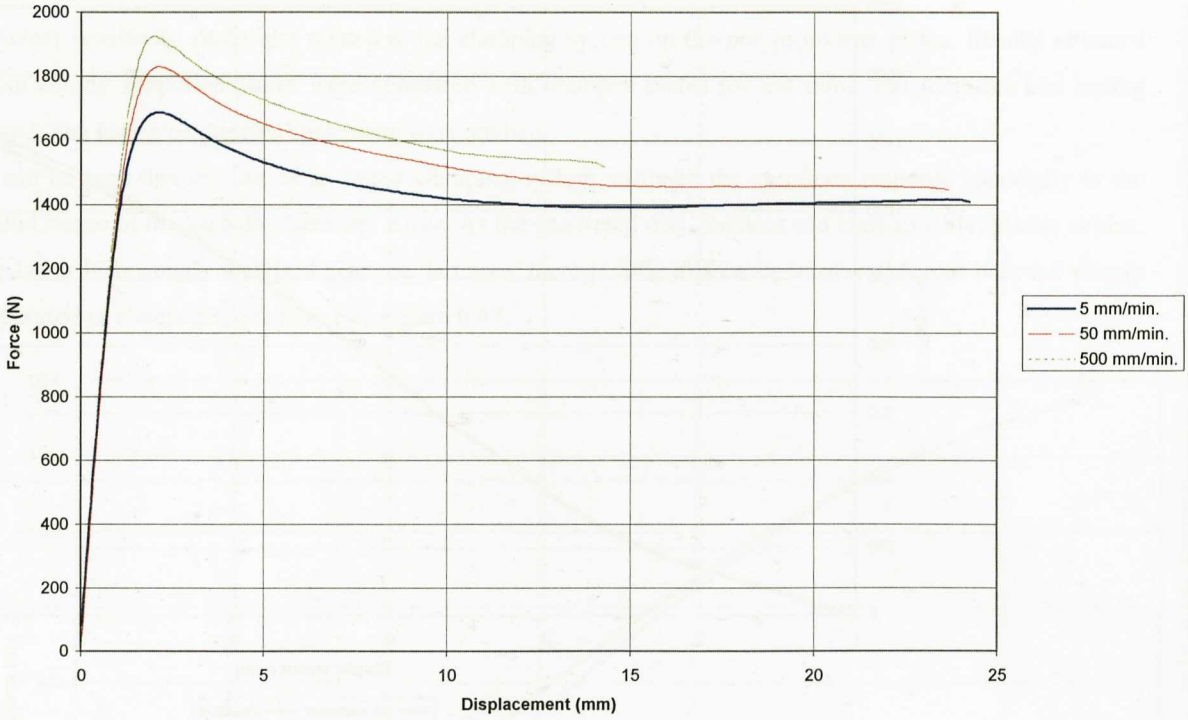

Figure 6.50: Representative force-displacement curves for the three tested speeds.

The calculation of engineering values of strain and stress was carried out using Equ. 2.6 and 2.7. As in the case of PP, force-displacement and engineering stress-strain curves offered continuously reducing force and stress values once the yield point was passed. A stabilisation or plateau area was observed which could, in principle be related to the neck propagation.

The calculation of true values of strain and stress data was performed using Equ. 2.10 and 2.11.

The calculated true stress-strain values gave considerable softening or peak down after the first maximum in stress. A hardening region was observed up to rupture, which could be related to the neck formation and cold-drawing.

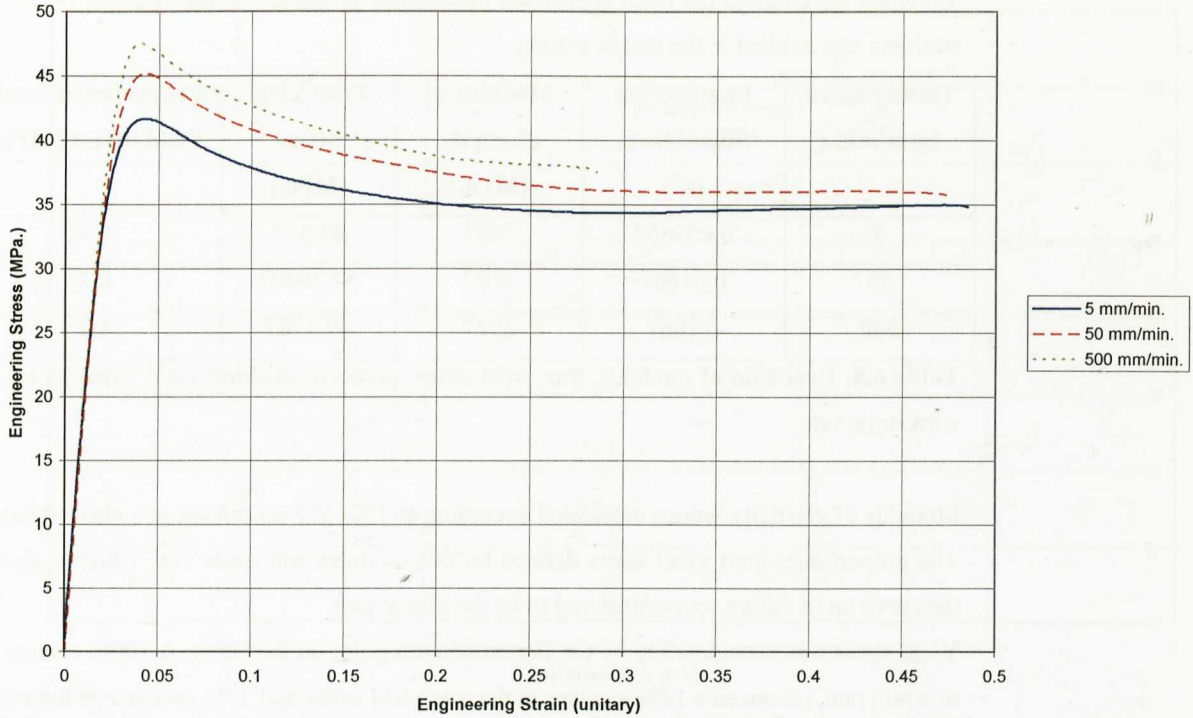

Figure 6.51: Representative engineering stress-strain curves for the three testing speeds.

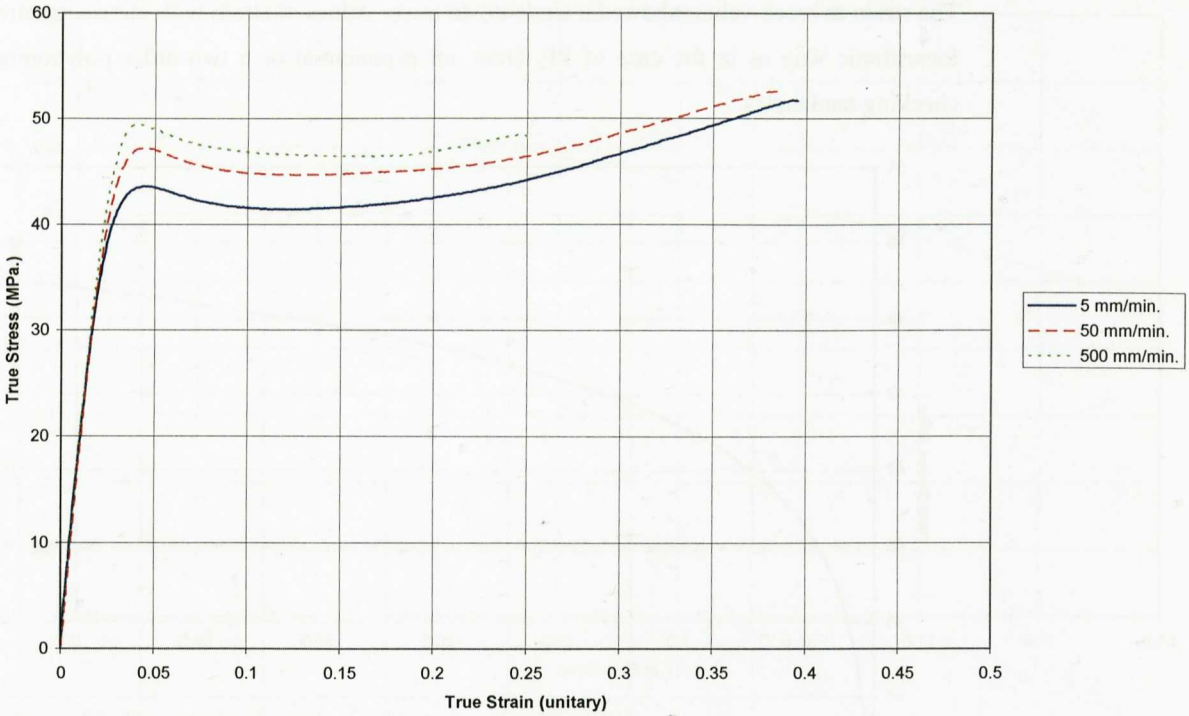

Figure 6.52: True stress-strain curves for the three testing speeds.

6.3.4.1.1. Determination of some Characteristic Data from Tensile Tests.

The comments about engineering strain rate and true strain rate have been stated in the section 6.3.1.2.1 related to the PP material. Here again, engineering strain rate will be used as reference.

Table 6.8 summarises the most significant mechanical properties of the selected PC/ABS in concern to the straining rate applied in the tensile testing.

Testing speed (mm/min.)	Engineering Strain Rate (s^{-1})	Modulus of elasticity (MPa.)	True Yield Stress (MPa.)	Proportional Limit Yield Stress (MPa.)	True Strain at Break (unitary)
5	0.001667	2087	43.557	8.3	0.3953
50	0.01667	2087	47.20405	8.3	0.3876
500	0.1667	2087	49.4787	8.3	0.25

Table 6.8: Evolution of modulus, true yield stress, proportional-limit yield stress and strain at break values with strain rate.

Modulus of elasticity values calculated according to ISO 527 do not show a clear variation with strain rate. The proportional-limit yield stress defined by this modulus was quite low, which suggested that the rest of the curve up to failure was considered to be the plastic part.

Yield stress was considered to be the first maximum point on the curve. A 100% change in the testing speed or strain rate, produced a 12% increase in the true yield stress and 37% decrease in the strain at break.

The evolution of yield stress with strain rate gave, as in the case of PP, an increasing effect with some logarithmic-type tendency, although the collected data corresponded only to three tensile testing speeds. The Eyring's relation gave the same tendency.

The strain at break values showed a tendency to lower values of strain with increasing strain rates but not in a logarithmic way as in the case of PP. Here, an exponential or a two-order polynomial fit was better for checking tendencies.

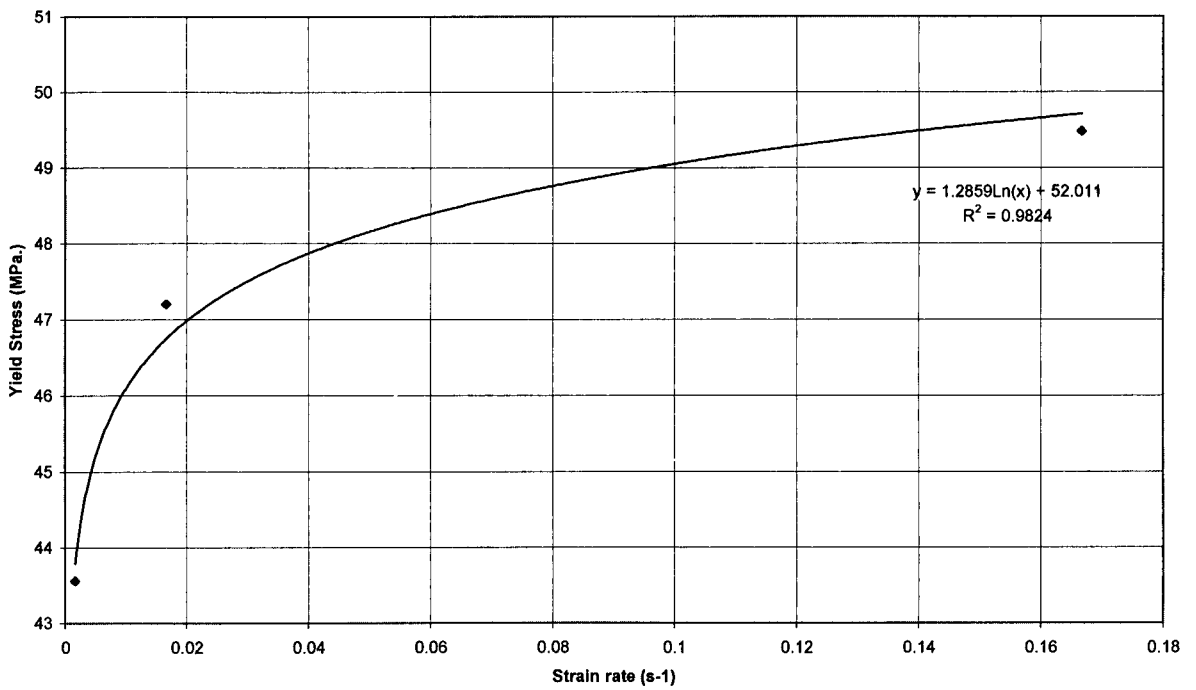

Figure 6.53: True yield stress versus strain rate, PC/ABS.

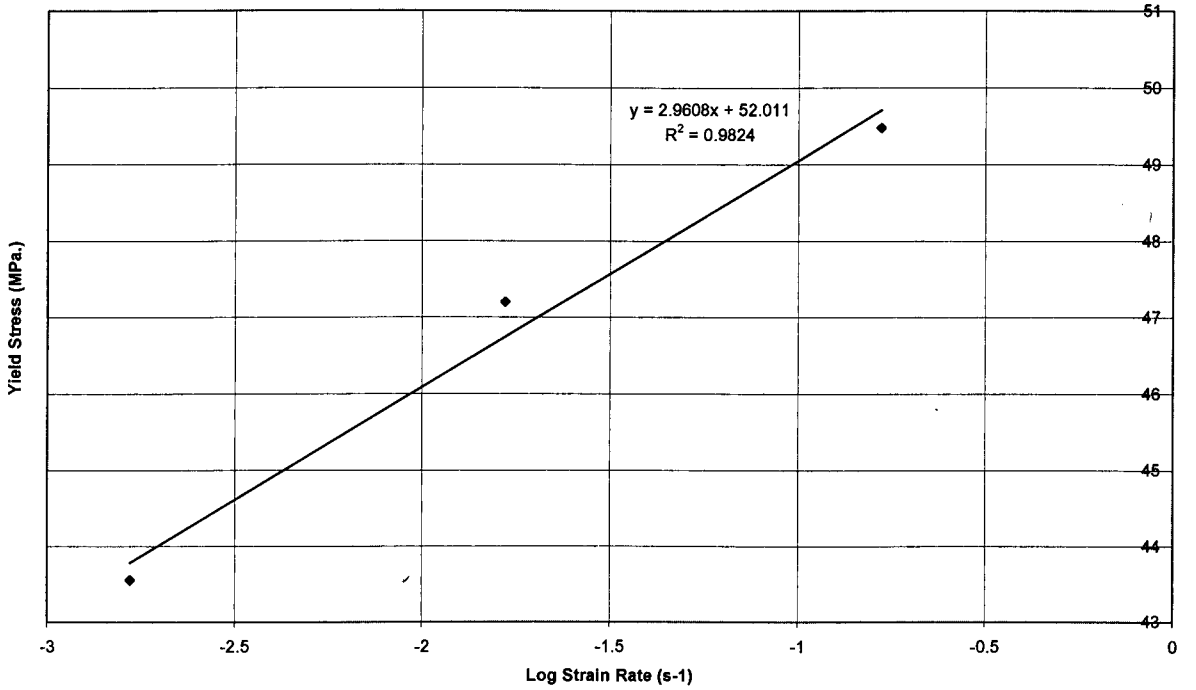

Figure 6.54: True yield tress versus strain rate, according to the Eyring's equation, PC/ABS.

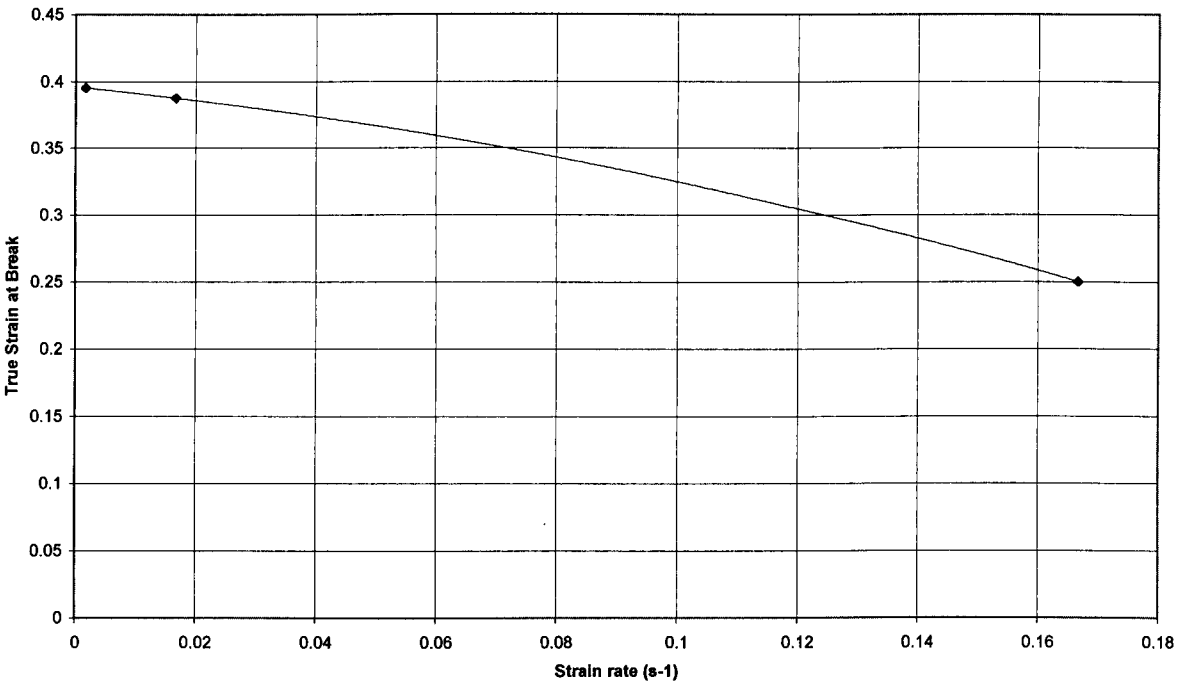

Figure 6.55: True strain at break versus strain rate, PC/ABS.

6.3.4.1.2. Data preparation for ANSYS.

For the selected PC/ABS material the following should be the necessary data to implement the tensile test values in the elasto-plastic constitutive models of ANSYS:

- Elastic modulus: 2087 MPa.
- Elastic Poisson's ratio: 0.4. From material manufacturers' data sheets.

As it was assumed the use of a multilinear isotropic hardening behaviour,

- A set of true stress vs. true strain points up to failure were defined.

This description offered a yield stress value of 8.333 MPa. and the post yield behaviour was directly calculated from engineering data, ignoring any consideration of non-homogeneities due to necking. The result is the following curve for the 5 mm/min. test:

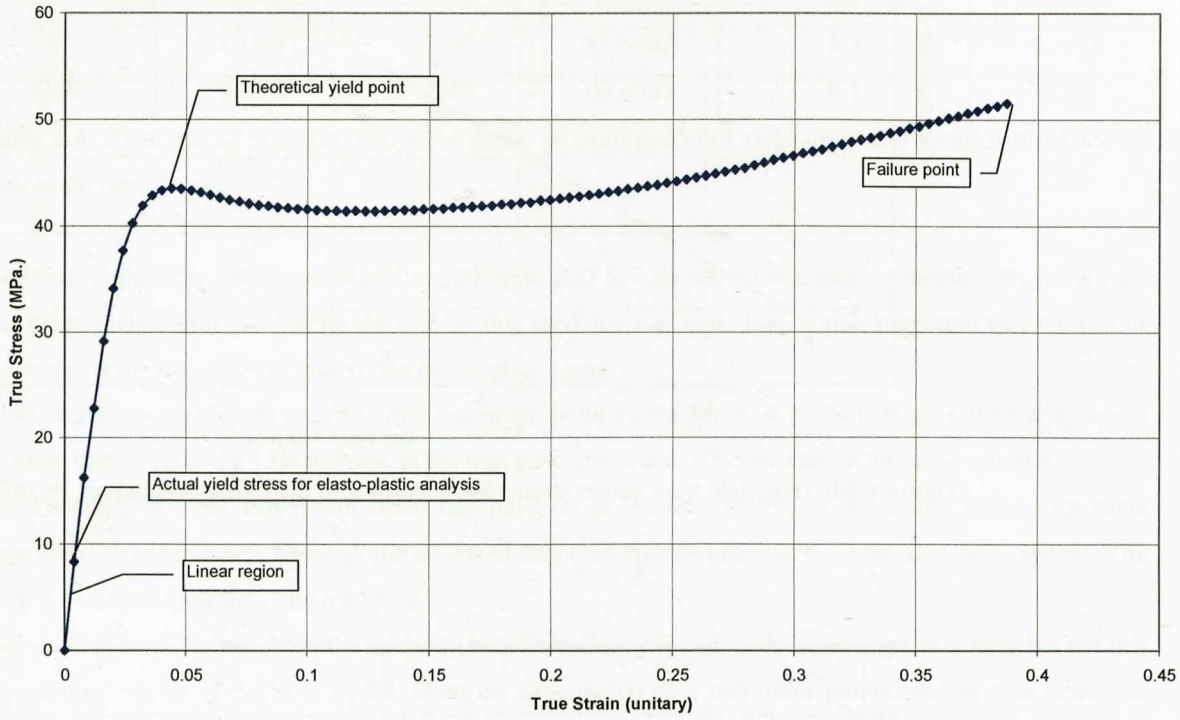

Figure 6.56: Definition of the elasto-plastic curve for ANSYS. PC/ABS.

6.3.5. Bending Testing of PC/ABS.

The same testing conditions and procedures as described for PP were applied in this section for the studied PC/ABS.

6.3.5.1. Results.

The PC/ABS specimens showed no failure in terms of breakage when bent up to 18 mm. Considerable whitening was observed especially in the tensile area of the specimen.

Figure 6.57: Bent PC/ABS specimen at 18 mm displacement.

Figure 6.58 shows the load-displacement traces at the three testing speeds.

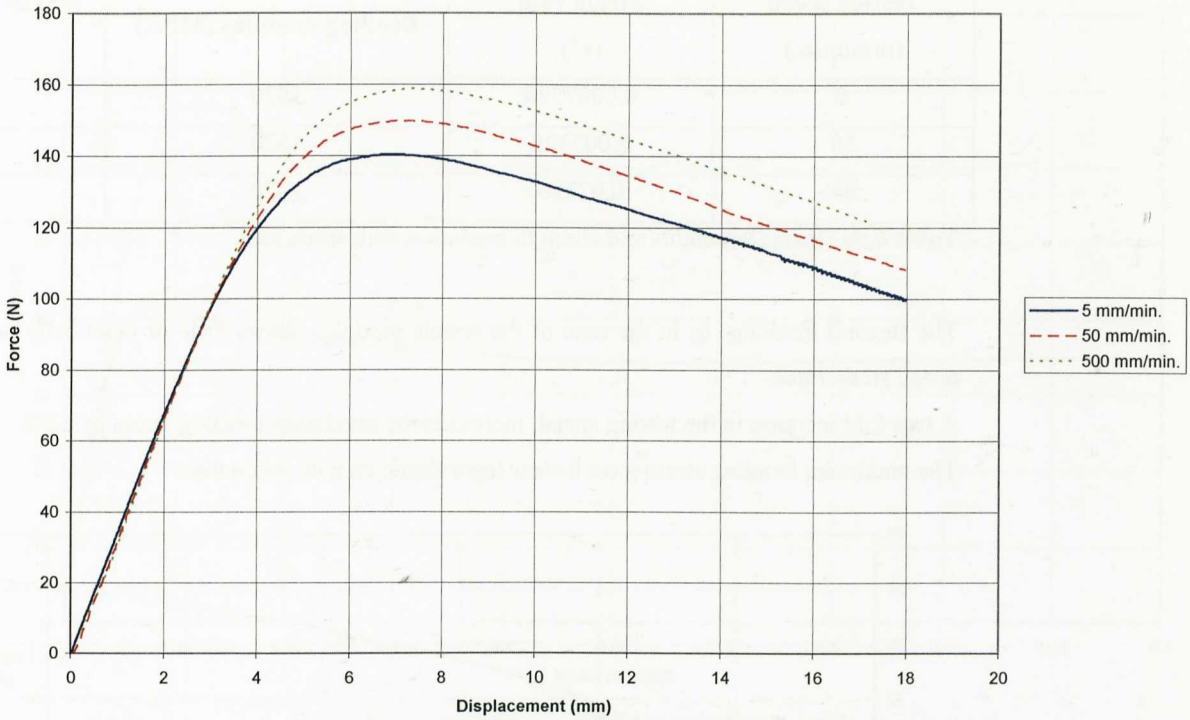

Figure 6.58: Representative load-displacement results at testing speeds of 5, 50 and 500 mm/min. It can be observed that increase in the testing speed had an increasing effect on the maximum bending force. No failure was observed in the specimens.

The bending stress-strain curves were calculated using Equations 2.35 and 2.36.

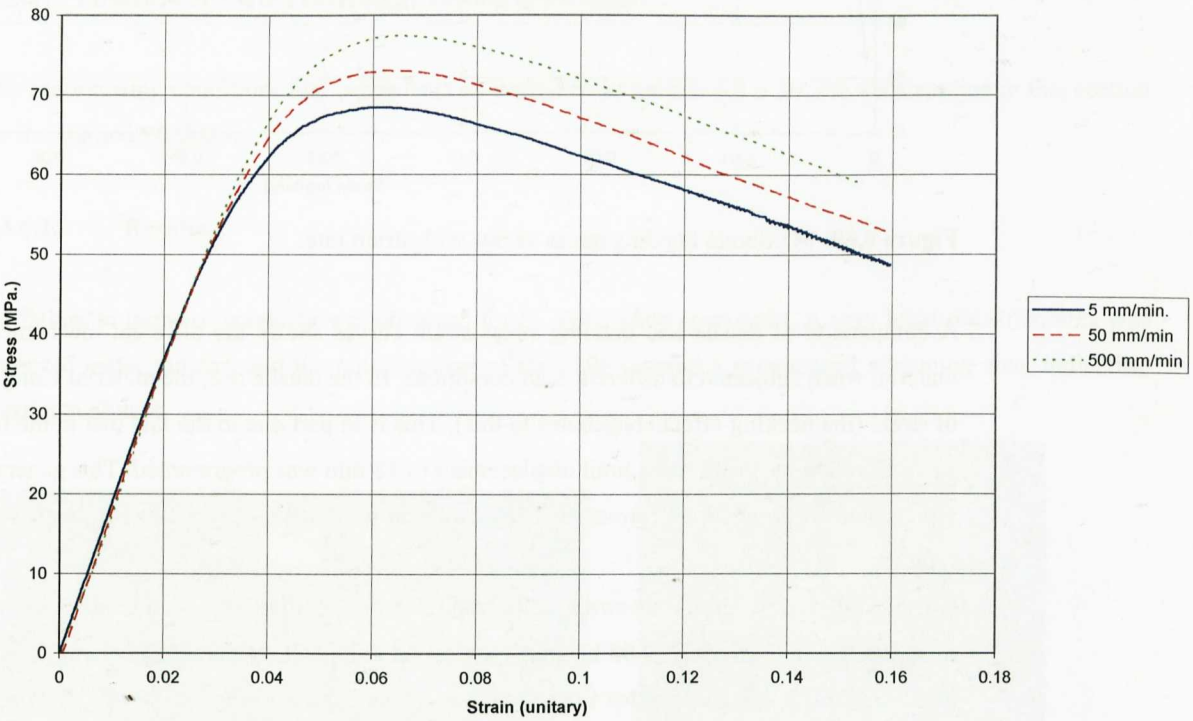

Figure 6.59: Representative stress-strain results for increasing testing velocities of 5, 50 and 500 mm/min.

The strain rate effect on flexural modulus (according to ISO 178 standard) and the maximum stress values are summarised in table 6.9.

Testing speed (mm/min.)	Strain rate (s^{-1})	Bending modulus (MPa.)	Maximum bending stress (MPa.)
5	0.0007396	1820	68.41
50	0.007396	1820	73.04
500	0.07396	1820	77.43

Table 6.9: Flexural modulus and strength evolution with strain rate.

The flexural modulus, as in the case of the tensile modulus shows little or practically no variation with the tested strain rates.

A two fold increase in the testing speed, increased the maximum bending stress by 12%.

The maximum bending stress gave a clear logarithmic fit with strain rate.

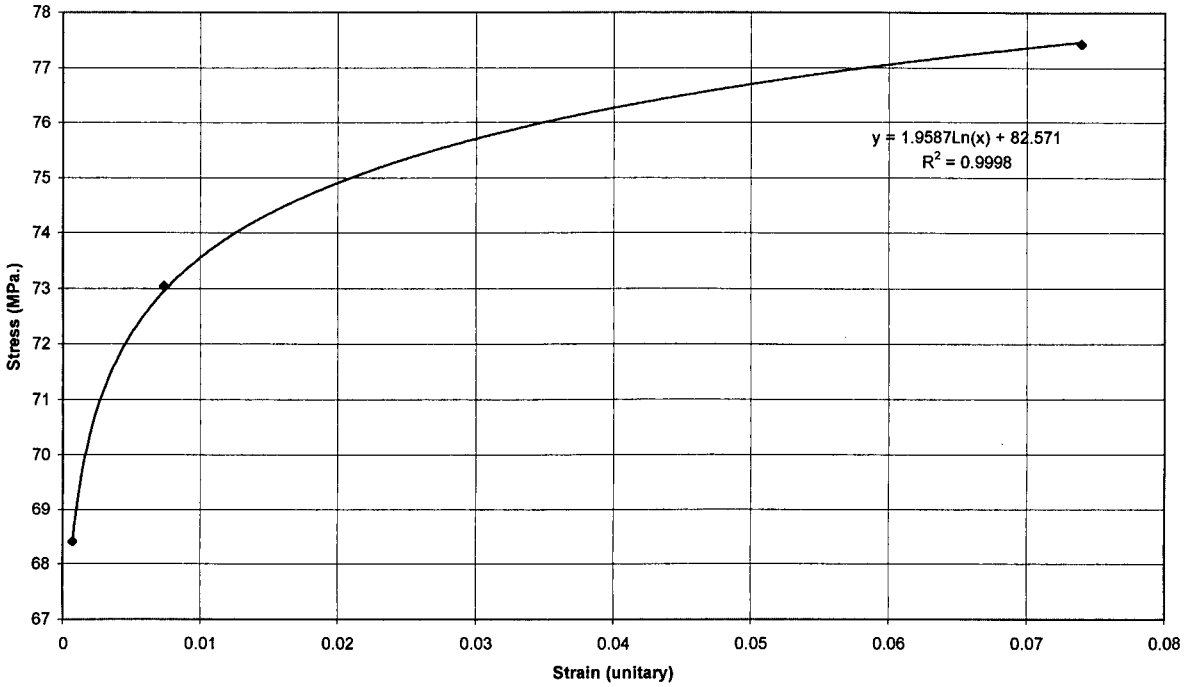

Figure 6.60: Maximum bending stress versus with strain rate.

A comparison of tensile and bending stress-strain curves shows the different mechanical behaviour of the material when subjected to different load conditions. In the tensile test, the material elongates to higher levels of strain (the necking effect contributes to this). This is in part due to the fact that in the bending test, the test was controlled by speed and a limit displacement of 18 mm was programmed. This generated the limit strains represented in Figure 6.59 (around 0.156), while in the tensile test, the experiment was carried out up to rupture.

On the other hand, the stress-strain calculation for the bending test is limited to the linear region of the experiment (approximately, 0.05 in strain) as beyond this point, calculations are not accurate enough. For the elastic region, it can be said that the initial modulus is similar to the tensile test. Beyond this point bending stresses are in a higher level than tensile stresses. In the tensile test the maximum stress is around 44 MPa. for the 5 mm/min. test, while in the bending test the maximum stress value is found to be around 68 MPa. In the flexural test, compressive behaviour is also present and this can contribute to this difference in maximum stresses beyond the linear region.

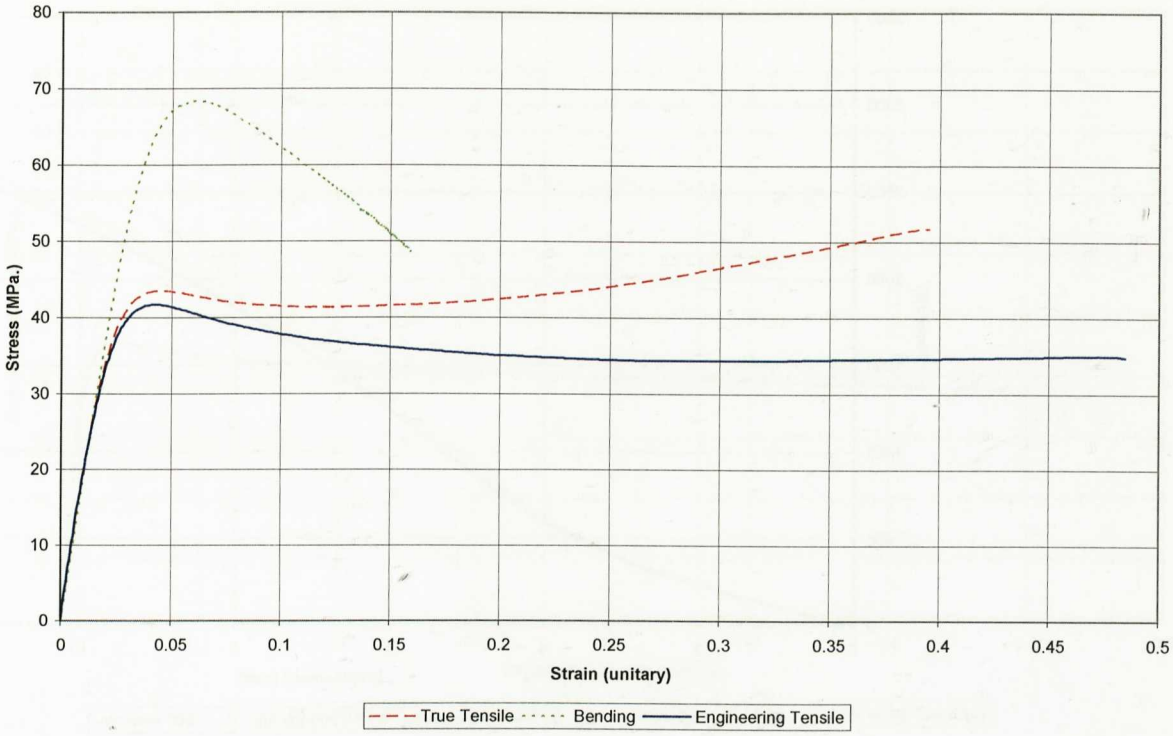

Figure 6.61: Tensile and bending stress-strain curves at 5 mm/min, PC/ABS.

From the simulation viewpoint, the objective was to correlate the experimental bending force-displacement curves in bending with the input of true stress-strain data from tensile tests.

6.3.6. Puncture or Plate Penetration Testing of PC/ABS

The same testing conditions and procedures as described in section 6.3.3 for PP were applied in this section for the studied PC/ABS.

6.3.6.1. Results.

No failure in terms of breakage was observed for PC/ABS plate specimens. A very localised strain area was observed under the dart and the outer surface of the plate showed a pronounced whitening area, indicating crazing evolution.

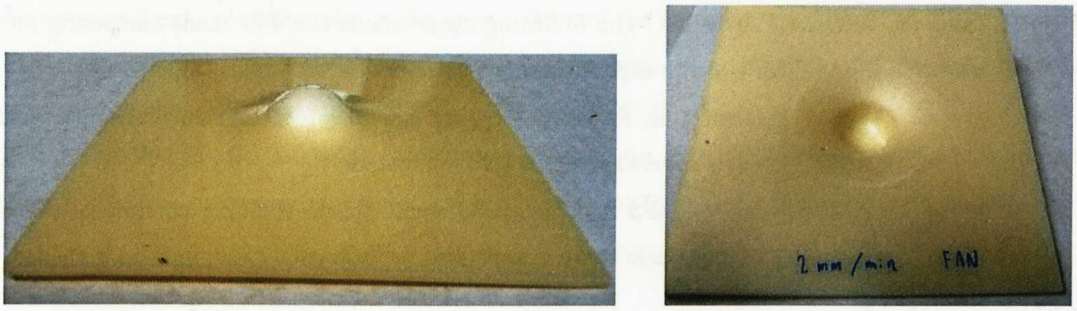

Figure 6.62: Punctured PC/ABS specimen. A 20 mm diameter dart was used at 2 mm/min.

In the following graph three representative force-displacement curves are plotted per each testing speed.

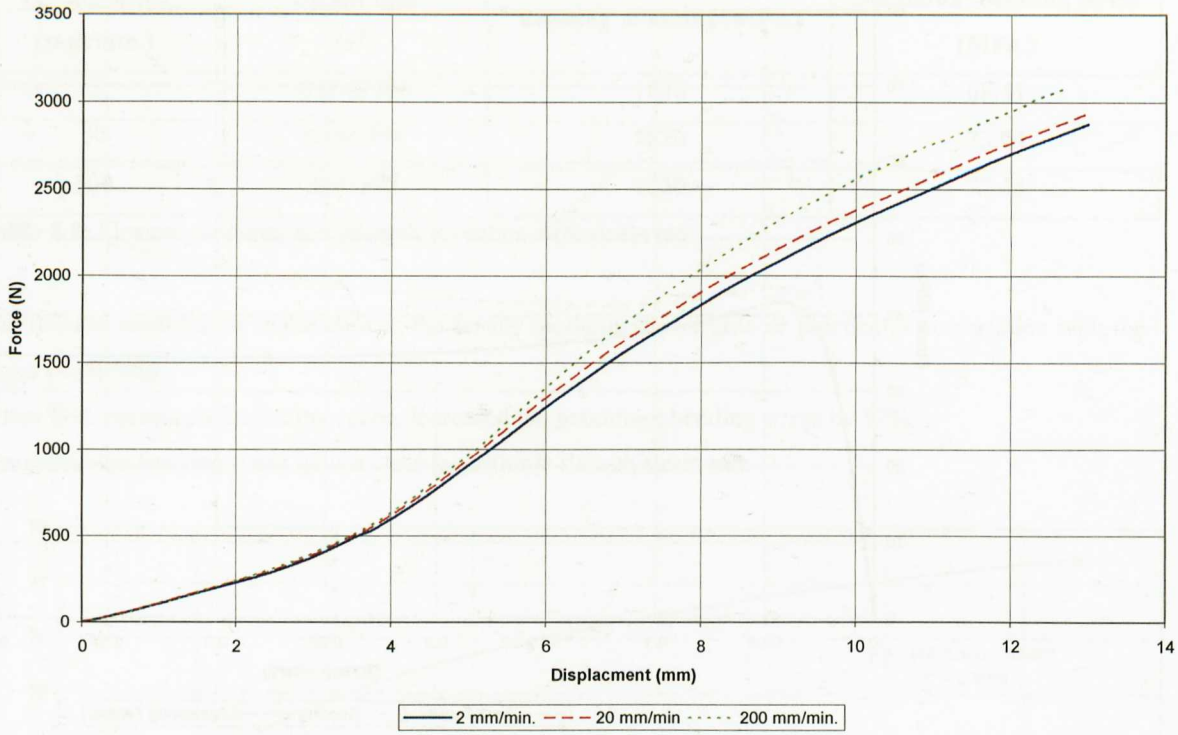

Figure 6.63: Representative load-displacement traces for PC/ABS at the tested velocities of 2, 20 and 200 mm/min. An indenter with a diameter of 20 mm was used and the specimens were simply supported on the base annular plate.

As in the case of PP, load-displacement curves for PC/ABS are linear up to 2 mm for the three testing speeds. This could be considered the elastic response of the plate. Beyond this displacement value, a non-linear behaviour is observed with force values increasing with increasing speed of the test. This non linear behaviour corresponds to the yielding and necking behaviour of PC/ABS when subjected to puncture action.

A 100% increase in the testing speed supposed an increase of a 7% in the maximum force for a displacement of 13 mm.

The main goal of the puncture tests was to generate force-displacement data for simulations in ANSYS and LS-DYNA.

6.3.7. Appendix 6.1: Comparison between commercial data and experimental own tensile testing.

Tensile data both for the studied PP and the PC/ABS materials are available at www.campusplastics.com or using the software CAMPUS®. The following observations could be made comparing the engineering data extracted from CAMPUS with experimentally determined values in this study:

- A good agreement in the elastic region can be observed. However, the yield stress value in CAMPUS data is somewhat higher for both materials.
- CAMPUS data is valid for elastic and small plastic straining conditions. For studies where the plastic area of the tensile curve is important, experimental determination is needed.

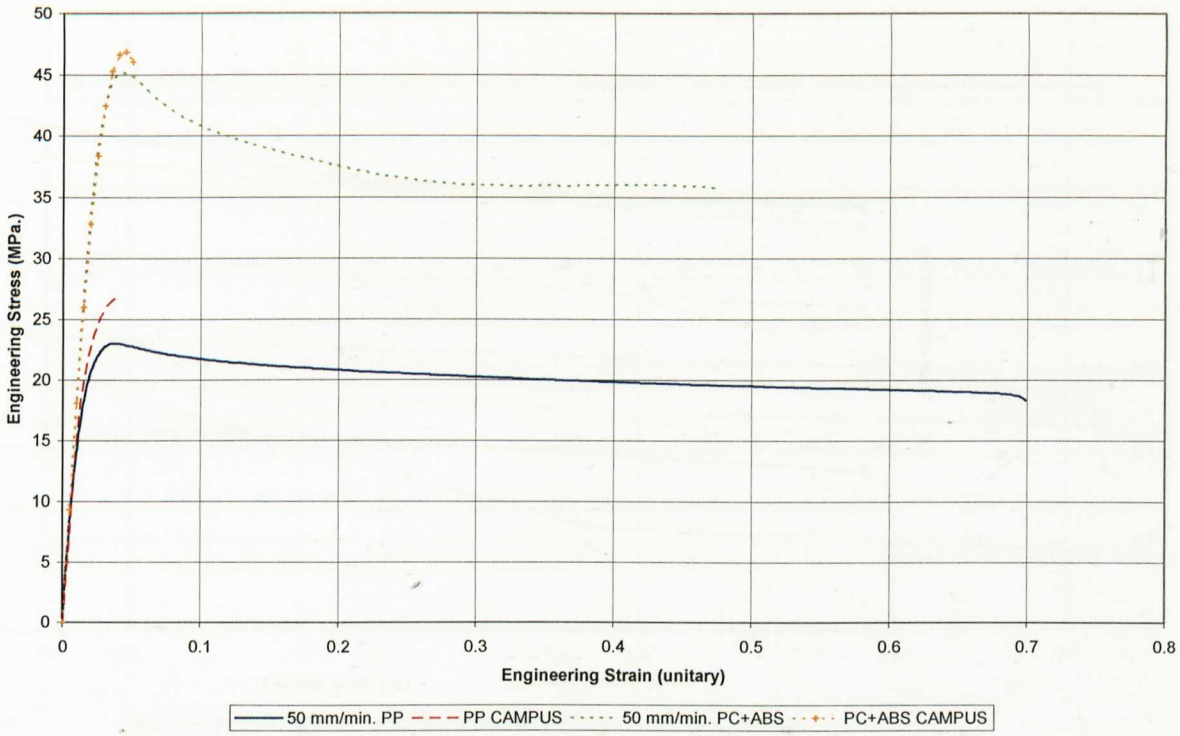

Figure 6.64: Comparison of CAMPUS and own experimental tensile curves for PP and PC/ABS.

6.3.8. Appendix 6.2: Temperature and rate effects on PP and PC/ABS.

It was described in the first part of this thesis work that mechanical behaviour of thermoplastic materials is very sensitive to any change in temperature or rate of testing. In section 2.3 the Eyring's model was described which has been often used to describe temperature and rate effects on yielding. This appendix describes some experimental results obtained in this study for PP and PC/ABS when tensile tested at different temperatures and strain rates.

The selected testing velocities were the used along this work: 5, 50 and 500 mm/min.

The selected testing temperatures were: -40, -20, 0, 23 and 60ºC. A temperature chamber was used in conjunction with the universal testing machine. Nitrogen cooling was used to obtain the low testing temperatures. These tests were performed at the Polymer Centre Laboratory in London Metropolitan University.

The drawback of using the temperature chamber was the inability to use a clip-on extensometer system inside to measure the developed strains in the gage section of the multipurpose specimens. Thus, the strain values reported here refer to the clamping distance (115 mm). Consequently, the testing strain rates were (considering the testing speed): 0.000725, 0.00725 and 0.0725 s^{-1}.

For the studied PP, the following results were obtained for the yield stress at varying temperatures and the logarithm of the strain rate (which was a way of evaluating the validity of the Eyring's model):

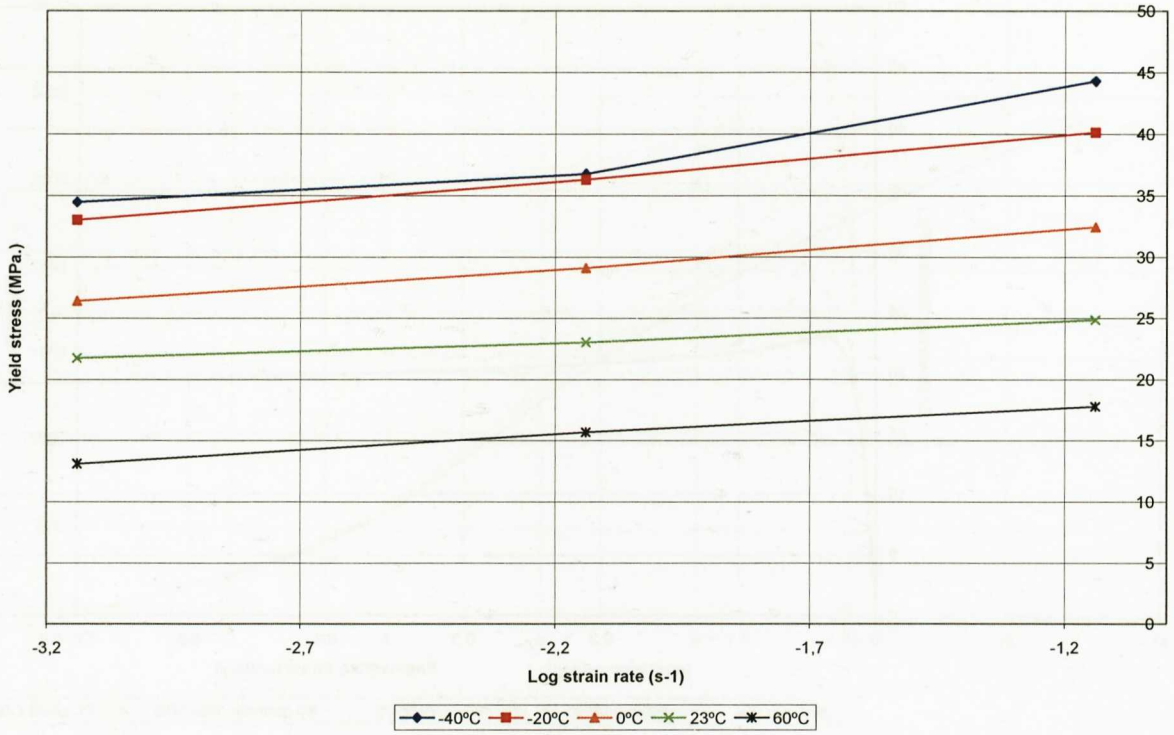

Figure 6.65: Evolution of the yield stress with the logarithm of the applied strain rate at different temperatures, PP.

The reported yield stress data was considered to be the maximum in the engineering stress-strain curves.

It can be observed that for the PP, there was a linear tendency of increasing the yield stress with the logarithm of the strain rate. This tendency was only broken by the test at -40°C. In this case, difficulties were found to correctly clamp the specimens at such a low temperature and this could cause some measurements errors.

The strain at break values were also measured. It was observed that in this case no linear relationship could be observed between strain values and the logarithm of the used strain rate:

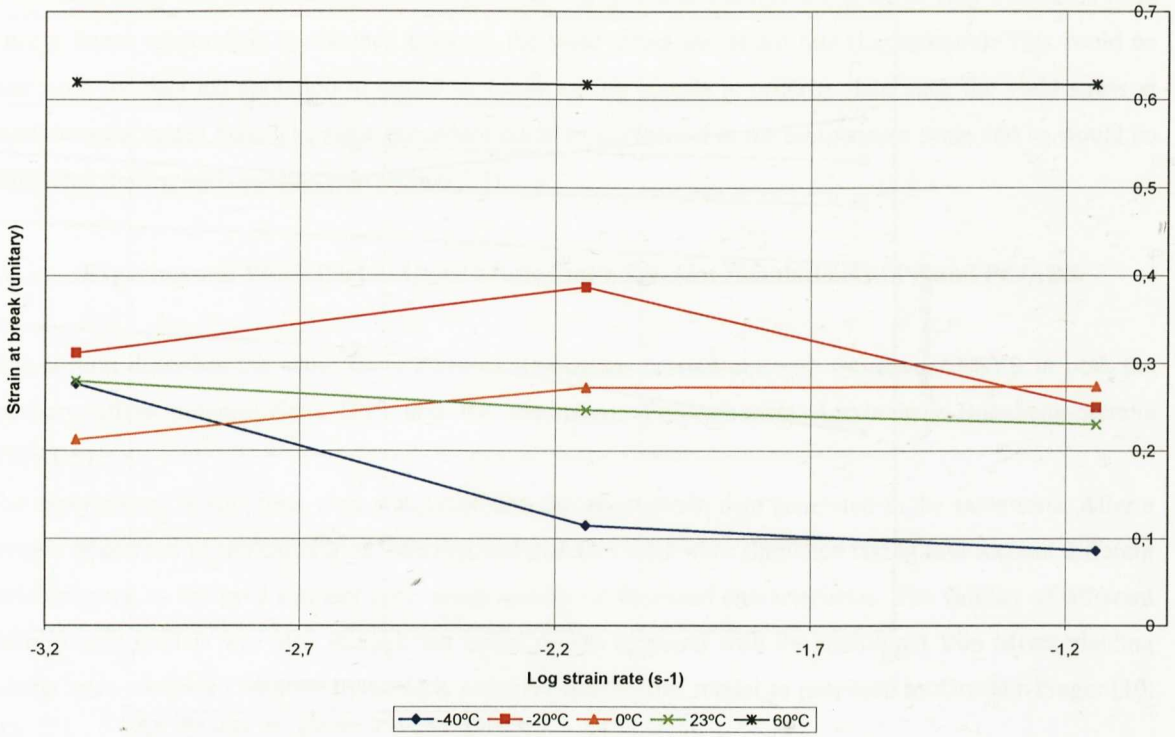

Figure 6.66: Evolution of the strain at break values with the logarithm of the applied strain rate at different temperatures, PP.

Even not applying logarithms it was checked that no proper tendency could be extracted due to the high scatter in strain to failure values; curves tended to cross each other avoiding any tendency derivation.

For the selected PC/ABS, it can be observed that again a linear relationship was observed on the yield stress when plotted against the logarithm of the strain rates at different temperatures. Again, the tests at -40°C presented some measurement difficulties.

For strain at break values no linear tendency was observed when plotted against the logarithm of the strain rates at different temperatures.

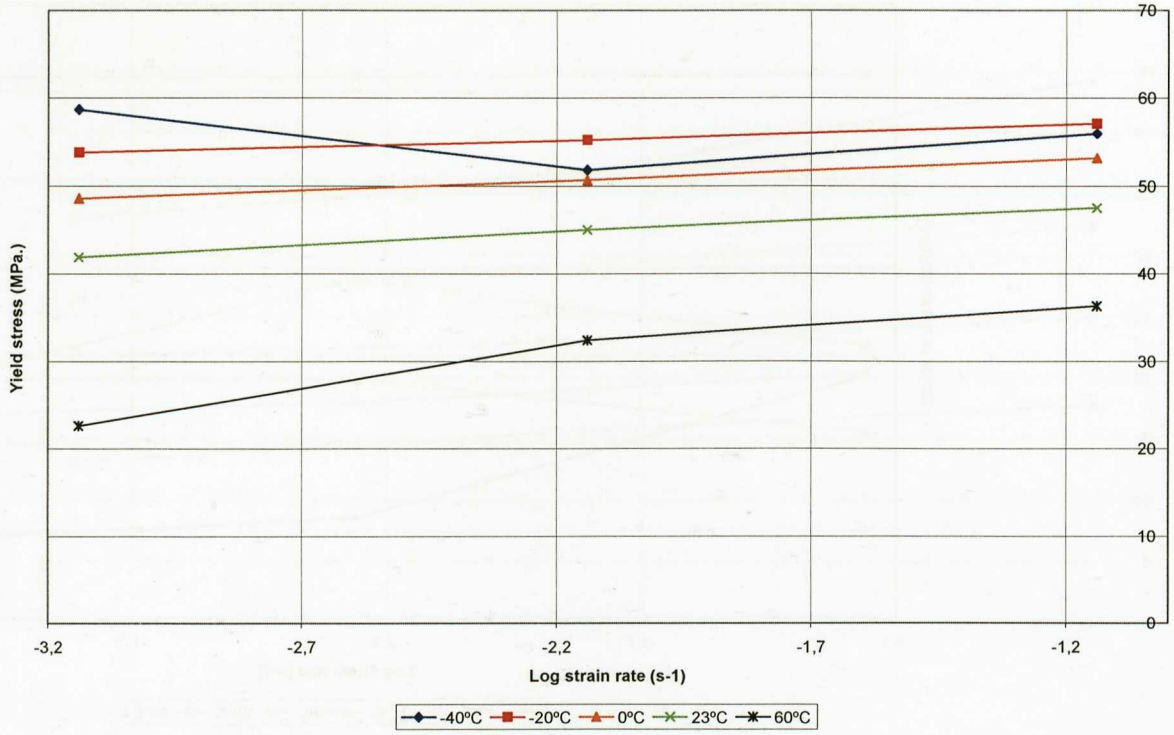

Figure 6.67: Tensile yield stress versus the logarithm of the applied strain rate at different temperatures for PC/ABS.

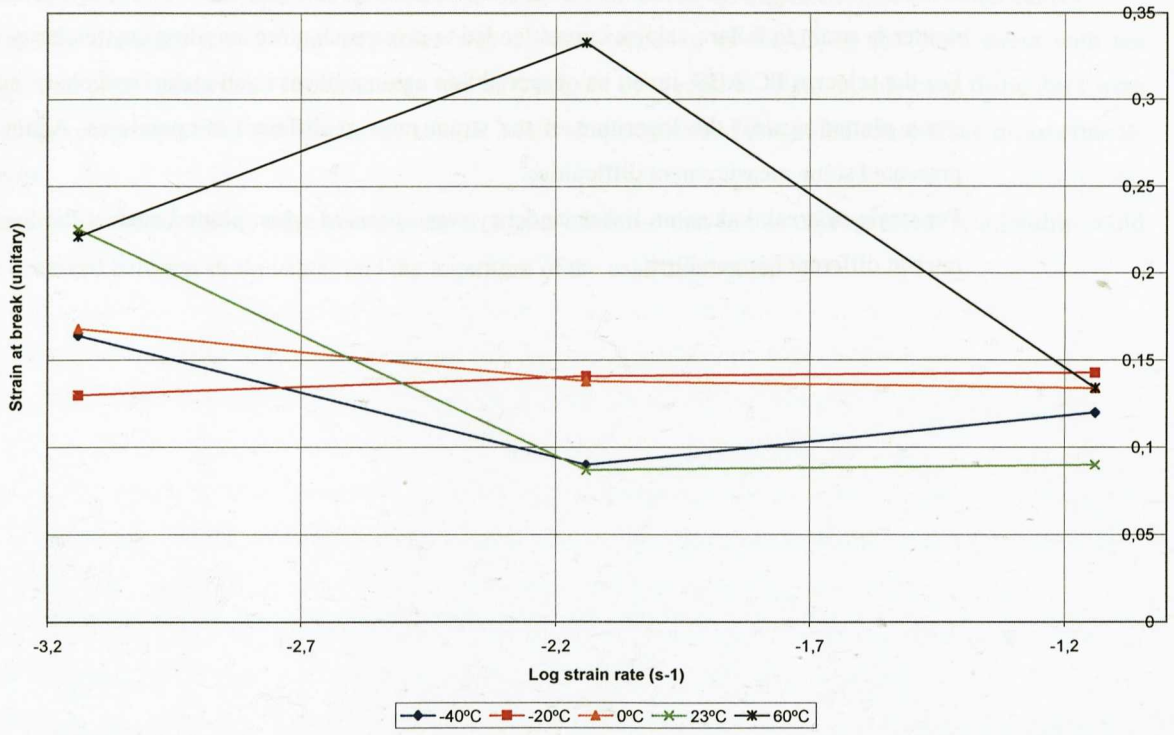

Figure 6.68: Strain at break versus the logarithm of the applied strain rate at different temperatures for PC/ABS.

It was noted that no proper relationship could be observed even without applying logarithms due to the high scatter in strain to failure values; curves tended to cross each other avoiding any tendency derivation.

It was concluded that within the selected range of testing speeds and temperatures the Eyring's model is valid since a linear relationship is obtained between the yield stress and strain rate (logarithmic). This could be later used for data extrapolation to higher or lower testing speeds in order to determine the yield stress at conditions not tested here. The same procedure could be performed in the temperature scale and so would be completed the Eyring's scheme (see section 2.3).

6.4. Experimental Work Part 2: Quasi-Static Finite Element Simulations of PP and PC/ABS.

This section describes the static finite element simulations carried out with the code ANSYS in both the semi-crystalline polypropylene (PP) and the amorphous Polycarbonate+Acrylonitrile-Butadiene-Styrene (PC/ABS).

The experimental tensile tests were simulated with the stress-strain data generated in the same tests. After a process of correction and calibration, bending and puncture tests were simulated taking into account different variables such as the used element type, mesh density or frictional characteristics. The validity of different elasto-plastic models was also studied; the initial results obtained with the traditional Von Mises yielding criteria were compared with the hydrostatic sensitive constitutive model as proposed by Drucker-Prager [10, 26].

6.4.1. Quasi-Static Tensile Test Calibration in ANSYS. Polypropylene.

6.4.1.1. Material Definition.

Any material model to be implemented in the finite element analysis should be calibrated at first in order to check its validity for predicting the experimental data. The simplest, is the tensile test calibration method. As the majority of material models require input of uniaxial tensile data, a common practice is to simulate by finite elements the same experimental test from which true stress-strain data are generated.

In the present study, the first attempt was to simulate the stress-strain curve obtained in tension at 5 mm/min. The first step was to convert the engineering stress-strain data using the classical conversion formula. This assumes that volume incompressibility was considered in plasticity.

A Multilinear Isotropic (MISO) constitutive material model was selected for the elasto-plastic modelling of the material data. A true stress-true total strain curve consisting of 80 pairs of data points was created in ANSYS with the first point corresponding to the proportional limit's yield point of the material (9.183 MPa.). This is an artefact for this elasto-plastic model for a correct definition of the elastic region, as described previously. In addition to this data, elastic data is also needed for the MISO model. A tensile elastic modulus (EX in ANSYS), of 1458.1 MPa. and an elastic Poisson's ratio (PRXY in ANSYS), of 0.38 were also defined. These elastic constants were obtained from the tensile test performed at a speed of 5 mm/min.

6.4.1.2. Finite Element Modelling.

The main objective of the tensile test simulation was to correlate up to the breakage point the full tensile process of the specimen. For this purpose 3D solid element types had to be selected since 3D shell type elements are not useful for simulating the non-homogeneous and triaxial states of straining that occur when a neck is developed in the specimen.

An eight node SOLID 185 element type was selected in ANSYS for meshing the ISO 3167 specimen geometry. A global element size of 1 mm was used for meshing a quarter part of the specimen. Only a quarter part of the specimen was modelled due to symmetry considerations; the specimen is equal in the thickness and in the width directions but although it is also symmetric in the length direction, one side of the specimen is fixed and the other side is moving, so this direction was modelled and not considered symmetric for modelling purposes.

Symmetric boundary conditions were imposed on the surfaces of symmetry plane. Additionally, in order to simulate the clamping system used in the experimental test, the nodes corresponding to those areas were fully constrained. A pilot node was also created to collect the reaction forces that were generated when applying gradually a final displacement value of 40 mm, corresponding to the experimental specimen failure point.

Figure 6.69: Finite element model of the tensile test specimen. SOLID 185 type elements were used.

6.4.1.3. Results.

Force-displacement results obtained in ANSYS and in the experimental test were compared in order to check the validity of this elasto-plastic model for reproducing the tensile test. It was observed that:

1. The stiffness of the initial region of the curve was slightly under-predicted by the simulation response.
2. The high straining region where necking occurred did not correlated closely since a sudden decrease in the simulated curve was observed.

It was observed that this decrease was due to the fact than in the simulation, for displacement regions above 9 mm, the input stress-strain data was insufficient to represent the high straining zone. ANSYS extrapolates with a zero slope curve when the material is being strained above the input stress-strain data. This zero slope extrapolation was responsible of the decrease in the simulation curve. Thus, the material input curve had to be corrected adding stress-strain data points above the initial input curve. The curve was extended with a slope curve of 44.4 MPa. This slope value was calculated from the tendency of the stress-strain curve before failure and iteratively comparing the simulation results with the experimental ones.

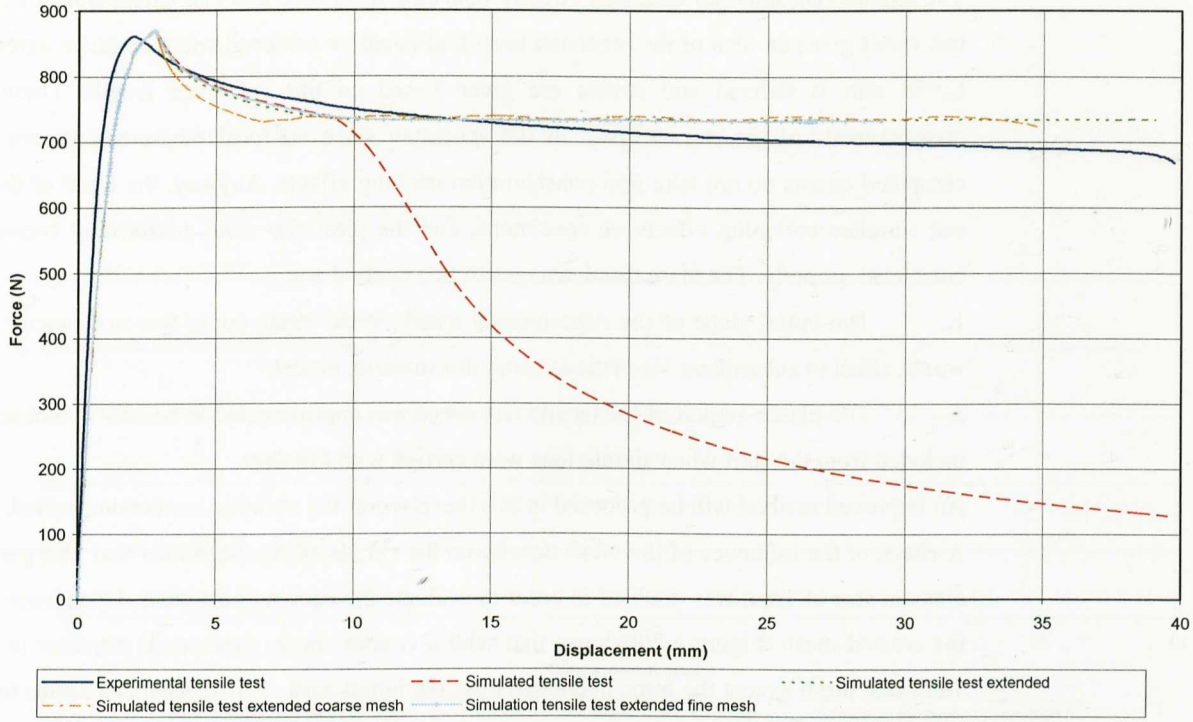

Fig. 6.70: Comparison of experimental and simulated tensile test curves.

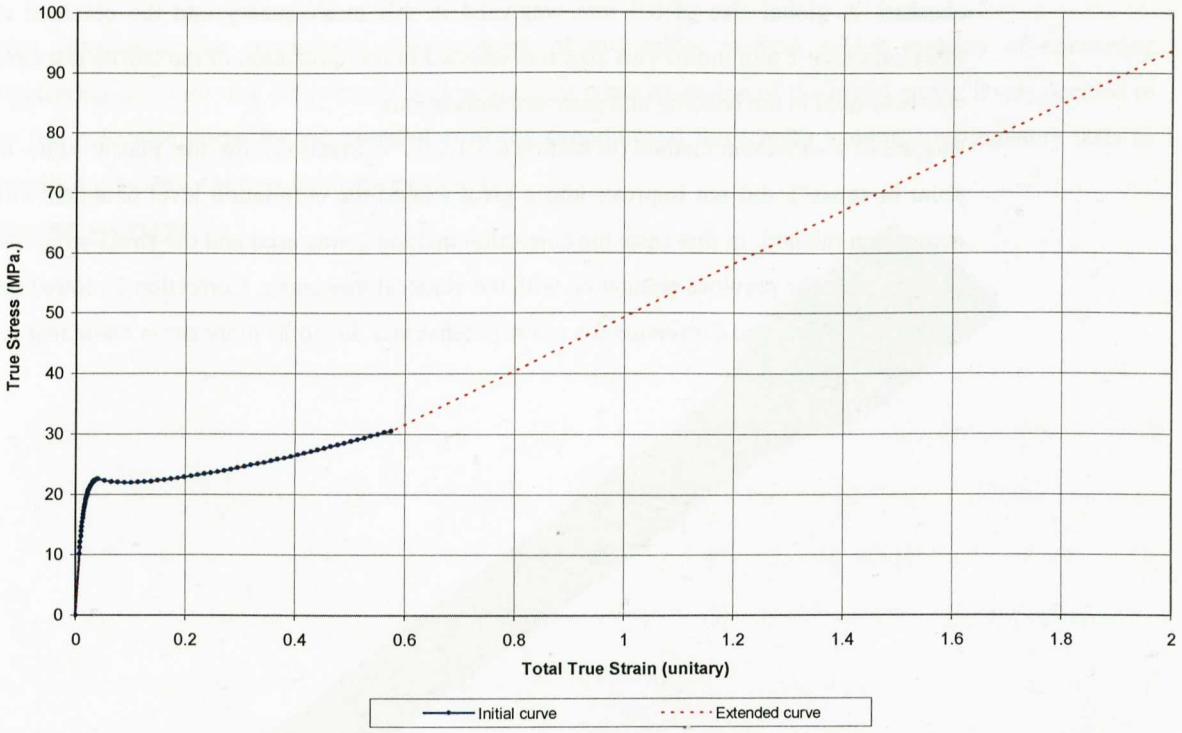

Fig. 6.71: The initial curve from the tensile test was necessary to be extended in order to correlate properly the experimental tensile test.

The comparison of force-displacement data in Fig. 6.72 gives an idea about the correlation level that could be achieved with the use of a true stress-strain curve obtained from the classical conversion of engineering data (volume incompressibility in plasticity), in conjunction with a MISO elasto-plastic model.

The engineering material data was directly collected from load cell and extensometer measurements. Thus, this result gives an idea of the precision level that could be achieved when common extensometry is used; a L_0=50 mm is defined and strains are given based on this reference length. These strains are mean measurements of the strains given in the specimen since no local measurements are performed, so the computed strains do not take into consideration necking effects. Anyway, the input of the calculated curves can simulate softening effects on specimens, and the plasticity zone, performing corrections, can also be correlated properly. The main disadvantages of this method are:

1. The initial slope of the experimental tensile stress-strain curve was not exactly reproduced, which would affect to subsequent simulations using this material model.
2. The plastic region of the tensile test curve was approximated in some way but some error would be included from the start when simulations were carried with this data.

An improved method will be proposed in this thesis work: the iterative correction method.

A check of the influence of the mesh density on the simulated tensile results was also performed. The initial element size of 1mm was doubled in order to evaluate the necking behaviour dependence on the precision of the created mesh. Figure 6.70. shows that with a coarser mesh, the overall response is very similar to the 1mm fine mesh except the force decreased after the initial peak. This mechanism seems to be sensitive to the mesh quality. In this work, the 1 mm mesh is considered to be fine enough for representing the different specimen geometries, while the 2 mm mesh is somewhat rough. Thus, the 1mm mesh results and its correlation with the experimental curve are considered satisfactory. Additionally a finer mesh was also checked. A global size of 0.5 mm was used in this mesh quality and the obtained results were almost identical to the 1 mm mesh. This size was selected in the simulation of the tensile test since this mesh quality was later used in the bending and puncture simulations.

The use of a correction method (in section 6.3.1.2.3. "Corrections for the plastic zone from the maximum point in stress"), did not improve into a great extend the correlation level obtained with the classical true conversion method. In this case, the correction method 2 was used and the stress-strain data was extended as in the case of the previous simulation with the classical true curve. Correction 1 offered a too soft response in the plasticity area and Correction 3 a too stiff behaviour due to its more strain hardening response.

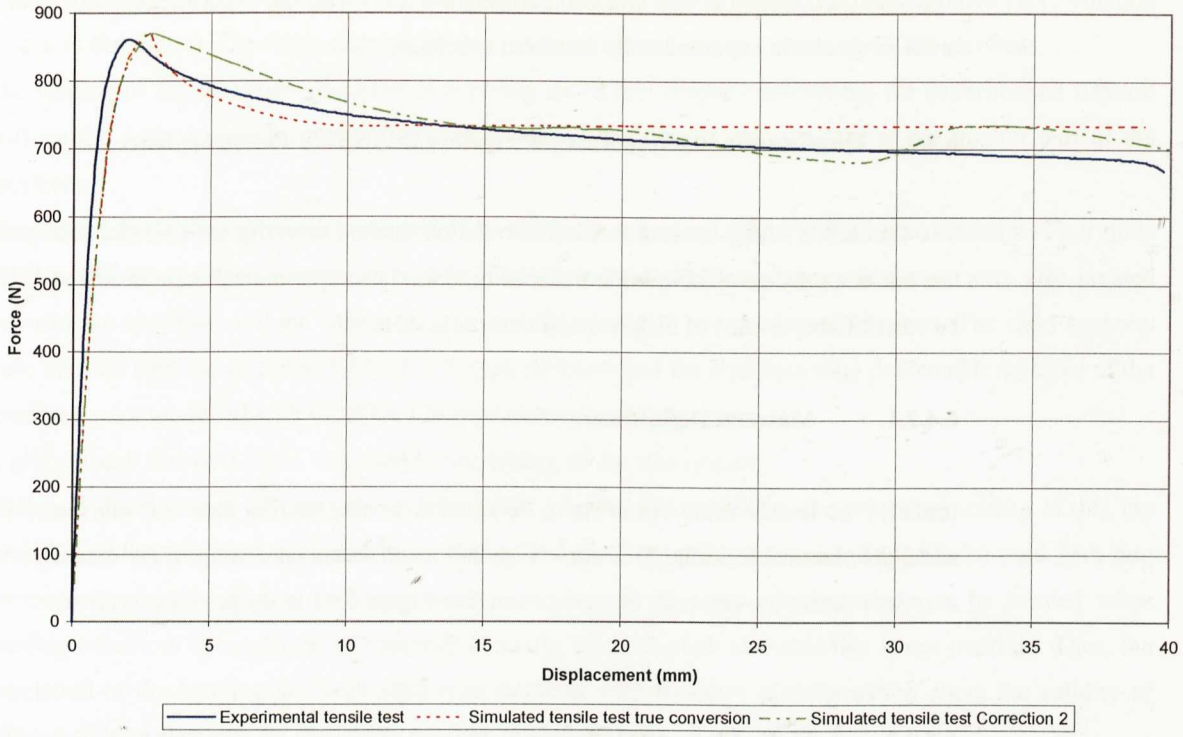

Figure 6.72: Correlation of the experimental tensile test with the MISO model. The classical true conversion method and Correction 2 method are compared.

Even considering the commented disadvantages of this initial method, which consists of converting engineering data into true data directly and performing some extension of the initial curve, it was decided to use the generated curve for the correlation of the experimental three point bending and puncture tests as described previously and so, evaluate its validity.

Figure 6.73: Simulated tensile test in PP. Von Mises stress contours can be observed.

The simulated response was in a good correlation level with the experimental behaviour. See Figure 6.16 in order to check the experimentally fractured specimen.

6.4.2. Quasi-Static Bending Test Correlation in ANSYS. Polypropylene.

The simulation of the flexural test is a correlation method to verify the material data generated in the tensile test and the selected elasto-plastic material models. The experimental data presented in the section 6.3.2 will be correlated by means of different simulations in ANSYS.

6.4.2.1. Material Definition.

Initially, the tensile stress-strain curve obtained from engineering data was converted into true expressions using the classical formula. This curve also had a correction consisting of the extension of the plasticity area in order to calibrate correctly the tensile test (see Figure 6.71 in the previous section).

6.4.2.2. Finite Element Modelling.

Two approaches were considered for modelling the flexural specimen. The first approach defined the specimen with the use of solid hexahedral elements. Eight node SOLID 185 type elements were selected in ANSYS for this purpose. Contact elements were also created between the specimen and the central support and the specimen and the lateral supports. The rigid supports were meshed with the so called TARGE 170 type elements and the corresponding deformable surfaces of the specimen were modelled with CONTA 174 type elements.

A global mesh size of 0.5 mm was used for modelling all the test system. This produced a very good quality mesh in the specimen; when bending characteristics are needed to capture by simulation, a sufficient element number have to be located through the thickness (usual recommendation is > 2 elements). In this case, eight hexahedral elements were located through the thickness of the specimen.

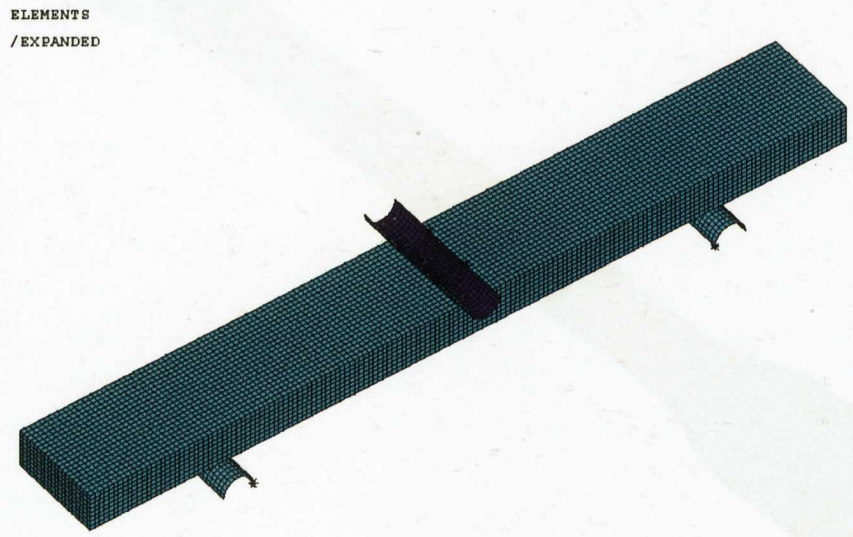

Figure 6.74: Finite element model of the flexural test specimen. SOLID 185 type elements were used for meshing the plastic part.

Due to symmetry, only a quarter of the full geometry was modelled in ANSYS (an expanded representation is seen in the figure). The finite element for this model consisted of 8442 nodes and 7262 elements.

The loading of the specimen consisted of applying an 18 mm displacement (from the experimental flexural test) on the central rigid support. Additional symmetry conditions were applied to the quarter part of the specimen.

The second modelling approach consisted of meshing the specimen with 3D shell type elements. Four node SHELL 181 type elements were selected in ANSYS for this purpose. Contact elements were also created between the specimen and the central support and the specimen and the lateral supports. The rigid supports were meshed with the so called TARGE 170 type elements and the corresponding deformable surfaces of the specimen were modelled with CONTA 174 type elements.

A global mesh size of 0.5 mm was used for modelling all the test system.

The main disadvantage of using this type of shell element for modelling the present specimen is that the thickness of the specimen is considerable, 4 mm, and shell type elements are intended to be used with thin components. Additionally, a sufficient number of through thickness elements have to be located when bending behaviour is needed to be captured correctly but with shell elements this is not possible. Thus, the simulation of the bending test with shell type elements will also give us information about the validity of using shell type elements for modelling medium thickness parts.

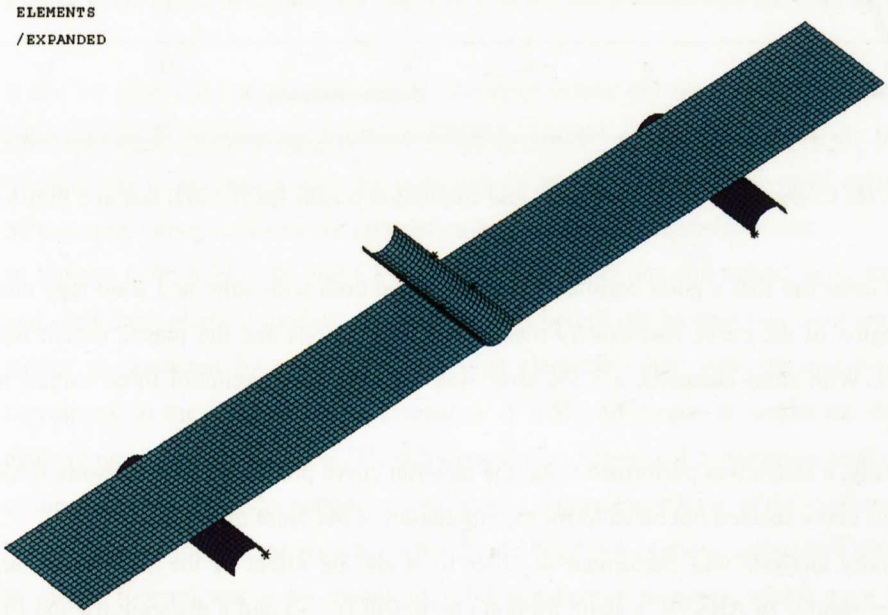

Figure 6.75: Finite element model of the flexural test specimen. SHELL 181 type elements were used for meshing the plastic part.

Due to symmetry considerations, only a quarter of the full geometry was modelled in ANSYS (an expanded representation is seen in the figure). The finite element for this model consisted of 1314 nodes and 1762 elements.

The loading of the specimen consisted of applying an 18 mm displacement (from the experimental flexural test) on the central rigid support. Additional symmetry conditions were applied to the quarter part of the specimen.

No strain rate sensitivity was included in the MISO model. No frictional effects were included between the specimen and the supports.

6.4.2.3. Results.

First simulation results were obtained performing a comparison analysis between solid and shell type elements.

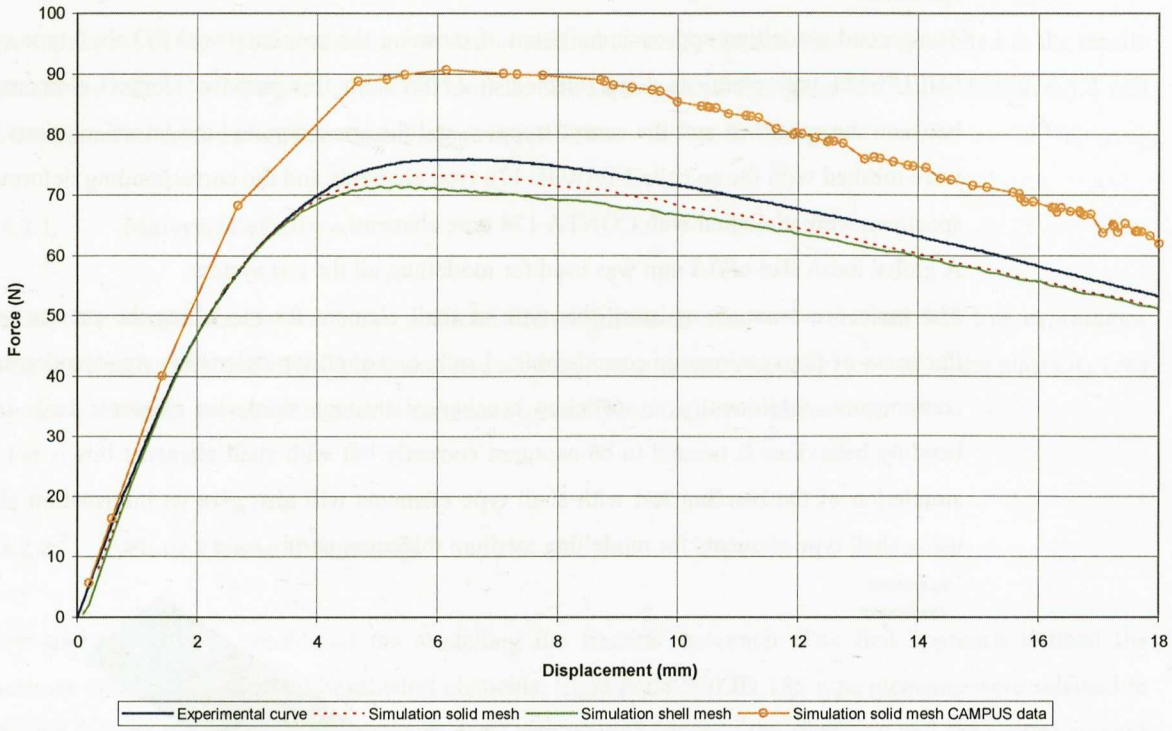

Figure 6.76: Comparison of experimental and simulation results for flexural test at 5 mm/min.

It can be observed that a good correlation was obtained both with solid and shell type elements. The initial elastic region of the curve was exactly matched by simulations and the plastic region was also adequately described. With solid elements, a 3.3% error was found in the maximum force values, to 6.5 % for shell elements.

Additionally, a check was performed using the material curve provided in the software CAMPUS (see Figure 6.64). This curve seemed not be valid for the simulation of the 5mm/min. tests.

A sensitivity analysis was performed in order to study the effect of the frictional characteristics on the simulation results. In ANSYS, a static friction coefficient (μ_{static}) and a dynamic friction ($\mu_{dynamic}$) coefficient can be defined for the contact interfaces. For this study an arbitrary value of 0.60 was selected for μ_{static} and a half value of 0.30 for $\mu_{dynamic}$. An additional study was performed using half values for both coefficients; μ_{static}=0.30, $\mu_{dynamic}$=0.15

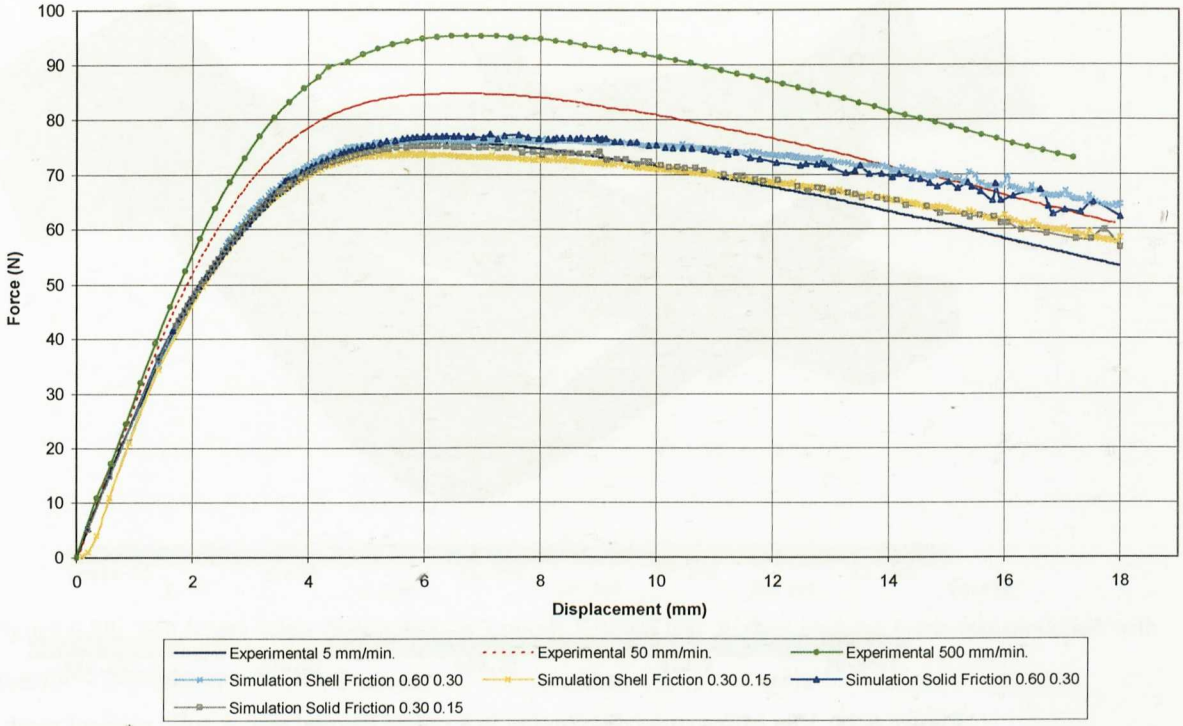

Figure 6.77: Effect of the friction coefficient on the simulated results for solid and shell type elements.

It can be observed that the addition of frictional values did not improve the simulation response; both for solid and shell element types. The simulated curves tend to be stiffer in the plastic region which is not qualitatively in agreement with the experimental results. Additionally, force values tend to approximate the 50 mm/min. curve, reducing the correlation level with the 5 mm/min. curve.

In Figures 6.78, 6.79, 6.80 and 6.81, the Von Mises stresses and strains generated using both type of solid and shell finite element models are represented, where it can be seen that there are differences in stresses and strains as predicted by solid and mesh type elements (shell type element results should comparatively correspond to the solid top surface results). A 6.5% difference in maximum stress values exists for each element type. Approximately a 21% difference exists between the maximum total strains on the upper surface of the solid model and the maximum total strains on the upper layer of the shell model. These differences can be attributed to the lack of accuracy when modelling thick sections using shell elements. The appropiate way to model flexural test is by means of solid hexahedral elements, which gave the best approximation to experimental force-displacement data.

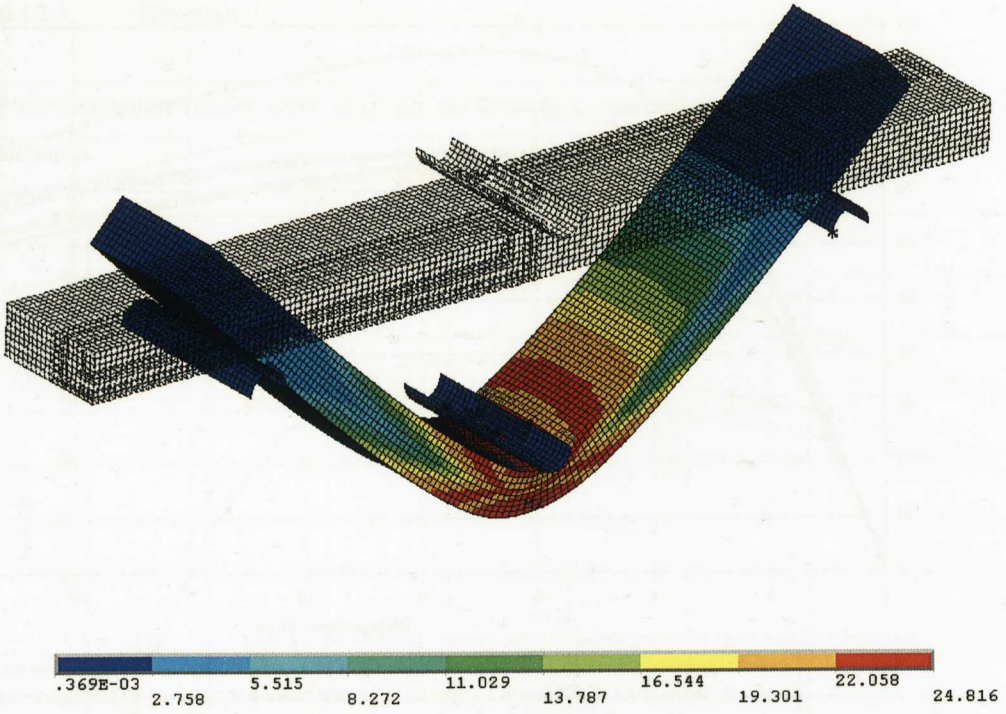

Figure 6.78: Von Mises stress distribution in 3 points flexural test. A solid element mesh was modelled with an applied displacement of 18 mm.

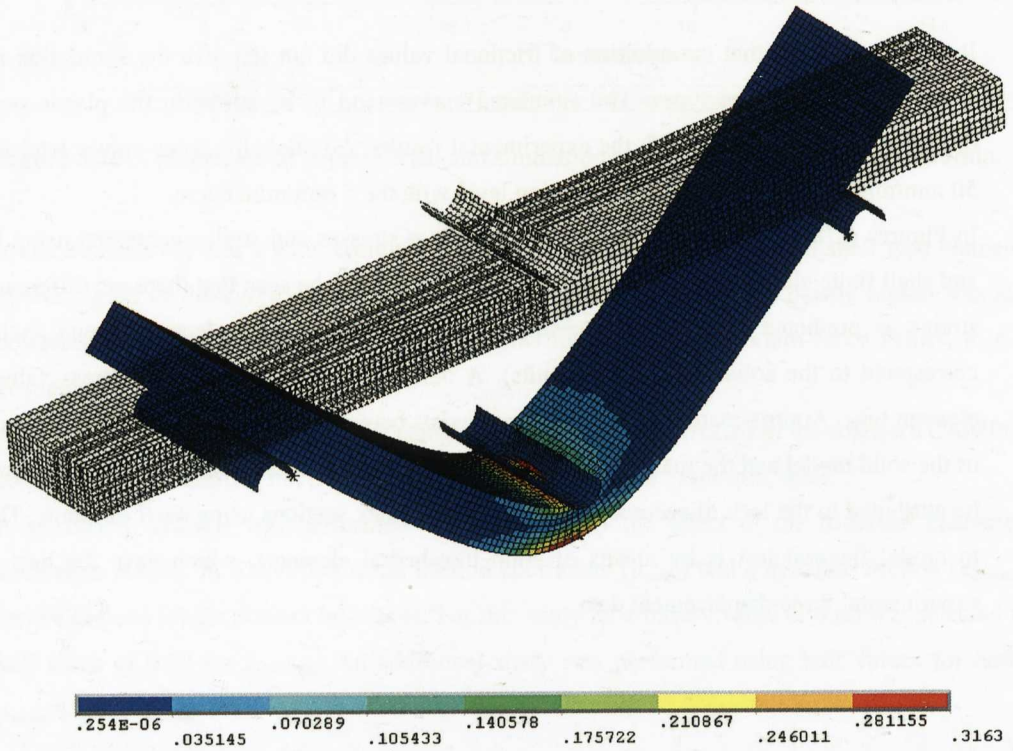

Figure 6.79: Von Mises total strain distribution in 3 points flexural test. A solid element mesh was modelled with an applied displacement of 18 mm.

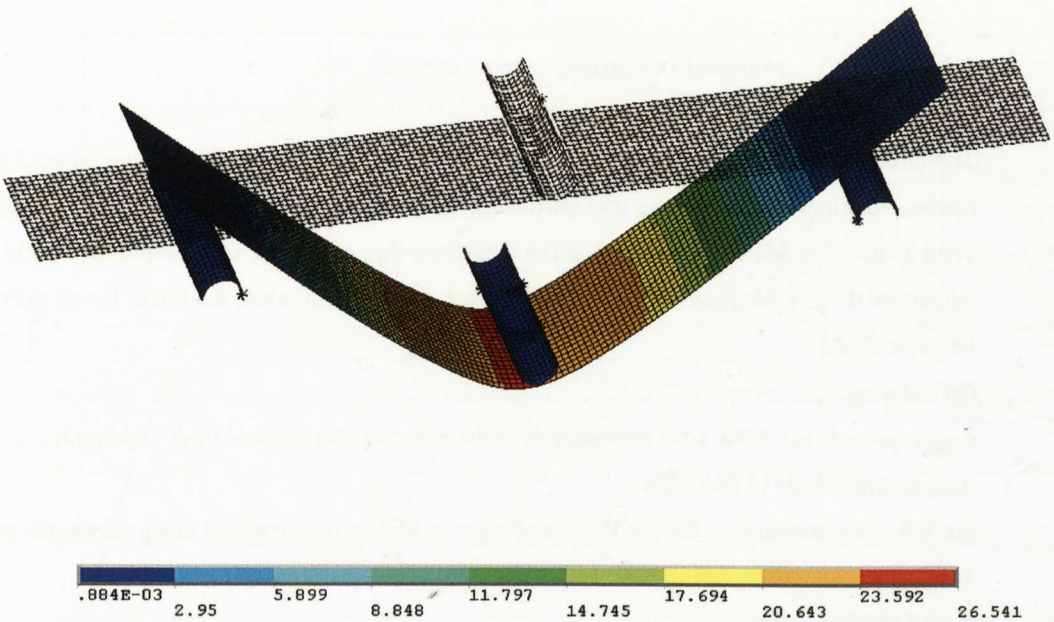

Figure 6.80: Von Mises stress distribution in 3 points flexural test. A shell element mesh was modelled with an applied displacement of 18 mm.

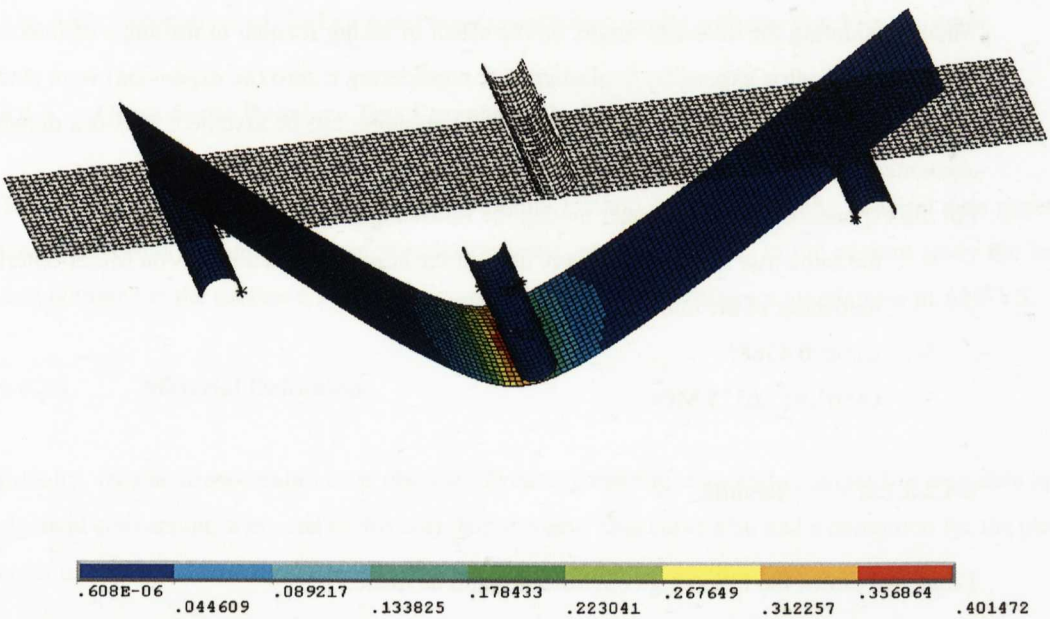

Figure 6.81: Von Mises total strain distribution in 3 points flexural test. A shell element mesh was modelled with an applied displacement of 18 mm.

6.4.2.3.1. Bending Simulation. Use of a Hydrostatic Sensitive Constitutive Model: Drucker-Prager. Polypropylene.

The aim of this study was to examine the effect of accounting for hydrostatic effects with the use of a proper constitutive model in ANSYS. The first simulations were carried out with the MISO elasto-plastic model considering the Von Mises yield criteria. As stated earlier in the theoretical section of the thesis (2.2.1.5.), thermoplastic materials are sensitive to hydrostatic stresses. This contributes to differences in tensile and compressive yield stresses. The bending test was considered an ideal experiment to test these effects since the specimen is subjected principally to both tensile and compressive loads.

6.4.2.3.1.1. Material Definition.

The Drucker-Prager material model was used to model the different yield values in tensile and compressive modes. No compression testing was performed. Instead, a general relation between compressive and tensile yield as given in [5] was used. Using the data from this reference, the compressive yield stress for PP was calculated to be 1.34 times the tensile yield stress. With this in mind, the linear Drucker-Prager material card was calculated.

Considering,

σ_{yield} tensile=9.183 MPa. (this corresponds to the selected proportional limit yield point), and

σ_{yield} compressive=12.665 MPa.

the following parameters for the Drucker-Prager model were calculated using relationships given in Chapter 4.

σ_y=6.735 MPa.

β=0.0841

θ=10.75°

c=5.554 MPa.

when considering the dilatancy angle, θ_f, the effect of taking it equal to the angle of internal friction, θ, (this supposes volumetric expansion in plasticity) or considering it zero (no expansion) were studied.

In the linear Drucker-Prager model, no material hardening can be assumed. This is a drawback which can be accounted for using exponential Drucker-Prager model.

For the exponential Drucker-Prager model, the following parameters were defined:

- the same true stress-strain curve used in the simulations with the Von Mises criteria (this defines the hardening of the material).
- $C_1=\alpha$=0.4368°
- $C_2=\sigma'_y$=17.6375 MPa.

6.4.2.3.1.2. Results.

From the results, the following conclusions could be made:

- the use of a perfectly plastic model with no hardening (as the case of the linear Drucker-Prager model) does not give satisfactory results. The bending response of the material was in a higher level of forces. A check was performed in order to determine the differences with a Von Mises model and considering again no hardening. The bending response was even in a lower position.
- with the linear Drucker-Prager model, there was practically no effect on changing the volumetric expansion option.
- the experimental data was fitted better using the exponential Drucker-Prager model than the Von Mises criteria. The use of a hydrostatic sensitivity yield model tends to stiffen the bending response of the material. This is beneficial since the results obtained from the Von Mises model were always lower than the experimental curves.

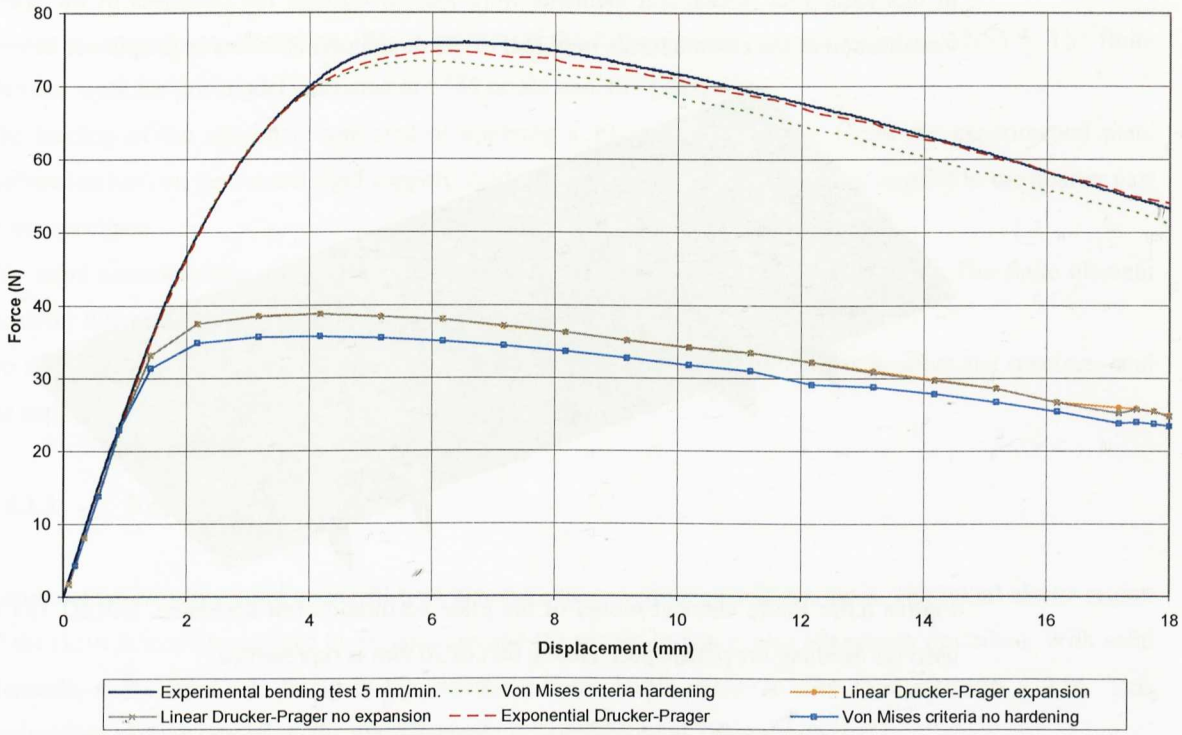

Fig. 6.82: Comparison of the Drucker-Prager constitutive model with the Von Mises criteria.

6.4.3. Quasi-Static Puncture Test Correlation in ANSYS. Polypropylene.

The simulation of the puncture test is a correlation method for validating the material data generated in the tensile test, and the application of the elasto-plastic material models. In the present study the experimental data obtained in the section 6.3.3 will be correlated by means of different simulations in ANSYS.

6.4.3.1. Material Definition.

Initially, tensile stress-strain curve obtained from engineering data and converted to true data applying the classical conversion, was used in this correlation study. This curve also had a correction for the plastic area in order to calibrate correctly the tensile test. See Figure 6.71.

6.4.3.2. Finite Element Modelling.

Two approaches were considered for modelling the square shaped plate specimen. The first approach defined the specimen with the use of solid hexahedral elements. Eight node SOLID 185 type elements were selected in ANSYS for this purpose. Contact elements were also created between the specimen and the penetrating dart and the specimen and the base support. The rigid supports were meshed with the so called TARGE 170 type elements and the corresponding deformable surfaces of the specimen were modelled with CONTA 174 type elements.

A global mesh size of 0.5 mm was used for modelling the region in contact with the hemispherical indenter. A coarser mesh was used for the rest of the specimen (2 mm). This produced a very good quality mesh in the critical regions of the specimen. When bending characteristics are needed to capture by simulation, a sufficient element number have to be located through the thickness (usual recommendation is > 2 elements).

In this case, four hexahedral elements were located through the thickness of the specimen. For a better visualisation of the created mesh, only half of the model part is shown in the picture below:

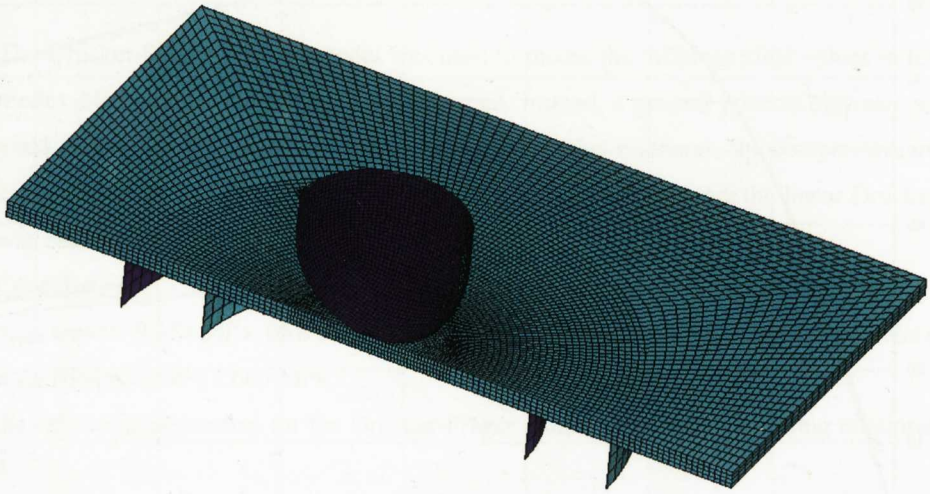

Figure 6.83: Finite element model of the plate perforation test specimen. SOLID 185 type elements were used for meshing the plastic part. Here a dart of 20 mm is represented.

Due to symmetry considerations, only a quarter part of the full geometry was modelled in ANSYS. The finite element mesh for this model consisted of 19494 nodes and 17671 elements.

The loading of the specimen consisted of applying a 13 mm displacement (from the experimental plate perforation test) on the central rigid support. Additional symmetry conditions were applied to the quarter part of the specimen. The same considerations were taken into account for the 11.7mm diameter dart model. The finite element mesh for this model consisted of 19494 nodes and 17671 elements again.

The second modelling approach consisted of meshing the specimen with 3D shell type elements. Four node SHELL 181 type elements were selected in ANSYS for this purpose. Contact elements were also created between the specimen and the central support and the specimen and the base support. The rigid supports were meshed with the so called TARGE 170 type elements and the corresponding deformable surfaces of the specimen were modelled with CONTA 174 type elements.

A global mesh size of 0.5 mm was used for modelling the region in contact with the hemispherical striker. Coarser mesh was used for the rest of the specimen (2 mm). This produced a very good quality mesh in the critical regions of the specimen.

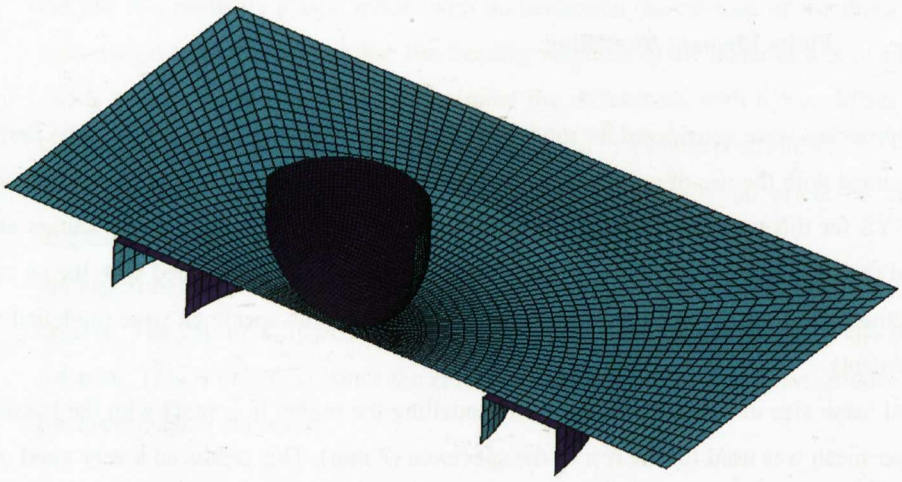

Figure 6.84: Finite element model of the plate perforation test specimen. SHELL 181 type elements were used for meshing the plastic part. Here a dart of 20 mm is represented.

Due to symmetry considerations, only a quarter of the full geometry was modelled in ANSYS. The finite element mesh for this model consisted of 8488 nodes and 4072 elements.

The loading of the specimen consisted of applying a 13 mm displacement (from the experimental plate perforation test) on the central rigid support. Additional symmetry conditions were applied to the quarter part of the specimen.

The same considerations were taken into account for the 11.7mm diameter dart model. The finite element mesh for this model consisted of 8488 nodes and 4072 elements again.

No strain rate sensitivity was incorporated in the MISO model. Frictional effects between the specimen and the supports were not considered.

6.4.3.3. Results.

Results obtained using solid and shell type elements show a good correlation level. The initial elastic region of the curve is exactly matched by simulations and the plastic region is also adequately described. With solid elements, a 5% error was found in the maximum force levels, whereas with shell elements a 9 %. This comparison was performed on the experimental curve produced at 20 mm/min.

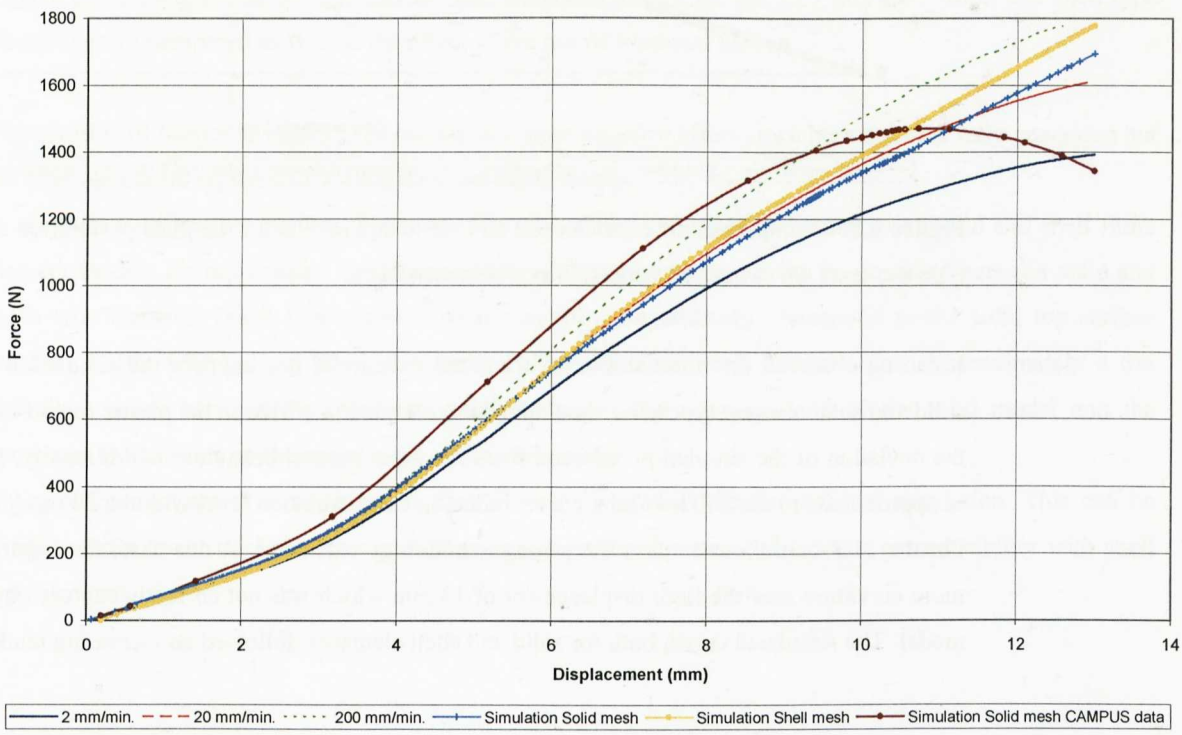

Figure 6.85: Comparison of experimental and simulated results for the plate perforation test. Solid and shell type elements were compared.

The tensile input curve tested at 5 mm/min. seems to be a high testing speed for correlating the slowest curve at 2 mm/min. Once again, data from the software CAMPUS gave a higher response than the experimental curves.

It can be seen that shell type elements offered a stiffer response than solid elements in this case (the contrary behaviour was given in the bending test). This has to be considered in terms of element straining under the dart and the intrinsic shell elements' behaviour.

A sensitivity analysis was performed in order to study the effect of the frictional characteristics on the simulation results. In ANSYS, a static friction coefficient (μ_{static}) and a dynamic friction ($\mu_{dynamic}$) coefficient can be defined in the contact interfaces. For this study an arbitrary value of 0.30 was selected for μstatic and a half value of 0.15 for $\mu_{dynamic}$. No higher frictional values were selected since the simulated response was initially located in an intermediate state between 2 and 200 mm/min., matching the 20 mm/min. curve.

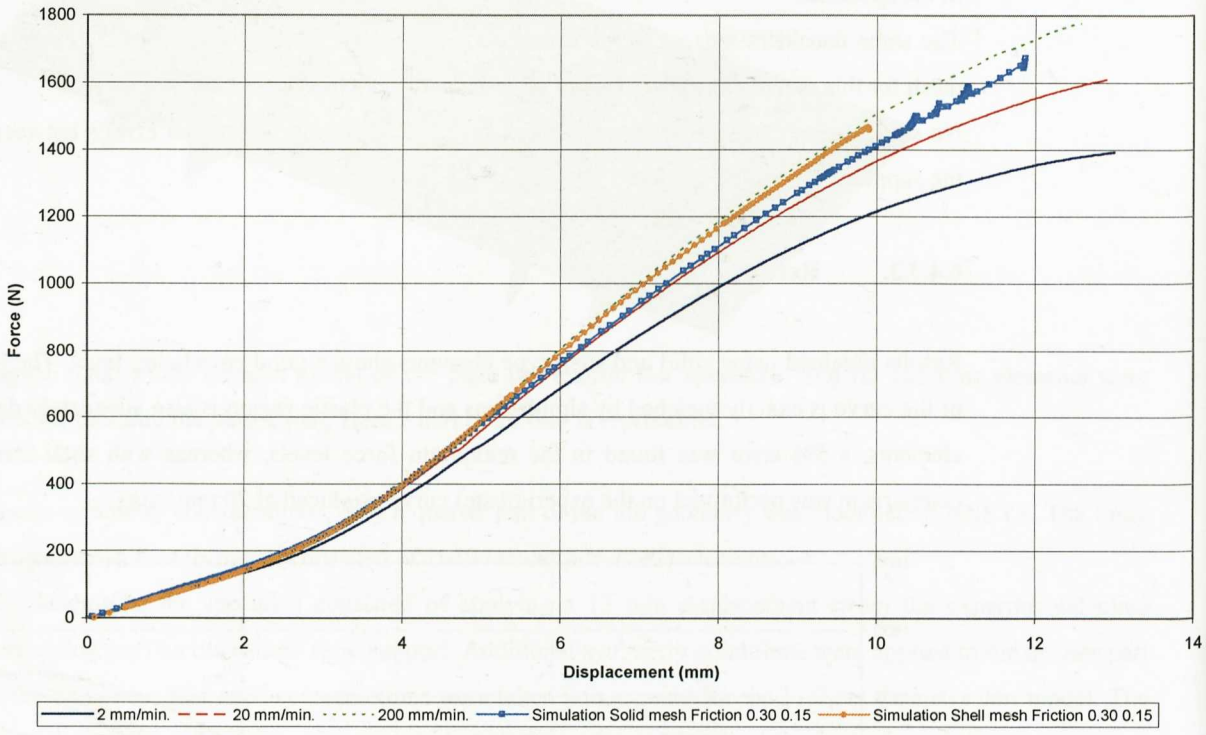

Figure 6.86: Comparison of experimental and simulated results for the plate perforation test. Solid and shell type elements are compared with frictional characteristics.

It can be observed that the addition of frictional values did not improve the simulation response; both for solid and shell element types, the simulated curves tended to stiffen in the plastic region which could produce the deviation of the simulation response from the experimental behaviour. Additionally, force values tended to approximate to the 200 mm/min. curve, reducing the correlation level with the 20 mm/min. curve.

For the 11.7 mm diameter dart, the same methodology was used. In this case, the experimental curves had more curvature near the limit displacement of 13 mm which was not correctly captured by the finite element model. The simulated curve, both for solid and shell elements, followed an increasing tendency.

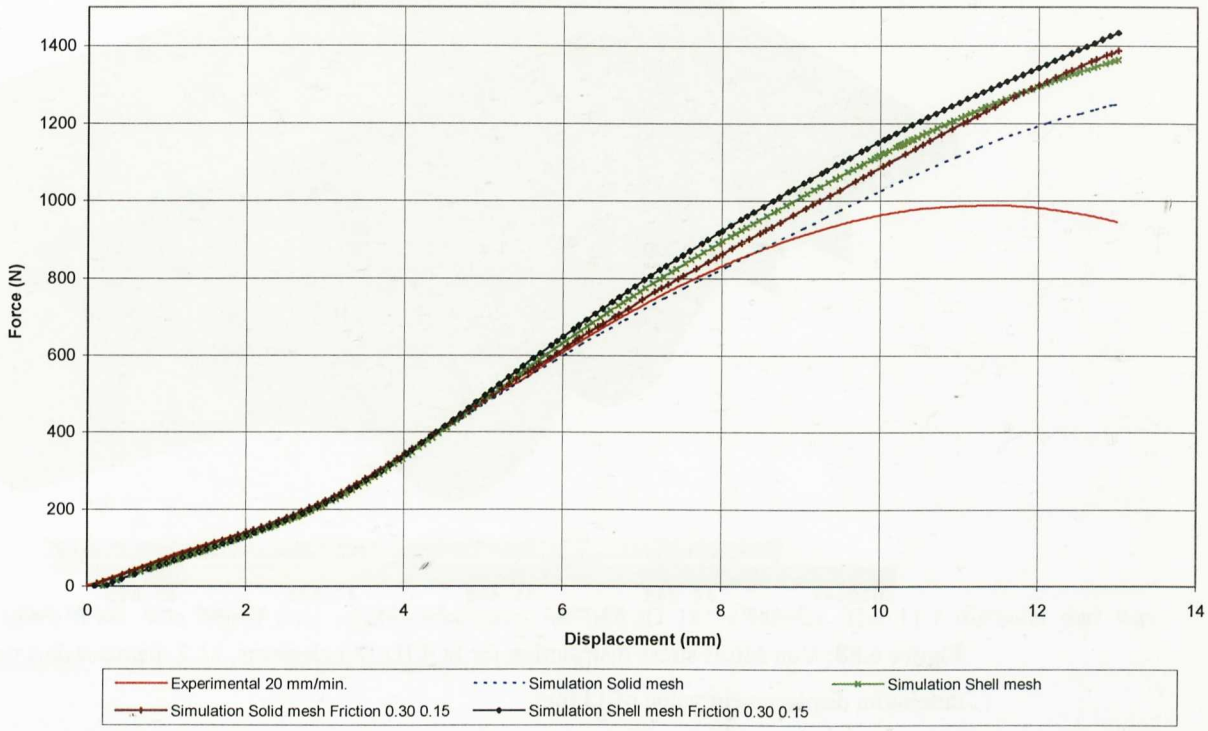

Figure 6.87: Comparison of experimental and simulated curves for the 11.7 mm dart. Solid and shell type elements were compared as well as the effect of the use of frictional values.

The addition of frictional values even produced a more negative effect since higher forces were generated but the ultimate plastic region still did not matched qualitatively.

In the following graphs, the Von Mises stresses and strains generated in both type of solid and shell finite element models are represented. Differences both in stresses and strains can be observed between solid and mesh type elements (shell type element results should comparatively correspond to the solid top surface results). A 1% difference in maximum stress values exists for each element type. Approximately a 6% difference exists between the maximum total strains on the upper surface of the solid model and the maximum total strains on the upper layer of the shell model.

These differences are now much lower than those registered in the flexural test simulation. This can be attributed to a lower thickness specimen in the plate perforation test and a better reproducibility with shell type elements.

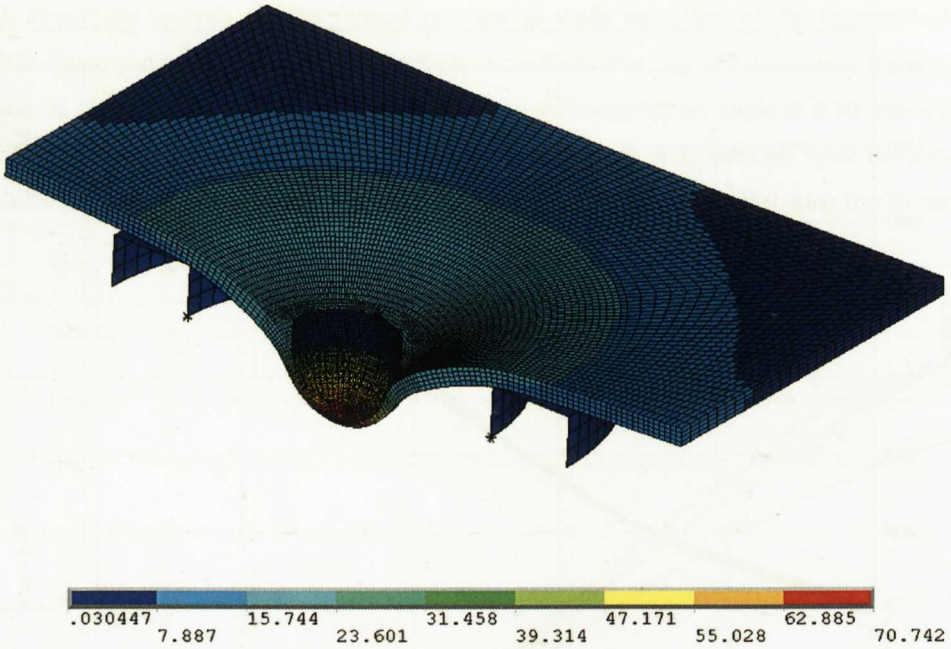

Figure 6.88: Von Mises stress distribution for SOLID 185 elements. 11.7 diameter dart was modelled, with a maximum displacement value of 13 mm.

A closer representation of the deformed specimens gives the location of maximum stresses at the centre of the specimen where the dart is acting.

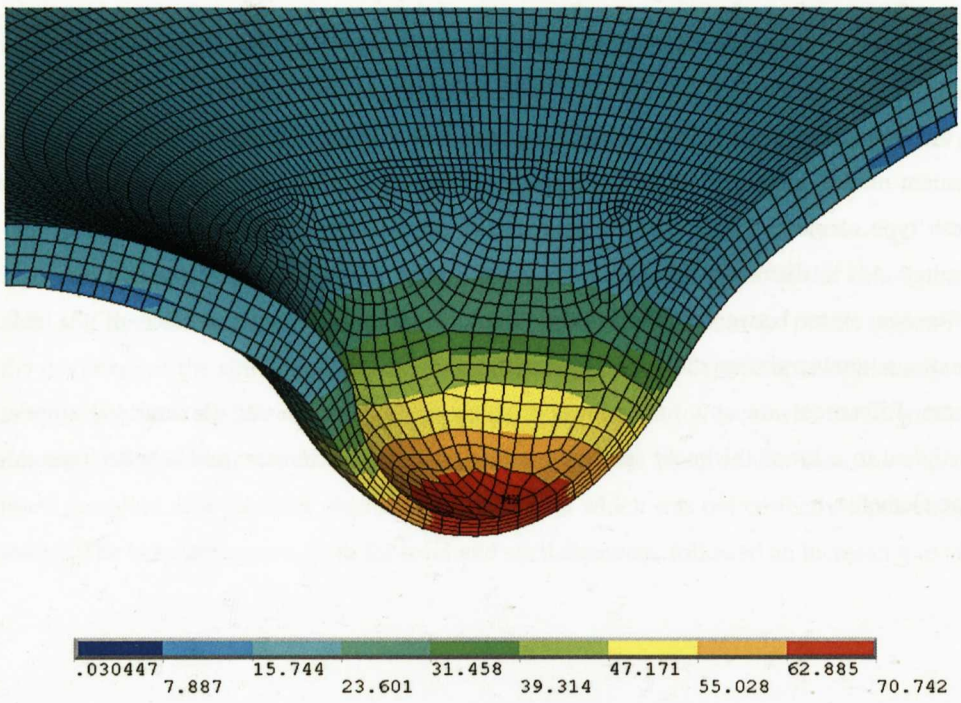

Figure 6.89: Von Mises stress distribution for SOLID 185 elements. The 11.7 diameter dart was modelled, with a maximum displacement value of 13 mm.

The Von Mises total strain distribution is also located around the dart action. High maximum strain levels are given (141%).

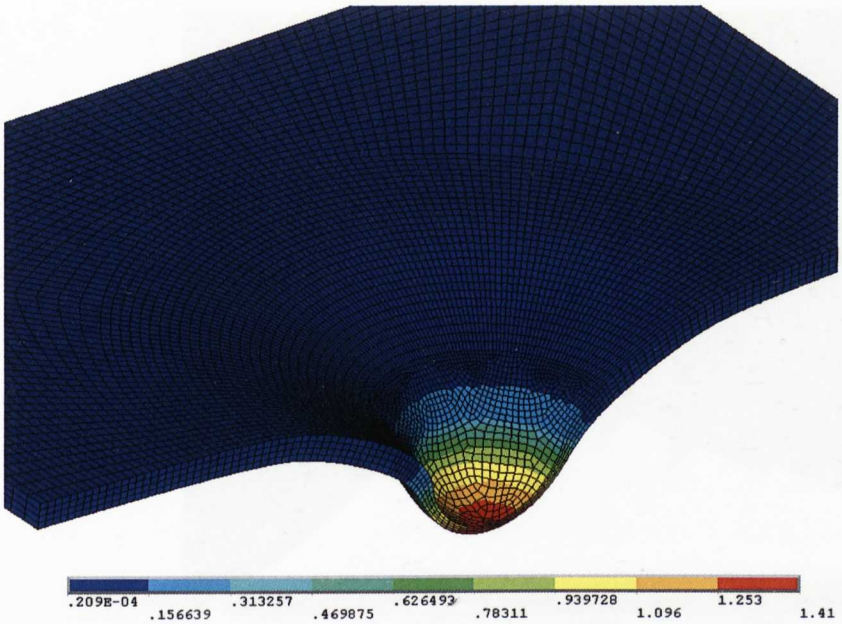

Figure 6.90: Von Mises total strain distribution for SOLID 185 elements. The 11.7 diameter dart was modelled, with a maximum displacement value of 13 mm.

For SHELL 181 elements,

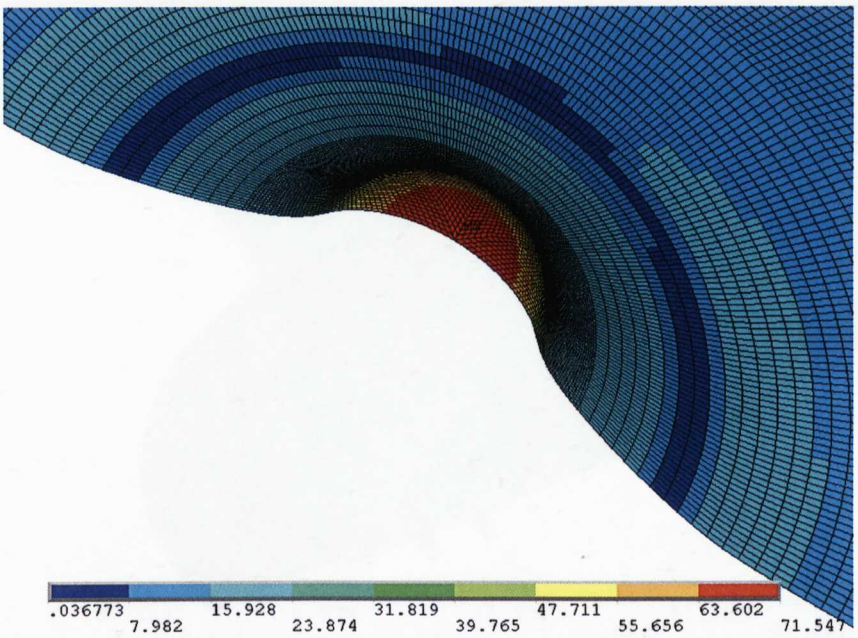

Figure 6.91: Von Mises stress distribution for SHELL 181 elements. 11.7 diameter dart was modelled, with a maximum displacement value of 13 mm.

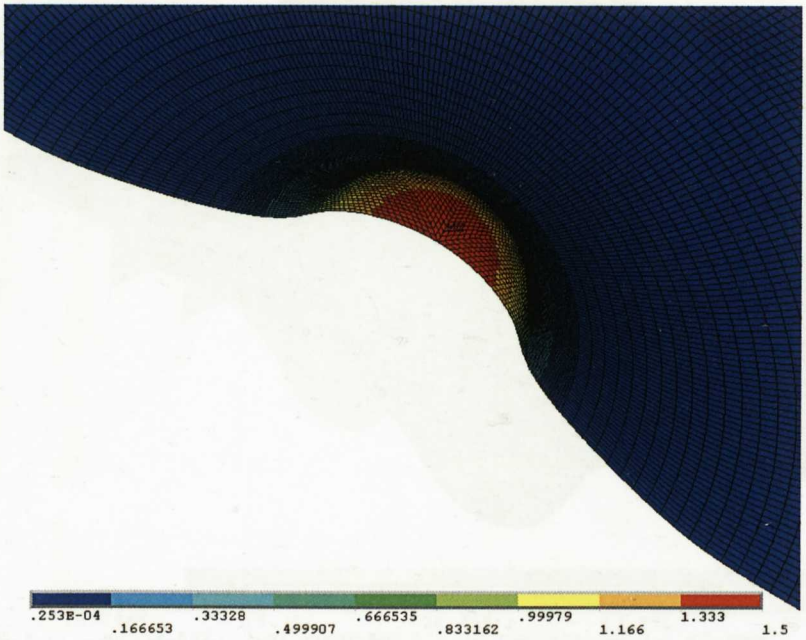

Figure 6.92: Von Mises total strain distribution for SHELL 181 elements. The 11.7 diameter dart was modelled, with a maximum displacement value of 13 mm.

The effect of clamping the specimens on the force-displacement behaviour was also studied in ANSYS. In the following picture the created solid mesh can be observed. In addition to the previous model, a top surface was created which simulated the clamping effect of the real metallic part in the testing device. This was a rigid surface modelled with TARGE 170 type elements. Correspondent CONTA 174 flexible surface were also modelled in the specimen in order to detect contact between the two surfaces.

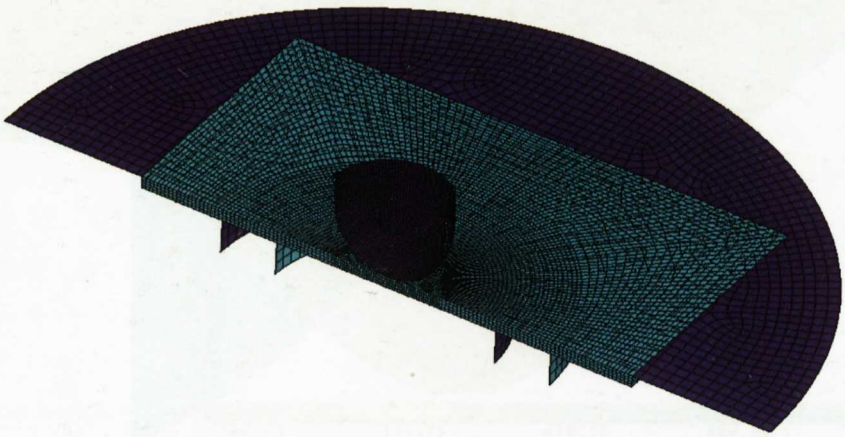

Figure 6.93: 3D solid mesh model of the clamped specimen. A 20 mm dart was modelled.

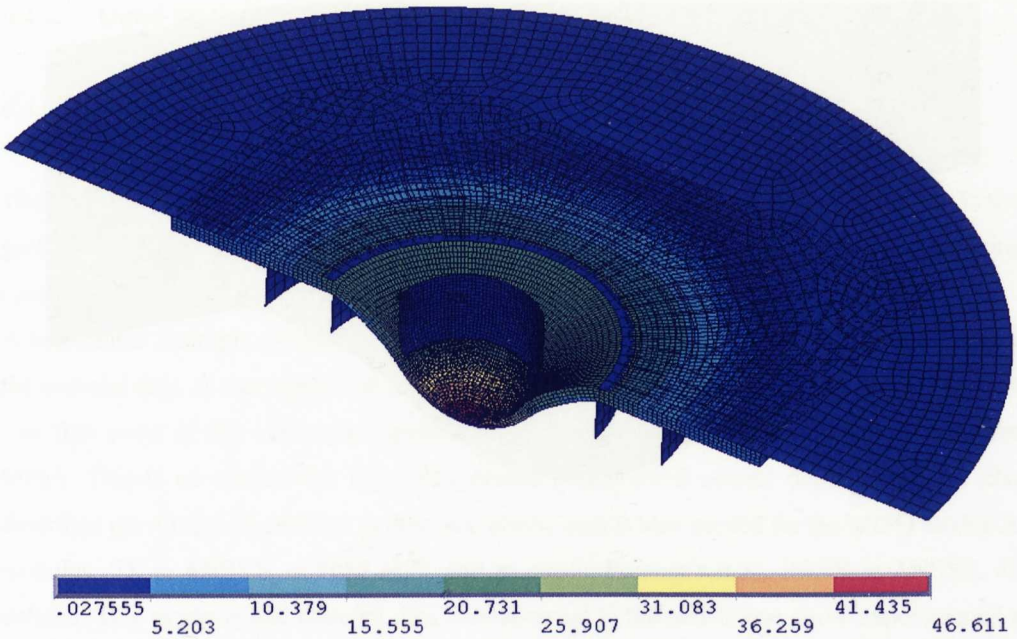

Figure 6.94: Von Mises stress distribution for the clamped specimen. A 20 mm dart was modelled.

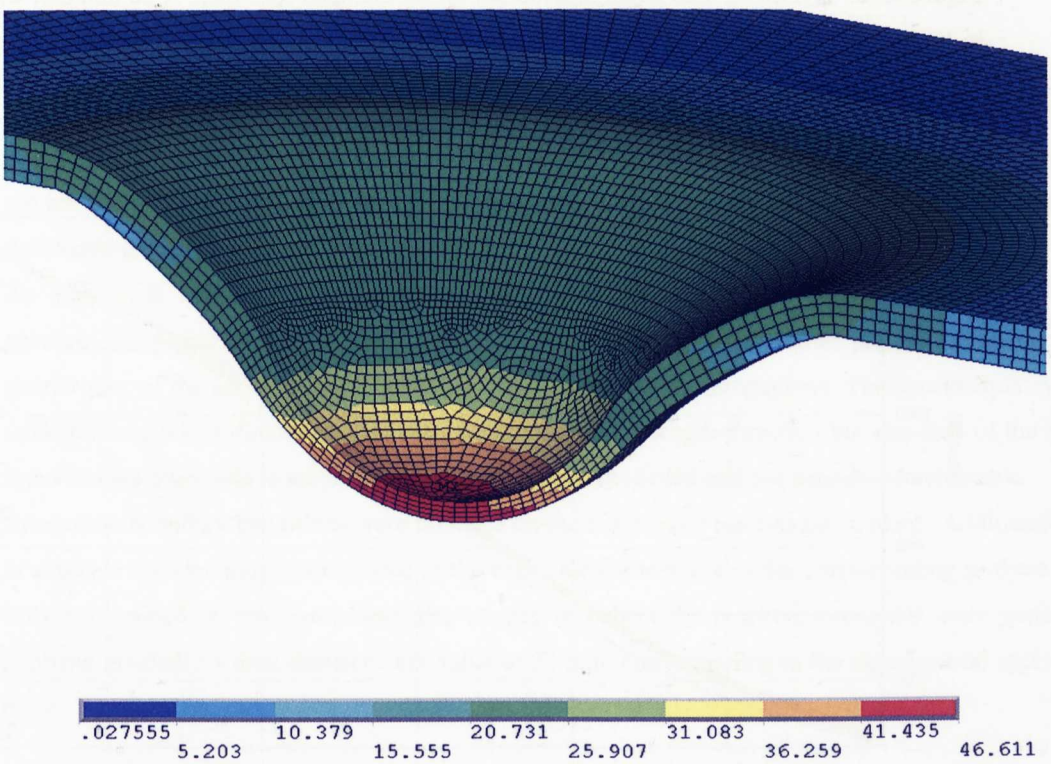

Figure 6.95: Von Mises stress distribution for the clamped specimen. A 20 mm dart was modelled.

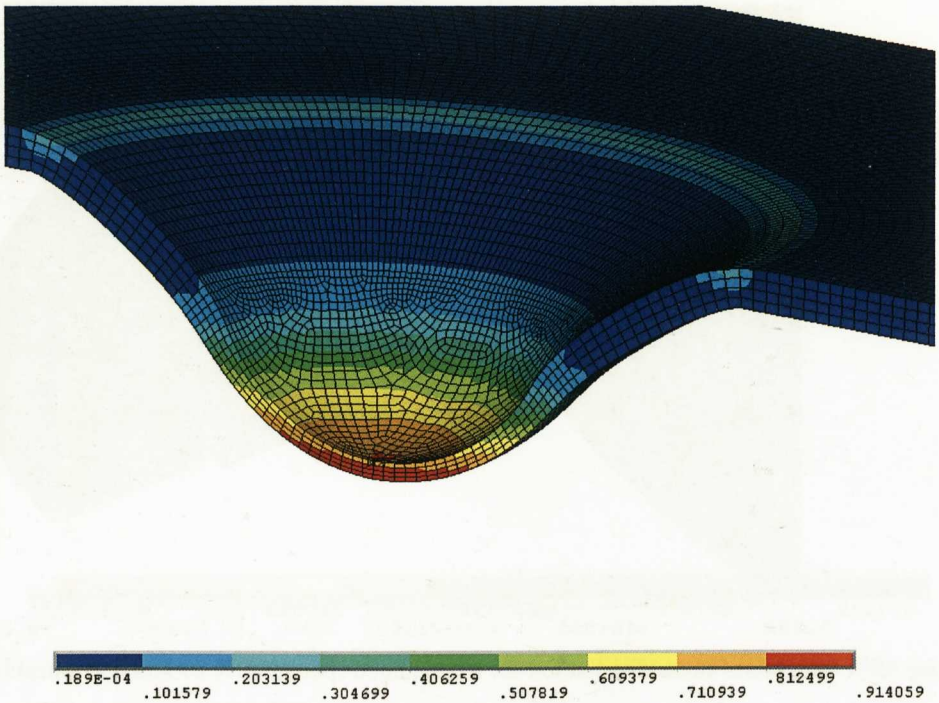

Figure 6.96: Von Mises total strain distribution for the clamped specimen. A 20 mm dart was modelled.

In Figure 6.97, the experimental curve is compared with the simulation results for a 20mm dart. Clamping effects were studied using True material data for the calculation.

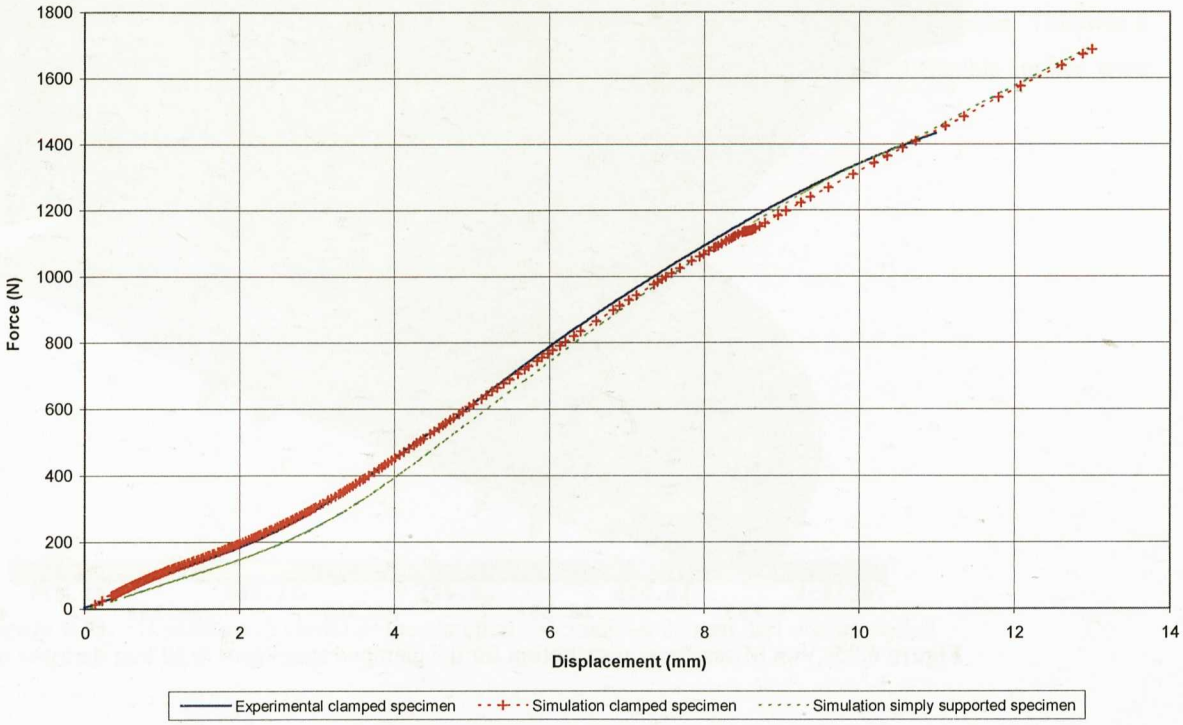

Figure 6.97: Comparison of experimental and simulation results for clamped specimens. As reference, the simply supported specimen simulation results are included.

It can be observed that the simulation was able to reproduce the effect of clamping the specimen. The initial load-displacement curve stage was correctly represented in ANSYS. As displacement values were increased, the difference decreased between clamped and unclamped simulation results, which was also given in the experimental results. See Figure 6.47.

6.4.4. Quasi-Static Tensile Test Calibration in ANSYS. PC/ABS.

6.4.4.1. Material Definition.

The same material definition considerations applied to PP were used with PC/ABS. The first simulation was performed using true stress-strain data converted from engineering stress-strain data using the classical conversion formula. Thus, volume incompressibility was considered in plasticity.

A Multilinear Isotropic (MISO) constitutive material model was selected for the elasto-plastic modelling of the material data. A true stress-true total strain curve consisting of 98 pairs of points was created in ANSYS. The first point of this curve corresponded to the proportional limit's yield point of the material (8.3332 MPa.). This is an artefact for this elasto-plastic model for a correct definition of the elastic region, as described previously. In addition to this data, elastic data is also needed for the MISO model. A tensile elastic modulus, EX in ANSYS, of 2087 MPa. and an elastic Poisson's ratio, PRXY in ANSYS, of 0.4 were also defined. This experimental material data corresponded to the tensile test curve experimented at a speed of 5 mm/min.

6.4.4.2. Finite Element Modelling.

The main objective of the tensile test simulation was to correlate the corresponding test up to the failure point of a tensile specimen. For this purpose 3D solid element types had to be selected since 3D shell type elements are not useful for simulating the non-homogeneous and triaxial states of straining that occur when a neck is developed in the specimen.

An eight node SOLID 185 element type was selected in ANSYS for meshing the ISO 3167 specimen geometry. A global element size of 1 mm was used for meshing a quarter part of the specimen. Only a quarter part of the specimen was modelled due to symmetry considerations. The specimen is symmetric in thickness and width directions. It is also symmetric in the length direction but one side of the specimen is fixed and the other side is moving so this direction was modelled and not considered symmetric.

Symmetric boundary conditions were imposed on the surfaces of the symmetry plane. Additionally, in order to simulate the clamping system used in the experimental test, the nodes corresponding to those areas were fully constrained. A pilot node was also created to collect the reaction forces that were generated when applying gradually a final displacement value of 24 mm. corresponding to the experimental specimen failure point.

6.4.4.3. Results.

Force-displacement results obtained in ANSYS and in the experimental test were compared in order to check the validity of this elasto-plastic model for reproducing the tensile test.

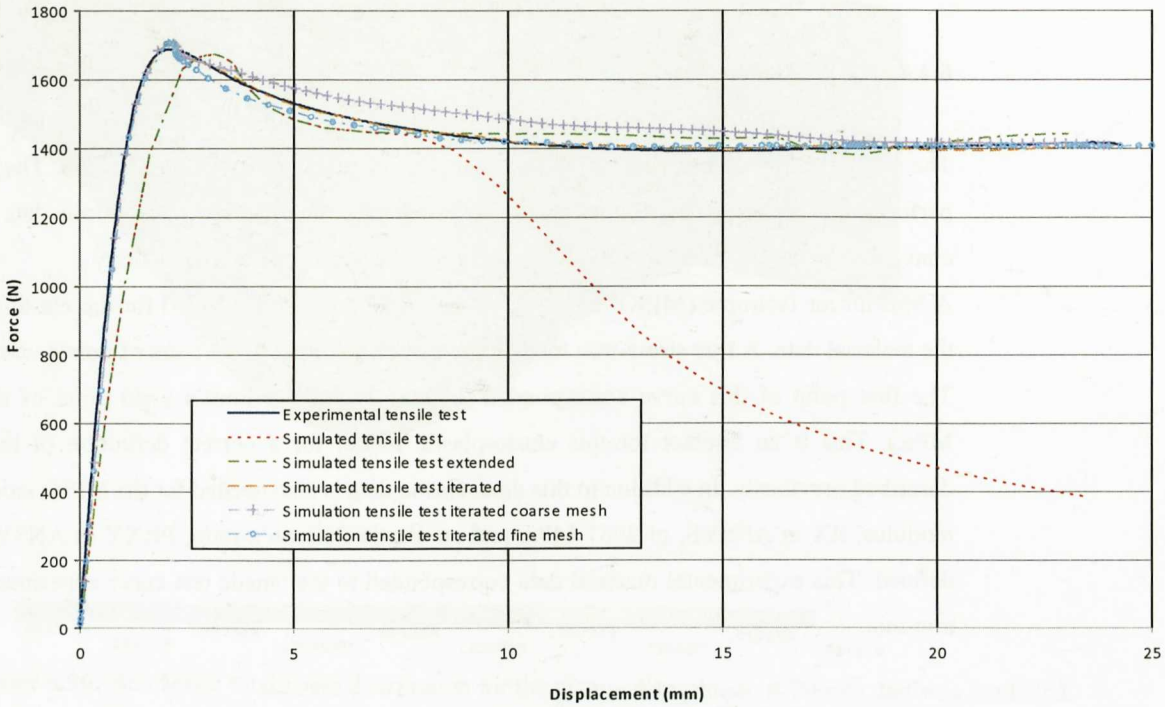

Fig. 6.98: Comparison of experimental and simulated tensile curves for PC/ABS at 5 mm/min.

It was observed that:

1. The stiffness of the initial region of the curve is now considerably under estimated by the simulation response.
2. The high straining region of the load-displacement curve where necking occurred did not correlated accurately since a sudden decrease in the simulated curve was observed.

It was noted that this decrease was due to insufficient stress-strain data points inputted for displacement regions above 12 mm to represent the high straining zone. ANSYS extrapolates with a zero slope curve when the material is being strained above the input stress-strain data. This zero slope extrapolation was responsible for the decrease in the simulation curve. Thus, the material input curve had to be corrected adding stress-strain data points beyond the initial input curve. The curve was extended with a gradient of 66.8 MPa. This gradient value was calculated from the tendency of the stress-strain curve before failure and iteratively comparing the simulation results with the experimental ones.

The extension of the initial curve gave better results, especially in the plasticity region but still the initial stage of straining was not properly correlated.

Again, the tensile test simulation is dependent on the mesh quality, especially in the necking region. The use of a coarser mesh of 2mm, gives a poorer representation of the decrease in force after the initial peak (Figure 6.98). The use of a finer mesh of 0.5mm gives a higher force decrease in the necking envelope but is admissible due to the scatter in the experimental tensile testing itself.

Here, an iterative method was proposed in order to match the experimental tensile force-displacement curve. The main idea is based on the work performed by Trantina and Nimmer [30] and as a results of the present thesis work, the following paper was also published by Arriaga [31] in concern to the proposed iterative method.

6.4.4.3.1. The iterative method.

The mechanical relationships between constitutive behaviour, onset of necking and the post-yield stability of the tensile specimen can be studied starting with a simple bilinear elastic-plastic constitutive model.

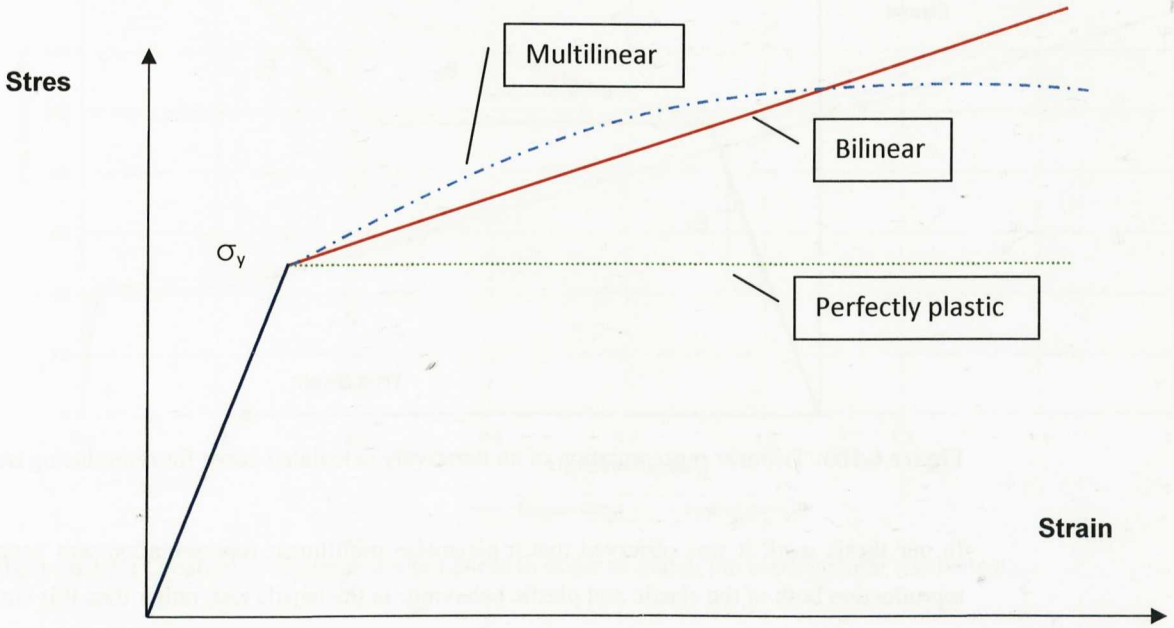

Figure 6.99: Different elasto-plastic approximations to define the stress-strain behaviour in a FEA code [30].

Variations in the predicted load versus the crosshead displacement behaviour of the tensile specimen as a function of the initial hardening modulus (E_2 in the bilinear constitutive model) can be studied. With elastic modulus and yield stress held constant, there is significant difference in the post-yield load-displacement behaviour as the value of E_2 is varied from $+2\sigma_y$ to $-2\sigma_y$. For a hardening modulus with a value twice the yield stress, the load-displacement behaviour is similar to that seen in many metals; hardening is given with homogeneous plastic deformation.

If hardening modulus is considered equal to the yield stress of the material, the maximum in the load-displacement curve now takes place at the yield point and the load decreases as the crosshead displacement increases. There is no longer any region of homogeneous plastic deformation, instead localised necking occurs simultaneously with yield.

As the hardening modulus is reduced below the value of the yield stress, the maximum load and the neck formation always coincide with initial yield, and the post yield slope of the loads-displacement curve becomes increasingly negative. This type of behaviour is often visible in the load-displacement behaviour of ductile polymers.

A true stress-strain characterised by increasing values of the post yield modulus as a function of true strain is necessary for a neck to stabilise and propagate. To quantify the effects of this mechanism, a trilinear relationship between the true stress and the true strain can be modelled. The third stage modulus E_3 and the amount of true strain between yield and third stage hardening, ε_d, can be varied parametrically.

Basically, defining values for E_3 one can iteratively adjust the experimentally observed neck propagation and strain hardening. A value of twice the yield stress of the material for this modulus, gives as a result that the load reaches a finite minimum and then remains constant. Higher values of E_3 can reproduce the strain hardening of some materials.

The draw strain, defines as ε_d also plays an important role in the post yield deformation and load-carrying capability. Lower values of ε_d result in smaller load reductions prior to stabilisation and less crosshead displacement prior to final stiffening.

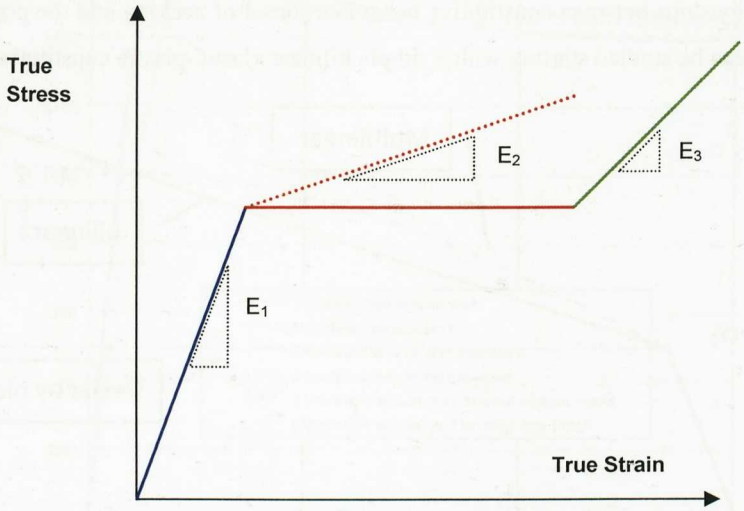

Figure 6.100: Trilinear representation of an iteratively calculated curve for reproducing necking effects [30].

In our thesis work it was observed that a piecewise multilinear representation was necessary for a correct reproduction both of the elastic and plastic behaviour in the tensile test, rather than this simplified approach.
In our approach, the tensile curve is divided in three main regions:
Region 1: up to the maximum in force. The simulation is just carried to the displacement correspondent to the maximum in force, and the input stress-strain curve is adjusted in order to match the experimental trace.
Region 2: reduction down of force, necking. The simulation is carried on to describe the necking region of the curve, which is usually obtained defining a correct gradient around the yield stress defined in the material card. This reproduces the fall in stress values. Similar to E_2.
Region 3: strain hardening, stiffening. The gradient of the curve needs to be increased in order to capture the force raise as the neck propagates along the specimen. Similar to E_3.
The following curve was necessary for matching the experimental force-displacement trace:

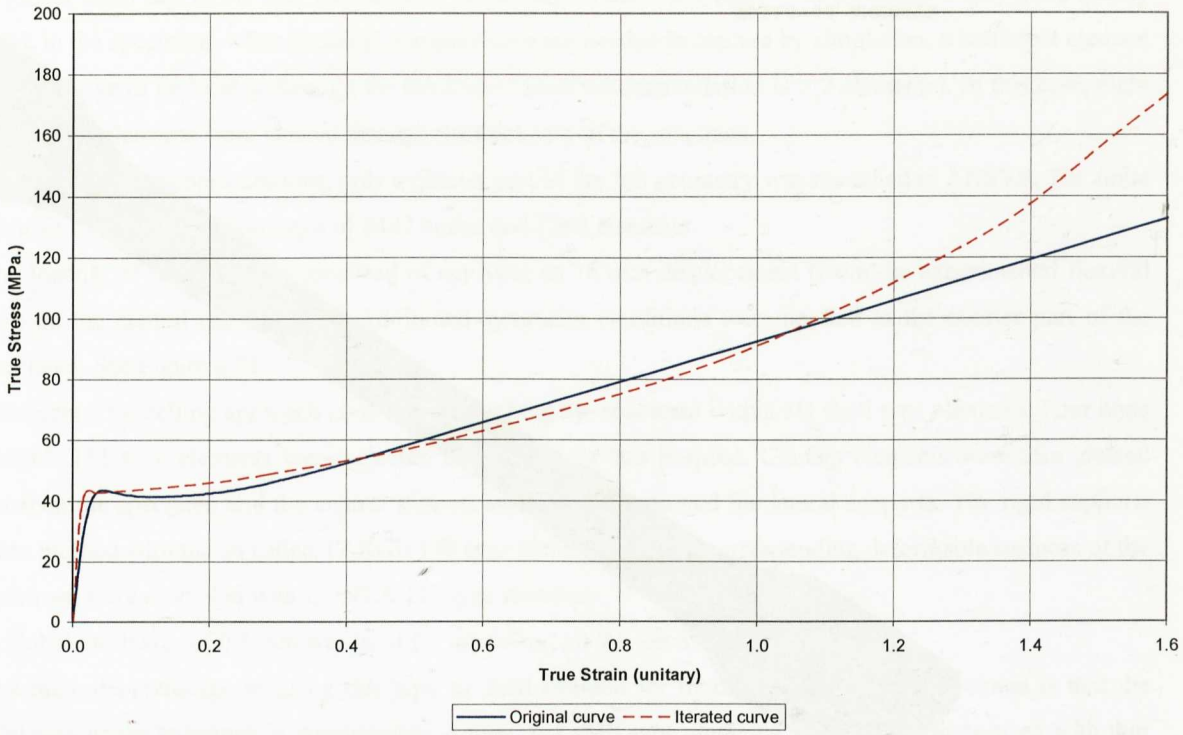

Figure 6.101: Creation of an iterated input curve in order to match the experimental tensile test.

The results obtained with this curve can be seen in the previous Figure 6.94. It can be observed that the iterative curve matches properly the experimental tensile test curve.

For the tensile test simulation in ANSYS, the necking behaviour of the PC/ABS material was correctly reproduced from the deformed shape viewpoint. A necked area was clearly visible with the corresponding section reduction. See Figure 6.102. This simulated behaviour was similar to the observed experimental neck, see Figure 6.49. In the experiments, necking can start in any point of the gauge length due to any material fault or non-symmetry, while the FEA model is perfect and the neck starts at the center of the specimen.

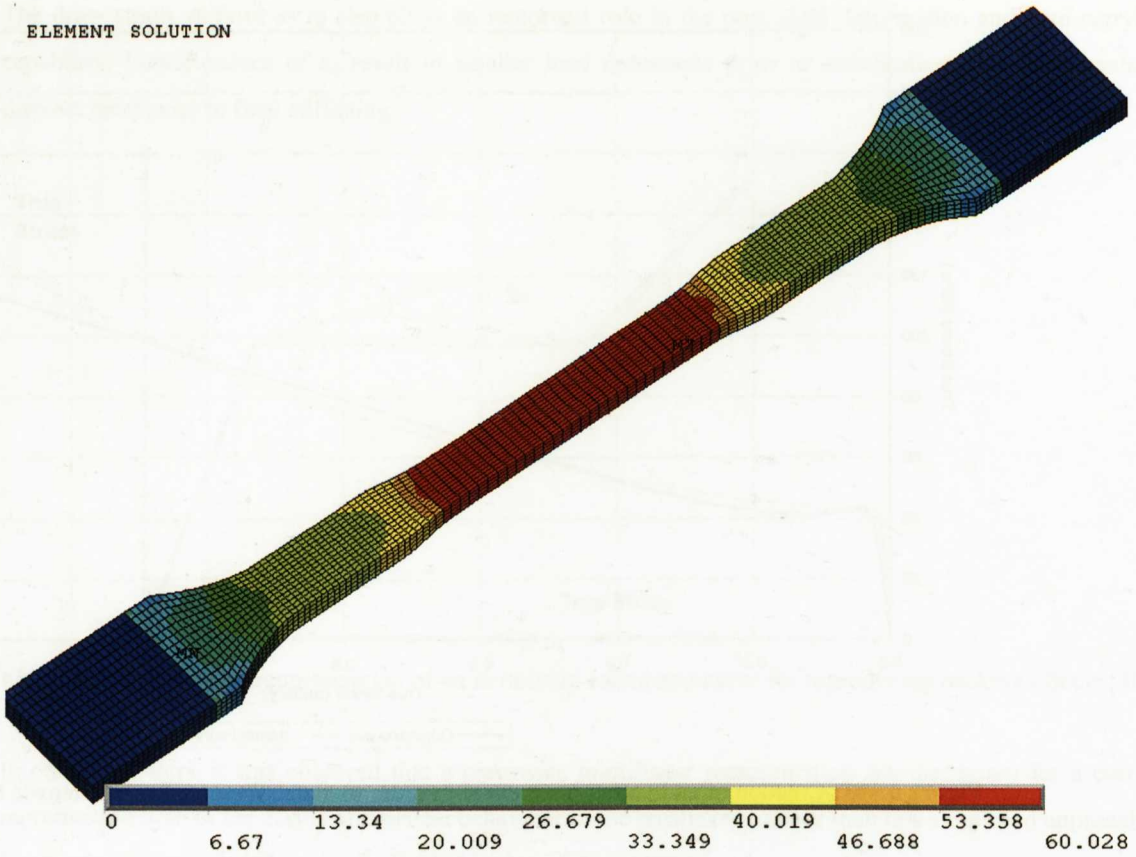

Figure 6.102: Von Mises stress distribution in ANSYS. The necking behaviour was appropriately simulated.

6.4.5. Quasi-Static Bending Test Correlation in ANSYS. PC/ABS.

The simulation of the flexural test is a correlation method for validating the material data generated in the tensile test and the elasto-plastic material models. In the present study the experimental data obtained in the step 6.3.5 will be correlated by means of different simulations in ANSYS.

6.4.5.1. Material Definition.

Initially, the tensile stress-strain curve obtained from engineering data and converted applying the classical true conversion, was used in this correlation study. This curve also had a correction consisting on the extension of the plasticity area in order to calibrate correctly the tensile test.
Additionally, an iterated curve was also used, since this curve correlated in a more accurate way the experimental tensile test.

6.4.5.2. Finite Element Modelling.

Two approaches were considered for modelling the flexural specimen. The first approach defined the specimen with the use of solid hexahedral elements. Eight node SOLID 185 type elements were selected in ANSYS for this purpose. Contact elements were also created between the specimen and the central support and the specimen and the lateral supports. The rigid supports were meshed with the so called TARGE 170 type elements and the corresponding deformable surfaces of the specimen were modelled with CONTA 174 type elements.

A global mesh size of 0.5 mm was used for modelling all the test system. This produced a very good quality mesh in the specimen; when bending characteristics are needed to capture by simulation, a sufficient element number have to be located through the thickness (usual recommendation is > 2 elements). In this case, eight hexahedral elements were located through the thickness of the specimen.

Due to symmetry considerations, only a quarter part of the full geometry was modelled in ANSYS. The finite element for this model consisted of 8442 nodes and 7262 elements.

The loading of the specimen consisted of applying an 18 mm displacement (from the experimental flexural test) on the central rigid support. Additional symmetry conditions were applied to the quarter part of the specimen. See Figure 6.74.

The second modelling approach consisted of meshing the specimen with a 3D shell type elements. Four node SHELL 181 type elements were selected in ANSYS for this purpose. Contact elements were also created between the specimen and the central support and the specimen and the lateral supports. The rigid supports were meshed with the so called TARGE 170 type elements and the corresponding deformable surfaces of the specimen were modelled with CONTA 174 type elements.

A global mesh size of 0.5 mm was used for modelling all the test system.

The main disadvantage of using this type of shell element for modelling the present specimen is that the thickness of the specimen is considerable, 4 mm, and shell type elements are intended to be used with thin components. Additionally, a sufficient number of through thickness elements have to be located when bending behaviour is needed to be captured correctly but with shell elements this is not possible. Thus, the simulation of the bending test with shell type elements will also give us information about the validity of using shell type elements for modelling medium thickness parts.

Due to symmetry considerations, only a quarter part of the full geometry was modelled in ANSYS (an expanded representation is seen in the figure). The finite element for this model consisted of 1314 nodes and 1762 elements.

The loading of the specimen consisted of applying an 18 mm displacement (from the experimental flexural test) on the central rigid support. Additional symmetry conditions were applied to the quarter of the specimen studied. See Figure 6.75.

No strain rate sensitivity was included in the MISO model. No frictional effects were included between the specimen and the supports.

6.4.5.3. Results.

First simulation results were obtained performing a comparison in between solid and shell type elements.

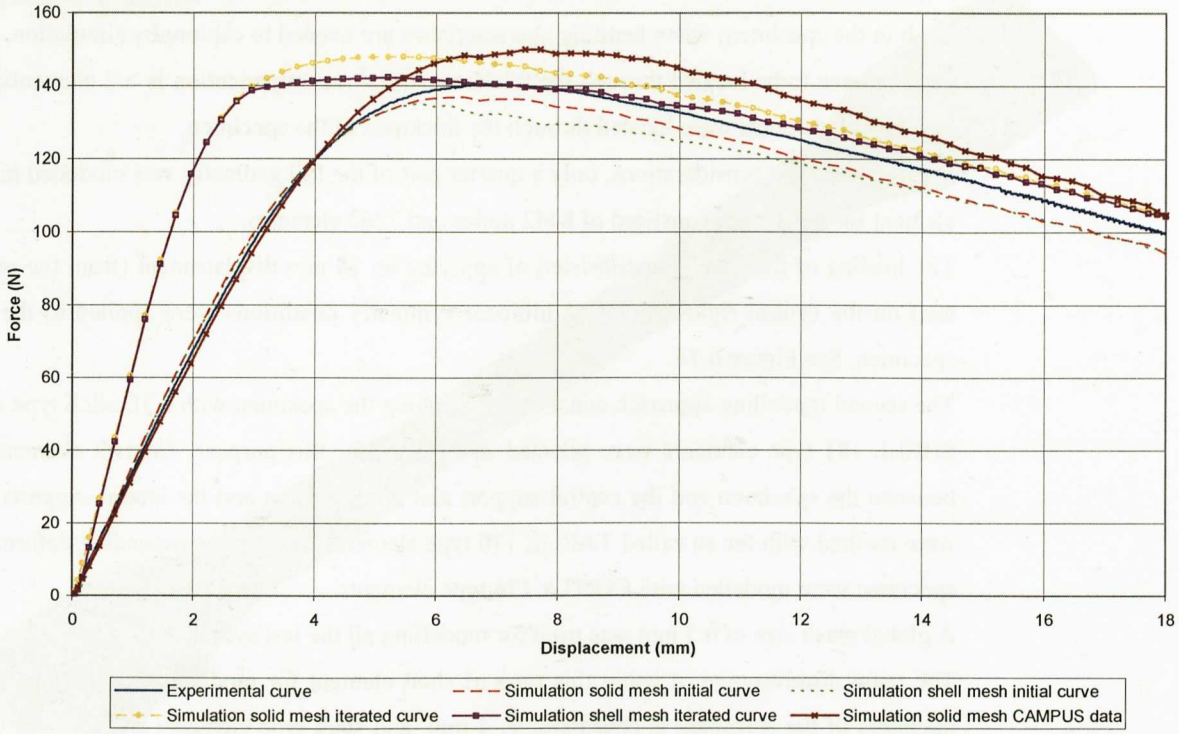

Figure 6.103: Comparison of experimental and simulation results for flexural test at 5 mm/min. The material data input was done with the original curve and with the iteratively calculated one.

It can be observed that a good correlation level was obtained both with solid and shell type elements when using the original stress-strain curve. The initial elastic region of the curve was exactly matched by simulations and the plastic region was also adequately described. With solid elements, a 2.6% error was found in the maximum force levels, whereas with shell elements a 6.4 %.

But with the input of the iteratively adjusted stress-strain curve, although the tensile behaviour was perfectly matched, the response in the initial stages of bending produced values with a higher stiffness than experimental data. This denotes that a very precise uniaxial tensile calibration is not always adequate for simulating other testing modes such as bending.

In this case, CAMPUS data input offered a higher response than the 5 mm/min. Curve but could be very close to the 50 mm/min. curve.

A sensitivity analysis was performed in order to study the effect of the frictional characteristics on the simulation results. In ANSYS, a static friction coefficient (μ_{static}) and a dynamic friction ($\mu_{dynamic}$) coefficient can be defined in the contact interfaces. For this study an arbitrary value of 0.60 was selected for μstatic and a half value of 0.30 for $\mu_{dynamic}$. An additional study was performed using half values for both coefficients; μ_{static}=0.30, $\mu_{dynamic}$=0.15

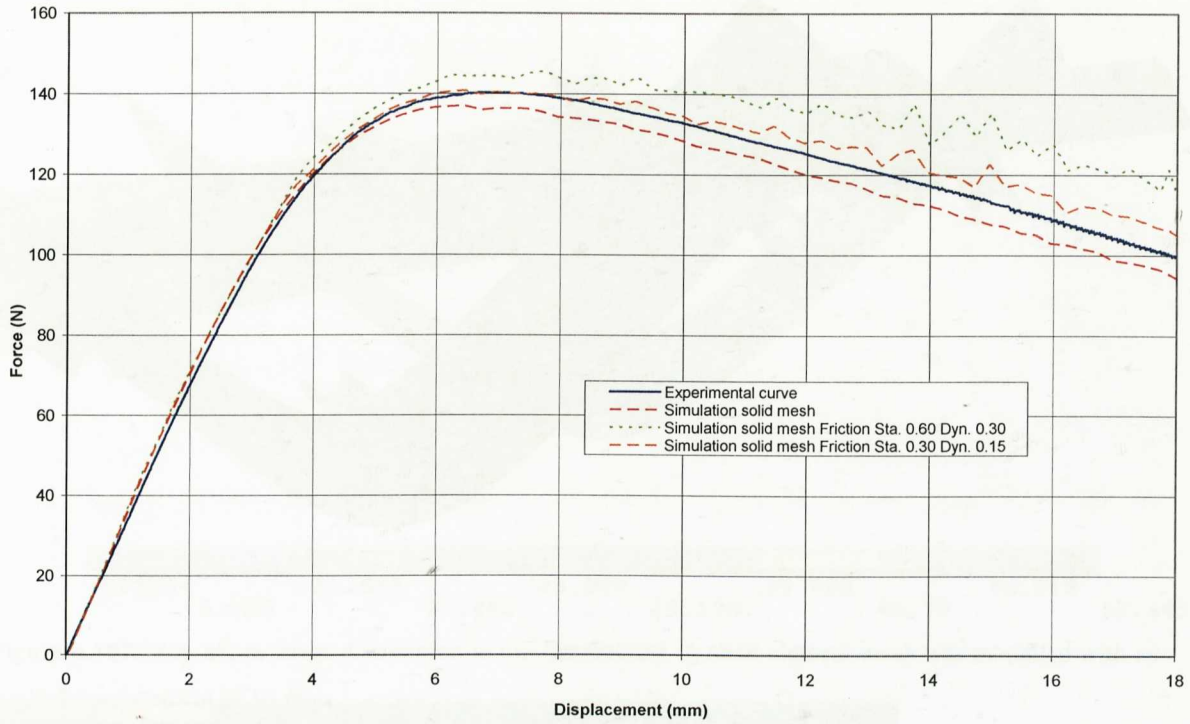

Figure 6.104: Effect of the friction coefficient on the simulated results for solid elements.

It can be observed that the addition of frictional values did not improve considerably the simulation response. For solid elements, the simulated curves tended to stiffen in the plastic region which was not qualitatively in agreement with the experimental behaviour. Anyway, low frictional values tended to approximate in a better manner the experimental curve since the initial simulation of no friction effects in conjunction with the used tensile stress-strain curve always gave a lower response than experimental.

In the following graphs, the Von Mises stresses and strains generated in both type of solid and shell finite element models are represented. Differences both in stresses and strains can be observed between solid and mesh type elements (shell type element results should comparatively correspond to the solid top surface results). A 9% difference in maximum stress values exists for each element type. Approximately a 21% difference exists between the maximum total strains on the upper surface of the solid model and the maximum total strains on the upper layer of the shell model.

These differences can be attributed to the modelling of a considerable thickness model with shell elements. The proper way to model the flexural test for collecting adequately the bending stresses, strains, forces and displacements is by means solid hexahedral elements, which gave the best approximation to experimental force-displacement data.

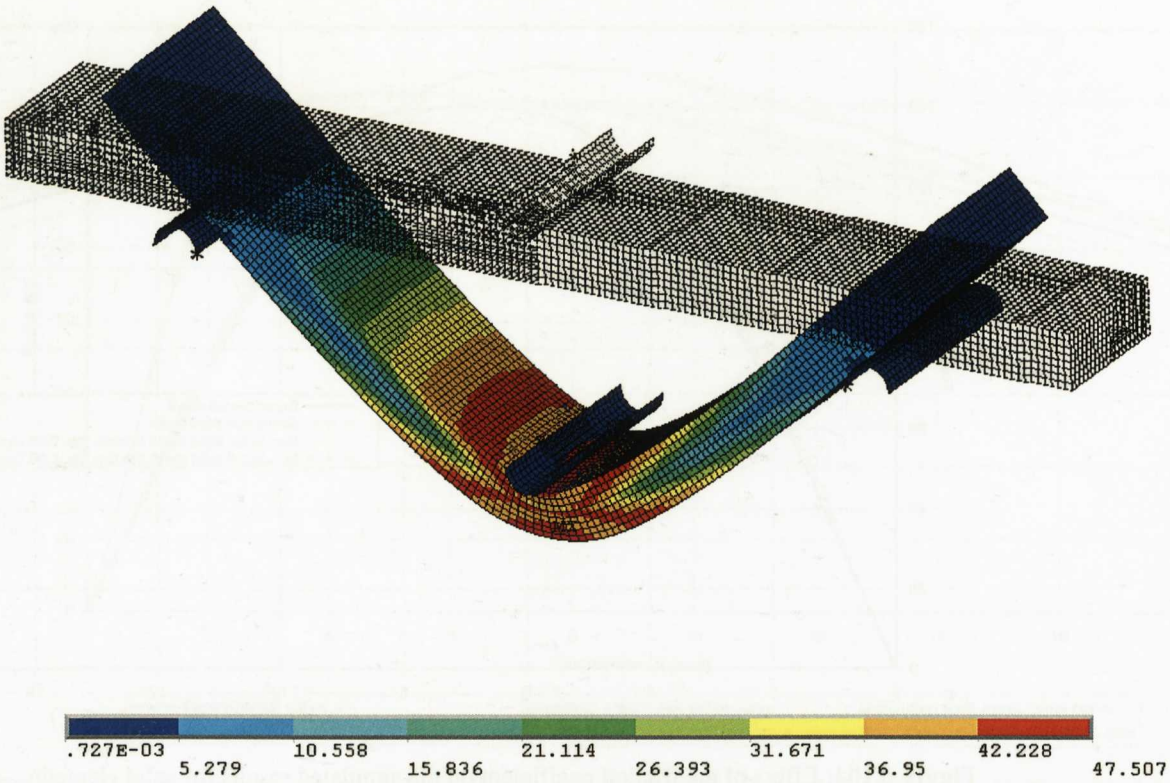

Figure 6.105: Von Mises stress distribution in the flexural test. A solid element mesh was modelled with an applied displacement of 18 mm.

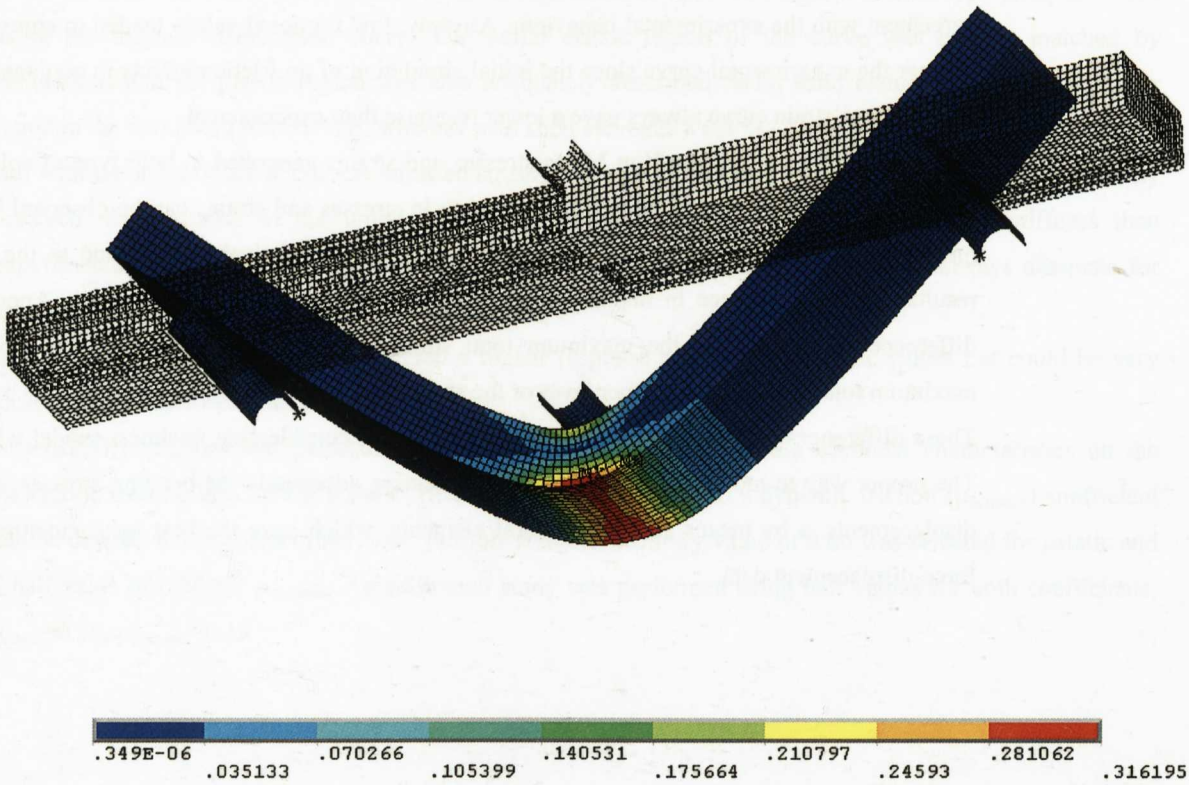

Figure 6.106: Von Mises total strain distribution in the flexural test. A solid element mesh was modelled with an applied displacement of 18 mm.

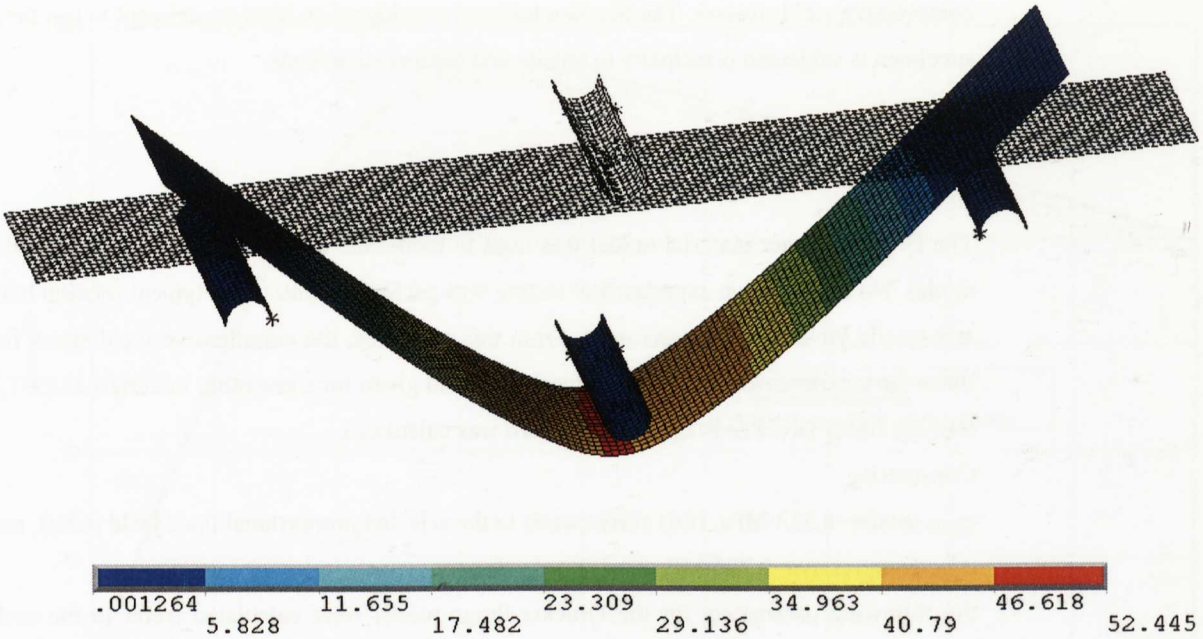

Figure 6.107: Von Mises stress distribution in the flexural test. A shell element mesh was modelled with an applied displacement of 18 mm.

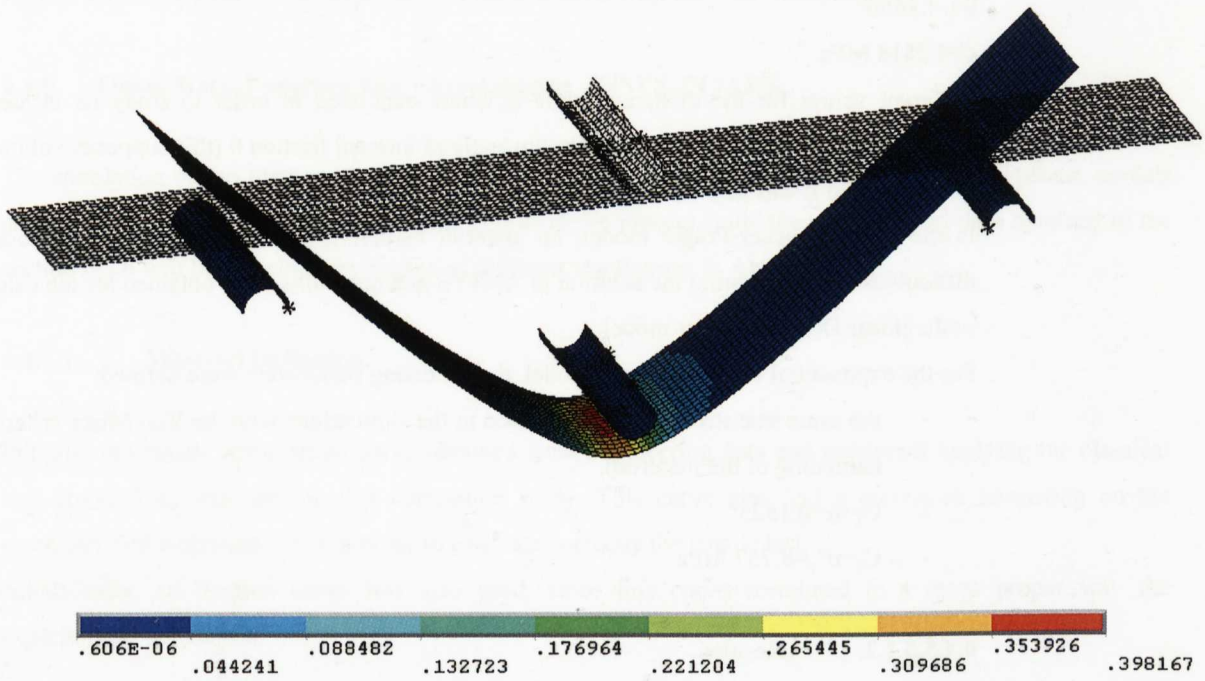

Figure 6.108: Von Mises total strain distribution in the flexural test. A shell element mesh was modelled with an applied displacement of 18 mm.

6.4.5.3.1. Bending Simulations. Use of a Hydrostatic Sensitive Constitutive Model: Drucker-Prager. PC/ABS.

The aim of this study was to check the effect of accounting for hydrostatic effects with the use of a proper constitutive model in ANSYS. The first simulations had been carried out with the MISO elasto-plastic model and considering the Von Mises yield criteria. As has been stated in the theoretical sections of the thesis, thermoplastic materials are sensitive to hydrostatic stresses. This contributes to differences in tensile and

compressive yield stresses. The bending test was considered an ideal experiment to test these effects since the specimen is subjected principally to tensile and compressive loads.

6.4.5.3.1.1. Material Definition.

The Drucker-Prager material model was used to model the different yield values in tensile and compressive modes. No compressive experimental testing was performed. Instead, a typical relation between compressive and tensile yield from [6] was used. From this reference, the compressive yield stress for PC/ABS is 1.11 times the tensile yield stress. This behaviour is also given for some other materials as PBT, PC or ABS. With this, the linear Drucker-Prager material card was calculated.

Considering,

σ_{yield} tensile=8.333 MPa. (this corresponds to the selected proportional limit yield point), and

σ_{yield} compressive=9.226 MPa.

the following parameters for the Drucker-Prage model were calculated (refer to the section 4.5 about the Drucker-Prager model and the calculation of parameters):

σ_y=5.0558 MPa.

β=0.0294

θ=-4.2656°

c=4.2818 MPa.

Different values for the dilatancy angle θ_f where examined in order to study its influence in simulation results. It was considered to be equal to the angle of internal friction θ (this supposes volumetric expansion in plasticity) and it was also checked to assume it to be zero (no expansion).

In the linear Drucker-Prager model, no material hardening can be assumed. This produced convergence difficulties when obtaining the solution in ANSYS and no results were obtained for the calculated parameters of the linear Drucker-Prager model.

For the exponential Drucker-Prager model, the following parameters were defined:

- the same true stress-strain curve used in the simulations with the Von Mises criteria (this defines the hardening of the material).
- $C_1=\alpha$=0.1525°
- $C_2=\sigma'_y$=8.757 MPa.

6.4.5.3.1.2. Results.

Pertaining to the obtained results, the following points could be observed:

- no results could be obtained for the linear Drucker-Prager material model.
- the exponential or extended Drucker-Prager did work. The simulation response was even closer to the experimental curve than the response obtained with the Von Mises model.

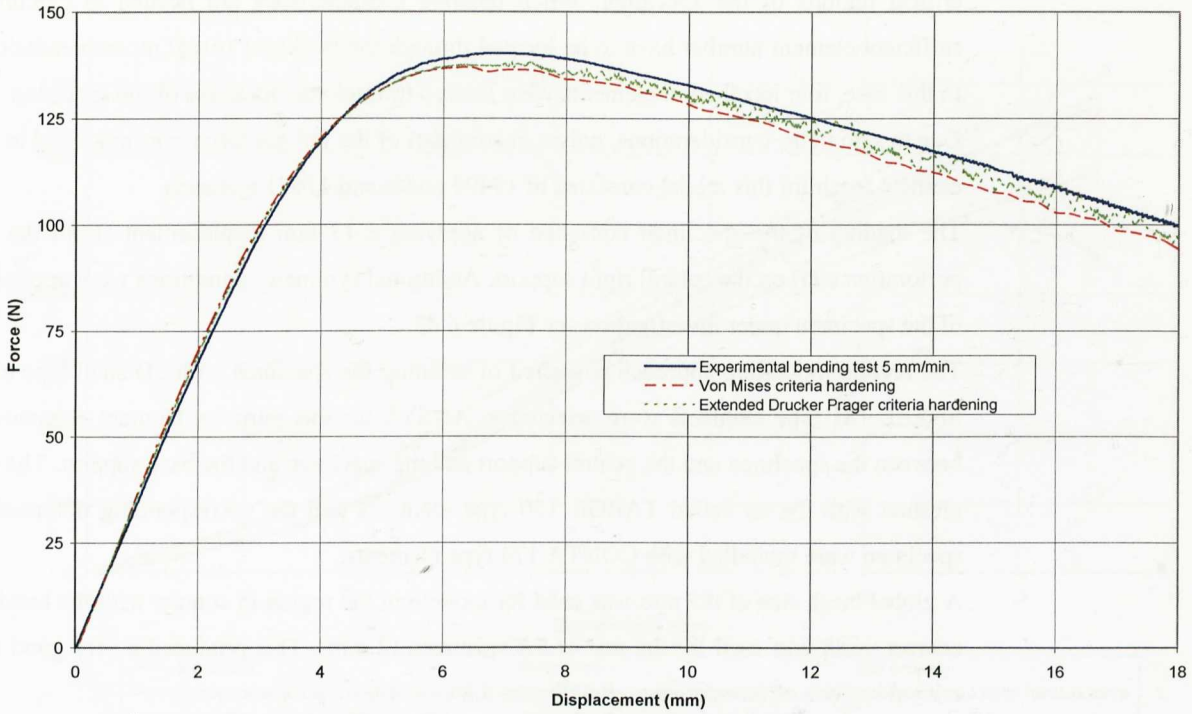

Figure 6.109: Comparison of the Drucker-Prager criteria with the Von Mises model.

6.4.6. Quasi-Static Puncture Test Correlation in ANSYS. PC/ABS

The simulation of the plate perforation test is a correlation method for validating the elasto-plastic models and the material data generated in the tensile test. In the present study the experimental data obtained in the section 6.3.6 will be correlated by means of different simulations in ANSYS.

6.4.6.1. Material Definition.

Initially, the tensile stress-strain curve obtained from engineering data and converted applying the classical true conversion, was used in this correlation study. This curve also had a correction consisting on the extension of the plasticity area in order to calibrate correctly the tensile test.
Additionally, an iterated curve was also used, since this curve correlated in a more proper way the experimental tensile test.

6.4.6.2. Finite Element Modelling.

Two approaches were considered for modelling the square shaped plate specimen. The first approach defined the specimen with the use of solid hexahedral elements. Eight node SOLID 185 type elements were selected in ANSYS for this purpose. Contact elements were also created between the specimen and the penetrating dart and the specimen and the base support. The rigid supports were meshed with the so called TARGE 170 type elements and the corresponding deformable surfaces of the specimen were modelled with CONTA 174 type elements.
A global mesh size of 0.5 mm was used for modelling the region in contact with the hemispherical striker. A coarser mesh was used for the rest of the specimen (2 mm). This produced a very good quality mesh in the

critical regions of the specimen. When bending characteristics are needed to capture by simulation, a sufficient element number have to be located through the thickness (usual recommendation is > 2 elements). In this case, four hexahedral elements were located through the thickness of the specimen.

Due to symmetry considerations, only a quarter part of the full geometry was modelled in ANSYS. The finite element mesh for this model consisted of 19494 nodes and 17671 elements.

The loading of the specimen consisted of applying a 13 mm displacement (from the experimental plate perforation test) on the central rigid support. Additional symmetry conditions were applied to the quarter part of the specimen under investigation see Figure 6.83.

The second modelling approach consisted of meshing the specimen with 3D shell type elements. Four node SHELL 181 type elements were selected in ANSYS for this purpose. Contact elements were also created between the specimen and the central support and the specimen and the base support. The rigid supports were meshed with the so called TARGE 170 type elements and the corresponding deformable surfaces of the specimen were modelled with CONTA 174 type elements.

A global mesh size of 0.5 mm was used for modelling the region in contact with the hemispherical striker. A coarser mesh was used for the rest of the specimen (2 mm). This produced a very good quality mesh in the critical regions of the specimen. See Figure 6.84.

Due to symmetry considerations, only a quarter part of the full geometry was modelled in ANSYS. The finite element mesh for this model consisted of 8488 nodes and 4072 elements.

The loading of the specimen consisted of applying a 13 mm displacement (from the experimental plate perforation test) on the central rigid support. Additional symmetry conditions were applied to the quarter part of the specimen.

No strain rate sensitivity was included in the MISO model. No frictional effects were included between the specimen and the supports.

6.4.6.3. Results.

The obtained results for solid and shell type elements; the curve shapes were closely reproduced using the original curve data; however the simulation results tended to produce higher force values. Moreover, the input of a testing curve at 5 mm/min. correlates better the experimental puncture test at 200 mm/min. than lower testing speed curves. Additionally, the use of shell elements again produced stiffened again the stiffer. The initial elastic region of the curve is exactly matched by simulations. With solid elements, a 12% error was found in the maximum force levels, whereas shell elements produced a 16 % error. This comparison was performed with the experimental curve tested at 20 mm/min.

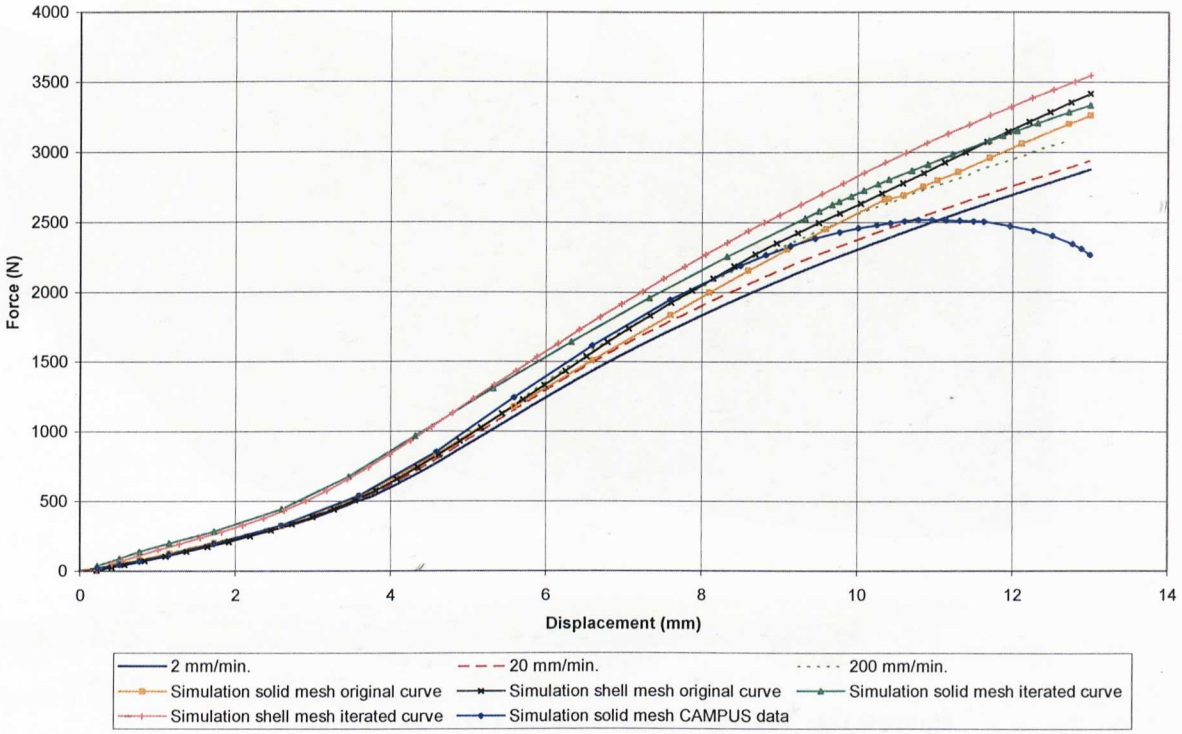

Figure 6.110: Comparison of experimental and simulated results for the plate perforation test. Solid and shell type elements were compared as well as the effect of the input tensile curve.

When using the iterated curve for calibrating the tensile test, a stiffer response was obtained than the experimental curves in every case. The initial linear region was not correctly correlated and the plasticity area was over predicted. This implies, as in bending test, the iterated curve was correct for correlating the experimental tensile test but with other modes of deformation gave higher responses than the experimental behaviour.

CAMPUS data offered an acceptable correlation level approximately up to 9 mm displacement. From this point onwards, as the material input curve has no additional data points, ANSYS extrapolates a zero slope curve and thus the force-displacement curve tends to decrease in stiffness, which was no observed experimentally.

The following figure plots the Von Mises stress distribution for a 13mm displacement with solid elements.

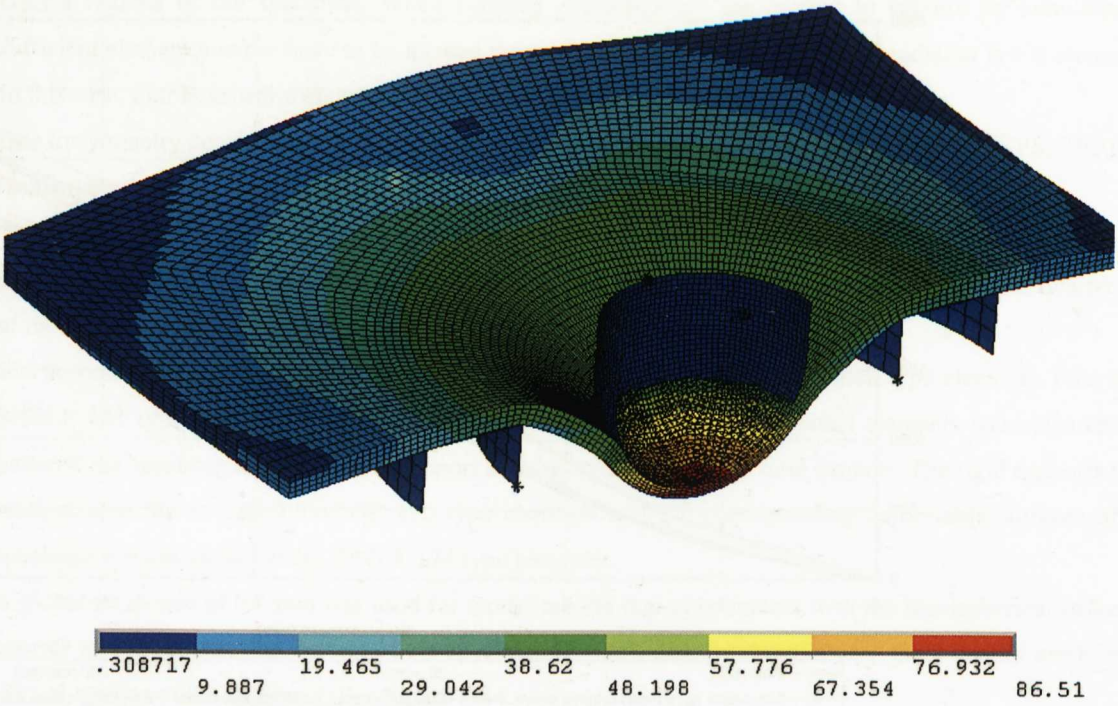

Figure 6.111: Von Mises stress distribution with solid elements.

The following figure plots the Von Mises total strain distribution for a 13mm displacement with solid elements.

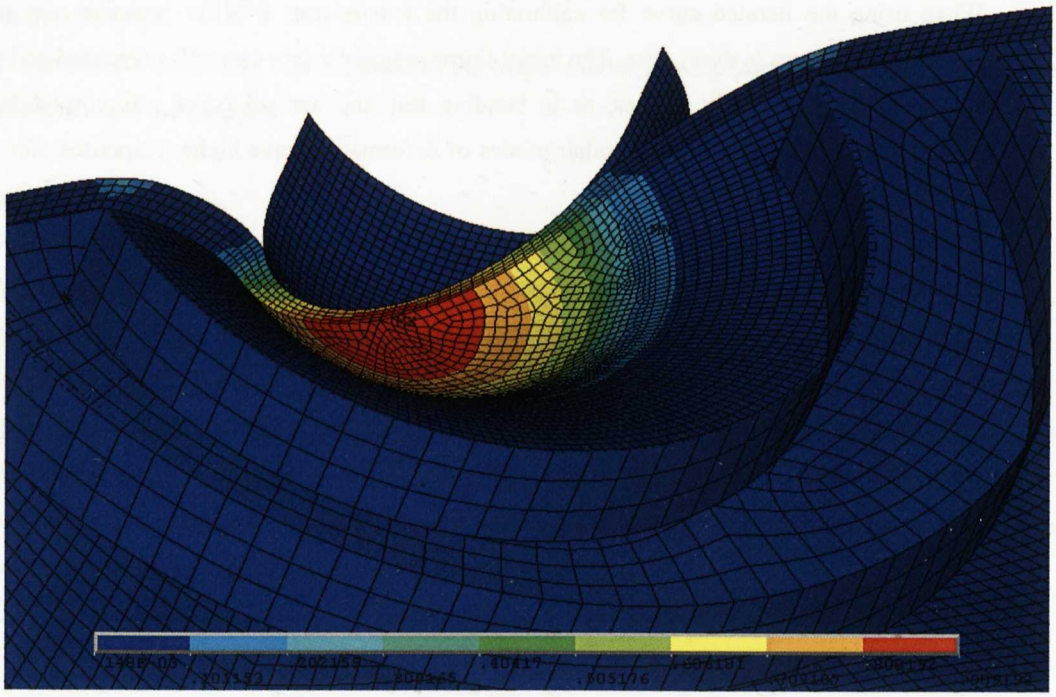

Figure 6.112: Total strain distribution with solid elements.

With shell elements, higher stress and strain levels were calculated. A 5% difference exists between stress values for solid and shell elements. A 7% difference exists in strains values calculated with solid and shell elements. The differences are lower than when simulating the bending test, due to the lower thickness of the specimen in the puncture tests and the better reproducibility with shell elements.

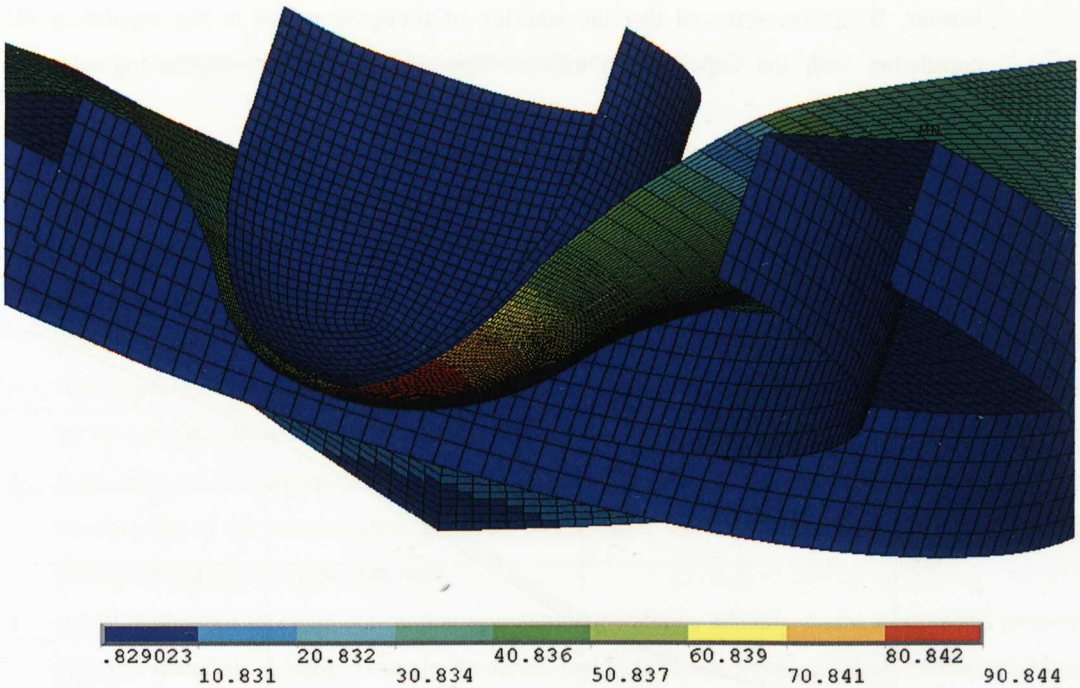

Figure 6.113: Von Mises stress distribution with shell elements.

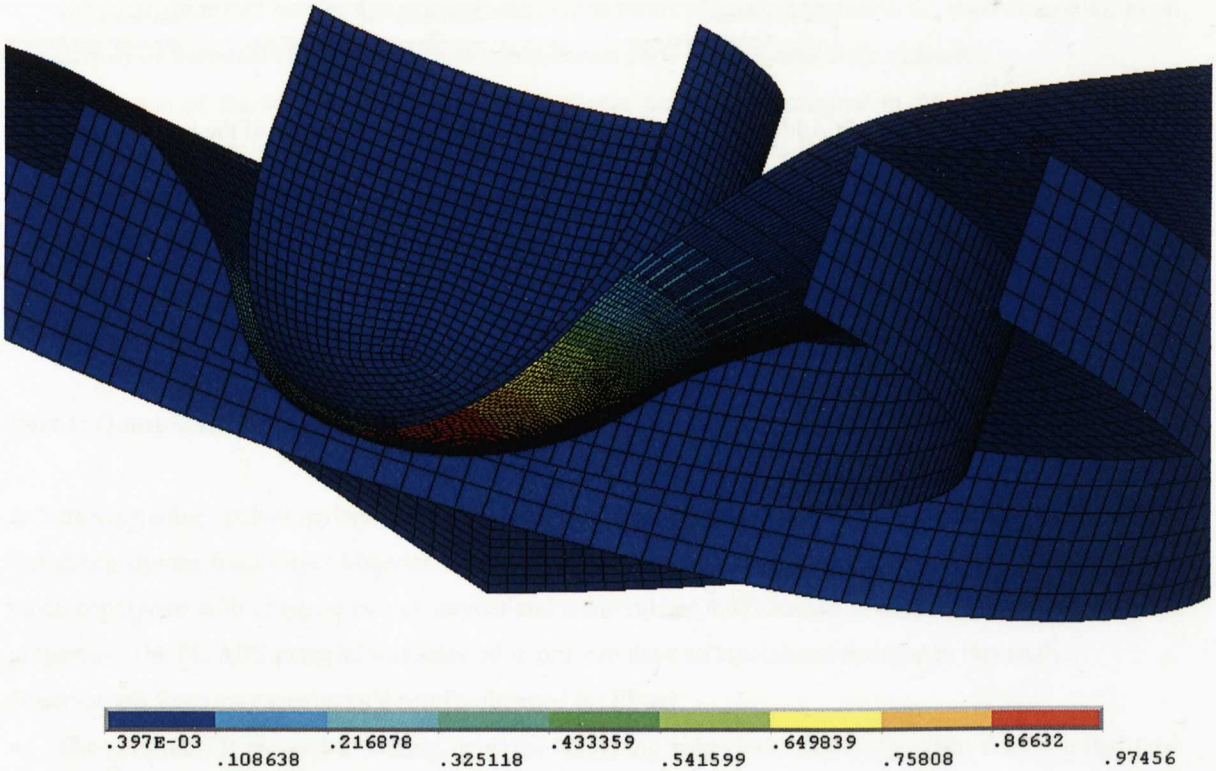

Figure 6.114: Von Mises strain distribution with shell elements.

Frictional effects. A sensitivity analysis was performed in order to study the effect of the frictional characteristics on the simulation results. In ANSYS, a static friction coefficient (μ_{static}) and a dynamic friction ($\mu_{dynamic}$) coefficient can be defined to the contact interfaces. In this study an arbitrary value of 0.60 for μ_{static} and a half value 0.30 for $\mu_{dynamic}$. An additional study was performed using half values for both coefficients; μ_{static}=0.30, $\mu_{dynamic}$=0.15

Results. It can be observed that the addition of frictional values to the simulation did not improve the correlation with the experimental curves. The tendency was to obtain higher force values than the experimental traces.

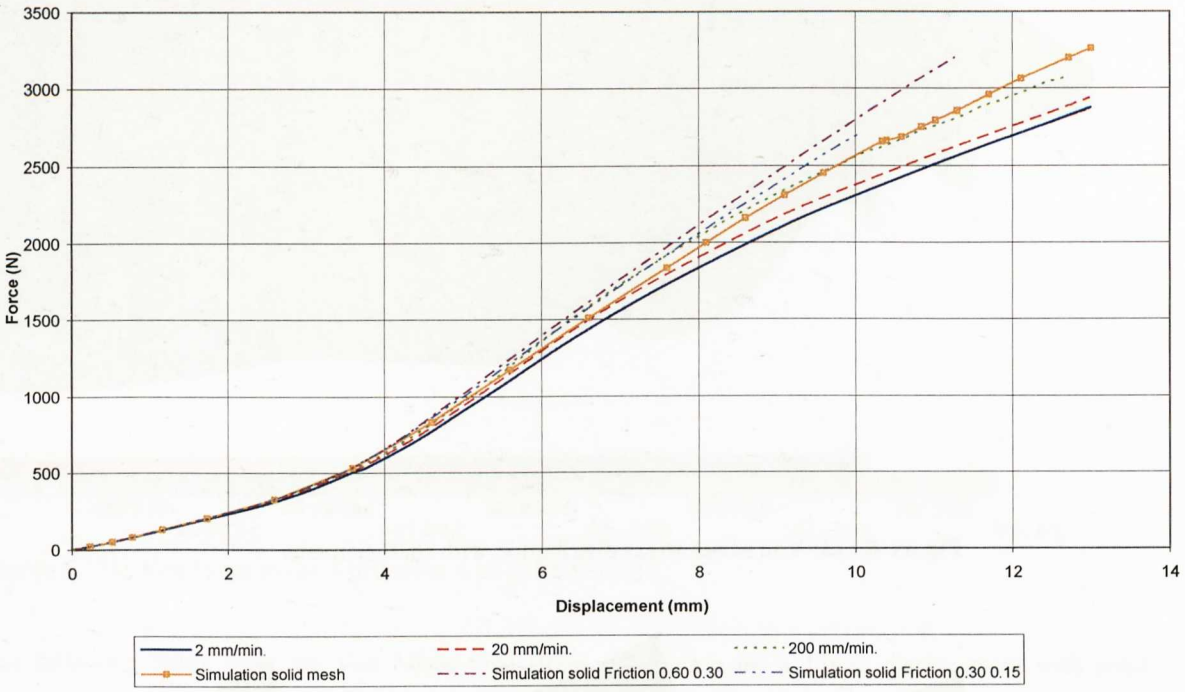

Figure 6.115: Addition of frictional values to the initial simulation of the puncture test.

Chapter 7: Discussion of results: Experimental Work Part 1 & 2.

This section describes the main conclusions extracted both from the experimental testing and simulation scheme carried out in the quasi-static part of the thesis work.

The main objectives that there were established within this study were:

- Identification of the slow rate mechanical properties of the selected materials. Tensile, bending and puncture experimental procedures were used for this purpose. Tensile testing was considered as a fundamental procedure to generate uniaxial stress-strain data, in terms of "true" data which could later be used in finite element analysis codes as ANSYS.
- Evaluation of the uniaxial tensile test data to simulate with finite elements the correlation tests as the bending test or the puncture test of plates. In this point different corrections were evaluated in order to obtain appropriate uniaxial true data.
- Initial evaluation of strain rate and temperature dependency of some basic mechanical properties of the selected materials. Elastic Young's modulus, yields stress or strain at break values were evaluated in order to clarify some tendencies at the slow rate regime.
- Development of a finite element procedure in order to obtain adequate correlation between experimental tests and simulated results. Basic considerations in terms of mesh type (solid vs. shell elements), mesh density or frictional characteristics between different parts of the model were evaluated.
- Evaluation of the validity of different elasto-plastic models implemented in ANSYS. These material constitutive models were developed to model metallic materials. In this thesis, they have been adopted for evaluating their response when modeling thermoplastic materials. Additionally, more sophisticated material models as the Drucker-Prager model were evaluated. This model takes into account some considerations that usual elasto-plastic models based on the Von Mises yield criteria do not take and which are important to model plastics' behaviour; different yielding in tensile and compressive modes.

Part 1: Quasi-Static Testing of PP and PC/ABS.

A semicrystalline polypropylene from the manufacturer Borealis and a Polycarbonate+Acrylonitrile-Butadiene-styrene from Bayer Material Science were tested in quasi-static conditions. The PP material was a block copolymer with ethylene as comonomer and some rubber modification in order to improve the impact properties. The PC/ABS material was selected in order to have an amorphous material in this study.

Observations from the experimental results obtained for PP are:

- The selected PP showed a crazing or stress-whitening behaviour, especially when tensile tested (see Figure 6.16). This denoted some rubber modification of the base material in order to improve the impact properties.
- The final fracture of the specimen was accompanied by some local reduction at a point of the gauge length.
- Tensile test data was generated at three testing velocities of 5, 50 and 500 mm/min. A clip-on extensometer was used in order to generate strain data and a load cell in order to obtain force data and then calculate stress values. This step of obtaining valid stress-strain data was the most complicated phase as finite element codes as ANSYS require "true" data input.

- The clip-on extensometer offered overall strain values in between two positions, but these values were not true local strain values as for example for PP some necking was given at the final stages of deformation.
- Engineering stress values obtained from force data and the original specimen's cross section, needed to be converted into true stress values. The initial consideration was the assumption of a constant deformation volume preservation during the plastic stage of the tensile test, so that the classical equations in Equ. 2.10 and Equ. 2.11 could be used.
- An iterative method to obtain true stress-strain data was proposed.

- It was observed that as the testing speed was held constant in the tensile tests, the engineering strain rate was also constant but the true strain rate decreased exponentially (see Figure 6.21).
- Yield stress values at different testing velocities were calculated using the Considére's construction. Elastic modulus values were calculated according to the ISO standard 527.
- The elastic tensile modulus followed a natural logarithmic relation with the engineering strain rate for the tested speeds. In a similar way, the true yield stress also followed a natural logarithmic relation with the engineering strain rate. The strain at break tendency was also a natural logarithmic curve but in this case, at higher testing speeds, lower strain values were obtained.
- The Eyring's relation seemed to be valid in the range of the tested velocities. An approximate linear tendency could be established for the true yield stress values in front of the logarithmic values of the strain rates. This gave an idea about the possibility of interpolating for different testing velocities inside the tested regime to obtain yield stress data, and also some way for extrapolating to higher testing velocities, but additional testing data should also be recommendable in the later case.
- As elasto-plastic models require separated elastic and plastic data, a concept of "proportional yield point" was included. Using the linear elastic modulus value (calculated as stated in ISO 527), a "fictitious" yield point was calculated, which was lower than the theoretical yield point. This artifact was studied in order to represent the tensile curve with a linear elastic part and a non-linear plastic section. This always over predicts the generated plastic strains but it is a way to not under-predict the stiffness of the material considering a linear portion up to the maximum in the curve. See Figure 6.27. Similar logarithmic tendencies were observed with the new calculated yield stress values with the natural logarithm of the engineering strain rate.
- Data preparation for ANSYS simulations: a multilinear isotropic material model was selected which gave the possibility to use different stress-strain points to define the input curve. The first choice was to use the classical conversion from engineering to true data. See Figure 6.30.
- Additional corrections were performed to this classical conversion in order to take into account in a more detailed way the necking behaviour of the material. These conversions seemed not to be very useful for the selected material as the necking behaviour was not predominant. See later simulation results.
- Bending testing of PP. The displacement of the loading central support was given by the stroke of the moving part of the machine. Force was recorded in the load sensor attached to this central support. This data was later converted into stress-strain data adopting the classical formula of a beam under 3 point bending, equations 2.35 and 2.36.
- The same testing velocities as in the tensile mode were used, and again, stress-whitening was observed in the central region of the deformed shape of the specimens. See Figure 6.35. Bending modulus and maximum bending stress values followed again a natural logarithmic trend when plotted against the used

engineering strain rates. In this case, this logarithmic tendency was even more precise than in the tensile case.

- It was observed that tensile and bending stress-strain curve shapes differed to a great extent. A major contribution to this was that bending stress-strain data was obtained using linear formulas while real experimental data was non-linear. Additional effects of different strain rate levels, compressive behaviour in bending or different straining levels also contributed to this difference. See Figure 6.41.
- Puncture testing of PP. The displacement of the loading hemispherical dart was given by the stroke of the moving part of the machine. Force was recorded in the load sensor attached to this dart. Three testing velocities were used, 2, 20 and 200 mm/min. Lower testing velocities than in the tensile and bending modes were used, from one point to have a differing speed scheme and evaluate the reproducibility by finite element simulations, and from another point due to the fact that higher testing velocities were somewhat dangerous in the used testing device.
- Polypropylene plates showed a clear whitening effect when puncture tested although no total fracture was given for the tested strain levels.
- The effect of the testing speed on the force-displacement curves at different velocities was that a stiffening effect was observed above displacements of 3 mm at higher speeds. The initial linear region was almost identical for the three testing velocities. See Figure 6.44.
- The differently injected specimens gave very similar results; there was no difference in between force-displacement data for fan gate plates or laterally injected specimens. Figure 6.45.
- When using two dart diameters (20 and 11.7 mm), with a lower diameter dart, lower failure force values were recorded due to the easier penetration of the dart in the plastic material. Figure 6.46.
- Concerning the clamping system, the use of an upper clamping device stiffened the plate's response in the initial region of the curve. For higher straining levels, as plastic strains were being localized in the dart area, this difference was decreasing. Figure 6.47.
- Friction properties in between the plate specimen and the supports were modified with the use of Vaseline. This produced lower force values than obtained when without lubrication, but the difference was of the order of the experimental scatter. Figure 6.48.

The experimental results obtained for PC/ABS, have been discussed in the section for PP, however the followings are particular for PC/ABS,

- The selected PC/ABS material showed a necking behaviour when tensile tested and once passed through the yield point. See Figure 6.49.
- At first, the obtained force-displacement curves were converted into engineering stress-strain curves and then to true stress-strain data using the same procedure outlined for PP. Additionally, an iterative method was proposed for this material due to its pronounced necking.
- In terms of strain rate sensitivity, the modulus of elasticity remained almost independent of the changing testing speed. True yield stress tendency was to vary logarithmically with the engineering strain rate and the true strain at break decreasing with increasing strain rate followed a polynomial relation. As in the case of PP, the Eyring's model could be used for establishing yield stress-strain rate relations inside the experimental regime used or outside this range by performing extrapolations, but always bearing in mind that only three testing speeds were evaluated in this study, at room temperature.

- The slow rate tensile test curve was obtained from the classical conversion equations 2.10 and 2.11. The true stress-strain curve was inputted in ANSYS as a multilinear isotropic model based on the Von Mises yield criteria. See Figure 6.56.
- Bending. Considerable whitening was observed especially in the tensile area of the specimen. Figure 6.57.
- Bending modulus remained almost non sensitive to the used strain rates. Maximum bending stress values followed a logarithmic relation with the engineering strain rate.
- As for PP, there were clear differences between bending and tensile stress-strain curves. The reasons mentioned for PP could also be applied in this case. Tensile stress-strain curves seemed to be more precise for large strain material behaviour since bending curves are obtained from linear elasticity equations.
- Polycarbonate+Acrylonitrile-Butadiene-Styrene plates showed a clear stress whitening effect when punctured although no failure was observed at the strain levels tested. Figure 6.62.
- The effect of the testing speed on the force-displacement curves at different velocities was that a stiffening effect was given above displacements of 3.5 mm. The initial linear region was almost identical for the three testing velocities. See Figure 6.63.
- A short appendix was included in section 6.3.7 comparing commercial data and the experimental tests performed in this thesis work. Although the elastic region for both materials was similar between CAMPUS data and own values, yield stress values were somewhat higher when checking CAMPUS data for both materials. CAMPUS data could be valid for elastic and small plastic straining conditions. For studies where the plastic area of the tensile curve was important, experimental own testing was needed.
- In appendix 6.3.8, a deeper study was performed on the strain rate and temperature dependency of the selected materials.
    - It could be observed that for the PP, there was a linear tendency for yield stress to increase with the logarithm of the strain rate.
    - Additionally, strain at breaks values were also measured. It was observed that in this case no linear relationship could be observed between strain values and the logarithm of the used strain rate.
    - For the selected PC/ABS, it could be observed that some linear relationship existed between the yield stress and the logarithm of the strain rates, at different temperatures.
    - For strain at break values no linear tendency was observed when plotted against the logarithm of the strain rates at different temperatures.

Part 2: Quasi-Static Finite Element Simulations of PP and PC/ABS.

- The finite element simulation code ANSYS was used for the simulation of the experimental tensile, bending and puncture tests for both materials.
- The main objective was to evaluate the validity of the use of a classical metallic approach,
    - volume preservation in plasticity > classical conversion from engineering to true stress-strain data.
    - same behaviour in tensile and compressive yielding > Von Mises criteria.

when simulating the described tests.

- Additionally, a more sophisticated approach (iterative method) was proposed in conjunction with the use of a special yielding criterion suitable for thermoplastic materials, the Drucker-Prager model.

Simulations results for PP,

- The comparison of experimental tensile force-displacement data and the simulated behaviour showed an overall good approximation level. See Figure 6.70. and comments. It was necessary to extend the initially measured tensile curve in order to correlate properly the large straining region.
- The use of a clip-on extensometer, the calculation of engineering stress-strain curves and later use of the classical conversion to true data seemed to be valid for this material. Disadvantages, the initial slope of the tensile curve was not properly simulated and it was necessary to extent the experimental curve, see Figure 6.71, to match the large strain experimental curve.
- Mesh sensitivity in tensile mode. Different simulations were carried out using different mesh densities. The decrease in force after the maximum seemed to be mesh dependant. For the selected mesh densities the rest of the curve remain almost insensitive to the change in mesh density.
- The use of an input curve in ANSYS from a correction method (section 6.3.1.2.3) did not improve the correlation level with the tensile test. Figure 6.72.
- Bending simulations. The use of the extended true stress-strain curve gave a very good match to the experimental slow rate bending test. See Figure 6.76. This was even better with solid elements than with shell structures. The thickness of the specimen was too thick for shell type element modeling.
- The use of arbitrary frictional values did not improve the correlation level between simulated and experimental bending tests. The initial consideration of no friction between different parts gave adequate results.
- The use of the Drucker-Prager criterion even improved these results. This denoted that in testing modes were additional states of deformation as compression or shear could be present (bending), it was recommendable to use more sophisticated elasto-plastic models. See Figure 6.82.
- Puncture simulations. The simulation response was located in higher values than the experimental force-displacement curve. The use of an input curve tested at 5 mm/min. seemed to produce a better correlation with the the puncture curve at 20 mm/min. than the curve at 2 mm/min. Shell elements even gave a stiffer response than solid elements and the use of frictional values again did not improve the correlation level between experiments and simulations. Figure 6.85.
- For the smaller dart of diameter 11.7 mm, the simulation did not capture correctly the curvature of the force-displacement trace at the final stage of deformation. Figure 6.87.
- The effect of clamping the specimen on the upper side was correctly captured by the simulation in ANSYS. Figure 6 97.

Simulations results for PC/ABS,

- An iterative method was proposed for the selected PC/ABS material. As the necking behaviour was predominant after the maximum force, this plastic region up to rupture was iteratively simulated in ANSYS, changing the input curve in order to approximate with a number of iterations to the experimental tensile curve. This method was described in section 6.4.4.3.1.

- Thus, two input curves were used in the simulations: the direct curve from the tensile tests (load sensor and clip-on extensometer) and performing conversions and extensions to obtain a true stress-strain curve. And an iterated curve, which was obtained iteratively adjusting the input curve to match the experimental force-displacement curve.
- The comparison of experimental tensile force-displacement data and the simulated behaviour showed an optimum approximation level when using the iterated curve. On the other hand, the extended curve did not represent properly the initial portion of the curve up to the maximum in force. Again, the necking behaviour was sensitive to the used mesh density. Fine meshes of 1 or 0.5 mm gave the best correlation.
- Bending simulations. A good correlation level was obtained both with solid and shell type elements when using the original or classically calculated true stress-strain input curve. The iterated input curve offered a too stiff response in the initial region of the bending force-displacement curve up to the maximum in force. This denotes that a very precise unixial tensile calibration is not always adequate for simulating other testing modes as bending.
- When using the original input curve, as in the case of PP, solid elements offered a better approximation to the test curve. Figure 6.103.
- The addition of frictional characteristics did not improve the simulation response compared to the experimental behaviour.
- The use of a hydrostatic sensitive constitutive model as the Drucker-Prager model, improved the simulation results in bending mode. A better approximation to the experimental test curve was obtained than that offered by the Von Mises criteria. This denotes that in bending dominated modes the use of such a model was recommendable both for semicrystalline and amorphous materials. See Figure 6.109.
- Puncture or dart penetration simulations. The iterated input curve offered again a too stiff response, especially in the initial region of the force-displacement response. The original curve input represented correctly the experimental curve shapes but force levels were in a higher level than the slowest testing speed. The tendency was to correlate in a better way the curve at 200 mm/min.
- Shell elements offered as in the case of PP, stiffer response than solid elements. This was not adequate for the simulation of the experimental behaviour. In a similar way, the addition of friction properties did not improve the correlation between simulation and test.

Literature References.

[1] Michael Junginger, Heinrich Werner and Frank Huberth. "Measurement Technique for Local Strain Determination and its application to Plastic Materials in the Automotive Industry". Presentation at CRASH-MAT 2001.

[2] S. S. Sternstein and L. Ongchin. "Yield Criteria for Plastic Deformation of Glassy High Polymers in General Stress Fields". Polymer Prepints. Vol10, N°2, Sep 1965.

[3] Poisson's ratios of Bayer Thermoplastics. Application Technology Information. Bayer AG.

[4] N. G. McCrum, C. P. and C. B. Bucknall. "Prinpicles of Polymer Engineering". Edited by Oxford Science Publications.

[5] S.I. Krishnamachari. "Applied Stress Analysis of Plastics. A Mechanical Engineering Approach". Edited by: Van Nostrand Reinhold.

[6] Joseph T. Woods and Gerald G. Trantina. "Material Characterization for Predicting Impact Performance of Plastic Parts". SAE Document N° 1999-01-3178.

[7] R. R. P. Rodenburg. "Development Process of Seamless Airbag Covers. Description of tools and generation of material properties using high strain rate tensile testing". Report N° MT 04.12. TU/e Internship Report July 2004.

[8] N. J. Mills. "Plastics. Microstructure and Engineering Applications". Edited by: Edward Arnold.

[9] G. Dean, R. Mera and E Arranz. "Determination of the Properties of Plastics at High Strain Rates". NPL Report MAT(A) 115. September 2002.

[10] G. Dean and B. Read. "Modelling the Behaviour of Plastics for Design under Impact." Polymer Testing, Volume 20, N° 6, 2001, pp 677-683(7).

[11] G. Dean and M. N. Charalambides. "Development of Test Methods for Design under High Rates of Loading. Data Requirements for the Use of Finite Element Methods to Predict the Impact Performance of Plastics". NPL Report CMMT(A) 58. April 1997.

[12] Y. Duan, A. Saigal, R. Greif and M.A. Zimmerman. "Impact Behavior and Modeling of Engineering Polymers". Polymer Engineering and Science, Vol 43, N° 1, 2003, pp.

[13] Y. Duan, A. Saigal, R. Greif and M.A. Zimmerman. "Analysis of Multiaxial Impact Behavior of Polymers". Polymer Engineering and Science, Vol. 42, N°2, 2002, pp. 395-402.

[14] C. G'Sell , J.M. Hiver and A. Dahoun. "Experimental characterization of deformation damage in solid polymers under tension, and its interrelation with necking". International Journal of Solids and Structures, Volume 39, 2002, pp. 3857–3872.

[15] Lobo, H. and Hurtado, J. "Characterization and Modeling of Non-linear Behavior of Plastics". ABAQUS User Conference, Boston (2006).

[16] Gerald G. Trantina and Joseph T.Woods. "Standard Test Procedures for Relevant Material Properties for Structural Analysis". SPE/ANTEC Proceedings 1998.

[17] Pádraig Naughton, Rony Van Daele, John McCallum and Daryl Hertema. "Characterisation of Talc-Filled Impact-Modified Polypropylene for Use in Engineering Analyses". SAE Document N° 980986.

[18] G. Menges, M. Weng and Th. Fölster. "Deformation Behaviour of Thermoplastics for Non-Uniform Stress Distributions". Kunststoffe German Plastics 80 (1990) 9.

[19] W. Michaeli, Th. Fölster and B. Lewen. "Simulating the Long-Term Behaviour of Plastics. Determination of isochronous stress-strain diagrams from accelerated tensile tests". Kunststoffe German Plastics 79 (1989) 7.

[20] Walter Michaeli and Markus Gliβmann. "Concept for the numerical description of the true stress/strain behaviour of semi-crystalline thermoplastics". Polymer Testing, Volume 20, N° 5, 2001, pp. 591-596.

[21] G. Dean, R. Hunt and R. Shastrit. "Illustrations of the Application of Finite Element and Processing Simulation Analyses to Plastics". NPL Report CMMT(A)266 June 2000.

[22] Torodd Berstad. "Implementation of constitutive model for thermoplastics with some preliminary results". 9th LS-DYNA International Conference, 2006.

[23] Paul Wyluda and Dan Wolf. "Examination of Finite Element Analysis and Experimental Results of Quasi-statically Loaded Acetal Copolymer Gears". MSC Software White Paper.

[24] Gervais Milcent. "Evaluation of Constitutive Laws of Plastic Materials for Crashworthiness Simulations". EuroPAM Conference, 2004, Paris.

[25] Frank J. Ferfecki. "A Finite Element Material Model and Method for Predicting the Cumulative Behavior of Energy Absorbing Components in Thermoplastic Bumper Systems Subjected to Multiple Impacts". SAE Document N° 2001-01-0352.

[26] P. A. Du Bois, M. Koesters, T. Frank and S. Kolling. "Crashworthiness Analysis of Structures made from Polymers". 3. LS-DYNA Anwenderforum, Bamberg, 2004.

[27] Test Standard. ISO 527. Plastics - Determination of tensile properties.

[28] A. Arriaga. "Finite-element analysis of quasi-static characterisation tests in thermoplastic materials: Experimental and numerical analysis results correlation with ANSYS". Polymer Testing, Volume 26, Issue 3, May 2007, Pages 284-305.

[29] Paul A. du Bois. "Workshop on Crashworthiness Simulation". 22nd CAD-FEM Users' Meeting 2004, Dresden, 10 Nov.

[30] Gerry Trantina and Ron Nimmer. "Structural Analysis of Thermoplastic Components". Edited by Mc Graw Hill Inc.

[31] A. Arriaga et al. "Impact testing and simulation of a polypropylene component. Correlation with strain rate sensitive constitutive models in ANSYS and LS-DYNA". Polymer Testing 29 (2010) 170–180.

PART II: Impact Studies in Thermoplastic Materials. Experimental Testing and Finite Element Analysis.

Index of Contents.

Index of Tables.

Index of Figures.

Abstract.

The primary aim of the study was to evaluate the validity of the elasto-plastic constitutive models implemented in the Finite Element Analysis (FEA) software ANSYS® and LS-DYNA®. This was carried out comparing experimental high speed tensile, Charpy and Puncture impact test results with the corresponding FEA calculations. The studies were carried out in concern to the high rate testing and finite element analysis of two thermoplastic materials. The selected materials were a blend of Polycarbonate (PC) and Acrylonitrile-Butadiene-Styrene (ABS), these were respectively Bayblend® T45 from Bayer Material Science, an amorphous polymer and a Polypropylene (PP) copolymer, BE677AI from Borealis, a semi-crystalline polymer.

The uniaxial tensile behavior of both materials was used to generate material data input for the simulation software. Tensile testing ranged from a slow strain rate to a high rate according to the ISO 18872 standard. Due to post yield uncertainties when measuring true values of stress and strain with conventional extensometric devices, the iterative approach presented in the PART I of the thesis, was used here as a solution for measuring large local strains in plastic tensile specimens.

The experimental Charpy impact test and the plate Puncture test with hemispherical dart, were used as correlation tests with simulations in order to validate not only the used constitutive elasto-plastic models used based on the Von Mises yield criteria (MISO + Perzyna constitutive model in ANSYS or MAT_024 in LS-DYNA), but also to check the influence of different simulation variables. The parameters studied were the element type and the friction between different parts. Additionally, another constitutive models were also studied, such as MAT_089 (to consider strain rate effects on yielding and failure) or MAT_187 (SAMP) to evaluate another yielding criteria, considering compression and shear effects on the yield surface.

It was observed that for both materials, consideration needed to be made of strain rate effects on yielding to obtain an initially acceptable correlation with Charpy and Puncture tests. These results were improved with the use of iteratively correlated stress-strain curves at different strain rates. Additionally, the extrapolation method described in ISO 18872 was also found to be adequate since acceptable results were obtained in the correlation of the Puncture tests.

The use of more complex mathematical models such as MAT_089 or MAT_187 did not offer improvements for the studied experiments in comparison to the classical MAT_024 model. However, the complexity of MAT_187 makes it ideal for covering most of the particularities of thermoplastic materials behaviour and needs to be studied in further work.

Chapter 8: Introduction.

The use of thermoplastic polymers for crash padding applications is increasing in the automotive sector. The motivation for this usage resides particularly in different passive safety regulations; for example, the FMVSS (Federal Motor Vehicle Safety Standard) for interior occupant impact in vehicles and the FMVSS 581 and ECE-R 42 (European Regulation) for bumper impact. In order to fulfill these standards, thermoplastic materials need to be designed in complex structures that, when impacted, produce stipulated and non harmful deceleration levels in the occupants.

The design process for these structures includes finite element based simulations as a means of predicting part performance and reducing the number of physical prototypes necessary in certification tests. However, there are currently some shortcomings in the generation of adequate material data for feeding various simulation codes (PAM-CRASH, RADIOSS, LS-DYNA, ABAQUS-EXPLICIT, DYTRAN, AUTODYN, etc.).

In part, this problem arises from the mechanical characterisation methods used for plastic materials. Although quasi-static levels of straining rate are well covered with standardisation (e.g., different ASTM or ISO standards for tensile testing), thermoplastic materials testing at high strain rates (as required for impact applications) is not covered by a specific standard. To date, two different "standards" have been proposed: a recommended practice from the Society of Automotive Engineers, SAE J-2749 "High Strain Rate Tensile Testing of Polymers", and an ISO standard, ISO 18872, "Plastics – Determination of tensile properties at high strain rates" [87, 88]. However, it can be said that so far, each development centre focusing on high speed thermoplastic testing follows its own individual in house testing methods and the proposed standards are not strictly followed.

Additional problems arise from the modelling of thermoplastic material properties and the implementation of the constitutive models in finite element simulation programs. Plastic materials show very particular features which should be accounted for in precise impact simulations. Features include strain rate sensitivity, necking or strain localisation, temperature sensitivity and anisotropy due to filler distribution. These aspects are extensively explained in the literature review Chapter 9. Different phenomenological models have been developed and implemented in codes such as LS-DYNA [3, 4, 10, 18, 25, 46, 47] but as the base materials' behaviour is so complex, no model covers all the required aspects. In industry related applications, development times are critical and the tendency is to use the simplest elasto-plastic models with some strain rate dependency.

The present study deals with a blend of Polycarbonate (PC) and Acrylonitrile-Butadiene-Styrene (ABS), Bayblend® T45 from Bayer Material Science, as an amorphous polymer and a Polypropylene (PP) copolymer, BE677AI from Borealis, as a semi-crystalline polymer.

Three main areas were evaluated in order to check the validity of the different material models and simulation variables in ANSYS (implicit approach) and LS-DYNA (explicit approach).

The first area relates to the generation of input data for FEA. Obtaining stress-strain data for the simulation of impact events needs the material to be tested at different speeds or straining rates.

The second area is related to the treatment of the tensile test data at different strain rates in order to use it with disposable material models in ANSYS and LS-DYNA.

And the third section is related to the correlation of relatively simple experimental impact tests (such as Charpy or Puncture tests) in order to evaluate the validity of the material models implemented in the described software.

Charpy and Puncture test were selected in order to evaluate different deformation modes; mainly bending in Charpy tests (the case of notched specimens is more complex due to triaxial stresses and crack propagation) and biaxial loading in Puncture tests.

Chapter 9: Literature Review of Part II.

This chapter has been categorised into three sections for a more ordered description of the literature review:

1. Thermoplastic Materials Constitutive Modelling in FEA for High Strain Rate Applications, where the different material constitutive modelling approaches for crash applications published in literature are described.
2. Characterisation Methods and Finite Element Procedures in Impact Analyses, where the different work methodologies found in literature related to material testing, use of different FEA codes, and material models, are described.
3. High Strain Rate Test Methods, where the different test methodologies and instruments found in literature are described.

9.1. Thermoplastic Materials Constitutive Modelling in FEA for High Strain Rate Applications.

Thomas Goral [1] addressed materials modelling of engineering thermoplastics for finite element analysis when subjected to high speed or impact loading. The selected material was a Polycarbonate (PC), which was modelled in different ways (increasing model complexity) for evaluating a head-impact test in LS-DYNA. Initially, the author described the uniaxial tensile behaviour of unfilled thermoplastics in four regions:

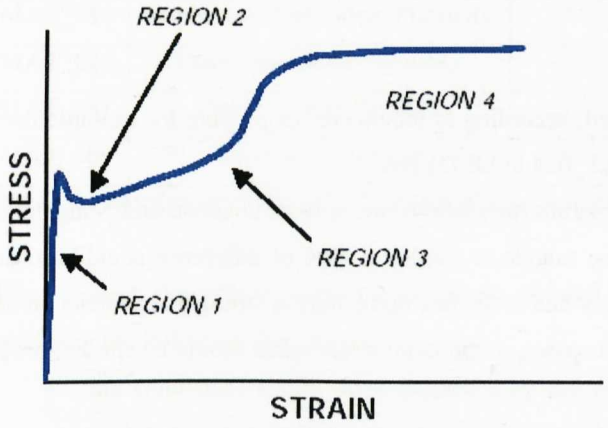

Figure 9.1: Different regions in a nominal stress-strain curve of a ductile thermoplastic material [1].

Region 1: defined as an elastic zone where despite non linearity, recoverable straining is given upon load removal.
Region 2: starts when the yield stress is reached and passed through. A drop in stresses is observed due to the neck formation in the specimen.
Region 3: strain hardening due to molecular orientation, stress rises.
Region 4: depicts a stabilisation of the strain hardening effect.

Goral emphasised the strain rate effects on the stress-strain curves: the yield stress increased with strain rate until the ductile-to-brittle transition was reached. He did not observe variation in the elastic region and as a general rule, the statement that the yield stress increases 7% with a decade of increase in strain rate was presented.

The different approximations for modelling the elasto-plastic behaviour of the PC were as follows:

- perfectly elastic material: Young's modulus, Poisson's ratio and density.
- perfectly plastic model: Young's modulus, Poisson's ratio, density and zero slope curve above yield point.
- piecewise linear plasticity model: Young's modulus, Poisson's ratio, density and stress-strain points for defining the entire plastic curve.
- piecewise linear plasticity model plus scaling of the yield stress with strain rate: Young's modulus, Poisson's ratio, density, stress-strain points for defining the entire plastic curve and a multiplier for the yield stress depending on the strain rate. This model accounted for the variation of yield stress with strain rate.

Note: these two last approximations were also adopted in the present thesis work to simulate Charpy and Puncture impact tests.

The experimental head-impact tests were conducted at 7.1 m/s. Force-displacement and acceleration-time curves were compared with the simulation results obtaining the best correlation in the material model with piecewise definition and strain rate effects.

Pádraig Naughton [2] outlined an approach to model some of the effects of strain rate in the simulation of thermoplastics in high speed crash applications. He divided the strain rate effects into three categories:

- effect on overall stress level.
- effect on failure strain.
- effect on modulus.

The first category could be covered, according to the author, employing for example the Cowper-Symonds constitutive model included in MAT_024 in LS-DYNA.

Related to failure strain, at higher strain rates lower values were obtained and Naughton exposed that even within the same material, from one sample to another a 20% of difference could be observed in measured strain to break values. This is mainly due to the fact that failure is strongly dependent on internal faults in the specimen's structure. For design purposes, a minimum strain value should be chosen, probably, plus a safety factor.

Modulus was also affected by the strain rate, leading to stiffer behaviour at high strain rates. The problem remains that in thermoplastics the elastic region is not linear and from the FEA viewpoint two general simplifications can be adopted for defining this region:

- a single secant modulus up to the yield point.
- using an initial modulus at low stress values and defining the rest of the non-linear region as it would be plastic.

The first choice underestimates the stiffness of the material and the second approximation defines more plastic straining than in reality.

The author tested both approaches testing and simulating a knee impact on a glove box door (16 Kg. at 5-8 m/s.). The loading of the structure was modelled in a better manner with the second option but it underestimated the rebound in the unloading phase due to the generation of excessive plastic strains. He concluded that a non linear elastic region definition was needed in FEA codes.

Xinran (Sharon) Xiao [3] examined the effect of strain rate in the simulation of the standard FMVSS 201 with different material models in LS-DYNA. The material parameters investigated include yield stress, Young's modulus and failure strain.

FMVSS 201 is a requirement for reducing occupant injuries from head impacts inside the vehicle. As thermoplastics are increasingly being used in interior applications, the available material models that could be interesting for plastics were studied in this research.

The first difficulty experienced by the author was the inability to model the modulus or failure strain variation with strain rate in most material models.

The second difficulty resided in the hydrostatic stress component dependency on yielding in many plastics.

And the last commented difficulties resulted from the material softening upon yielding and the adiabatic heating and additional softening at relatively slow strain rates (0.1-10 s^{-1}). This could cause stress-strain curves to cross each other at different strain rates, which in turn leads to problems in interpolation algorithms. The author studied three elasto-plastic material models implemented in LS-DYNA: MAT_019, MAT_024 and MAT_089. He took into account the pressure sensitivity in yielding using a user programmed subroutine. The author summarised the capabilities of some strain rate models in the following table:

Material Number	Material Title	Strain Rate Dependency				Softening
		Yield Stress	Young's Modulus	Failure Strain	Failure Stress	
MAT_019	Strain Rate Dependent Plasticity	Y	Y	-	Y	-
MAT_024	Piecewise Linear Plasticity	Y	-	Y	-	-
MAT_081	Plasticity with Damage	Y	-	-	-	Y
MAT_089	Plasticity Polymer	Y	-	Y	-	-

Table 9.1: Attributes of the different material laws implemented in LS-DYNA [3].

Head impact simulations with the described material models where compared to experimental results obtaining the following conclusions:

- the simulation results were improved by not only taken into account the yield stress dependence with strain rate but also the failure strain and modulus dependence, so, MAT_019 was the best choice (followed by MAT_024 and MAT_089 respectively).
- the Von Mises criterion modification did not give improvements through the use of shell elements where low hydrostatic components were present.
- the use of a maximum strain rate single curve gave poor results; different strain rate curves were needed compromising the strain rate ranges of the real part.

In another reference [4], the same author also explained the possible suitability for plastics' impact simulation of the material model MAT_015 in LS-DYNA. This is the so called Johnson-Cook law which has the strain rate dependency on yield stress and failure strain and additionally can describe softening. No results were presented for this model.

Y. Duan, A. Saigal, R. Greif and M.A. Zimmerman [5] carried out several impact correlation studies with their so called model DSGZ (see Section 3.1). The experimental impact tests were based on multiaxial drop

dart tests (ASTM D3763) in different materials like ABS or Polybutylene terephthalate (PBT). They studied different testing conditions (speeds and temperatures) as well as different modelling parameters (remarking the effect of the selected friction coefficient between the dart and the plastic plate) for the simulation of the real event.

The authors also proposed a thermo-mechanical coupling model for taking into account the heat generation during high strain rate testing and its influence on the stress-strain curve of the material. At high strain rates the heat generation should be taken into account with the following relation:

$$\Delta T = \beta \frac{(\bar{\sigma}^{old} + \bar{\sigma}^{new})\Delta\bar{\varepsilon}^{pl}}{2\rho c} \qquad \text{Equ. 9.1.}$$

where ρ is material density, c is specific heat, β is the fraction of dissipated plastic energy which converts into thermal energy, $\bar{\sigma}^{old}$ is the equivalent stress at the beginning of a strain increment, $\bar{\sigma}^{new}$ is the equivalent stress at the end of the strain increment, and $\Delta\bar{\varepsilon}^{pl}$ is the increment of equivalent plastic strain. This equation in conjunction with the DSGZ model, decreases the equivalent stress as a temperature rise is given due to the generation of rapid local plastic strains.

The authors proposed a value of 0.9 for β due to the lack of available data.

As the DSGZ model describes uniquely the deformation behaviour of the thermoplastic material, additional information is needed for the failure simulation of the material. The authors used a failure criterion based on maximum plastic strains:

$$\psi = \frac{\sum \Delta\bar{\varepsilon}^{pl}}{\bar{\varepsilon}_{\max}^{pl}} \qquad \text{Equ. 9.2.}$$

where $\bar{\varepsilon}_{\max}^{pl}$ is a prescribed maximum equivalent plastic strain, $\Delta\bar{\varepsilon}^{pl}$ is the increment of equivalent plastic strain and ψ is an indicator of material failure. If the sum of plastic strain increments equal or pass the prescribed value (i.e. $\psi \geq 1$) elements are removed from calculations.

Note: a similar criteria was adopted in the present thesis work. For example, in LS-DYNA a certain plastic strain limit can be specified in MAT_024. Elements that pass this value are deleted from calculation which simulates material failure or eroding.

In general they found good agreement between experimental and simulation results in ABAQUS using the DSGZ model with thermo-mechanical coupling plus the failure criterion (implemented with subroutines created in the programming language FORTRAN). The model response was located in almost all conditions in an intermediate position between the test scatter.

They remarked the influence of the hydrostatic pressure sensitivity variable (if it was not taken into account, overestimates of 24% were obtained in force-displacement traces) and the influence of the friction coefficient (a zero value underestimated by 17% the force values).

The thermo-mechanical coupling did not greatly improve the simulations results for the tested temperatures and strain rates.

In the present thesis no thermo-mechanical coupling will be considered.

Dr. Jerome P. J. Coulton [6] presented a paper related to the analysis and results of the modelling of an aliphatic polyketone (Carilon EP) at high strain rates and low temperatures. LS-DYNA was used as the explicit code for plate perforation simulations where two different material models were evaluated: Johnson-Cook and Kruphowsky.

The author concluded that although there were many material models that comprised some of the high rate polymeric aspects in different FEA codes as LS-DYNA or PAM-CRASH, there was not given any detail on how to obtain the constants needed in the different laws.
The author proposed the simulation of the tensile test as a way to correlate the complex experimental deformation modes within the polymer.
Instrumented Puncture tests were also evaluated as a way to compare the material model capability of modelling impact tests.
Note: this approximation was adopted in the present thesis work. Additionally, Charpy impact tests were also carried out and simulated in ANSYS and LS-DYNA.

Scott Burr et. al. [7, 8] carried out a sensitivity and correlation study of a finite element code (LS-DYNA) to thermoplastic material parameter inputs under high speed impact events.
They remarked that material parameters for high-speed impact events were by far the most difficult input parameters to generate in FEA. For the elastic region of the material response, Young's modulus, Poisson's ratio, and yield strength values are required. For the plastic region of the material response, a true stress/true strain relationship. If any of the material parameters vary as a function of strain rate, those rate dependencies also need to be accounted for in the model.
They proposed as an alternative technique the finite element method itself. A specimen was subjected to a dynamic impact, often an instrumented dart impact, while the load and displacement of the impactor were recorded. A finite element model of this system was created to simulate the impact event. In essence, every element in the system model now became a strain gauge. Material properties were modified by trial and error to obtain a response that correlated with the load-displacement curve obtained in the physical tests.

The crash modelling of plastics has also been treated from a "rubbery" point of view by some authors like **Heiner Müllerschön, Armin Dangel, Nils Karajan, Alexander Hummel and Andreas Wüst** [9]. The material of study was a Lupolen from Basell (High Density Polyethylene, HDPE) which is used for fuel tanks in DaimlerChrysler Commercial Vehicles. Lupolen is a strain rate dependent material and up to a relatively high level of deformation, strains are almost fully reversible. Thus, the viscoelasticity of this material was treated in LS-DYNA by means of the *MAT_ODGEN_RUBBER model which is used generally for the description of the hyperelastic and visco-elastic behaviour of rubbers.

Frank Huberth, Stefan Hiermaier and Marika Neumann [10] presented an overview on existing material models for thermoplastics applicable on shell elements in LS-DYNA. Specifically, the problem of parameter derivation from experimental data was discussed.
From our thesis viewpoint, the different material models description that the authors exposed are very interesting and a brief summary will be explained below.

Material models in LS-DYNA.
The material model *MAT_024 (*MAT_PIECEWISE_LINEAR_PLASTICITY) in LS-DYNA was often used for the crash and impact simulation with thin walled structures and is intensely used still today. This material model describes the elastic deformation as linear. Strain rate effects are considered by shifting the yield stress. Analogously, the pure elastic deformation increases with the strain rate. The plastic material behaviour can be described with true stress- strain curves for different strain rates by a separate plastic strain

part. When using *MAT_024 for thermoplastic materials it is recommend to activate the viscoplastic option (VP=1) to improve the results and reduce oscillations.

For *MAT_024 a maximum plastic strain criteria, a time step based element elimination and the possibility of a user defined failure subroutine as well as no consideration of failure are disposable. This appears to be sufficient but a user defined failure subroutine is not an option for normal daily use and the maximum strain criteria is more suitable for brittle failure behaviour.

The authors remarked that the experimental determination of one value for maximum plastic strain was not that easy in tensile tests for example as the results scatter frequently by more than 30%.

The strain rate influence on the failure strain is included in a material model, developed not for metals but for plastics, *MAT_089 (*MAT_PLASTICITY_POLYMER). In comparison with *MAT_024 the only benefit of this model from a practical point of view is the possibility to include a rate dependent failure. The controllability for *MAT_024 offers the user more options.

Another model specifically developed for plastics is *MAT_101 (*MAT_GEPLASTIC_SRATE_200a). This model includes strain rate effects, different criteria for element elimination against strain rate, principal stress and plastic strain. A special feature is the definition of unloading moduli as a function of the plastic strain. Basis for the model is a stress-strain curve but additional parameters have to be determined, like the pressure sensitivity factor.

A kind of successor of *MAT_024 is *MAT123 (*MAT_MODIFIED_LINEAR_PLASTICITY). The main disadvantage of *MAT_123 compared to *MAT_024 is the currently unused VP option. The enhancements of *MAT_123 are additional failure options. The latest improvement is the inclusion of rate dependence of the plastic thinning failure.

*MAT_081 (*MAT_PLASTICITY_WITH_DAMAGE) is an elasto-visco-plastic material model that is comparable to *MAT_024 but includes an additional damage approach. Reaching a defined strain softening is introduced until material rupture. This softening should consider cavitation in the material under loading. Voids occur mainly under tensile loading but the model considers no different load cases.

Consideration of a load dependent material behaviour for tension and compression is given in *MAT_124 (*MAT_PLASTICITY_COMPRESSION_TENSION). This model offers the user the possibility to define yield stresses for tension and compression separately. The elastic constants are identical for both. Strain rate effects are modelled by a Cowper-Symonds model. The separated consideration of tension and compression could be useful for bending dominated loading cases.

For pure elastic problems a viscoelastic material model could be used. The only one available for shells is *MAT_076 (*MAT_GENERAL_VISCOELASTIC).

A new material model has been implemented into LS-DYNA as a user defined constitutive model by **S. Kolling, A. Haufe, M. Feucht & P.A. Du Bois** [11]. From the author's viewpoint, all effects associated with thermoplastics can be approximately considered in a simple material model: necking by an elastic-plastic law, unloading behaviour by a damage model and pressure dependent behaviour e.g. by a standard Drucker-Prager model.

A new constitutive model, termed as SAMP-1 (Semi-Analytical Model for Polymers with C1-differentiable yield surface) was developed by the authors (all the constitutive material model formulation is described in the corresponding paper), being an interesting contribution the consideration of the crazing phenomena. Many plastics and PP-EPDM in particular, show a localised deformation process called crazing. The material will typically change colour and turn white in the craze. From a mechanical point of view crazing can be

identified with a permanent increase of volume (volumetric plastic straining) and a low biaxial strength. To simulate crazing it may therefore be desirable to consider biaxial test data in the numerical model. In SAMP-1 the hardening curve resulting from a biaxial tensile test is therefore optional as input. The curve should give yield stress as a function of volumetric strain.

The strain rate dependency of SAMP-1 was investigated by the simulation of dynamic tests (tensile, compression and shear) in PP-EPDM. Some limitations of the model from the authors' viewpoint are:

– The input data is based on test results that are partly difficult to obtain. The latter is primarily true for shear and biaxial loading but also for compressive loads and for any dynamic load involving stress relaxation processes.

– The application is limited to ductile plastics that are initially isotropic and remain isotropic throughout the deformation process. This will not be the case for most polymeric materials.

From the same reference, in the year 2002 a PhD. thesis with the topic characterisation and modelling of unreinforced thermoplastics for numerical simulation of crash was concluded by Michael Junginger. He developed a material model that included a stress state dependency for tension, compression and shear. Strain rate and temperature were also considered. A logarithmic strain rate and linear temperature dependency with yield stress was used.

Input data determination.

The experimental data is generated by tensile tests in most cases. These tests are mainly performed at constant speed but not at constant strain rate. The authors proposed an interpolation scheme to generate curves for constant strain rates.

Some tests were performed recently at EMI (Ernst Mach Institute, Freiburg, Germany) to estimate the crazing dilatation under tensile load. Two optical measurement systems were used to determine the tensile strain, thickness reduction and the lateral reduction in a PC+ABS blend. The analysis of the segment volume leaded to an increase in volume up to more than 30% for quasi static loading.

G. D. Dean and L. E. Crocker [12] presented the results of a United Kingdom DTI (Department of Trade and Industry) project related to the impact characterisation and FEA modeling of thermoplastic materials. Measurements of true stress vs. true strain were carried out under tension, compression and shear on a rubber-toughened propylene-ethylene copolymer (used for the manufacture of motor vehicle interior door trims). Results were analysed to determine the properties and parameters required by selected elastic-plastic models (Von Mises, linear Drucker-Prager and cavitation model) for the simulation of impact performance using finite element methods. The procedure used for the determination of properties at high strain rates involved:

1. Modelling the shape of experimental hardening curves at low and moderate strain rates.
2. Determining the variation of model parameters with strain rate.
3. Deriving hardening behaviour at high strain rates by extrapolation.

These curves were fitted using the Equation 3.1:

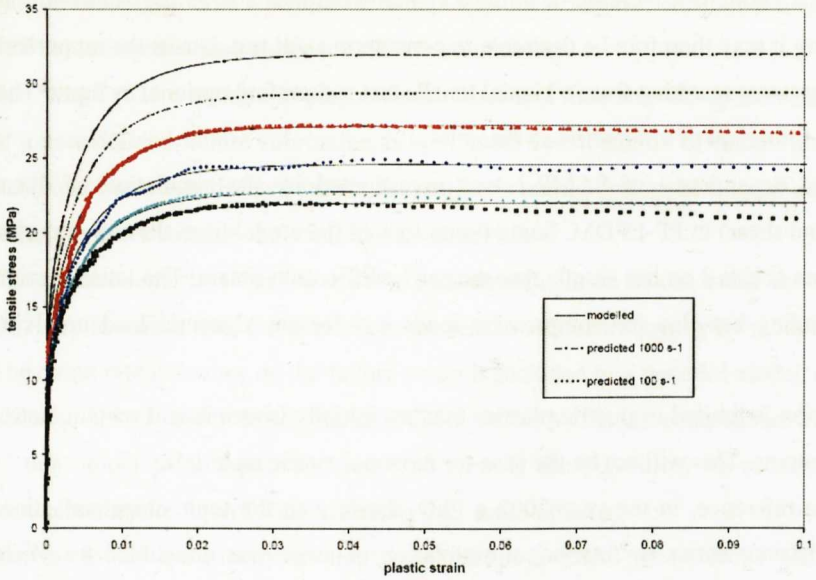

Figure 9.2: True stress-plastic strain curves generated from Equation 3.1. Extrapolations to 100 and 1000 s^{-1} were performed [12].

Note: this methodology was also tested in the present thesis work. It is mainly based on the ISO 18872 standard, which includes the necessary constitutive models.

Analysis of these measurements revealed that the increase in the flow stress σ_f with strain rate could be accurately modelled by the Eyring function.

The authors also performed a sensitivity analysis of the different parameters that could be considered in a FEA. Here, some results from their work are illustrated:

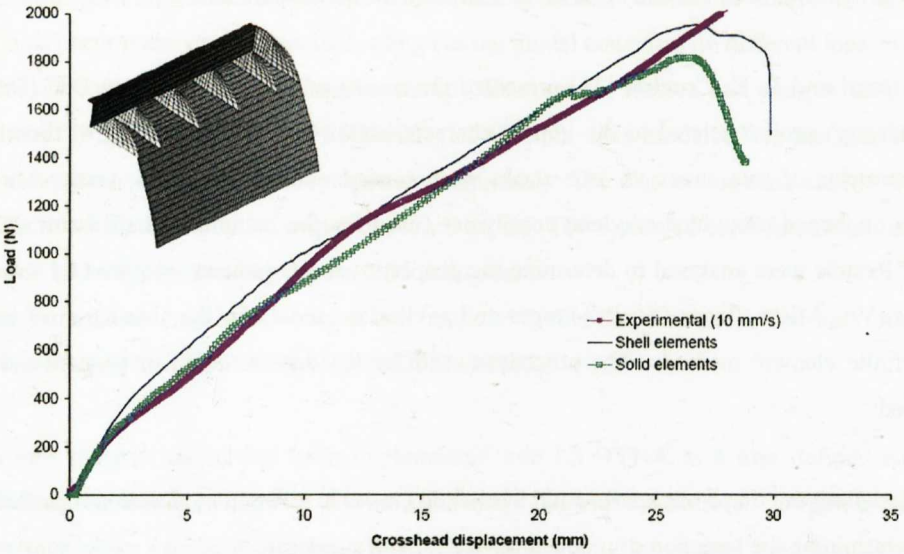

Figure 9.3: Comparison of predicted (ABAQUS) and measured values using different element types [12].

- Element type. Although shell elements were able to predict the overall deformation of the component well, solid elements performed better in stress and strain analyses. See Figure 9.3.
  It can be also be observed that the tested speed was not of the high rate range (10 mm/s.).

- Material parameters. The use of a low-rate curve underestimated the peak loads in the component. When more care was taken in selecting a single rate curve, then reasonable predictions could be

obtained. As it is difficult to estimate the varying strain rates within a complex shape during impact loading, it is always prudent to include rate-dependent data if possible. See Figure 9.4.

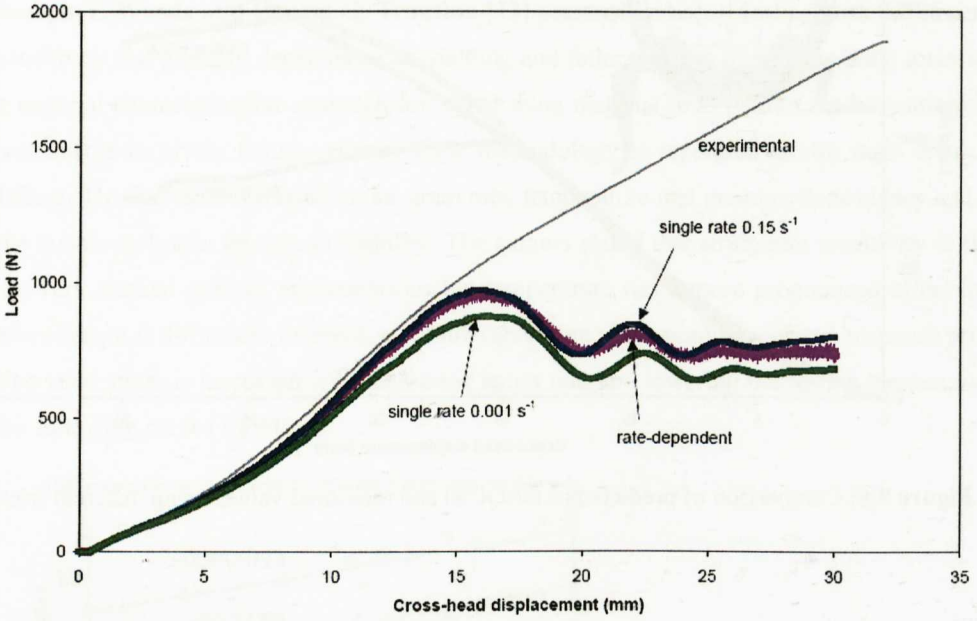

Figure 9.4: Comparison of predicted (ABAQUS) and measured values using different material strain rate approximations [12].

- Material model. For the studied plastic component the so called cavitation model (which was developed by the authors and considers crazing effects) was the best choice to represent the force-displacement behaviour of the impacted part. See Figure 9.5.

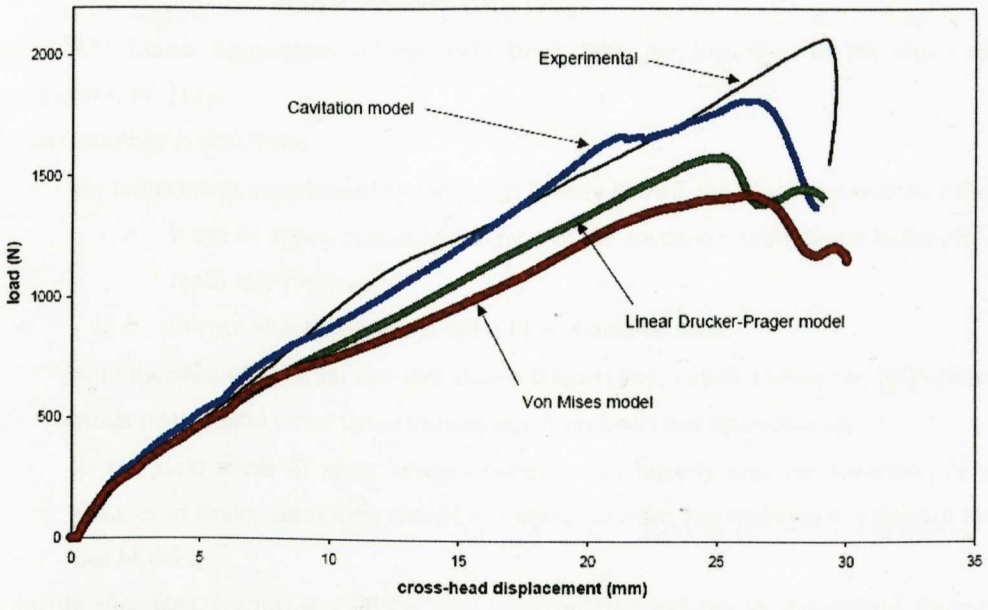

Figure 9.5: Comparison of different material laws with experimental impact test [12].

- Friction. Taking into account some friction between different parts, FEA results were improved. See Figure 9.6.

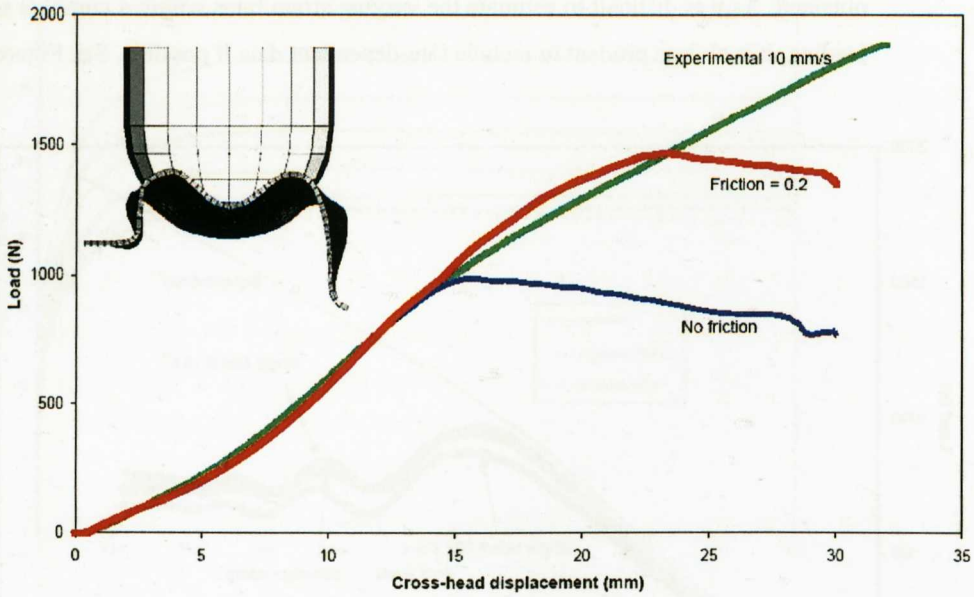

Figure 9.6: Comparison of predicted (ABAQUS) and measured values using different friction values [12].

9.2. Material Characterisation Methods and Finite Element Procedures in Impact Analyses.

Joseph T. Woods and Gerald G. Trantina [13] presented a paper dealing with the strain rate, temperature sensitivity and pressure dependence on yielding and failure modes of thermoplastic materials. They outlined a material characterisation approach for establishing material deformation modes, anticipated failure modes and ductile or brittle failure criteria. Their methodology is separated in two main areas: deformation and failure. The first area is related to the strain rate, temperature and pressure dependency and the second one to the ductile or brittle fracture probability. The authors stated that strain rate sensitivity in the elastic range is not very marked in most thermoplastics but temperature has a more pronounced effect in modulus values. Moreover, it is difficult to establish modulus values due to the nonlinear elastic response prior to yielding.
The yield stress is increased with increasing strain rate and lowering the testing temperature, they presented the following curves for PC:

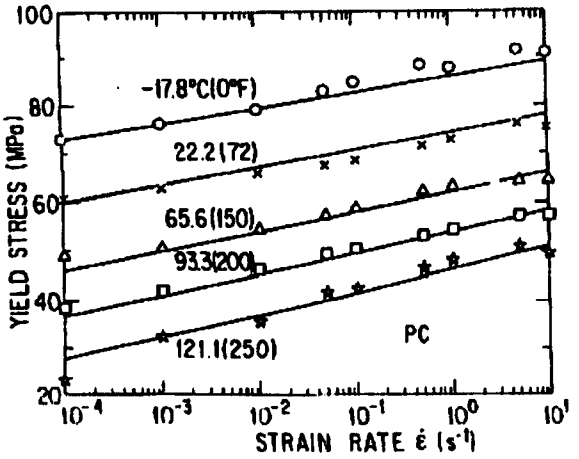

Figure 9.7: Linear dependency of the yield stress with the logarithm of the strain rate at different temperatures, PC [13].

The methodology is as follows:

- the temperature experienced by the part is usually known, the strain rate must be calculated:
  - it can be approximated by the ratio of the maximum strain found in the part and the time to reach that strain level.
  - in case of complex geometries, FEA should be used.
- with the calculated strain rate and known temperature, tensile testing can be performed. The tested strain rates should cover the calculated one from lower and upper bounds.
- as the yield stress of many thermoplastics varies linearly with the logarithm of strain rate, few decades of strain rate testing should be carried out, then extrapolation to higher or lower strain rates can be done.

In ductile situations, tearing is a further step after yielding and can be determined from strain to failure measurements. They developed a methodology for defining a tearing ductile failure criterion based on equivalent plastic strain to failure:

- impact testing is performed in three geometries: circular disk, disk with a hole and three-point notched beam bending (Charpy).
- different temperatures and strain rates are used.
- displacement at failure is recorded in each case.

- FEA is performed in each test condition and at the corresponding experimental failure displacement, the equivalent plastic strain given by the software is recorded.
- if the failure criterion is consistent, there should not be differences between different tests (unless brittle failures are given in some conditions).
- equivalent plastic strains are plotted as a function of strain rate.
- if enough samples are tested the failure strain can be treated statistically, establishing means and standard deviations.

For brittle failure, they established that fracture occurs when the maximum principal stress in a component reaches a critical rate dependent value. If maximum principal stress levels within the part are kept below the critical value then brittle failure is not a concern.

The methodology for brittle failure is as follows:

- three point bend testing of notched specimens at the desired temperatures and strain rates.
- the displacement at break is recorded.
- FEA of the three point bending test. A mesh refinement is needed in the notch area.
- the simulation results are compared with experimental tests and at the displacements at break, and the maximum principal stresses are recorded.
- as in the previous case, if consistent data is achieved in between different geometries, a plot of maximum principal stresses versus strain rate can be obtained.

The authors tested this methodology with a plastic bumper for a pendulum impact at -30°C and a testing speed of 5-7 ft/s. They were able to predict failure location and time fairly well in broken parts using failure criterion based on lower bound measures (from the distribution of measured failure values in the described methodology).

Stephen M. Pitrof and Michael C. Lee [14] presented a new methodology for characterising thermoplastic materials for impact simulations:

- the first step consists of carrying out quasi-static tensile tests in small samples cut from injection moulded parts (12x2x1.5 mm gauge length).
- Young's modulus is calculated from a stress correspondent to a strain of 1%.
- engineering data is converted to true data assuming incompressibility in the plastic regime.
- the next step consists on developing strain rate dependant data (modulus variation with strain rate). A servo-hydraulic instrument is used for applying sinusoidal vibration to a previously elastically loaded sample:
    - the elastic strain in the initial equilibrium state should be around 0.5%.
    - the superimposed sinusoidal strain amplitude should be around 0.2%.
    - a certain frequency should be used.
    - the vibration needs to be of a sufficient duration to make an acceptable measurement without causing the specimen to significantly change temperature.
- the strain rate is calculated from the frequency of the alternating stress.
- the stress is based on the storage and loss modulus.
- as the yield strain is fixed at 1%, the variation of the Young's modulus with frequency or strain rate is calculated from the measured stress.

This method is quite simple and straight forward and the authors proposed it as an alternative to the expensive and time consuming methods like Split-Hopkinson systems. It can be said that the strain range of the presented method is far below crash applications where all the energy is almost absorbed in the plastic regime. In other words, the testing method is adequate for the non-linear viscoelastic region characterisation but ignores viscoplastic effects.

The authors employed the generated material data in the simulation of knee bolsters in LS-DYNA and ABAQUS. The material treatment was elasto-plastic in both codes (MAT_024 in LS-DYNA and similar in ABAQUS) with no rate dependency in modulus, which was in contrast with the used test method used. Anyway, an overall good correlation was obtained with experimental deceleration-time curves. Improvements were needed in material modelling regarding the strain rate sensitive modulus, fracture and elasto-plastic contributions.

O. Schang, et al. [15] studied the mechanical behaviour of a ductile Polyamide 12 during impact. They focused on the application of a constitutive equation determined during low speed tensile tests, to a model of the polymer deformation behaviour during impact. The study consisted of three steps:

- tensile tests for the determination of the parameters in the constitutive equation.
- validation of the law at higher strain rates by testing and numerical simulation, and taking into account heat power dissipation.
- multiaxial impact testing and correlation with numerical results.

The constitutive model was based on the G' Sell-Jonas equation (see Equation 3.13). Failure was not taken into account in this study.

J.C. Viana, A.M. Cunha and N. Billon [16] continued in the path of the above mentioned work. Again, the G' Sell-Jonas law was selected for the description of the stress-strain curve with dependence on straining rate and temperature. Here, the effect of processing conditions on the properties of the plastic samples was taken into account by relating mould filling simulations in C-MOLD with the material law's coefficients as follows:

- two thermomechanical indices were selected in the mould-filling code: the crystallinity degree of the core and the level of orientation of the skin layers.
- stress-strain tests were performed at different temperatures and strain rates using samples obtained at different processing conditions. The G' Sell law's parameters were identified.
- the filling thermomechanical coefficients and the parameters of the material law were related with a polynomial type function.

The authors studied the dart drop test behaviour of two geometries obtaining satisfactory results.

In the present thesis work, no processing effects have been considered.

Frank Lutter; Michael Münker and Martin Wanders [17] worked on the simulation and material characterisation strategies for modelling the crash behaviour of automotive components (with special consideration to hybrid metal-plastic front-ends). They considered the rate and temperature dependency and the importance of measuring adequately the local stresses and strains as well as failure characteristics.

Their simulation method was based first on the modelling of the tensile test. If deviations were observed with experimental results (especially in materials suffering necking) they modified the input data iteratively in order to match the experimental force-displacement curve.

Note: a similar method was used in the present thesis work.

They observed that when a tensile specimen is stretched and a neck is formed, at the point where the necking takes place, the strain rate is up to 30 times higher than the technical or engineering strain rate at which the test specimen is stretched as a whole.

They investigated that for a PC/ABS, considering a constant elastic modulus, an exponential relationship existed between temperature shift and the change in the loading rate within certain limits. The authors proposed the Williams-Landel-Ferry superposition principle in order to estimate for example high strain rate properties (where technical difficulties appear for measuring adequate stress-strain data), testing at low temperatures.

P.A. du Bois, M. Koesters, T. Frank and S. Kolling [18] performed a comparative review of material models for polymers subjected to impact loading. For thermoplastics, they gave an overview of suitable plasticity material laws in LS-DYNA and showed how the behaviour can be characterised approximately by using metal plasticity. But in thermoplastics, non-linear elasticity exists and commonly used material laws based on von Mises plasticity are not precise enough from the authors' viewpoint.

Taking the three-point bending test, they proposed the use of a Drucker-Prager material model that takes the compressibility and the different behaviour of the material under tensile and compressive stress into account. Because of the higher yield stress under compression, it was not possible to precisely simulate the bending test using von Mises plasticity based on the tensile test. If a Drucker-Prager model was used, where, taken from the experiment, the yield stress under compression was 1.3 times the yield stress under tension, the bending test could be simulated in good agreement.

A similar study was performed in Sections 6.4.2.3.1 and 6.4.5.3.1 of this thesis.

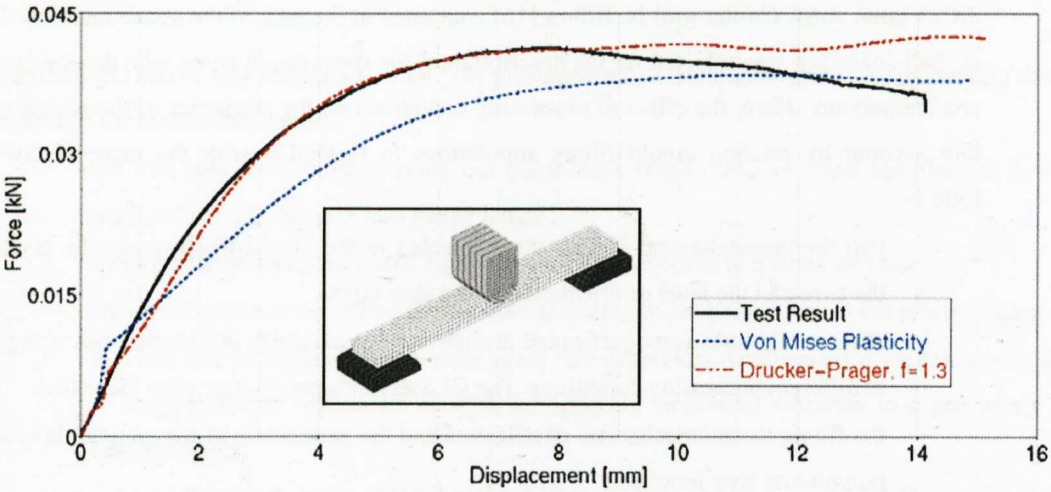

Figure 9.8: Comparison of experimental and simulated bending test results. The Drucker-Prager model gives a better approximation than the Von Mises law [18].

Julio C. Abajo Alonso, Alberto Negro Marne, Alberto Mansilla Gallo and Isabel Gobernado Mitre [19] developed a complete methodology, based on characterisation tensile tests at different strain rates under static and dynamic experimental conditions, implementation of the obtained behaviour laws in the PAM-CRASH finite element code, and final validation of results for the design optimization of an automotive A-pillar trim.

The authors remarked that at the present there is no a standard for conducting dynamic tensile tests at determined strain rates for obtaining suitable stress-strain curves for FEA. However, international associations as SAE (Society of Automotive Engineers) and ESIS (European Structural Integrity Society) are

showing a great interest in the definition of a methodology for the characterisation of thermoplastic materials at high strain rates.

Masahiro Fujii, Syunichi Kawano and Hiroshi Fujino [20] performed a benchmark problem for crush analysis of plastic parts for automotive.

In their work, several tensile and compression tests were carried out to evaluate the effect of strain rate and temperature on the mechanical properties of plastic materials. Then, crush tests of a plate with ribs made of rubber toughened polypropylene were carried out to prepare benchmark data.

They emphasised on:

- the effect of moulding conditions; mechanical properties often vary even in the same part as can be seen in different specimens cut from different zones.
- the effect of strain rate.
- the effect of ambient temperature and furthermore, temperature rises during test due to visco-elastic phenomenon and low conductivity of thermoplastics.

They obtained true stress-strain relationship from: extension, from gauge lengths of 25 mm, and load, from load-washer during tensile test, assuming volume conservation conditions.

They studied different simulation variables as the mesh size, the strain rate dependency or the effect of imperfections in a ribbed test piece:

- effects of mesh size were not significant within the range of size of mesh selected in this report.
- they observed possibilities to reduce computational time by selecting appropriate typical strain rates. Further studies were needed.
- consideration of small initial imperfection at the contact area significantly affected the analysis results. Detailed representation of this geometry at finite element modelling was necessary in crush analysis.

Markus Brinkmann (IKV) [21] presented the modelling aspects of the mechanical behaviuor of thermoplastics in dynamic applications.

The method was based on measurements of force-displacement values in a high speed testing machine at different strain rates, conversion to true stress-strain, simulation of the tensile tests, and correlation with the experimental tests to get the material card.

Note: a similar method was used in the present thesis work.

This method was then evaluated again in more complex geometries (airbag covers):

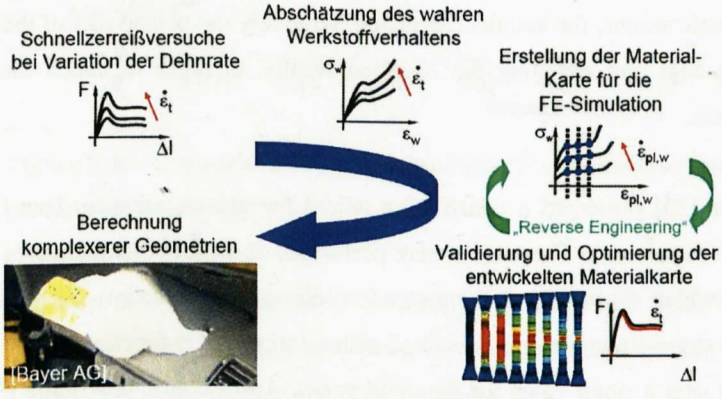

Figure 9.9: Process for the determination of adequate stress-strain curves at different strain rates. Tensile test simulation is the basis [21].

For the evaluation of the material card, both from plasticity and failure viewpoint, the author used a dart drop test in ribbed and non-ribbed rectangular plates (PC+ABS, PP, PA). It can be seen that the force-displacement curves were approximately matched in some cases although optimisation was needed. Moreover, great differences were observed in between solid and shell type element results. *This behaviour was also observed in the simulation results of the present thesis.*

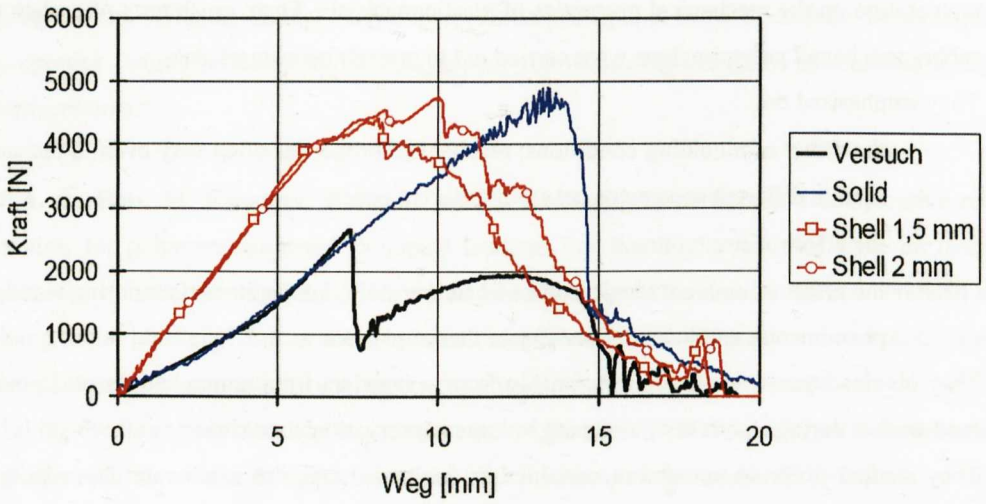

Figure 9.10: Comparison of experimental (black) and simulation results using different element types [21].

Slimane Bekhouche, Yvon Chevalier and Pierre Guellec [22] presented a complete approach for the design of car bumpers loaded by small impacts. It was based on non linear explicit dynamic FEA and an experimental procedure to define behaviour laws. This approach was validated by several realistic tests on complex structures under low speed or quasi-static loading, taking into account geometrical, contact and behavioural non-linearities.

The authors distinguished three general impact types:

- violent crashes (speeds beyond 50 km/h.), where the objective is to protect the occupants conserving the cabinet's integrity avoiding sudden accelerations.
- moderate crashes (speeds around 15 km/h.), where the objective is to minimise vehicle reparation costs.
- impacts at low speeds (4-8 km/h.), where there should not be apparent damages in the car.

The selected material constitutive law was a simplified version of the Johnson-Cook model.

At small strains, the classical conversion from engineering to true stress-strains was used, assuming volume preservation. At high plastic strains, the authors calculated iteratively the plastic part of the curve simulating the experimental tensile tests and adjusting the obtained results, in order to match the lateral straining behaviour of the specimens.

T. Pyttel and S. Weyer [23] presented a constitutive model for glassy polymers based on experimental investigations of tensile coupon tests. These tests were performed at different temperatures and speeds. This model has two features which distinguish it from standard elasto-plastic models. First, the temperature is included and second, the stress-strain curve is described with an appropriate function.

Their constitutive model uses a small value for the yield stress. Accordingly, nearly the whole stress strain curve is prescribed by the hardening curve. For the hardening behaviour of the material a function given by G'Sell is used.

The change in temperature during simulation is calculated as an adiabatic overheating. This change in temperature is directly connected to equivalent plastic strain rate, $\dot{\varepsilon}^p$, and heat capacity, Q, and calculated as:

$$\dot{T} = Q \cdot \dot{\varepsilon}^p \qquad \text{Equ. 9.3.}$$

Spingler, P Drazetic and E Markiewicz [24] used the method in Figures 9.11 and 9.12 for predicting the dart impact behaviour of the so called "gutter" parts:

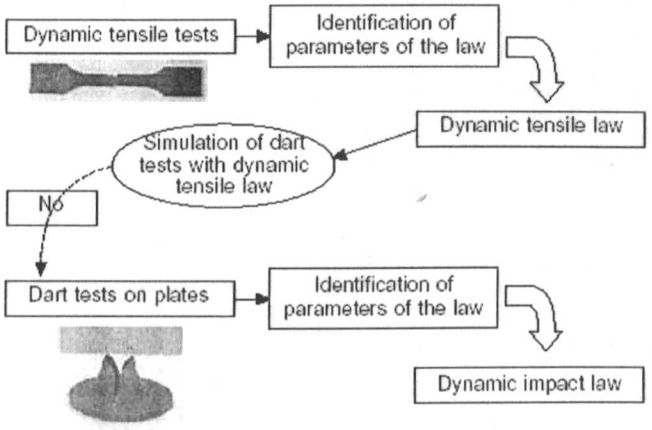

Figure 9.11: Process for the determination of tensile dynamic parameters from the simulation of dart impact tests [24].

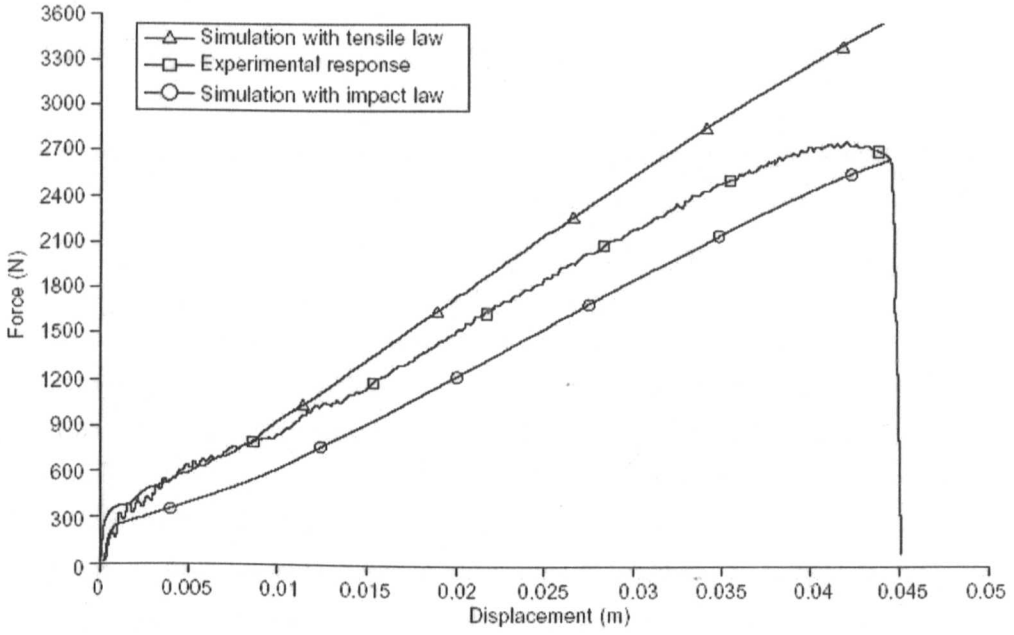

Figure 9.12: Comparison of experimental results and simulated ones using different material input data from previous methodology [24].

The two laws were unable to accurately reproduce the behaviour of the gutter under impact loading. According to the authors, there were many reasons to explain such differences:

- not the same loadings (Tensile-Puncture);
- thermal difference during loadings;

- not the same strain rate range;
- not taking into account anisotropy during mould filling.

A new methodology developed by the authors takes into account the heating of the material during the testing,

- it is considered that the self-heating of the material during the test has the same consequences as the effect of the external temperature on the behaviour.

as well as the anisotropy generated in the moulding of the specimens and parts,

- taking into account the different flow directions and testing the samples extracted from those different orientations.

Closer approximation to experimental data was obtained.

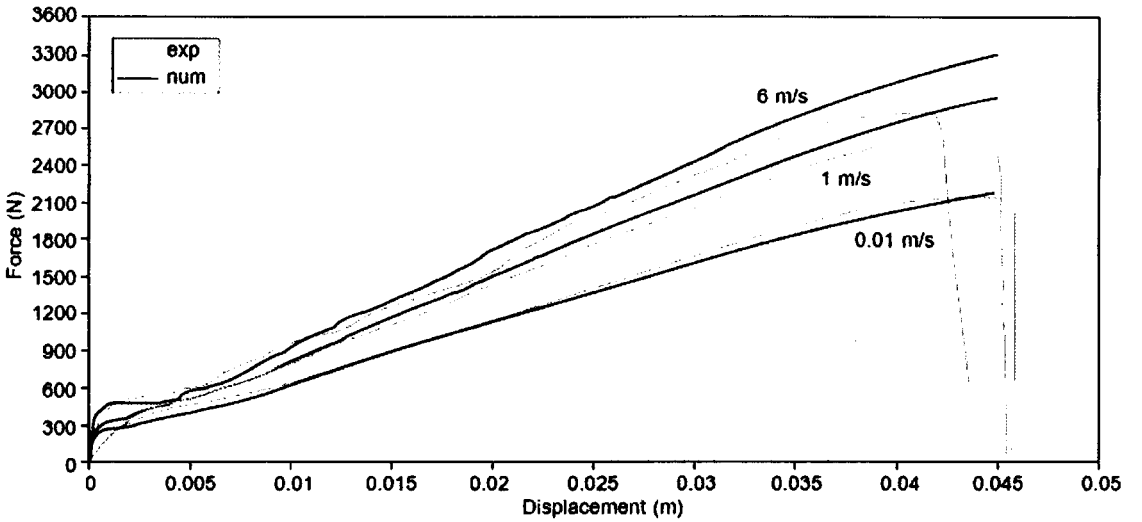

Figure 9.13: Results obtained on the gutter taking into account self-heating and material anisotropy [24].

Stefan Glaser [25] proposed an integrative crash simulation of reinforced thermoplastics taking into account the importance of process induced material data:

- in a first step, the fibre orientation within the part is determined by a mould-fill simulation using MOLDFLOW, the most widely used commercial mould-fill simulation software. The computation takes into account the properties of the moulding compound (melt viscosity, fibre content, etc.), as well as the process parameters such as injection speed and holding pressure.
- secondly, the information gained about the fibre orientation in the moulded state is then used in a non-linear anisotropic material model developed by BASF. The specifically devised software module is called FIBER. With the help of this module, the mechanical properties of the resin/fibre composite are calculated from the various fibre orientations. It is thus possible to take into account the process-related material properties during the computation.
- in a third and final step, a structural analysis of the part is carried out with either LS-DYNA or ABAQUS, two common commercial finite-element software packages, to which the BASF's material model extension has been added.

Related to the high strain rate material characterisation, they used a servo-hydraulic testing machine in conjunction with an optical strain measurement system.

Jin Sung Kim, Hoon Huh, Kang Wook Lee, Dae Yul Ha, Tae Jung Yeo and Soon Jo Park [26] proposed a useful method to obtain the true stress–true strain curve by modification of the experimental stress–strain

curve. A combination of finite element analysis and material constant optimisation was used. The results demonstrated that simulation with modified true stress–true strain curve was closely coincident with the experimental result while there was large discrepancy with the stress–strain curve before modification. See Figure 9.14

According to the authors, the stress–strain curves obtained with the ASTM IV standard specimen needed to be modified for a true stress–true strain relation. In order to modify the stress–strain curve using FEA, a new specimen was prepared:

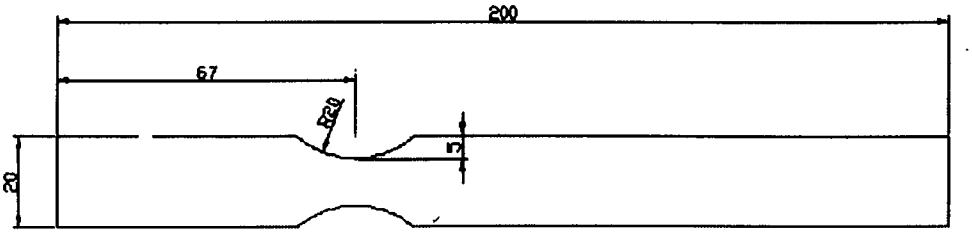

Figure 9.14: Proposed new specimen for use in FEA [26].

The new specimen was convenient for finite element analysis since necking always took place at the center of the arc region.

In order to consider the strain rate hardening effect, the Johnson–Cook model was adopted, Equation 9.4.

$$\sigma = (A + B\varepsilon_p^n)\left[1 + C\ln(\dot{\varepsilon}/\dot{\varepsilon}_0)\right](1 - T^{*m}) \qquad \text{Equ. 9.4.}$$

$$where T^* = \frac{T - T_{room}}{T_{melt} - T_{room}}$$

A, B, C, n and m are input constants and are needed to be calculated. ε_p is the plastic strain, $\dot{\varepsilon}$ is the current strain rate and $\dot{\varepsilon}_0$ is the reference or static strain rate.

Temperature effects are taken into account considering room temperature (T_{room}), melting temperature of the plastic (T_{melt}) and current temperature in the specimen (T).

The slope of the flow stress was predominantly determined by a value of B. For the reason, a value of B was modified in further analysis using an optimisation scheme.

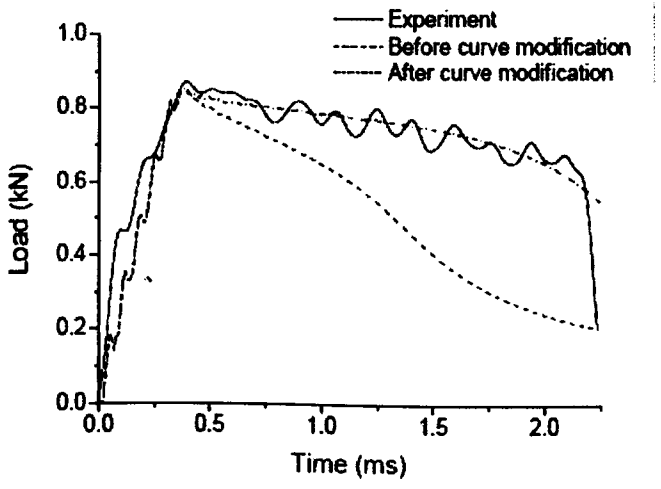

Figure 9.15: Comparison of experimental and simulated results [26].

It can be seen that the adjustment of a correct value for B gave satisfactory results.

9.3. High Strain Rate Test Methods.

This section exposes the most relevant and innovative testing methods found in literature in order to generate stress-strain data for thermoplastic materials in the high strain rate regime.
Although some standardisation trials are being carried out (Society of Automotive Engineers, SAE-J2749 or International Standarisation Organisation, ISO-18872), no specific standard exists for generating high strain rate data (are rather recommended practice guides than standards) and so, several authors propose their own methods and recommendations.
Moreover, the ISO 18872 standard is based on measuring stress-strain properties at low and moderate strain rates and using extrapolation equations to determine high strain rate data.

Susan I. Hill and co-workers [27,28,29] presented the general considerations in determining high strain rate material properties, mainly oriented to thermoplastic materials. Their work was focused on tensile data and the used specimens where in accordance with ASTM D 1822 Type L.
The University of Dayton Research Institute (UDRI), in conjunction with the Society of Automotive Engineers (SAE) and the High Strain Rate Plastics Committee (HSRPC), a sub-committee of SAE, developed a Practice Guide for High Rate Testing of Automotive Polymeric Materials which became a SAE-J Standard.
The Practice Guide provides the following recommendations for high rate tensile testing machines:

- use a damping method for strain rates above 10/s.
- use lightweight grips to minimise inertial effects.
- minimise the length of the load train.
- same specimen configuration at all strain rates.
- measure load with a high frequency response device (>100 KHz.).
- select a specimen that has a small enough gage area to ensure that at least 10 or 15 stress waves propagate through the gage section before yielding occurs.
- tests at four orders of magnitude of plastic strain rate for covering the strain rate of interest.
- use five replicates per condition.
- direct strain measurement to failure.

M. Keuerleber, P. Eyerer and J. Bühring [30] presented the strain rate and temperature behaviour of different thermoplastics (airbag cover materials) tested in servo-hydraulic systems. They used additionally DSC and DMA analyses to evaluate the glass transition temperature and its change at different frequencies (or strain rates). In this way, the influence of the rate of loading on the shift of the T_g could be observed and so the change in the material behaviour from ductile to brittle. At higher frequencies, a shift to higher glass transition temperatures was observed.
When evaluating the local and lateral strains generated in a sample tested at high speed, the authors pointed out that a high speed digital camera should be used, where a compromise between accuracy (pixels) and number of measured points (pictures per second) had to be found. Finally, the authors remarked that care must be taken with location of the illumination system of the camera which generates heat and can vary the material's behaviour.

Francois Barthelat and Hubert Lobo [31] presented a method for generating high strain rate data in a PP using a falling weight 3 point bend test. A heavy crosshead was dropped from a variable height (for obtaining different testing speeds) and impacted a beam type specimen supported on two cylindrical rods. The loading nose of the crosshead was instrumented with an accelerometer, from which different load measurements could be calculated.

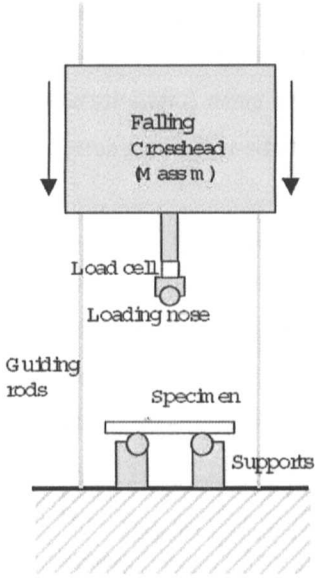

Figure 9.16: Scheme of the falling weight 3 point flexural test [31].

The momentum conservation gives:

$m_c \cdot a(t) = m_c g - F(t)$ Equ. 9.5.

where m_c is the mass of the falling crosshead, a(t) is the measured acceleration in the crosshead, g is the gravity and F(t) is the force at the loading nose.

Integrating once gives the speed:

$$v(t) = v_0 + gt - \frac{1}{m_c}\int_0^t F(t)dt \qquad \text{Equ. 9.6.}$$

where v_0 is the speed measured by the flag system located in the testing machine.

Integrating a second time gives the displacement of the crosshead from the flag:

$$x(t) = v_0 t + \frac{1}{2}gt^2 - \frac{1}{m_c}\int\int_0^t F(t)dt \quad \text{Equ. 9.7.}$$

The deflection at the centre of the beam is then obtained by removing the distance flag-specimen from x(t).

As the force measurement is performed at the loading nose and not directly in the specimen, the authors checked the inertial effects at the nose:

$m_{ln} \cdot a(t) = m_{ln} g + F(t) - P(t)$ Equ. 9.8.

where m_{ln} is the mass of the loading nose and P(t) the force exerted by the specimen.

using again $m_c \cdot a(t) = m_c g - F(t)$ (Equation 9.5)

$$P(t) = (1 + \frac{m_{ln}}{m_c})F(t) \qquad \text{Equ. 9.9.}$$

as m_{ln} is very small compared to m_c, $P(t) \approx F(t)$.

The authors completed the data acquisition by converting the force-displacement curves to stress-strain traces considering linear elasticity laws. They considered perfect plasticity at yield so the stresses could be calculated as:

$$\sigma = \frac{FL}{wt^2} \qquad \text{Equ. 9.10.}$$

where F is the measured force, L the span distance, w the specimen's width and t the thickness.

Assuming small deformations, the engineering strain at the outer fibre of the beam is given by:

$$\varepsilon = \frac{6td}{L^2} \qquad \text{Equ. 9.11.}$$

where d is the displacement at the centre.

The strain rate at the outer fibre can be calculated by

$$\dot{\varepsilon} = \frac{6tv}{L^2} \qquad \text{Equ. 9.12.}$$

where v is the testing speed.

They obtained the following results:

- the modulus increased with strain rate, which was consistent with viscoelasticity.
- the yield stress increased with strain rate following the Eyring's relation.
- the strain at yield increased at very low strain rates and not significantly at higher rates.

Massimo Nutini and Mario Vitali [32] presented a methodology for the measurement of true stress-strain tensile properties at high strain rates in polyolefins for automotive applications.

They remarked the need of high strain rate material data at different temperatures for the simulation of crash events in the automotive sector, where plastic components are being used extensively.

Application	Strain rate (s^{-1})
Bumper pendulum	1
ECE21 pedestrian impact	10
FMVSS201 (specific cases), Airbags	100

Table 9.2: Typical strain rates found in common impacts [32].

Application	Temperature (°C)
Bumper	-30 to 23
Instrument panels, interior parts	-30 to 85

Table 9.3: Typical temperature requirements for plastic parts [32].

As engineering stresses and strains are only valid for the small strain elastic region, true values are needed for crash simulation, where the generated strains are usually high and the material constitutive models require true data.

The authors proposed two approaches for obtaining true stress-strain data:

1. by conversion of engineering data supposing volume conservation in plasticity, in conjunction with the inverse problem method. *This approach was used within this research.*
2. by direct measurement using a high speed data acquisition camera system.

The first approach is based on measuring the engineering stress and strain, converting it to true data and simulating the tensile test (rate dependency is taken into account). Then, material true data is adjusted in order to match the experimental force-displacement curve.

The second approach is based on measuring directly the generated strains in the tensile specimen. Longitudinal and transversal strains can be obtained (the thickness strain is considered to be equal to the transversal strain) using the camera system, from which the following calculations can be performed: true stress, true strain, true strain rate and true Poisson's ratio.

Christopher Clark, Paul E. Johnson and Colin Frost [33] presented the results obtained in high strain rate testing (up to 50/sec.) of different plastics: PC, ABS, PC+ABS, PBT and PC+PBT.First they remarked that it was difficult, if not impossible, to accurately estimate performance based on extrapolated slow strain rate data. For example, previous work carried out by Stokes and Neid at strain rates of 0.1/sec and 1/sec, resulted in a rule of thumb prediction of a 7% increase in ultimate tensile strength for every tenfold increase in strain rate, but a survey of automotive customers indicated that this analysis typically over-predicted component deflection and under-predicted loads at failure.

An important concept that they exposed was that a high speed impact may result in a high strain rate in one object, and low strain rate in another. In energy management applications such as instrument panels and knee bolters, component geometry and stress concentrations are different than those for bumpers, resulting in different strain rates for events that occur at similar speeds.

Christopher L. Clark and Deborah J. Locke [34] conducted another study to evaluate several materials at strain rates and temperatures representative of upper interior conditions under head impact. The results of this study showed that engineering thermoplastics behave more consistently and predictably at higher strain rates than do polyolefins and were much less rate sensitive than the olefinic materials:

- the guideline of a seven-percent increase in tensile strength per decade increase in strain rate was supported by the data and was valid at room temperature for the engineering thermoplastics. It was not applicable to polyolefins.
- the seven-percent rule did not apply to any material at elevated temperatures.
- a five-percent per decade increase in modulus was supported by the new data for engineering thermoplastics (also in elevated temperatures).
- the five-percent rule did not apply to polyolefins at any temperature.

S. Sundararajan, K. Aekbote, C. C. Chou, G. G. Lim, J. Chickola and L. A. Walker [35] determined the dynamic tensile characteristics of various door trim materials and recommended a practical test methodology. ABS and PP were studied in a servo-hydraulic test system from MTS. The maximum stress of these materials increased from quasi-static to dynamic test conditions (as much as 100%). The dynamic stiffness of PP increased two times from quasi-static tests. No significant change in stiffness was observed for ABS during quasi-static and dynamic tests at different strain-rates.

They found that:

- the maximum stress increases significantly with increase in the strain rate till the strain rate reaches a critical value. Further increase in strain rate tests does not increase the maximum stress significantly. This critical strain rate has yet to be determined.

B. C. Duncan and A. Pearce [36] carried out a comparative study between servo-hydraulic high rate and drop testing systems when generating stress-strain data for design under impact loading. Their study covered the testing of engineering thermoplastics (PC, PC+ABS and ABS) as well as adhesives (epoxy, acrylic and polyurethane based) at high strain rates (up to 100 s^{-1}).

They found that related to stress-strain curves up to failure, the noise in the drop impact tests is generally far greater than in the high rate tests but similar curve shapes could be obtained using padding materials.

The authors described some other general considerations related to the lateral strain measurements: Poisson's ratio at large strains tended to be lower than in the elastic region and the assumption that material volume is constant in many material models did not hold. Measurements at low strain rates tended to indicate little rate sensitivity in the relationship between lateral and tensile strain. For some materials, such as ABS, plots of lateral strain against tensile strain showed two regions with different gradients:

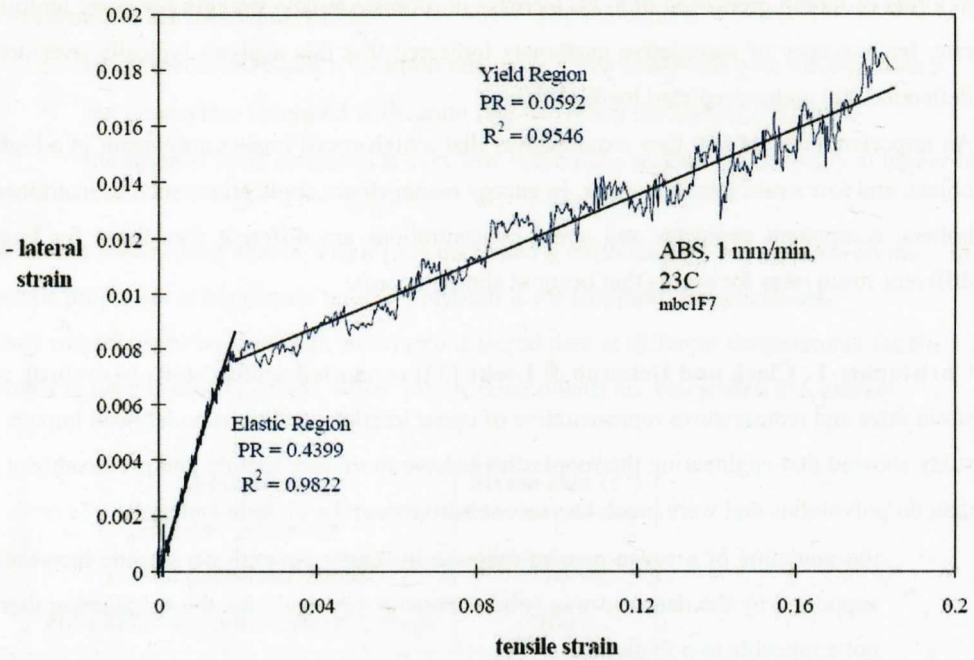

Figure 9.17: Evolution of the Poisson's ratio from low to high strains in ABS [36].

At low strains, the elastic Poisson's ratio is around 0.4 but after yield (where crazing/cavitation occurs leading to an increase in volume) the slope of lateral strain against strain is aproximately 0.1. This is significantly lower than usually assumed, and estimating true stress using the elastic Poisson's ratio alone will give significant errors at large strains.

The authors proposed that low strain rate data can be used to estimate lateral strains at high rates.

Another complication arises from measurements of along-thickness direction strains which are higher (in some materials like PC) than the lateral strains (width direction). The authors did not investigate this observation as to state it as a material property, due to process variables or an artefact of the measurement.

S. M. Walley, J. E. Field, P. H. Pope and N. A. Safford [37] studied the rapid deformation behaviour of various polymers in compression. The authors remarked that a strain rate regime that is physically interesting

was often been ignored, that is around 10 s^{-1}, where the transition from isothermal to adiabatic deformation takes place. Moreover, at strain rates higher than ca. 10^{-1} s^{-1}, the timescale for the flow of heat away from the specimen becomes greater than the duration of the experiment, so that significant temperature rises are to be expected. This will tend to produce strain softening when the rate of deformation is large, so that the stress-strain curve at a high strain rate could fall below the curve determined for a lower strain rate when a certain strain is exceeded.

A high-speed camera was used to film the deformation. The compressive strain rate may be found as a function of time by measuring the diameter of the specimen from the photographic negatives. Compressive strain was defined as:

$\varepsilon_c = \ln(h_0 / h)$ Equ. 9.13.

where h_0 is the original height and h the deformed height. If volume is conserved during deformation and the sides remain vertical, then:

$A_0 h_0 = Ah$ Equ. 9.14.

where A_0 is the original area and A the deformed area of the specimen. If the loading is perfectly uniaxial, the specimen deforms as a circular disc, so that the first equation becomes:

$\varepsilon_c = 2\ln(d / d_0)$ Equ. 9.15.

where d_0 is the original diameter and d the deformed diameter. Differentiating this equation with respect to time, strain rate can be calculated:

$\dot{\varepsilon} = 2(\dot{d} / d_0)$ Equ. 9.16.

Using this formula, the strain rates achieved in the apparatus were ca. 5 x $10^3 s^{-1}$ for 1 mm thick specimens and 2.5 x $10^3 s^{-1}$ for 2 mm thick specimens. These strain rates are considerably lower than those from typical impact applications.

Additional compression testing references can be found in the work carried out by S. F. Lee and G. **M. Swallowe** [38]. They developed a dropweight system to obtain stress–strain data for polymeric materials under high strain rate impact. The system consisted of a combination of a high-speed camera and a dropweight instrumented with an accelerometer. Sample deformation during impact was recorded photographically, and the images were then scanned into a computer in order to measure sample deformation strain. The combination of the accelerometer signal and the camera results allowed sample deformation stress to be measured.

The samples were tested in compression mode, where from diameter deformation measurements, axial strains were calculated assuming a Poisson's ratio of 0.5 in plastic strains.

Keith N. Knapp II, A. Gabrielle and Daeyong Lee [39] presented and compared three methods of obtaining tensile stress-strain response of polymers at large deformations:

- standard displacement controlled engineering stress-strain tension tests, using standard uniform section test samples.
- displacement controlled tension tests, measuring local true strain and local true stress data, using hourglass shaped test samples.
- true constant strain rate controlled tests that measure local true strain and local true stress, using hourglass shaped test samples.

The third testing method used the hourglass test specimen; however, instead of performing the test at a uniform crosshead rate on an Instron 4204 load frame (second method), an Instron 1331 load frame was used. The controllers for the 1331 load frame were modified to allow the input of an external control signal. This external control signal was created using a personal computer equipped with LabView and a National Instruments data acquisition card to provide a control signal for the rate at which the width of the sample changed with respect to time.

To achieve a true constant strain rate, an exponential input signal was required for the command signal. In this manner the servo-hydraulic system controlled the actuator's position to maintain the required change in width of the sample. Tests were run using this method at true tensile strain rates of 0.002 and 0.02 sec-1.

The researchers found this method the most suitable for generating different iso-strain rate curves as input data for material models. The other test methods did not allow a constant strain rate curve generation since no strain control was exerted in the test sample.

The authors affirmed that there was currently a limitation on the rates at which these constant true strain rate tension tests may be conducted. Therefore, extrapolation of the existing model was necessary and then verify experimentally.

M. Junginger [40] presented a measurement technique for local strain determination in plastic materials. The author remarked that the measurement of strains using the Linear Variable Differential Transformer (LVDT), i.e. measuring the crosshead displacement, could lead to inaccurate results especially in materials showing necking and cold drawing.

The measurement method of the author consisted of:

- non-contact video controlled system, Kodak Ektapro HS 4550 (f= 30-40500 Hz.)
- digital black and white images of the sample surface at different experimental times.
- commercial grey scale correlation software (ARAMIS from GOM).

The testing speed specified by the author was slow: 30 mm/min. It was not described the system's performance at high strain rates.

Although at low strains (modulus measurements) there was not a significant difference, the LVDT system was not capable of measuring the "real" hardening behaviour of the material:

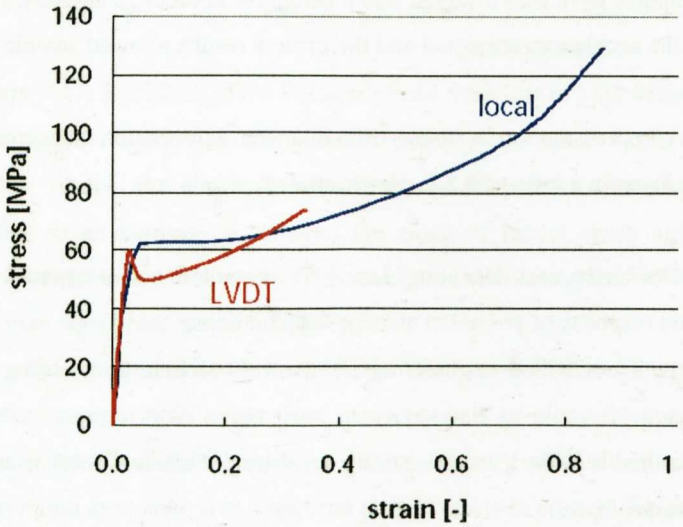

Figure 9.18: The LVDT system gave much more lower strain values than the local measuring system. Strains were under predicted and the necking behaviour could not be captured [40].

Using this technique, higher strains and strain rates were observed in comparison to standard methods using the LVDT signal.

K. Thoma [41] presented results from the measurement of mechanical parameters in the range of high and highest strain rates. He summarised the maximum velocities, strain rates and typical impact durations that could be found in different applications.

	Maximum velocities (m/s)	**Typical load duration (s)**	**Maximum strain rates (1/s)**
Structural engineering: pneumatic hammer impact	5	$5x10^{-3}$	1
Automotive industry: crash	20	$5x10^{-2}$	500
Terminal ballistic: projectile penetration	2000	$1x10^{-4}$	1000000
Manufacturing technology: machining	-	-	1000000
Astronautics: meteorite impact	10000	$1x10^{-6}$	10000000

Table 9.4: Different speeds, durations and strain rates generated in several impact cases [41].

The author observed that in the simulation of the tensile test, a setup-specific oscillation of the force signal appeared at the force gauge. One possibility of avoiding these oscillation problems could be an indirect force measurement; as shown in Figure 9.19 this could be achieved by measuring the strain with the help of a second strain gauge positioned at a point on the sample that was only elastically deformed. Assuming an entirely elastic strain in this widened sample area, the tensile force could be calculated together with the modulus of elasticity. The appearance of oscillations at the force gauge and their effects on the measuring result could thus be prevented:

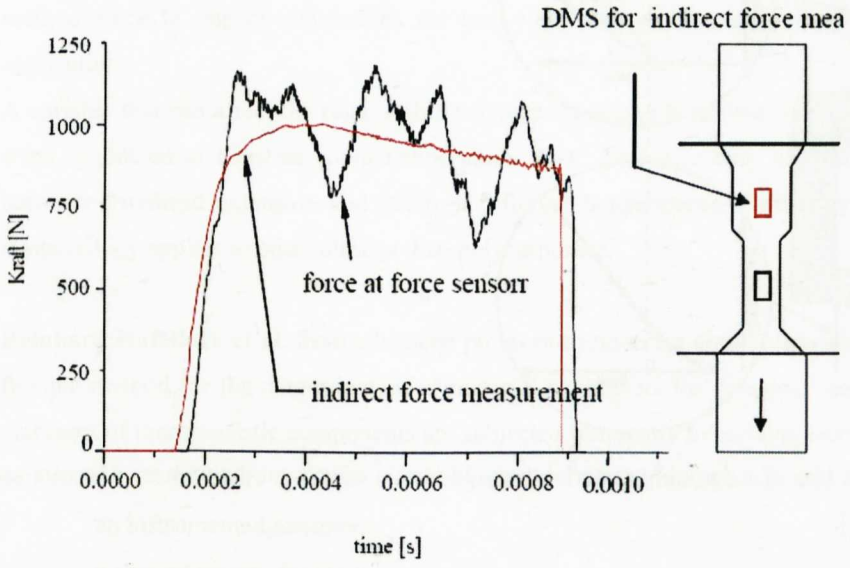

Figure 9.19: Strain gauge (DMS) location in the elastic part of the specimen in order to measure non-oscillating forces [41].

G. D. Dean and R. D. Mera [42] presented a test methodology for characterising the failure of tough plastics at high strain rates. Such data is required for finite element simulations of impact situations. A new tensile specimen geometry, intended to provide a uniform strain region at high strains, was described (which was

later adopted by the standard ISO 18872). High-speed photography and digital image correlation (DIC) strain mapping were used to accurately determine strain at failure. The tensile tests were carried out in a servo-hydraulic machine.The pictures were processed using a digital image correlation system supplied by LaVision. The software divides the initial image of the specimen into square elements whose size can be selected by the user. The software then correlates the movement of each element during the test to determine displacement vectors. Axial and transverse strain distributions can then be derived from the deformation maps. For the determination of strains in this test, an area 6 mm wide and 3 mm high in the centre of the specimen was chosen. The mean axial and transverse strains within this area were determined for each image taken during the test. Using the lateral strain measurements from each image, true stresses could be derived.

Ph. Béguelin, M. Barbezat and H. H. Kausch [43] studied the mechanical behaviour of polymers and composites at intermediate strain rates. They illustrated the application of a high speed servohydraulic testing machine and an optical extensometer. The authors described an important factor when using servo-hydraulic systems with "slack adapters" or "pick up" devices (in tensile testing mode an acceleration stroke is needed for the actuator to reach the desired testing speed, and after this, the specimen is engaged with the grips): the damping of the noise that produces the impact of the slack when engaging the specimen. With the insertion of a viscoelastic material between the contact surfaces, the impact was dampened and thus the track rod was smoothly accelerated:

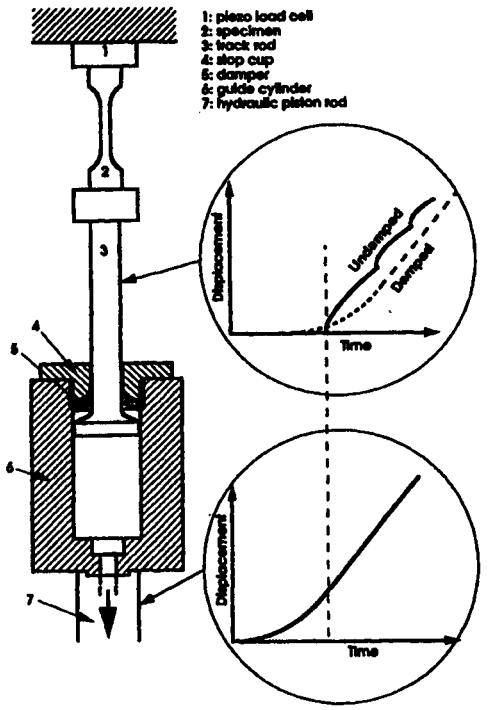

Figure 9.20: Use of a damping material to avoid inertia effects on the pick up unit of a servo-hydraulic test machine [43].

The contact material used in this study was a filled polyurethane elastomer, with a low crosslinking density.

J. Fitoussi, F. Meraghni, Z. Jendli, G. Hug and D. Baptiste [44] performed a research concerned with the development and optimisation of an experimental methodology devoted to the micro and macroscopic characterisation of composites under high-speed loadings. The optimisation aimed at minimising the amplitude of measurements perturbation in order to give rise to homogeneous stress/strain fields within the

tested specimen (a servo-hydraulic machine was used for high speed testing). Each specimen was instrumented by a strain gauge positioned on its central zone. Composite specimen geometry was optimised as a result of numerical computations using ABAQUS finite element code. The optimisation procedure relied upon coupling FE numerical results and experimental data.

The objective was to match experimental measurements of force and displacements imposing velocities to the simulation model (a tensile specimen). The strain distribution in the specimen was checked in order to obtain a homogeneous state and the different dimensions of the specimen geometry (radius, length, cross-section) were adjusted automatically.

Luke Perkins and Hubert Lobo [45] developed a novel technique to measure tensile properties of plastics at high strain rates. They used an inferential technique that correlated strain to extension at low strain rates and showed that this could be extended to measure strain at higher strain rates. To obtain high strain rate properties, specimens were tested first on a Universal Testing Machine using a clip-on extensometer to find how strain related to crosshead displacement. Using the data from that test, a polynomial was used to relate strain to crosshead displacement. Using the polynomial best-fit curve, strain measurements were obtained using crosshead displacement data from the high speed experiment. These tests showed that an extensometer could be used to establish the relationship between crosshead extension and strain. Once this correlation was made an extensometer was no longer necessary provided that the relationship between crosshead displacement and strain was independent of strain rate (they have seen this is true for the material and test conditions described in the correspondent paper). After peak stress was achieved, the correlation between nominal strain and measured strain was not good. This was because after the yield point the measured strain values for the different testing methods varied greatly. These variations resulted from error in extensometry and may be caused by extensometer slip or by deterioration of the markings used for the video extensometer. A good correlation could only be obtained in the post yield region. This is an important handicap for this method since in impact simulations the post-yield part of the test is fundamental in energy absorption applications.

A variable that can affect the relationship between crosshead extension and strain is temperature. These tests were conducted at constant room temperature, 23°C; therefore they did not demonstrate any correlation between crosshead extension and strain at different temperatures. Further, it needs to be shown that this methodology applies to other plastics than polycarbonate.

Reinhard Hafellner et al. from advanced polymer engineering GmbH (a.p.e.) [46, 47] presented a new and flexible method for the determination of material parameters for dynamic simulation. The author remarked that most of thermoplastic components are subjected frequently to bending loads, so they developed a special pendulum system (where specimens are subjected to flexural loads) consisting on:

- an instrumented hammer.
- a camera system for strain measurements.
- a temperature chamber.
- simultaneous simulation of the impact event.

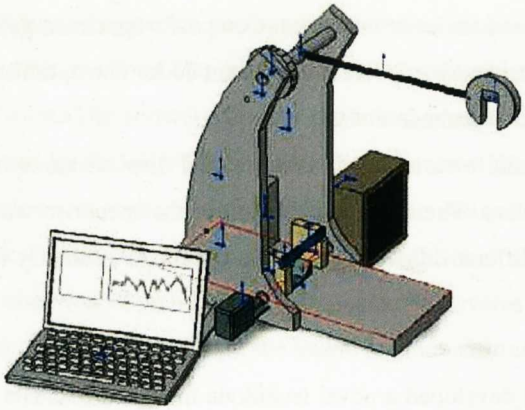

Figure 9.21: Scheme of the test system consisting on the simultaneous simulation of impact bending [46].

The developed special pendulum test system was named IMPETUS, for testing polymeric materials in the velocities range between 0.1-10000 mm/s. This pendulum system was connected to a simulation code in order to generate "automatically" the material cards. Basically the method consisted of simulating the 3 point bending impact tests in LS-DYNA and adjusting the input material data automatically for matching the experimental curves. The material input should also be validated with other geometries as dart drop tests.

In a thesis report from **R. R. P. Rodenburg** [48] several details are given in concern to high strain rate thermoplastic testing, instrumentation, material specific issues and constitutive modeling. Here, the test data shown in the report is exposed in order to illustrate the differences in stress-strain behaviour that can be found in the same material depending on the used strain rate and temperature.

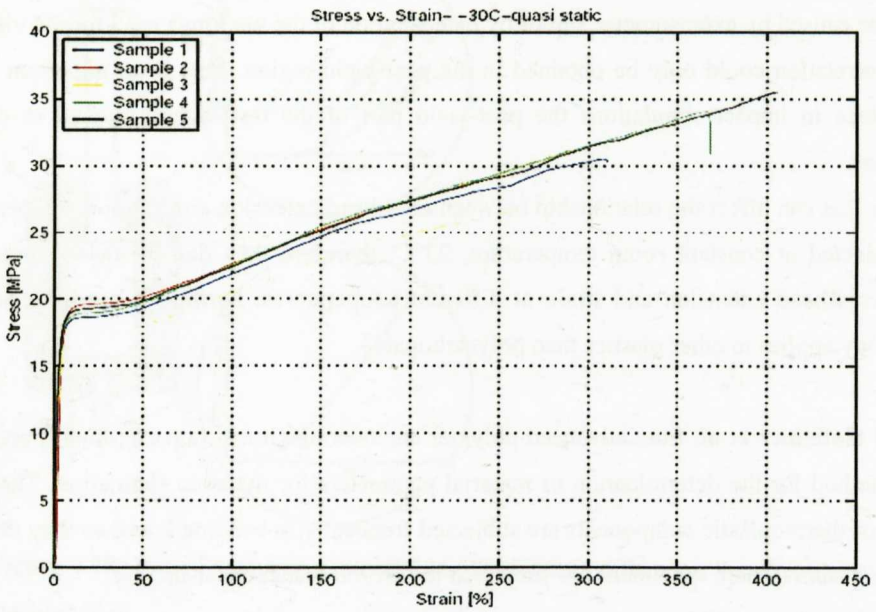

Figure 9.22: Quasi static tensile test results of a TPO skin at -30°C [48].

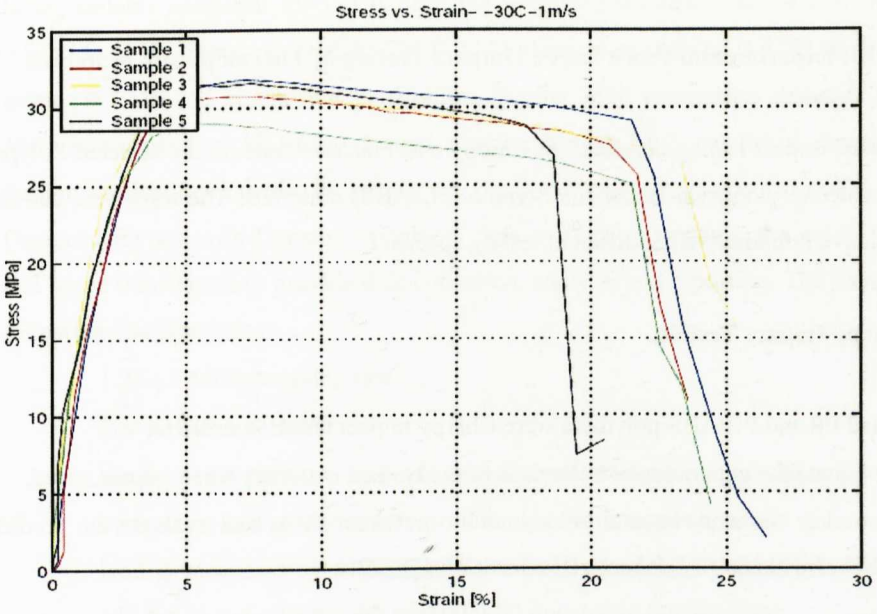

Figure 9.23: High strain rate (10/s) tensile test results of a TPO skin at -30°C [48].

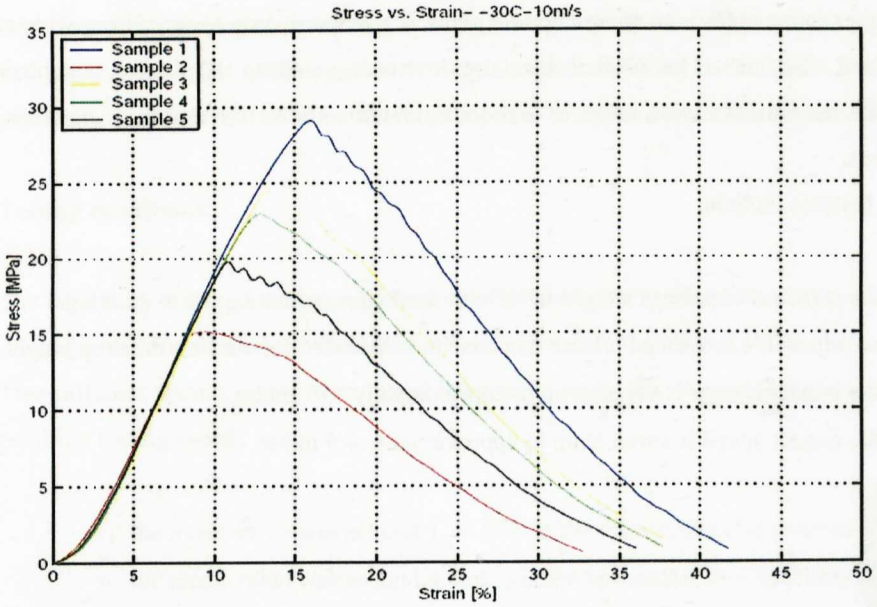

Figure 9.24: High strain rate (100/s) tensile test results of a TPO skin at -30°C [48].

Chapter 10: Experimental Work Part 1: Impact Testing of Thermoplastic Materials.

In this thesis, impact testing consisted of Charpy and Puncture tests on the selected Polypropylene (PP) and Polycarbonate/Acrylonitryle-Butadiene-Styrene (PC/ABS) materials. The tests were carried out at 23°C and at 50% relative humidity, using different testing speeds.

10.1. Charpy Impact Testing.

The selected PP and PC/ABS polymers were Charpy impact tested in order to,

- evaluate the experimental behaviour of the studied materials when impact tested.
- simulate the experimental behaviour by means of FEA, and evaluate the predictive capability of different elasto-plastic material constitutive models.

A Dynatup® Model 8200 Impact Test Instrument from INSTRON was used for testing thermoplastic samples in Charpy configuration. *Note: the testing machine was used from the collaborative work with Maier Technology Centre (MTC) in Ajangiz, Spain.* This is a vertical drop tower with a wide range of adjustable energies and velocities. The 8200 is ideal for low energy testing of plastics, composites, ceramics, and metals. The instrument's wide range of test configurations allows for testing of both specimens and actual components.
Principal features include:

- the standard crosshead weight is variable from approximately 0.7 to 12.6 Kg.
- an adjustable crosshead release mechanism is included for varying the drop height.
- the impact energy is variable up to approximately 136 Joules.
- the impact speed is variable up to approximately 4.5 m/sec.

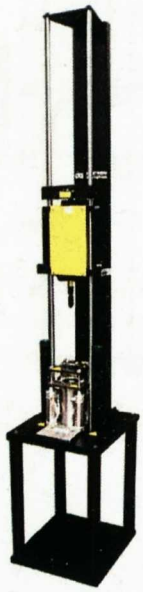

Figure 10.1: Commercial Dynatup impact tester, Model 8200.

Using suitable specimen support fixtures the following standards can be met: ASTM D 256 Izod plastics, ASTM D 6110 Charpy plastics, ASTM D 2444 plastic pipe, ASTM D 3763 High Speed Puncture of Plastics, Boeing® BMS-256 composites penetration, Boeing 7620 composites damage, ISO 179 Izod plastics, ISO 180 Charpy plastics, ISO 6603-2 rigid plastics, NASA ST-1 composite damage, and other standard and custom applications can also be met.

Designed for use with Dynatup Impulse™ data acquisition systems, the model 8200 is equipped with load and speed transducers to provide data collection, analysis and reporting. The data acquisition systems has the following characteristics:

- 1.25 - 5 MHz sampling rate.
- 500 KHz. bandwidth.
- standard unit performs single or two-channel analog signal conditioning.
- connection to a second unit to provide up to four input channels.
- load is measured by a INSTRON load cell (model 8902-01, with a maximum load capability of ±15.6 KN and a sensitivity of 0,005kN), located in the impactor.
- initial speed is measured by a flag system.

The test specimens' dimensions were according to the ISO 527 Type A standard (see section 6.2.1) and were manufactured by injection moulding. A straight length of 80 mm was cut from the total length in order to test in Charpy mode. Half of the specimens were notched according to the ISO 179 Type A standard, where the notch base radius is of 0.25 mm, the notch depth of 2 mm and the notch angle is of 45°.

Testing conditions.

The laboratory atmosphere was adjusted to be 23°C and 50% relative humidity.

10 specimens were tested per condition.

Two different testing heights were used in order to study the strain rate effects on the Charpy samples. The resulting testing speeds were:

- v_1: the mean value was around 1.75 m/s. in the un-notched test specimens from PC+ABS.
- v_2: the mean value was around 4.4 m/s. in the un-notched test specimens from PC+ABS.
- v_1: the mean value was around 1.78 m/s. in the notched test specimens from PC+ABS.
- v_2: the mean value was around 4.4 m/s. in the notched test specimens from PC+ABS.

- v_1: the mean value was around 1.77 m/s. in the un-notched test specimens from PP.
- v_2: the mean value was around 4.42 m/s. in the un-notched test specimens from PP.
- v_1: the mean value was around 1.8 m/s. in the notched test specimens from PP.
- v_2: the mean value was around 4.4 m/s. in the notched test specimens from PP.

All the tests were performed using a total mass of 7.668 Kg.

These conditions were different from those stated in the ISO 179 standard, but in this thesis work the objective was to correlate own defined experimental impact conditions, with simulations in ANSYS and LS-DYNA.

The used test system can be seen in Figure 10.2:

Figure 10.2: Test system configuration, the specimen clamping device and the dart can be seen in the centre.

The Charpy impactor as well as the supports were in accordance with the ISO 179 standard.

Recorded data and obtained results in the Charpy tests.

The following data was reported by the software of the testing machine:

- Force-time data (KN-ms).
- Force-displacement data (KN-mm).
- Energy-time data (J-ms).
- Speed-time data (m/s-ms).

Calculations performed by the software: velocities and displacements were derived from accelerations, which were calculated from the load cell's measurements.

Acceleration in m/s^2 can be obtained from:

$$a = \frac{F \cdot 1000}{M} \qquad \text{Equ. 10.1.}$$

where F is the force measured by the load cell, in KN, and M is the mass dropped, in Kg.

Speed in m/s can be calculated from:

$$v = \frac{(t_1 - t_0)}{1000} \cdot a + v_0 \qquad \text{Equ. 10.2.}$$

where v_0 is the previous Speed and t_1-t_0 represents the gradient in time (difference between actual and previous data).

Displacement in mm can be obtained from:

$$d = (t_1 - t_0) \cdot v + d_0 \qquad \text{Equ. 10.3.}$$

where d_o is the previous time step's displacement.

Energy in J is calculated from force and the calculated displacements:

$$E = F(d_1 - d_0) \cdot E_0 \qquad \text{Equ. 10.4.}$$

where E_0 is the previous time step's energy.

10.1.1. Charpy Test Results for PC/ABS.

The following graphs from Figure 10.3 to 10.8 show the different results obtained for the studied PC/ABS. Un-notched and notched specimens were evaluated. The results shown are for an intermediate sample from the 10 specimens tested per condition.

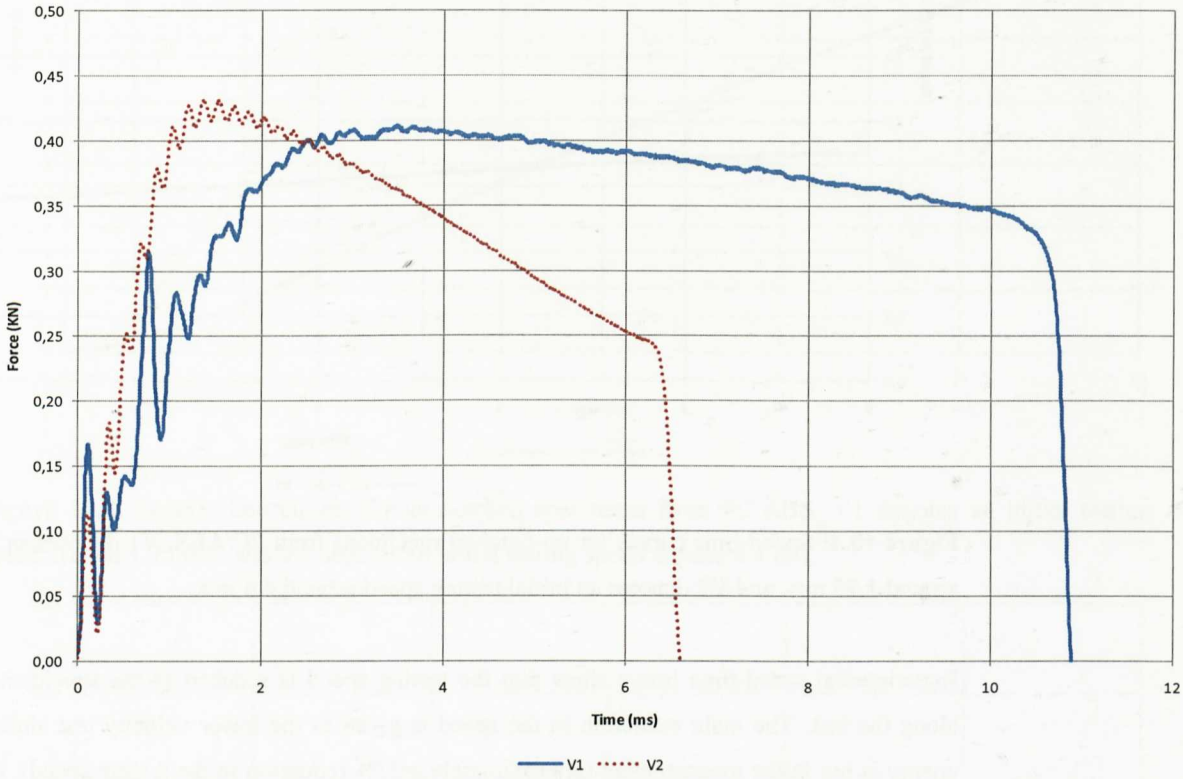

Figure 10.3: Force-time curves for un-notched specimens from PC/ABS. V1 denotes an initial testing speed around 1.75 m/s. and V2 denotes an initial testing speed around 4.4 m/s.

From force-time curves, it can be observed that at both testing speeds the specimen's failure mode was without breakage; after the initial inertial and subsequent peaks there is a yielding behaviour and posterior plastic deformation until a limit bending deformation is obtained.

Observation of the first inertial peak showed that at the higher testing speed, higher inertial peaks were recorded but also a higher scatter was observed. In this case, a lower peak than that at the lower speed is observed in the graph, but the reason this curve was selected was that the curve trace was comparatively cleaner and smoother than the other testing traces at the same speed.

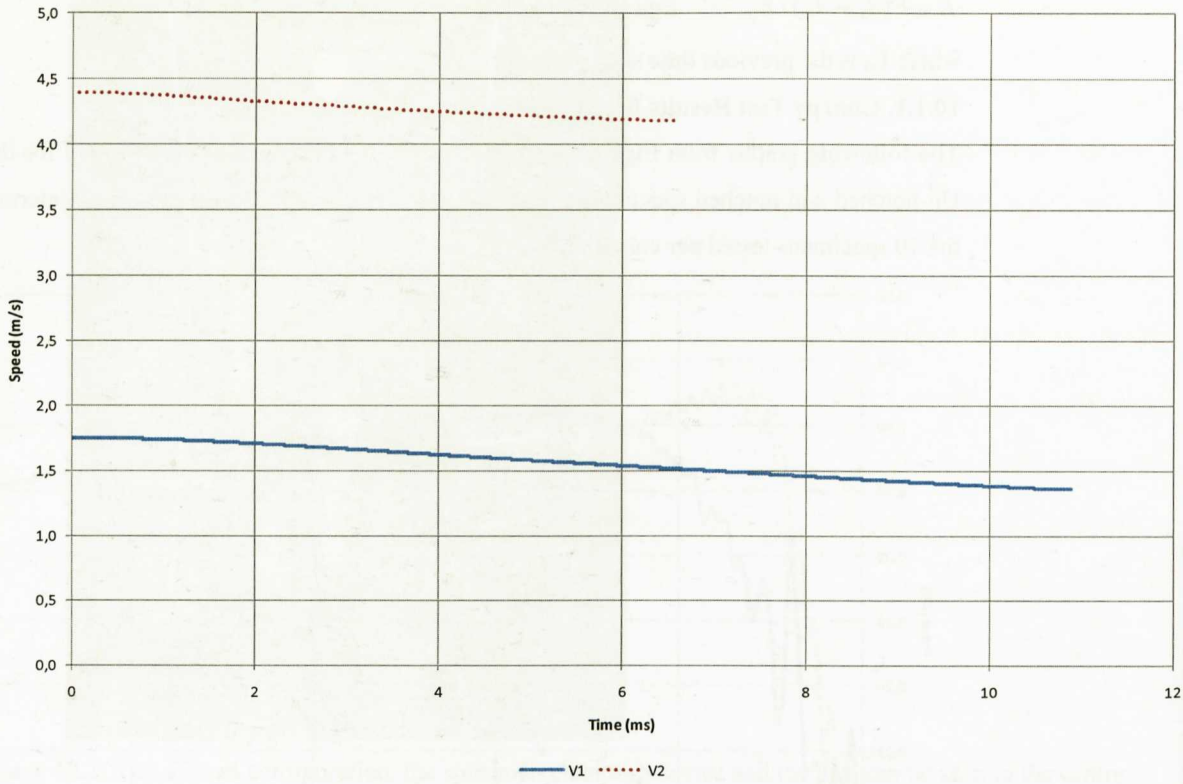

Figure 10.4: Speed-time curves for un-notched specimens from PC/ABS. V1 denotes an initial testing speed around 1.75 m/s. and V2 denotes an initial testing speed around 4.4 m/s.

Experimental speed-time traces show that the testing speed is reduced as the specimen is being deformed along the test. The main reduction in the speed is given in the lower velocity test since the lowest kinetic energy is put in the measurement (approximately a 22% reduction in the testing speed). In the higher testing speed a 4.5% reduction is given.

In terms of energy, a value of 6 J was recorded up to the maximum deformation instant in the lower testing speed, and a value of 9 J in the higher testing velocity.

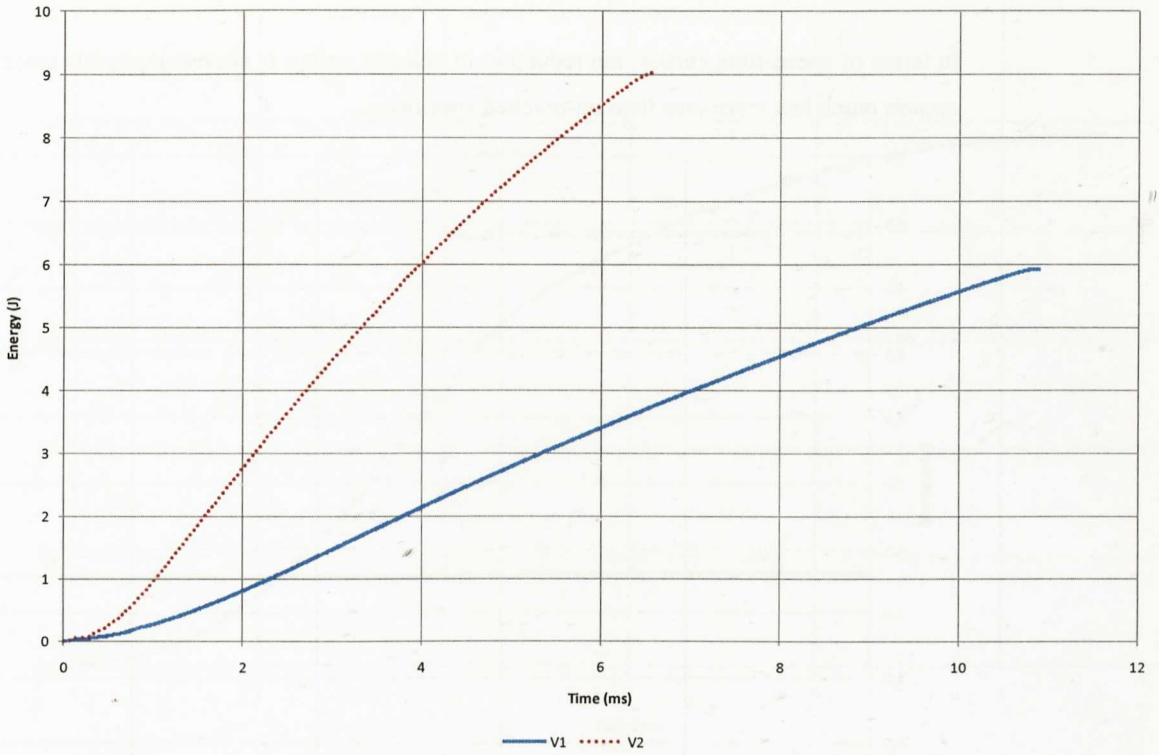

Figure 10.5: Energy-time curves for un-notched specimens from PC/ABS. V1 denotes an initial testing speed around 1.75 m/s. and V2 denotes an initial testing speed around 4.4 m/s.

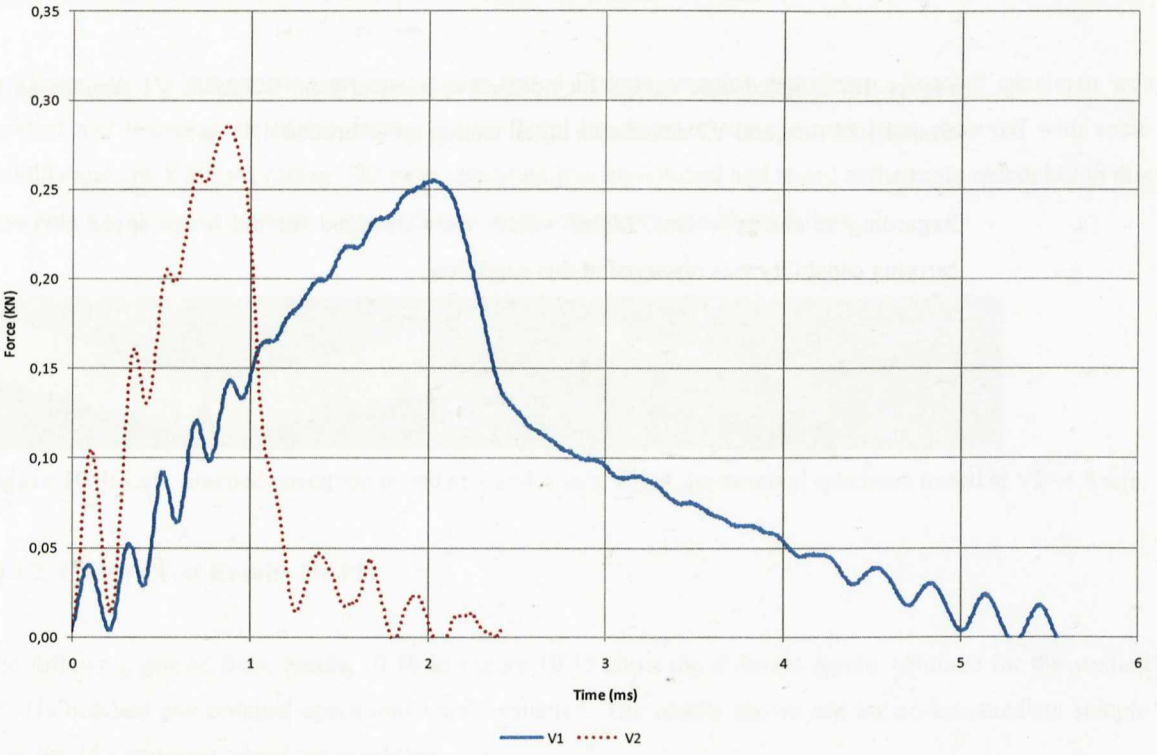

Figure 10.6: Force-time curves for notched specimens from PC/ABS. V1 denotes an initial testing speed around 1.81 m/s. and V2 denotes an initial testing speed around 4.41 m/s.

Force-time curves for the notched specimens show a partial failure after the initial inertial and subsequent peaks, followed by a stable cracking (especially in the case of the lower testing speed). For the higher testing speed, this cracking up to the final failure is not as stable as in the lower testing speed, as a more sudden decrease in force values is observed.

In terms of speed-time curves, the reduction in velocity values is almost negligible since notched specimens oppose much less resistance than un-notched specimens.

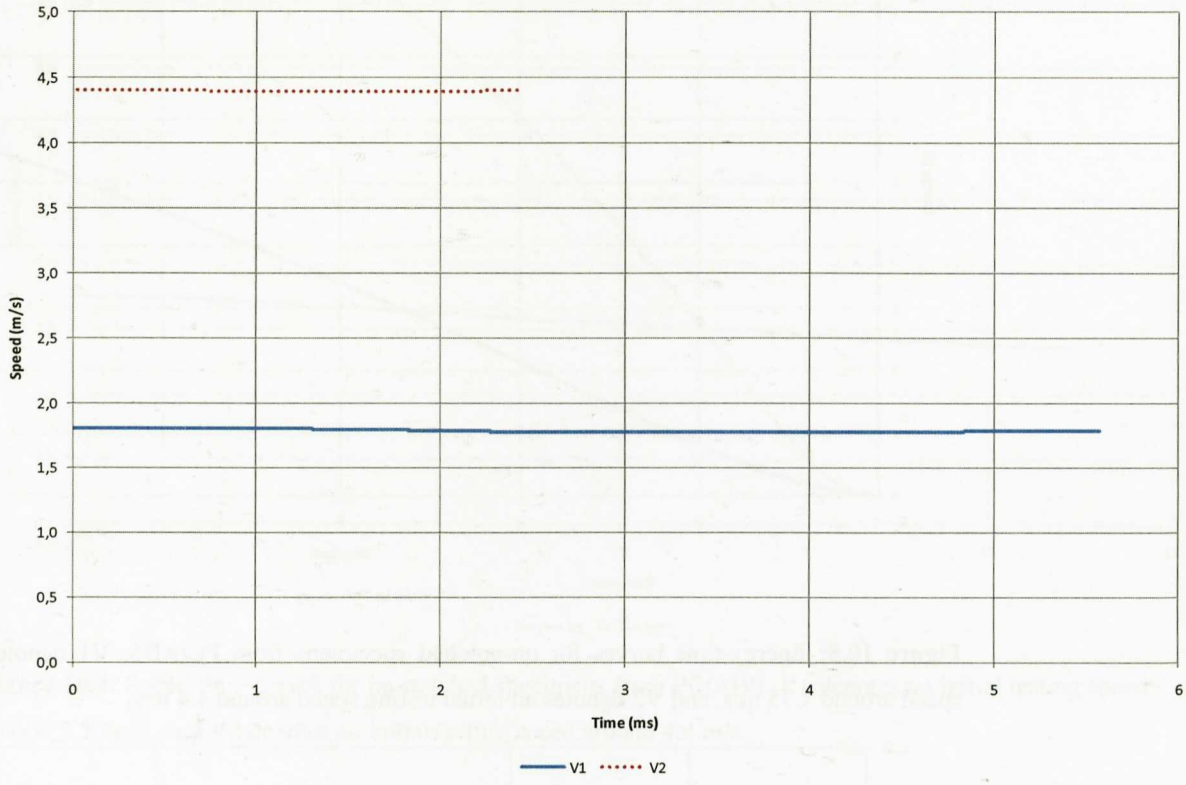

Figure 10.7: Speed-time curves for notched specimens from PC/ABS. V1 denotes an initial testing speed around 1.81 m/s. and V2 denotes an initial testing speed around 4.41 m/s.

Regarding to energy values, higher values were obtained for the lower speed curve since a higher load carrying capability was observed at this condition.

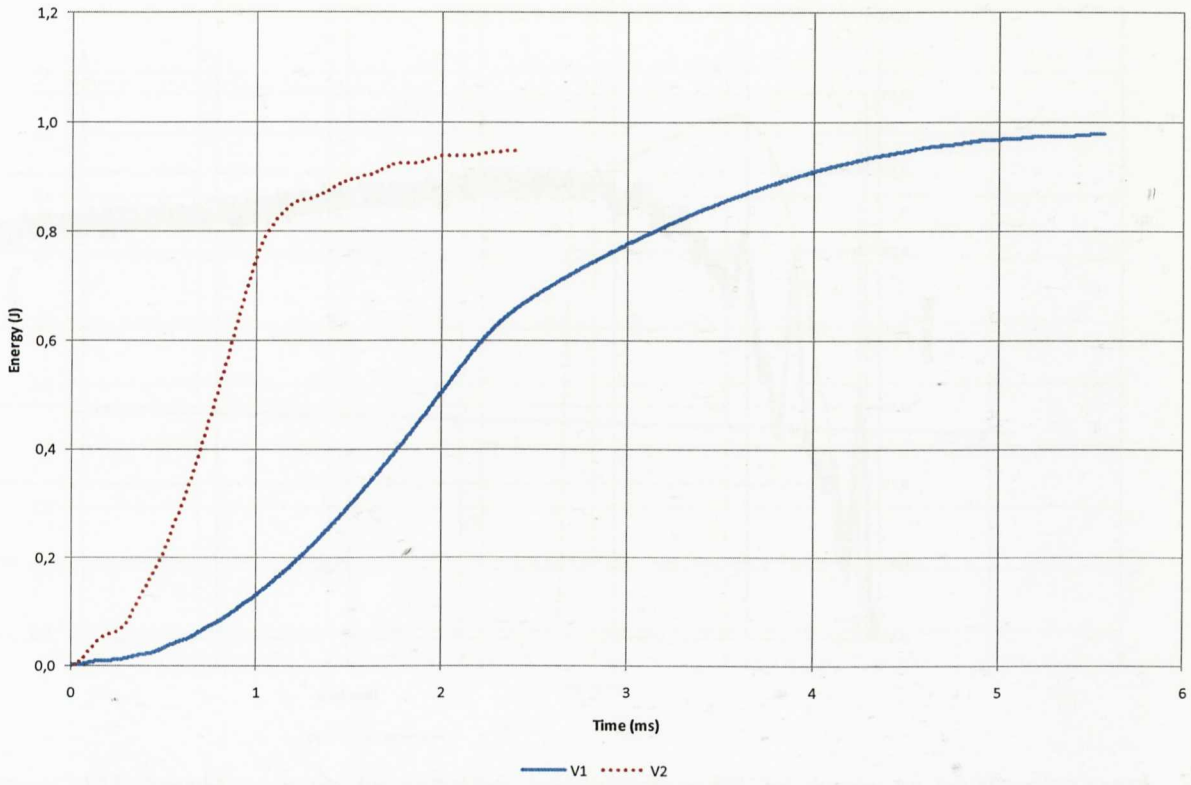

Figure 10.8: Energy-time curves for notched specimens from PC/ABS. V1 denotes an initial testing speed around 1.81 m/s. and V2 denotes an initial testing speed around 4.41 m/s.

In Figure 10.9, a comparative picture of two tested Charpy samples are shown. The left specimen was notched and tested at the higher testing speed. Total breakage of the specimen was observed with some yielding and crack arrest process. The right specimen was un-notched and tested at the same speed, but in this case only a yielding and plastic deformation process was observed without failure.

Figure 10.9: Left, notched specimen tested at V2=4.4 m/s. Right, un-notched specimen tested at V2=4.4 m/s.

10.1.2. Charpy Test Results for PP.

The following graphs from Figure 10.10 to Figure 10.15 show the different results obtained for the studied PP. Un-notched and notched specimens were evaluated. The results shown are for an intermediate sample from the 10 specimens tested per condition.

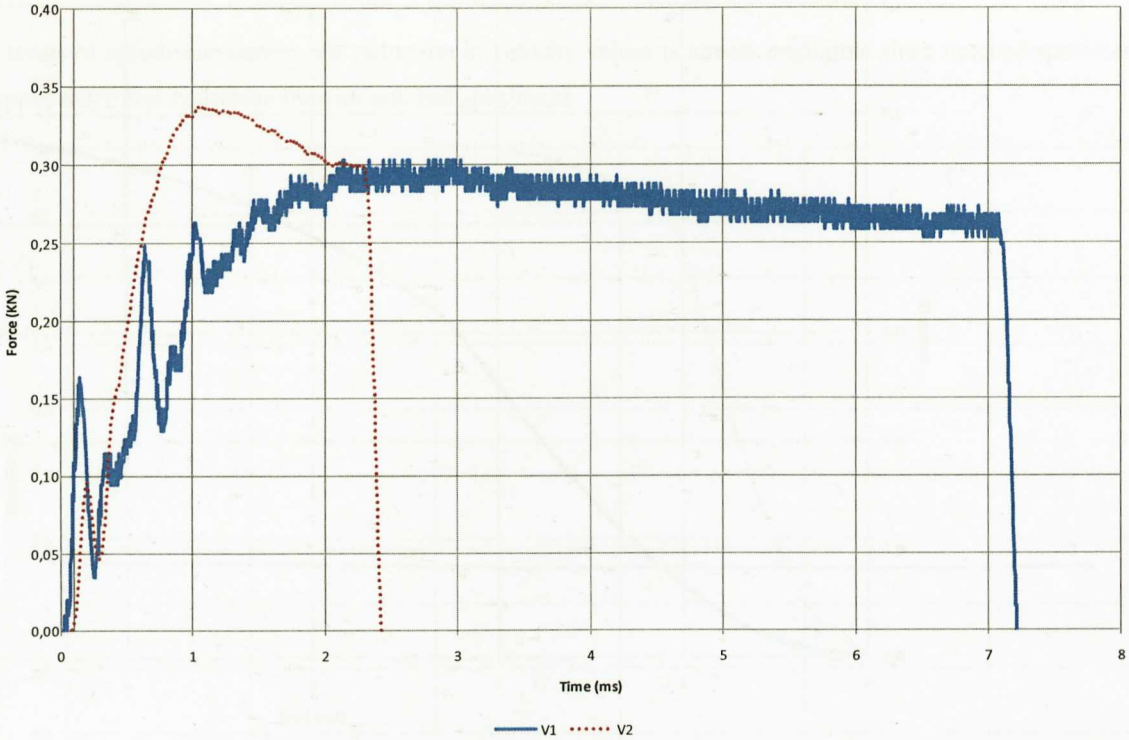

Figure 10.10: Force-time curves for un-notched specimens from PP. V1 denotes an initial testing speed around 1.77 m/s. and V2 denotes an initial testing speed around 4.42 m/s.

From force-time curves, it can be observed that at both testing speeds the specimen's failure mode was with total breakage; after the initial inertial and subsequent peaks there is a yielding behaviour and posterior plastic deformation. Specimen failure is given after some crack arrest.

Regarding to the first inertial peak it was observed that at the higher testing speed, higher inertial peaks were recorded but also a higher scatter. In this case a lower peak than that at the lower speed is observed in the graph, but the reason to select this curve was that the curve trace was comparatively cleaner and smoother than the other testing traces at the same speed.

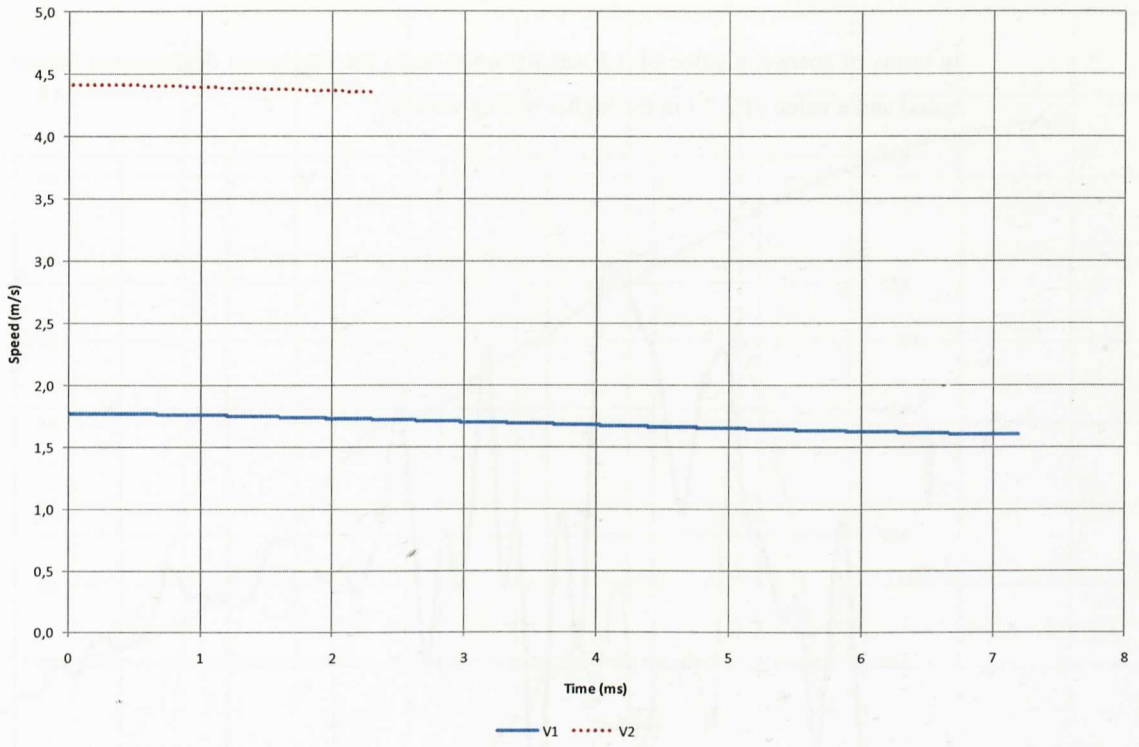

Figure 10.11: Speed-time curves for un-notched specimens from PP. V1 denotes an initial testing speed around 1.77 m/s. and V2 denotes an initial testing speed around 4.42 m/s.

Testing speed-time traces show that the testing speed is reduced as the specimen is being deformed along the test. The main reduction in the speed is given in the lower velocity test since the lowest kinetic energy is put in the measurement (approximately a 10% reduction in the testing speed). In the higher testing speed a 1% reduction is given.

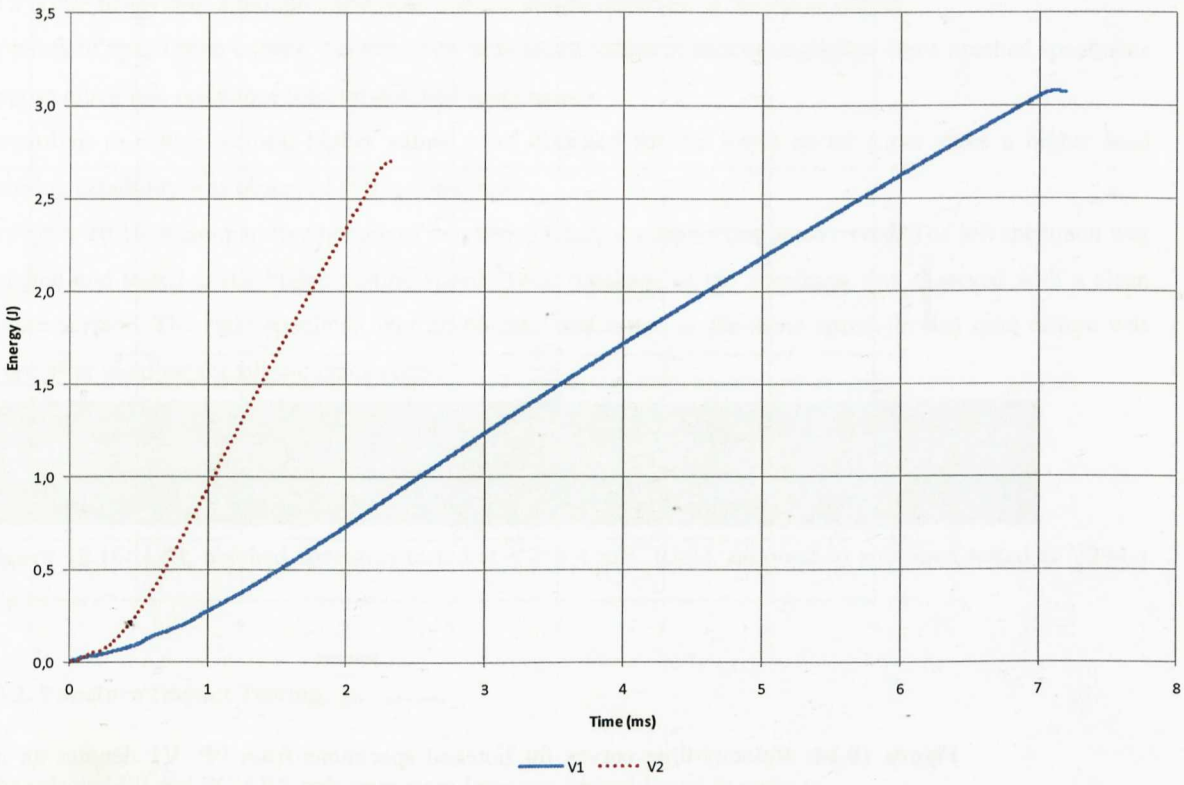

Figure 10.12: Energy-time curves for un-notched specimens from PP. V1 denotes an initial testing speed around 1.77 m/s. and V2 denotes an initial testing speed around 4.42 m/s.

In terms of energy, a value of 3 J was recorded up to the maximum deformation instant in the lower testing speed and a value of 2.7 J in the higher testing velocity.

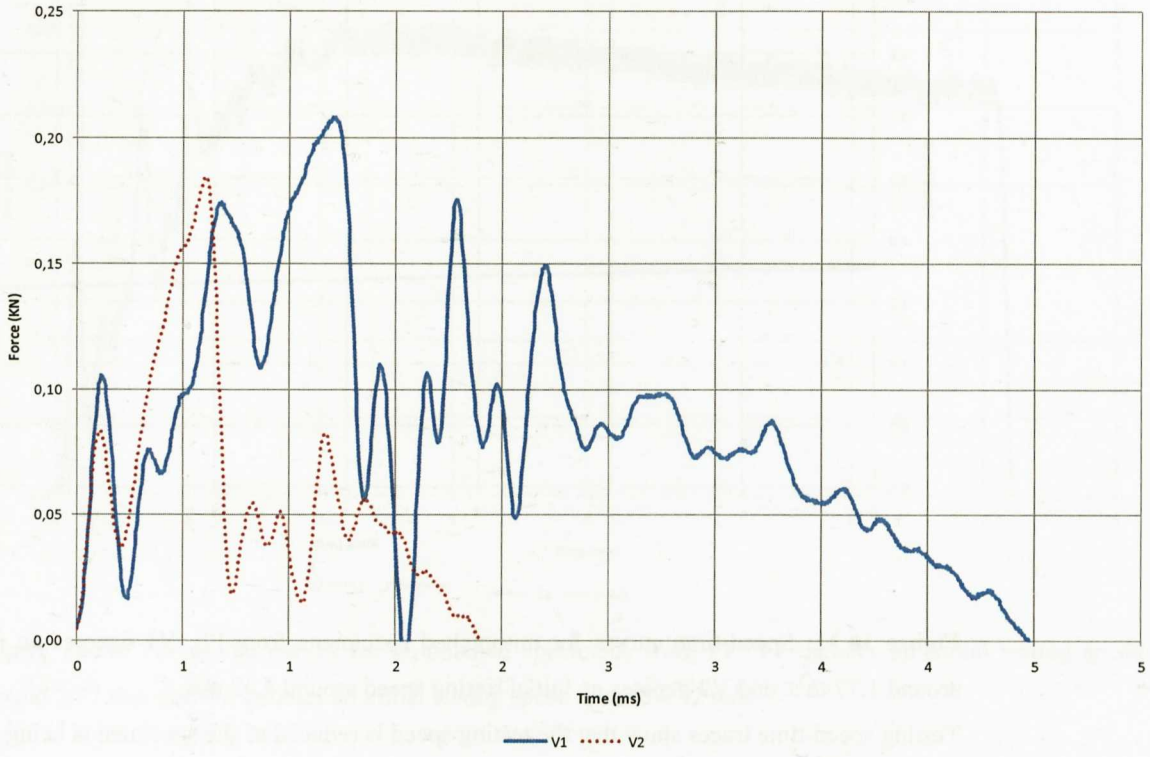

Figure 10.13: Force-time curves for notched specimens from PP. V1 denotes an initial testing speed around 1.77 m/s. and V2 denotes an initial testing speed around 4.41 m/s.

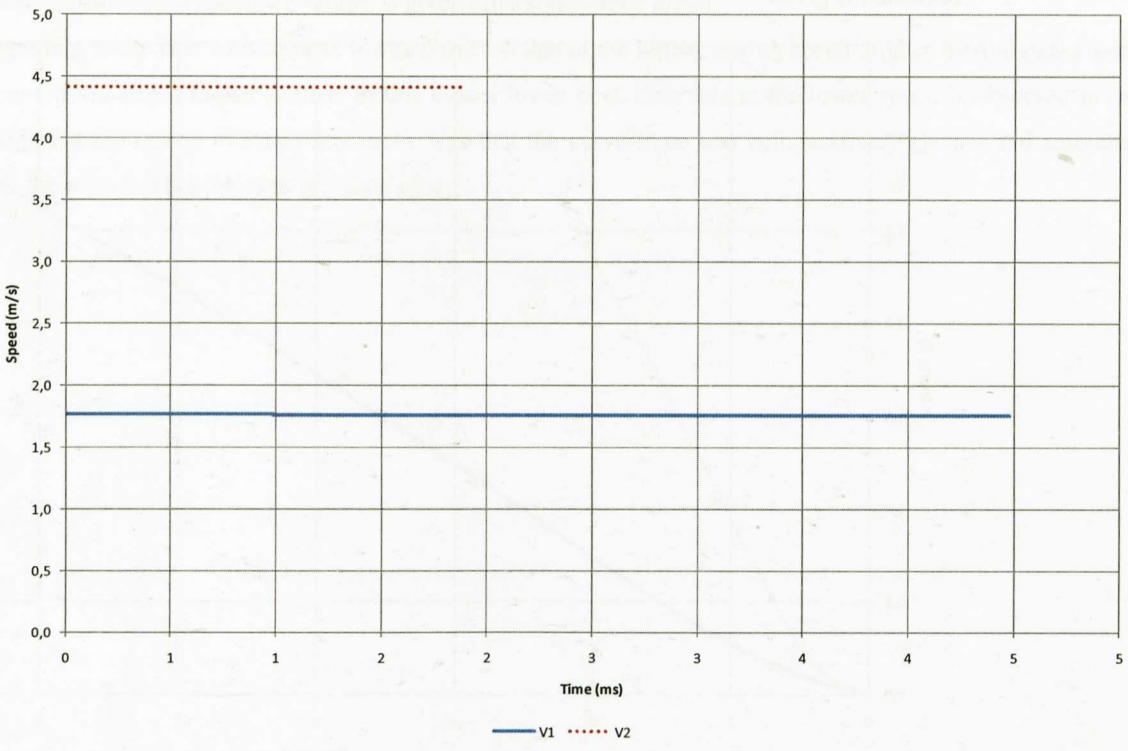

Figure 10.14: Velocity-time curves for notched specimens from PP. V1 denotes an initial testing speed around 1.77 m/s. and V2 denotes an initial testing speed around 4.41 m/s.

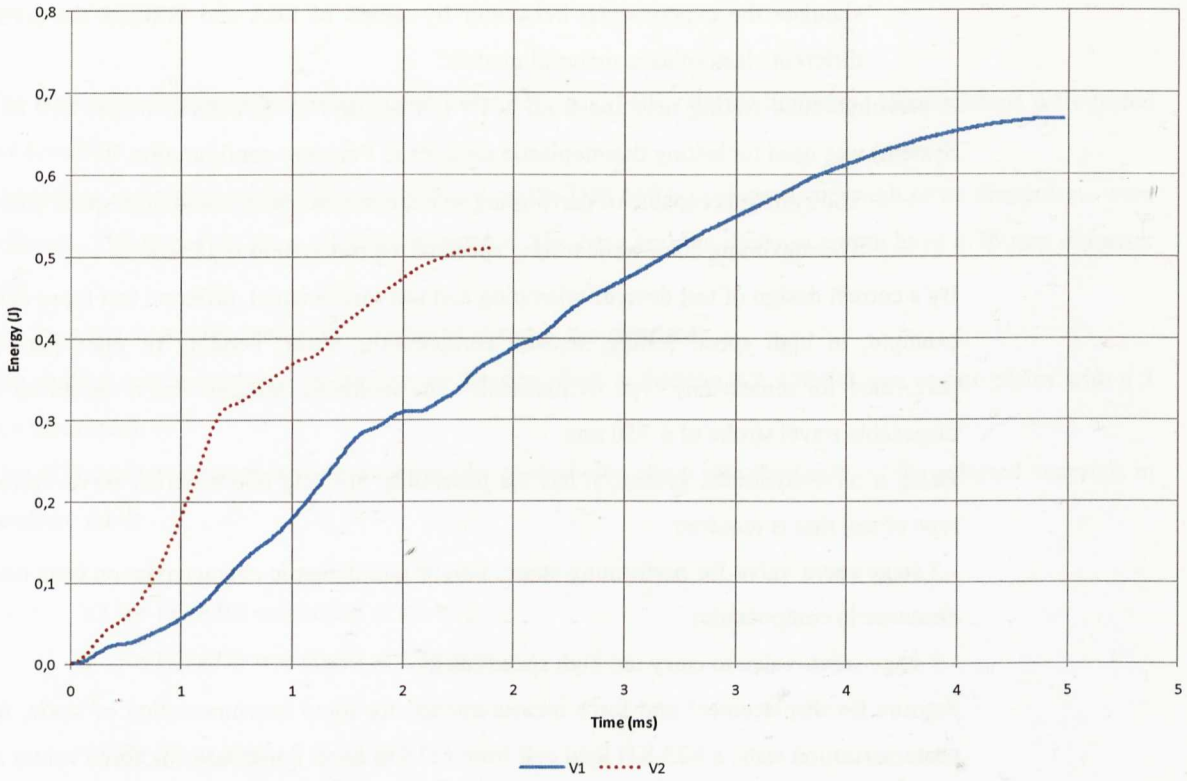

Figure 10.15: Energy-time curves for notched specimens from PP. V1 denotes an initial testing speed around 1.77 m/s. and V2 denotes an initial testing speed around 4.41 m/s.

Force-time curves for the notched specimens show a brittle-like behaviour after the initial inertial and subsequent peaks. This denotes some transition from ductile behaviour at the lower testing speed of 1.77 m/s, to a brittle behaviour, although some plastic arrest can be observed in the curve shapes.

In terms of speed-time curves, the reduction in velocity values is almost negligible since notched specimens oppose much less resistance than un-notched specimens.

Regarding to energy values, higher values were obtained for the lower speed curve since a higher load carrying capability was observed at this condition.

In Figure 10.16, a comparative picture of two tested Charpy samples can be observed. The left specimen was notched and tested at the higher testing speed. Total breakage of the specimen was observed with a clean failure surface. The right specimen was un-notched and tested at the same speed. In this case failure was given after yielding and plastic crack arrest.

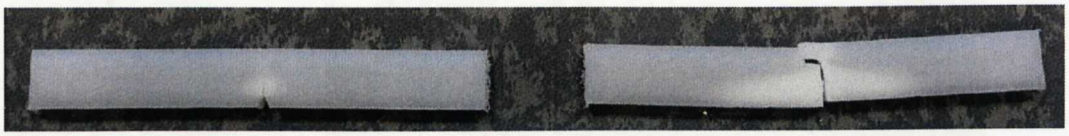

Figure 10.16: Left, notched specimen tested at V2=4.4 m/s. Right, un-notched specimen tested at V2=4.4 m/s.

10.2. Puncture Impact Testing.

The selected PP and PC/ABS polymers were Puncture impact tested in order to,

- evaluate the experimental behaviour of the studied materials when dart impact tested.

- simulate the experimental behaviour by means of FEA and evaluate the predictive capability of different elasto-plastic material models.

A servohydraulic testing machine from MTS (on demand manufactured model 819.10 High Rate Testing System) was used for testing thermoplastic samples in Puncture configuration.

- The system is capable of performing static, dynamic, fatigue and high speed characterisation tests.
- The maximum achievable testing speed of the test system is 18 m/s.

By a correct design of test devices (clamping and test instruments), different test types can be carried out. For example, in high speed testing, tensile, compression, shear, bending or plate perforation tests can be performed for almost any type of materials. The hydraulic actuator has a capability of ± 40 KN and a disposable travel stroke of ± 350 mm.

Being a servo-hydraulic system, it has the possibility of using two different servo-valves depending on the type of test that is required:

- 2 stage servo-valve for performing static, fatigue and dynamic characterisation tests (useful for example in elastomeric components).
- 3 stage servo-valve to carry out high speed tests.

Sensors for displacement and force measurements: for force instrumentation of static, fatigue and dynamic characterisation tests, a ±25 KN load cell from MTS is used. For measuring force values at high speed tests a piezo-electric load washer model 9361B of ±60 KN from KISTLER was used.

The actuator displacement is measured by an innovative method (magnetostrictive principle) from MTS, which is called the Temposonics® and substitutes the historically used LVDT concept.

In dynamic characterisation tests (elastomers), a DYTRAN accelerometer is mounted in the actuator in order to obtain precise displacement values. This accelerometer measures in a ±50G range and is used when testing frequencies in the range of 10-300 Hz. are required.

The data acquisition system (National Instruments PCI 6110 card) is able to measure 5.000.000 points/second (which is especially useful in high rate tests).

This testing machine is capable of maintaining the testing velocity constant along the specimen deformation and failure process.

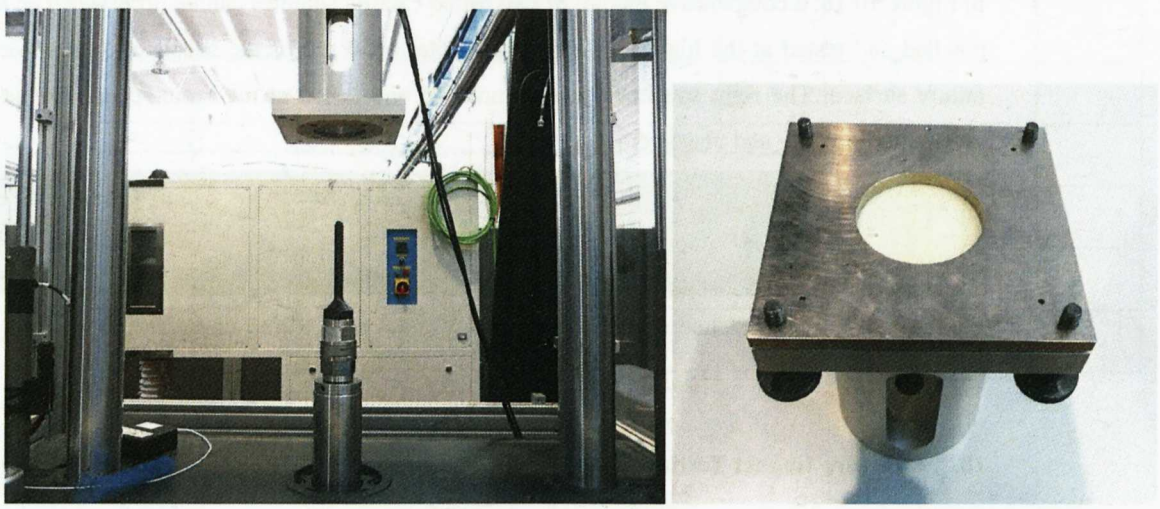

Figure 10.17: Puncture system. Right, mounting on the testing machine. Left, clamping system of the plastic sample.

Testing conditions.

The laboratory atmosphere was sadjusted to be 23°C and 50% relative humidity. 10 specimens were tested per condition.

The testing system principle was mainly based on the ISO 6603-2 standard, although some dimensions were different. The impactor has a 12.7mm diameter. The base and the upper supports have a 76 mm diameter hole.

The impactor was lubricated with vaseline as stated in the standard.

The studied specimens were of the type of the described in Section 6.2. (90x90 mm square plates with a 2 mm thickness).

Two different testing speeds were used in order to study the strain rate sensitivity of the selected materials in Puncture mode:

- V1 for PC/ABS was stated at 1.1 m/s.
- V2 for PC/ABS was stated at 4.04 m/s.

- V1 for PP was stated at 1.1 m/s.
- V2 for PP was stated at 4.4 m/s.

10.2.1. Puncture Test Results for PC/ABS.

Figures 10.18 and 10.19 show the Force-time and Force-displacement results obtained for the studied PC/ABS at the two selected testing speeds. Displacement values were measured from the hydraulic actuator's position.

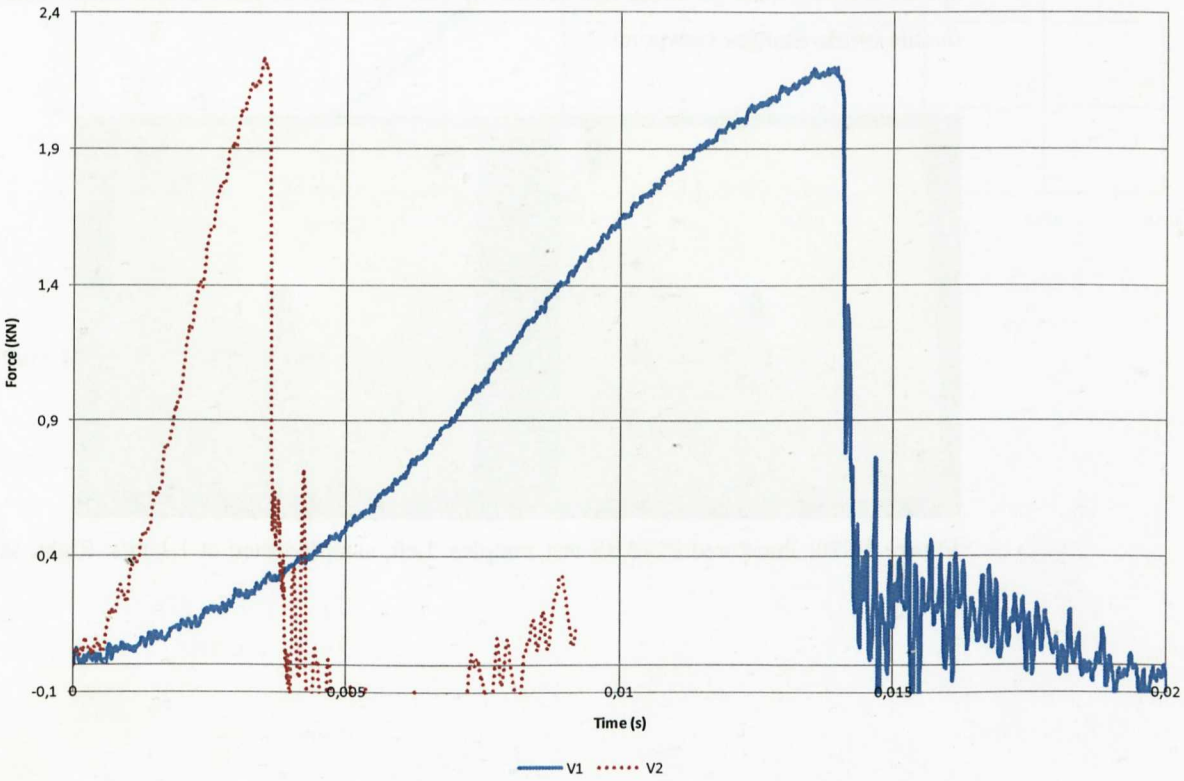

Figure 10.18: Force-time Puncture curves for PC/ABS. V1 = 1.1 m/s. and V2 = 4.04 m/s.

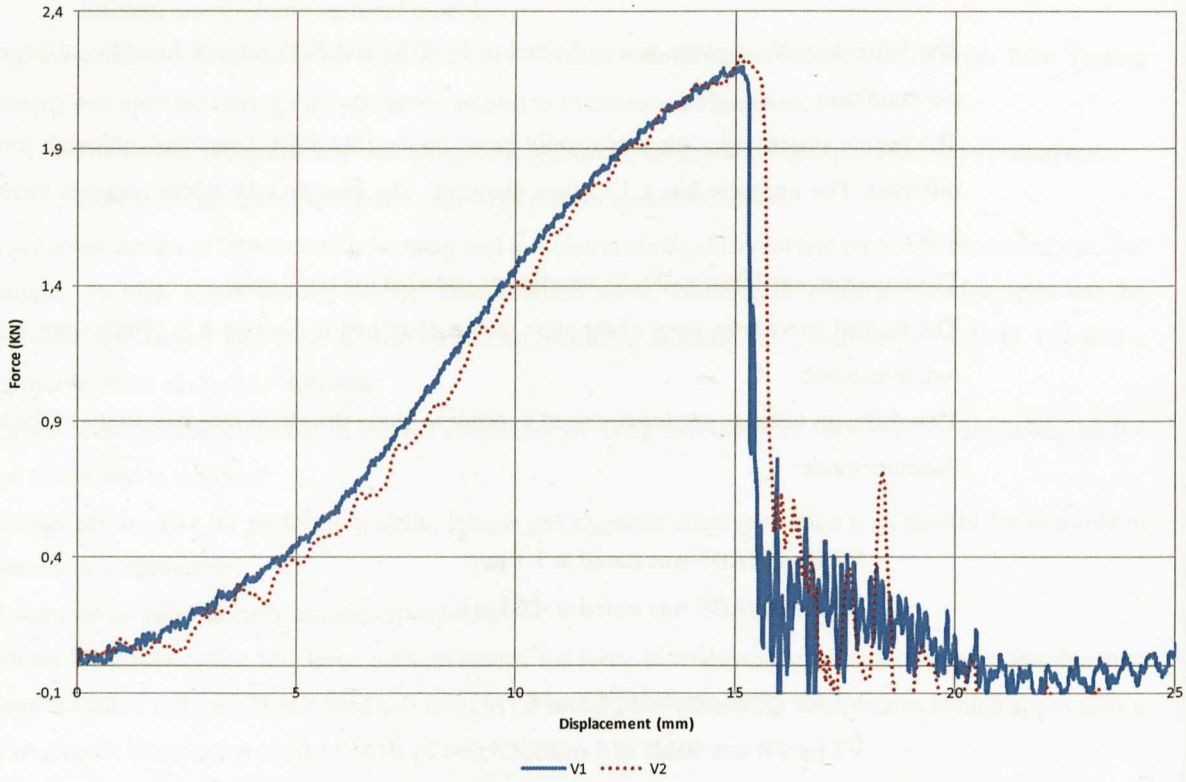

Figure 10.19: Force-displacement Puncture curves for PC/ABS. V1 = 1.1 m/s. and V2 = 4.04 m/s.

From Figures 10.18 and 10.19, it can be observed that at both testing speeds the curve shape is very similar. Specimens break with yielding and subsequent unstable cracking.

In Figure 10.20 a comparative view of two PC/ABS specimens tested at the different speeds are shown. It can be observed that the failure mode is very similar in both specimens, denoting that this material at this testing speeds shows almost no strain rate sensitivity both in terms of force-displacement data, and from possible ductile-brittle changes viewpoint.

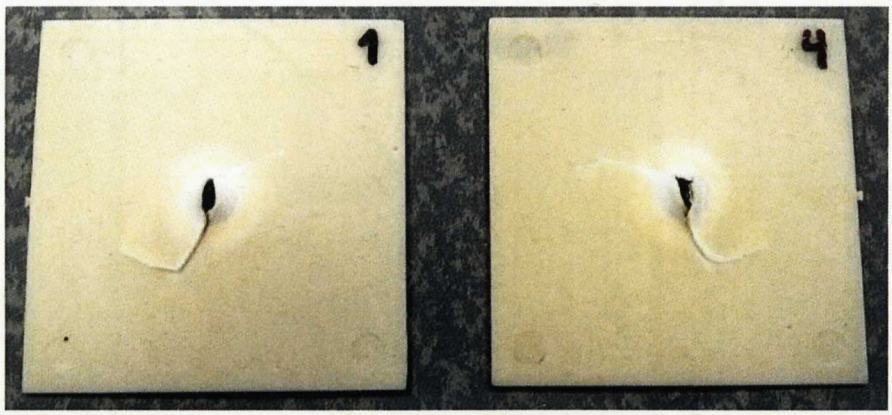

Figure 10.20: Punctured PC/ABS test samples. Left, sample tested at 1.1 m/s. Right, sample tested at 4.04 m/s.

Figure 10.21: Punctured PC/ABS test sample, detailed view.

10.2.2. Puncture Test Results for PP.

The following graphs from Figure 10.22 to 10.23 show the Force-time and Force-displacement results obtained for the studied PP at the two selected testing speeds.

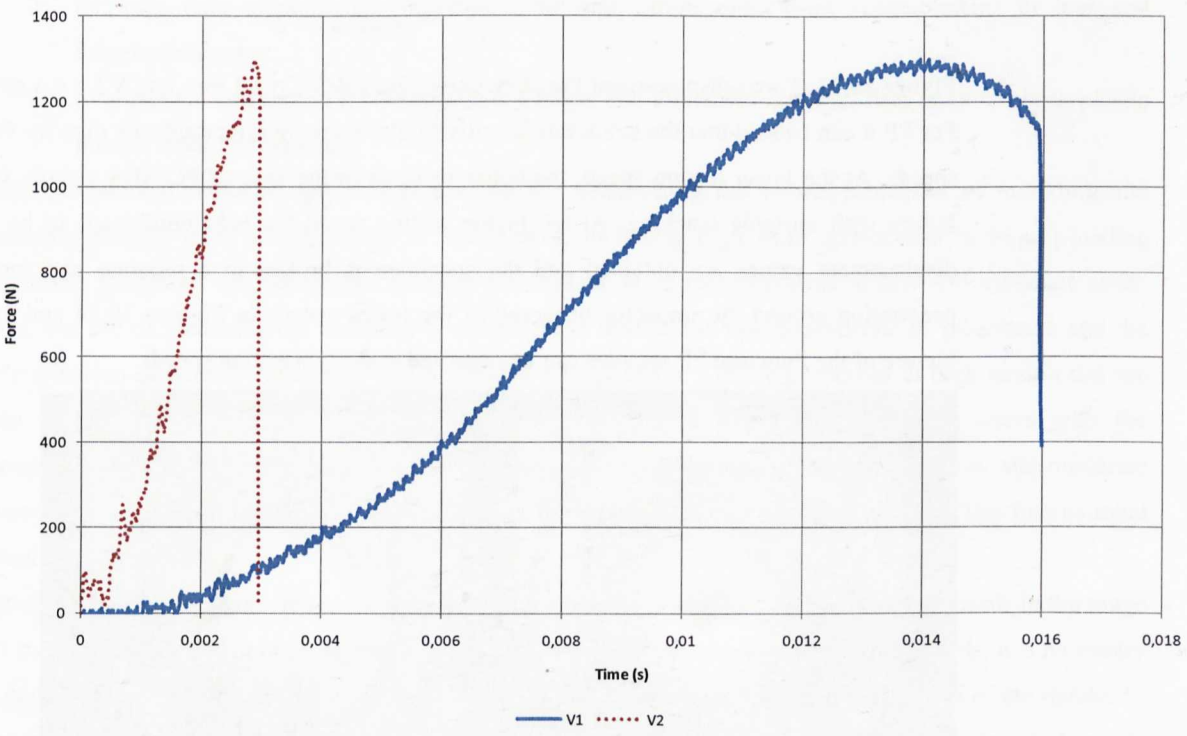

Figure 10.22: Force-time Puncture curves for PP. V1 = 1.1 m/s. and V2 = 4.4 m/s.

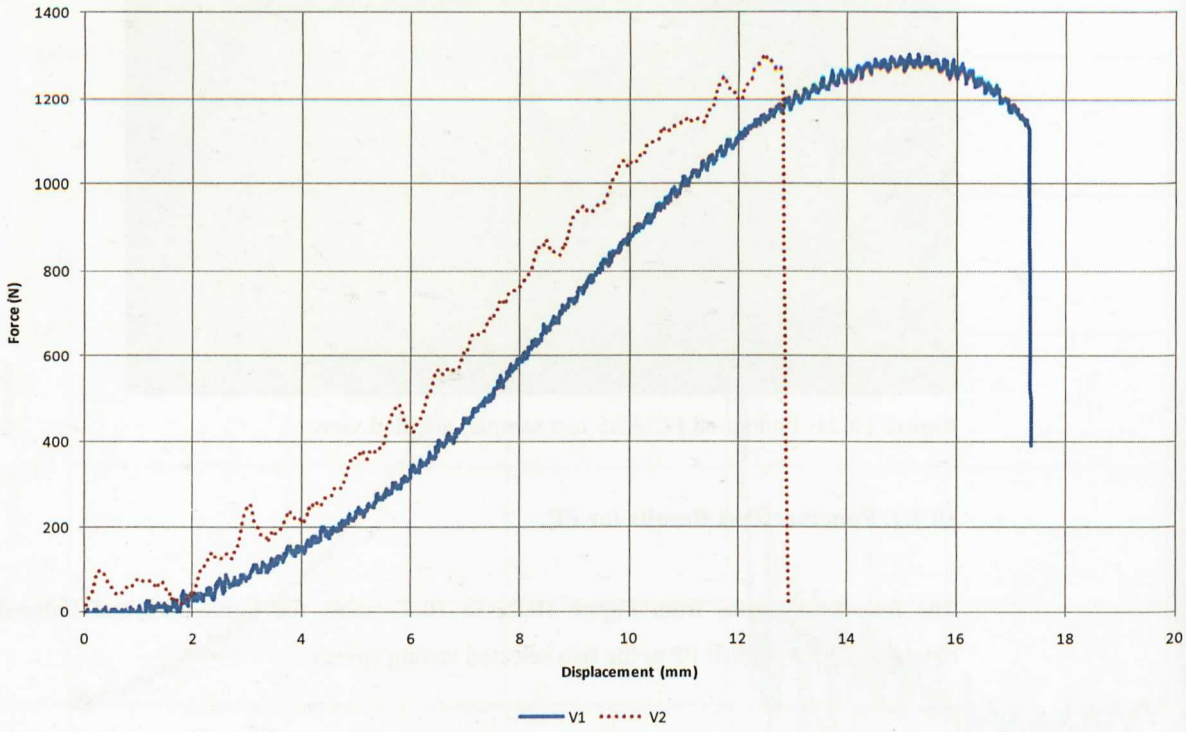

Figure 10.23: Force-displacement Puncture curves for PP. V1 = 1.1 m/s. and V2 = 4.4 m/s.

For PP it can be said that the strain rate sensitivity plays a more important role than for PC/ABS at the tested speeds. At the lower testing speed, the behavior is, as in the case of PC/ABS, ductile yielding with a final failure with unstable cracking. At the higher testing speed the behaviour tends to be more brittle, lower displacement values are obtained and the specimen is broken in a separate part instead of the ductile penetration around the impactor observed in the lower speed. In Figures 10.24 and 10.25 a comparative picture of the Puncture PP samples can be observed at the two testing speeds.

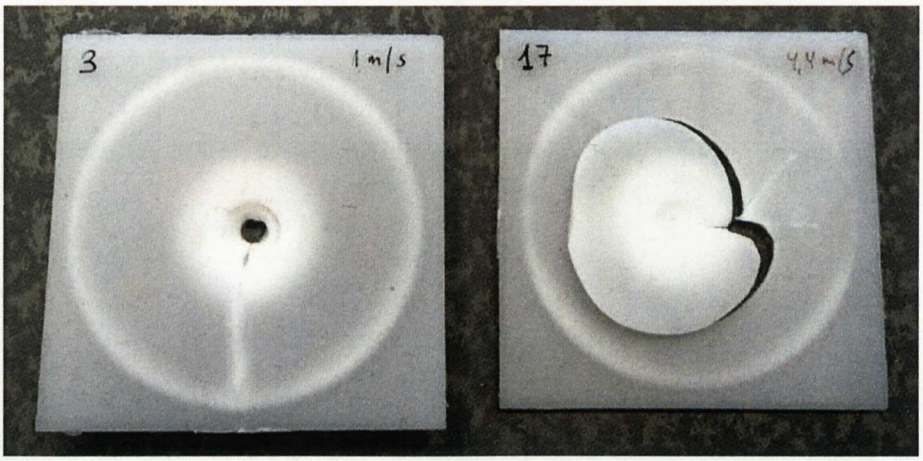

Figure 10.24: Punctured PP test samples. Left, sample tested at 1.1 m/s. Right, sample tested at 4.4 m/s.

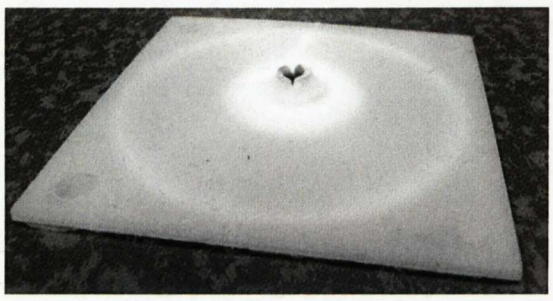

Figure 10.25: Punctured PP test sample at the lower testing speed, detailed view.

10.3. Tensile Testing at High Strain Rates.

The objective of tensile testing at high strain rates was to obtain true stress-strain curves at different strain rates in order to feed the constitutive material models implemented in ANSYS and LS-DYNA.

The method followed in this section is based on the standard ISO 18872:2007 Plastics - Determination of tensile properties at high strain rates.

Although it has been stated that nowadays there is still no specific standard for testing at high strain rates and generation of true stress-strain data for input in impact FEA, ISO developed this procedure which is mainly based on the research work carried out by Dean et al. [12]. The use of this standard is still under discussion, very little information can be found in the literature where this methiod is used [49]. Research centers are not confident with described extrapolation methods and perform their own testing [10].

In this thesis work the objective is to study the validity of the procedure described in the standard,

1. To generate true stress-strain data at different strain rates, covering data required by Charpy and Puncture impact tests.
2. Evaluate data extrapolation capabilities to high strain rates from measurements at low and intermediate rates.
3. Evaluate the correlation level simulating Charpy and Punctures test with data input to elasto-plastic models from this standard.

This International Standard specifies procedures for determining the tensile properties of moulding and extrusion plastics over a wide range of strain rates, including high rates appropriate to impact-loading situations. Properties are determined through a combination of measurements at low and moderate strain rates, the use of mathematical functions to model these results, the rate-dependence of parameters and the determination of parameters at high strain rates by extrapolation. Tensile properties at high strain rates are then derived by calculation. In this way, the experimental problems and associated errors with the measurement of properties at high rates are avoided. The measurement of properties at low and moderate strain rates is based on ISO 527-2, which identifies the types of plastics materials to which this International Standard is applicable.

Tensile stress versus strain curves are measured in accordance with ISO 527-2 at selected speeds in the range 0,1 mm/s to 100 mm/s. In order to maximise the accuracy of these results at the higher speeds, it is necessary to pay attention to certain features of the design of the test assembly as described in Clause 5 of the standard.

According to Clause 5, servo-hydraulic testing machines usually need to be employed to achieve test speeds above 10 mm/s. At test speeds above around 10 mm/s, errors may arise in the measurement of force. These are associated with the presence of resonance modes in the force transducer, the test specimen and components in the test assembly. To maximise the speed range over which measurements of satisfactory accuracy can be made, attention should be paid to the design of the test assembly so that it incorporates a high stiffness (e.g. piezoelectric) force transducer and components of low mass and high rigidity.

In this standard, measurements are also made of the variation of Poisson's ratio with strain. Values of true stress and true plastic strain are calculated from these results at each strain rate. In this thesis work, instead of using extensometric devices to measure strains and thus Poisson's ratio, an iterative process was used to determine true stress-strain data correlating experimental force-displacement results in ANSYS and LS-DYNA.

In ISO 18872, a mathematical function is used to accurately model the shape of each stress/plastic strain curve. The variation of parameters in this function with strain rate is also modelled to enable the values of parameters at higher strain rates to be determined by extrapolation. Stress/strain curves at these higher strain rates can then be derived by calculation.

At strains above the yield strain, where the stress reaches a maximum or increases only slowly with strain, the strain distribution in the gauge region in standard specimens becomes non-uniform. In extreme situations, this is visible as a neck, and is the reason that International Standards refer to recording the nominal strain (see ISO 527-1:1993, 4.10) through measurements of changes in the grip separation. These strain values have an unknown error which, for some materials, can be very large. Where higher accuracy is required, the ISO 18872 standard proposes an alternative specimen geometry. This specimen has a uniform thickness but the width is reduced from 10 mm to 8 mm by a circular waist cut at the centre of the specimen length. The specimen thickness is not critical, so it can be machined from the central region of type 1A or 1B specimens.

In this thesis work the original multipurpose type specimens were used (see section 6.2) as the slow rate testing part was also carried out with this type of specimens.

According to the standard, specimens shall be tested at speeds of 0.1 mm/s, 1 mm/s, 10 mm/s and 100 mm/s. If results at the highest speed are unreliable, or if greater confidence is required in the analysis of results, additional speeds may be used which should be selected from the values 0.3 mm/s, 3 mm/s and 30 mm/s. In this thesis work, an additional speed of 300 mm/s. was also used

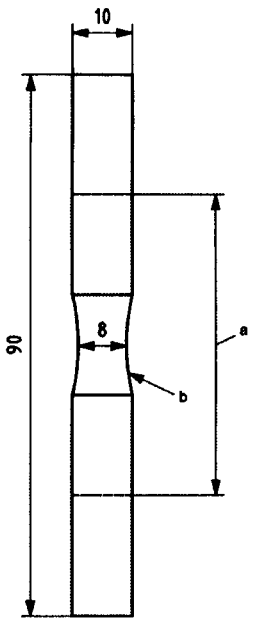

Figure 10.26: ISO 18872 recommended specimen for the generation of true stress-strain data at high strain ranges. A, grip separation (50 mm) and b, radius (35 mm).

Testing conditions.

The MTS 819.10 servohydraulic system was used for tensile testing at different speeds.

The laboratory atmosphere was adjusted to be 23°C and 50% relative humidity. 10 specimens were tested per condition.

The following testing speeds were used: 0.1, 0.3, 1, 3, 10, 30, 100 and 300 mm/s.

Up to 10mm/s a standard load cell from MTS model ±25 KN was used. Above 10mm/s a piezo-electric load cell from KISTLER model 9361B was used for load measurements and a displacement sensor from MTS

Temposonics®. This is due to higher sensitivity of piezo load cells to fast testing events. On the contrary, piezo load cells are not sensitive enough for slow rate testing.

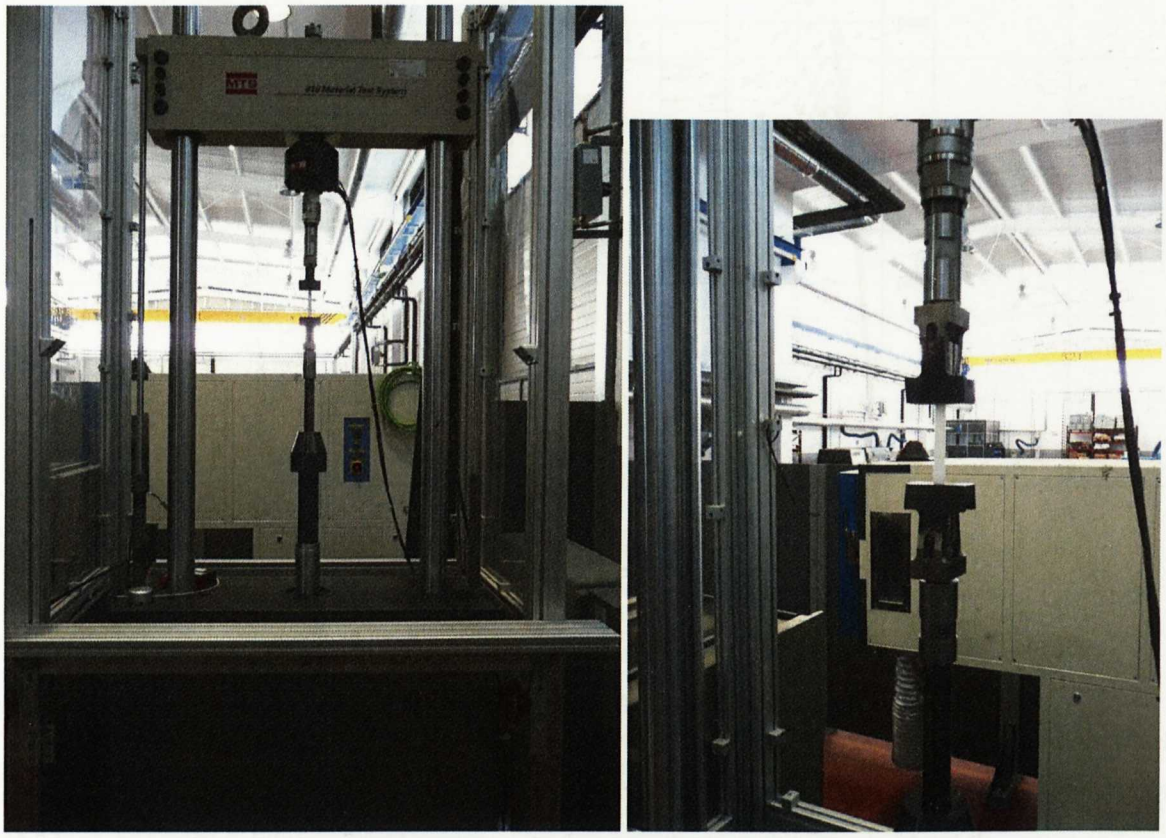

Figure 10.27: Tensile testing scheme. Left, view of the servohydraulic testing machine. Right, tensile testing clamps and specimen.

The specimens were fixed in a 115 mm distance between clamps (as stated in the ISO 527 standard) and time, force and displacement data was recorded up to the rupture point. No extensometric device was included for strain measurements.

10.3.1. High Strain Rate Tensile Test Results for PC/ABS.

Figure 10.28 shows the obtained force-displacement curves for PC/ABS at the selected testing speeds. From the tested 10 specimens, intermediate curves are represented.

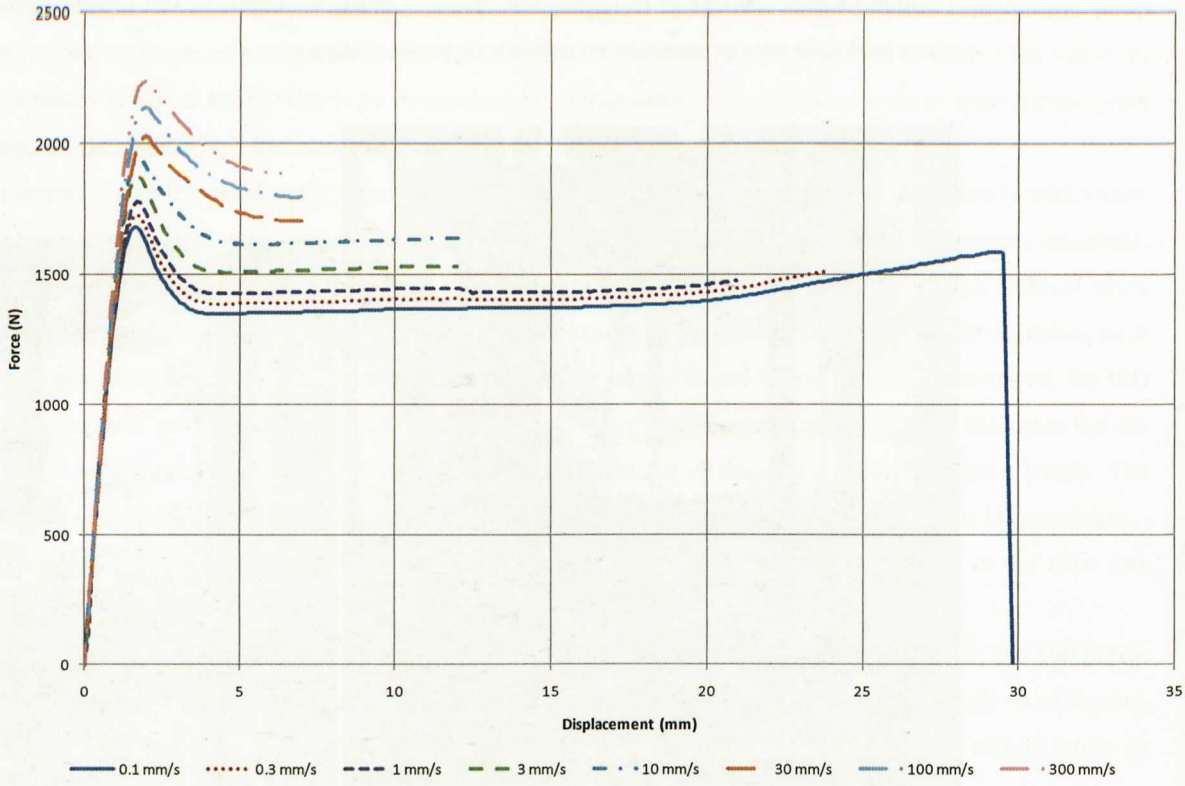

Figure 10.28: Force-displacement results for PC/ABS. Testing speeds from 0.1 to 300 mm/s. 23°C and 50% R.H.

It can be observed that as the testing speed is increased the force peak in the yield region also increases which denotes that the yield behaviour of this material is rate sensitive. Failure strains are also decreased in a great extent as testing rate is increased but in this case the scatter in test data is considerable.

The experimental force-displacement curves were later correlated in ANSYS iteratively adjusting the input stress-strain curve in order to match the experimental traces in Figure 10.28. The process was repeated for each testing speed.

10.3.2: High Strain Rate Tensile Test Results for PP.

Figure 10.29 shows the obtained force-displacement curves for PP at the selected testing speeds. From the tested 10 specimens, intermediate curves are represented.

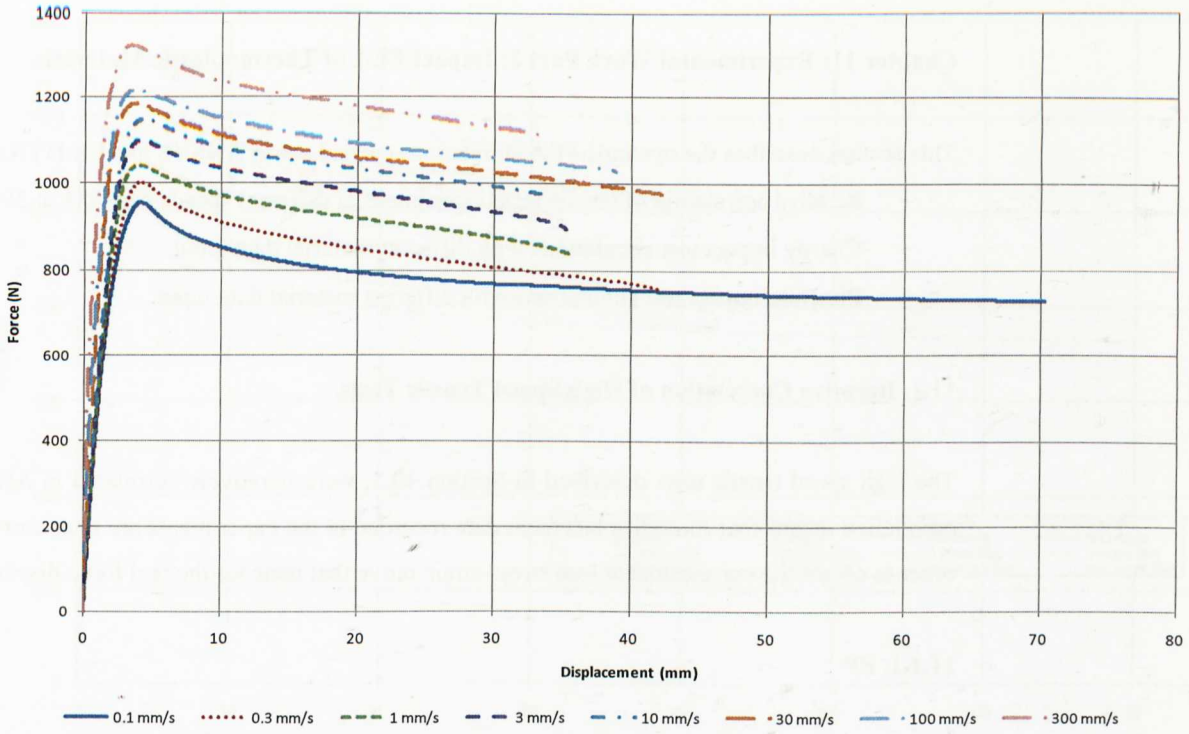

Figure 10.29: Force-displacement results for PP. Testing speeds from 0.1 to 300 mm/s. 23°C and 50% R.H.

It can be observed that as the testing speed is increased the force peak in the yield region also increases which denotes that the yield behaviour of this material is rate sensitive. Failure strains are also decreased as testing rate is increased but in this case the scatter in test data is considerable.

The experimental force-displacement curves were later correlated in ANSYS iteratively adjusting the input stress-strain curve in order to match the experimental traces in Figure 10.29. The process was repeated for each testing speed.

Chapter 11: Experimental Work Part 2: Impact FEA of Thermoplastic Materials.

This section describes the dynamic FEA simulations carried out in ANSYS and LS-DYNA in concern to the:

- iterative correlation of tensile tested specimens at different speeds from 0.1 to 300 mm/s.
- Charpy impact test simulations with different material data input.
- Puncture impact test simulations with different material data input.

11.1. Iterative Correlation of High Speed Tensile Tests.

The high speed tensile tests described in Section 10.3, were iteratively correlated in ANSYS. This iterative correlation means that force-displacement data recorded in the experiments are later correlated in ANSYS in order to obtain the correspondent true stress-strain curve that matches the real force-displacement graph.

11.1.1. PP

This iterative process was performed accordingly to the method described in Section 6.4.4.3.1.
The material definition and finite element model creation were the same used in Sections 6.4.1.1 and 6.4.1.2. In this case the process was repeated for each curve at different testing speeds. As a result, true stress-strain curves were obtained as input to correlate the different tensile tests. These stress-strain curves were later used to simulate Charpy and Puncture impact tests.
Figure 11.1 shows the different stress-strain curves obtained to correlate the force-displacement graphs in Figure 11.2.

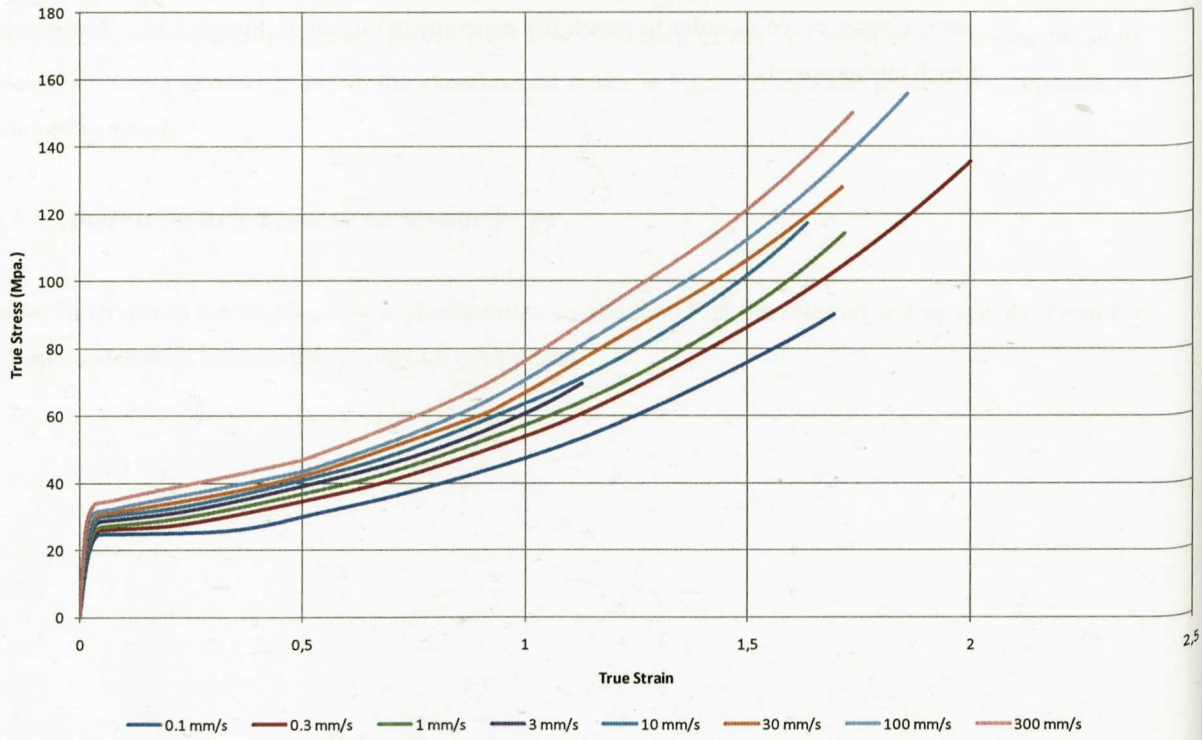

Figure 11.1: True stress-strain curves for PP resulting from the iterative process to match the experimental force-displacement curves.

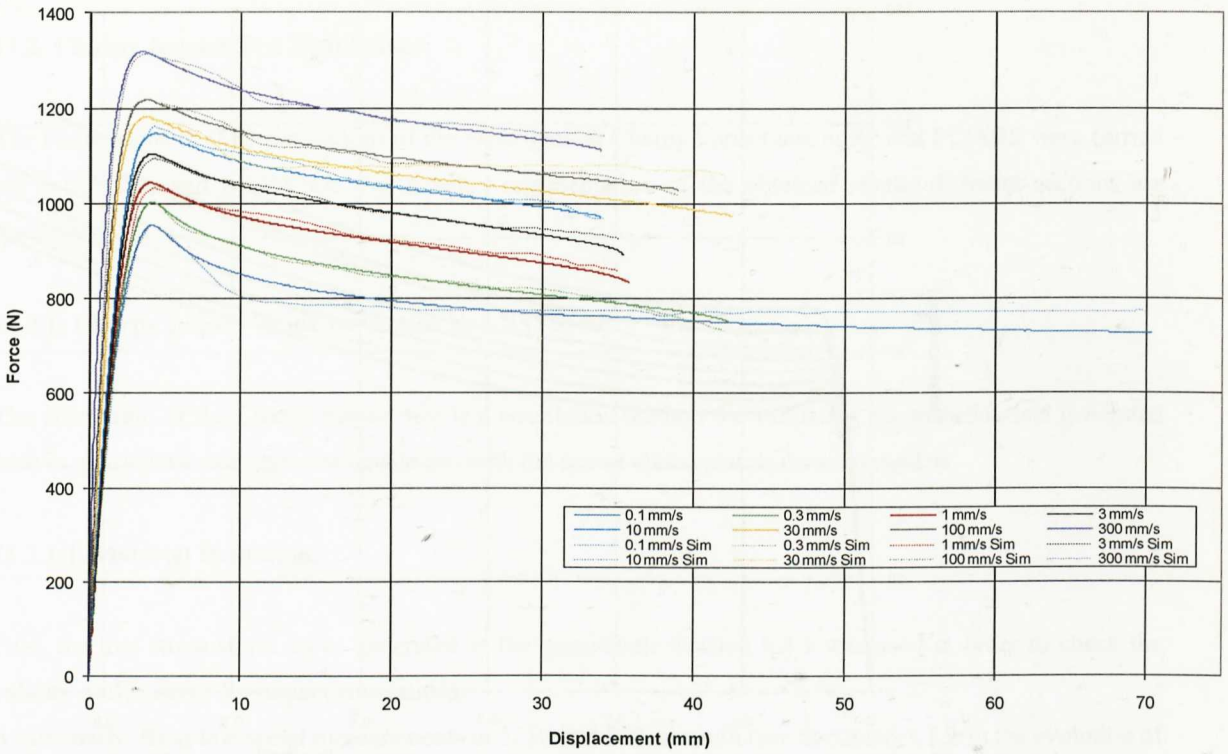

Figure 11.2: Correlation for PP between experimental tensile test curves from 0.1 to 300 mm/s and simulation results obtained in ANSYS using stress-strain curves from Figure 11.1.

It can be observed that with the use of the true stress-strain curves in Figure 11.1, a good correlation level was obtained between experimental and simulated force-displacement results.

11.1.2. PC/ABS

The same procedure followed with PP was performed in PC/ABS. The iterative process was performed accordingly to the method described in Section 6.4.4.3.1.

The material definition and finite element model creation were the same as those used in Sections 6.4.4.1 and 6.4.4.2. In this case, the process was repeated for each curve at different testing speeds. As a result, true stress-strain curves were obtained as input to correlate the different tensile tests. These stress-strain curves were later used to simulate Charpy and Puncture impact tests.

Figure 11.3 shows the different stress-strain curves obtained in the correlation process.

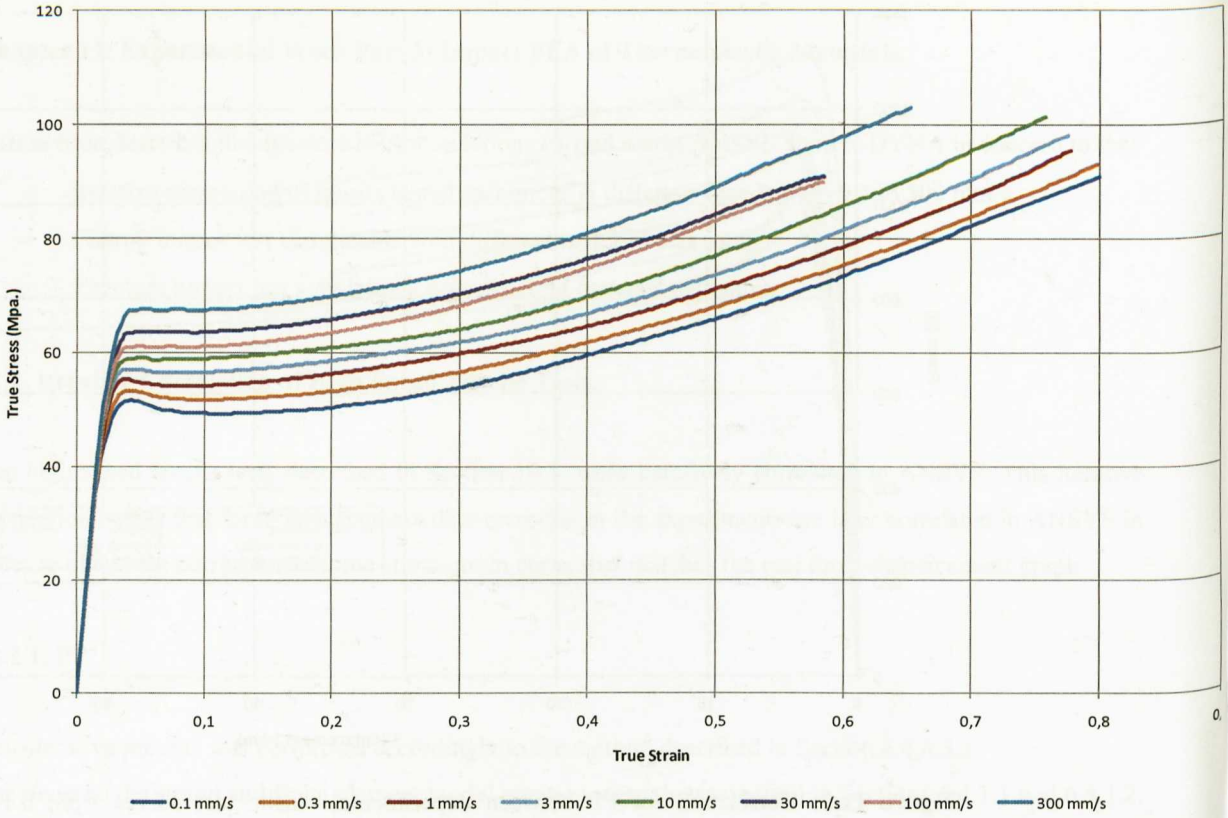

Figure 11.3: True stress-strain curves for PC/ABS resulting from the iterative process to match the experimental force-displacement curves.

11.2. Charpy Impact Test Simulations.

The Finite Element (FE) simulations of the experimental Charpy impact test in PP and PC/ABS were carried out in ANSYS and LS-DYNA. For a better representation of the obtained results different sections are presented.

11.2.1. Charpy Impact Test Correlation in ANSYS. PP.

The simulation of the Charpy impact test is a correlation method for validating the material data generated both in quasi-static and high rate tensile test with the use of elasto-plastic material models.

11.2.1.1. Material Definition.

First, the true stress-strain curve generated in the quasi-static Section 6.4.1 was used in order to check the validity of this curve for impact simulations.
Additionally, from low speed measurements at 5, 50 and 500 mm/min (see Section 6.3.1.2.1) the evolution of yield stress with strain rate was also studied using the Perzyna viscoplastic model (see Section 4.4).
From Table 6.5, the following values were used to fit the Perzyna model:
5 mm/min→0.001667s-1→9.183MPa.
50 mm/min→0.01667s-1→11.99MPa.
500 mm/min→0.1667s-1→12.217MPa.
Although the fit quality was not very good, the objective was to evaluate the effect of taking into account strain rate effects in the impact simulation.
The fit gave an m value of 0.37 and a γ value of 3.93. Figure 11.4 reflects the fit obtained in the software KaleidaGraph 4.0.
Thus, the first approach was to use a MISO material model in ANSYS to represent the true stress-strain curve of the material in Figure 6.71. In addition to this elasto-plastic definition, a tensile elastic modulus of 1458.1 MPa. and a Poisson's ratio of 0.38 were also defined.
The second approach was to add a Perzyna viscoplastic model to this definition, considering an m value of 0.37 and a γ value of 3.93.

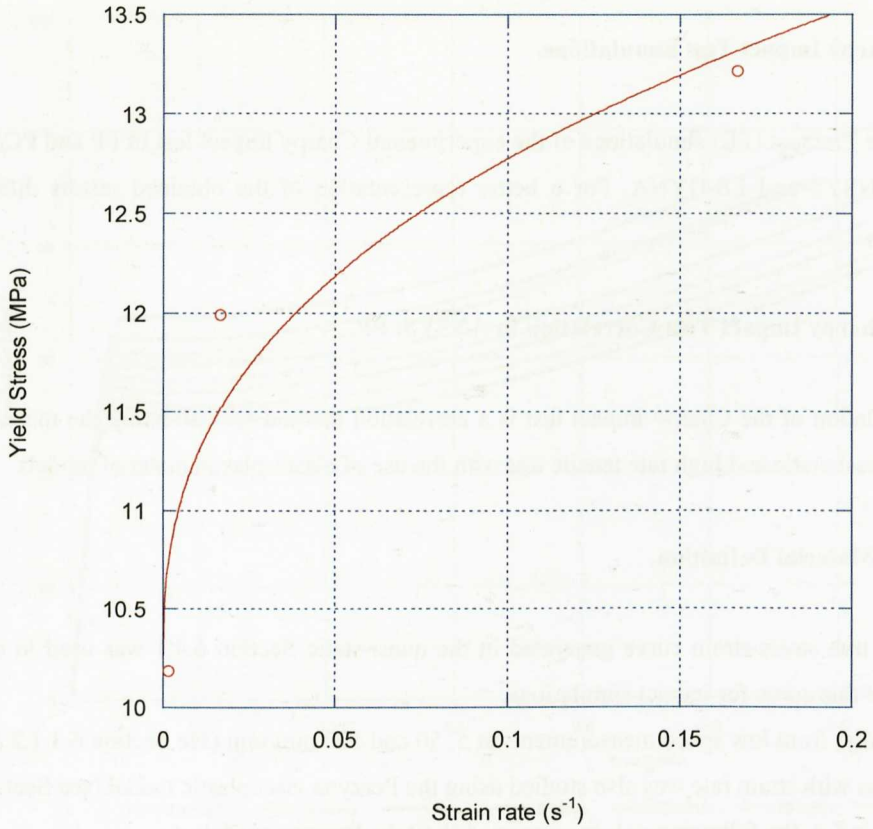

Figure 11.4: Perzyna fit for three slow rate yield values of PP.

A density value of 0.905×10^{-9} Tn/mm^3 was also specified for PP (from material data sheets) which is necessary in a dynamic analysis for inertial effects to be taken into account.

11.2.1.2. Finite Element Modelling.

The Charpy impact test geometry was modeled in ANSYS. Both the un-notched and notched geometries were represented by finite element models in order to study the virtual impact behaviour and compare with experimental results.

The un-notched specimen and the impactor were meshed with SOLID 185 (8 node hexahedral) type elements. Contact elements were created between the impactor and the specimen and the specimen and the base supports (TARGE 170 and CONTA 174 type elements). See Figure 11.5.

A global mesh size of 0.5 mm was used for modeling all the test system. This produced a very good quality mesh in the specimen; when bending characteristics are needed to capture by simulation, a sufficient element number have to be located through the section (usual recommendation is > 2 elements). In this case, 20 hexahedral elements were located through the impacted section of the specimen.

Due to symmetry, only a quarter of the full geometry was modelled in ANSYS (an expanded representation can be seen in Figure 11.5). The finite element for this model consisted of 11862 nodes and 9408 elements.

The loading of the specimen consisted of,

- applying a 7.668 Kg. mass to the impactor.
- applying the correspondant initial velocity to the impactor (1.77 m/s in the lower speed case and 4.42 m/s in the higher speed case).
- applying gravity in the system.

Additional symmetry conditions were also applied to the quarter part of the specimen.

A large displacement transient analysis was performed in each case, specifying the correspondent simulation time (in seconds); 0.0075 s in the lower speed case and 0.0023 s in the higher speed case.

Figure 11.5: Finite element model for the un-notched Charpy test configuration, PP and PC/ABS.

The notched specimen and the impactor were also meshed with SOLID 185 (8 node hexahedral type elements). Contact elements were created between the impactor and the specimen and the specimen and the base supports (TARGE 170 and CONTA 174 type elements).

A global mesh size of 0.5 mm was used again for modeling all the test system. In this case a fine mesh was created in the notch area in order to represent adequately the radius of the notch (see Figures 11.6 and 11.7).

Due to symmetry, only a quarter of the full geometry was modelled in ANSYS (an expanded representation is seen in Figure). The finite element mesh for this model consisted of 16186 nodes and 12817 elements.

The loading of the specimen consisted of,

- applying a 7.668 Kg. mass to the impactor.
- applying the correspondant initial velocity to the impactor (1.77 m/s in the lower speed case and 4.42 m/s in the higher speed case).
- applying gravity in the system.

Additional symmetry conditions were also applied to the quarter part of the specimen.

A large displacement transient analysis was performed in each case, specifying the correspondent simulation time (in seconds); 0.0045 s in the lower speed case and 0.002 s in the higher speed case.

Figure 11.6: Finite element model for the notched Charpy test configuration, PP and PC/ABS.

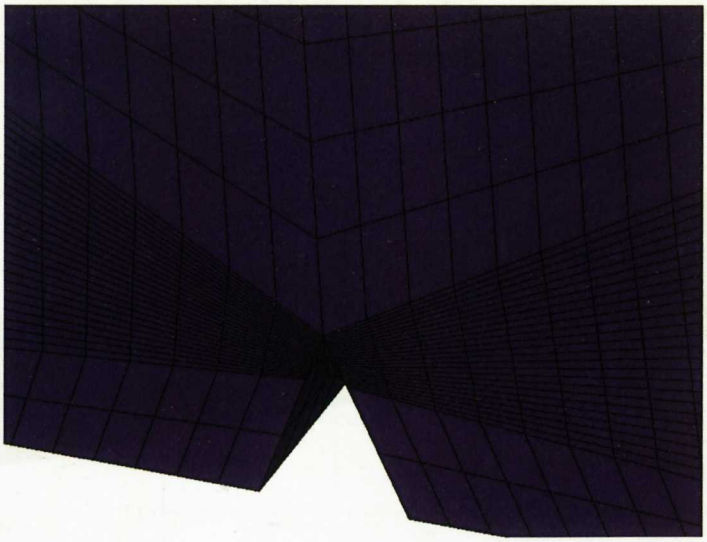

Figure 11.7: Mesh detail in the notch area.

11.2.1.3. Results.

For the *unnotched specimen at the lower testing speed*, the curve traces shown in Figures 11.8 and 11.9 were obtained.

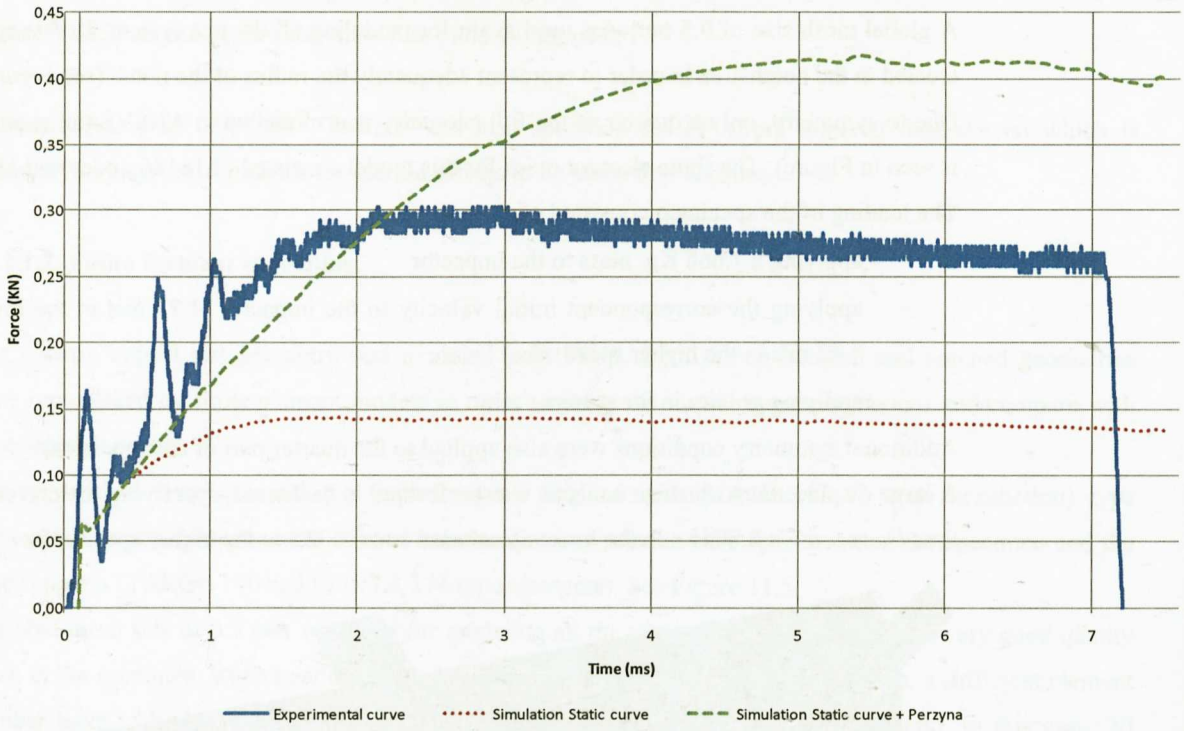

Figure 11.8: Comparison of experimental and simulation force-time results in ANSYS for the lower speed un-notched test, PP.

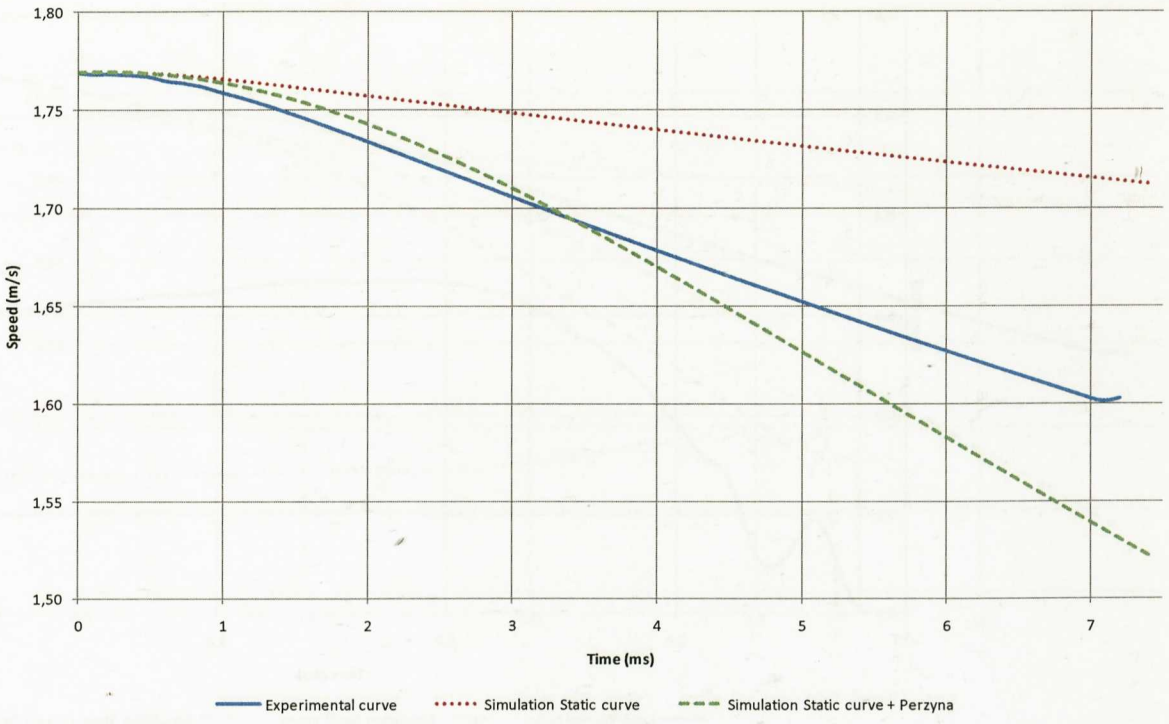

Figure 11.9: Comparison of experimental and simulation speed-time results in ANSYS for the lower speed un-notched test, PP.

The input of a static curve gives lower force values than experimental results. Additionally, the initial force peak is represented by simulation (although lower peak values are registered) but subsequent peaks are not simulated.

Speed-time curves differ considerably when a single static curve is used. With the use of a viscoplastic Perzyna model, force-time results are not improved in the initial peak area and in the plastic deformation region a scaling effect is clearly visible: force values rise to even higher values than experimental results. This is an indicative that extrapolations with the Perzyna model give too high yield stress values with increasing strain rates.

The speed-time curve tends to match closer the experimental curve.

For the *un-notched specimen at the higher testing speed*, the curve traces shown in Figure 11.10 were obtained.

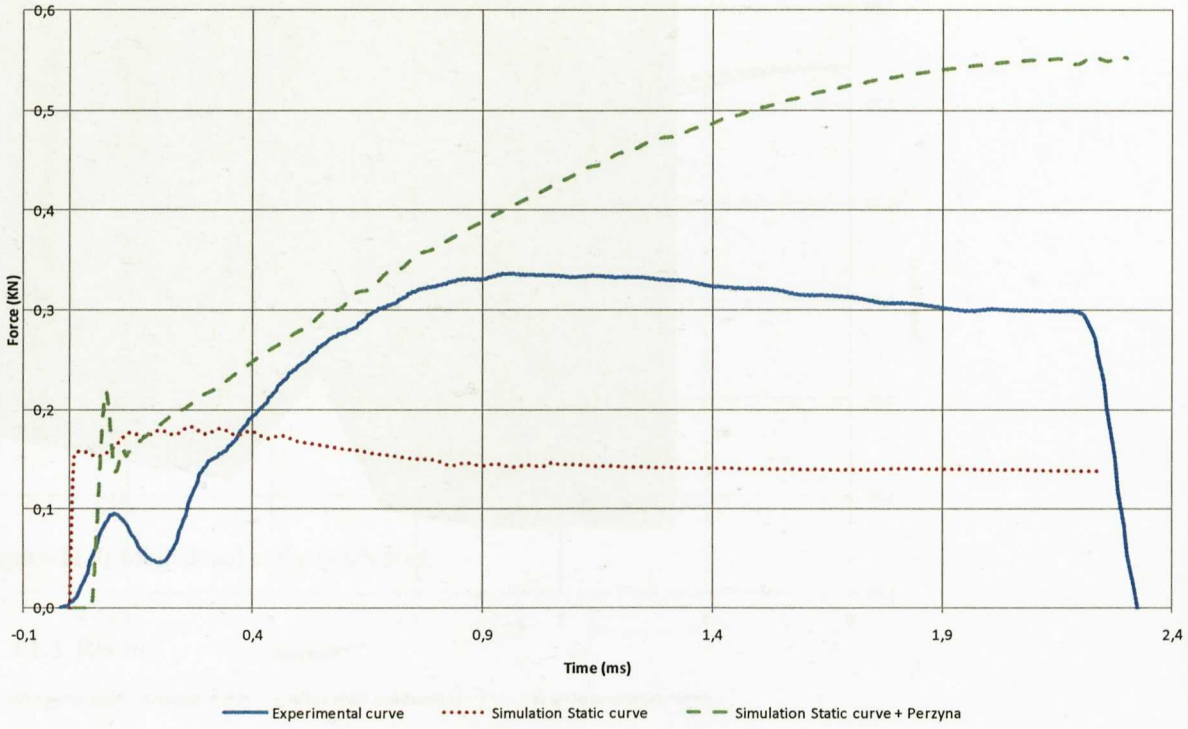

Figure 11.10: Comparison of experimental and simulation force-time results in ANSYS for the higher speed un-notched test, PP.

The input of a static curve now gives higher initial force peak values than experimental results. Some experimental curves also showed higher peak values than the selected intermediate curve.

The plastic deformation area until rupture is represented by lower force values. However the experimental tendency at this testing speed of having an initial peak with no subsequent peaks is now correlated in a better way. Speed-time curves differ considerably when a single static curve is used.

With the use of a viscoplastic Perzyna model, force-time results are improved in the initial peak area and in the plastic deformation region but higher values than experimental results are recorded. Speed-time curve tends to match closer the experimental curve.

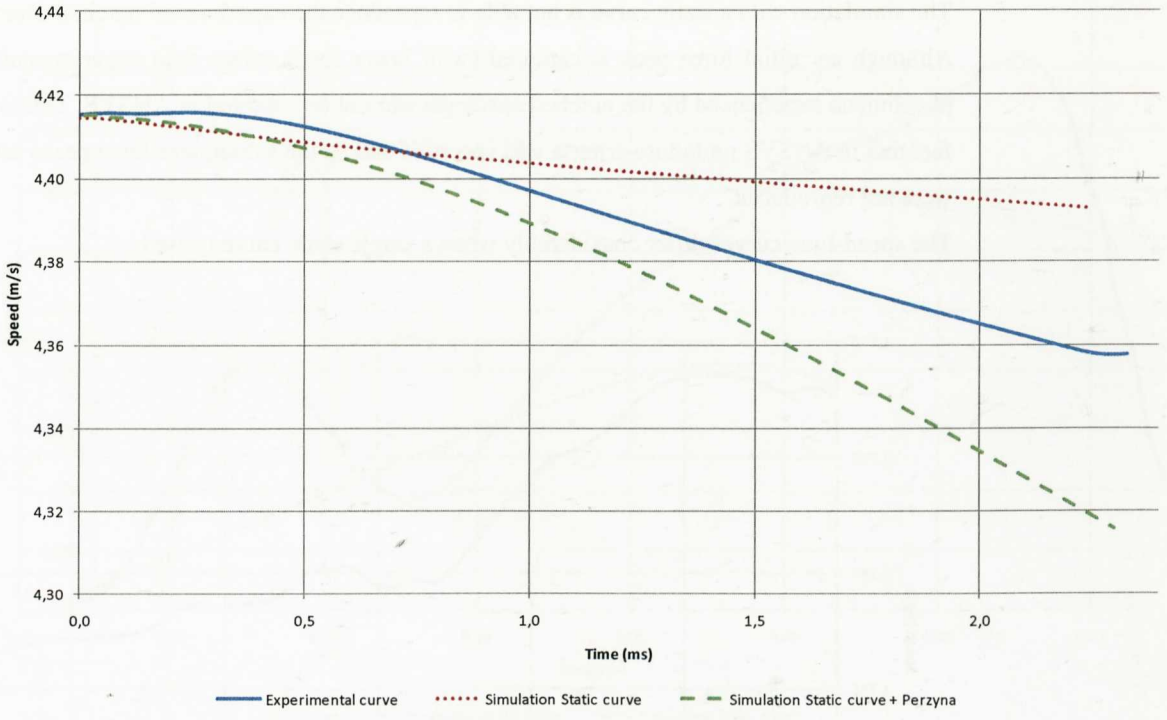

Figure 11.11: Comparison of experimental and simulation speed-time results in ANSYS for the higher speed un-notched test, PP.

For the *notched specimen at the lower testing speed*, the curve traces shown in Figure 11.12 and 11.13 were obtained. In this case the Perzyna model did not give acceptable results since no convergence was achieved in the solution.

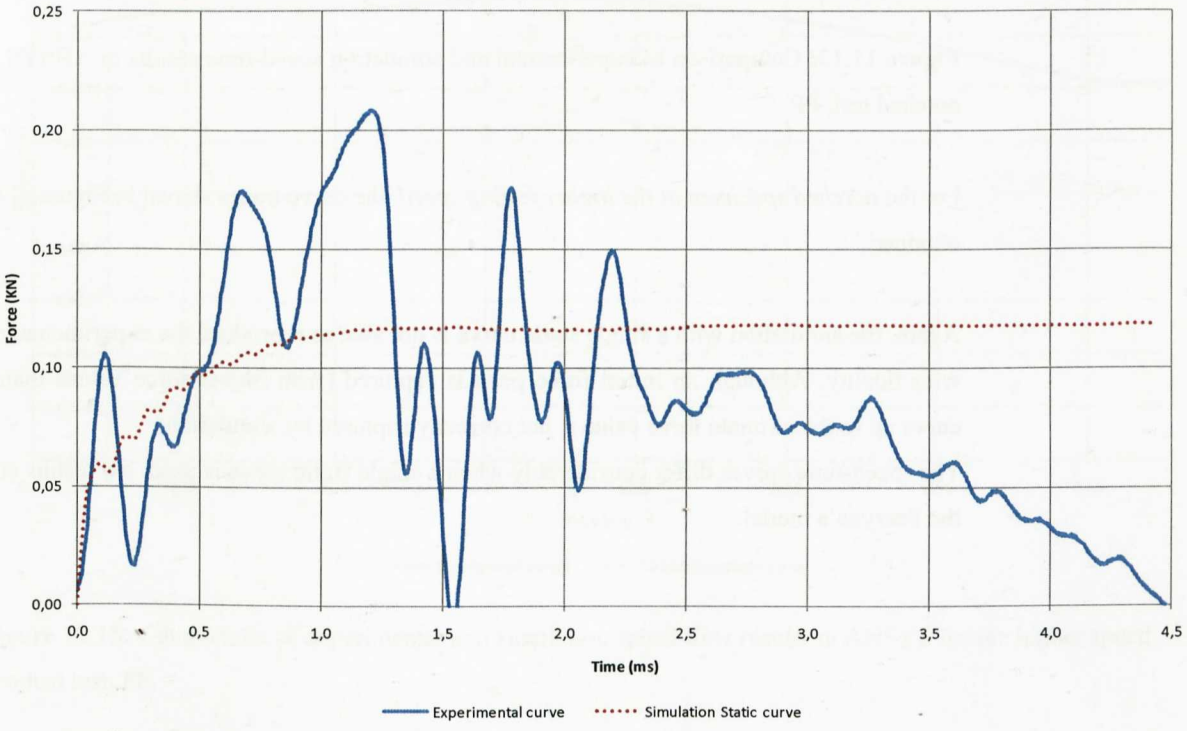

Figure 11.12: Comparison of experimental and simulation force-time results in ANSYS for the lower speed notched test, PP.

The simulation with a static curve is not able to reproduce the experimental notched Charpy test with fidelity. Although an initial force peak is captured (with lower force values than experimental), the later breaking phenomena experienced by the notched specimen can not be captured in ANSYS. This is probably due to the fact that in ANSYS no failure criteria was specified and so the subsequent force peaks associated with failure were not reproduced.

The speed-time curves differ considerably when a single static curve is used.

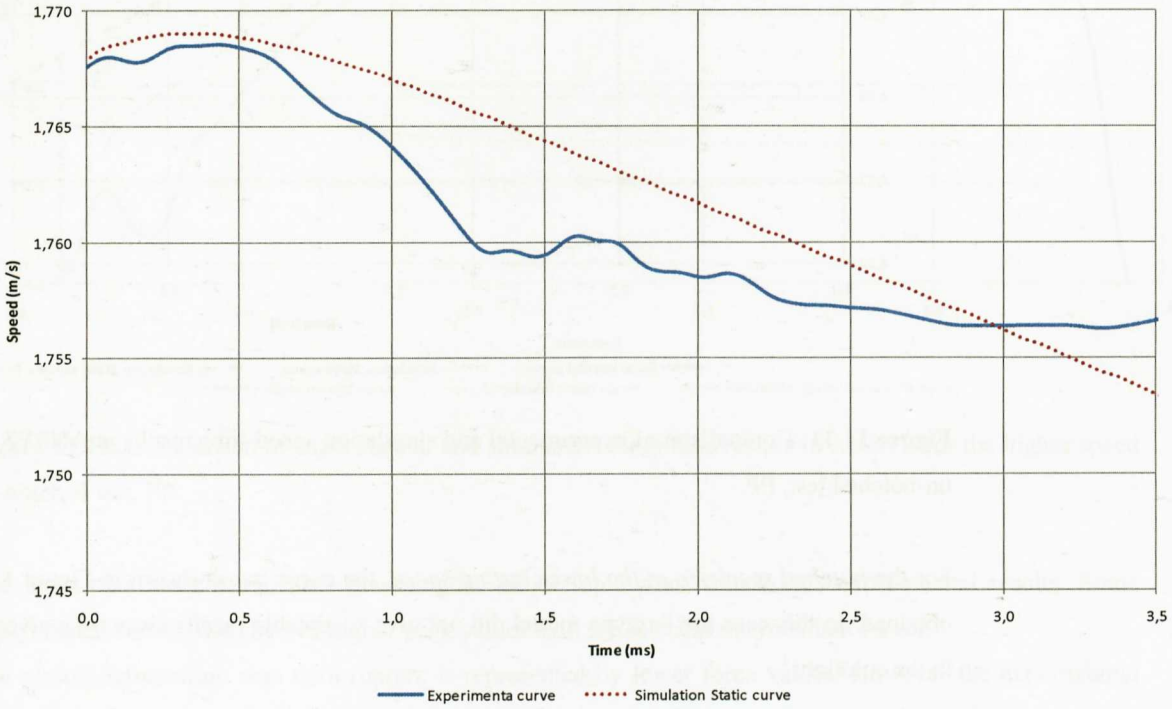

Figure 11.13: Comparison of experimental and simulation speed-time results in ANSYS for the lower speed notched test, PP.

For the *notched specimen at the higher testing speed*, the curve traces shown in Figures 11.14 and 11.15 were obtained.

Again, the simulation with a single static curve is not able to reproduce the experimental notched Charpy test with fidelity. Although an initial force peak is captured (with higher force values than experimental), the curve up to the ultimate force value is not correctly captured by simulation.

The speed-time curves differ considerably when a single static curve is used. No results could be obtained for the Perzyna's model.

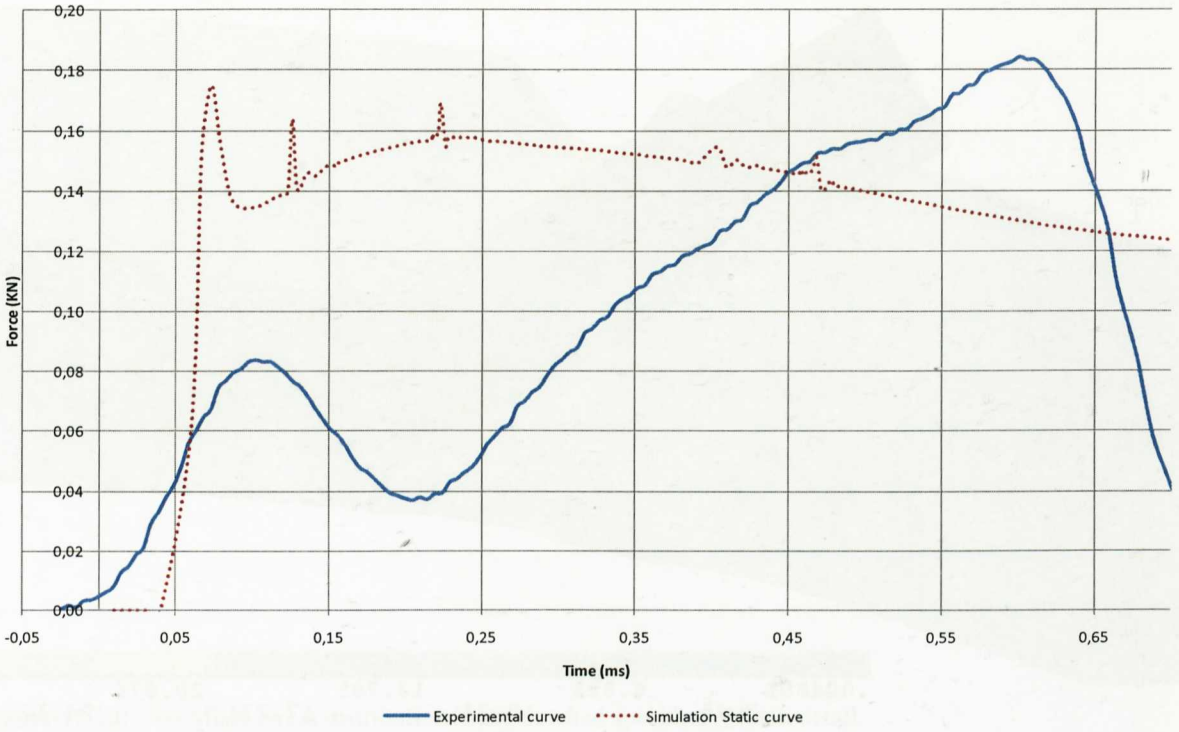

Figure 11.14: Comparison of experimental and simulation force-time results in ANSYS for the higher speed notched test, PP.

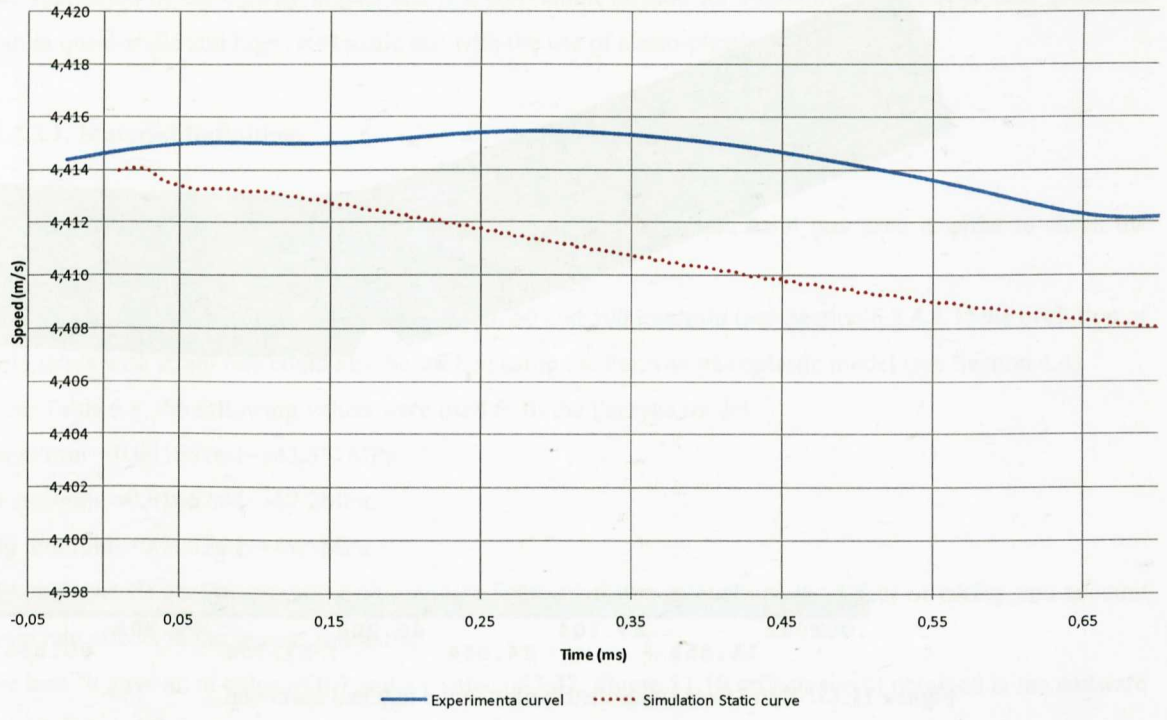

Figure 11.15: Comparison of experimental and simulation speed-time results in ANSYS for the higher speed notched test, PP.

Figures 11.16, 11.17 and 11.18 show for illustrative purposes the Von Mises stresses obtained both in the un-notched and notched specimens. Similar stress patterns were obtained for both materials.

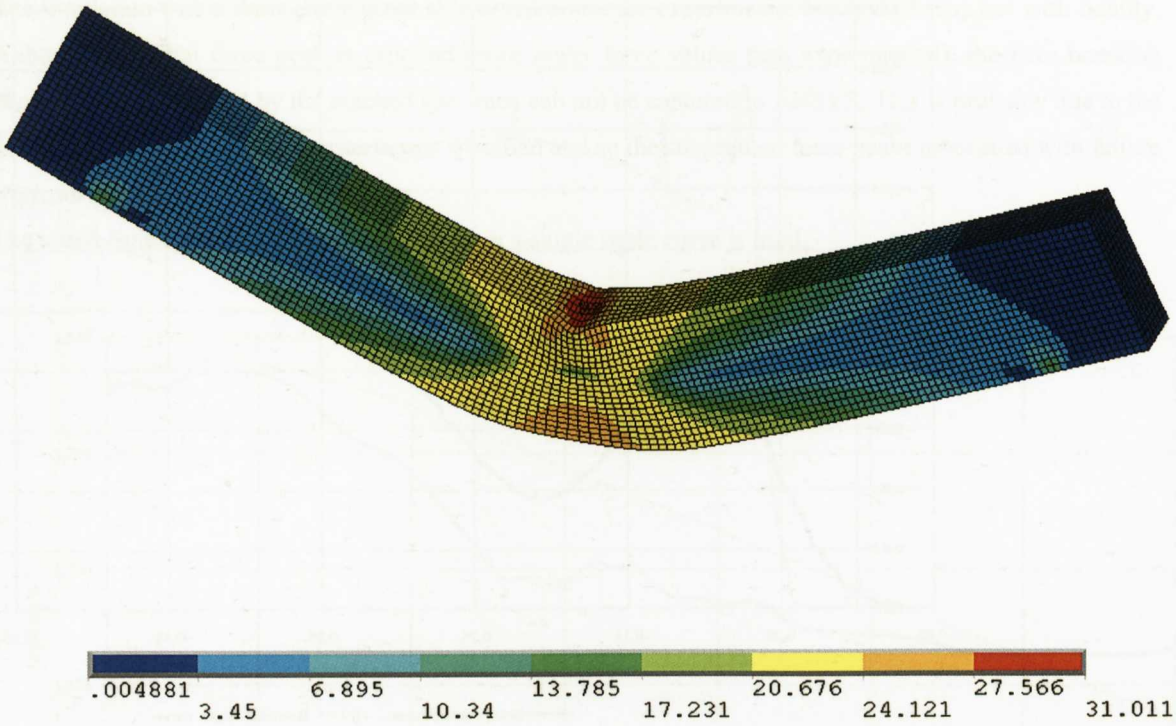

Figure 11.16: Von Mises stress distribution in the un-notched specimen. Under the impactor, a permament indentation induced strained area can be observed.

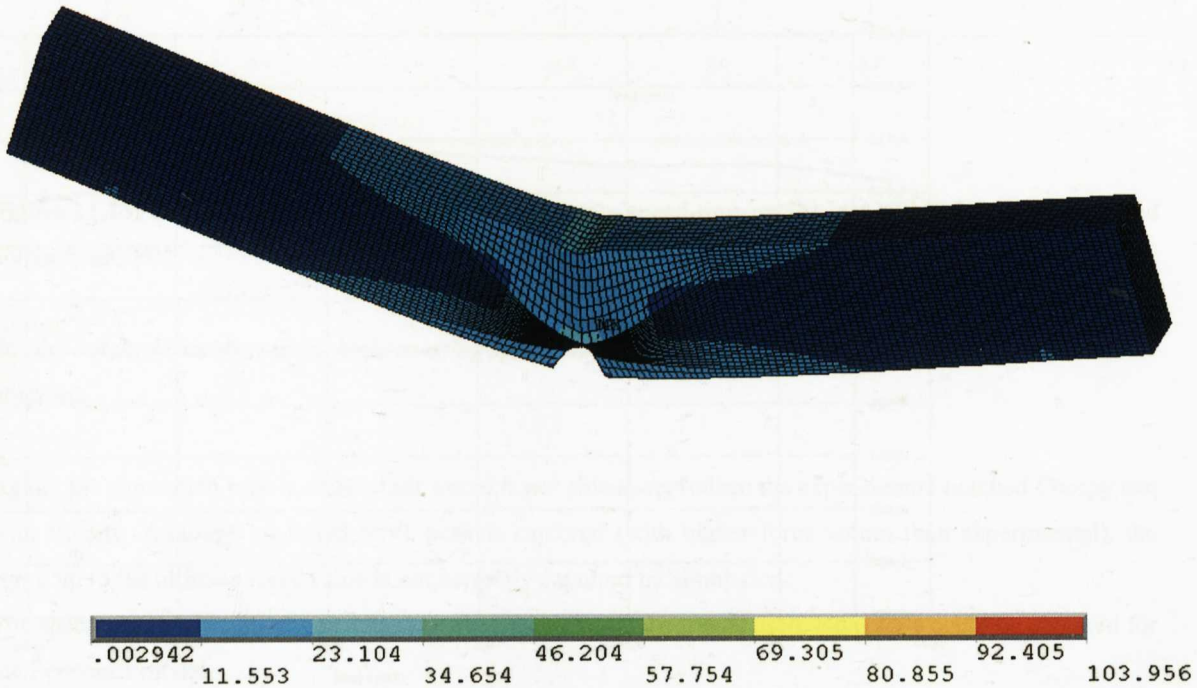

Figure 11.17: Von Mises stress distribution in the notched specimen.

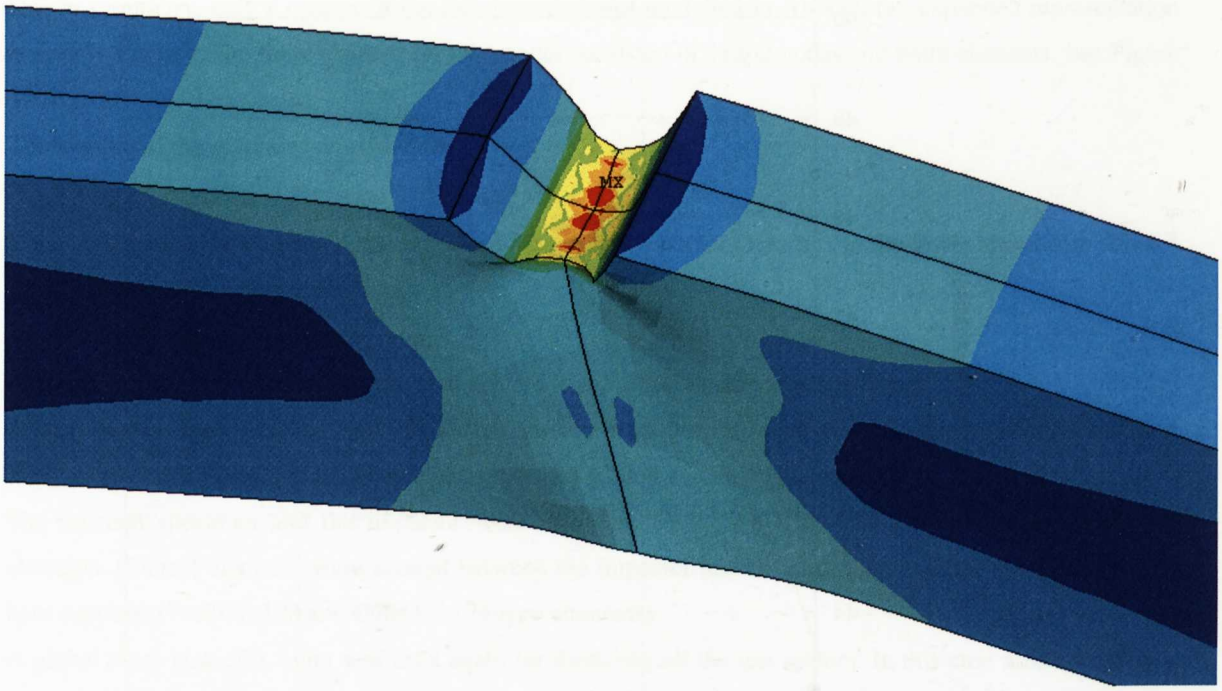

Figure 11.18: Von Mises stress distribution in the notched specimen. Notch detail.

11.2.2. Charpy Impact Test Correlation in ANSYS. PC/ABS.

The simulation of the Charpy impact test is a correlation method for validating the material data generated both in quasi-static and high rate tensile test with the use of elasto-plastic material models.

11.2.2.1. Material Definition.

First, the true stress-strain curve generated in the quasi-static Section 6.4.4 was used in order to check the validity of this curve for impact simulations.

Additionally, from low speed measurements at 5, 50 and 500 mm/min (see Section 6.3.4.1.1) the evolution of yield stress with strain rate could also be studied using the Perzyna viscoplastic model (see Section 4.4).

From Table 6.8, the following values were used to fit the Perzyna model:

5 mm/min→0.001667s-1→43.557MPa.

50 mm/min→0.01667s-1→47.2MPa.

500 mm/min→0.1667s-1→49.5MPa.

Although the fit quality was not very good, the objective was to evaluate the effect of taking into account strain rate effects in the impact simulation.

The best-fit gave an m value of 0.7 and a γ value of 2.32. Figure 11.19 reflects the fit obtained in the software KaleidaGraph 4.0

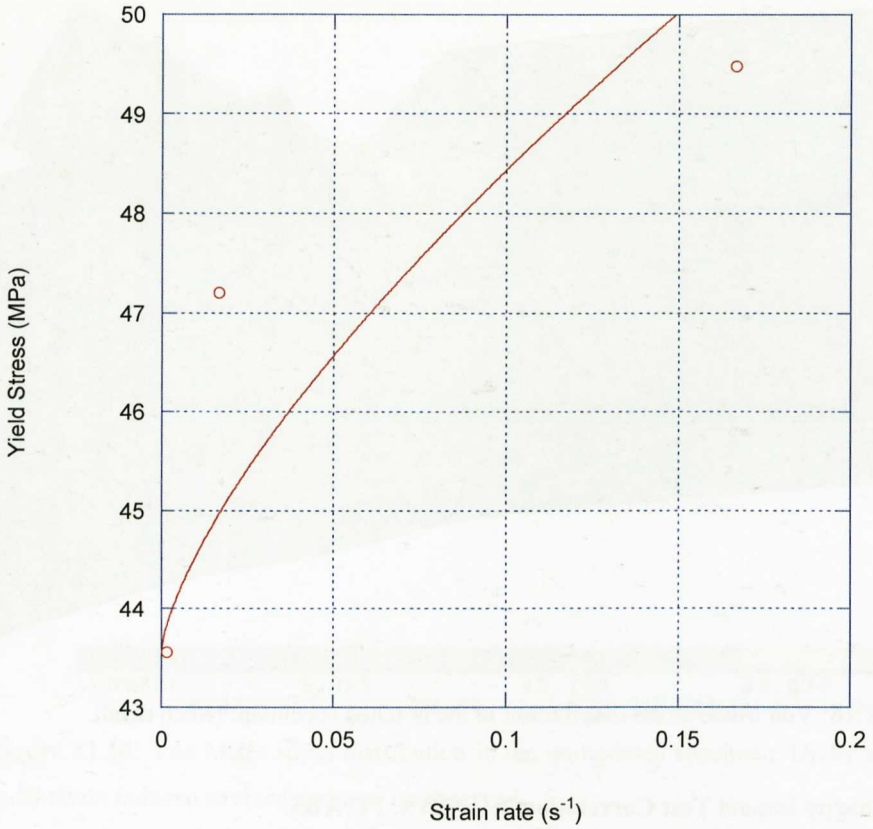

Figure 11.19: Perzyna fit for three slow rate yield values of PC+ABS.

Thus, the first approach was to use a MISO material model in ANSYS to represent the true stress-strain curve of the material in Figure 6.101. In addition to this elasto-plastic definition, a tensile elastic modulus of 2087 MPa. and a Poisson's ratio of 0.4 were also defined.

The second approach was to add a Perzyna viscoplastic model to this definition, considering an m value of 0.7 and a γ value of 2.32.

A density value of 1.1×10^{-9} Tn/mm^3 was also specified for PC/ABS (from material data sheets) which is necessary in a dynamic analysis for inertial effects to be taken into account.

11.2.2.2. Finite Element Modelling.

The Charpy impact test geometry was modeled in ANSYS. Both the un-notched and notched geometries were represented by finite element models in order to study the impact behaviour and compare with experimental results.

The un-notched specimen and the impactor were meshed with SOLID 185 (8 node hexahedral) type elements. Contact elements were created between the impactor and the specimen and the specimen and the base supports (TARGE 170 and CONTA 174 type elements).

A global mesh size of 0.5 mm was used for modeling all the test system. This produced a very good quality mesh in the specimen; when bending characteristics are needed to capture by simulation, a sufficient element number have to be located through the section (usual recommendation is > 2 elements). In this case, 20 hexahedral elements were located through the impacted section of the specimen.

Due to symmetry, only a quarter of the full geometry was modelled in ANSYS (an expanded representation is seen in Figure). The finite element for this model consisted of 11862 nodes and 9408 elements. See Figure 11.5.

The loading of the specimen consisted of,

- applying a 7.668 Kg. mass to the impactor.
- applying the correspondant initial velocity to the impactor (1.75 m/s in the lower speed case and 4.4 m/s in the higher speed case).
- applying gravity in the system.

Additional symmetry conditions were also applied to the quarter part of the specimen.

A large displacement transient analysis was performed in each case, specifying the correspondent simulation time (in seconds); 0.011 s in the lower speed case and 0.0066 s in the higher speed case.

The notched specimen and the impactor were also meshed with SOLID 185 (8 node hexahedral) type elements. Contact elements were created between the impactor and the specimen and the specimen and the base supports (TARGE 170 and CONTA 174 type elements).

A global mesh size of 0.5 mm was used again for modeling all the test system. In this case a fine mesh was created in the notch area in order to represent adequately the radius of the notch (see Figures 11.6 and 11.7).

Due to symmetry, only a quarter of the full geometry was modelled in ANSYS (an expanded representation is seen in Figure 11.6). The finite element for this model consisted of 16186 nodes and 12817 elements.

The loading of the specimen consisted of,

- applying a 7.668 Kg. mass to the impactor.
- applying the correspondant initial velocity to the impactor (1.81 m/s in the lower speed case and 4.41 m/s in the higher speed case).
- applying gravity in the system.

Additional symmetry conditions were also applied to the quarter part of the specimen.

A large displacement transient analysis was performed in each case, specifying the correspondent simulation time (in seconds); 0.0055 s in the lower speed case and 0.0023 s in the higher speed case.

11.2.2.3. Results.

For the *un-notched specimen at the lower testing speed*, the curve traces shown in Figures 11.20 and 11.21 were obtained.

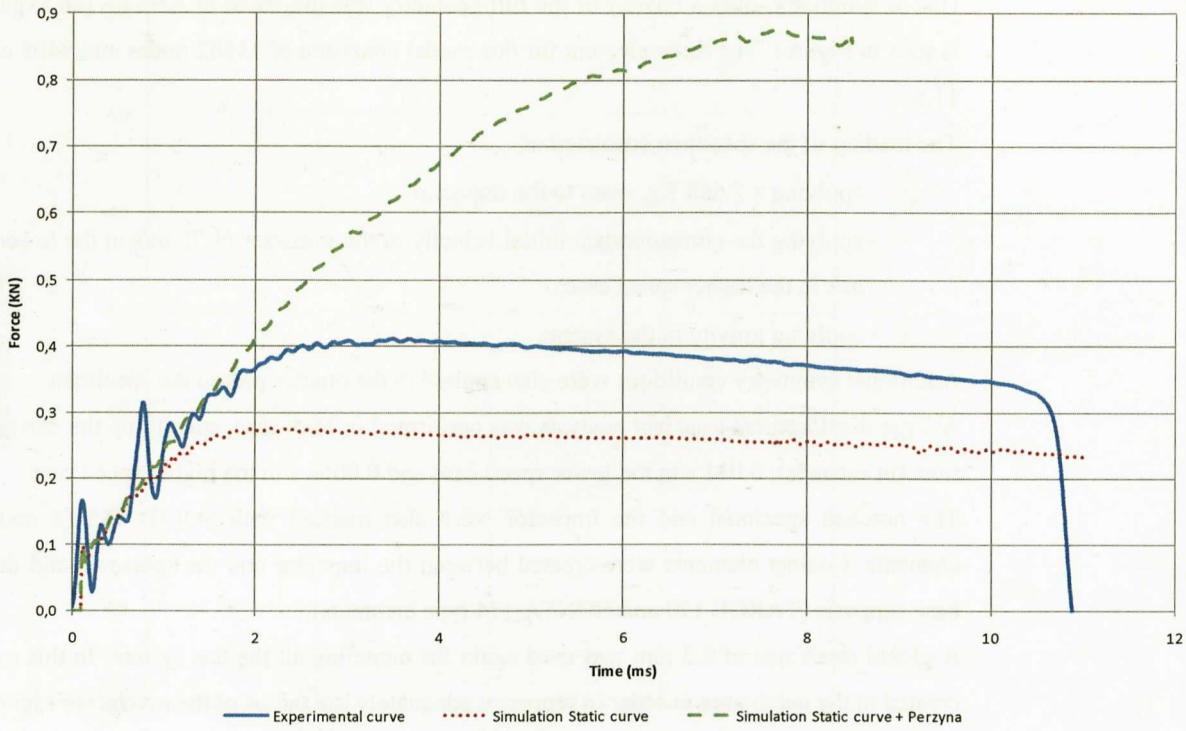

Figure 11.20: Comparison of experimental and simulation force-time results in ANSYS for the lower speed un-notched test, PC/ABS.

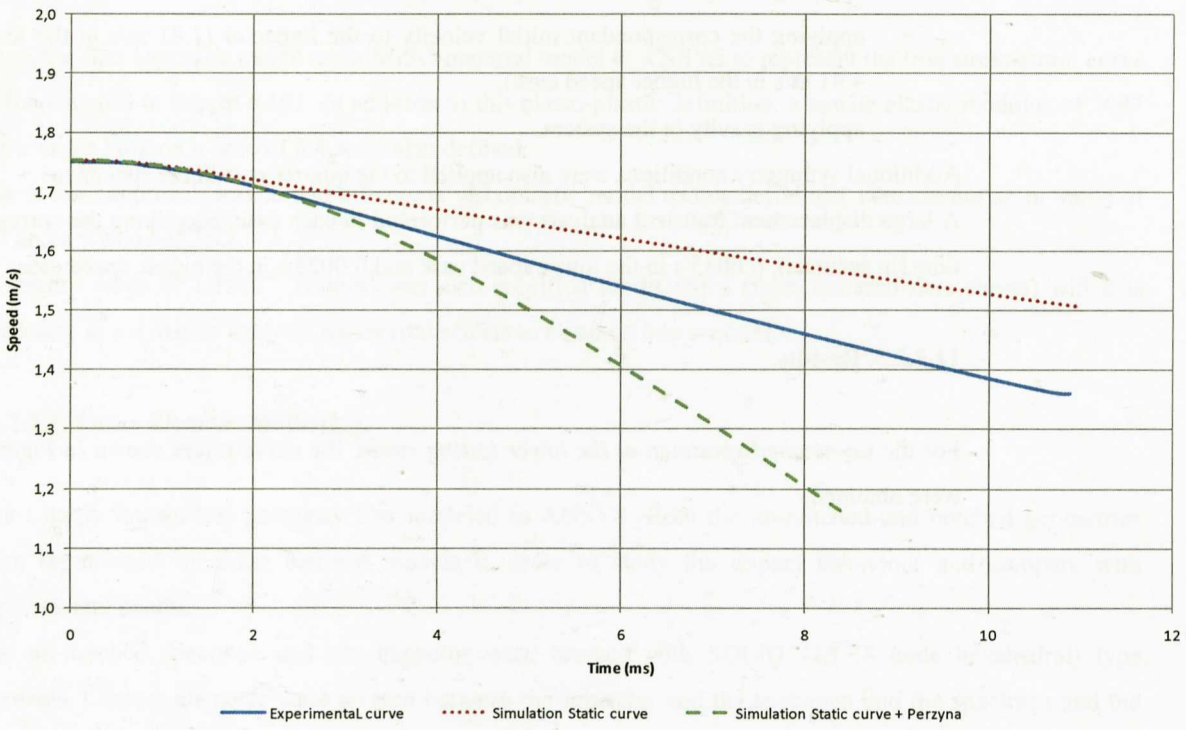

Figure 11.21: Comparison of experimental and simulation speed-time results in ANSYS for the lower speed un-notched test, PC/ABS.

The input of a static curve gives lower force values than experimental results. Additionally, the initial force peak is represented by simulation (lower peak values are registered) but subsequent peaks are not simulated. Speed-time curves differ considerably when a single static curve is used. With the use of a viscoplastic Perzyna model, force-time results are not improved in the initial peak area and in the plastic deformation

region a scaling effect is clearly visible, consequently, force values rise to even higher values than experimental results. This an indicative that extrapolations with the Perzyna model give too high yield stress values with increasing strain rates.

The speed-time curves differ again considerably.

For the *un-notched specimen at the higher testing speed*, the curve traces shown in Figure 11.22 and 11.23 were obtained.

In this case the Perzyna model did not give acceptable results since no convergence was achieved in the solution. The input of a static curve gives higher initial peak force values than experimental results but in this case subsequent peaks were captured. In the plastic deformation region, up to ruputure, simulation values are lower than experimental force results. The speed-time curves differ considerably when a single static curve is used.

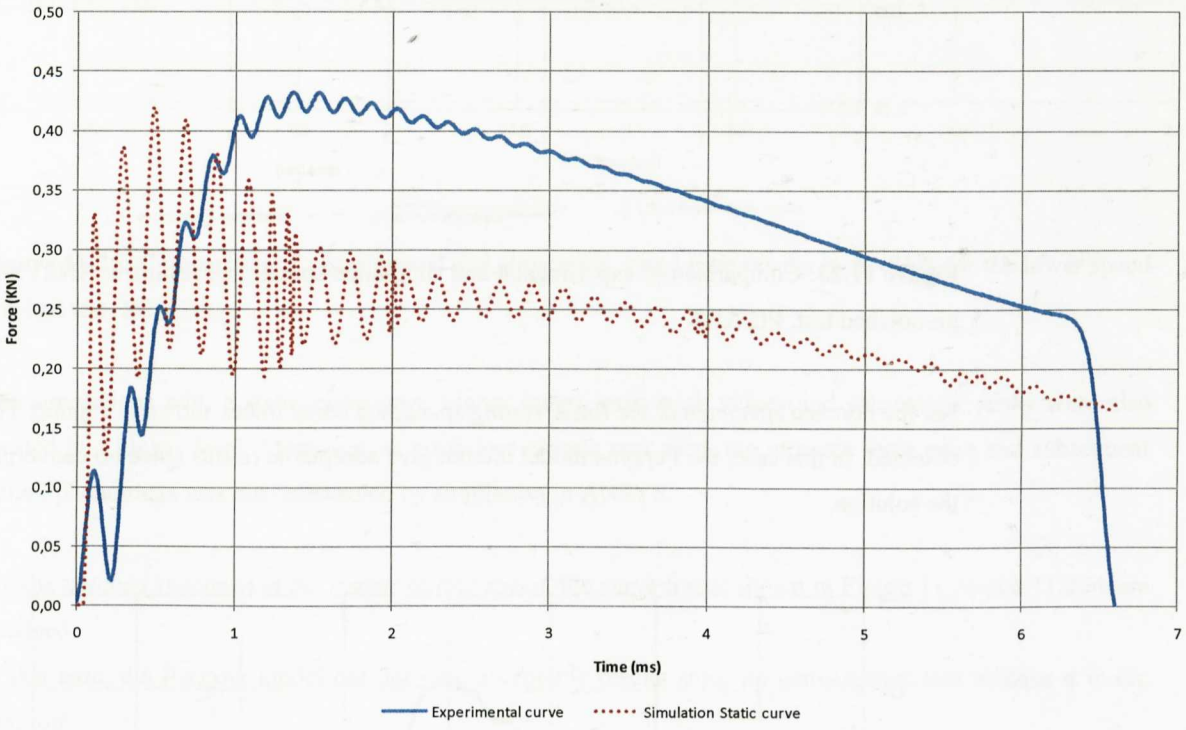

Figure 11.22: Comparison of experimental and simulation force-time results in ANSYS for the higher speed un-notched test, PC/ABS.

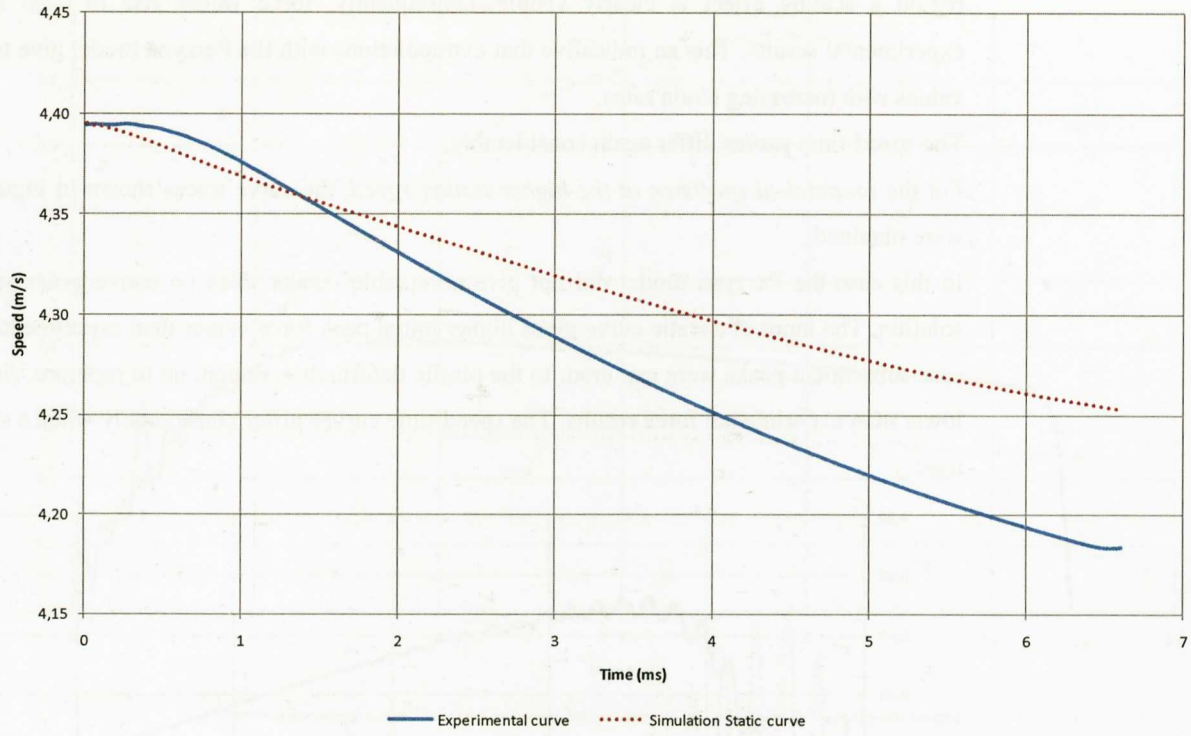

Figure 11.23: Comparison of experimental and simulation speed-time results in ANSYS for the higher speed un-notched test, PC/ABS.

For the *notched specimen at the lower testing speed*, the curve traces shown in Figures 11.24 and 11.25 were obtained. In this case, the Perzyna model did not give acceptable results since no convergence was achieve in the solution.

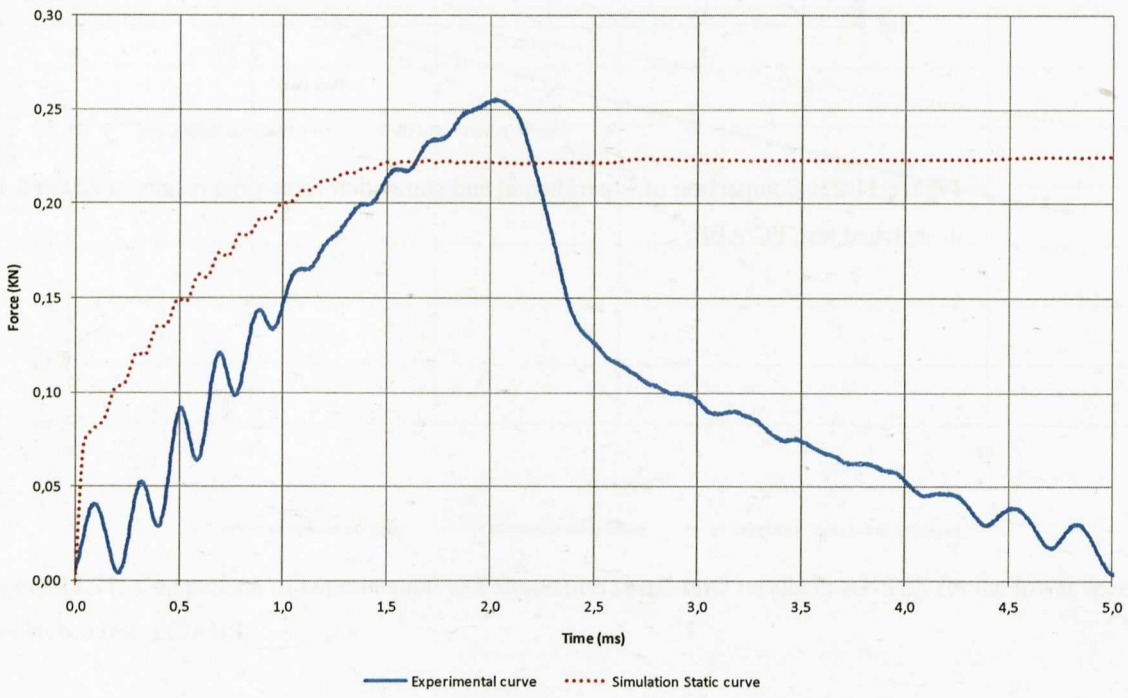

Figure 11.24: Comparison of experimental and simulation force-time results in ANSYS for the lower speed notched test, PC/ABS.

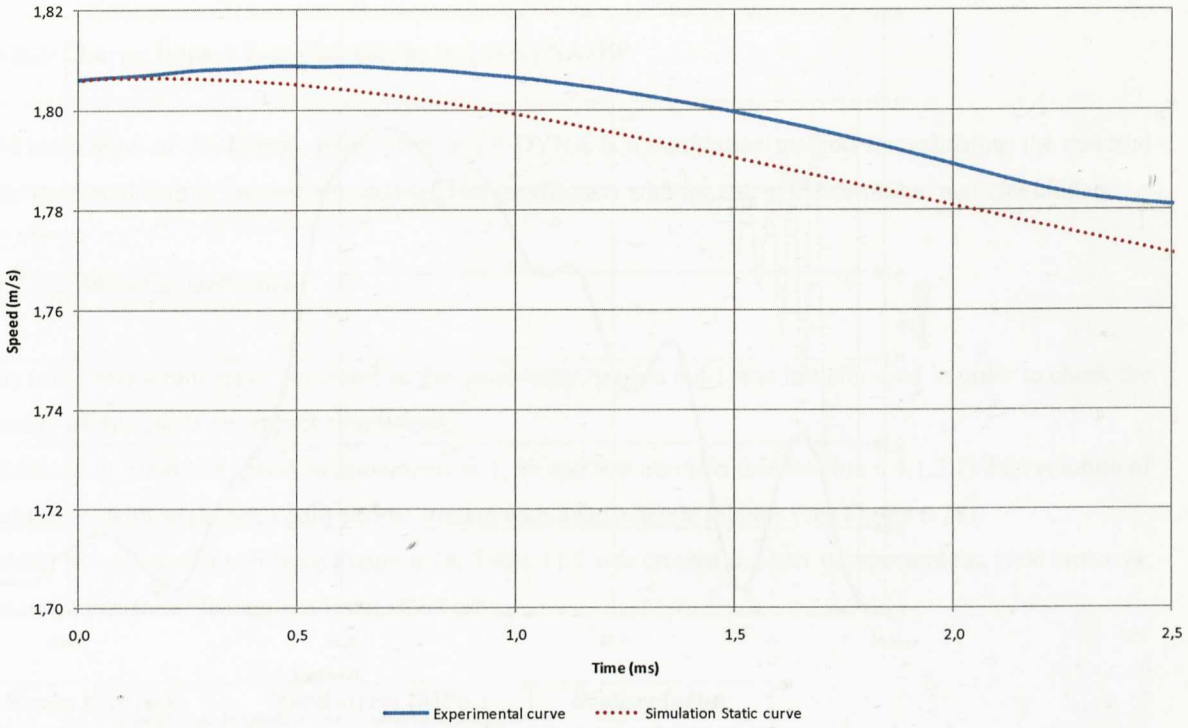

Figure 11.25: Comparison of experimental and simulation speed-time results in ANSYS for the lower speed notched test, PC/ABS.

The simulations with a static curve gave higher initial force peak values and subsequent peaks were also located in a higher level. Moreover, as no failure criteria was used, the ultimate force peak and subsequent failure phenomena was not reproduced by simulation in ANSYS.

For the *notched specimen at the higher testing speed*, the curve traces shown in Figure 11.26 and 11.27 were obtained.

In this case, the Perzyna model did not give acceptable results since no convergence was achieve d in the solution.

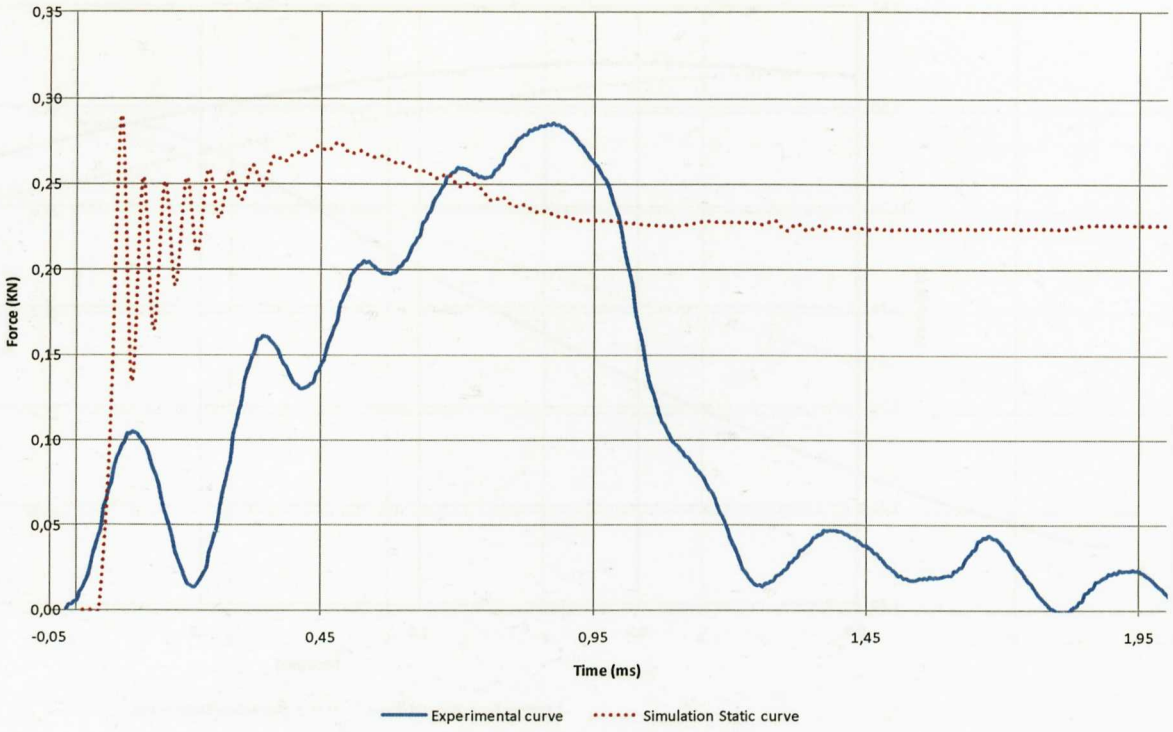

Figure 11.26: Comparison of experimental and simulation force-time results in ANSYS for the higher speed notched test, PC/ABS.

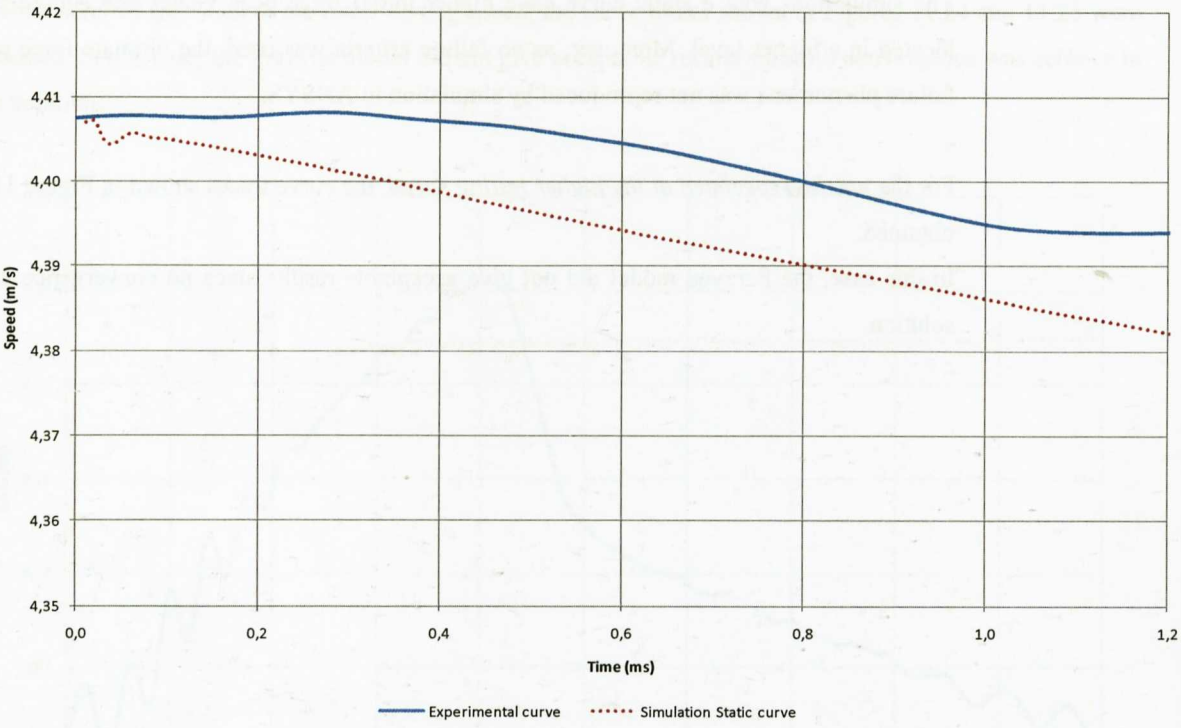

Figure 11.27: Comparison of experimental and simulation speed-time results in ANSYS for the higher speed notched test, PC/ABS.

Again, the simulation with a static curve is not able to reproduce the experimental notched Charpy test with fidelity. Although an initial inertial force peak and subsequent peaks were captured (with higher force values than experimental), the curve up to the ultimate force value is not correctly captured by simulation.
The speed-time curves differ considerably when a single static curve is used.

11.2.3. Charpy Impact Test Correlation in LD-SYNA. PP.

The simulation of the Charpy impact test in LS-DYNA is a correlation method for validating the material data generated both in quasi-static and high rate tensile tests with the use of elasto-plastic material models.

11.2.3.1. Material Definition.

The true stress-strain curve generated in the quasi-static Section 6.4.1 was initially used in order to check the validity of this curve for impact simulations.
Additionally, from low speed measurements at 5, 50 and 500 mm/min (see Section 6.3.1.2.1) the evolution of yield stress with strain rate could also be studied with a logarithmic relation (see Figure 6.28).
Taking into account the fit from Figure 6.28, Table 11.1 was created in order to represent the yield stress vs. the strain rate for different decades of strain rate.

Strain rate (s-1)	Yield stress (MPa.)	Scaling factor
0.001667	9.183	1
0.01667	11.99	1.177
0.1667	12.217	1.3
1.667	13.83*	1.5
15.67	15.35*	1.61
166.7	17.86*	1.75
1667	19.38*	1.9

Table 11.1: Yield stress scaling factor with strain rate, PP.

*denotes extrapolated values using data fits from Figures 6.28 and 6.29, which were calculated according to the **Eyring's model**.

Thus, the first approach was to use an elasto-plastic material model to represent the true stress-strain curve of the material in Figure 6.71. In addition to this elasto-plastic definition, a tensile elastic modulus of 1458.1 MPa. and a Poisson's ratio of 0.38 were also defined.
The second approach was to add a scaling factor table to the yield stress definition in function of the generated strain rates. See Table 11.1.
A third approach was also studied, which was based on the input of the iterated curves calculated in Section 11.1.1. Each iteratively calculated curve was inputted in a tabulated form in true stress-plastic strain format. Strain rates were calculated from the simulation results of the tensile specimens. Strain rate values were calculated according to the standard ISO 18872. This standard defines the plastic strain rate as the gradient of a plot of the true plastic strain against time at the value for plastic strain corresponding to the peak in stress or, if no peak is observed, the yield stress.
Note: The plastic strain rate varies throughout the test and generally increases at a maximum rate in the region of the peak in stress or the yield stress.
All of these approaches were carried out using the so called MAT_024 model in LS-DYNA.

In MAT_024, an elasto plastic material with an arbitrary stress versus strain curve and arbitrary strain rate dependency can be defined. The most general approach is to use table definitions to represent the experimental true stress - plastic strain curves depending on different strain rates. Anyway, a base static curve can also be used in addition to a yield scaling table which gives almost identical results. Additionally, instead of using curves and tables, Cowper-Symonds coefficients can be inputted, these are calculated from experimental data in a previous step.
In the Cowper-Symonds model, where MAT_024 is based, the dynamic yield stress, σ_{YD}, can be calculated from:

$$\sigma_{YD} = \sigma_{YS}\left(1+\left(\frac{\dot{\varepsilon}_p}{C}\right)^{1/P}\right) \qquad \text{Equ. 11.1}$$

Where σ_{YS} is the static yield stress, $\dot{\varepsilon}_p$ is the plastic strain rate and C and P are the Cowper-Symonds constant to be calculated from experimental data [50].

When using tables to account for rate effects, intermediate values are automatically found by interpolating between curves. If the strain rate value falls out of range, automatic extrapolation is not used; rather, either the first or last curve determines the yield stress depending on whether the rate is low or high, respectively.
Failure in MAT_024: A plastic strain to failure can also be defined. When the plastic strain reaches this value, the element is deleted from the calculation.

A density value of 0.905×10^{-9} Tn/mm^3 was also specified for PP (value obtained from material data sheets) which is necessary in a dynamic analysis for inertial effects to be taken into account.

11.2.3.2. Finite Element Modelling.

The Charpy impact test geometry was modeled in LS-DYNA. Both the un-notched and notched geometries were represented by finite element models in order to study the virtual impact behaviour and compare with experimental results.
The un-notched specimen was meshed with SOLID 164 type elements (full integration 8 node hexahedral elements). The impactor and the base supports were meshed with rigid shell type elements. Automatic contact elements were created between the impactor and the specimen and the specimen and the base supports.
A global mesh size of 1 mm was used for modeling all the test system. The finite element for this model consisted of 3738 nodes and 2623 elements.
Due to symmetry, only a quarter of the full geometry was modelled in LS-DYNA (an expanded representation is seen in Figure 11.28).
The loading of the specimen consisted of,

- applying a 7.668 Kg. mass to the impactor.
- applying the correspondant initial velocity to the impactor (1.77 m/s in the lower speed case and 4.42 m/s in the higher speed case).
- applying gravity in the system.

Additional symmetry conditions were also applied to the quarter part of the specimen.

An explicit impact analysis was performed in each case, specifying the correspondent simulation time (in seconds); 0.0075 s in the lower speed case and 0.0023 s in the higher speed case.

For the un-notched specimen, the mesh shown in Figure 11.28 was created.

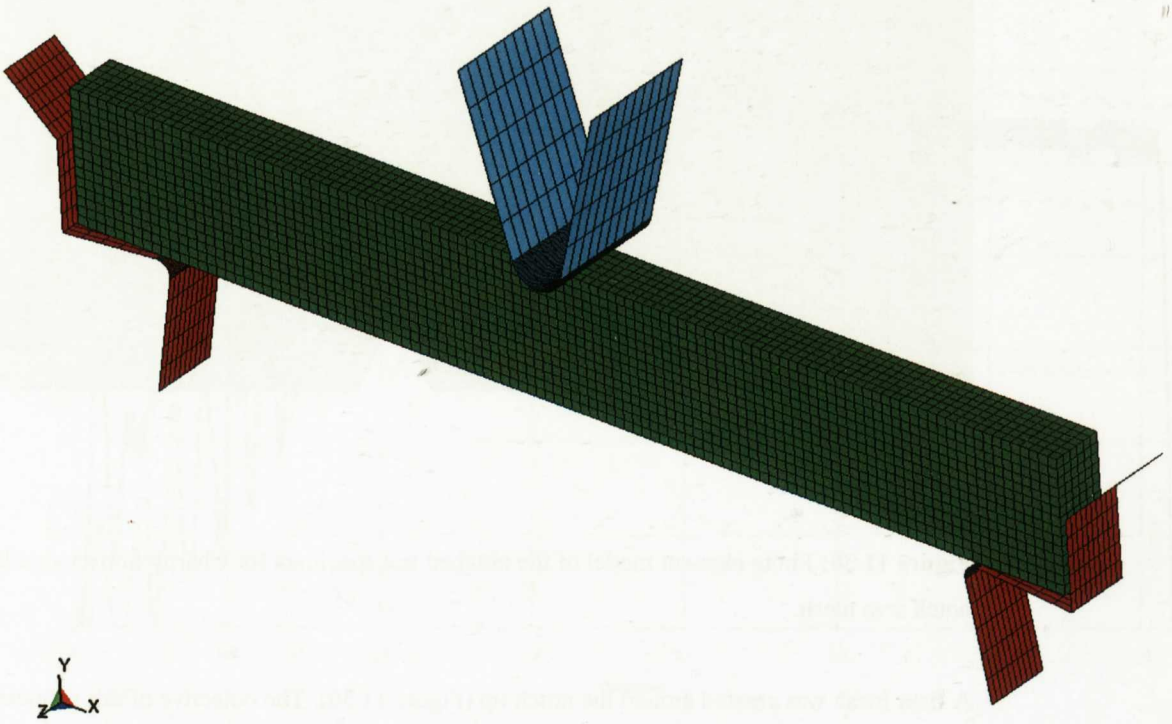

Figure 11.28: Finite element model of the un-notched test specimen for Charpy impact simulation.

For the notched specimen, the mesh shown in Figure 11.29 was created.

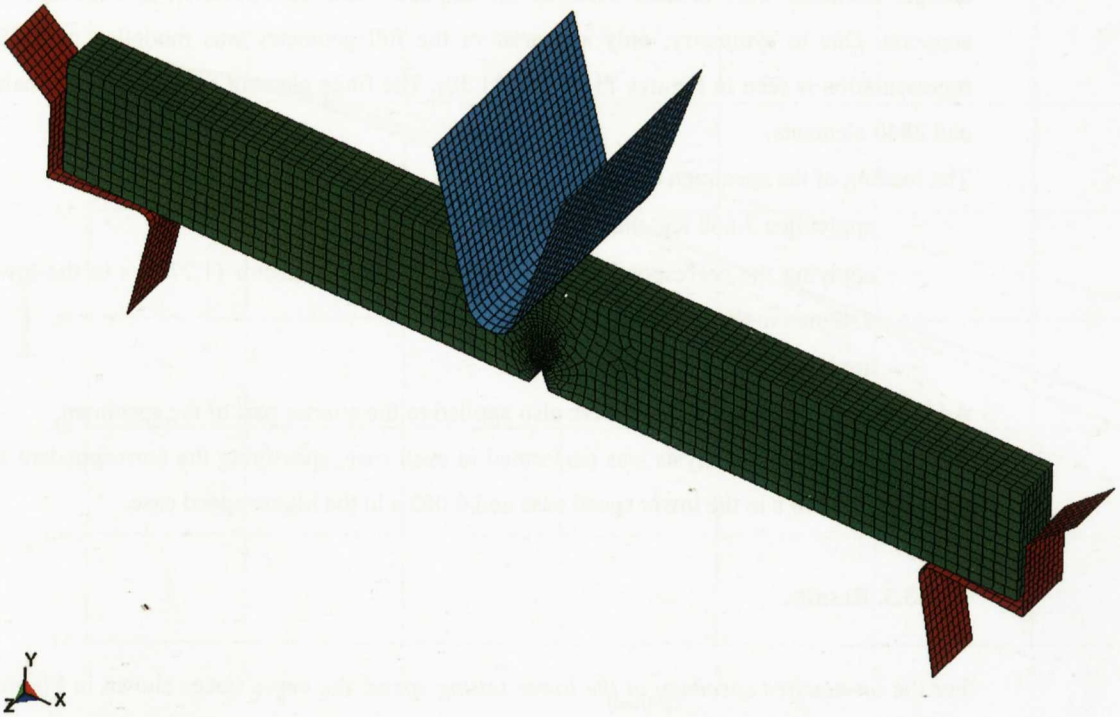

Figure 11.29: Finite element model of the notched test specimen for Charpy impact simulation.

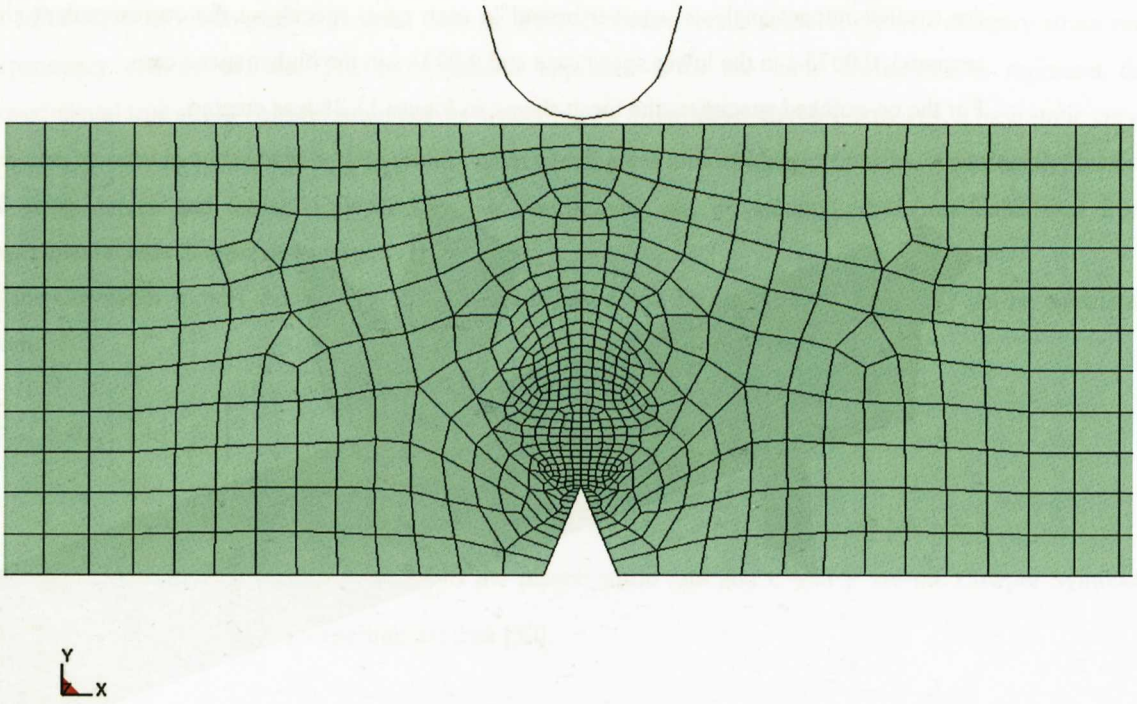

Figure 11.30: Finite element model of the notched test specimen for Charpy impact simulation. Detail of the notch area mesh.

A finer mesh was created around the notch tip (Figure 11.30). The objective of this refinement was to capture properly the crack arrest when the failure criteria was used in the Charpy simulation.

The notched specimen was meshed with SOLID 164 type elements (full integration 8 node hexahedral elements). The impactor and the base supports were meshed with rigid shell type elements. Automatic contact elements were created between the impactor and the specimen and the specimen and the base supports. Due to symmetry, only a quarter of the full geometry was modelled in ANSYS (an expanded representation is seen in Figures 11.29 and 11.30). The finite element for this model consisted of 3869 nodes and 2840 elements.

The loading of the specimen consisted of,

- applying a 7.668 Kg. mass to the impactor.
- applying the correspondant initial velocity to the impactor (1.77 m/s in the lower speed case and 4.42 m/s in the higher speed case).
- applying gravity in the system.

Additional symmetry conditions were also applied to the quarter part of the specimen.

An explicit dynamic analysis was performed in each case, specifying the correspondent simulation time (in seconds); 0.0045 s in the lower speed case and 0.002 s in the higher speed case.

11.2.3.3. Results.

For the *un-notched specimen at the lower testing speed*, the curve traces shown in Figures 11.31 and 11.32 were obtained.

It can be seen that comparatively a considerable improvement was obtained in contrast with the previous results in ANSYS. Here, the initial inertia force peak and subsequent peaks are adequately correlated in LS-DYNA. The input of a static curve gives lower force values than experimental results, but the addition of a

scaling factor improves the simulation curve. Using the curves obtained iteratively from tensile test at different speeds gives the best results. Anyway, the first part of the force-time curve needs to be scaled to higher values since it is not quantitatively well represented.

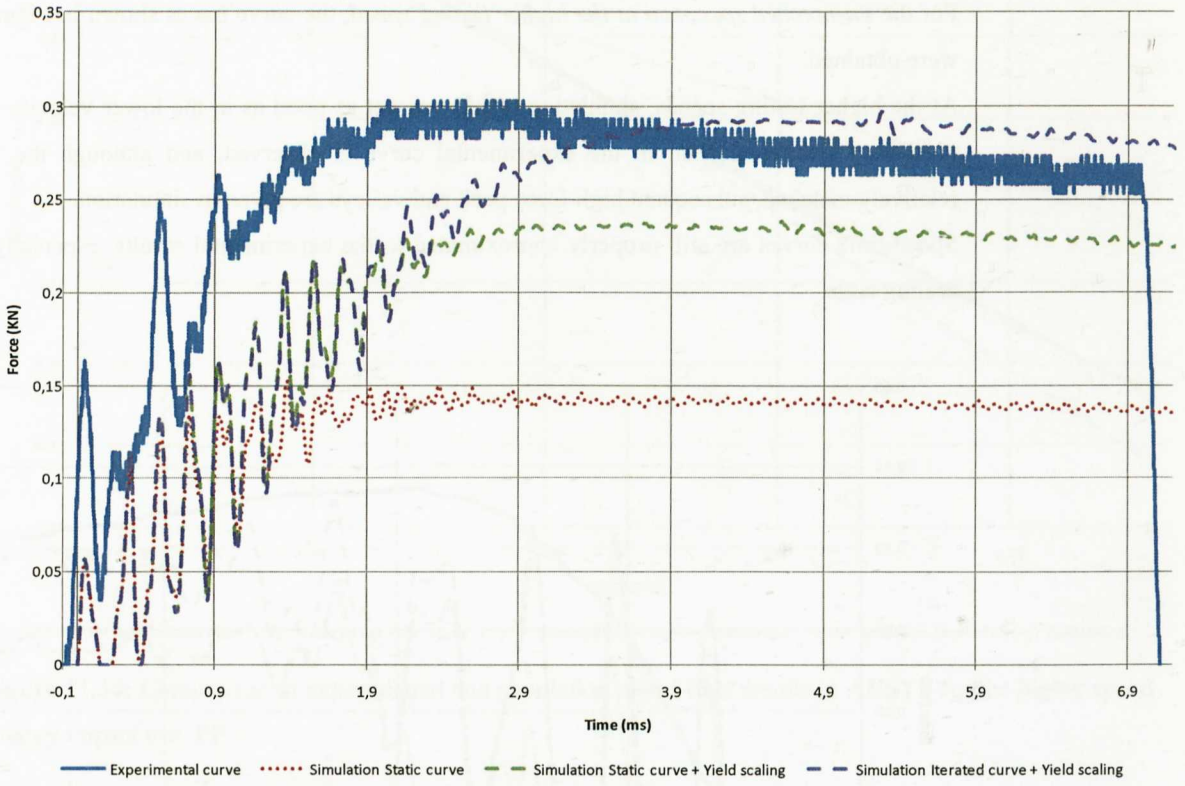

Figure 11.31: Comparison of experimental and simulation force-time results in ANSYS for the lower speed Charpy impact test, PP.

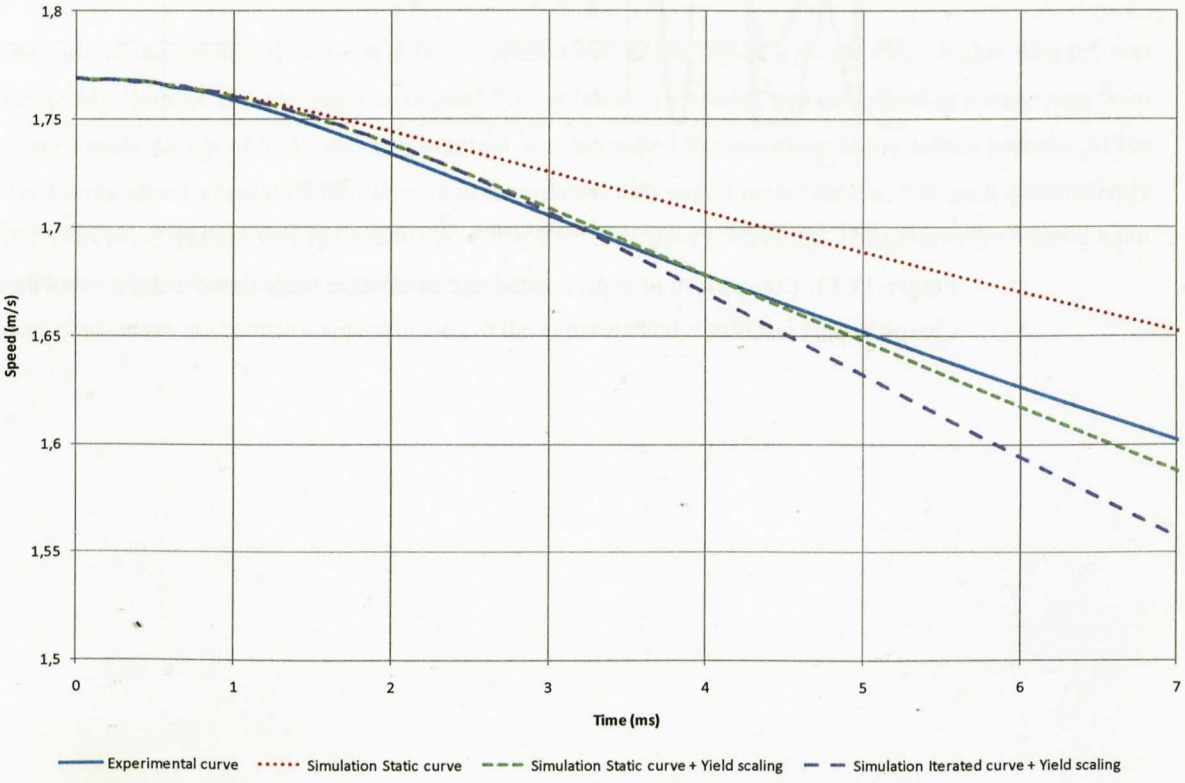

Figure 11.32: Comparison of experimental and simulation speed-time results in ANSYS for the lower speed Charpy impact test, PP.

Speed-time curves are now properly approximated to the experimental results, especially when using a rate scaling table.

For the *un-notched specimen at the higher testing speed*, the curve traces shown in Figures 11.33 and 11.34 were obtained.

At the higher testing speeds, simulation results are not as good as in the lower velocity case. A much more oscillatory behaviour than in the experimental curve is observed, and although the first initial peak is relatively matched, subsequent high force peak and valleys are given in simulation.

Speed-time curves are still properly approximated to the experimental results, especially when using a rate scaling table.

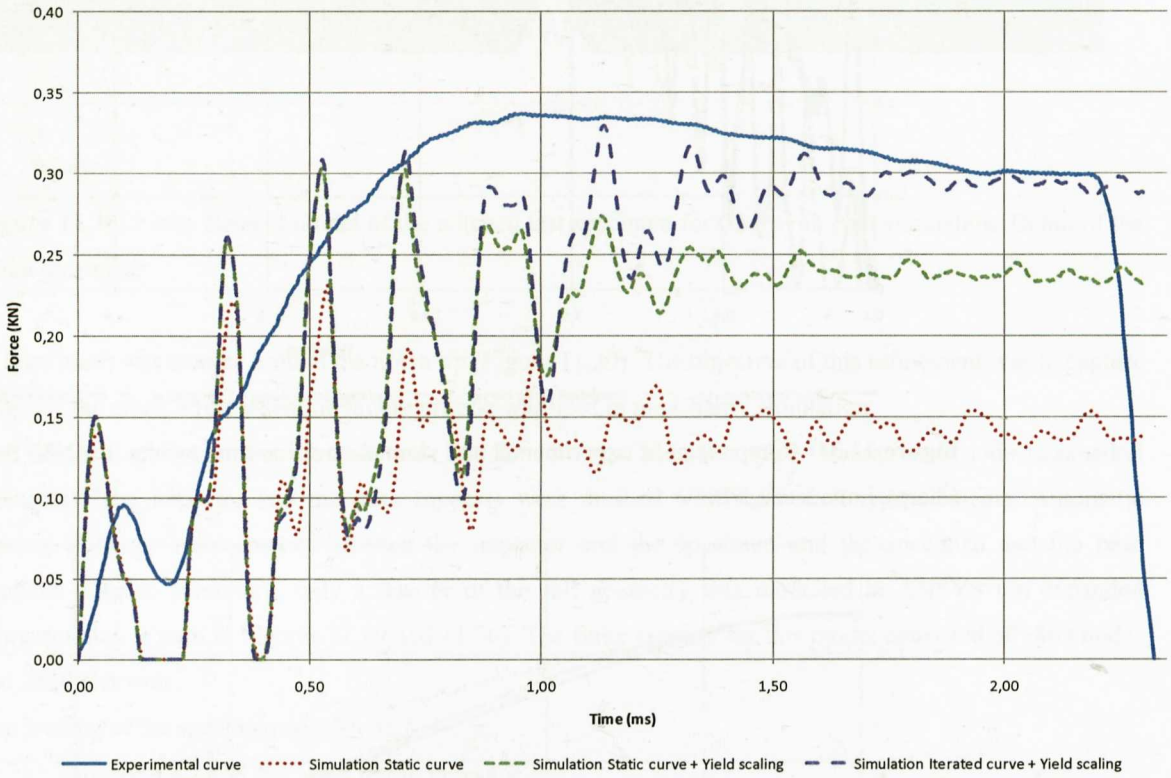

Figure 11.33: Comparison of experimental and simulation force-time results in ANSYS for the higher speed Charpy impact test, PP.

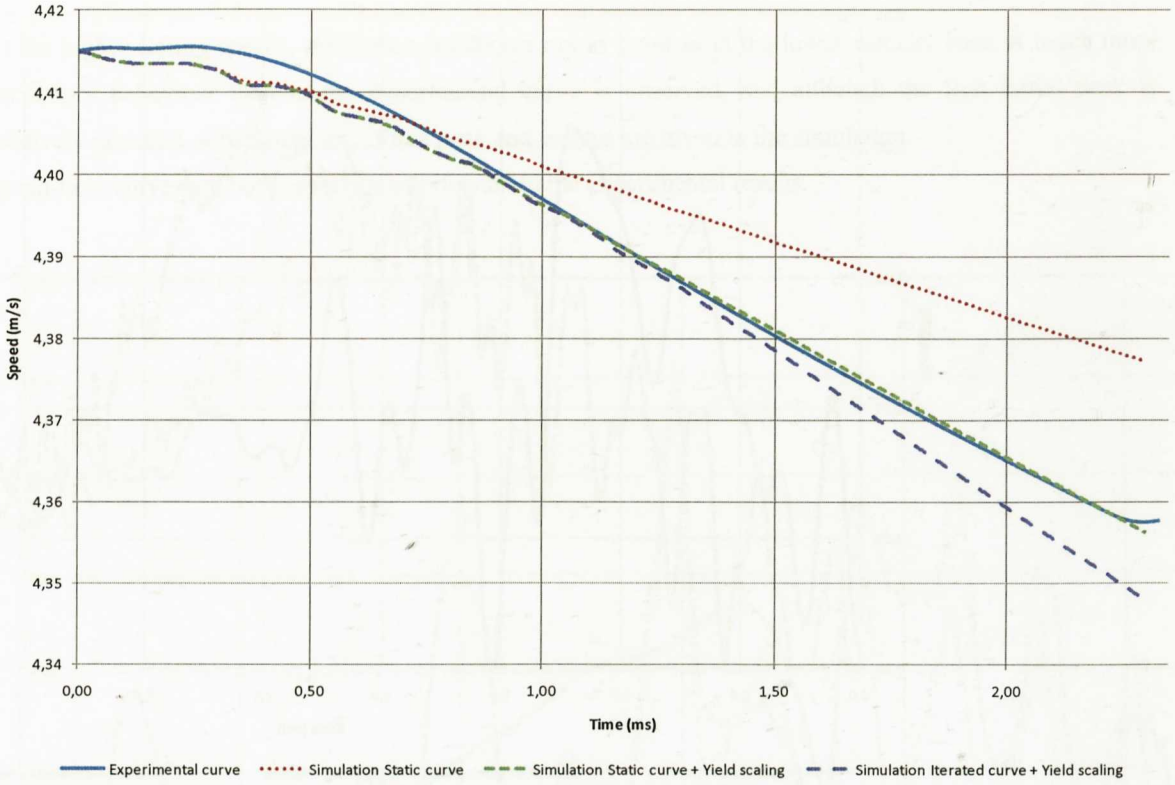

Figure 11.34: Comparison of experimental and simulation speed-time results in ANSYS for the higher speed Charpy impact test, PP.

For the *notched specimen at the lower testing speed*, the curve traces shown in Figure 11.35 and 11.36 were obtained.

In the case of the notched specimens, a failure criteria was added. When a plastic strain higher than 0.5 was given in any element, this element was deleted from solution. This value was calculated as a mean data from the quasi-static curves at 5, 50 and 500 mm/min. and permitted the modeling of the failure process. At the lower testing speed, simulation results were in accordance with experimental results. Although quantitatively differences exist, qualitatively the overal curve shape is reproduced adequately. The iteratively obtained input curves gave higher force values in the failure process.
Speed-time curves are properly approximated to the experimental results.

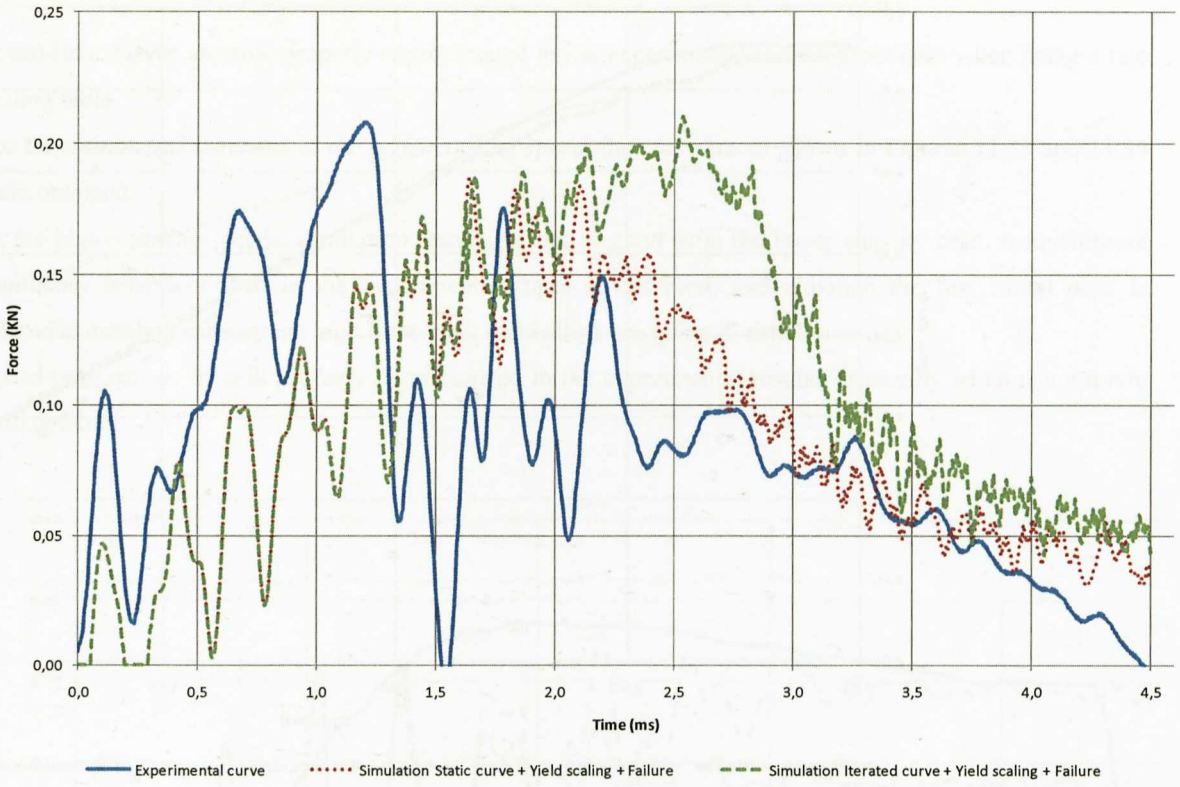

Figure 11.35: Comparison of experimental and simulation force-time results in ANSYS for the lower speed Charpy impact test, PP.

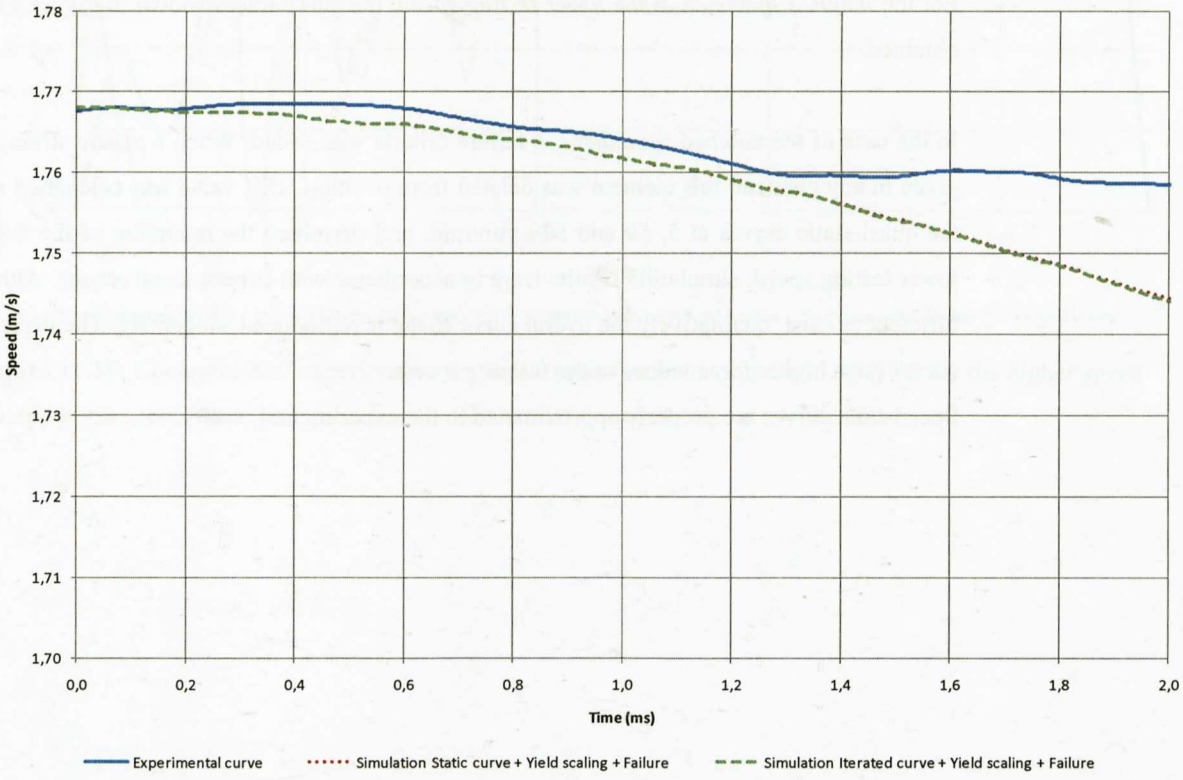

Figure 11.36: Comparison of experimental and simulation speed-time results in ANSYS for the lower speed Charpy impact test, PP.

For the *notched specimen at the higher testing speed*, the curve traces shown in Figure 11.37 and 11.38 were obtained.

At the higher testing speeds, simulation results are not as good as in the lower velocity case. A much more oscillatory behaviour than in the experimental curve is observed, and although the first initial peak is relatively matched, subsequent high force peak and valleys are given in the simulation.
Speed-time curves are not properly approximated to the experimental results.

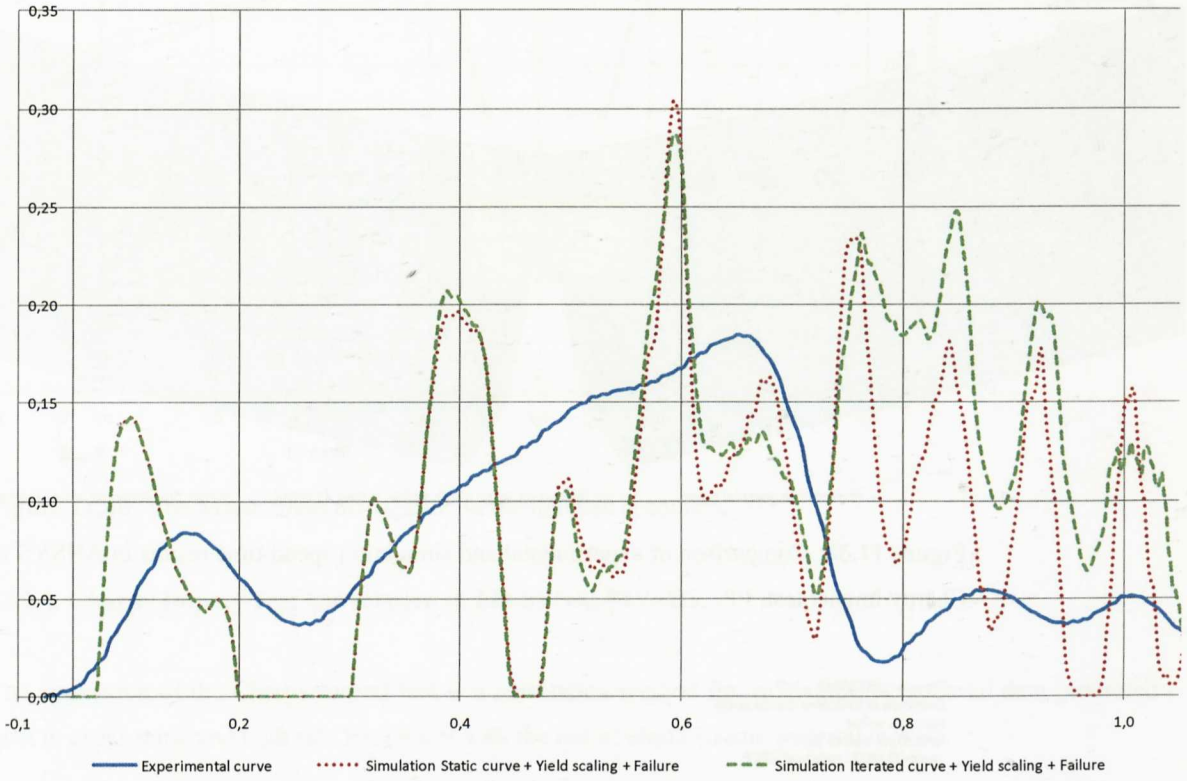

Figure 11.37: Comparison of experimental and simulation force-time results in ANSYS for the higher speed Charpy impact test, PP.

Figures 11.39 and 11.40 show for illustrative purposes the Von Mises stresses obtained both in the un-notched and notched specimens. These stress patterns were given for both materials.

Figure 11.40 represents the notch opening process when the specimen is impacted. The described failure criteria was used which deleted the elements exceeding a prescribed plastic strain value (0.5)

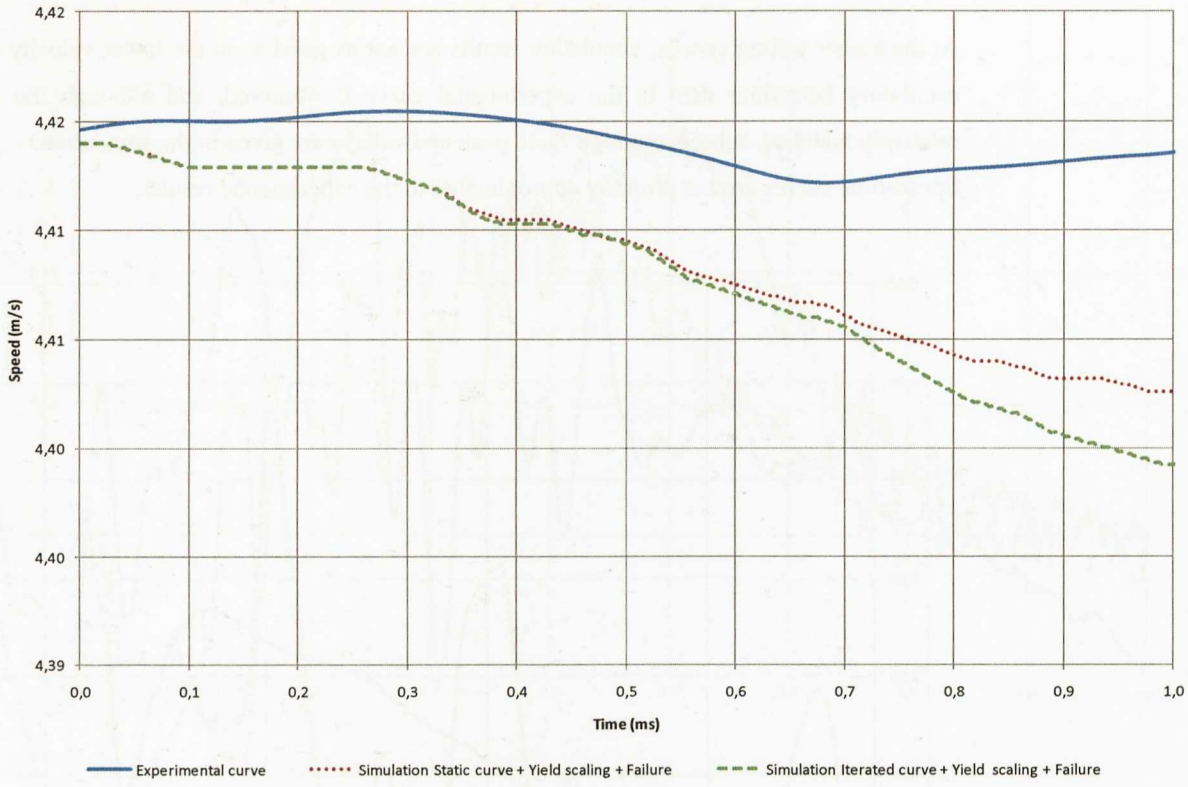

Figure 11.38: Comparison of experimental and simulation speed-time results in ANSYS for the higher speed Charpy impact test, PP.

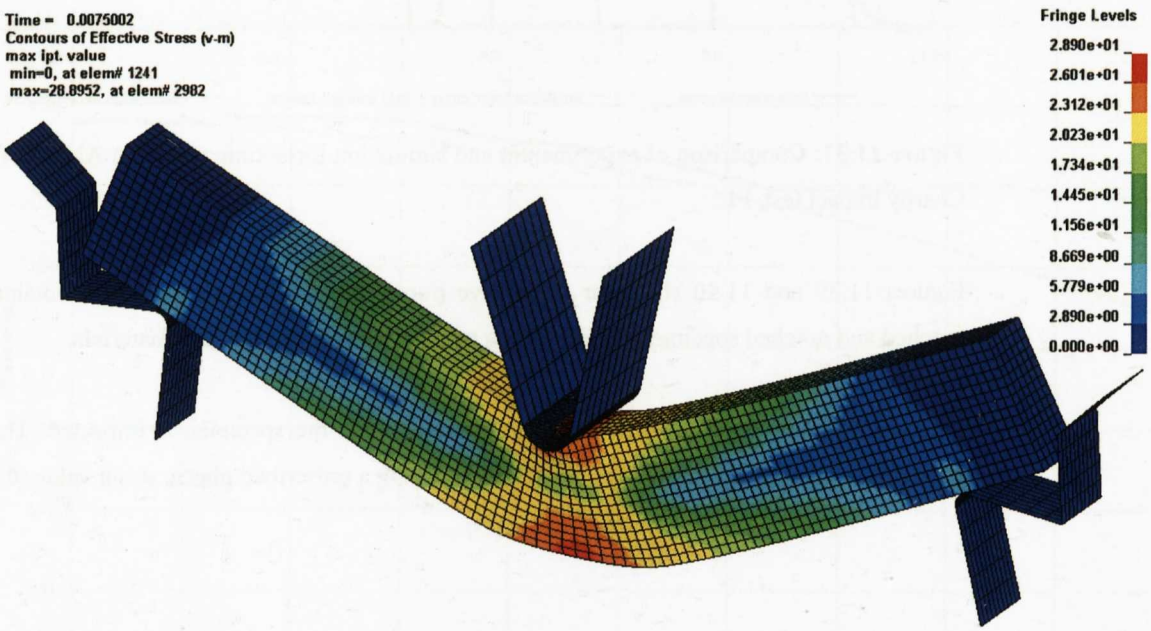

Figure 11.39: Von Mises stress distribution in the un-notched specimen. Under the impactor, a permament indentation induced strained area was observed.

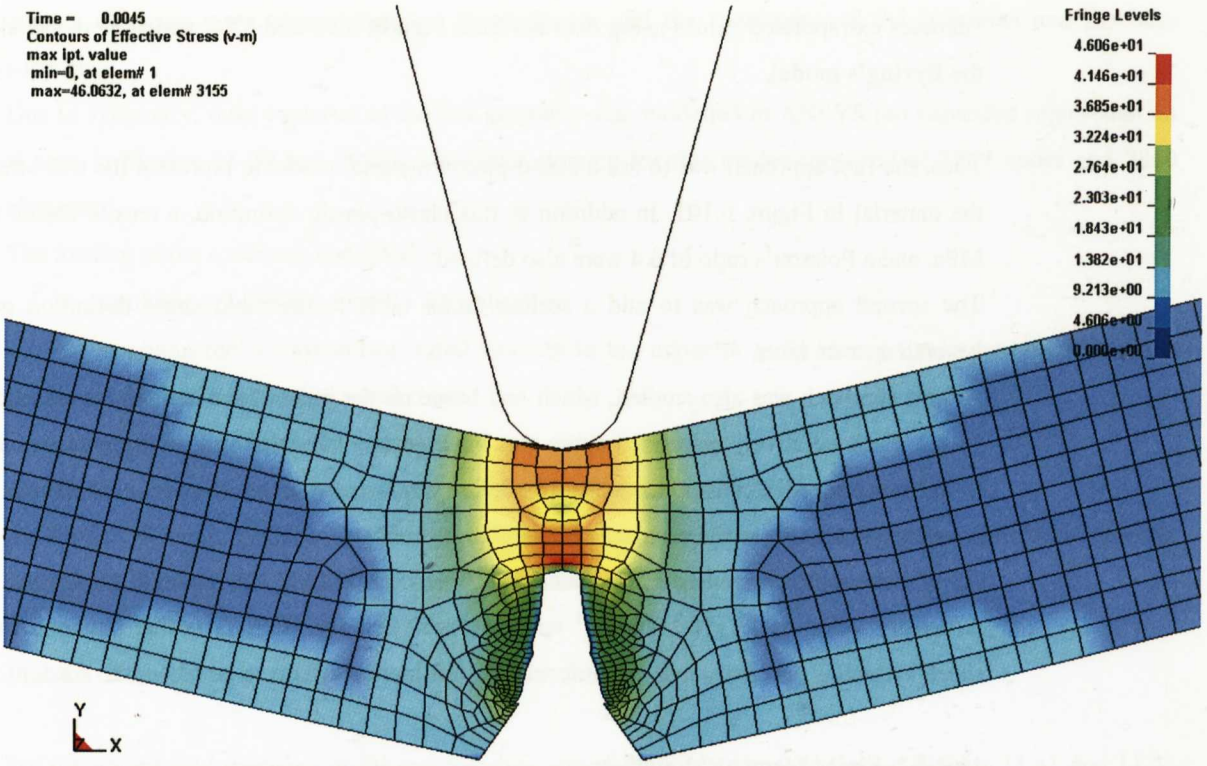

Figure 11.40: Von Mises stress distribution in the notched specimen.

11.2.4. Charpy Impact Test Correlation in LD-SYNA. PC/ABS.

The simulation of the Charpy impact test is a correlation method for validating the material data generated both in quasi-static and high rate tensile test with the use of elasto-plastic material models.

11.2.4.1. Material Definition.

First, the true stress-strain curve generated in the quasi-static Section 6.4.4 was used to check the validity of this curve for impact simulations. See Figure 6.101.

Additionally, from low speed measurements at 5, 50 and 500 mm/min (see Section 6.3.4.1.1) the evolution of yield stress with strain rate could also be studied with a logarithmic relation (see Figures 6.53 and 6.54).

Taking into account the fit from Figure 6.53, Table 11.2 was created to represent the yield stress vs. the strain rate for different decades of strain rate.

Strain rate (s-1)	Yield stress (MPa.)	Scaling factor
0.001667	43.557	1
0.01667	47.204	1.084
0.1667	49.479	1.136
1.667	52.668*	1.209
15.67	55.629*	1.277
166.7	58.59*	1.345
1667	61.551*	1.413

Table 11.2: Yield stress scaling factor with strain rate, PC/ABS.

*denotes extrapolated values using data fits from Figures 6.53 and 6.54, which were calculated according to the **Eyring's model.**

Thus, the first approach was to use a elasto-plastic material model to represent the true stress-strain curve of the material in Figure 6.101. In addition to this elasto-plastic definition, a tensile elastic modulus of 2087 MPa. and a Poisson's ratio of 0.4 were also defined.

The second approach was to add a scaling factor table to the yield stress definition in function of the generated strain rates.

A third approach was also studied, which was based on the input of the iterated curves calculated in Section 11.1.2. Each iteratively calculated curve was inputted in a tabulated way in true stress-plastic strain format. Strain rates were calculated from the simulation results of the tensile specimens. Strain rate values were calculated according to the standard ISO 18872.

All of these approaches were carried out using the so called MAT_024 model in LS-DYNA.

A density value of $1.1x10^{-9}$ Tn/mm^3 was also specified for PC/ABS (value obtained from material data sheets) which is necessary in a dynamic analysis for inertial effects to be taken into account.

11.2.4.2. Finite Element Modelling.

The Charpy impact test geometry was modeled in LS-DYNA. Both the un-notched and notched geometries were represented by finite element models in order to study the impact behaviour and compare with experimental results.

The un-notched specimen was meshed with SOLID 164 type elements (full integration 8 node hexahedral elements). The impactor and the base supports were meshed with rigid shell type elements. Automatic contact elements were created between the impactor and the specimen and the specimen and the base supports.

A global mesh size of 1 mm was used for modeling all the test system. The finite element for this model consisted of 3738 nodes and 2623 elements. Due to symmetry, only a quarter of the full geometry was modelled in LS-DYNA (an expanded representation is seen in Figure 11.28).

The loading of the specimen consisted of,

- applying a 7.668 Kg. mass to the impactor.
- applying the correspondant initial velocity to the impactor (1.75 m/s in the lower speed case and 4.42 m/s in the higher speed case).
- applying gravity in the system.

Additional symmetry conditions were also applied to the quarter part of the specimen.

An explicit impact analysis was performed in each case, specifying the correspondent simulation time (in seconds); 0.011 s in the lower speed case and 0.0066 s in the higher speed case.

For the notched specimen, the mesh shown in Figure 11.29 was created.

A finer mesh was created around the notch tip. The objective of this refinement was to capture properly the crack arrest when a failure criteria was used in the Charpy simulation.

The notched specimen was meshed with SOLID 164 type elements (full integration 8 node hexahedral elements). The impactor and the base supports were meshed with rigid shell type elements. Automatic

contact elements were created between the impactor and the specimen and the specimen and the base supports.

Due to symmetry, only a quarter of the full geometry was modelled in ANSYS (an expanded representation is seen in Figures 11.29 and 11.30). The finite element for this model consisted of 3869 nodes and 2840 elements.

The loading of the specimen consisted of,

- applying a 7.668 Kg. mass to the impactor.
- applying the correspondant initial velocity to the impactor (1.81 m/s in the lower speed case and 4.41 m/s in the higher speed case).
- applying gravity in the system.

Additional symmetry conditions were also applied to the quarter part of the specimen.

An explicit dynamic analysis was performed in each case, specifying the correspondent simulation time (in seconds); 0.0055 s in the lower speed case and 0.0023 s in the higher speed case.

11.2.4.3. Results.

For the *un-notched specimen at the lower testing speed*, the curve traces shown in Figures 11.41 and 11.42 were obtained.

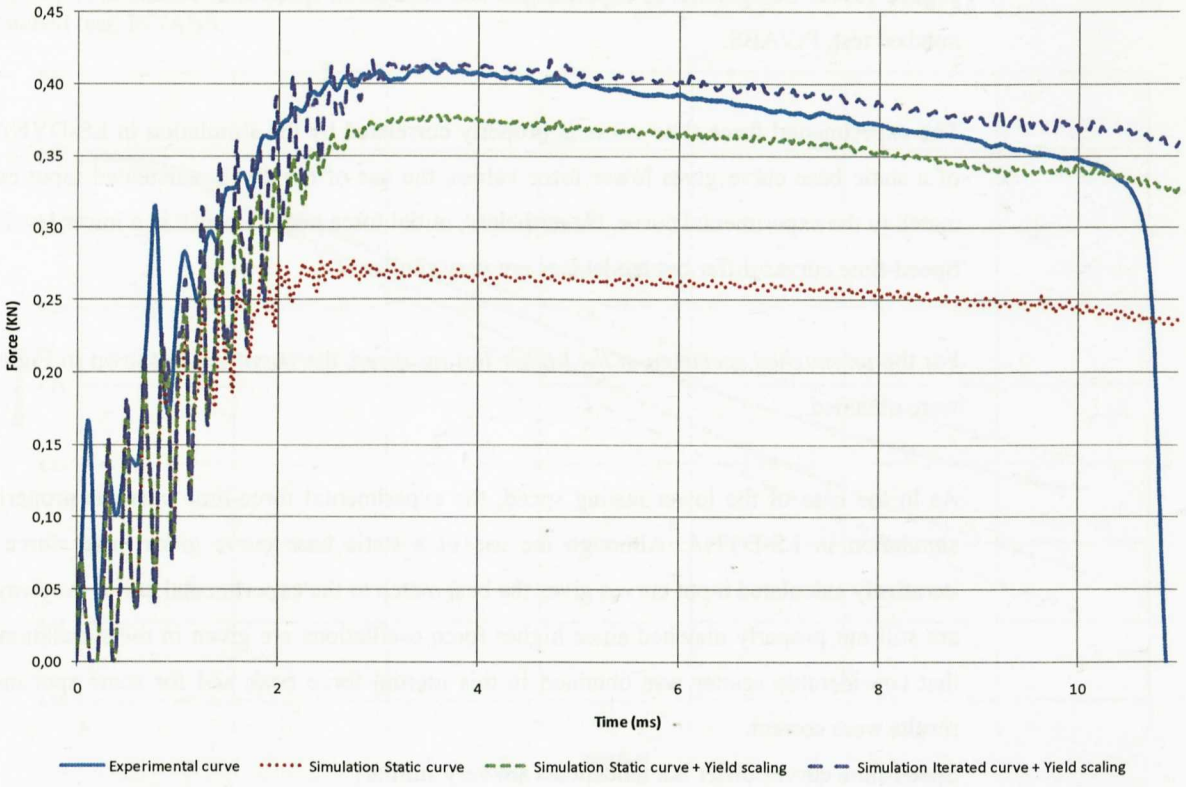

Figure 11.41: Comparison of experimental and simulation force-time results in ANSYS for the lower speed notched test, PC/ABS.

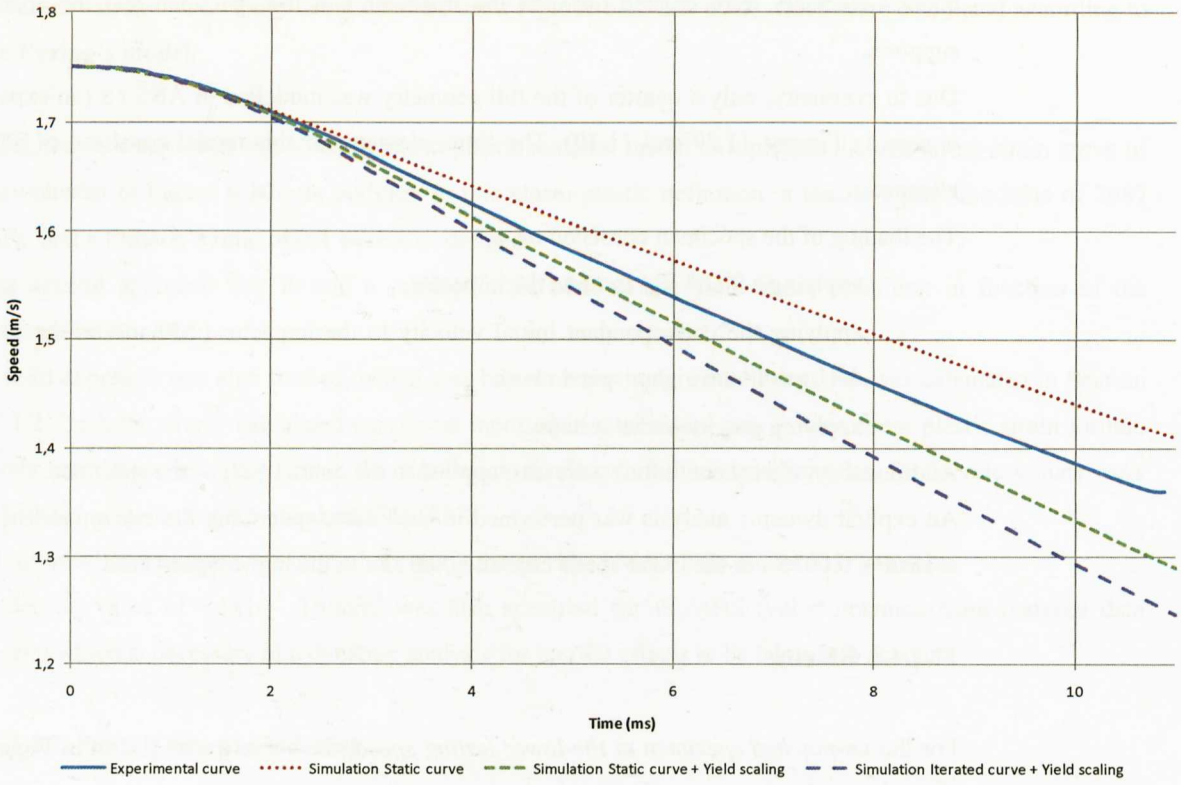

Figure 11.42: Comparison of experimental and simulation speed-time results in ANSYS for the lower speed notched test, PC/ABS.

The experimental force-time curve is properly correlated by the simulation in LS-DYNA. Although the use of a static base curve gives lower force values, the use of iteratively calculated input curves gives the best match to the experimental curve. Nevertheless, initial force peaks are still in a lower level than experimental. Speed-time curves differ but tendencies are very similar.

For the *un-notched specimen at the higher testing speed*, the curve traces shown in Figures 11.43 and 11.44 were obtained.

As in the case of the lower testing speed, the experimental force-time curve is properly correlated by the simulation in LS-DYNA. Although the use of a static base curve gives lower force values, the use of iteratively calculated input curves gives the best match to the experimental curve. Anyway, initial force peaks are still not properly matched since higher force oscillations are given in the simulation. It has to be noted that considerable scatter was obtained in this inertial force peak and for some specimens the simulations results were correct.
Speed-time curves differ but tendencies are very similar.

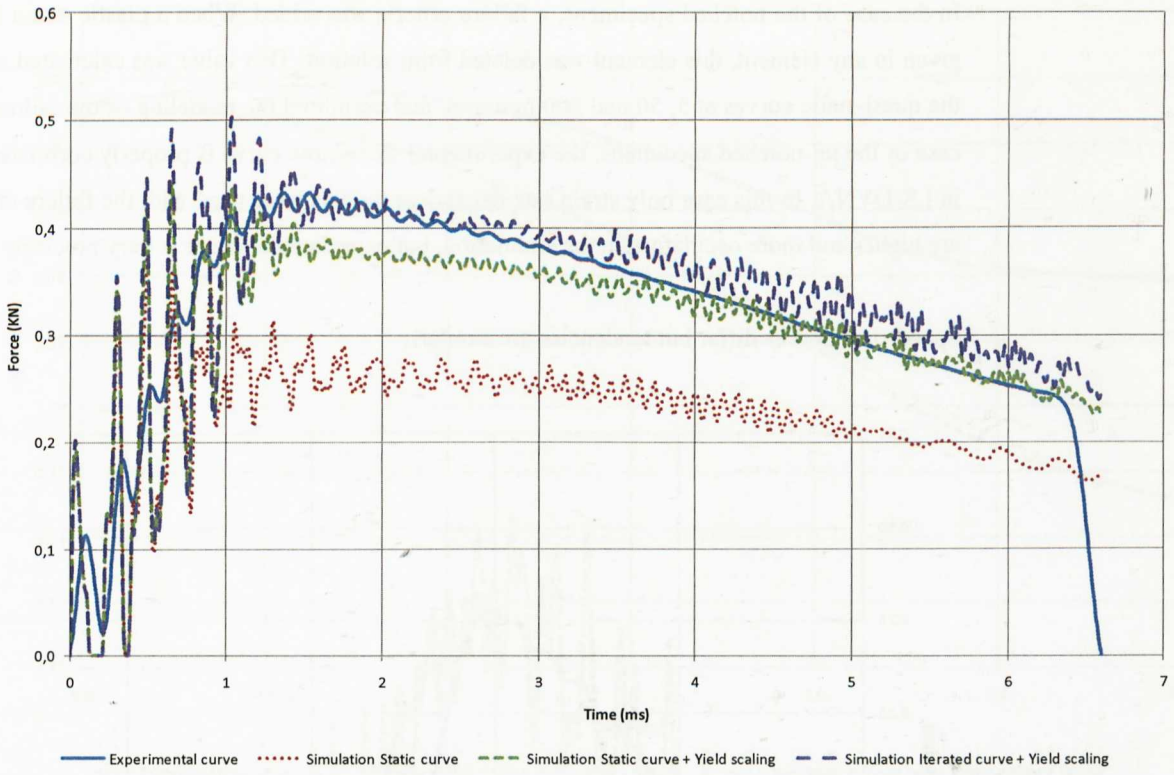

Figure 11.43: Comparison of experimental and simulation force-time results in ANSYS for the higher speed notched test, PC/ABS.

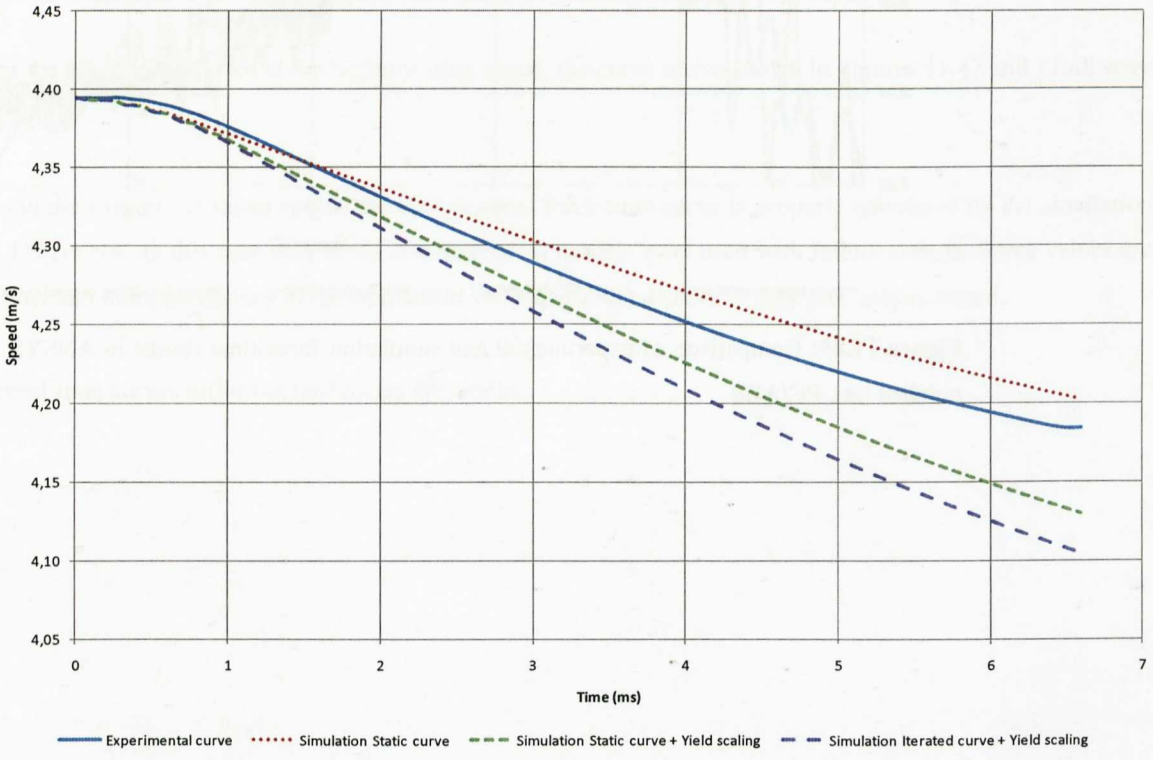

Figure 11.44: Comparison of experimental and simulation speed-time results in ANSYS for the higher speed notched test, PC/ABS.

For the *notched specimen at the lower testing speed*, the curve traces shown in Figures 11.45 and 11.46 were obtained.

In the case of the notched specimens, a failure criteria was added. When a plastic strain higher than 0.5 was given in any element, this element was deleted from solution. This value was calculated as a mean data from the quasi-static curves at 5, 50 and 500 mm/min. and permitted the modeling of the failure process. As in the case of the un-notched specimens, the experimental force-time curve is properly correlated by the simulation in LS-DYNA. In this case only strain rate dependent models were used with the failure criteria. Force values are higher and more oscillatory in the simulation, but experimental curve is very precisely matched.

Speed-time curves differ but tendencies are similar.

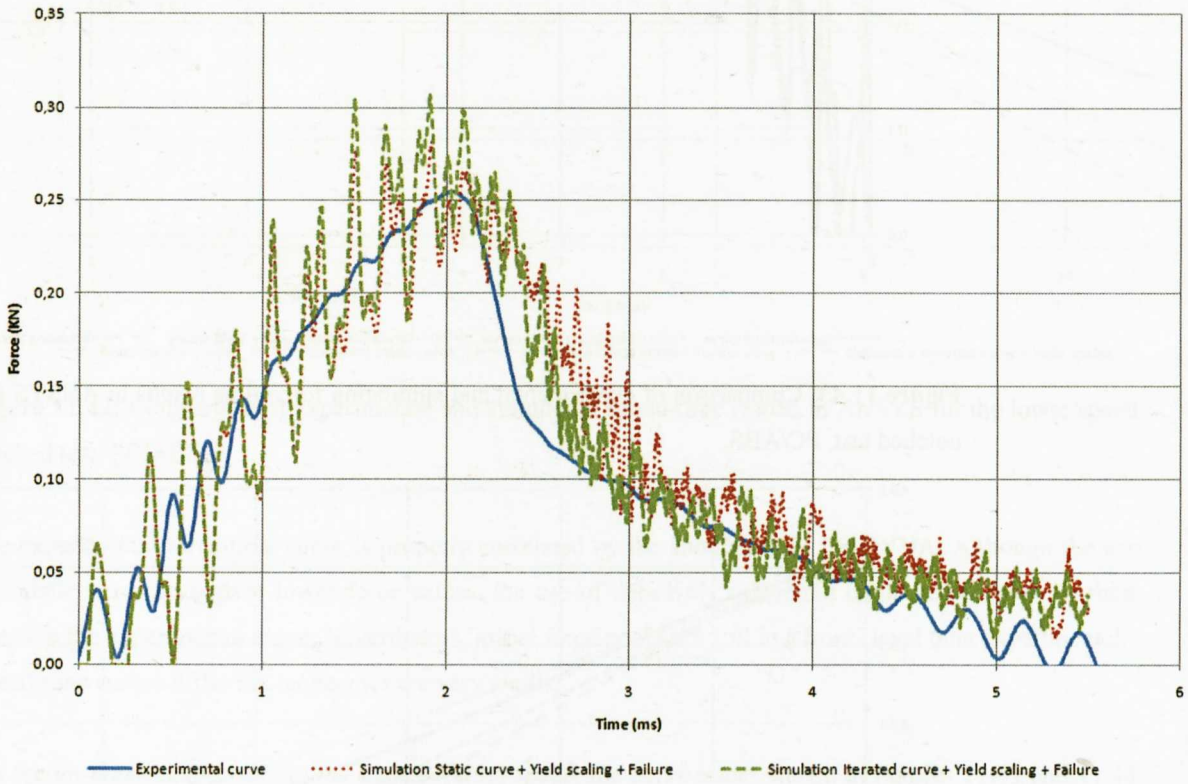

Figure 11.45: Comparison of experimental and simulation force-time results in ANSYS for the lower speed notched test, PC/ABS.

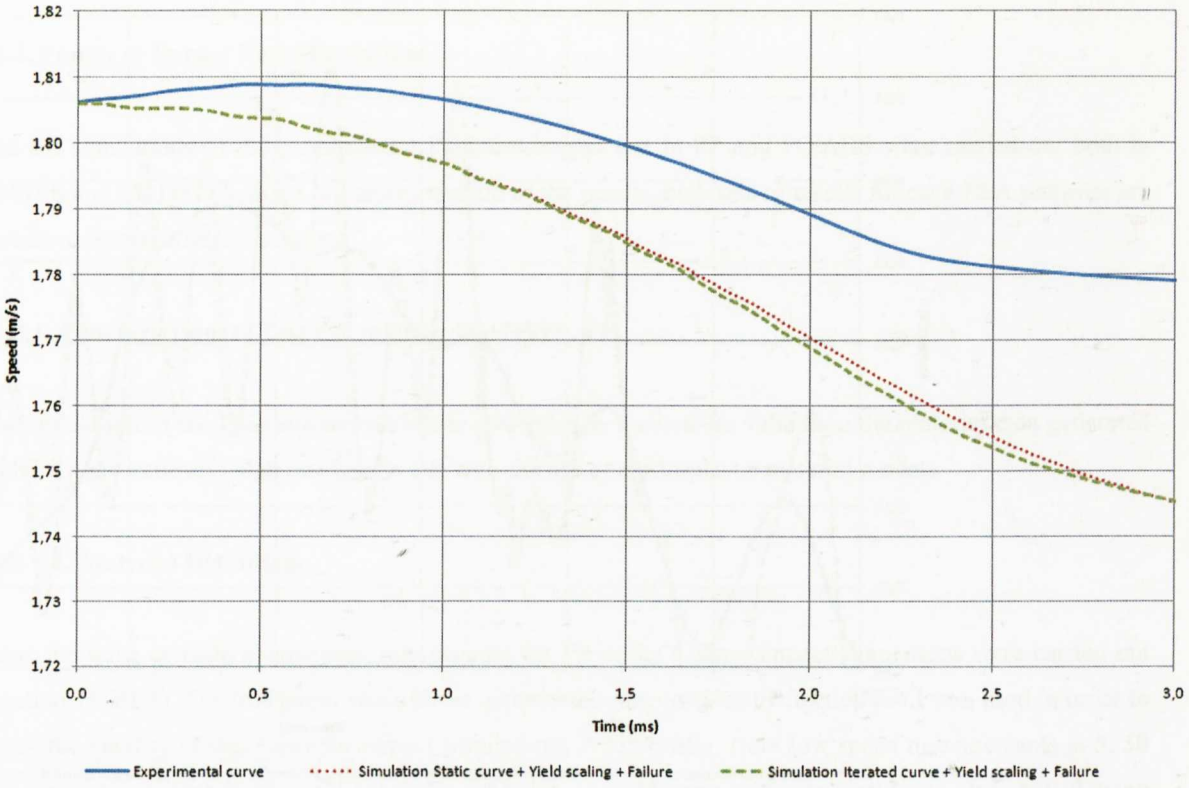

Figure 11.46: Comparison of experimental and simulation speed-time results in ANSYS for the lower speed notched test, PC/ABS.

For the notched specimen at the higher testing speed, the curve traces shown in Figures 11.47 and 11.48 were obtained.

As in the case of the lower speed, the experimental force-time curve is properly correlated by the simulation in LS-DYNA. In this case only strain rate dependent models were used with failure criteria. Force values are higher and more oscillatory in the simulation, but experimental curve is very precisely matched.

Speed-time curves differ but tendencies are similar.

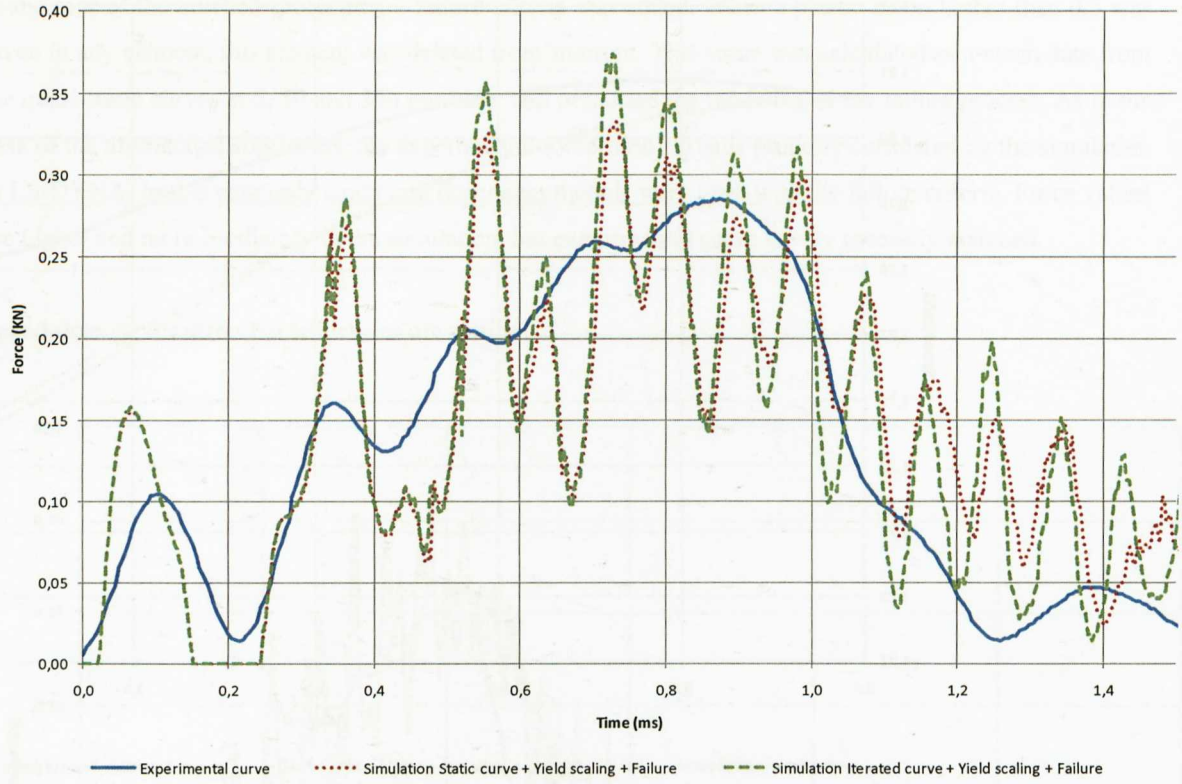

Figure 11.47: Comparison of experimental and simulation force-time results in ANSYS for the higher speed notched test, PC/ABS.

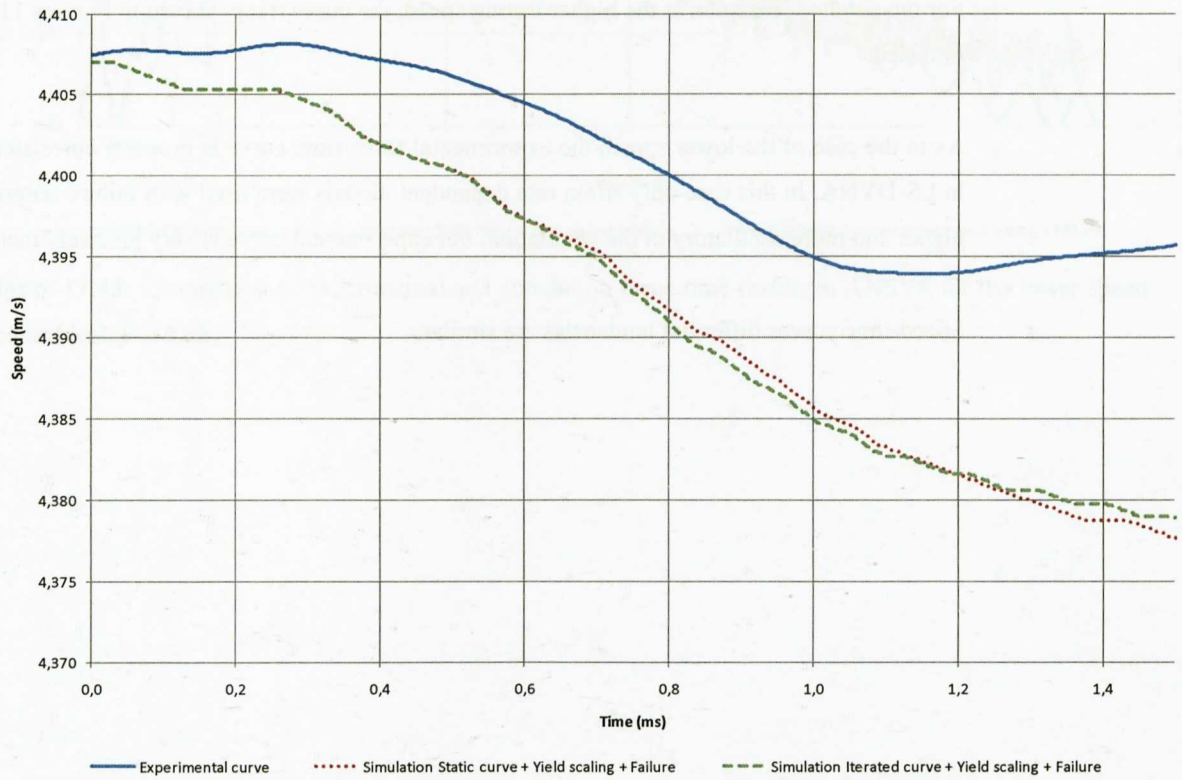

Figure 11.48: Comparison of experimental and simulation speed-time results in ANSYS for the higher speed notched test, PC/ABS.

11.3. Puncture Impact Test Simulations.

The FE simulations of the experimental Puncture impact test in PP and PC/ABS were carried out both in ANSYS and LS-DYNA. For a full representation of the results, both sets of results for each FEA software are discussed in two different sections.

11.3.1. Puncture Impact Test Correlation in ANSYS. PP.

The simulation of the Puncture impact test is a correlation method for validating the material data generated both in quasi-static and high rate tensile test with the use of elasto-plastic material models.

11.3.1.1. Material Definition.

Here, the same considerations taken into account for PP in the Charpy impact simulations were carried out (Section 11.2.1.1). The true stress-strain curve generated in the quasi-static Section 6.4.1 was used in order to check the validity of this curve for impact simulations. Additionally, from low speed measurements at 5, 50 and 500 mm/min (see Section 6.3.1.2.1) the evolution of yield stress with strain rate was also studied using the Perzyna viscoplastic model (see Section 4.4).
The fit gave an m value of 0.37 and a γ value of 3.93. Figure 11.4 reflects the fit obtained in the software KaleidaGraph 4.0.
Thus, the first approach was to use a MISO material model in ANSYS to represent the true stress-strain curve of the material in Figure 6.71. In addition to this elasto-plastic definition, a tensile elastic modulus of 1458.1 MPa. and a Poisson's ratio of 0.38 were also defined.
The second approach was to add a Perzyna viscoplastic model to this definition, considering an m value of 0.37 and a γ value of 3.93.

A density value of 0.905×10^{-9} Tn/mm^3 was also specified for PP (value obtained from material data sheets) which is necessary in a dynamic analysis for inertial effects to be taken into account.

11.3.1.2. Finite Element Modelling.

The Puncture impact test geometry was modeled in ANSYS by finite element models in order to study the experimental impact behaviour and compare with experimental results.
The specimen and the impactor were meshed with SOLID 185 (8 node hexahedral type elements). Contact elements were created between the impactor and the specimen and the specimen and the base supports (TARGE 170 and CONTA 174 type elements). See Figure 11.49.
A global mesh size of 2 mm was used for modeling all the test system, except in the specimen contact region with the impactor, where a mesh size of 0.5 mm was specified. Thus, the mesh size was of the adaptative type from 0.5 at high stress gradients to 2 mm at low stress gradients. This produced a very good quality mesh in the specimen; when bending characteristics are needed to be captured by simulation, a sufficient element number have to be located through the section (usual recommendation is > 2 elements). In this case, 4 hexahedral elements were located through the impacted section of the specimen.

Due to symmetry, only a quarter of the full geometry was modelled in ANSYS (an expanded half representation can be seen in Figure 11.49). The finite element for this model consisted of 10250 nodes and 11002 elements.

The loading on the specimen consisted of,

- applying a constant impact velocity to the impactor (1.0865 m/s in the lower speed case and 4.3534 m/s in the higher speed case).
- applying gravity in the system.

Additional symmetry conditions were also applied to the quarter part of the specimen.

A large displacement transient analysis was performed in each case, specifying the correspondent simulation time (in seconds); 0.016 s in the lower speed case and 0.003 s in the higher speed case.

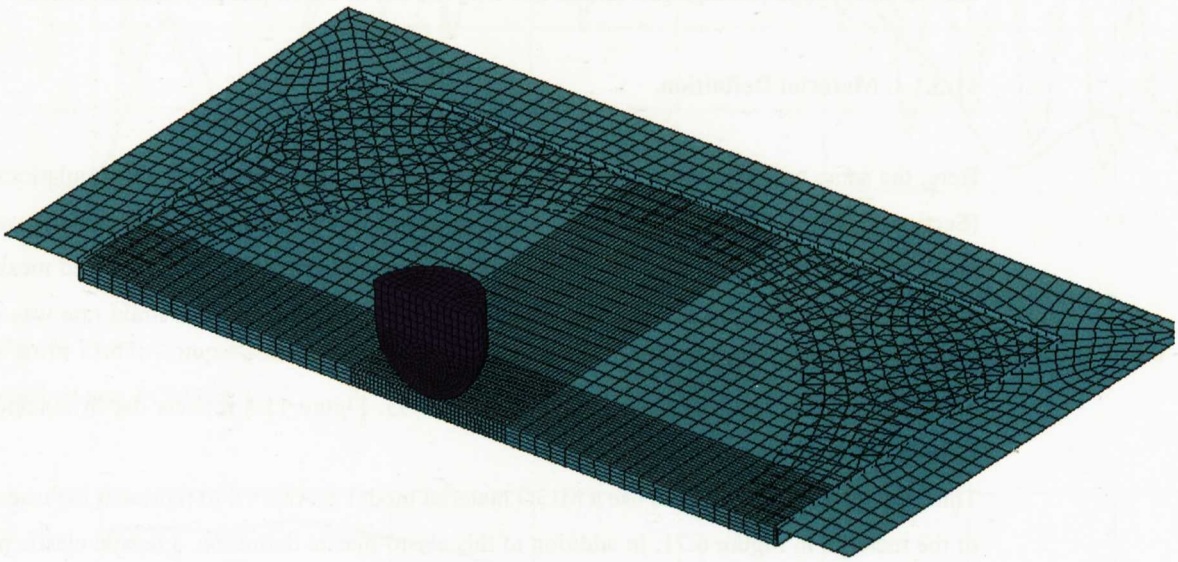

Figure 11.49: Finite element model for the Puncture test configuration, solid elements, PP.

The Puncture specimen was also meshed with SHELL 181 elements (4 node type elements) in order to check the differences between using solid or shell elements. Contact elements were created between the impactor and the specimen and the specimen and the base supports (TARGE 170 and CONTA 174 type elements).

The same mesh considerations for the solid elements were adopted here too. Due to symmetry, only a quarter of the full geometry was modelled in ANSYS (an expanded half representation can be seen in Figure 11.50). The finite element for this model consisted of 4059 nodes and 6289 elements.

The same loading considerations for the solid elements were adopted here too.

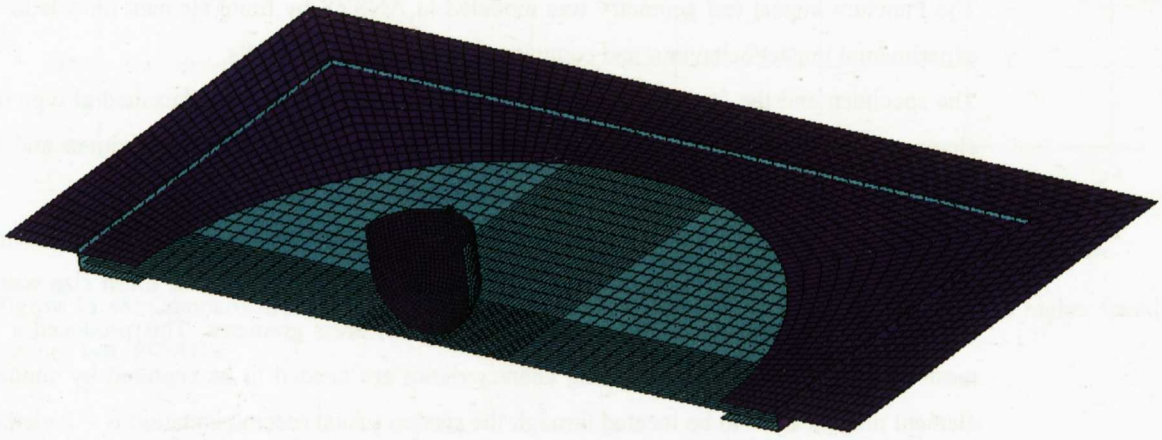

Figure 11.50: Finite element model for the Puncture test configuration, shell elements, PP.

11.3.1.3. Results.

For the *Punctured specimen at the lower testing speed*, the curve traces shown in Figure 11.51 were obtained.

No full convergence was achieved in the simulations, neither for solid elements nor for shells. Originally, with shell elements very high force oscillations were obtained, the curve shown in Figure 11.51 was obtained after smoothing in KaleidaGraph 4.0.

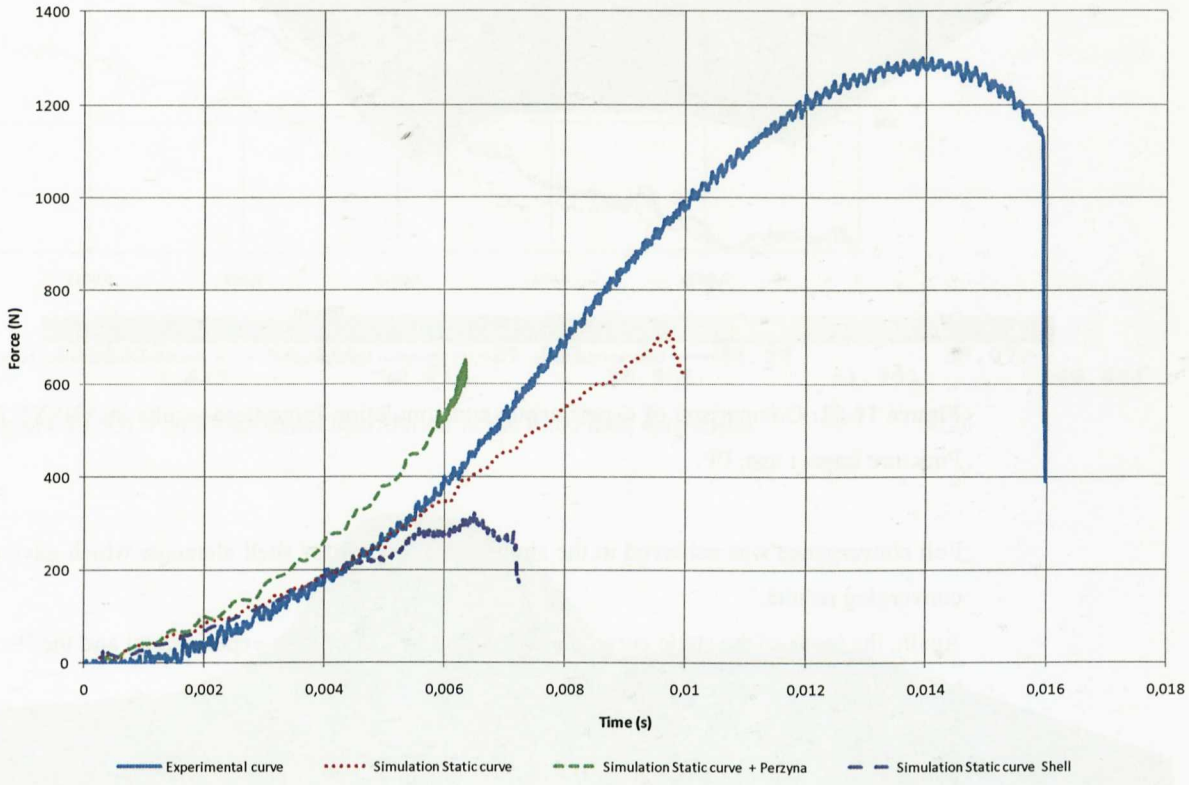

Figure 11.51: Comparison of experimental and simulation force-time results in ANSYS for the lower speed Puncture impact test, PP.

It can be seen that using a static input curve predicts lower force values than experimental. On the other hand, the use of the Perzyna model gives higher force values than experimental, indicating that yield stress values extrapolated with this model are too high.
Shell elements are not adequate for these simulations in ANSYS. Very oscillatory results are obtained.

For the *Punctured specimen at the higher testing speed*, the curve traces shown in Figure 11.52 were obtained.

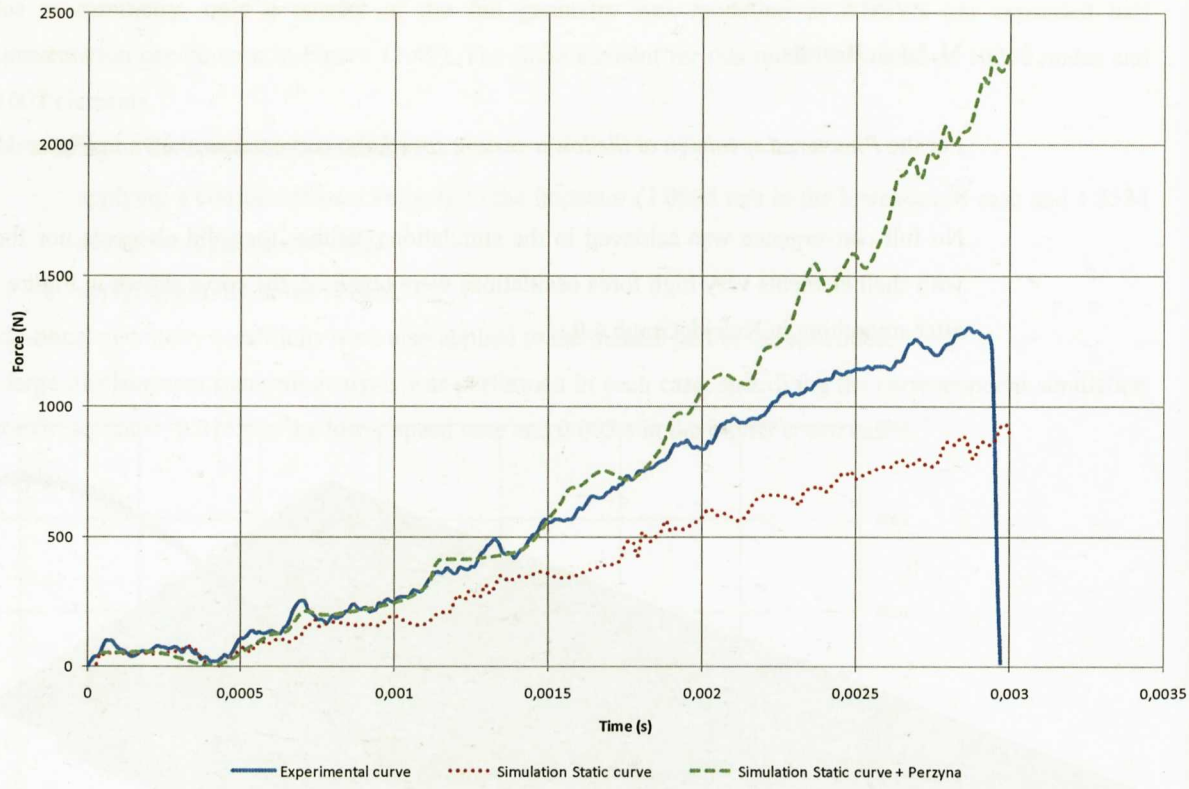

Figure 11.52: Comparison of experimental and simulation force-time results in ANSYS for the higher speed Puncture impact test, PP.

Full convergence was achieved in the simulations, except for shell elements which gave erroneous and non-converging results.

Again, the input of the static curve gives lower force values than experimental and the Perzyna model gives a too stiff response as strains are higher.

Figures 11.53 and 11.54 show the Von Stress distribution that is obtained in ANSYS for the Puncture test in PP. Similar stress patterns were obtained for PC/ABS.

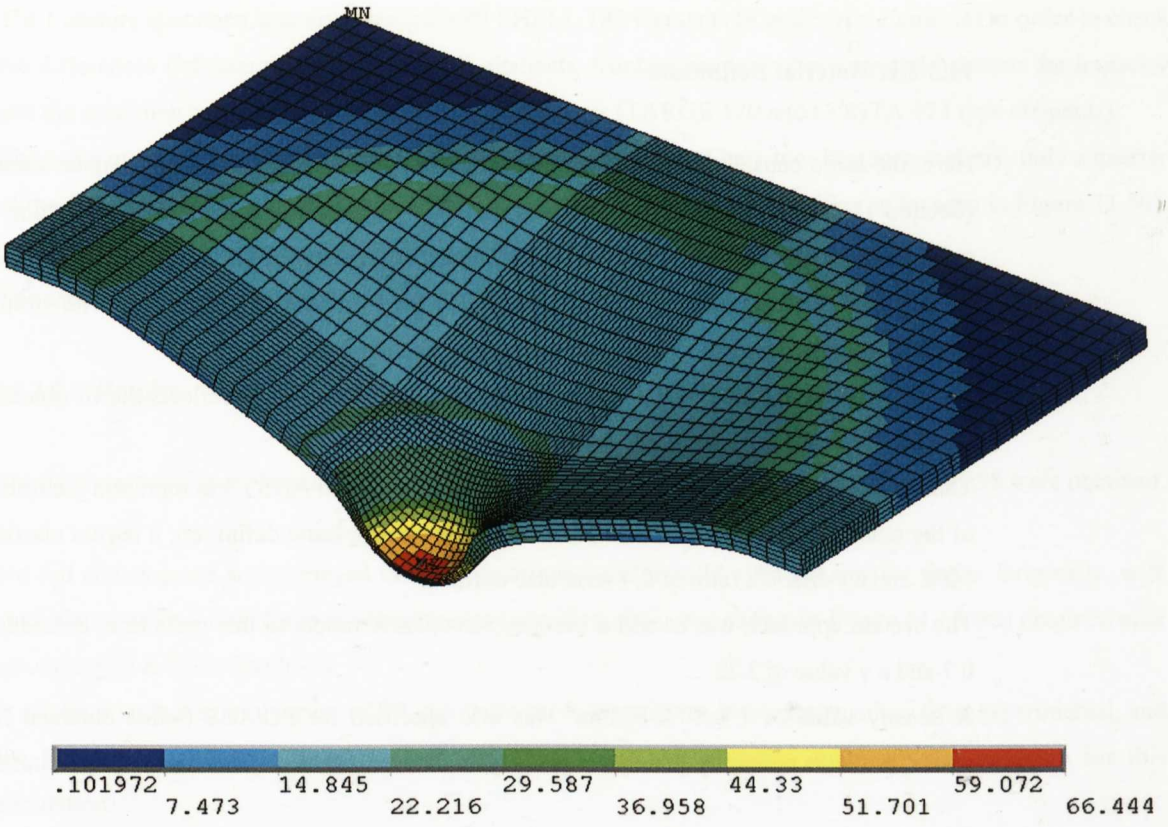

Figure 11.53: Von Mises stress distribution in the Punctured specimen.

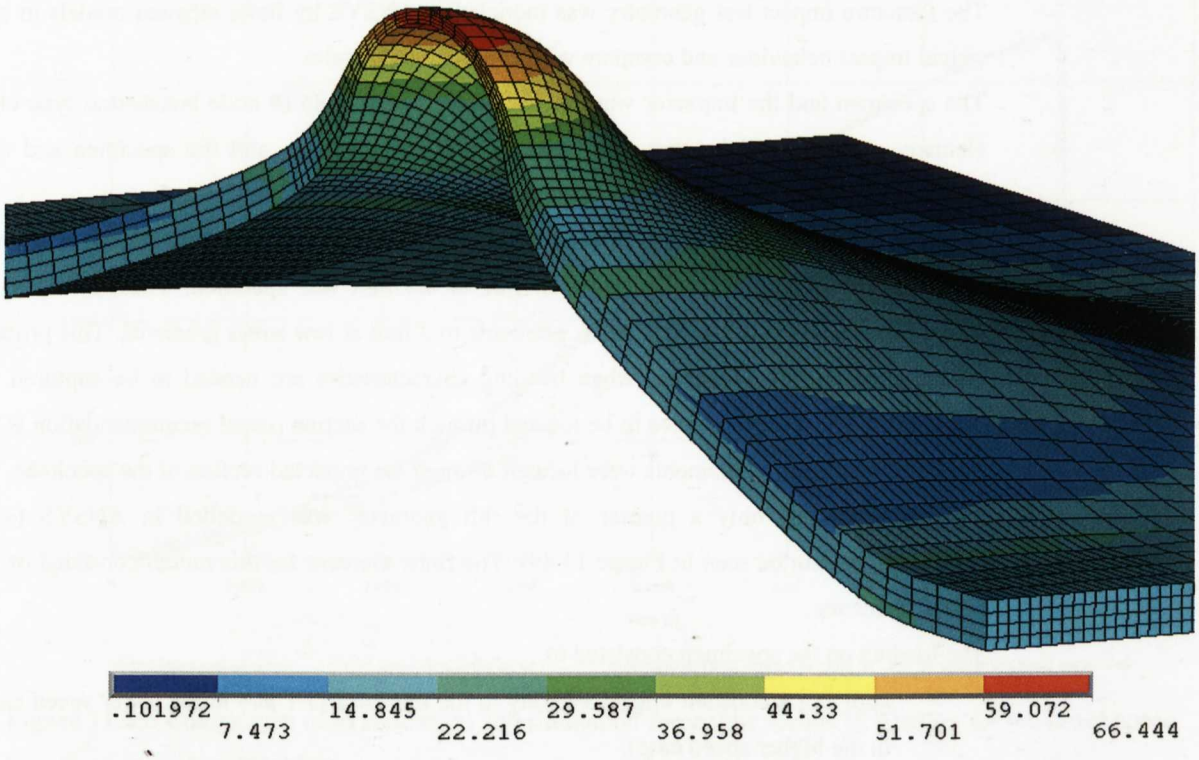

Figure 11.54: Von Mises stress distribution in the Punctured specimen.

11.3.2. Puncture Impact Test Correlation in ANSYS. PC/ABS.

The simulation of the Puncture impact test is a correlation method for validating the material data generated both in quasi-static and high rate tensile test with the use of elasto-plastic material models.

11.3.2.1. Material Definition.

Here, the same considerations taken into account for PC/ABS in the Charpy impact simulations were done (Section 11.2.2.1). First, the true stress-strain curve generated in the quasi-static Section 6.4.4 was used in order to check the validity of this curve for impact simulations. Additionally, from low speed measurements at 5, 50 and 500 mm/min (see Section 6.3.4.1.1) the evolution of yield stress with strain rate was also be studied using the Perzyna viscoplastic model (see Section 4.4).

The fit gave an m value of 0.7 and a γ value of 2.32. Figure 11.19 reflects the fit obtained in the software KaleidaGraph 4.0.

Thus, the first approach was to use a MISO material model in ANSYS to represent the true stress-strain curve of the material in Figure 6.101. In addition to this elasto-plastic definition, a tensile elastic modulus of 2087 MPa. and a Poisson's ratio of 0.4 were also defined.

The second approach was to add a Perzyna viscoplastic model to this definition, considering an m value of 0.7 and a γ value of 2.32.

A density value of 1.1×10^{-9} Tn/mm^3 was also specified for PC/ABS (value obtained from material data sheets) which is necessary in a dynamic analysis for inertial effects to be taken into account.

11.3.2.2. Finite Element Modelling.

The Puncture impact test geometry was modeled in ANSYS by finite element models in order to study the virtual impact behaviour and compare with experimental results.

The specimen and the impactor were meshed with SOLID 185 (8 node hexahedral type elements). Contact elements were created between the impactor and the specimen and the specimen and the base supports (TARGE 170 and CONTA 174 type elements). See Figure 11.49.

A global mesh size of 2 mm was used for modeling all the test systems, except in the specimen contact region with the impactor, where a mesh size of 0.5 mm was specified. Thus, the mesh size was of the adaptative type from 0.5 at high stress gradients to 2 mm at low stress gradients. This produced a very good quality mesh in the specimen; when bending characteristics are needed to be captured by simulation, a sufficient element number have to be located through the section (usual recommendation is > 2 elements). In this case, 4 hexahedral elements were located through the impacted section of the specimen.

Due to symmetry, only a quarter of the full geometry was modelled in ANSYS (an expanded half representation can be seen in Figure 11.49). The finite element for this model consisted of 10250 nodes and 11002 elements.

The loading on the specimen consisted of,

- applying a constant impact velocity to the impactor (1.1 m/s in the lower speed case and 4.035 m/s in the higher speed case).
- applying gravity in the system.

Additional symmetry conditions were also applied to the quarter part of the specimen.

A large displacement transient analysis was performed in each case, specifying the correspondent simulation time (in seconds); 0.014 s in the lower speed case and 0.0036 s in the higher speed case.

The Puncture specimen was also meshed with SHELL 181 elements (4 node type elements) in order to check the differences between using solid or shell elements. Contact elements were created between the impactor and the specimen and the specimen and the base supports (TARGE 170 and CONTA 174 type elements).
The same mesh considerations for the solid elements were adopted here too. Due to symmetry, only a quarter of the full geometry was modelled in ANSYS (an expanded half representation can be seen in Figure 11.50).
The finite element for this model consisted of 4059 nodes and 6289 elements.
The same loading considerations for the solid elements were adopted here too.

11.3.2.3. Results.

For the *Punctured specimen at the lower testing speed*, the curve traces shown in Figure 11.55 were obtained.

No full convergence was achieved in the simulations, not for solid elements nor for shells. Originally, with shell elements very high force oscillations were obtained, the curve shown in Figure 11.68 was obtained after smoothing in KaleidaGraph 4.0.
It can be seen that as in the case of PP, the static curve input gives lower force values than experimental, and the Perzyna model tends to give a too stiff response. Shell elements again are not adequate for this simulation.

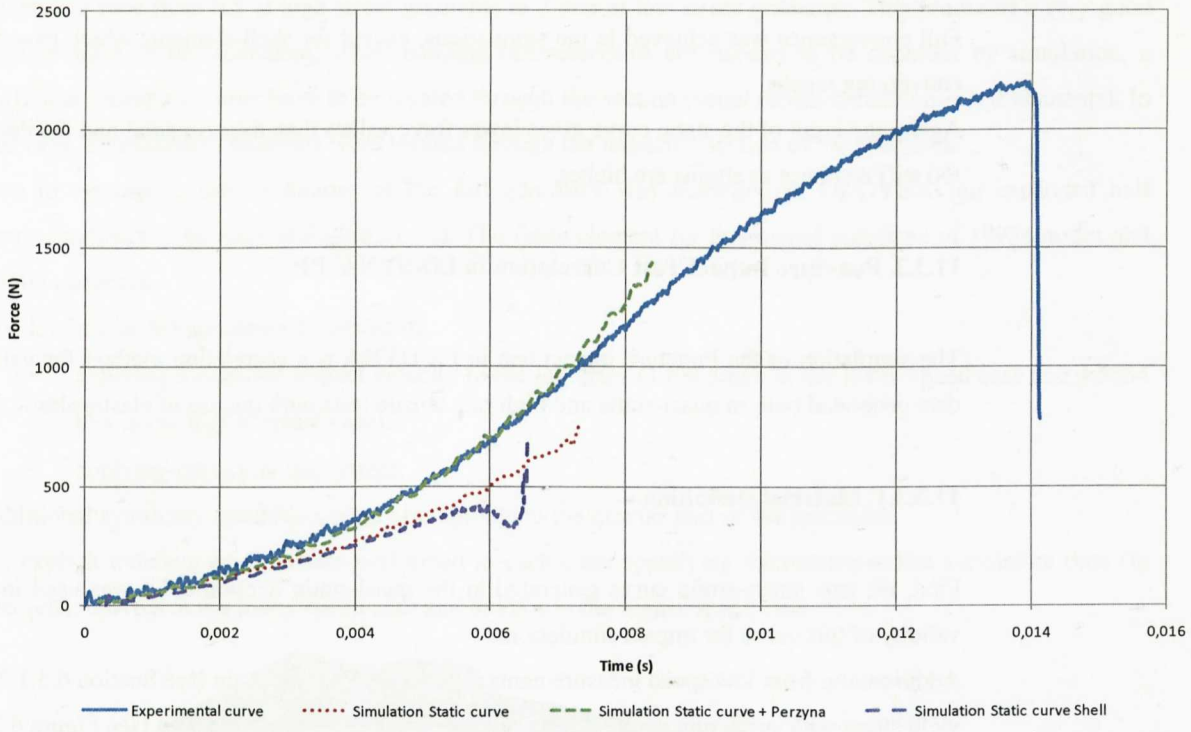

Figure 11.55: Comparison of experimental and simulation force-time results in ANSYS for the lower speed Puncture impact test, PC/ABS.

For the *Punctured specimen at the higher testing speed*, the curve traces shown in Figure 11.56 were obtained.

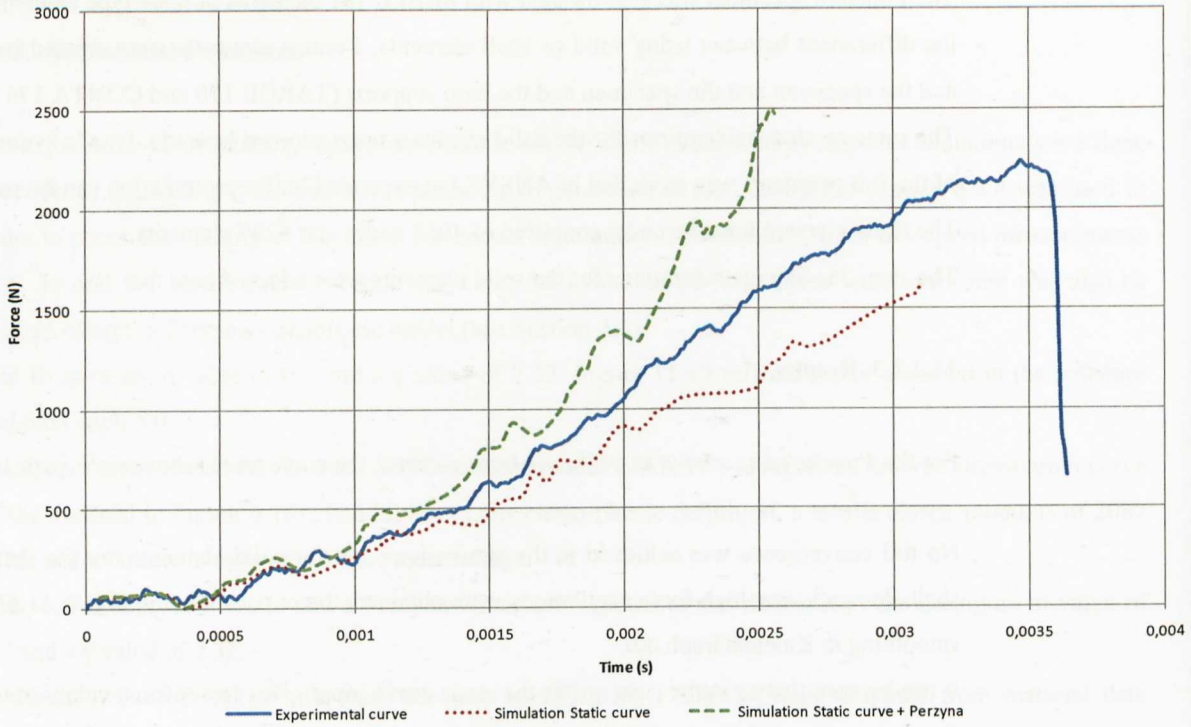

Figure 11.56: Comparison of experimental and simulation force-time results in ANSYS for the higher speed Puncture impact test, PC/ABS.

Full convergence was achieved in the simulations, except for shell elements which gave erroneous and non-converging results.

Again, the input of the static curve gives lower force values than experimental and the Perzyna model gives a too stiff response as strains are higher.

11.3.3. Puncture Impact Test Correlation in LD-SYNA. PP.

The simulation of the Puncture impact test in LS-DYNA is a correlation method for validating the material data generated both in quasi-static and high rate tensile tests with the use of elasto-plastic material models.

11.3.3.1. Material Definition.

First, the true stress-strain curve generated in the quasi-static Section 6.4.1 was used in order to check the validity of this curve for impact simulations.

Additionally, from low speed measurements at 5, 50 and 500 mm/min (see Section 6.3.1.2.1) the evolution of yield stress with strain rate could also be studied with a logarithmic relation (see Figure 6.28).

Taking into account the fit from Figure 6.28, Table 11.1 was created in order to represent the yield stress vs. the strain rate for different decades of strain rate.

Thus, the first approach was to use a elasto-plastic material model to represent the true stress-strain curve of the material in Figure 6.71. In addition to this elasto-plastic definition, a tensile elastic modulus of 1458.1 MPa. and a Poisson's ratio of 0.38 were also defined.

The second approach was to add a scaling factor table to the yield stress definition in function of the generated strain rates. Table 11.1.

A more complex extrapolation method was also used, which is based on previous work performed by Grean et al. [12] and the ISO 18872 standard. The calculation of the parameters for this method are described in Chapter 12.

A fourth approach was also studied, which was based on the input of the iterated curves calculated in Section 11.1.1.

All of these approaches were carried out using the so called MAT_024 model in LS-DYNA.

A density value of 0.905×10^{-9} Tn/mm^3 was also specified for PP (obtained from material data sheets) which is necessary in a dynamic analysis for inertial effects to be taken into account.

11.3.3.2. Finite Element Modelling.

The Puncture impact test geometry was modeled in LS-DYNA by finite element models in order to study the impact behaviour and compare with experimental results.

The specimen was meshed with SOLID 164 type elements (full integration 8 node hexahedral elements). The impactor and the base supports were meshed with rigid shell type elements. Automatic contact elements were created between the impactor and the specimen and the specimen and the base supports.

A global mesh size of 2 mm was used for modeling all the test systems, except in the specimen contact region with the impactor, where a mesh size of 0.5 mm was specified. Thus, the mesh size was of the adaptative type from 0.5 at high stress gradients to 2 mm at low stress gradients. This produced a very good quality mesh in the specimen; when bending characteristics are needed to be captured by simulation, a sufficient element number have to be located through the section (usual recommendation is > 2 elements). In this case, 4 hexahedral elements were located through the impacted section of the specimen.

Due to symmetry, only a quarter of the full geometry was modelled in LS-DYNA (an expanded half representation can be seen in Figure 11.57). The finite element for this model consisted of 19954 nodes and 15609 elements.

The loading on the specimen consisted of,

- applying a constant impact velocity to the impactor (1.0865 m/s in the lower speed case and 4.3534 m/s in the higher speed case).
- applying gravity in the system.

Additional symmetry conditions were also applied to the quarter part of the specimen.

An explicit transient analysis was performed in each case, specifying the correspondent simulation time (in seconds); 0.016 s in the lower speed case and 0.003 s in the higher speed case.

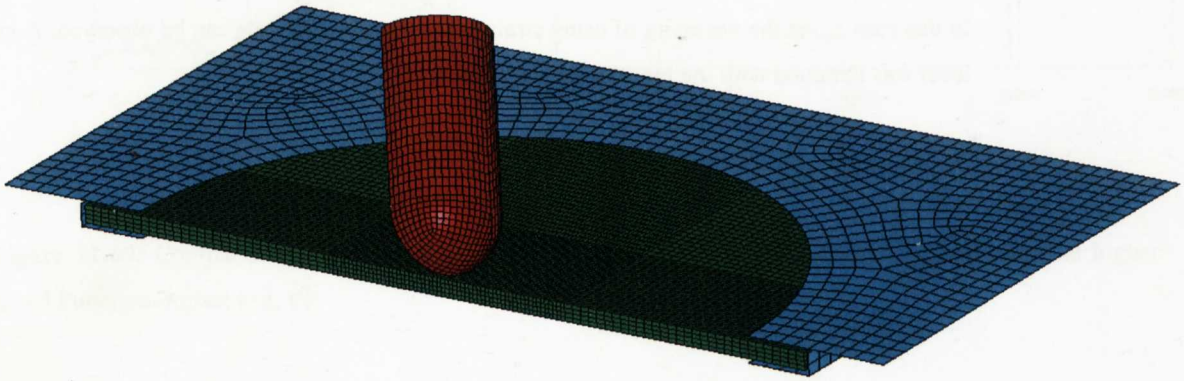

Figure 11.57: Finite element solid model of the test system for Puncture impact simulation.

The Puncture specimen was also meshed with shell elements (4 node type elements) in order to check the differences between using solid or shell elements. Contact elements were created between the impactor and the specimen and the specimen and the base supports.

The same mesh considerations for the solid elements were adopted here too. Due to symmetry, only a quarter of the full geometry was modelled in LS-DYNA (an expanded half representation can be seen in Figure 11.58). The finite element for this model consisted of 9721 nodes and 9380 elements.

The same loading considerations for the solid elements were adopted here again.

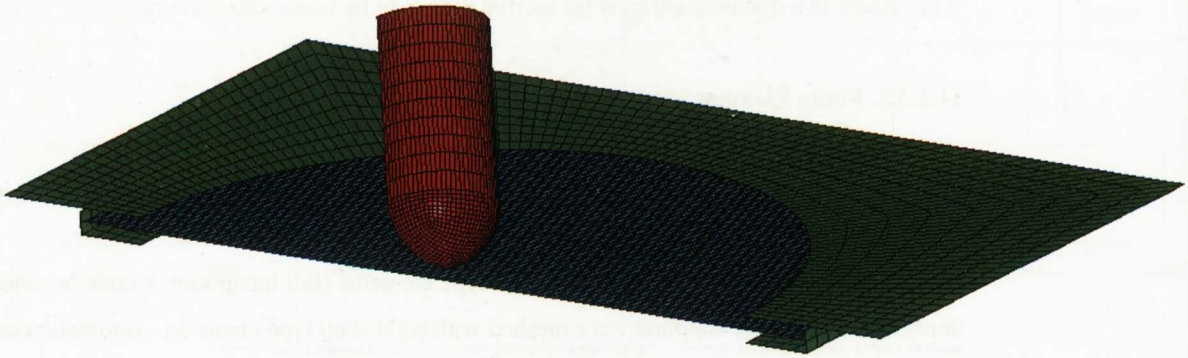

Figure 11.58: Finite element shell model of the test system for Puncture impact simulation.

11.3.3.3. Results.

For the *Punctured specimen at the lower testing speed*, the curve traces shown in Figure 11.59 were obtained.

Results obtained in LS-DYNA are considerably better than those obtained in ANSYS. Although the use of a static curve gives low force values, taking into consideration strain rate dependency, the experimental curve is closely followed except in the near to failure region. The use of a failure value just cuts the curve suddenly in a certain value and it is not able to reproduce the negative slopes observed in the experimental curve. This indicates that some damage mechanism is present in the experimental behaviour which can not be captured in simulation.

Shell elements give a too stiff behaviour.

For the *Punctured specimen at the higher testing speed*, the curve traces shown in Figure 11.60 were obtained.

In this case again the necessity of using strain rate dependant models can be observed. A good approximation level was obtained with the input of the iterated curves.

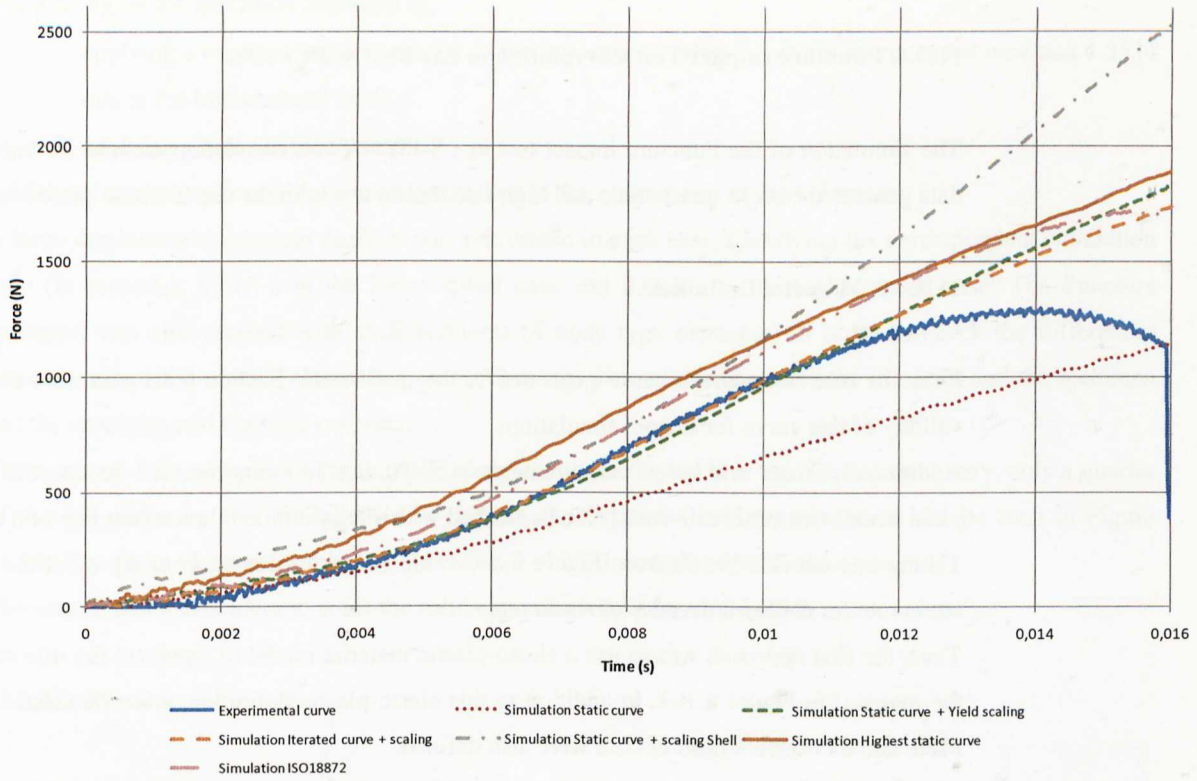

Figure 11.59: Comparison of experimental and simulation force-time results in LS-DYNA for the lower speed Puncture impact test, PP.

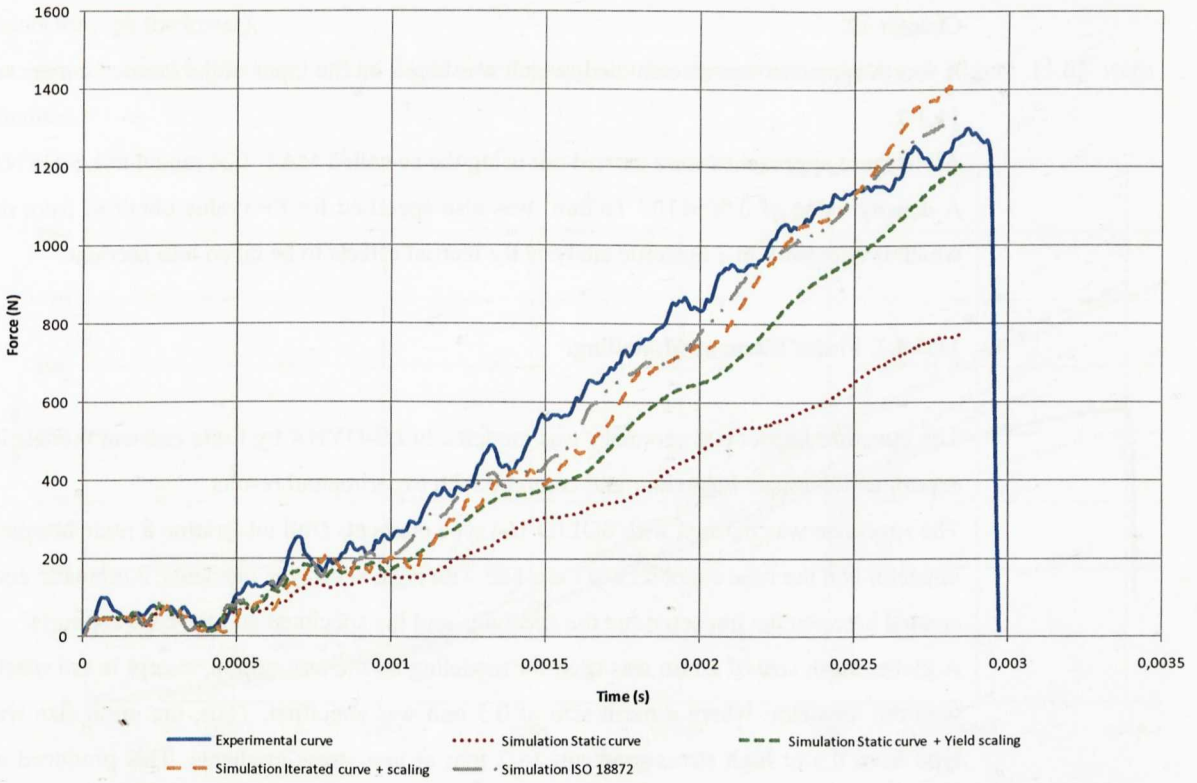

Figure 11.60: Comparison of experimental and simulation force-time results in LS-DYNA for the higher speed Puncture impact test, PP.

11.3.4. Puncture Impact Test Correlation in LD-SYNA. PC/ABS.

The simulation of the Puncture impact test in LS-DYNA is a correlation method for validating the material data generated both in quasi-static and high rate tensile test with the use of elasto-plastic material models.

11.3.4.1. Material Definition.

First, the true stress-strain curve generated in the quasi-static Section 6.4.1 was used in order to check the validity of this curve for impact simulations.
Additionally, from low speed measurements at 5, 50 and 500 mm/min (see Section 6.3.4) the evolution of yield stress with strain rate could also be studied with a logarithmic relation (see Figure 6.53).
Taking into account the fit from Figure 6.53, Table 11.2 was created in to represent the yield stress vs. the strain rate for different decades of strain rate.
Thus, the first approach was to use a elasto-plastic material model to represent the true stress-strain curve of the material in Figure 6.101. In addition to this elasto-plastic definition, a tensile elastic modulus of 1458.1 MPa. and a Poisson's ratio of 0.38 were also defined.
The second approach was to add a scaling factor table to the yield stress definition in function of the generated strain rates. Table 11.2.
A more complex extrapolation method was also used, which is based on previous work performed by Grean et al. [12] and the ISO 18872 standard. The calculation of the parameters for this method are described in Chapter 12.
A fourth approach was also studied, which was based on the input of the iterated curves calculated in Section 11.1.2.
All of these approaches were carried out using the so called MAT_024 model in LS-DYNA.
A density value of 0.905×10^{-9} Tn/mm^3 was also specified for PP (value obtained from material data sheets) which is necessary in a dynamic analysis for inertial effects to be taken into account.

11.3.4.2. Finite Element Modelling.

The Puncture impact test geometry was modeled in LS-DYNA by finite element models in order to study the experimental impact behaviour and compare with experimental results.
The specimen was meshed with SOLID 164 type elements (full integration 8 node hexahedral elements). The impactor and the base supports were meshed with rigid shell type elements. Automatic contact elements were created between the impactor and the specimen and the specimen and the base supports.
A global mesh size of 2 mm was used for modeling all the test system, except in the specimen contact region with the impactor, where a mesh size of 0.5 mm was specified. Thus, the mesh size was of the adaptative type from 0.5 at high stress gradients to 2 mm at low stress gradients. This produced a very good quality mesh in the specimen; when bending characteristics are needed to capture by simulation, a sufficient element number have to be located through the section (usual recommendation is > 2 elements). In this case, 4 hexahedral elements were located through the impacted section of the specimen. Due to symmetry, only a quarter of the full geometry was modelled in LS-DYNA (an expanded half representation is seen in Figure 11.57). The finite element for this model consisted of 19954 nodes and 15609 elements.

The loading on the specimen consisted of,

- applying a constant impact velocity to the impactor (1.0865 m/s in the lower speed case and 4.3534 m/s in the higher speed case).
- applying gravity in the system.

Additional symmetry conditions were also applied to the quarter part of the specimen.

A large displacement transient analysis was performed in each case, specifying the correspondent simulation time (in seconds); 0.016 s in the lower speed case and 0.003 s in the higher speed case. The Puncture specimen was also meshed with shell elements (4 node type elements) in order to check the differences between using solid or shell elements. Contact elements were created between the impactor and the specimen and the specimen and the base supports.

The same mesh considerations for the solid elements were adopted here too. Due to symmetry, only a quarter of the full geometry was modelled in LS-DYNA (an expanded half representation can be seen in Figure 11.58). The finite element for this model consisted of 9721 nodes and 9380 elements.

The same loading considerations for the solid elements were adopted here too.

11.3.4.3. Results.

For the *Punctured specimen at the lower testing speed*, the curve traces shown in Figure 11.61 were obtained. In this case, strain rate dependant models offered a too stiff response, especially at large strain levels but again the static curve was insufficient to correlate adequately the experimental curve. Shell elements offered again a too stiff response. A default element formulation was used (Belytschko-Tsai, with 4 integration points through thickness).

For the *Punctured specimen at the higher testing speed*, the curve traces shown in Figure 11.62 were obtained.

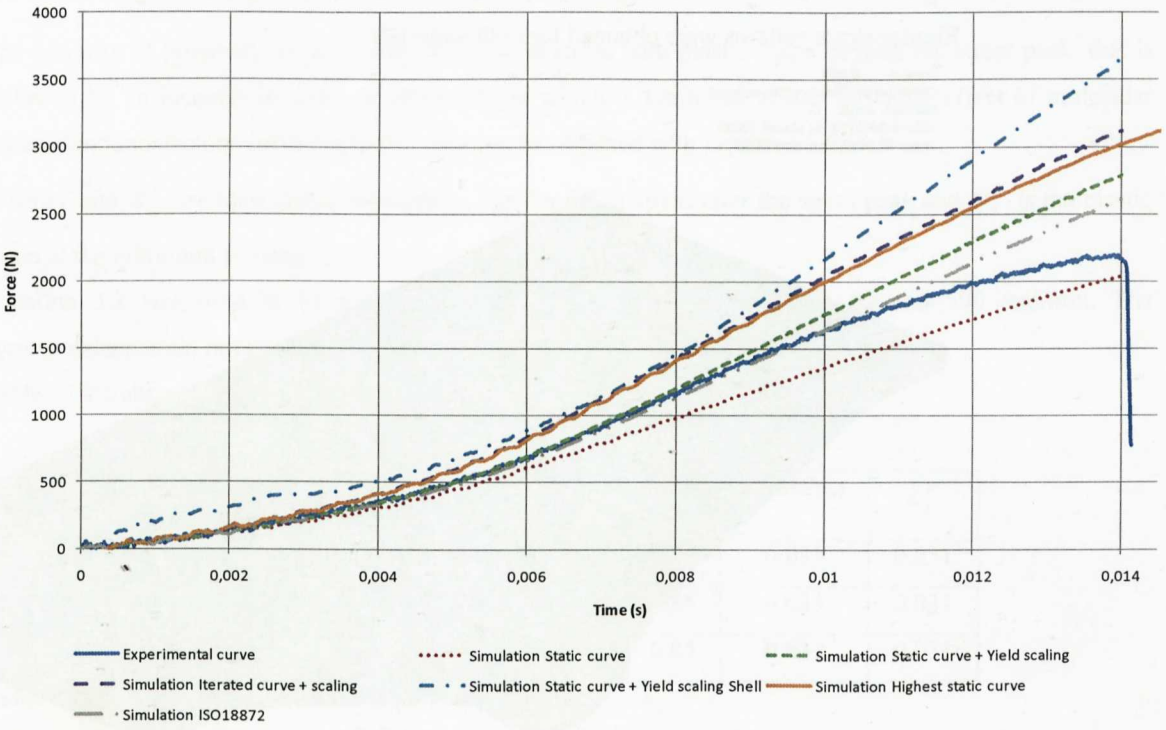

Figure 11.61: Comparison of experimental and simulation force-time results in LS-DYNA for the lower speed Puncture impact test, PC/ABS.

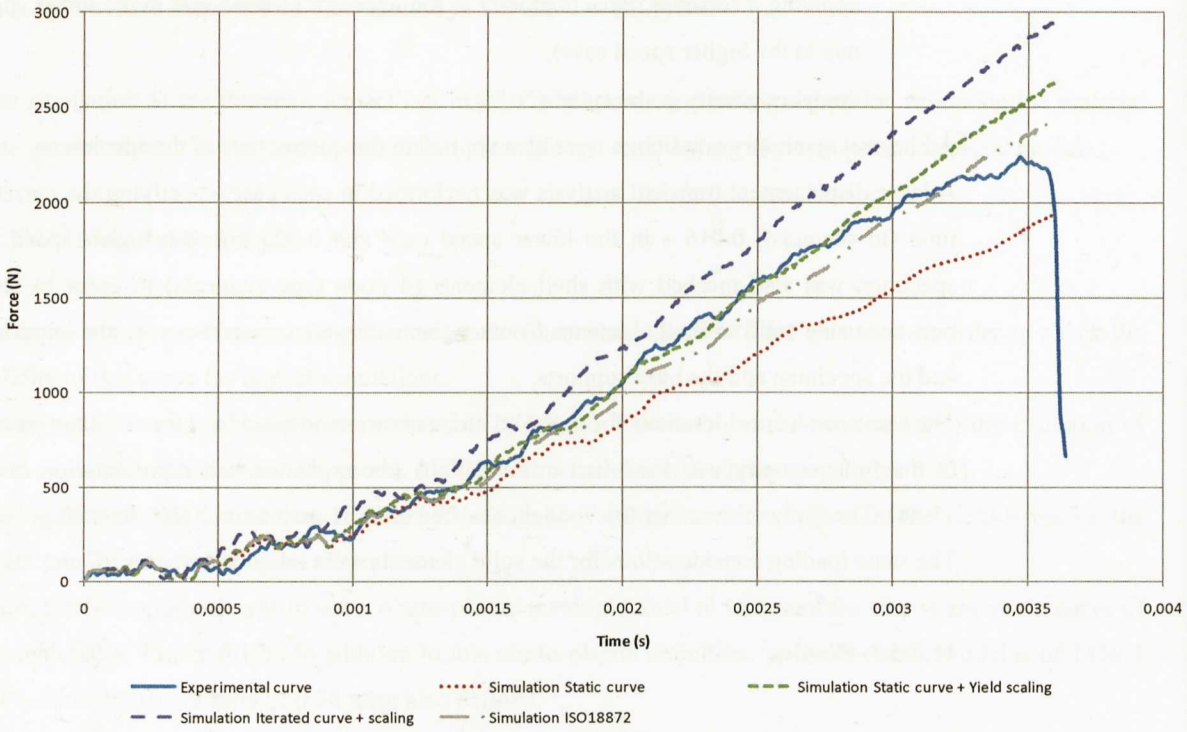

Figure 11.62: Comparison of experimental and simulation force-time results in LS-DYNA for the higher speed Puncture impact test, PC/ABS.

Although the use of a base static curve in addition with a strain rate scaling table gives proper approximation to the experimental test, the best match was obtained with the method extrapolation method proposed in the ISO 18872 standard. This tendency was also confirmed with the results obtained in the Puncture simulations in PP.

Figure 11.63 shows for illustrative purposes, the Von Mises stresses obtained in the Punctured specimen. Similar stress patterns were obtained for both materials.

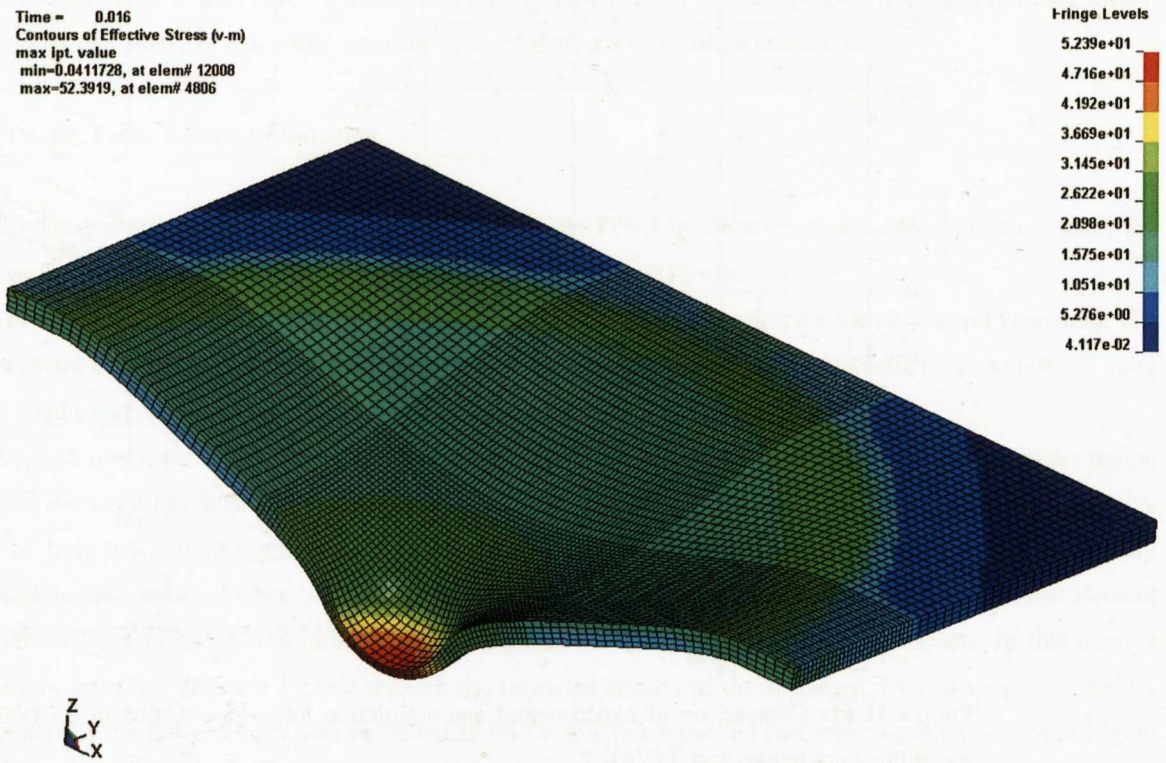

Figure 11.63: Von Mises stress distribution in the Punctured specimen.

Chapter 12: Calculation of material model parameters according to ISO 18872.

This standard has been used in Section 10.3 to generate force – displacement data at different testing speeds. Later, this data was iteratively correlated in order to obtain true stress - strain data at different strain rates.
The standard can also be used to model with a mathematical function the true stress - plastic strain curve at a quasi-static speed. If different measurements are performed at different testing speeds (or strain rates), the Eyring's equation is used in the standard in order to generate different stress-strain curves in function of the generated strain rates.
From this research viewpoint, with the obtained iterated curves at different testing rates it was not specifically necessary to use a modeling mathematical function since FEA codes as LS-DYNA, and particularly using MAT_024, permit the tabular input of direct experimental stress-strain curves without any need of constants or parameter determination.
The use of the extrapolation method described in ISO 18872 was thought to be appropiate to check the validity of the procedure when slow strain rate is only available. Thus, the experimental testing carried out at the testing speeds of 5, 50 and 500 mm/min. for PP and PC/ABS was modeled with this method in order to compare it with the simple extrapolation method of fitting a logarithmic trend to yield stress values and using a static base curve in simulations.
It has to be remembered that both methods use the Eyring's equation for yield stress dependency with strain rate. The difference is given on the stress-strain curve shapes; using a base curve and logarithmic yield scaling with strain rate, only a base stress-strain curve is used, whereas in the procedure specified by ISO 18872, all curve shapes at different strain rates are modeled and can be used as input in FEA.

12.1. Calculations using Polypropylene (PP).

The majority of polymers show a small decrease in stress with plastic strain beyond the stress peak, this is followed by an increase in stress at larger strains which is attributed to the stiffening effect of molecular orientation. Satisfactory curve fits to this data can be obtained with Equation 3.2.
Where δ and ε_s^p are identifiable parameters: δ is the fall in stress after the stress peak and ε_s^p is the plastic strain at the minimum in stress.
Equation 3.2 was used to fit true stress-plastic strain curves tested at 5, 50 and 500 mm/min. The correspondant strain rates were 0.001667, 0.01667 and 0.1667 s^{-1} see Section 6.3.1.2.1.
Table 12.1 summarises the obtained parameter values.

Strain rate (s-1)	σ_0 (MPa.)	σ_f (MPa.)	ε_p^o	β	δ (MPa.)	ε_s^p
0.001667	9.1831	22.558	0.004	0.85	0.033	0.031
0.01667	10.99	22.693	0.004	0.85	0.033	0.031
0.1667	12.217	25.949	0.004	0.85	0.033	0.031

Table 12.1: Parameter values in the Equation 3.2, PP.

Similarly to the examples described in the ISO 18872 standard, no strain rate sensitivity was modeled in the parameters ε_p^o, β, δ and ε_s^p.

Taking into account a logarithmic variation of σ_0 and σ_f with strain rate, true stress - plastic strain curves were generated up to high strain rate values. See Figure 12.1.

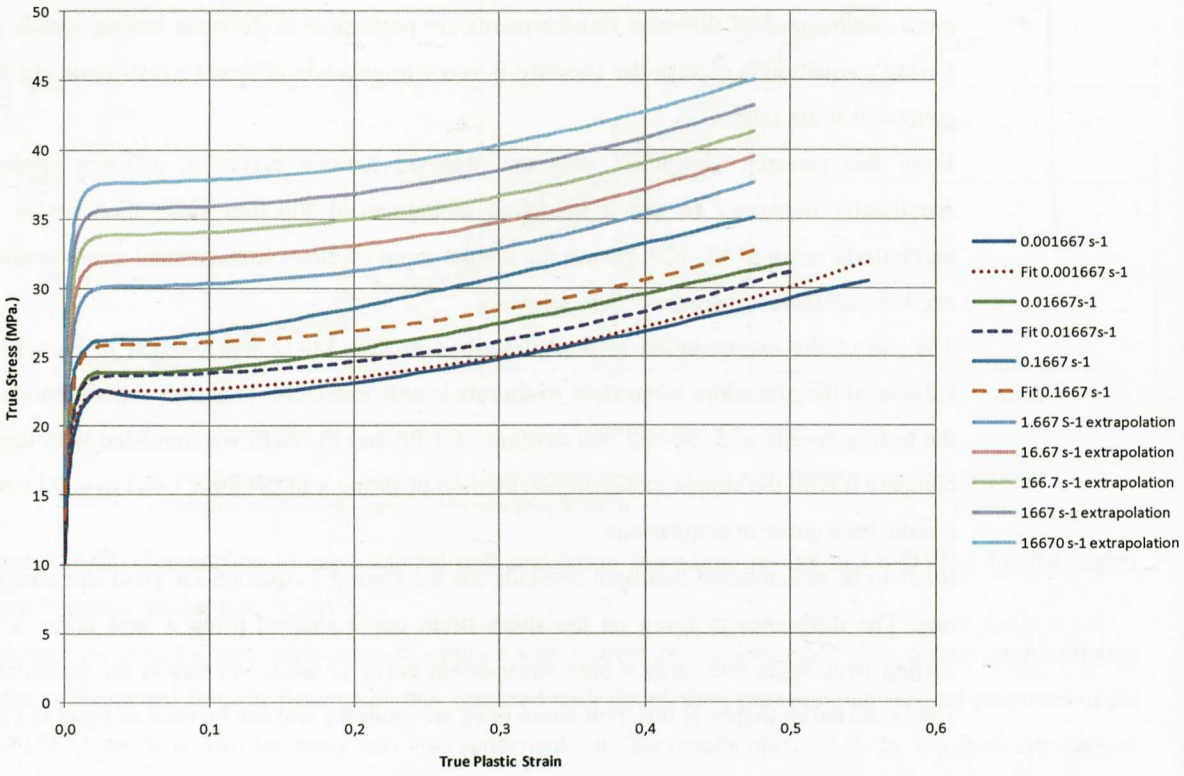

Figure 12.1: True stress - plastic strain curves for PP. Tensile data modellling according to ISO 18872.

The curve fits to the tested strain rates are not very precise, and optimisation of the material paramaters would be necessary for a more acceptable fit. The idea was to illustrate the possibility of constructing a series of curves with rate dependency, the later input in LS-DYNA, and the comparison with the basic approach of considering a single static curve + yield scaling.

These curves where input in LS-DYNA for the simulation of the puncture test at the two testing speeds, obtaining very satisfactory results. See Figures 11.59 and 11.60.

12.2. Calculations in PC/ABS.

Equation 3.2 was used to fit true stress-plastic strain curves tested at 5, 50 and 500 mm/min. The correspondant strain rates were 0.001667, 0.01667 and 0.1667 s^{-1} see Section 6.3.4.1.1.

Table 12.2 summarises the obtained parameter values.

Strain rate (s-1)	σ_0 (MPa.)	σ_f (MPa.)	ε_p^o	β	δ (MPa.)	ε_s^p
0.001667	8.333	43.557	0.003	0.9	1.8	0.108
0.01667	8.333	47.137	0.003	0.9	1.8	0.108
0.1667	8.333	49.313	0.003	0.9	1.8	0.108

Table 12.2: Parameter values in the Equation 3.2, PC/ABS.

As described in the ISO 18872 standard, no strain rate sensitivity was modeled in the parameters ε_p^o, β, δ and ε_s^p. Taking into account a logarithmic variation of σ_f with strain rate, true stress - plastic strain curves were generated up to high strain rate values. See Figure 12.2.

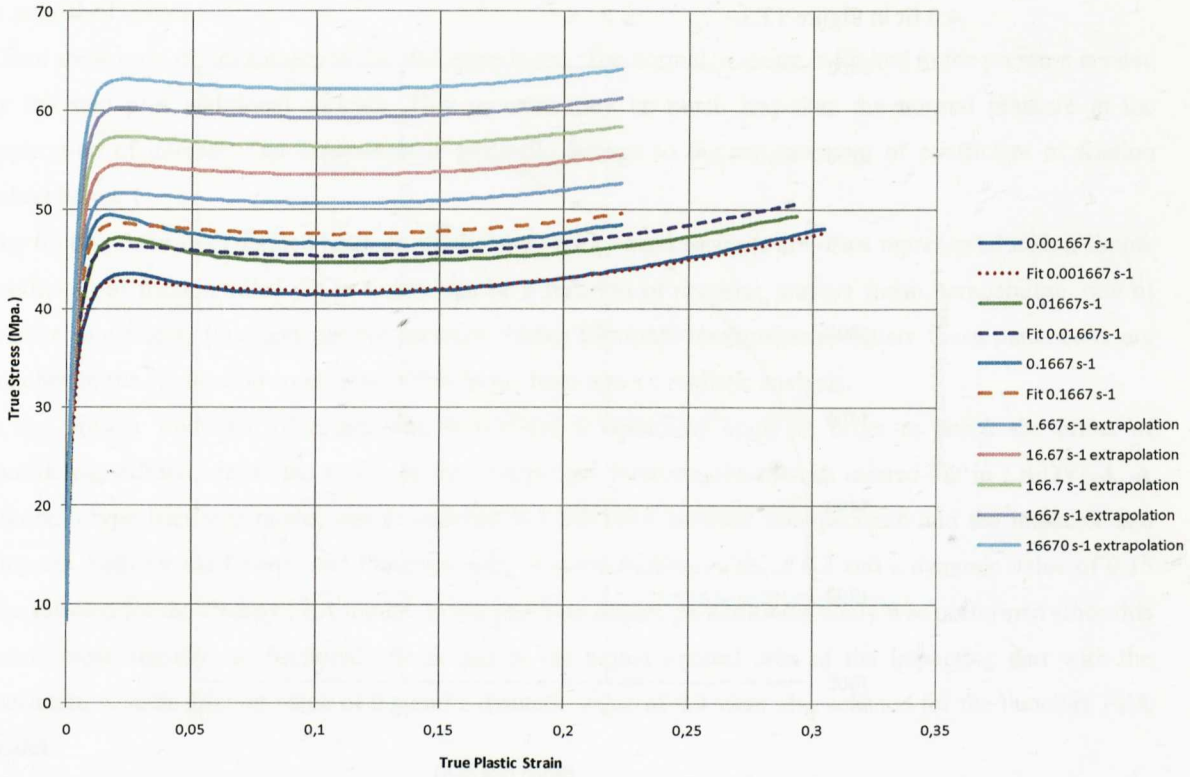

Figure 12.2: True stress - plastic strain curves for PC/ABS. Tensile data modellling according to ISO 18872.

The curve fits to the tested strain rates are not very precise, and optimisation of the material paramaters would be necessary for a more acceptable fit but the idea was to illustrate the possibility of constructing a series of curves with rate dependency the later input in LS-DYNA and the comparison with the basic approach of 1 static curve + yield scaling.

These curves where input in LS-DYNA for the simulation of the puncture test at the two testing speeds, obtaining very satisfactory results. See Figures 11.61 and 11.62.

12.3. Modelling elastic modulus variation with strain rate.

The ISO 18872 standard specifies a method for calculating strain rate dependent elastic modulus, which is based on extrapolating low speed data to high strain rates.

According to the standard, the variation of tensile modulus with strain rate is small for plastics materials at temperatures remote from a relaxation region. For those applications where accurate values are needed at high strain rates, these shall be determined by extrapolation of measured E values with Equation 12.1:

$$E = E_0\left(1 - k/\dot{\varepsilon}^n\right) \qquad \text{Equ. 12.1.}$$

Where E_0 is the static modulus, and k and n are parameters to be defined with a fit to experimental modulus values.

12.3.1. PP.

A check was performed in order to test if Equation 12.1 fitted adequately to the experimental modulus data measured in the iteratively corrected curves. Section 11.1.1.

A k value of -0.43, a n value of -0.34 and a R^2 value of 0.94 were obtained. See the following KaleidaGraph 4.0 fit in Figure 12.3.

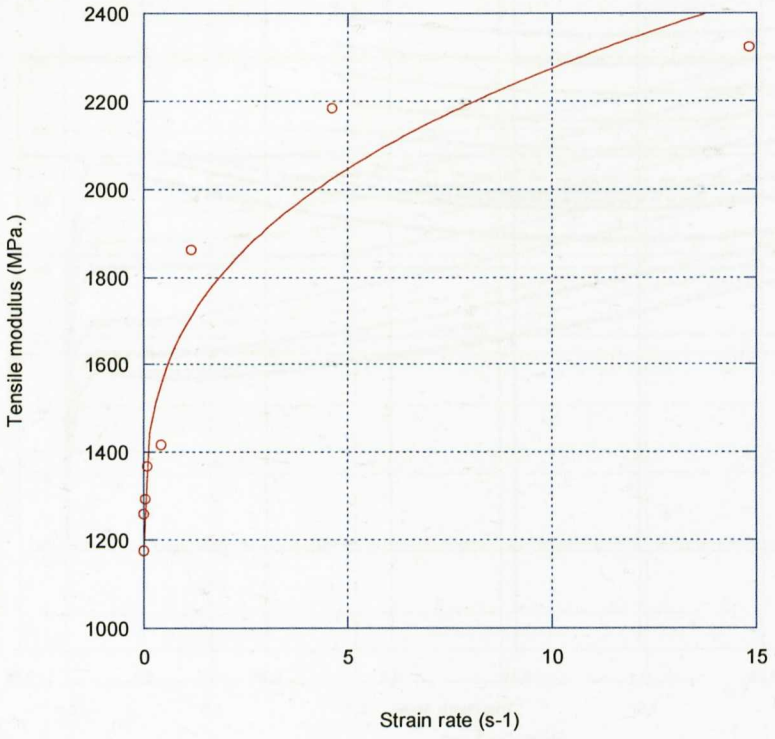

Figure 12.3: Equation 12.1 fit to experimental modulus values, PP.

The maximum tested nominal strain rate, around $15s^{-1}$ corresponded to the testing speed of 300 mm/s. Up to this strain rate the fit is adequate enough for general purposes. Care should be taken when extrapolating to higher strain rates since the tendency of the fit is to give too stiff responses.

12.3.2. PC/ABS.

No modulus variation with strain rate was observed in the experimental tests, so consequently, no mathematical modeling was performed.

12.4. A note on frictional effects in simulations.

The finite element simulations carried out in the preceding chapters were mainly focused on the study of material modeling considerations. Element type considerations were also taken into account comparing solid and shell elements. After some initial trials, fine enough mesh sizes were also used in order to capture proper flexural or puncture modes. For failure or crack arrest processes further mesh size studies are needed.

No considerations were made in respect to frictional effects, which could be important in certain applications [12]. Friction properties can be measured in standard conditions, for example, performing sled experiments as in the ISO 8295 standard. In the friction sled experiment, a sheet

of material is attached to a steel plate and dragged against a fixed surface of a second material. The normal force between the surfaces is created by the weight of the sled plus additional weights that may rest on the sled. The sliding resistance is measured using the load cell of a tensile tester that pulls the sled via a simple pulley arrangement. This is a popular friction experiment. The main advantages of the sled experiment are that the test is easy to set up and the test is easy to understand. The friction values are generally comparable to published values.

There are several disadvantages to the sled experiment. The normal pressure is limited to the pressure created by the sled plus additional weights. This pressure may be much less than the normal pressure in the application of interest. The experiment is generally limited to the measurement of coefficient of friction values below 1.

The frictional forces generated between plastic and various hard surfaces are often represented with a simple coefficient of friction value yet in reality can be a function of material, surface finish, temperature, rate of relative movement, time and normal pressure. Using frictional measurements where these parameters are matched to the application conditions will help to create a more realistic analysis.

In the present study the objective was to perform a sensitivity study in order to check the effect of considering different frictional values in the Charpy and Puncture simulations carried out in LS-DYNA. A Coulomb type frictional model was considered in LS-DYNA between the specimen and the impactor and supports, both for the Charpy and Puncture tests. A static friction value of 0.3 and a dynamic value of 0.15 was selected for the Charpy FEA model. In the puncture model, an additional study was performed since this test is more sensitive to frictional effects due to the higher contact area of the impacting dart with the specimen. A static friction value of 0.6 and a dynamic value of 0.3 were also selected for the Puncture FEA model

The simplest material modeling consideration was selected for comparing frictional effects; use of a single base quasi-static stress-strain curve. For notched specimens, strain rate effects and failure were also considered.

12.4.1. Charpy test simulation considering frictional effects.

For PP, force-time results can be observed from Figures 12.4 to 12.7, both for un-notched and notched specimens at the two tested speeds of 1.1 and 4.4 m/s.

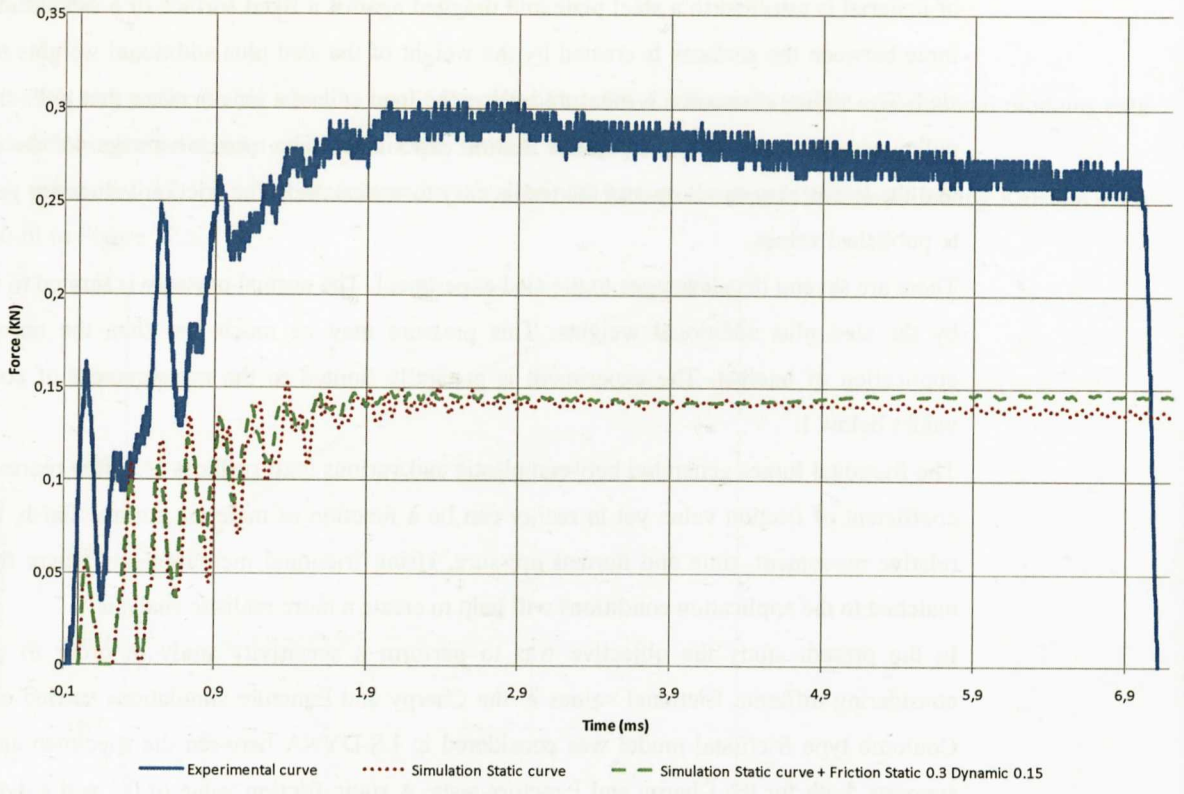

Figure 12.4: Force-time results including frictional effects. Un-notched specimen, lower speed, PP.

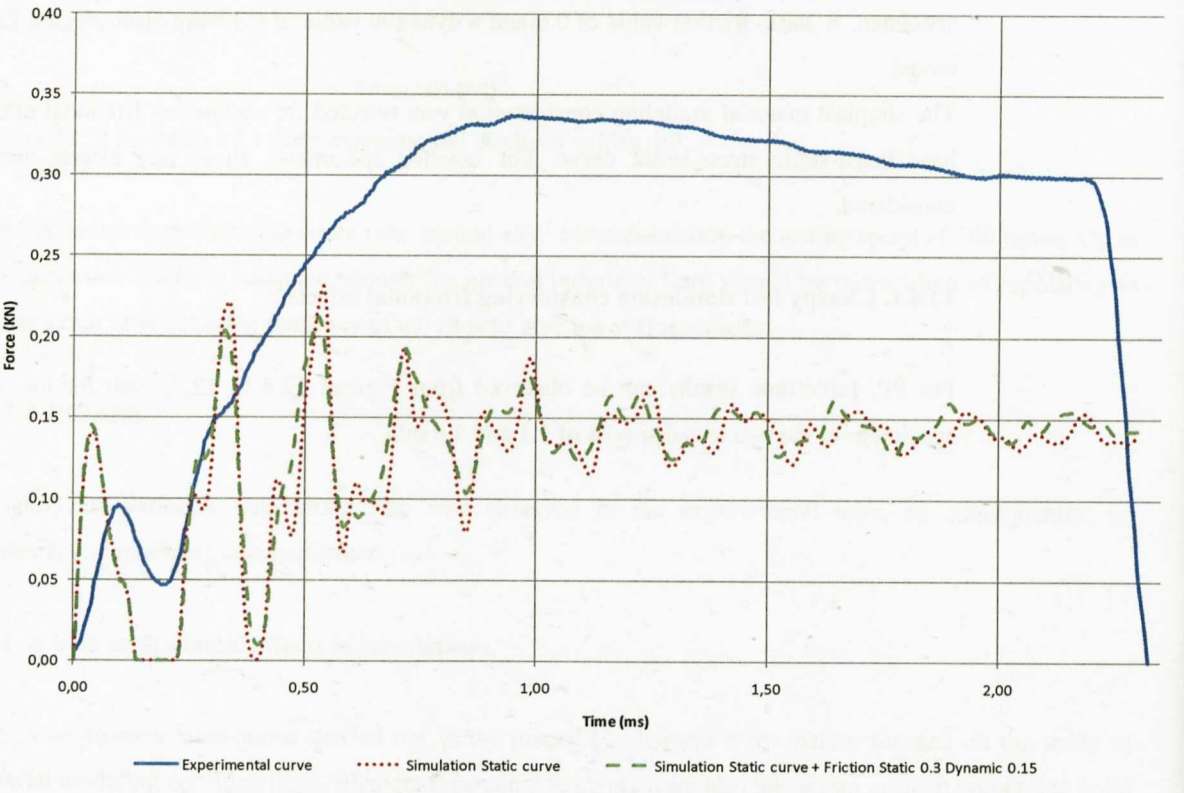

Figure 12.5: Force-time results including frictional effects. Un-notched specimen, higher speed, PP.

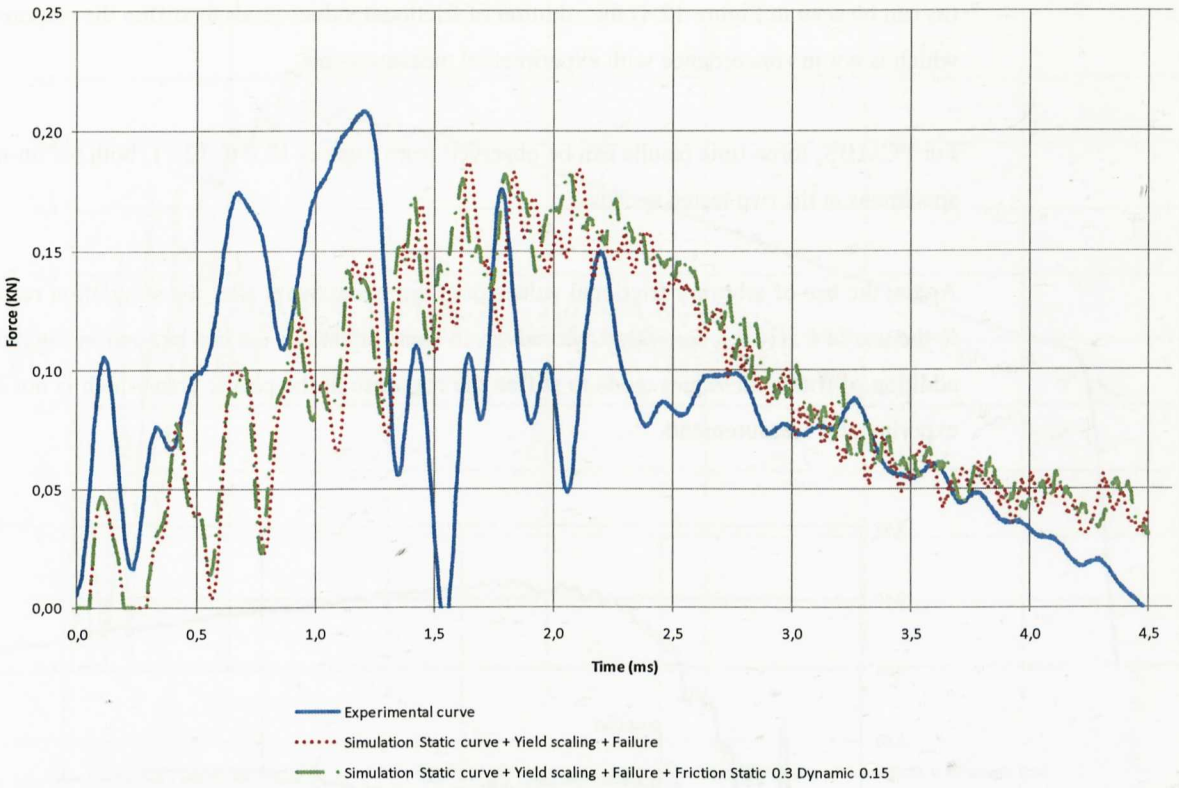

Figure 12.6: Force-time results including frictional effects. Notched specimen, lower speed, PP.

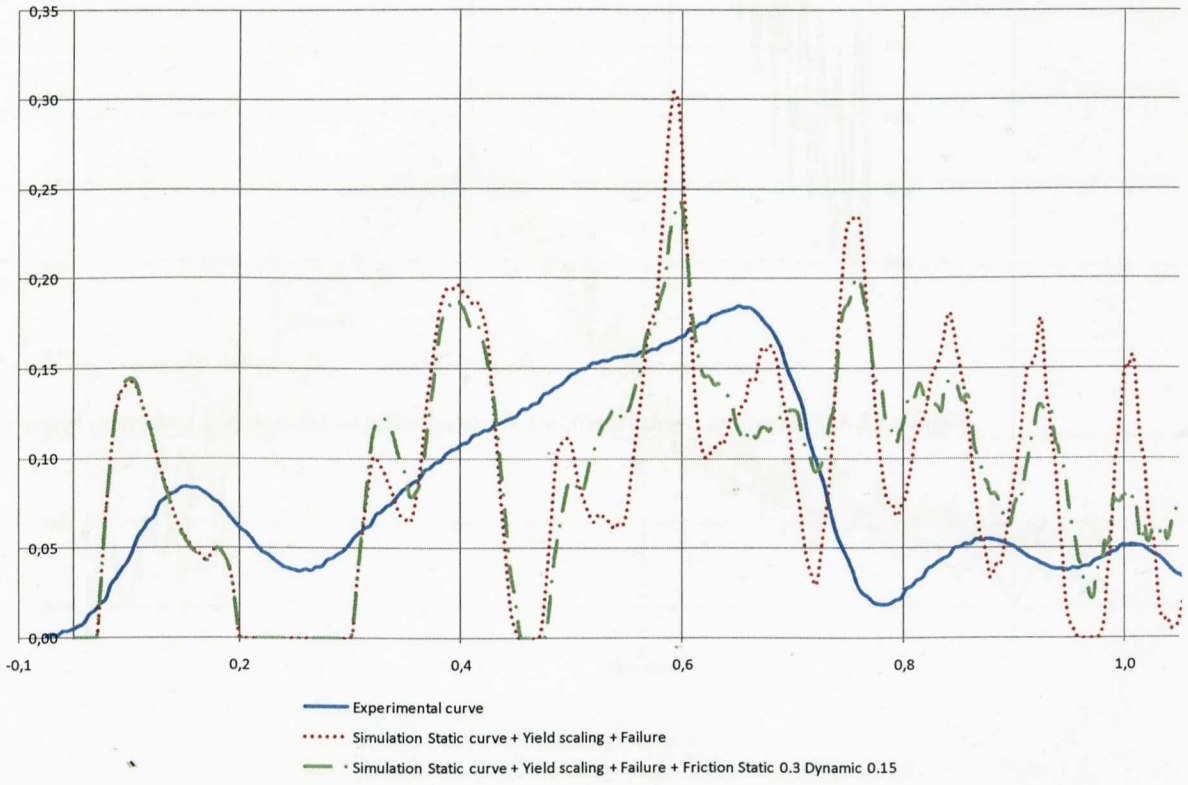

Figure 12.7: Force-time results including frictional effects. Notched specimen, higher speed, PP.

It can be observed that for Charpy test simulations, the use of arbitrary frictional values does not excessively alter the simulation response in comparison to the use of a zero friction value. Moreover, in some situations

(as can be seen in Figure 12.4) the addition of frictional values tends to stiffen the response in the plastic area which is not in concordance with experimental measurements.

For PC/ABS, force-time results can be observed from Figures 12.8 to 12.11, both for un-notched and notched specimens at the two tested speeds.

Again, the use of arbitrary frictional values does not excessively alter the simulation response in comparison to the use of a zero friction value. Moreover, in some situations (as can be seen in Figures 12.8 and 12.9) the addition of frictional values tends to stiffen the response in the plastic area which is not in concordance with experimental measurements.

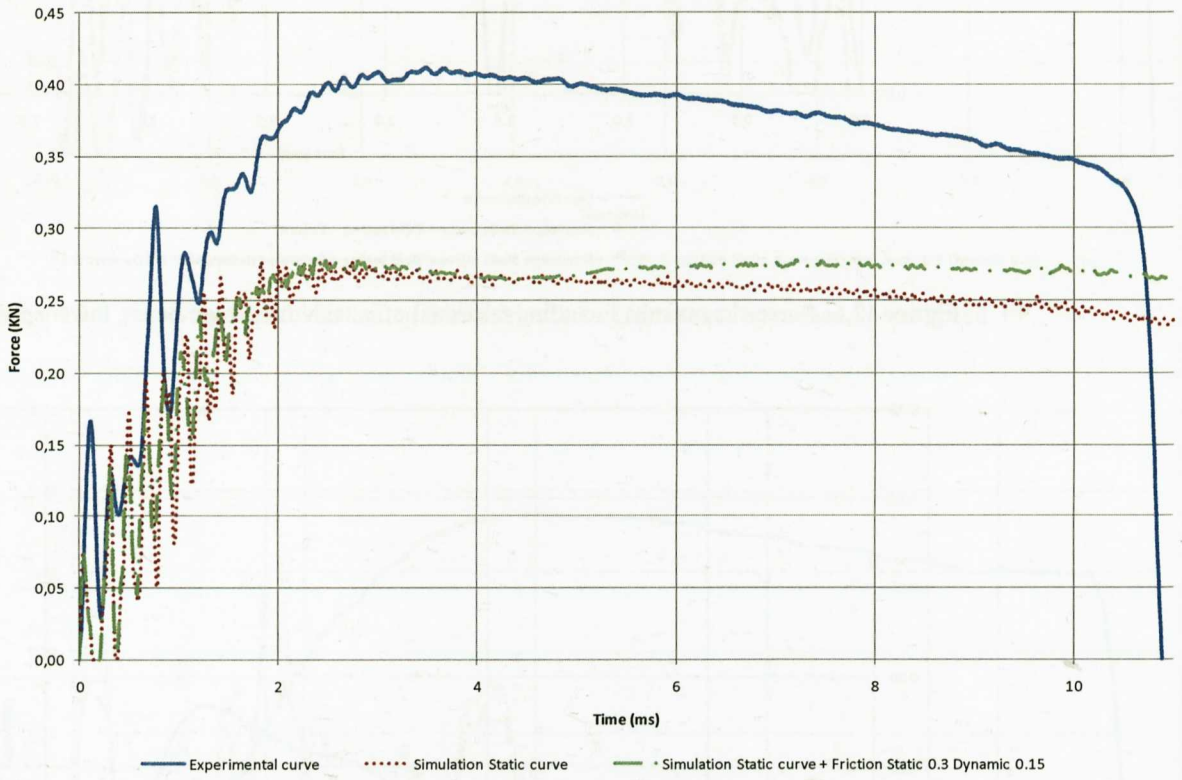

Figure 12.8: Force-time results including frictional effects. Un-notched specimen, lower speed, PC/ABS.

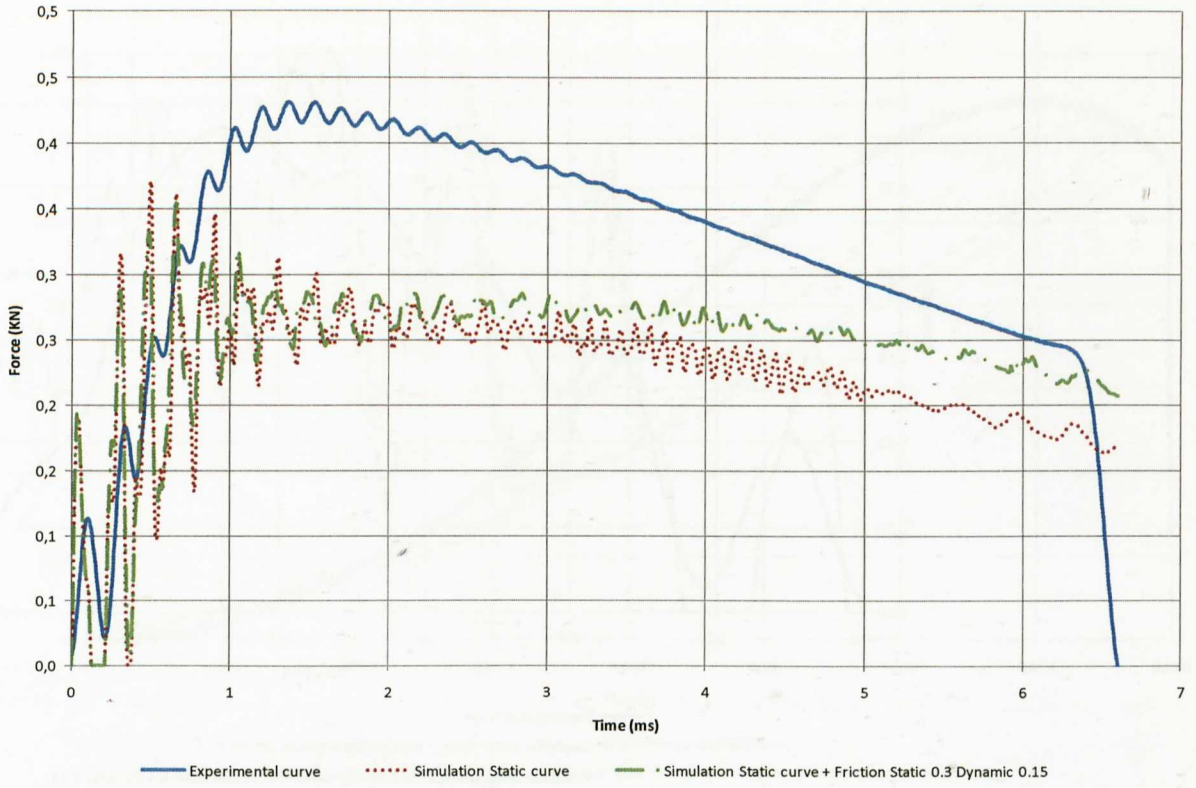

Figure 12.9: Force-time results including frictional effects. Un-notched specimen, higher speed, PC/ABS.

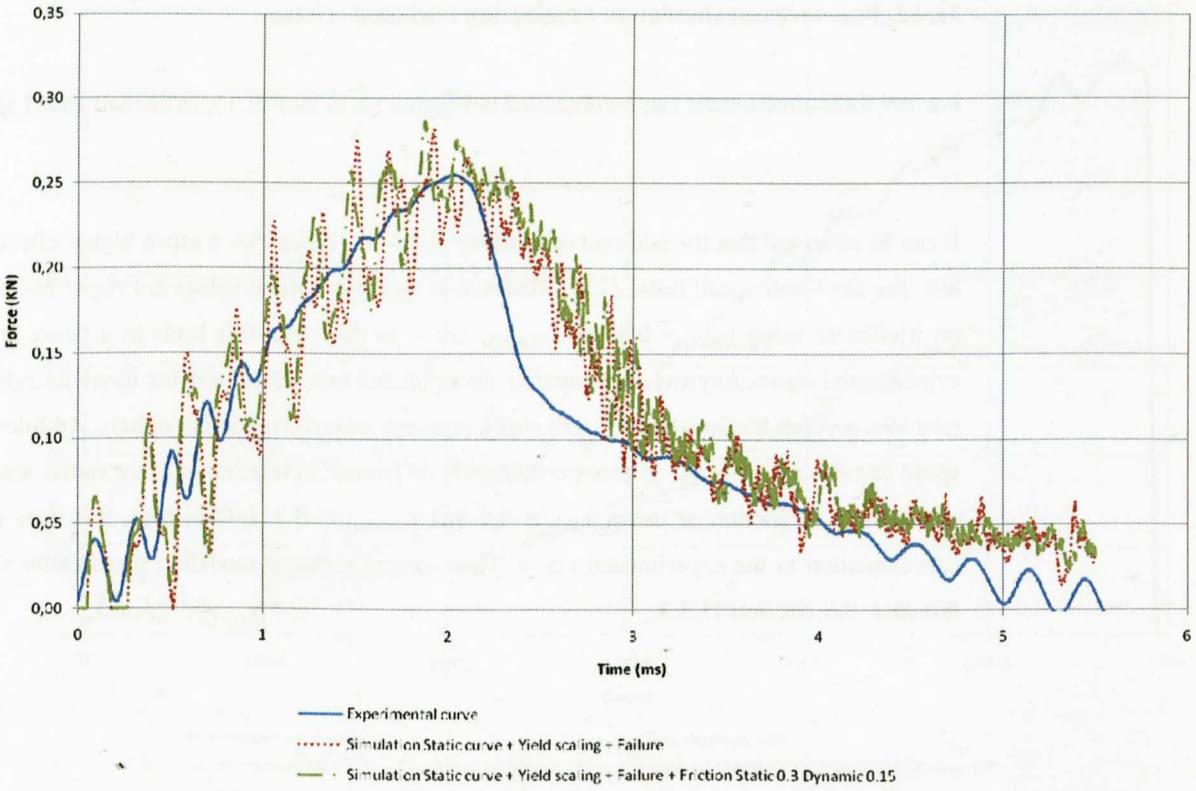

Figure 12.10: Force-time results including frictional effects. Notched specimen, lower speed, PC/ABS.

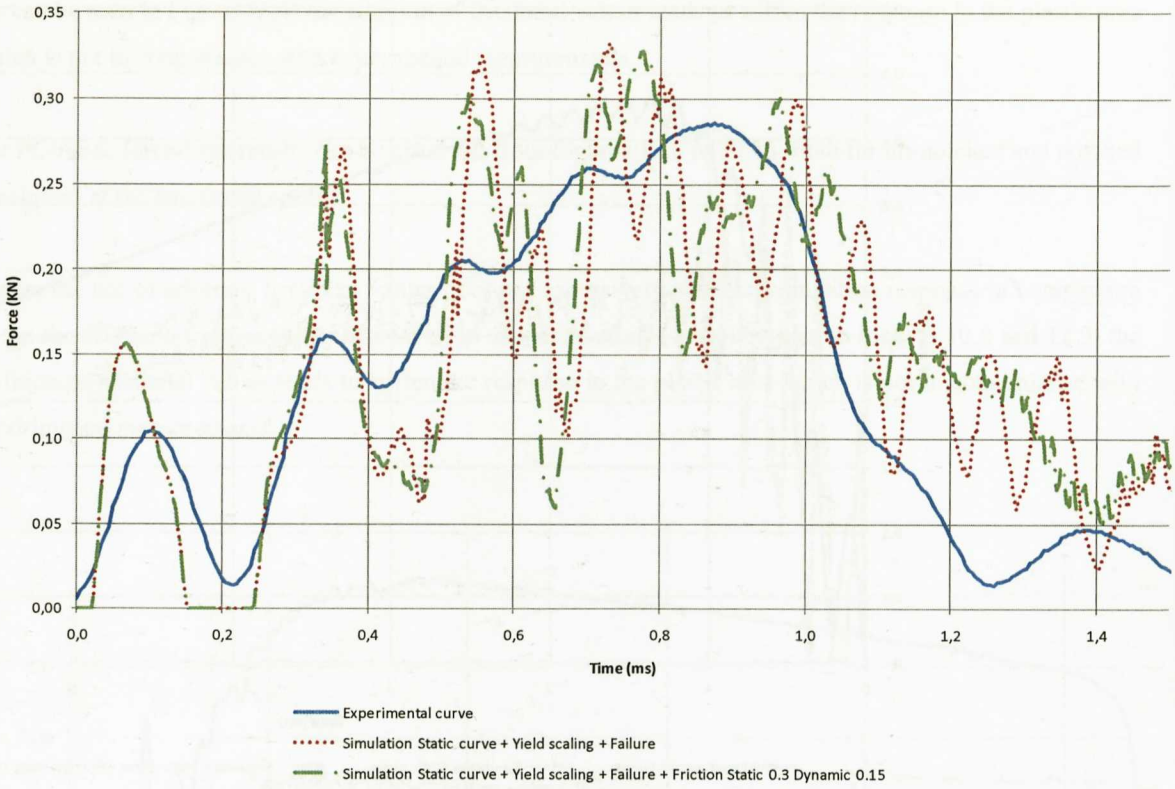

Figure 12.11: Force-time results including frictional effects. Notched specimen, higher speed, PC/ABS.

12.4.2. Puncture test simulation considering frictional effects.

For PP, force-time results can be observed in Figures 12.12 and 12.13, at the two tested speeds of 1.1 and 4.4 m/s.

It can be observed that the addition of arbritary frictional values has a much higher effect than in the Charpy test. For the lower speed tests, 17% difference in maximum force values are registered between considering no friction or using $\mu_{static} = 0.6$ and $\mu_{dynamic} = 0.3$. In this case, this leads to a better approximation to the experimental curve. Anyway, this could be not predicted beforehand and the usual consideration is first not to take into account frictional effects and check properly material modeling effects. Additionally, for the higher speed test this effect is not so pronounced; 10% difference in maximum force values are registered between considering no friction or using $\mu_{static} = 0.6$ and $\mu_{dynamic} = 0.3$. In this case, this does not lead to a better approximation to the experimental curve. Thus, proper material modeling gives better simulation results in this case. See Section 11.3.3.

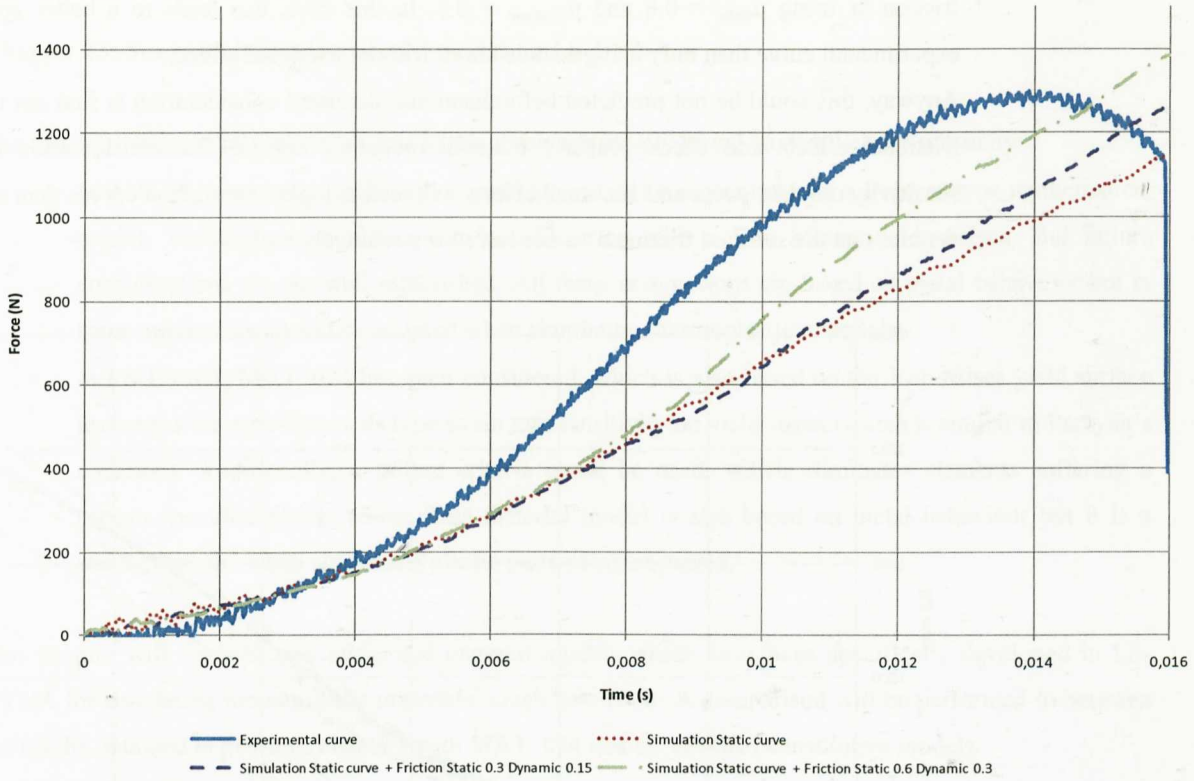

Figure 12.12: Force-time results including frictional effects. Lower speed, PP.

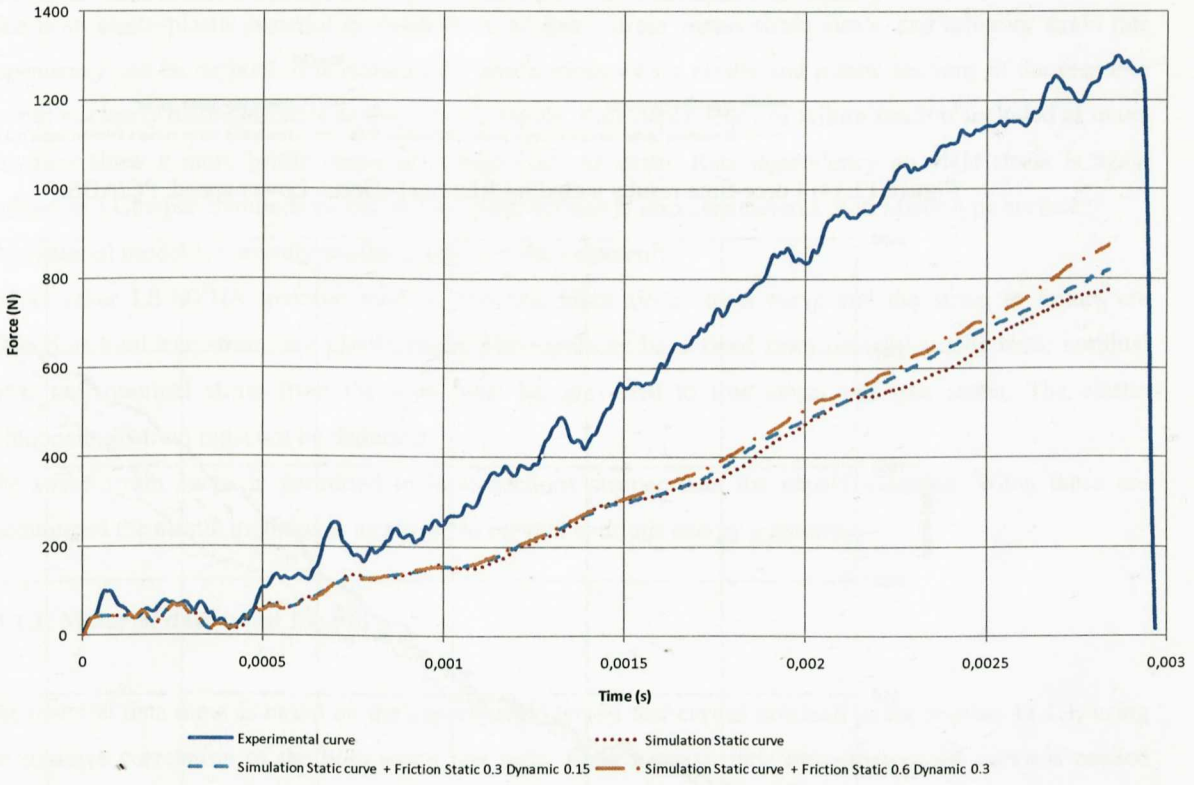

Figure 12.13: Force-time results including frictional effects. Higher speed, PP.

For PC/ABS, force-time results can be observed in Figures 12.14 and 12.15, at the two tested speeds.

Again, the addition of arbitrary frictional values has a much higher effect than in the Charpy test. Both for the lower and higher test speeds, 19% difference in maximum force values are registered between considering no

friction or using μ_{static} = 0.6 and $\mu_{dynamic}$ = 0.3. In this case, this leads to a better approximation to the experimental curve than only using a static curve without frictional effects.

Anyway, this could be not predicted beforehand and the usual consideration is first not to take into account frictional effects and check properly material modeling effects. The consideration of both strain rate sensitivity on yield stress and frictional effects will lead to higher simulation curves than experimental, which denotes that the selected frictional values have been relatively high.

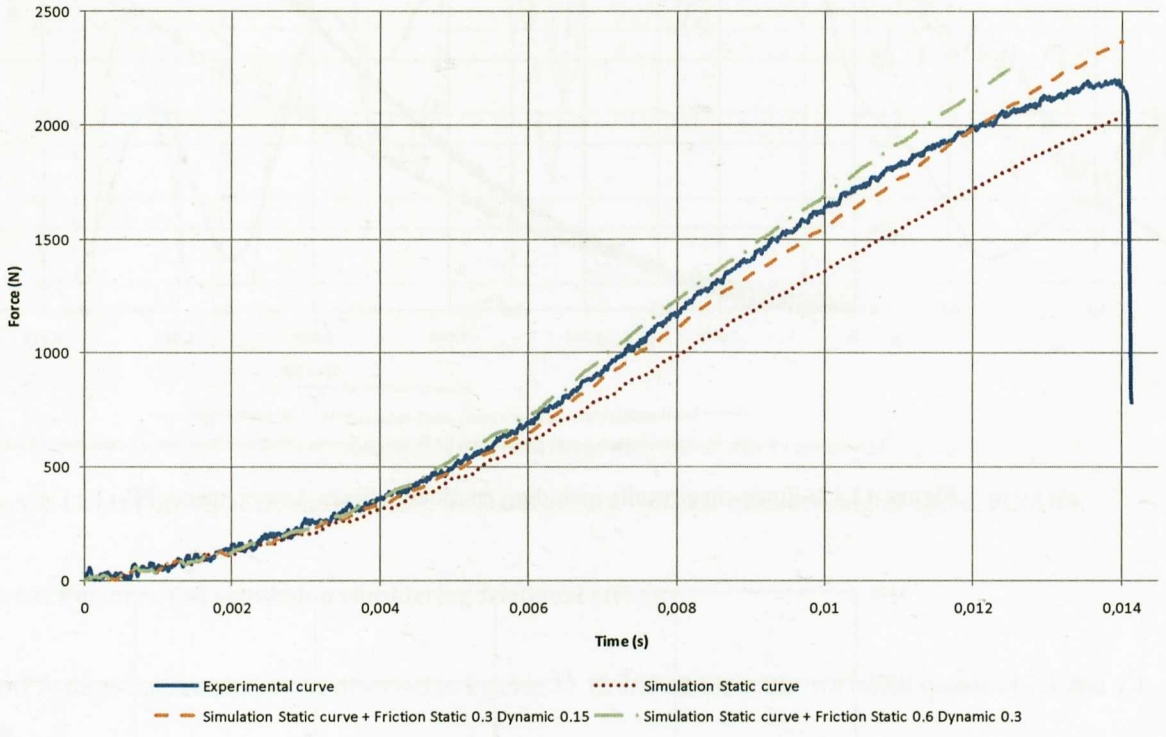

Figure 12.14: Force-time results including frictional effects. Lower speed, PC/ABS.

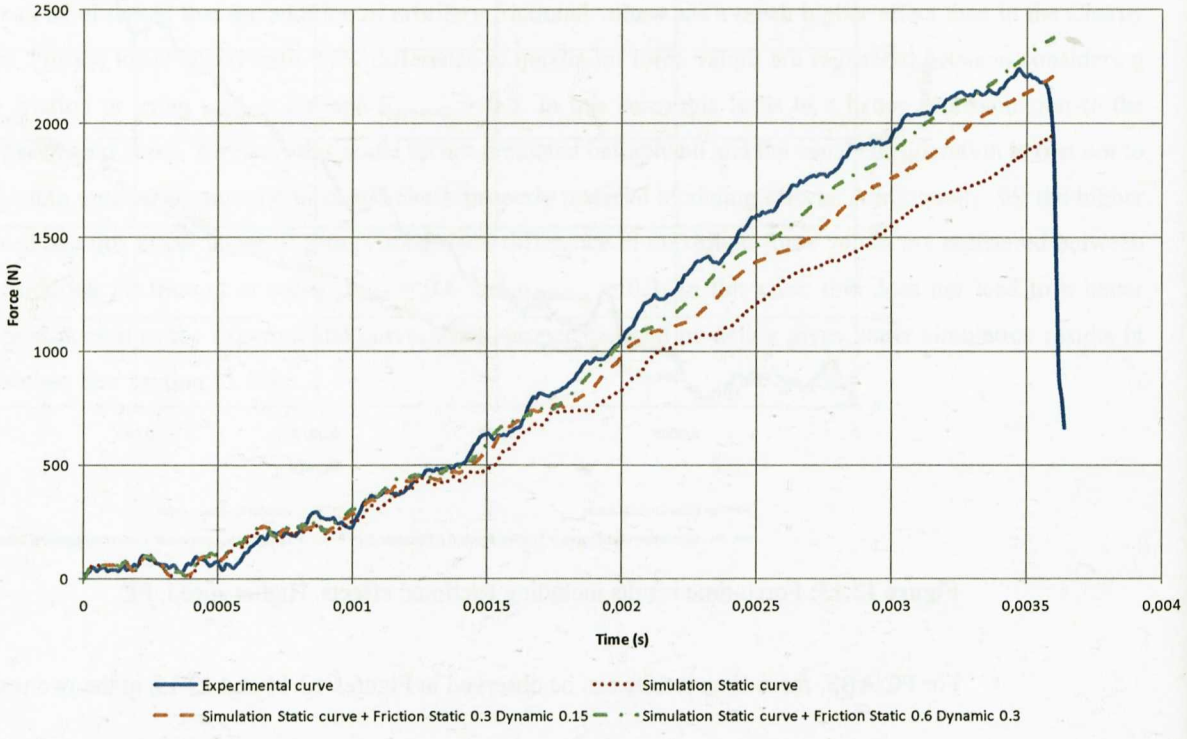

Figure 12.15: Force-time results including frictional effects. Higher speed, PC/ABS.

Chapter 13: Study of different material models in LS-DYNA.

The constitutive material models studied in this thesis are mainly based on metal elasto-plasticity:

- In ANSYS, strain rate sensitivity on yield stress can be accounted with a Perzyna type mathematical model. Yielding can be taken into consideration with a Von Mises yield surface. But failure considerations are not well established. All these assumptions are based on metal behaviour but in some applications could be adopted when simulating thermoplastic materials.
- In LS-DYNA, MAT_024 has been considered, which is also based on the Von-Mises yield surface and uses a Cowper-Symonds type strain rate sensitivity on yield stress (which is similar to Perzyna's equation). Additionally, a failure criteria could be used, which eliminates elements suffering a certain specified plastic strain. This material model is also based on metal behaviour but it is a standard model when simulating plastic parts being impacted.

This chapter will describe two additional material models which have been specifically developed in LS-DYNA for simulating thermoplastic materials' crash behaviour. A comparison will be performed in between the results obtained in previous chapters with MAT_024 and the selected constitutive models.

13.1. MAT_089 (*MAT_PLASTICITY_POLYMER).

This is an elasto-plastic material model with an arbitrary stress versus strain curve, and arbitrary strain rate dependency can be defined. It is intended for applications where elastic and plastic sections of the response are not as clearly distinguishable as they are for metals. Rate dependency of failure strain is included as many polymers show a more brittle response at high rates of strain. Rate dependency on yield stress is again defined as a Cowper-Symonds model and the yield surface is also considered a Von Mises type surface.
The material model is currently available only for shell elements.
Unlike other LS-DYNA material models, both the input stress-strain curve and the strain to failure are defined as total true strain, not plastic strain. The input can be defined from uniaxial tensile tests; nominal stress and nominal strain from the tests must be converted to true stress and true strain. The elastic component of strain must not be deducted.
The stress strain curve is permitted to have sections steeper than the elastic modulus. When these are encountered the elastic modulus is increased to prevent spurious energy generation.

13.1.1. Material data input for PP.

The material data input is based on the experimental tensile test curves obtained in the Section 11.1.1, using the iterative correlation of the high strain rate tests. First, a quasi-static true stress-strain curve is needed which is taken from the tests performed at 0.1 mm/s. This testing speed generates a nominal strain rate of 0.002 s^{-1}. See Figure 13.1.
Additionally a curve definition is needed in LS-DYNA for the strain rate dependency on yield stress. See Figure 13.2.
Finally, another curve definition is needed for the strain rate dependency of failure strain. The definition of strain rate dependency on failure is a complicated work. The specimens tested at different testing velocities

from low to high testing speeds (0.1-300 mm/s.) present a high experimental scatter in failure strain values. Additionally, in this thesis true stress-strain curves have been virtually generated iteratively correlating the experimental force-displacement curves. This also offers some scatter in failure strain values since the process is manual and there is always a certain error between simulation and experimental results, especially when necking and failure zones are wanted to be correlated.

In this case, it could not be observed that a clear dependency between increasing strain rate or testing velocity and the resultant failure strain existed (See Figure 11.1). However, a simple curve was developed in order to check strain rate effects on failure. A very small variation on failure strain with strain rate was defined. See Figure 13.3.

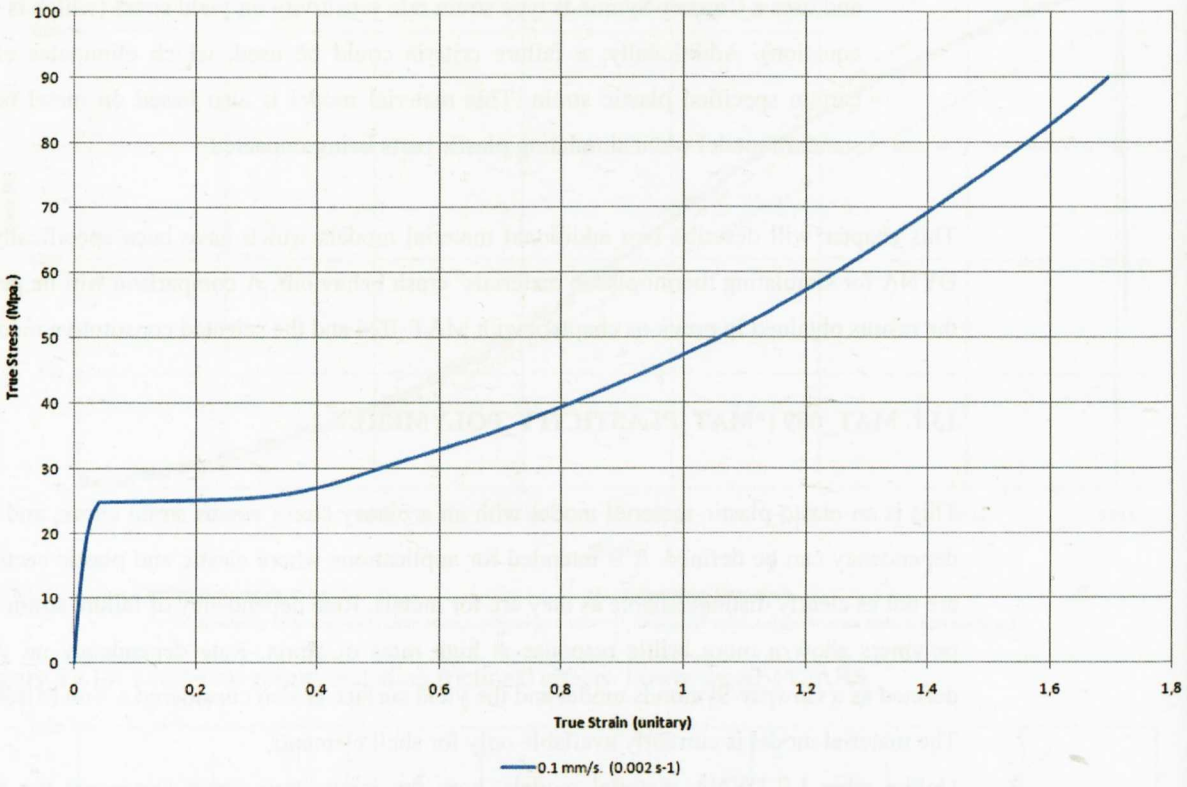

Figure 13.1: True stress – total true strain input for MAT_089 model, PP.

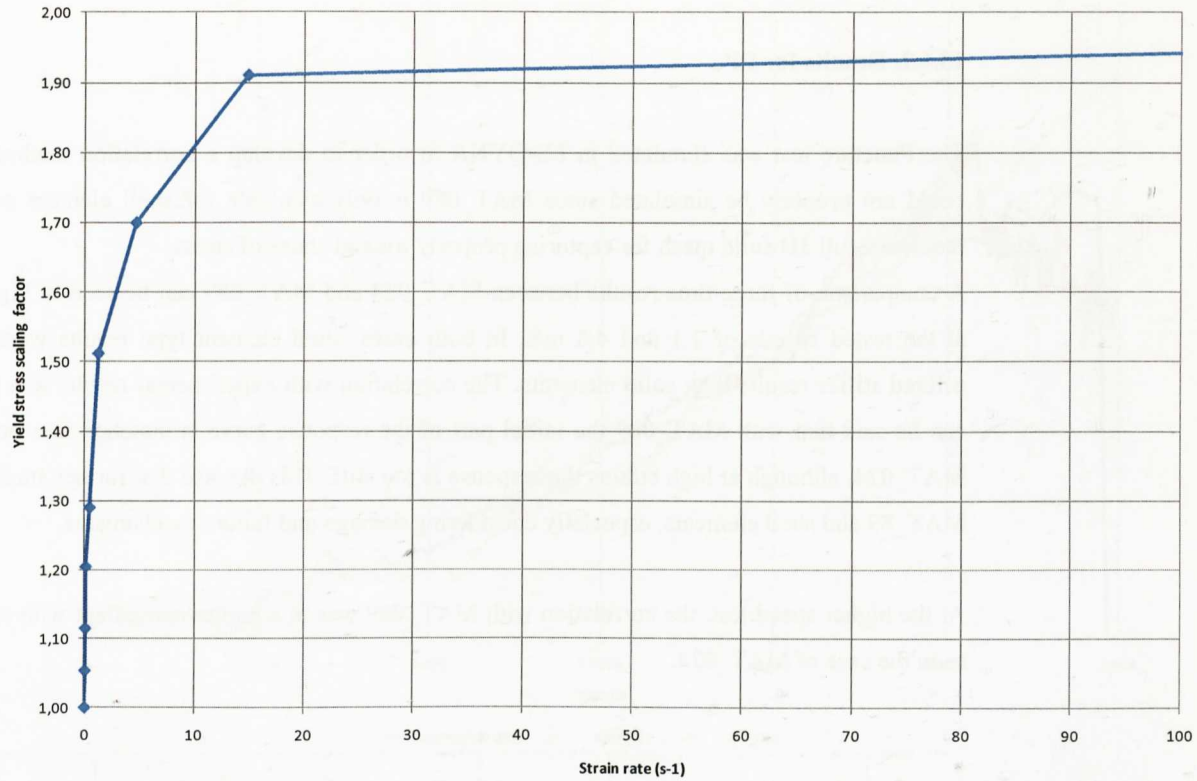

Figure 13.2: Definition of strain rate dependency on yield stress for MAT_089 model, PP.

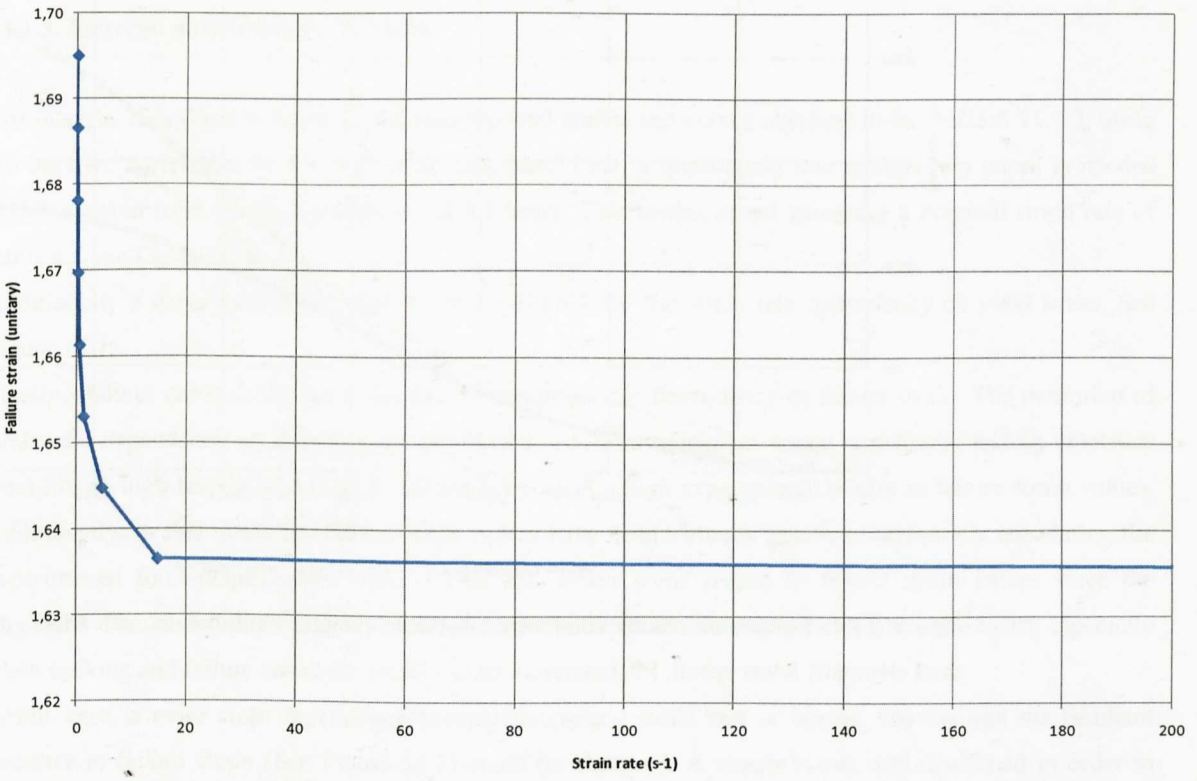

Figure 13.3: Definition of strain rate dependency on failure strain for MAT_089 model, PP.

13.1.2. Results for PP.

The Puncture test was simulated in LS-DYNA in order to develop a correlation method. The Charpy test could not properly be simulated since MAT_089 is only available for shell element and the Charpy test requires a full 3D solid mesh for capturing properly triaxial states of stress.

A comparison of force-time results between MAT_024 and MAT_089 can be seen in Figures 13.4 and 13.5 at the tested speeds of 1.1 and 4.4 m/s. In both cases, shell element type results were compared, which offered stiffer results than solid elements. The correlation with experimental results was not adequate but it can be said that with MAT_089 the initial part of the response curve is matched in a better way than with MAT_024, although at high strains the response is too stiff. This denotes that further studies are needed with MAT_89 and shell elements, especially considering damage and failure mechanisms.

At the higher speed test, the correlation with MAT_089 was in a higher agreement with experimental results as in the case of MAT_024.

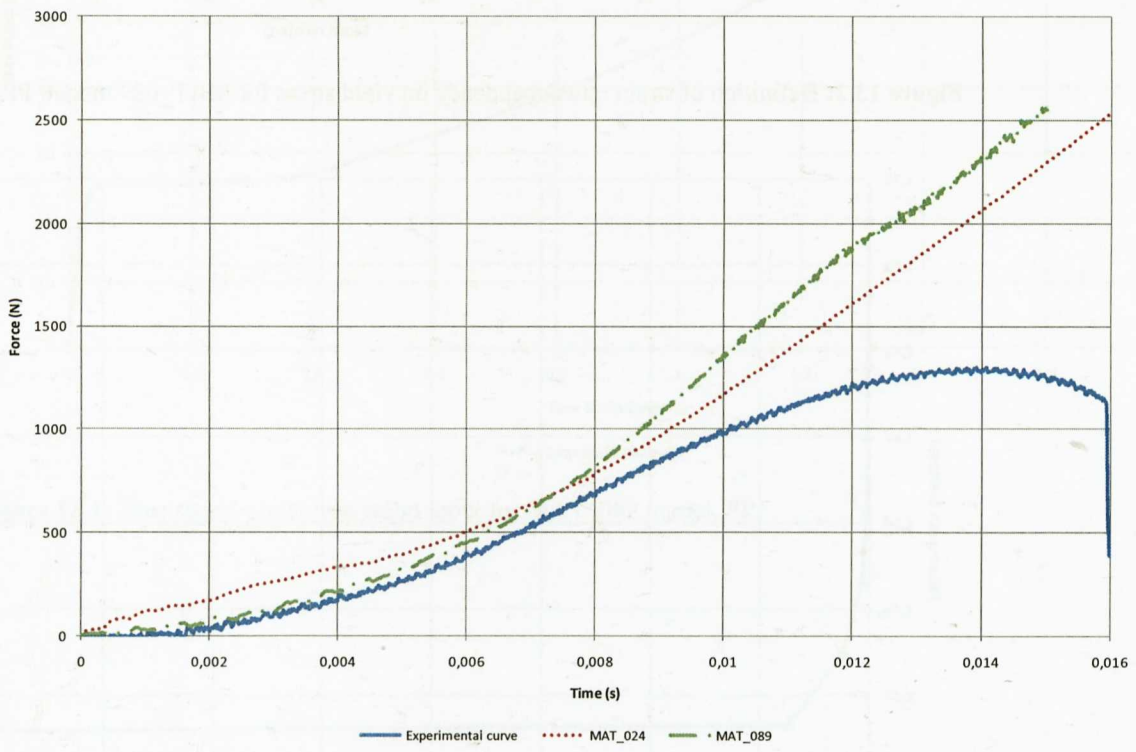

Figure 13.4: Force-time results comparison between puncture simulation with MAT_024 and MAT_089, shell elements, lower speed, PP.

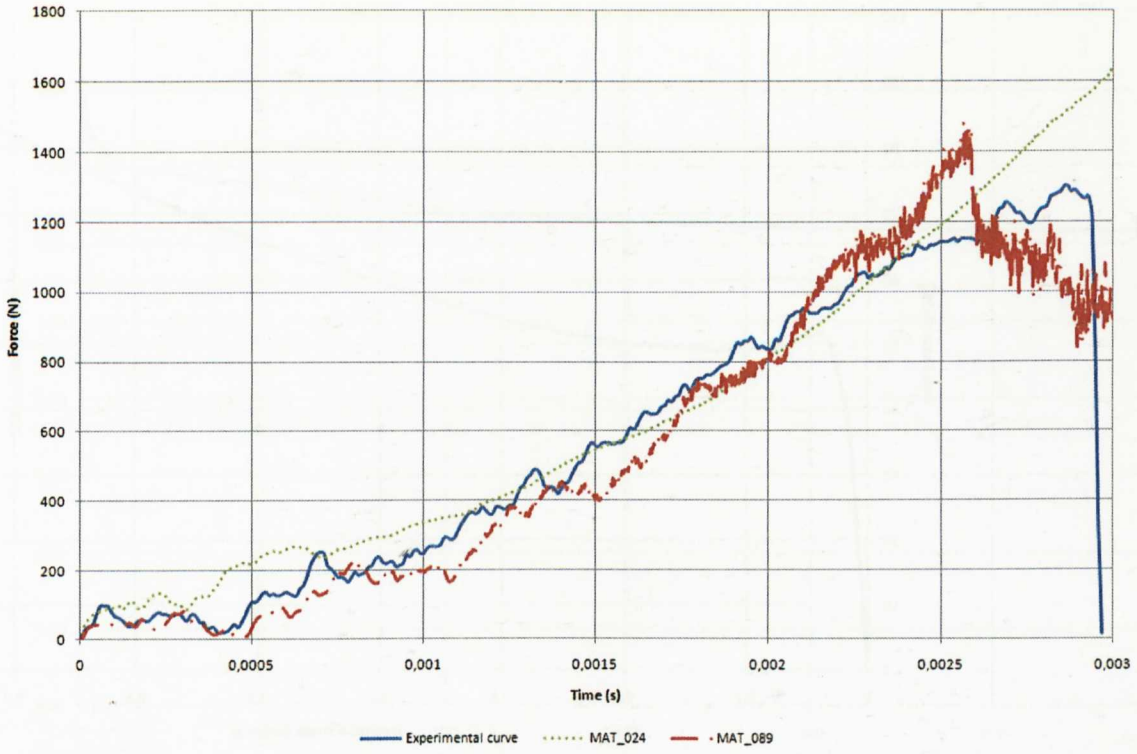

Figure 13.5: Force-time results comparison between puncture simulation with MAT_024 and MAT_089, shell elements, higher speed, PP.

13.1.3. Material data input for PC/ABS.

The material data input is based on the experimental tensile test curves obtained in the Section 11.1.2, using the iterative correlation of the high strain rate tests. First, a quasi-static true stress-strain curve is needed which is taken from the tests performed at 0.1 mm/s. This testing speed generates a nominal strain rate of 0.002 s^{-1}. See Figure 13.6.

Additionally a curve definition is needed in LS-DYNA for the strain rate dependency on yield stress. See Figure 13.7.

Finally, another curve definition is needed for the strain rate dependency of failure strain. The definition of strain rate dependency on failure is a complicated task. The specimens tested at different testing velocities from low to high testing speeds (0.1-300 mm/s.) present a high experimental scatter in failure strain values. Additionally, in this thesis true stress-strain curves have been virtually generated iteratively correlating the experimental force-displacement curves. This also offers some scatter in failure strain values since the process is manual and there is always a certain error between simulation and experimental results, especially when necking and failure zones are wanted to be correlated.

In this case, a more clear dependency between increasing strain rate or testing velocity and the resultant decrease in failure strain (See Figure 11.3) could be observed. A simple curve was developed in order to check strain rate effects on failure. See Figure 13.8.

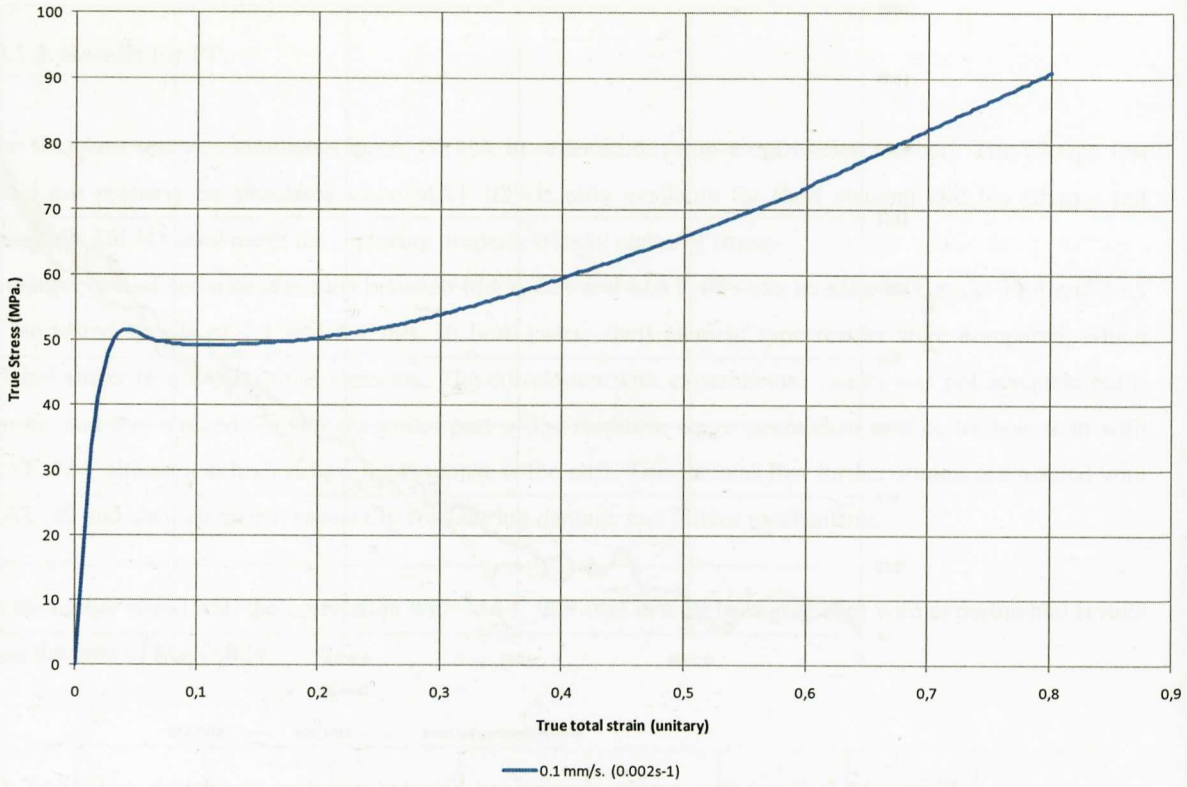

Figure 13.6: True stress – total true strain input for MAT_089 model, PC/ABS.

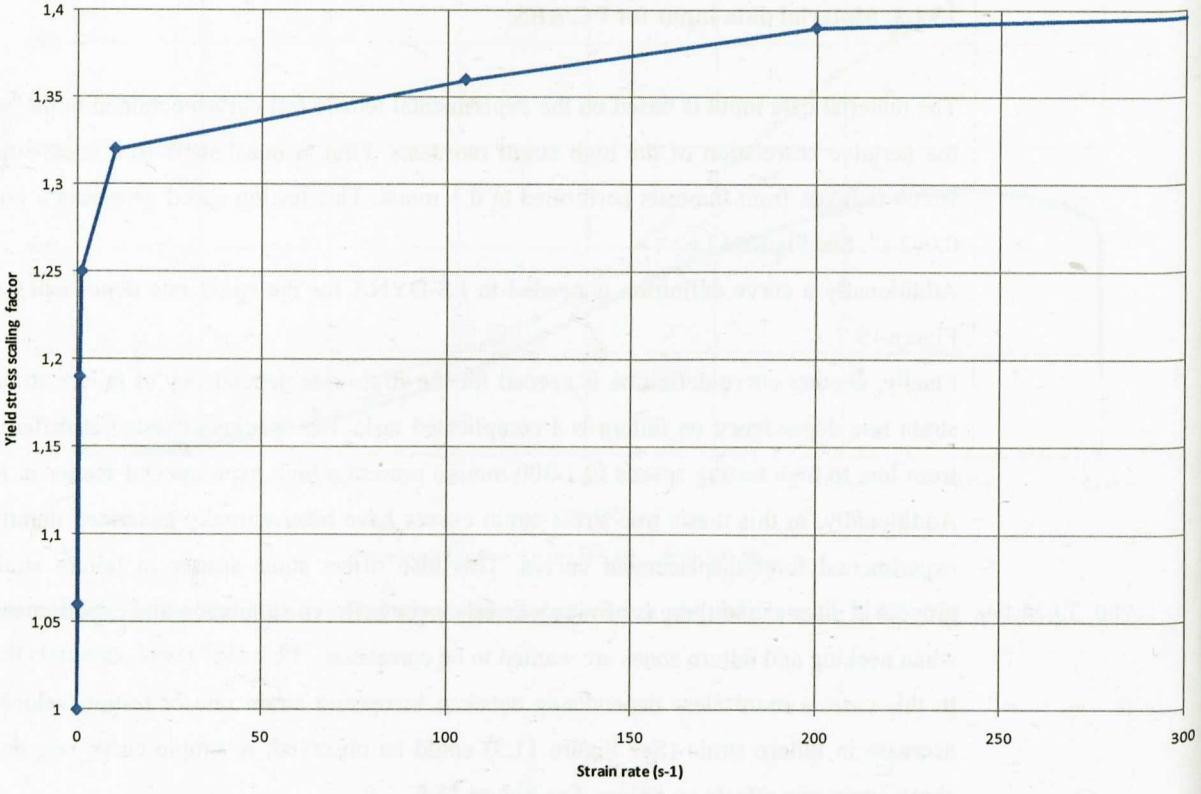

Figure 13.7: Definition of strain rate dependency on yield stress for MAT_089 model, PC/ABS.

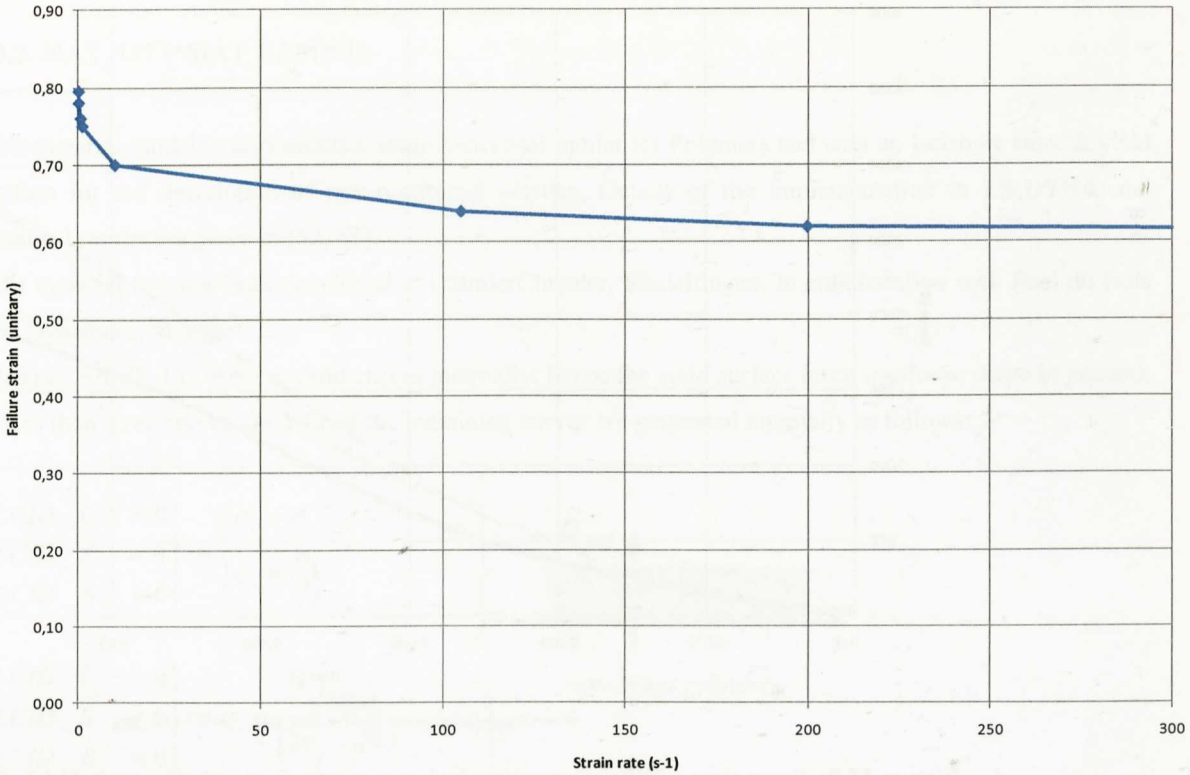

Figure 13.8: Definition of strain rate dependency on failure strain for MAT_089 model, PC/ABS.

13.1.4. Results for PC/ABS.

The Puncture test was simulated in LS-DYNA in order to develop a correlation method. Moreover, Charpy test could not properly be simulated since MAT_089 is only available for shell element and the Charpy test requires a full 3D solid mesh for capturing properly triaxial states of stress.

A comparison of force-time results between MAT_024 and MAT_089 can be seen in Figures 13.9 and 13.10. In both cases, shell element type results were compared, which offered stiffer results than solid elements. The correlation with experimental results was not adequate but it can be said that with MAT_089 the initial part of the response curve is matched in a better way than with MAT_024, although at high strains the response is too stiff. This denotes that further studies are needed with MAT_89 and shell elements, especially considering damage and failure mechanisms.

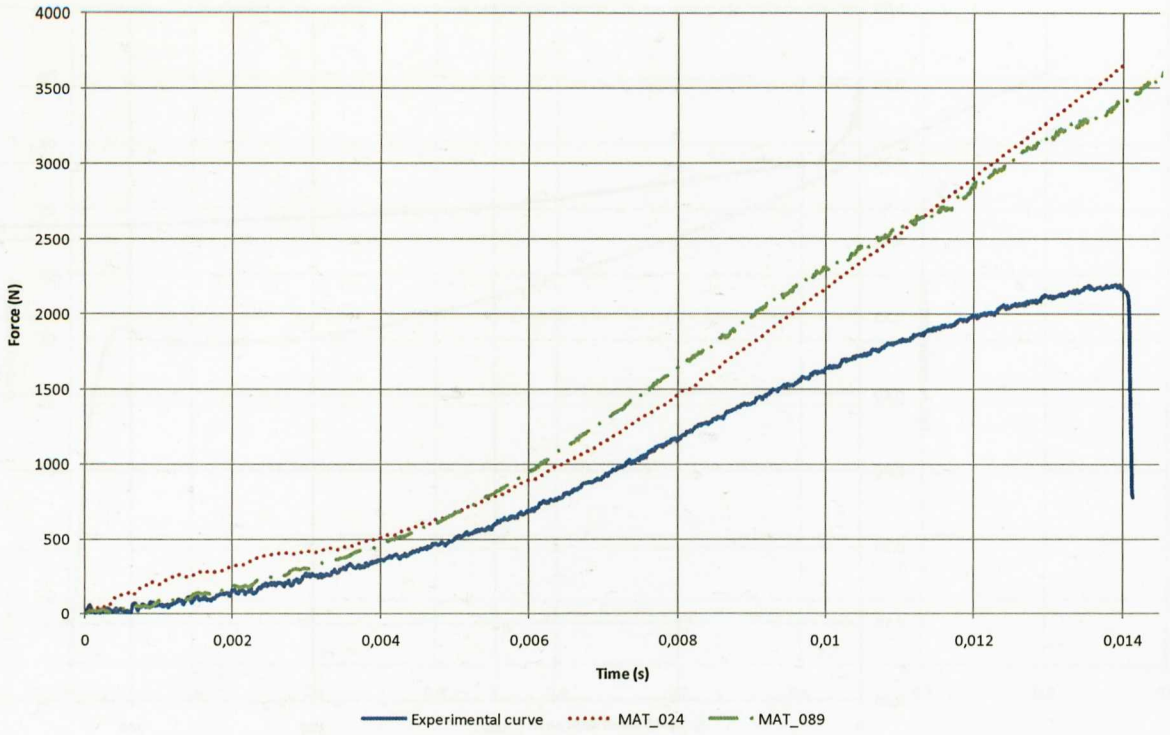

Figure 13.9: Force-time results comparison between puncture simulation with MAT_024 and MAT_089, shell elements, lower speed, PC/ABS.

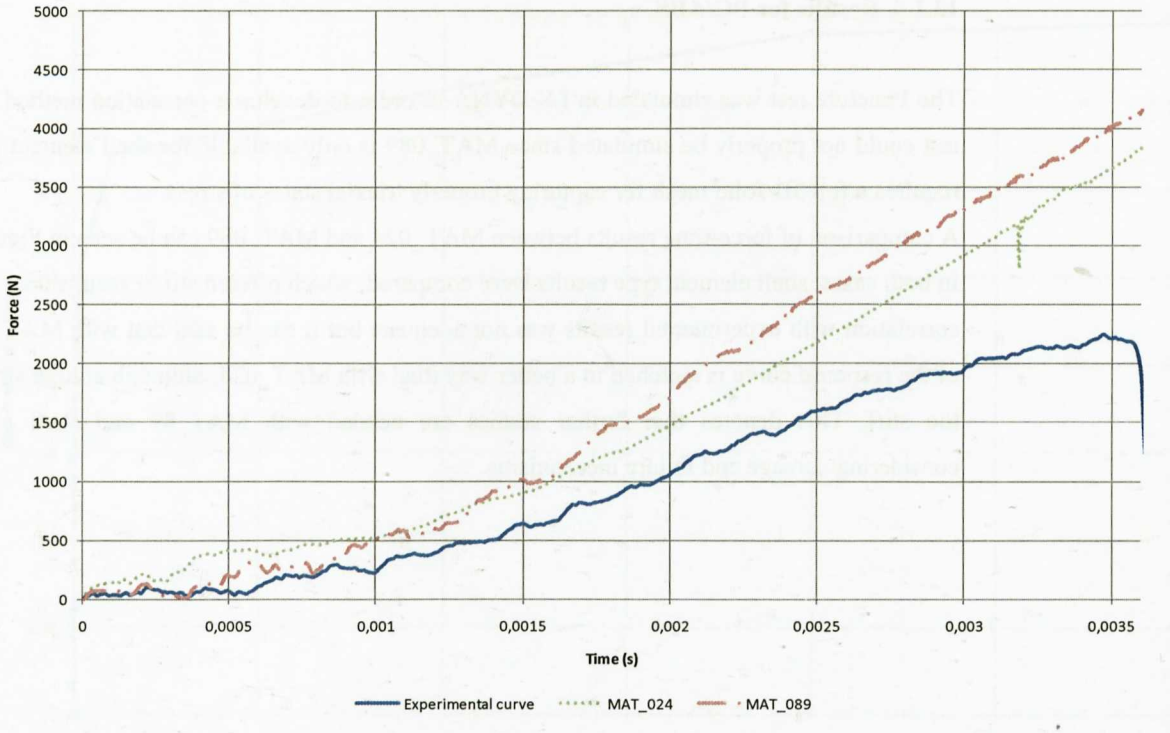

Figure 13.10: Force-time results comparison between puncture simulation with MAT_024 and MAT_089, shell elements, higher speed, PC/ABS.

13.2. MAT_187 (*MAT_SAMP-1)

This material model is also called a Semi-Analytical model for Polymers and uses an isotropic smooth yield surface for the description of non-reinforced plastics. Details of the implementation in LS-DYNA and obtained results are given in [52, 53].

This material law has been developed at DaimlerChrysler, Sindelfingen, in collaboration with Paul du Bois and Dynamore, Stuttgart.

Material SAMP-1 uses three yield curves internally; hence the yield surface has a quadratic shape in general. If less than three curves are defined the remaining curves are generated internally as follows:

$$\left.\begin{array}{ll} LCID\_C & =0 \\ LCID\_S & =0 \\ LCID\_B & =0 \end{array}\right\} \Rightarrow \begin{cases} \sigma_c = \sigma_t \\ \sigma_s = \dfrac{\sigma_t}{\sqrt{3}} \end{cases}$$

$$\left.\begin{array}{ll} LCID\_C & =0 \\ LCID\_S & \neq 0 \\ LCID\_B & =0 \end{array}\right\} \Rightarrow \sigma_c = \frac{\sqrt{3}\sigma_t\sigma_s}{\left(2\sigma_t - \sqrt{3}\sigma_s\right)}$$

$$\left.\begin{array}{ll} LCID\_C & \neq 0 \\ LCID\_S & =0 \\ LCID\_B & =0 \end{array}\right\} \Rightarrow \sigma_s = \frac{2\sigma_t\sigma_c}{\sqrt{3}\left(\sigma_t + \sigma_c\right)}$$

$$\left.\begin{array}{ll} LCID\_C & =0 \\ LCID\_S & =0 \\ LCID\_B & \neq 0 \end{array}\right\} \Rightarrow \begin{cases} \sigma_c = \dfrac{\sigma_t\sigma_b}{\left(3\sigma_b - 2\sigma_t\right)} \\ \sigma_s = \dfrac{\sigma_t\sigma_b}{\sqrt{3}\left(2\sigma_b - \sigma_t\right)} \end{cases}$$

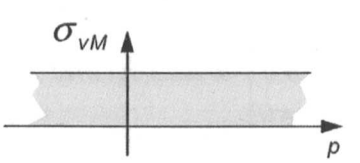

von Mises cylinder

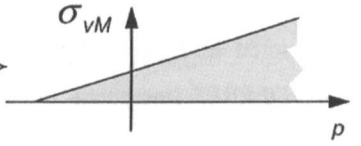

Drucker-Prager cone

Figure 13.11: SAMP-1 material model, generation of yield surfaces depending on the input stress-strain curves. LCID_C (compression curve), LCID_S (shear curve) and LCID_B (biaxial curve).

A linear yield surface in the invariant space spanned by the pressure and the Von Mises stress is generated using the available data point.

If more than two load curves are available, the following cases can be distinguished.

$$
\left.\begin{array}{ll} LCID\_C & \neq 0 \\ LCID\_S & = 0 \\ LCID\_B & = 0 \end{array}\right\} \Rightarrow SAMP-1
$$

$$
\left.\begin{array}{ll} LCID\_C & \neq 0 \\ LCID\_S & = 0 \\ LCID\_B & \neq 0 \end{array}\right\} \Rightarrow \sigma_s \frac{1}{\sqrt{3}} \sqrt{\frac{3\sigma_b^2 \sigma_c \sigma_t}{(2\sigma_b + \sigma_c)(2\sigma_b - \sigma_t)}}
$$

$$
\left.\begin{array}{ll} LCID\_C & = 0 \\ LCID\_S & \neq 0 \\ LCID\_B & \neq 0 \end{array}\right\} \Rightarrow \sigma_c = \frac{6\left(162\sigma_b^2\sigma_s^2 + \sigma_b\sigma_s^2\sigma_t\right)}{6\sigma_b\sigma_s^2 + 323\sigma_b^2\sigma_t + 3\sigma_s^2\sigma_t}
$$

$$
\left.\begin{array}{ll} LCID\_C & \neq 0 \\ LCID\_S & \neq 0 \\ LCID\_B & \neq 0 \end{array}\right\} \Rightarrow least\ squares
$$

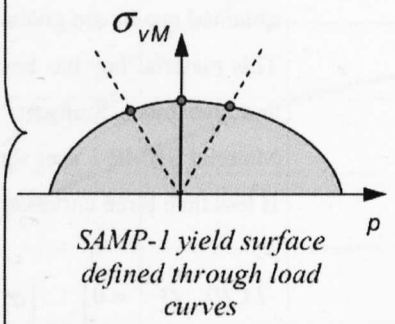

SAMP-1 yield surface defined through load curves

Figure 13.12: SAMP-1 material model, generation of yield surfaces depending on the input stress-strain curves. LCID_C (compression curve), LCID_S (shear curve) and LCID_B (biaxial curve).

If a LCID_D is given, then a damage curve as a function of equivalent plastic strain acting on the stresses is defined as depicted in Figure 13.13. EPFAIL (equivalent plastic strain at failure in the material card definition) and DEPRPT (increment of equivalent plastic strain) define the failure and fading behaviour of a single element:

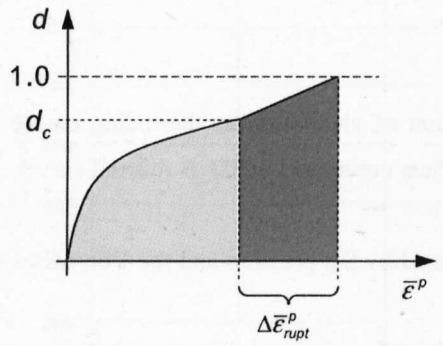

Figure 13.13: Damage parameter (d) evolution versus plastic strain.

This material model has a huge amount of input parameters and possibilities that make it difficult to handle with. The material card has 24 different parameters to fulfill which in some cases are very difficult to determine [90].

Additionally, since the generality of arbitrary curve inputs allows to generate unsolvable yield surfaces, SAMP may modify curves internally. This will always lead to warning messages at the beginning of the simulation run. One modification that is not allowed are negative tangents of the last two data points of the yield surface.

The complexity of the data input and the different parameters make it sometimes very difficult the achievement of correct simulation runs.

PP has not been studied with this material constitutive model. The material data card needs experimental data input from other test methods from tensile testing, i.e., compression, shear or biaxial test data. This data was not available for the studied PP material. However, for PC/ABS compression and shear data was available in literature [91].

13.2.1. Material data input for PC/ABS.

The material data input is based on the experimental tensile test curves obtained in the Section 11.1.2, using the iterative correlation of the high strain rate tests. Test data in Figure 11.3 was included in tabular format in order to characterize the strain rate sensitive behaviour in tension.
Additionally, a stress-strain curve from a compression test was also included. This test was performed at 0.1 mm/s and 23°C. See Figure 13.14.

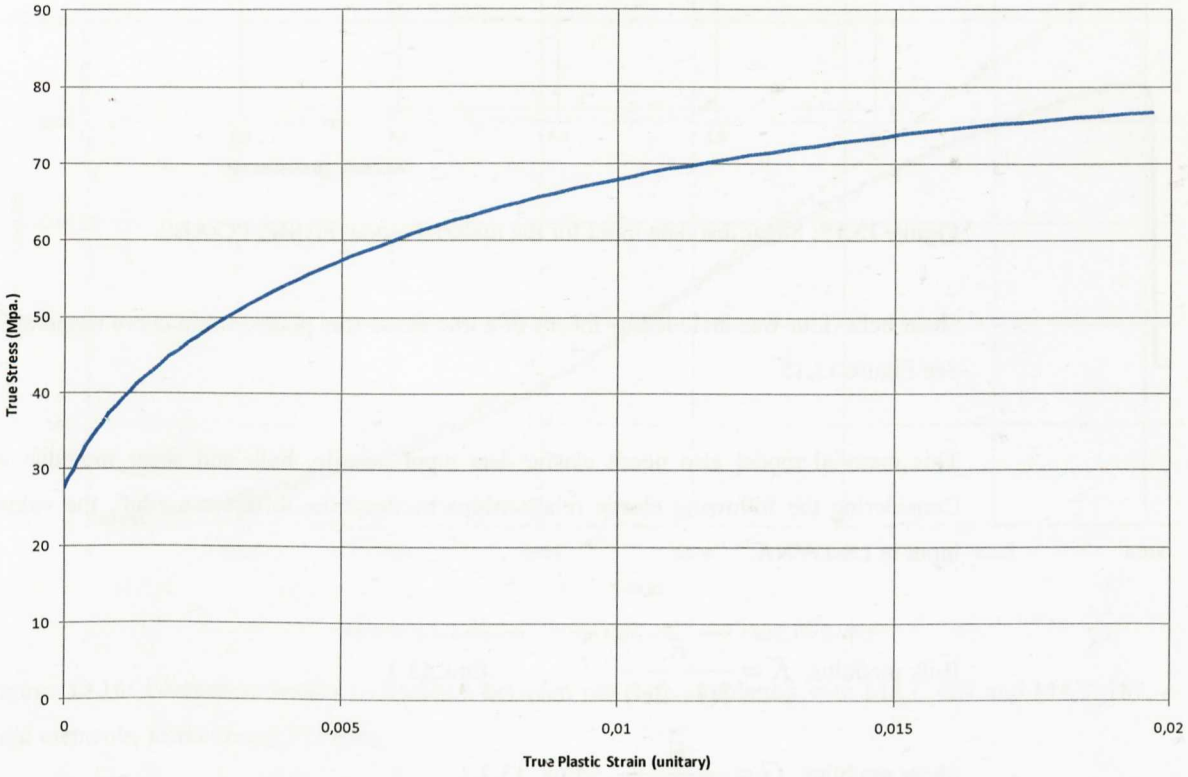

Figure 13.14: Compression test data input for the material model SAMP, PC/ABS.

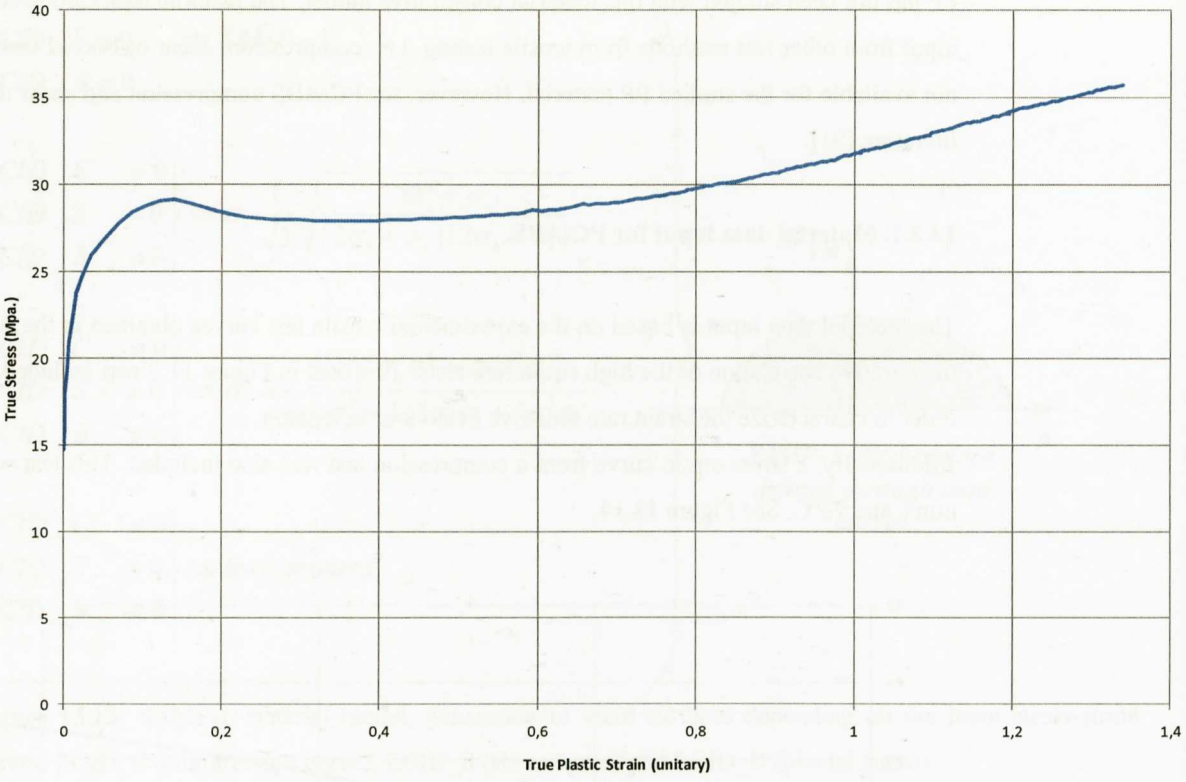

Figure 13.15: Shear test data input for the material model SAMP, PC/ABS.

Shear behaviour was included by means of a true stress-true plastic strain curve tested at 0.1 mm/s. and 23°C. See Figure 13.15.

This material model also needs elastic data input; tensile, bulk and shear modulus values are required. Considering the following elastic relationships between the different moduli, the values calculated where input in LS-DYNA.

Bulk modulus, $K = \frac{E}{3(1-2\upsilon)}$ Equ. 13.1.

Shear modulus, $G = \frac{E}{2(1+\upsilon)}$ Equ. 13.2.

Where ν is the elastic Poisson's ratio and E is the elastic tensile modulus. As E was defined to be 2520.78 Mpa., K was equal to 4201.3 MPa. and G was 900.28 MPa. (considering an elastic Poisson's ratio of 0.4 for this PC/ABS.

Although many other options are disposable in the SAMP material models only an additional parameter was included, DC=0.5, which acts like a failure plastic strain limit.
A density value of 1.1×10^{-9} Tn/mm^3 was also included.

13.2.2. Results for PC/ABS.

Puncture and Charpy tests were simulated in LS-DYNA in order to have a correlation comparison with experimental results.

13.2.2.1. Puncture test simulation.

A comparison of force-time results between MAT_024 and MAT_187 (SAMP) can be seen in Figures 13.16 and 13.17. In both cases, solid element type results were compared at the two tested speeds of 1.1 and 4.4 m/s. The simulation at the lower test speed had difficulties to complete the full run; only a portion of the full deformation curve can be compared with MAT_024, but it seems that the response with MAT_187 is stiffer than with MAT_024 and consequently does not match properly the experimental curve.

At the higher testing speed, the simulation with MAT_187 almost completes the full run. In comparison with MAT_024, the response is again stiffer and the correlation with the experimental curve is worse than using the simpler material model.

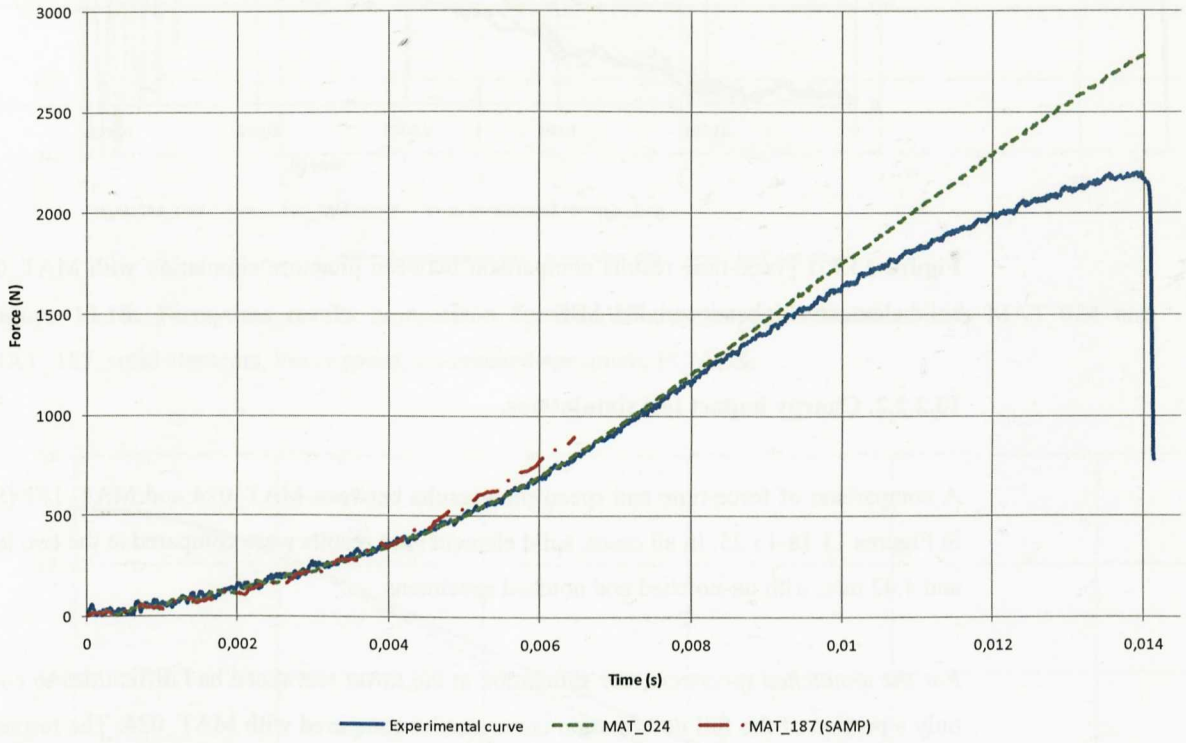

Figure 13.16: Force-time results comparison between puncture simulation with MAT_024 and MAT_187, solid elements, lower speed, PC/ABS.

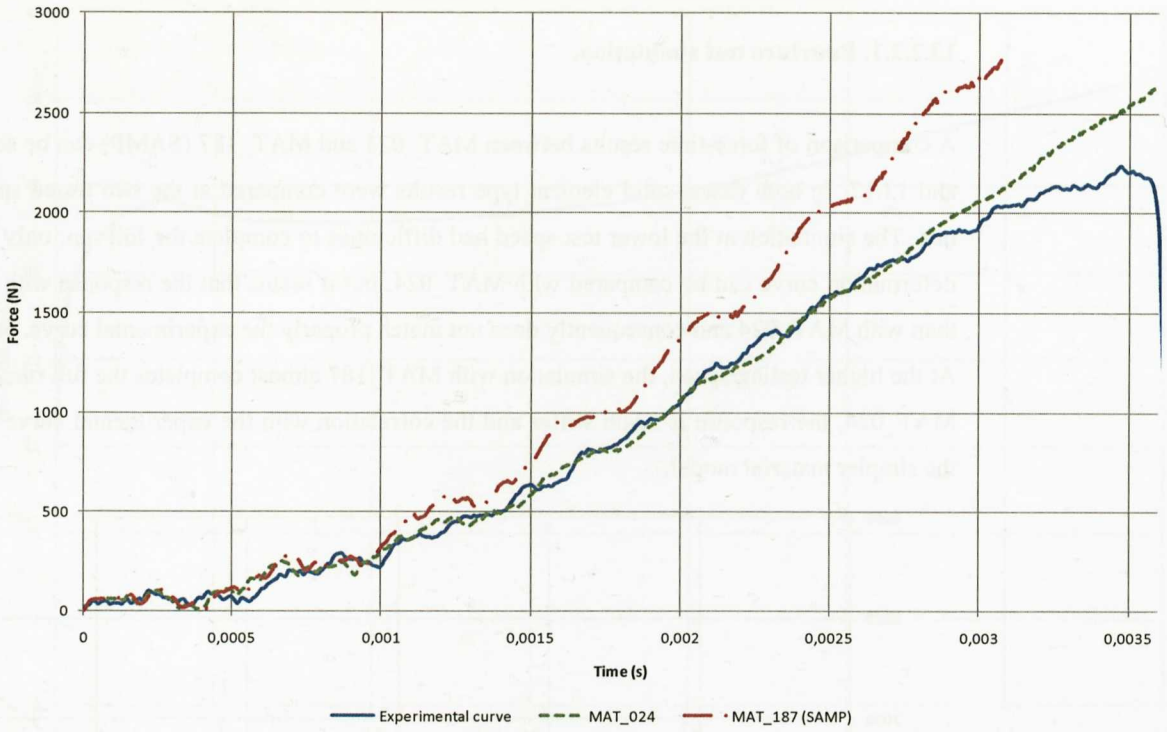

Figure 13.17: Force-time results comparison between puncture simulation with MAT_024 and MAT_187, solid elements, higher speed, PC/ABS.

13.2.2.2. Charpy impact test simulations.

A comparison of force-time and speed-time results between MAT_024 and MAT_187 (SAMP) can be seen in Figures 13.18-13.25. In all cases, solid element type results were compared at the two tested speeds of 1.75 and 4.42 m/s. with un-notched and notched specimens.

For the unnotched specimens, the simulation at the lower test speed had difficulties to complete the full run; only a portion of the full deformation curve can be compared with MAT_024. The response with MAT_187 similar to that with MAT_024; force-time curves are almost identical at the begininig although at higher deformation levels, the results with MAT_187 give lower force values. MAT_187 offers the best correlation with speed-time curves for the fully results completed.

The same considerations can be done for the test at the higher testing speed.

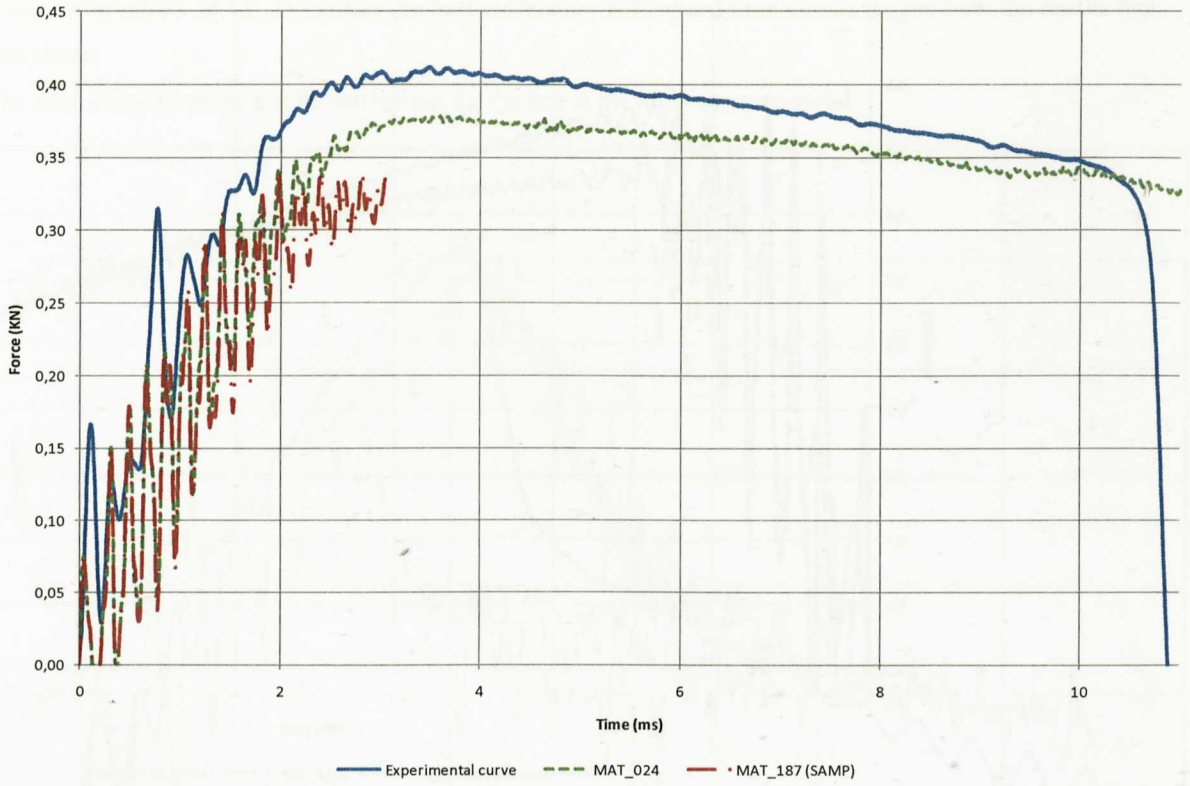

Figure 13.18: Force-time results comparison between Charpy impact simulation with MAT_024 and MAT_187, solid elements, lower speed, un-notched specimen, PC/ABS.

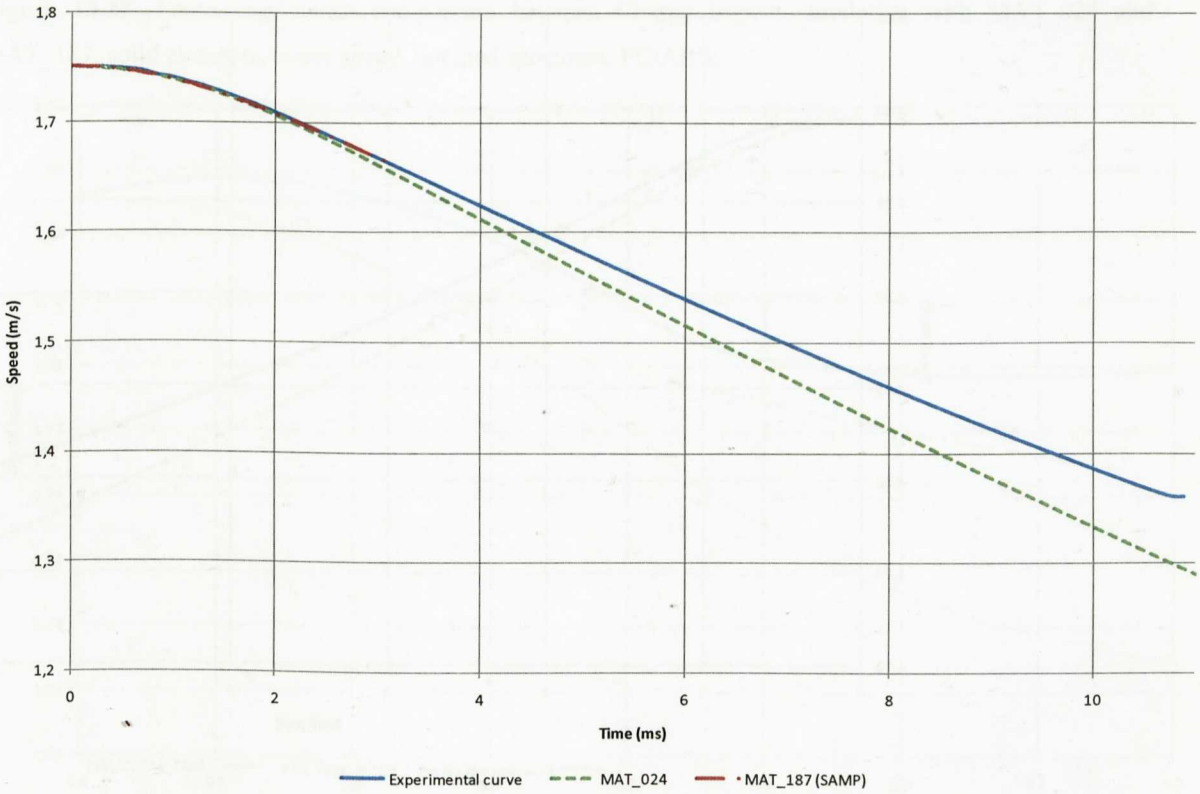

Figure 13.19: Speed-time results comparison between Charpy impact simulation with MAT_024 and MAT_187, solid elements, lower speed, un-notched specimen, PC/ABS.

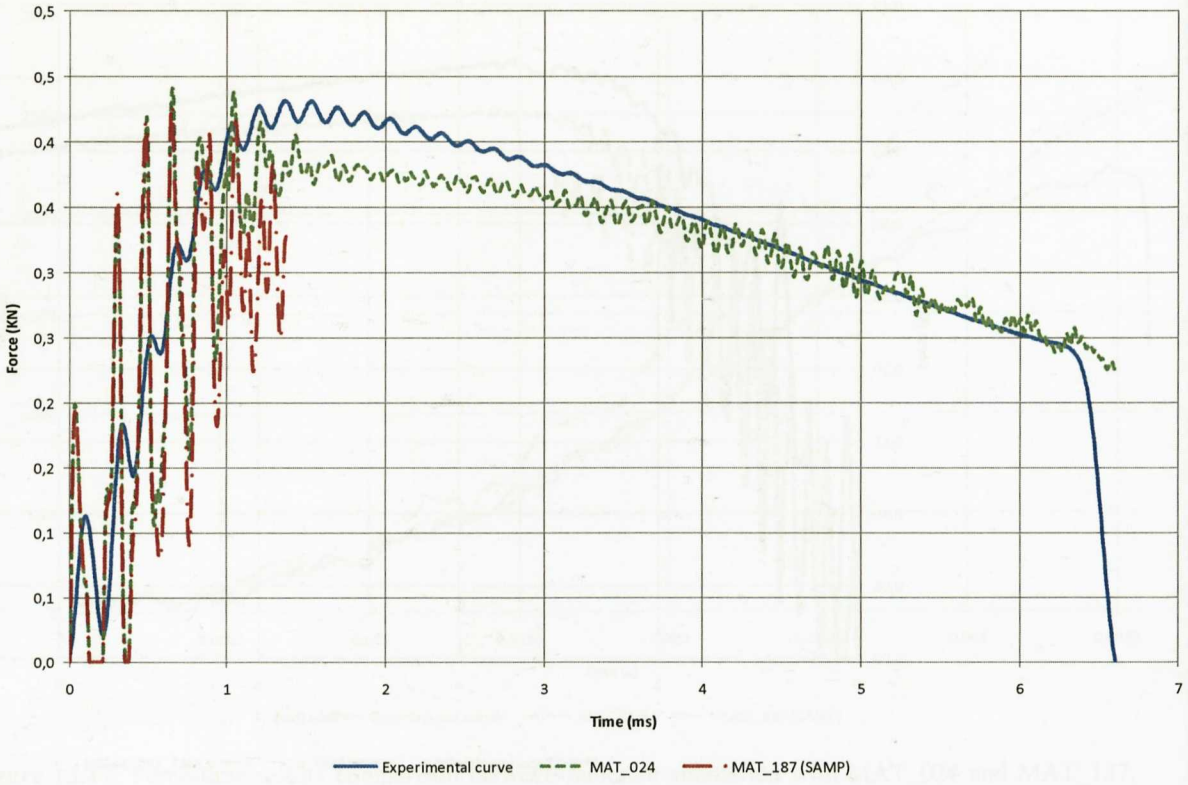

Figure 13.20: Force-time results comparison between Charpy impact simulation with MAT_024 and MAT_187, solid elements, higher speed, un-notched specimen, PC/ABS.

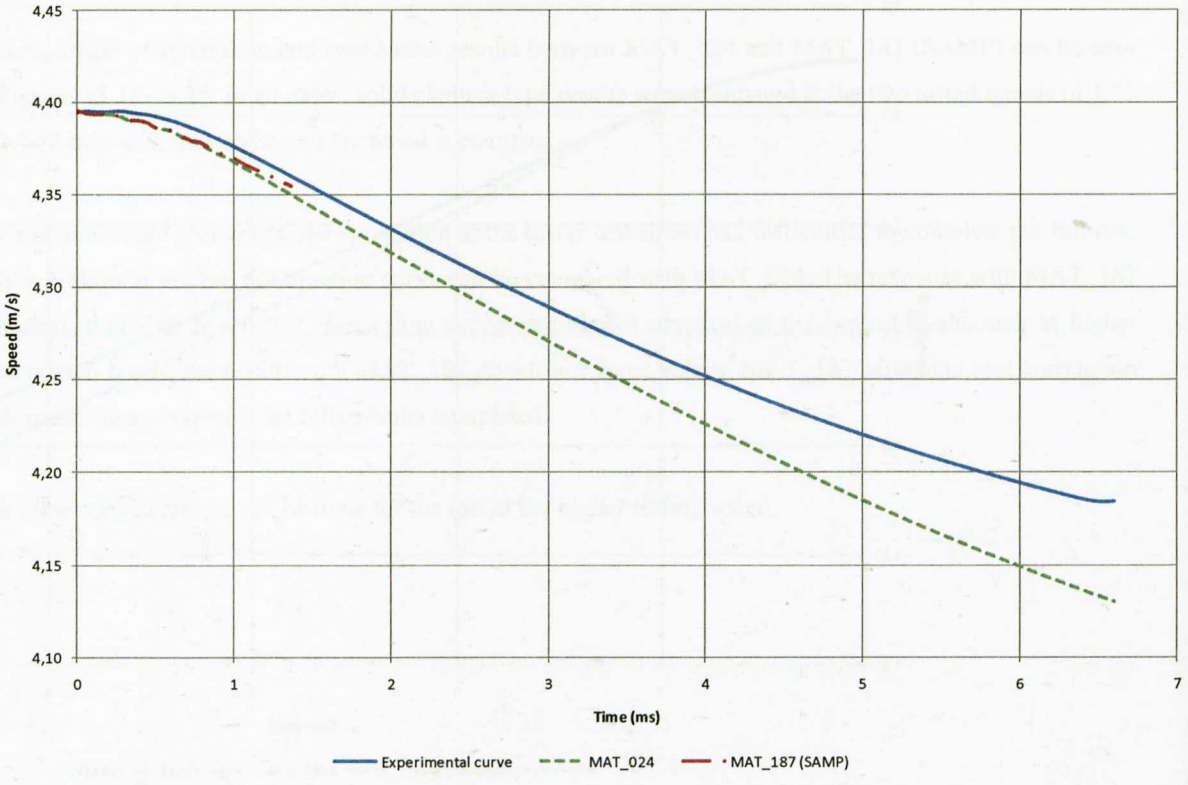

Figure 13.21: Speed-time results comparison between Charpy impact simulation with MAT_024 and MAT_187, solid elements, higher speed, un-notched specimen, PC/ABS.

For the notched specimen, the response with MAT_187 is similar to that with MAT_024; force-time curves are almost identical at the beginning although at higher deformation levels, the results with MAT_187 give

lower force values. MAT_187 offers the best correlation with speed-time curves for the time the results had completed.

The same considerations can be carried out for the test at the higher testing speed.

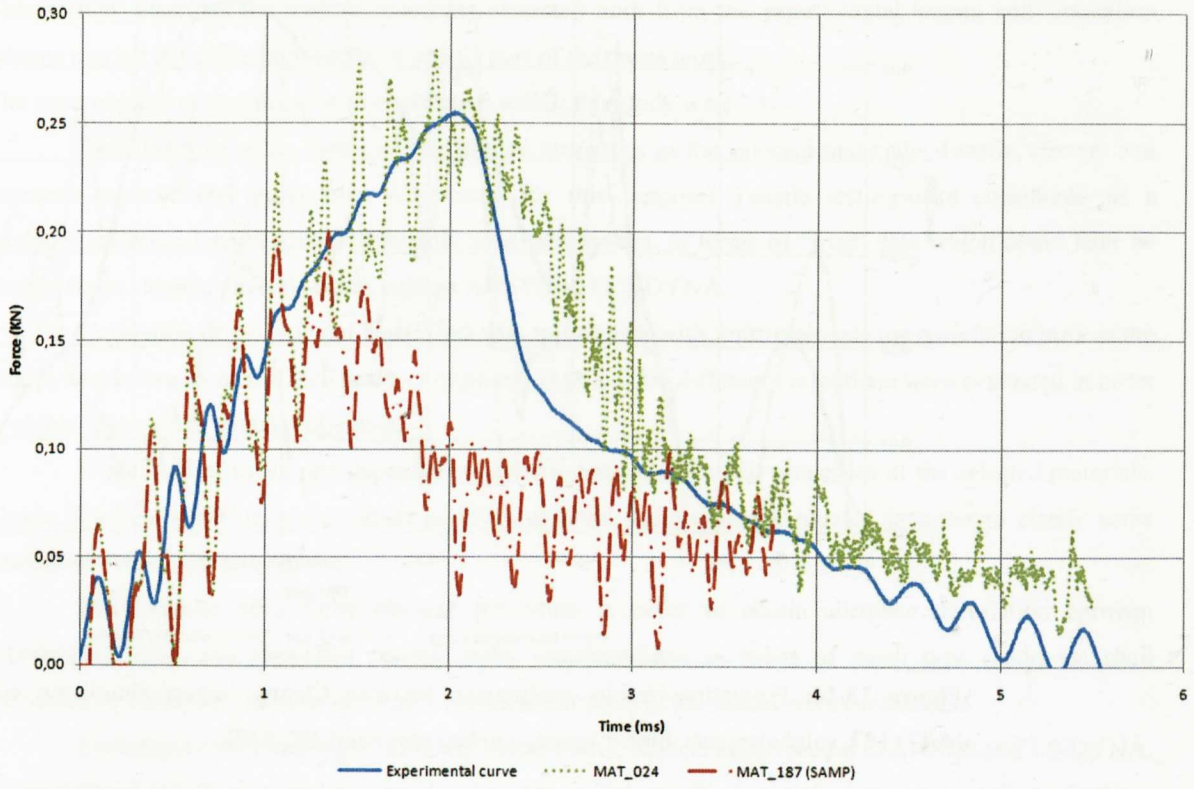

Figure 13.22: Force-time results comparison between Charpy impact simulation with MAT_024 and MAT_187, solid elements, lower speed, notched specimen, PC/ABS.

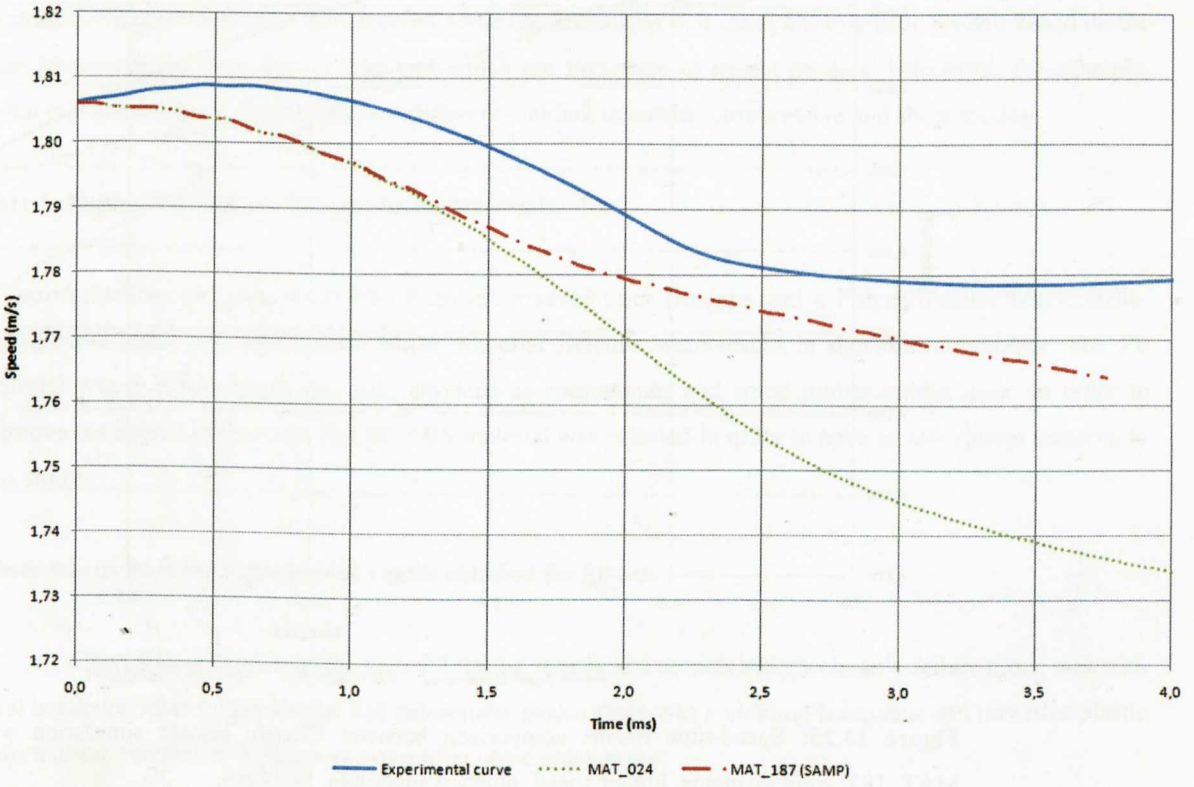

Figure 13.23: Speed-time results comparison between Charpy impact simulation with MAT_024 and MAT_187, solid elements, lower speed, notched specimen, PC/ABS.

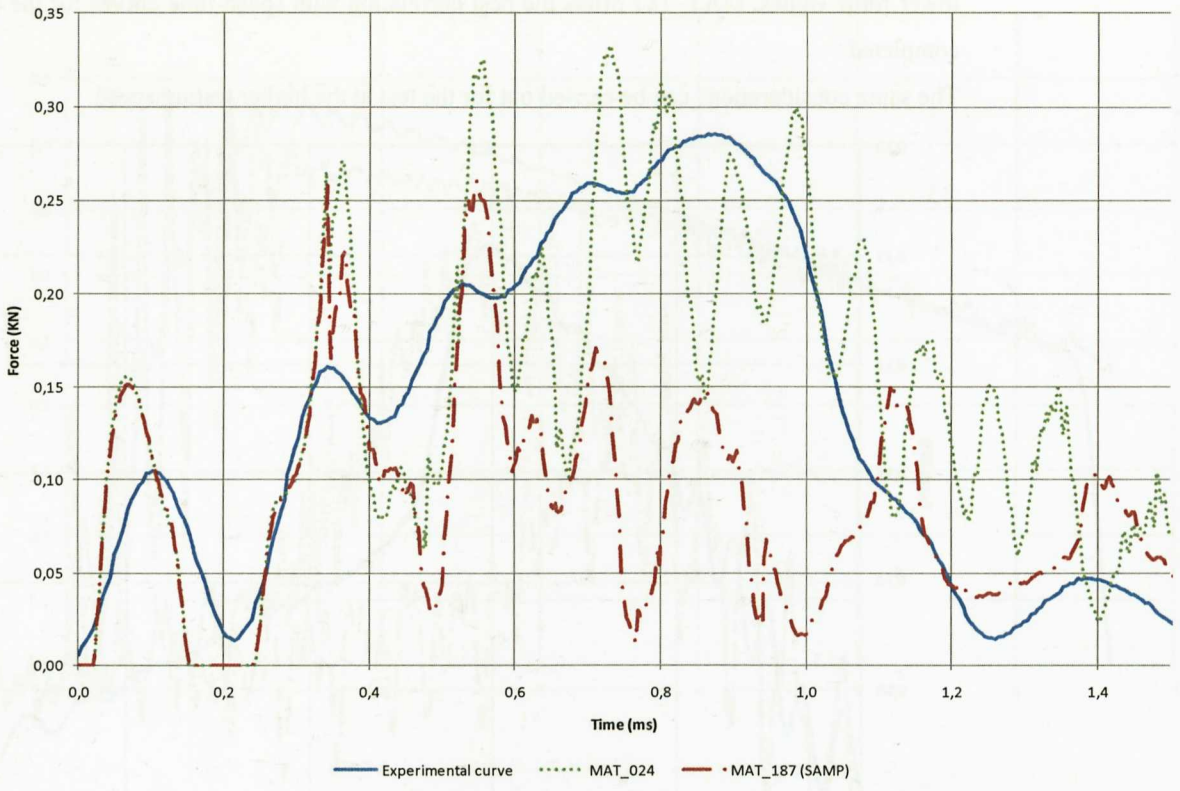

Figure 13.24: Force-time results comparison between Charpy impact simulation with MAT_024 and MAT_187, solid elements, higher speed, notched specimen, PC/ABS.

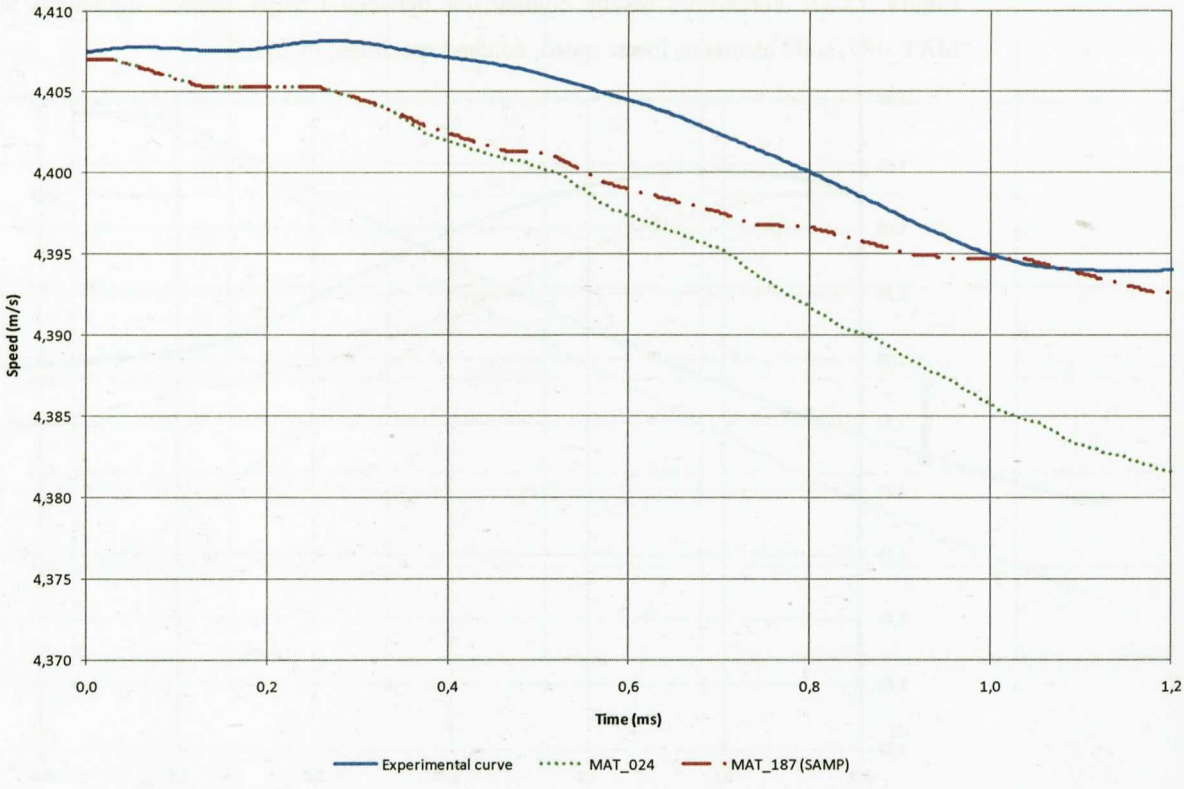

Figure 13.25: Speed-time results comparison between Charpy impact simulation with MAT_024 and MAT_187, solid elements, higher speed, notched specimen, PC/ABS.

Chapter 14: Discussion of Results. Experimental Work Part 1 & 2.

This section describes the main conclusions extracted both from the experimental testing and simulation scheme carried out in the high speed or impact part of the thesis work.

The main objectives that there were established within this study were:

- Identification of the high rate mechanical properties of the selected materials. Tensile, Charpy and Puncture experimental procedures were used for this purpose. Tensile testing was considered as a fundamental procedure to generate uniaxial stress-strain data, in terms of "true" data which could later be used in finite element analysis codes such as ANSYS and LS-DYNA.
- Evaluation of the uniaxial tensile test data to simulate with finite elements the correlation tests as the Charpy test in beams or the Puncture test of plates. In this point different corrections were evaluated in order to obtain appropriate uniaxial true data.
- Evaluation of strain rate dependency of some basic mechanical properties of the selected materials. Elastic Young's modulus, yields stress or strain at break values were evaluated in order to clarify some tendencies at the high rate regime.
- Development of a finite element procedure in order to obtain adequate correlation between experimental tests and simulated results. Basic considerations in terms of mesh type (solid vs. shell elements), or frictional characteristics between different parts of the model were evaluated.
- Evaluation of the validity of different elasto-plastic models implemented in ANSYS and LS-DYNA. These material constitutive models were developed to model metallic materials. In this thesis, they have been adopted for evaluating its response when modeling thermoplastic materials. Additionally, more sophisticated material models as the MAT_019 (*MAT_PLASTICITY_POLYMER) and MAT_187 (SAMP-1) were evaluated. These model takes into account some considerations that usual elasto-plastic models based on the Von Mises yield criteria do not take and which are important to model plastics' behaviour; for example, strain rate sensitivity of failure strain or different yielding in tensile, compressive and shear modes.

Part 1: Impact Testing of Thermoplastic Materials.

A semicrystalline polypropylene (PP) from the manufacturer Borealis and a Polycarbonate+Acrylonitrile-Butadiene-Styrene (PC/ABS) from Bayer Material Science were tested in dynamic conditions. The PP material was a block copolymer with ethylene as comonomer and some rubber modification in order to improve the impact properties. The PC/ABS material was selected in order to have an amorphous material in this study.

Observations from the experimental results obtained for PP are:

- Charpy impact tests: at the selected testing speeds, the un-notched specimen's failure mode was with total breakage: after initial inertial and subsequent peaks, there was a yielding behaviour and posterior plastic deformation. Specimen failure was given after some crack arrest.

Notched specimens showed a brittle-like behaviour after the initial inertial and subsequent peaks. This denoted some transition from ductile behaviour at the lower testing speed of 1.77 m/s, to a brittle behaviour,

although still some plastic arrest could be observed in the curve shapes. In Figure 10.16 two specimen failure modes were compared. From Figures 10.10 to 10.15 experimental graphical results were plotted.

- Puncture impact tests: it can be said that strain rate sensitivity plays a more important role than for PC/ABS at the tested speeds. At the lower testing speed, the behaviour is, as in the case of PC/ABS, ductile yielding with a final failure with unstable cracking. At the higher testing speed the behaviour tends to be more brittle, lower displacement values are obtained and the specimen breaks into two separate parts instead of the ductile penetration around the impactor observed in the lower speed. In Figures 10.24 and 10.25 a comparative picture of the Puncture PP samples can be observed at the two testing speeds. Figures 10.22 and 10.23 show the experimental graphs.
- High strain rate tensile tests: for PP, as the testing speed was increased, the yield stress was also increased, which denoted a positive strain rate dependency on yield stress. Consequently, this effect had to be accounted in posterior material modelling. Failure strains were also decreased as testing rate was increased, which indicated some negative dependency, but in this case the scatter in test data was considerably high to determine precise enough tendencies. Elastic modulus also indicated some positive dependency on increasing strain rate, i.e., the material tended to stiffen as the testing speed was increased. This effect was modeled in Section 12.3 of the thesis.

Observations from the experimental results obtained for PC/ABS are:

- Charpy impact tests: at the selected testing speeds, the un-notched specimen`s failure mode was without breakage: after initial inertial and subsequent peaks, there was a yielding behaviour and posterior plastic deformation until a limit bending deformation was obtained. Notched specimens showed a partial failure after the initial inertial and subsequent peaks, followed by a stable cracking (especially in the case of the lower testing speed). For the higher testing speed, this cracking up to the final failure was not as stable as in the lower testing speed, as a more sudden decrease in force values were recorded.

In Figure 10.9 two specimen failure modes were compared. From Figures 10.3 to 10.8 experimental graphical results were plotted.

- Puncture impact tests: it can be said that at both testing speeds the curve shape is very similar. This denotes that at the tested velocities of 1.1 and 4 m/s. the strain rate effects are almost negligible for the selected material. Specimens break with yielding and subsequent unstable cracking.

In Figures 10.20 and 10.21 a comparative picture of the punctured PC/ABS samples can be observed at the two testing speeds. Figures 10.18 and 10.19 show the experimental graphs.

- High strain rate tensile tests: for PC/ABS, as the testing speed was increased, the yield stress was also increased, which denoted a positive strain rate dependency on yield stress. Consequently, this effect had to be accounted in posterior material modelling. Failure strains were also decreased as testing rate was increased, which indicated some negative dependency, but in this case the scatter in test data was considerably high to determine precise enough tendencies. Elastic modulus did not indicate any dependency on increasing strain rate on the contrary to the observed behaviour in PP.

Part 2: Impact FEA of Thermoplastic Materials.

The finite element simulation codes ANSYS and LS-DYNA were used for the simulation of the experimental tensile, Charpy and Puncture tests for both materials.

The main objective was to evaluate the validity of the implemented material models in both codes. Additionally, different material input data generation was studied in order to evaluate the most adequate material testing scheme for validating impact tests.

Simulations results for PP,

- An iterative correlation method was developed for generating high strain rate stress-strain data. Tensile tests carried out at different testing speeds (according to ISO 18872) were simulated in ANSYS following the procedure described in the Part I of the thesis document. This method consisted of iteratively changing the input stress-strain curve for correlating the experimental force-displacement results. This process was repeated for each testing speed. Thus, true stress-strain data was generated as input for FEA. For PP, the curves shown in Figure 11.1 were obtained.
- Charpy impact test correlation in ANSYS: different material data input was evaluated in order to evaluate the correlation level with experimental impact tests. In general, a single stress-strain curve tested at quasi-static conditions did not offer an adequate correlation level. Taking into account strain rate dependency by means of a Perzyna type model did not improve the results, the achievement of solution convergence was complicated and the results tended to be considerably stiffer than experimental curves. In general terms, a poor correlation level could be obtained in ANSYS both for un-notched and notched specimens at the tested speeds. Due to this, the study was continued in LS-DYNA.
- Puncture impact test correlation in ANSYS: again, different material data input was evaluated in order to determine the correlation level with experimental impact tests. The same observations done in Charpy simulations results can be done here. In general, a single stress-strain curve tested at quasi-static conditions did not offer an adequate correlation level and convergence achievement was very complicated. Taking into account strain rate dependency by means of a Perzyna type model did not improve the results. In general terms, a poor correlation level could be obtained in ANSYS for the punctured specimens at the tested speeds, although at the higher speed the results were considerably better. Due to this, the study was continued in LS-DYNA.
- The use of different element types produced different model results; shell elements offered always too stiff responses (which have been seen in all the thesis work). This leads to us to recommend the use of solid elements even bearing in mind that the computational cost is higher but a better correlation of results is obtained.
- Charpy impact test correlation in LS-DYNA: different material data input was evaluated in order to evaluate the correlation level with experimental impact tests. In general, a single stress-strain curve tested at quasi-static conditions offered considerably lower force values than experimental. When taking strain rate effects using data at low strain rates and performing extrapolations with the Eyring's equation (Section 11.2.3.1), results were improved and the experimental curve was adequately approximated. The best correlation level was obtained when using the iterative method of tensile data generation at different testing speeds. For the notched specimens, this tendency was also corroborated and the use of a limit failure strain for element elimination was presented as a failure predictor.

- Puncture impact test correlation in LS-DYNA: again, different material data input was evaluated in order to evaluate the correlation level with experimental impact tests. The same observations done in Charpy simulations results can be done here. In general, a single stress-strain curve tested at quasi-static conditions offered lower force values than experimental. The best correlation level was obtained when taking into account strain rate effects with the Eyring's equation or using the iterative method presented here. In the Puncture test, an additional material data input was evaluated. This method consisted of testing tensile specimens at 5, 50 and 500 mm/min. and using the extrapolation equations presented in the standard ISO18872. Chapter 12.

It was observed that this method was also very valid for the correlation of the puncture test at the tested speeds.

- In concern to the use of different element types, shell elements offered always too stiff responses (which have been seen in all the thesis work). This makes us to recommend the use of solid elements even bearing in mind that the computational cost is higher but proper results are obtained.

Simulations results for PC/ABS,

- As adopted for PP, an iterative correlation method was developed for generating high strain rate stress-strain data. Tensile tests carried out at different testing speeds (according to ISO 18872) were simulated in ANSYS following the procedure described in the Part I of the thesis document. This method consisted of iteratively changing the input stress-strain curve for correlating the experimental force-displacement results. This process was repeated for each testing speed. Thus, true stress-strain data was generated as input for FEA. For PC/ABS, the curves shown in Figure 11.3 were obtained.
- Charpy impact test correlation in ANSYS: different material data input was evaluated in order to evaluate the correlation level with experimental impact tests. In general, a single stress-strain curve tested at quasi-static conditions did not offer an adequate correlation level. Taking into account strain rate dependency by means of a Perzyna type model did not improve the results, the achievement of solution convergence was complicated and the results tended to be considerably stiffer than experimental curves. In general terms, a poor correlation level could be obtained in ANSYS both for un-notched and notched specimens at the tested speeds. Due to this, the study was continued in LS-DYNA.
- Puncture impact test correlation in ANSYS: again, different material data input was evaluated in order to evaluate the correlation level with experimental impact tests. The same observations from Charpy simulations results can be repeated. In general, a single stress-strain curve tested at quasi-static conditions did not offer an adequate correlation level and convergence achievement was very complicated. Taking into account strain rate dependency by means of a Perzyna type model did not improve the results. In general terms, a poor correlation level could be obtained in ANSYS for the punctured specimens at the tested speeds, although at the higher speed the results were considerably better. Due to this, the study was continued in LS-DYNA.
- In concern to the use of different element types, shell elements offered always too stiff responses (which have been seen in all the thesis work). This makes us to recommend the use of solid elements even bearing in mind that the computational cost is higher but proper results are obtained.
- Charpy impact test correlation in LS-DYNA: different material data input was evaluated in order to evaluate the correlation level with experimental impact tests. In general, a single stress-strain curve tested at quasi-static conditions offered considerably lower force values than experimental. When taking strain rate

effects using data at low strain rates and performing extrapolations with the Eyring's equation (Section 11.2.4.1), results were improved and the experimental curve was adequately approximated. The best correlation level was obtained when using the iterative method of tensile data generation at different testing speeds. For the notched specimens, this tendency was also corroborated and the use of a limit failure strain for element elimination was presented as a failure predictor.

- Puncture impact test correlation in LS-DYNA: again, different material data input was evaluated in order to evaluate the correlation level with experimental impact tests. The same observations from Charpy simulations results can be repeated. In general, a single stress-strain curve tested at quasi-static conditions offered lower force values than experimental. The best correlation level was obtained when taking into account strain rate effects with the Eyring's equation or using the iterative method presented here. In the Puncture test, an additional material data input was evaluated. This method consisted of testing tensile specimens at 5, 50 and 500 mm/min. and using the extrapolation equations presented in the standard ISO18872. Chapter 12.

It was observed that this method was also very valid for the correlation of the puncture test at the tested speeds.

- In concern to the use of different element types, shell elements offered always too stiff responses (which have been seen in all the thesis work). This makes us to recommend the use of solid elements even bearing in mind that the computational cost is higher but proper results are obtained.

- Frictional effects in simulations, Section 12.4: it was observed that for PP and PC/ABS, the use of arbitrary frictional values in the Charpy test simulations did not considerably change the force-time responses in comparison to a zero friction value assumption. Moreover, in some situations, the addition of frictional values tend to stiffen the response in the plastic area which is not in concordance with experimental measurements.

It was observed that frictional effects are more marked in puncture simulations, although care must taken when selecting appropriate values since the tendency is always to stiffen the load-time traces, which can make to not properly correlate the experimental curve.

- Additional material models in LS-DYNA: it was studied the use of two material models which had been specifically developed for thermoplastic materials, MAT_089 and MAT_187.

MAT_089 was used with shell elements since it is not developed for solid type elements. It was observed that for both materials the tendency was to give even a stiffer response than with MAT_024 which was not adequate to correlate puncture force-time traces.

MAT_187 was used with solid type elements for PC/ABS and to correlate Charpy and Puncture tests. The main difficulty with this material model was to complete the full solution run; it is not very stable and very often error terminations were obtained. In comparison to MAT_024, the use of compression and shear input data did not improve the simulation results. Moreover, MAT_024 offer better approximation to experimental data.

In summary, a testing and simulation methodology was presented for correlating high speed impact events. A tensile test process was explained in order to generate stress-strain data at different testing speeds (taking some consideration from ISO 18872). This iterative method permitted the generation of proper material data which gave the best correlation level with experimental tests. It was remarked the necessity of considering strain rate effects both on yielding and failure (although this last point needs further studies). It was observed

that extrapolation methods based on the Eyring's equation or the mathematical models proposed in ISO 18872 could be adequate material data generation methods when high strain rate data is difficult to measure. It was determined that the use of simple metal-based material models as MAT_024 are adequate for obtaining proper correlation levels. When more detailed material behaviour description is needed, material models as MAT_187 could be used.

Chapter 15: General conclusions.

In the present study a work methodology based on both testing and simulation for the prediction of the mechanical behavior of thermoplastic materials has been developed. Two thermoplastic materials have been analysed, PP and PC+ABS, in quasi-static and high speed regimes. Additionally, thermal effects have also been evaluated.

In the quasi-static regime, it has been observed that the correlation level with tensile, bending and puncture test of plates was very precise with the use of simple elasto-plastic models which were historically developed for metallic materials. Nevertheless, with the use of more complex constitutive models, as with the addition of the Drucker-Prager yield criteria, simulation results were improved as in the case of bending dominated cases.

In the case of the correlation with the tensile test, it has been developed an iterative correction method that permits the correct calibration of this particular test where the measurements of local plastic strains are very difficult and expensive to achieve experimentally.

The simulation parameters as the element type, mesh density or frictional characteristics between different parts of the model, are controllable and can be evaluated performing different checks of its influence on the simulation results. In this study, it has been checked that the modification of the mentioned parameters do not improve noticeably the simulation results.

In summary, in the first part of the thesis, a methodology based on tensile measurements, corrections of the plastic area and calibration of the constitutuive model in different teting modes (bending, puncture) has been developed, where very precise comparative results have been obtained.

In the second part of the thesis, in concern to the crash regime studies, two correlation tests have been evaluated (Charpy impact and high speed puncture) with simulations in ANSYS and LS-DYNA. The methodology developed in the first part of the thesis has been adopted in order to combine it with the standard ISO 18872, both for the testing section and for the correct devellopment of the constitutive model and the procedure for extrapolations. It has been seen that this methodology offers very precise results when comparing impact experiments and simulations, especially with the use of the LS-DYNA code.

It has been observed that for the obtention of such and adequate correlation level, it is necessary to take into account specific dynamic effects on material properties as strain rate sensitivity on yield stress, elastic modulus or strain at break.

Simple elasto-plastic models based on metallic materials behavior offer very precise simulation results. Moreover, the use of complex models do not improve considerably the virtual responses, anyway, as these models are still under development and are including specific issues for polymeric materials, it woul be very interesting to evaluate additional material models in future works.

This methology avoids the use of expensive extensometric devices for the measurement of large local plastic strains and its use in design stages when developing plastic components, adding the automatisation of the iterative correction method proposed here, could result very attractive in terms of time and costs.

Companies that simulate with FEA codes the behavior of thermoplastic made components could make use now of a validated solution in different materials, testing regimes and loading conditions.

Conclusiones generales (Spanish).

En este estudio, se ha tratado de desarrollar una metodología de trabajo tanto en el apartado de ensayos como en el de simulación para la predicción del comportamiento mecánico de materiales termoplásticos. Se han analizado dos materiales plásticos, PP y PC+ABS, desde el punto de vista de régimenes cuasi-estático y de alta velocidad. También se ha evaluado el punto de vista térmico.

En el régimen cuasi-estático, se ha observado que la correlación entre resultados experimentales de tracción, flexión y perforación de placas es muy precisa con el uso de modelos elasto-plásticos simples históricamente desarrollados para materiales metálicos. Aun así, el uso de modelos más complejos como el criterio de fluencia de Drucker-Prager mejora los resultados por ejemplo en casos dominados por la flexión.

En el caso de la correlación con el ensayo de tracción, se ha desarrollado una metodología de corrección iterativa que permite calibrar adecuadamente este particular ensayo donde las mediciones de deformación son complicadas experimentalmente.

Los parámetros de simulación como el tipo de elemento, la densidad de malla o las características de fricción entre distintas piezas, son controlables y evaluables realizando diferentes pruebas de evaluación, pero se ha observado que en general no aportan mejoras aprecibles en los resultados obtenidos.

Por lo tanto, en la primera parte dedicada al régimen cuasi-estático, se ha desarrollado una metodología basada en mediciones de propiedades mecánicas en el ensayo de tracción, realización de correcciones de la zona plástica de la curva obtenida y calibración del modelo constitutivo del material en otros modos de deformación (flexión y perforación) donde se han obtenido unos resultados comparativos muy precisos.

En la seguna parte de la tésis concerniente al régimen de altas velocidades de ensayo (crash), se han utilizado dos ensayos de contrastación (Charpy y perforación de placas) de los resultados de simulación en ANSYS y LS-DYNA. Se ha utilizado la metodología de tracción desarrollada en la primera parte y mediante el uso de la norma ISO18872 para la realización de los ensayos y desarrollo del modelo constitutivo para extrapolaciones, se ha observado que la correlación con los resultados experimentales ha resultado muy adecuada, especialmente en el código LS-DYNA.

Se ha observado que para esta adecuada correlación, es necesario tener en cuanta el efecto de diferentes procesos dinámicos en el material como la dependencia de la tensión de fluencia, la deformación de rotura o el módulo elástico en la velocidad de deformación aplicada en el ensayo. Los modelos constitutivos básicos basados en el comportamiento de materiales metalicos ofrecen unos resultados muy aceptables que en muchos casos los modelos avanzados no mejoran, aun así, hay vías de mejora en estos modelos avanzados que será interesante cubrir en trabajos futuros.

Esta metodología evita la utilización de extensometría costosa para la medición de deformaciones locales en probetas y su utilización en fases de desarrollo de componentes mediante la automatización del procedimiento de corrección iterativa resultaría muy beneficiosa. Las empresas que simulan el comportamiento de sus componentes fabricados en materiales termoplásticos disponen de una solución contrastada en diferentes materiales, rangos de velocidades y modos de deformación.

Chapter 16: Future Studies.

This thesis has been divided into two parts in order to describe separately the quasi-static behaviour and the high rate behaviour of two selected thermoplastic materials. FEA simulations have been performed in order to study the correlation level that is obtained in simulating , tensile, flexural, Charpy or Puncture tests with the use of constitutive elasto-plastic material models. For that purpose, special attention has been paid to the generation of adequate material input data.

When considering future studies, it has to be said that in the quasi-static regime the use of Von Mises based material models have offered adequate results, although the implementation of material models as the Drucker-Prager equation improved slightly the simulation calculations. Thus, the use of more sophisticated constitutive models as MAT_187 (SAMP) should be interesting to study not only in high rate regimes but also in the quasi-static simulation scheme. This would lead us to study the influence of different material data input (tensile, compression, shear) on the numerical results.

The proposed iterative method for correlating experimental tensile test and consequently generating input stress-strain curves, has been demonstrated to be a valid method for properly correlating different testing modes both at slow or high testing speeds. However, direct measurement of stress-strain properties with adequate test equipment should also be considered for comparative purposes. This testing system should include high speed recording cameras to capture the specimen deformation process till rupture, and a digital image correlation system to experimentally determine 3D local strains. An internal project is being carried out in Leartiker (Lea Artibai Ikastetxea), as a continuation of this thesis research. The project deals with the measurement of local strains in tensile specimens. First results publication is expected to be performed by the end of year 2011.

Damage and failure mechanism have not been studied in depth in this thesis work; more attention has been paid to the deformation process of the specimens rather than the breaking phenomena. Although simple failure indicators have been used for example in MAT_024, MAT_89 or MAT_187, (where a limit plastic strain was specified as element elimination criteria to represent material break), this phenomena needs to be studied in further works. This should include strain rate dependency on failure strain, damage mechanisms implemented in SAMP_187, or brittle- ductile failure criteria.

Temperature effects should also be considered in future works. This study has been carried out mainly at 23°C although tensile experimental testing was also performed in other temperatures. As thermoplastic components are required to work at different conditions this study should be continued with different temperatures; low temperature behaviour is especially important when designing plastic parts due to brittle failure likelihood.

Processing effects should also be considered in future studies. The selected materials in this work were net plastics without any reinforcing filler as glass or mineral talc. The study should be open to the inclusion of additional materials with fibre contents in order to evaluate the anisotropic effects on the mechanical behaviour of the material at low and high strain rate testing and simulation. This work could be carried out

coupling used simulation codes as ANSYS or LS-DYNA with the commercial code DIGIMAT (Exstream Engineering, Luxembourg). This would lead us to pass the processing information (fibre orientations, residual stresses, weld lines, etc.) from an injection simulation program (MOLDFLOW, CADMOULD, SIGMASOFT, MOLDEX, etc.) to our structural software (for example LS-DYNA), developing our own material models (DIGIMAT).

Finally, the study should also consider the correlation of real use components as for example, bumpers, pillars or instrument panels. Our methodology was studied in a previous study [31] for a 20% mineral talc filled PP. The used component was not a real end use part but it was adequate for correlation studies. Further analyses are needed for evaluating the behaviour of different parts and materials to finally validate a work methodology.

Additional sections in Spanish.

Abstract (Spanish). Part I-

El objetivo principal de este estudio reside en la evaluación de la validez de los modelos elasto-plàsticos implementados en el software de Anàlisis por Elementos Finitos (AEF) ANSYS®. Este objetivo se ha llevado a cabo mediante la comparación de los resultados en ensayos experimentales de tracción, flexión y perforación o penetraciòn de placas con los correspondientes cálculos de AEF. Los análisis se han llevado a cabo en lo que concierne a ensayos a bajas velocidades y càlculo por elementos finitos en dos materiales termoplásticos. Los materiales seleccionados han resultado ser una mezcla de Policarbonato (PC) con Acrilonitrilo-Butadieno-Estireno (ABS), Bayblend T45 de Bayer Material Science, como polímero amorfo, y un Polipropileno (PP) copolìmero, BE677AI de Borealis, como ejemplo de polímero semicristalino.

El comportamiento uniaxial a tracción de los dos materiales se utilizò para la generación de datos de material para su entrada en el código de càlculo. Debido a la dificultad de predecir el comportamiento post-fluencia a la hora de medir las tensiones y deformaciones verdaderas con el uso de extensometrìa convencional, se presentó en este trabajo un método iterativo como solución a la medida de deformaciones locales plásticas considerables en las probetas de tracción.

El ensayo experimental de flexión en tres puntos y el ensayo de perforación de placas mediante dardo se utilizaron como métodos de correlación de las simulaciones con el fin de validar no sólo los modelos constitutivos elasto-plásticos basados en el criterio de fluencia de Von Mises, sino también como métodos para chequear la influencia de diferentes variables de simulación. Los parámetros estudiados resultaron ser el tipo de elemento, la densidad de malla, la fricción y las condiciones de contacto entre las diferentes piezas. Adicionalmente, se analizó un criterio de fluencia específico; el modelo Drucker-Prager sensitivo a presiones hidrostáticas.

Se observó que para ambos materiales el uso de la aproximación clásica para la obtención de valores verdaderos de tensión y deformación junto con el criterio de fluencia de Von Mises ofrecía unos resultados aceptables para los modos de ensayo estudiados. Aun así, las curvas experimentales de entrada no se ajustaban con precisión a los resultados de simulación de las probetas de tracción. Esto se solucionó mediante la utilización de un método iterativo para corregir las curvas de entrada en el código para ajustar perfectamente los ensayos experimentales de tracción. Aun siendo un procedimiento preciso para casos uniaxiales, se observó que para problemas de flexión o perforación este método ofrecía respuestas más rígidas que utilizando la aproximación clásica para la conversión de curvas tensión-defromación.

Por último, el criterio de Drucker-Prager fue capaz de capturar de un modo aun más preciso los problemas dominados por el modo de flexión que el criterio habitual de fluencia de Von Mises.

Abstract (Spanish). PART II.

El objetivo principal de este estudió resultó ser la evaluación de la validez de los modelos constitutivos elasto-plásticos implementados en los software de Análisis por Elementos Finitos (AEF) ANSYS® y LS-DYNA®. Esto se llevó a cabo comparando los resultados de ensayos experimentales de tracción a alta velocidad, impacto Charpy y ensayos de perforación de placas con los correspondientes cálculos de AEF. Los estudios se llevaron a cabo en lo concerniente a ensayos a altas velocidades y análisis por elementos finitos de dos materiales termoplásticos. Los materiales seleccionados han resultado ser una mezcla de

Policarbonato (PC) con Acrilonitrilo-Butadieno-Estireno (ABS), Bayblend T45 de Bayer Material Science, como polímero amorfo, y un Polipropileno (PP) copolìmero, BE677AI de Borealis, como ejemplo de polímero semicristalino.

El comportamiento a tracción uniaxial de ambos materiales se utilizó para la generación de datos de entrada de material para el programa de simulación. Los ensayos de tracción cubrieron el rango desde el régimen de velocidades bajas hasta velocidades altas de acuerdo a la norma ISO 18872. Debido a la dificultad de predecir el comportamiento post-fluencia a la hora de medir las tensiones y deformaciones verdaderas con el uso de extensometrìa convencional, el método iterativo presentado en la PARTE 1 de la tésis se utilizó como solución a la medida de deformaciones locales plásticas considerables en las probetas de tracción.

Los ensayos experimentales de impacto Charpy y perforación de placa por dardo fueron utilizados como ensayos de correlación con las simulaciones, con el objetivo de validar no sólo los modelos constitutivos elasto-plásticos basados en el criterio de fluencia de Von Mises (MISO + modelo constitutivo de Perzyna en ANSYS o MAT_024 en LS-DYNA), sino también para chequear la influencia de diferentes variables de simulación. Los parámetros estudiados fueron el tipo de elemento y la fricción entre diferentes piezas. Adicionalmente, se estudiaron otros modelos constitutivos como MAT_089 (para considerar efectos de la velocidad de deformación en la fluencia y el fallo) o MAT_187 (SAMP) para evaluar otro criterio de fluencia, en este caso considerando el efecto de compresión y cizalla en la superficie de fluencia.

Se observó que para ambos materiales se necesitaba tener en cuenta el efecto de la velocidad de deformación en la tensión de fluencia con el objeto de obtener inicialmente una correlación aceptable con los ensayos de impacto Charpy y penetración de placas. Los resultados se mejoraron con el uso de curvas iterativamnete correladas de tensión-deformación a diferentes velocidades de deformación. Adicionalmente, el método de extrapolación descrito en la norma ISO 18872 resultó ser adecuado para la correlación de los ensyos experimentales de perforación de placas a altas velocidades de deformación.

El uso de modelos de material más complejos como el MAT_089 o MAT_187 no ofreció mejoras para los experimentos estudiados en comparación al modelo básico MAT_024. Aun así, la complejidad del modelo MAT_187 lo hace ideal para cubrir la mayoría de las particularidades inherentes a los materiales termoplásticos y necesita de estudios adicionales en trabajos futuros.

Summary of the different chapters in Spanish.

Resumen de los capítulos de la tésis en Español.

Capítulo 1. Introducción (Parte I). Se presenta la problemática general existente a la hora de simular el comportamiento mecánico de los materiales termoplásticos mediante Análisis por Elementos Finitos (AEF). En este trabajo se plantea inicialmente la utilización de modelos constitutivos elasto-plásticos basados en el criterio de fluenica de Von Mises.

Capítulo 2. Definición del comportamiento mecánico de los polímeros termoplásticos. Se presentan las particularidades en el comportamiento mecánico de los materiales termoplásticos. Se describen las diferentes metodologías y normativas de ensayo.

Capítulo 3. Revisión literaria. En la primera parte se describen los modelos constitutivos que se han desarrollado para describir el comportamiento mecánico de los polímeros termoplásticos. En la segunda parte se explican los métodos de caracterización mecánica y simulación por elementos finitos que se han publicado

en la literatura. Adicionalmente, se comnetan las aproximaciones que se han desarrollado ara describir comportamientos como el fallo o el comportamiento a recuperación de carga.

Capítulo 4. Modelos constitutivos elasto-plásticos en el análisis por elementos finitos. Software ANSYS. Se describe la metodología de trabajo y teoría en ANSYS a la hora de trabajar con modelos elasto-plásticos.

Capítulo 5. Técnicas de análisis por elementos finitos y particularidades no –lineales. Se describe extensamente la teoría del método de los elementos finitos y su aplicación en el estudio de materiales termoplásticos.

Capítulo 6. Trabajo Experimental. Ensayos cuasi-estáticos y simulación por elementos finites de los materials termoplásticos. Se presenta el trabajo experimental completo llevado a cabo en la primera parte de la tesis. Se exponen los resultados obtenidos para ambos materiales.

Capítulo 7. Discusión de los resultados. Se comentan los resultados obtenidos para la primera parte de la tésis tanto en el apartado experimental como en el de la simulación.

Capítulo 8. Introducción (Parte II). Se presenta el estado del arte en cuanto a la simulación y ensayos en materiales termoplásticos sujetos a condiciones de carga de impacto (altas velocidades de deformación). La aproximación utilizada en este estudio seguirá la via utilizada en la Parte I en cuanto a modelos elasto-plásticos.

Capítulo 9. Revisión literaria. Esta revision se categoriza en tres apartados: modelos constitutivos para materiales termoplásticos en simulaciones por elementos finitos de eventos de impacto, métodos de caracterización y procedimientos de cálculo, y métodos de ensayos a altas velocidades.

Capítulo 10. Trabajo experimental, ensayos de impacto en materiales termoplásticos. Se expone el trabajo llevado a cabo en cuanto a la caracterización de los materiales seleccionados desde el punto de vista de ensayos Charpy, ensayos penetración de placas y ensayos de tracción a altas velocidades en los materiales seleccionados.

Capítulo 11. Trabajo experimental, AEF de impacto en materiales termoplásticos. Se expone el trabajo llevado a cabo en cuanto a las simulaciones de impacto en ANSYS y LS-DYNA en los materiales y ensayos seleccionados.

Capítulo 12. Cálculo de los parámetros del modelo constitutivo de acuerdo a la norma ISO 18872. En este apartado se calculan específicamente los coeficietnes necesarios en el modelo de material planteado en la norma.

Capítulo 13. Se estudian los modelos de material adicionales en LS-DYNA que permiten simular efectos mecánicos importantes en materiales termoplásticos. MAT_089, para el estudio de la sensitividad de la deformació de la rotura con la velocidad de deformación. MAT_187, datos de entrada y criterios de fallo adicionales.

Capítulo 14. En este apartdo se discuten tanto los resultados experimentales como la correlación con las simulaciones obtenidas con los diversos modelos de material y ensayos planteados.

Capítulo 15. Se plantean una serie de trabajos futuros que se observan como intereantes para el desarrollo posterior de la metodología planteada en la presente tésis.

Literature References.

[1] Thomas Goral. "Materials Modeling for Engineering Thermoplastics in FEA under High-Strain Loading". SAE Document N° 2000-01-1167.

[2] Pádraig Naughton. "Extension of Material Models and Finite Element Techniques to Improve the Simulation of High Speed Impact of Thermoplastic Materials". SAE Document N° 1999-01-0300.

[3] Xinran (Sharon) Xiao. "Plastic Material Modeling for FMVSS 201 Simulation". SAE Document N° 2002-01-0385.

[4] Xinran (Sharon) Xiao. "Plastic Material Modeling for Vehicle Crash Simulation Using LS- DYNA". ANTEC Conference 2001.

[5] Y. Duan, A. Saigal, R. Greif and M.A. Zimmerman. "Analysis of Multiaxial Impact Behavior of Polymers". Polymer Engineering and Science, Vol. 42, N°2, 2002, pp. 395-402.

[6] Jerome P. J. Coulton. "The Generation of a Material Model to Represent the Mechanical Behaviour of an Aliphatic Polyketone (Carilon EP) at High Strain Rate Events and Low Temperatures. 3rd Eurpean LS-DYNA Conference 2001.

[7] Scott Burr. "Taking a Hit : Modeling the Parameters of Thermoplastics in Car Crashes". Plastics Engineering 1997, vol. 53, n°9, pp. 43-46.

[8] Scott Burr and Gavin D. Vogel. "Material Model Development for Impact Analysis of Oriented Polypropylene Foam Structures". SAE 2001 World Congress.

[9] Heiner Müllerschön, Armin Dangel, Nils Karajan, Alexander Hummel and Andreas Wüst "Modelling of Plastics for Crash Simulation of Fuel Tanks". 3rd LS-DYNA Anwenderforum Bamberg 2004.

[10] Frank Huberth, Stefan Hiermaier and Marika Neumann. "Material Models for Polymers under Crash Loads. Existing LS-DYNA Models and Perspective". 4th LS-DYNA Anwenderforum Bamberg 2005.

[11] S. Kolling, A. Haufe, M. Feucht and P.A. du Bois. "SAMP-1: A Semi-analytical Model for the Simulation of Polymers". 4th LS-DYNA Anwenderforum Bamberg 2005.

[12] Dean, G.D, Crocker, L.E. "Prediction of the Impact Performance of Plastics Using Finite Element Methods". NPL Measurement Good Practice Guide, No. 87, February 2006.

[13] Joseph T. Woods and Gerald G. Trantina. "Material Characterization for Predicting Impact Performance of Plastic Parts". SAE Document N° 1999-01-3178.

[14] Stephen M. Pitrof and Michael C. Lee . "Experimental and Analytical Verification of Plastics Materials Models for Automotive Crashworthiness Applications". ANTEC Conference 2001.

[15] O. Schang, N. Billon, J. M. Muracciole and F. Fernagut. "Mechanical Behavior of a Ductile Polyamide 12 During Impact. Polymer Engineering & Science, Volume 36, Issue 4, pages 541–550, February 1996.

[16] Júlio C. Viana, António M. Cunha and Noelle Billon. "Experimental Characterization and Computational Simulations of the Impact Behavior of Injection-Molded Polymers". Polymer Engineering & Science, Volume 47, Issue 4, pages 337–346, April 2007.

[17] Frank Lutter, Michael Münker and Martin Wanders. "Simulation Right Through to Failure". Bayer ATI Document, also appeared in Kunststoffe International 2002/01, Page 22-24.

[18] P.A. Du Bois, S. Kolling, M. Koesters and T. Frank. "Material Behaviour of Polymers under Impact Loading". International Journal of Impact Engineering, Volume 32, Issue 5, May 2006, Pages 725-740. International Symposium on the Crashworthiness of Light-weight Automotive Structures.

[19] Julio C. Abajo Alonso, Alberto Negro Marne, Alberto Mansilla Gallo, Isabel Gobernado Mitre. "Metodología para el Desarrollo en Materiales Plásticos de Nuevos Componentes de Automoción con Requerimientos de Seguridad". Revista de Plásticos Modernos, Vol. 87 Número 576 (Junio 2004).

[20] Masahiro Fujii, Syunichi Kawano, Hiroshi Fujino. "Benchmark Problem for Crush Analysis of Plastic Parts for Automotive". JSAE Review 22 (2001) 23-27.

[21] Ernst Schmachtenberg, Markus Glißmann and Markus Brinkmann. "Modelling the Dynamic Material Behaviour of Thermoplastics in the FEA". Journal of Polymer Engineering, Vol. 26, Nos. 2-4, 2006, Special Issue: Papers Presented at the IKV 22nd Plastics Technology Colloquium, Aachen, Germany, March 10 - 12, 2004.

[22] Slimane Bekhouche, Yvon Chevalier, Pierre Guellec. "Analyse Non-Linéaire et Dimensionnement d'une Structure de Bouclier Automobile par Couplage Calculs-Essais". Mécanique & Industries, Volume 1, Issue 3, May 2000, Pages 295-302.

[23] T. Pyttel; S. Weyer. "Crash Simulation with Glassy Polymers – Constitutive Model and Application". International Journal of Crashworthiness, 1754-2111, Volume 8, Issue 5, 2003, Pages 433 – 442.

[24] G. Spingler; P. Drazetic; E. Markiewicz. "Dynamic Characterization of Polymers to Improve Numerical Simulations for Passive Safety". International Journal of Crashworthiness, 1754-2111, Volume 10, Issue 1, 2005, Pages 87 – 101.

[25] Stefan Glaser, Andreas Wüst. "Integrative Crash Simulation of Composite Structures. The Importance of Process Induced Material Data". 5th European LS-DYNA Conference, 2005.

[26] J. S. Kim, H. Huh, K. W. Lee, D. Y. Ha, T. J. Yeo, S. J. Park. "Evaluation of Dynamic Tensile Characteristics of Polypropylene with Temperature Variation". International Journal of Automotive Technology, August 2006, Volume 7, Number 5.

[27] Susan I. Hill, Peter Sjöblom. "Practical Considerations in Determining High Strain Rate Material Properties". SAE Document N° 981136.

[28] Hill, S.I., M.F. Pinnell, and A.J. Minch. "Standardization of High Strain Rate Tensile Testing of Polymers". Paper presented at the ANTEC, Society of Plastic Engineers, May 1-5, 2005.

[29] Pinnell, M.F., S.I. Hill, and A.J. Minch. "Special Concerns in High Strain Rate Tensile Testing of Polymers". Paper presented at the SAE World Congress, April 2006.

[30] M. Keuerleber, P. Eyerer, J. Biihring. "Measurement of Strain Rate-Dependent Material Properties for Polymers". ANTEC 2001 Presentation, May 6-9.

[31] F. Barthelat and H. Lobo: "High Velocity 3 Point Bending Test Using an Impact Tower", Society of Plastics Engineers, Annual Technical Conference, May 7-11 2000, Orlando, FL.

[32] Massimo Nutini, Mario Vitali. "Procedimiento para medir la tensión real/deformación real en ensayos de tracción a alta velocidad para poliolefinas en el mercado del automóvil". Jornadas "Los Plásticos en Automoción", Barcelona, 2003.

[33] Christopher Clark, Paul E. Johnson, Colin Frost. "High Strain-Rate Characterization of Thermoplastics Used for Energy Management Applications". SAE Document N° 940882.

[34] Christopher L. Clark, Deborah J. Locke. "High Strain Rate Testing of Engineering Thermoplastics for Head Impact Applications". SAE Document N° 960153.

[35] S. Sundararajan, K. Aekbote, C. C. Chou, G. G. Lim, J. Chickola and L. A. Walker. "High Strain-Rate Tensile Testing of Door Trim Materials". SAE Document N° 971064.

[36] B. C. Duncan and A. Pearce. "Comparison of Impact and High Rate Tests for Determining Properties of Adhesives and Polymers needed for Design under Impact Loading". NPL Report CMMT (A) 134, January 1999.

[37] S. M. Walley, J. E. Field, P. H. Pope and N. A. Safford. " Strain Rate Sensitivity of Polymers in Compression From Low to High Rates". DYMAT Journal Vol. 1, N° 3, September 1994, 211-227.

[38] G.M. Swallowe, and S.F. Lee, "Direct Measurement of High Rate Stress-Strain Curves using Instrumented Falling with and High Speed Photography", The Imaging Science Journal, 52(4), 2004, pp193-201, ISSN 1368-2199.

[39] Keith N. Knapp II, A. Gabrielle and Daeyon Lee. "Stress-Strain Response of Polymers for Predicting the Behavior of Integral Fasteners". ANTEC'97, Society of Plastic Engineers, 1997.

[40] M. Junginger, H. Werner, F. Huberth. "Measurement Technique for Local Strain Determination and its Application to Plastic Materials in the Automotive Industry". CRASH-MAT 2001, 24.-25. April, Freiburg.

[41] Klaus Thoma. "Measurement of Mechanical Parameters in the Range of High and Highest Strain Rates. Examples of Practical Application for a Wide Spectrum of Materials". Invited Paper given at the Material Testing Conference 2002, German Association for Materials Research and Testing, 5 - 6 December 2002, Bad Nauheim, Germany.

[42] R. D. Dean, G D, Mera. "Measurement of Failure in Tough Plastics at High Strain Rates". :NPL Report DEPC-MN 028, September 2005. ISSN: 1744-3910.

[43] Ph. Bkguelin, M. Barbezat and H. H. Kausch. "Mechanical Characterization of Polymers and Composites with a Servohydraulic High-Speed Tensile Tester". J. Phys. III Francel (1991) 1867-1880.

[44] J. Fitoussi, F. Meraghni, Z. Jendli, G. Hug, D. Baptiste. "Experimental Methodology for High Strain-Rates Tensile Behaviour Analysis of Polymer Matrix Composites". Composites Science and Technology 65 (2005) 2174–2188.

[45] Luke Perkins and Hubert Lobo. "A Novel Technique to Measure Tensile Properties of Plastics at High Strain Rates". ANTEC, Boston 2005.

[46] Reinhard Hafellner. "Neue Flexible Methoden der Materialdatenermittlung für die Dynamische Simulation". 3. LS-DYNA Anwenderforum, Bamberg 2004

[47] Peter Reithofer, Martin Fritz, Reinhard Hafellner "4a Impetus. Efficient Evaluation of Material Cards for Non-Reinforced and Reinforced Thermoplastics". 7th European LS-DYNA Conference, Salzburg, Austria, May 2009.

[48] R.R.P. Rodenburg. "Development Process of Seamless Airbag Covers. Description of Tools and Generation of Material Properties using High Strain Rate Tensile Testing". Report n° MT 04.13, TU/e Internship Report July 2004.

[49] M. Reiter and Z. Major. "Determination of Tensile Properties of Polymers at High Strain Rates". EPJ Web of Conferences 6, 39008 (2010).

[50] LS-DYNA® Keyword User's Manual. Volume I, June 2009 Version 971/Release 4 Beta, Livermore Software Technology Corporation (LSTC).

[51] M. Nutini, M. Vitali "Characterization of Polyolefins for Design under Impact: from True Stress/Local Strain Measurements to the F.E. Simulation with Ls-Dyna Mat. SAMP 1". 7. LS-DYNA Anwenderforum, Bamberg 2008.

[52] A. Haufe, P.A. Du Bois, S. Kolling and M. Feucht. "A Semi-Analytical Model for Polymers subjected to High Strain Rates". 5th European Ls-Dyna Users Conference.

[53] A. Haufe, P.A. Du Bois, S. Kolling and M. Feucht "SAMP-1: A Semi-Analytical Model for the Simulation of Polymers". 4. LS-DYNA Anwenderforum, Bamberg 2005.

[54] H. Daiyan, F. Grytten, E. Andreassen, O. V. Lyngstad, H. Osnes. "Numerical Simulation of Low Velocity Impact Loading OF Polymeric Materials". 7th European Ls-Dyna Conference.

[55] Mario Polanco-Loria, Arild Holm Claussen, Torodd Berstad and Odd Sture Hopperstad. "A Constitutive Model for Thermoplastics intended for Structural Applications". 7th European Ls-Dyna Conference.

[56] Sven Robert Raisch and Bernhard Möginger. "High rate tensile tests – Measuring equipment and evaluation". Polymer Testing, Volume 29, Issue 2, April 2010, Pages 265-272.

[57] Nadia Temimi-Maaref, Alain Burr, Noëlle Billon. "Damaging Processes in Polypropylene Compound: Experiment and Modeling". Polymer Science, Ser. A, 2008, Vol. 50, No. 5, pp. 558–567.

[58] L. Aretxabaleta, J. Aurrekoetxea, I. Urrutibeascoa and M. Sánchez-Soto. "Characterisation of the Impact Behaviour of Polymer Thermoplastics". Volume 24, Issue 2, April-April 2005, Pages 145-151.

[59] Adam Dustin Mulliken. "Low to High Rate Deformation of Amorphous Polymers: Experiments and Modelling". Master Thesis, MIT, 2004.

[60] Benedetta Marmiroli. "Correlazioni tra il processo di produzione, la microstruttura e le proprietà di materiali per la previsione del comportamento di manufatti in esercizio". Dottorato di Ricerca in Ingegneria Industriale, XVI ciclo, 2004.

[61] Z.N.Yin, T.J.Wang. "Deformation of PC/ABS Alloys at Elevated Temperatures and High Strain Rates". Materials Science and Engineering A 494 (2008) 304–312.

[62] J. P. F. Inberg, A. Takens, R. J. Gaymans. "Strain Rate Effects in Polycarbonate and Polycarbonate/ABS Blends". Polymer 43 (2002) 2795-2802.

[63] MarcusSchoßig, ChristianBiero, Wolfgang Grellmann, Thomas Mecklenburg. "Mechanical Behavior of Glass-Fiber Reinforced Thermoplastic Materials under High Strain Rates". PolymerTesting 27(2008) 893–900.

[64] D. Rittel, A. Dorogoy. "A Methodology to assess the Rate and Pressure Sensitivity of Polymers over a wide range of Strain Rates". Journal of the Mechanics and Physics of Solids 56 (2008) 3191–3205.

[65] Judith Pouwlien Frederika Inberg. "Fracture of Polycarbonate/ABS Blends". Thesis, University of Twente, Enschede, The Netherlands, April 2001.

[66] Nadia Temimi-Maaref. "Comportement thermo-mécanique et rupture de polypropylènes. Etude expérimentale et modélisation". Thesis, Ecole Doctorale 364 : Sciences Fondamentales et Appliquées.

[67] Elhem Ghorbel. "A Viscoplastic Constitutive Model for Polymeric Materials". International Journal of Plasticity 24 (2008) 2032–2058.

[68] Xinran Xiao. "Dynamic Tensile Testing of Plastic Materials". Polymer Testing 27 (2008) 164–178.

[69] E. Andreassen, H. Daiyan, F. Grytten, O.V. Lyngstad, R.H. Gaarder and E.L. Hinrichsen. "Mechanical Testing for Generating Input to Numerical Simulation Impact response of Injection-Moulded Components". Proceedings of the Polymer Processing Society 24th Annual Meeting ~ PPS-24 ~ June 15-19, 2008 Salerno (Italy).

[70] H.Louche, F.Piette-Coudol, R.Arrieux, J.Issartel. "An Experimental and Modeling Study of the Thermomechanical Behavior of an ABS Polymer Structural Component during an Impact Test". International Journal of Impact Engineering 36 (2009) 847–861.

[80] T. Glomsaker, E. Andreassen, M. Polanco-Loria, O. V. Lyngstad, R. H. Gaarder, E. L. Hinrichsen. "Mechanical Response of Injection-Moulded Parts at High Strain Rates". Extended abstract for PPS07ea, Gothenburg, Sweden, August 2007.

[81] Hiroyuki Mae, Kikuo Kishimoto. "Modeling and Simulation of Impact Failure Characteristic of Polypropylene by Elastoviscoplastic Constitutive Law". Journal of Solid Mechanics and Materials Engineering, Vol. 1, N° 1, 2007.

[82] Ismene Lage Cañellas. "Material Model Validation in Ls-Dyna for Car Interior Head Impact Situation". Master Thesis, Cranfield University, 2004/05.

[83] Hubert Lobo and Brian Croop. "A Robust Methodology to Calibrate Crash Material Models for Polymers". NAFEMS World Congress 2009, Greece.

[84] F. Grytten, H. Daiyan, M. Polanco-Loria and S. Dumoulin. "Use of digital image correlation to measure large-strain tensile properties of ductile thermoplastics". Polymer Testing Volume 28, Issue 6, September 2009, Pages 653-660.

[85] Qin-ZhiFang, T.J.Wang, H.G.Beom, H.P.Zhao. "Rate-dependent large deformation behavior of PC/ABS". Polymer 50 (2009) 296–304.

[86] M. Avalle, M. Peroni and A. Scattina "Mechanical models of the behaviour of plastic materials:influence of time and temperature". Latin American Journal of Solids and Structures 7 (2010) 41–61.

[87] ISO 18872. "Plastics. Determination of tensile properties at high strain rates."
Norma ISO

[88] SAE J 2749. "High Strain Rate Tensile Testing of Polymers".

[89] ANSYS software manual.

[90] LS-DYNA software manual.

[91] VDA project "Mechanische Charakterisierung thermoplastischer Kunststoffe für die Crash-Simulation".

Polymer Testing

Volume 26, Issue 3, May 2007, Pages 284-305.

Property Modelling

Finite-element analysis of quasi-static characterisation tests in thermoplastic materials: Experimental and numerical analysis results correlation with ANSYS

A. Arriaga, J.M. Lazkano, R. Pagaldai, A.M. Zaldua, R. Hernandez, R. Atxurra and A. Chrysostomou.

Abstract.

The use of structural calculation software based on finite-element analysis is nowadays a common practice when designing new industrial products processed from thermoplastic materials. In order to make an adequate prediction of the service behaviour of plastic components, it is necessary to carry out appropriate analysis when working with the software. This requires both the correct mechanical characterisation of the materials used for inputting the required properties in the calculation code, and the specification of the different solution characteristics.

In the present work, both areas have been studied in order to find a good correlation level between experimental mechanical test results in thermoplastic materials (principally two material types have been evaluated, a Polypropylene PP BE677AI from BOREALIS and a polycarbonate/acrylonitrile–butadiene-styrene PC/ABS T 45 from BAYER) and simulation of the same tests in the finite-element code ANSYS.

Initially, a series of conditions that can affect the quality of the material data input and, therefore, the simulation results are defined. These are the testing conditions of the plastic samples, the methods of measuring different strain values in the uniaxial tensile tests or the conversion from engineering measured data to "true" values that can be analysed in the software.

Next, two quasi-static validation tests are defined for the comparison of the simulation and experimental results: these are the 3-point bending test and the plate penetration test using semi-spherical darts. Following the bending and penetration experimental tests, simulation of the tests under the same conditions in ANSYS was conducted, taking into account the different variables that can change the results obtained and, therefore, the correlation with the physical tests. The accountable variables include the use of different element types in the simulation (solid, shell and plane axis-symmetric elements), the use of different friction coefficients between the plastic and metallic parts, or the use of different values for the elastic Poisson's ratio.

From the results obtained, it can be seen that the correlation level found in both materials and both testing modes, i.e. bending and penetration, is good both in the shape of the response curves and the quantitative values, even at high strain levels. A conclusion that can be extracted from the work is that the use of a correct friction coefficient is fundamental for good correlation between the experimental and simulation results. On the other hand, there are additional points to consider such as the use of different element types or the conversion of engineering values to "true" values where, for the tests described and the testing conditions used, no excessive differences are observed between one method and another.

Polymer Testing

Volume 29, Issue 2, April 2010, Pages 170-180.

Property Modelling

Impact testing and simulation of a polypropylene component. Correlation with strain rate sensitive constitutive models in ANSYS and LS-DYNA.

Aitor Arriaga, Rikardo Pagaldai, Ane Miren Zaldua, Alicia Chrysostomou, and Michael O'Brien.

Abstract.

A 20% mineral filled polypropylene homopolymer (Hifax XM2 U16 from LyondellBasell Industries) was studied. Correlation between experimental impact tests of components and tensile tests on specimens with simulations in ANSYS and LS-DYNA were conducted. The main goal of these tests was to evaluate the validity of elasto-plastic strain rate sensitive constitutive models implemented in both codes. Initially, strain localisation or necking phenomena were studied by simulating quasi-static tensile tests in ANSYS. An iterative method was used to match experimental force-displacement curves and so obtain true stress-strain curves as input for finite element analysis programs. Subsequently, the experimental impact testing of parts manufactured from the mineral filled polypropylene was simulated in ANSYS and LS-DYNA.

It was found that the viscoplastic strain rate sensitive Perzyna's model compared well with test results from force-time and velocity-time curves but did not adequately describe the high force levels developed, particularly at the start of the tests. Additional sensitivity analyses in terms of element type, contact stiffness and mesh density were also carried out. Yield stress rate dependency was evaluated using the material model MAT 24 in LS-DYNA and, in addition, yield stress and elastic modulus rate dependency was evaluated with MAT 19. Both models offered very similar results. An initial attempt to simulate failure was also carried out with MAT 24.